

NCAR-TN/IA-99
NCAR TECHNICAL NOTE

May 1975

Scientific Ballooning Handbook

Alvin L. Morris, Editor

ATMOSPHERIC TECHNOLOGY DIVISION

NATIONAL CENTER FOR ATMOSPHERIC RESEARCH
BOULDER, COLORADO

PREFACE

The scientific foundations for ascent by balloon were established as early as Archimedes; a practical application of his principles, however, was to await another twenty centuries. From the moment the Montgolfier brothers succeeded in flying balloons that could carry useful loads, scientists were eager to use them. Today, employing technological developments in materials, communications, and electronics, and taking advantage of new information about the circulation of the atmosphere, man has made balloon systems servants of science which can be used virtually anywhere on earth. He is even contemplating their use on other planets.

The current revolution in scientific ballooning has resulted in a technology that is, in its own right, important to many groups; unfortunately the literature of that technology is not readily available. Much of it was classified when written and received extremely limited distribution. In particular, reports of the excellent work done at the

University of Minnesota, although now declassified, are not generally accessible. Other important work has been published in scientific or trade journals that are not identified with ballooning.

It was my purpose when I undertook the preparation of this handbook to summarize the current technology of ballooning as completely as possible. I have been fortunate in obtaining contributions from experts in most of the technological areas I consider important. When no one could be found to contribute a section dealing with an important area, other contributors were asked to include in their sections pertinent material from the missing area. The most notable omission is a section on materials. Therefore, more information on materials is included in several other sections than the authors of those sections might otherwise have chosen to include.

Each contribution was reviewed by at least one person other than the author in an effort to minimize errors and avoid major omissions. The final content of each section was determined by the author, however.

To limit the size of the book, I have included only those techno-

logical areas which I feel are rather directly associated with scientific ballooning and about which information is not readily available. Thus, there are no general mathematical tables. Given the abundance of handbooks available in most technical libraries and the nearly universal use of high speed computers by technologists, this elimination seems justifiable.

Material for this handbook was selected and organized with several groups of people in mind. The scientist whose experiment will be flown on a balloon, the engineer who designs the balloon or the equipment to be flown, and flight operations engineers and technicians will all find useful information in it.

Principles have been emphasized, but "cookbook" procedures are also given for a few facets of balloon operations, e.g., selecting a parachute. Tables have been made short, but linear interpolation is acceptable in nearly all of them. Equations from which more complete data may be generated are usually included for the convenience of anyone using a computer.

The help of experts from many fields was essential in the compilation of this book, and I am grateful to each author for his contribution. Many others also contributed and while I cannot list all of their names, I would like to thank the following people for their special efforts: Justin Smalley, John Sparkman, and Karl Stefan for their critical review of the sections I wrote; Jay Chalmers and Matthew Reynolds for extensive computer programming aid; and Carolyn Morris for typing the manuscript, helping with the editing, and providing constant encouragement.

Alvin L. Morris

October 1972

CONTENTS

Section		Number of Pages	Number of Plates
I.	Evolution of Ballooning, <i>R. H. Upson</i>	48	26
II.	Theory of Balloon Flight, <i>A. L. Morris</i>	99	53
III.	Energy Balance and a Flight Model, <i>F. Kreith</i>	110	56
IV.	Lift Gases, <i>A. L. Morris</i>	43	24
V.	Balloon Design Considerations, <i>J. H. Smalley</i>	46	26
VI.	Scientific Balloon Instrumentation, <i>O. L. Cooper</i>	120	64
VII.	Stabilization and Orientation of Balloon-Borne Instruments, <i>R. A. Nidey</i>	57	34
VIII.	Superpressure Balloons, <i>V. E. Lally</i>	45	26
IX.	Hot-Air Ballooning, <i>R. G. McCarty</i>	39	21
X.	Parachutes, <i>A. L. Morris</i>	44	25
XI.	The Atmosphere, <i>A. L. Morris and S. B. Solot</i>	81	45
XII.	Tables, Graphs, and Miscellaneous, <i>A. L. Morris</i>	136	70

SECTION I

LIST OF SYMBOLS

EVOLUTION OF BALLOONING

by

Ralph H. Upton

List of Symbols ii

List of Figures iv

A. HISTORICAL INTRODUCTION 1

B. OPERATING CONDITIONS 4

C. ENVELOPE CONSTRUCTION 11

D. INSTRUMENTATION 15

E. FABRIC TESTING 16

F. INTERMEDIATE DEVELOPMENTS 19

G. INTRODUCTION OF THE NATURAL SHAPE 22

A CHRONOLOGY OF BALLOONING 34

A SHORT BIBLIOGRAPHY OF BALLOON HISTORY 46

REFERENCES 48

<u>Symbol</u>	<u>Description</u>	<u>Dimensions</u>
b	specific lift of gas	$ML^{-2}T^{-2}$
G	total weight carried at attachment point of balloon	MLT^{-2}
K	a shape constant [defined by Eq. (1)] which is determined by the design and operational conditions of a balloon	L^{-3}
m	subscript identifying its symbol with the equator of a balloon	
n	subscript identifying its symbol with the natural shape	
o	subscript identifying its symbol with a reference level far below a balloon's ceiling	
p	pressure	$ML^{-1}T^{-2}$
R_m	radius of curvature of a meridional section of a balloon	L
R_s	radius of a spherical balloon	L
s	gore length measured downward from the top of a balloon	L
s	subscript identifying its symbol with a sphere	
t_c	circumferential (horizontal) tension per unit of material width	MT^{-2}
t_m	meridional tension per unit of material width	MT^{-2}

t_s	meridional tension per unit of material width in a spherical balloon	MT^{-2}
V	volume (of gas or balloon)	L^3
V_o	volume of a balloon at a reference level far below the balloon's ceiling	L^3
V_s	volume of a spherical balloon	L^3
x	distance measured radially outward from the vertical axis of a balloon	L
x_o	radial distance from axis to balloon skin at level of zero differential pressure	L
x_l	radial distance from axis to edge of taut cap	L
y	distance measured upward	L
y_n	vertical distance measured from the top of a natural shape balloon to a point on the balloon skin. This distance may be given approximately by a cubic equation	L
y_o	vertical distance measured from the level of zero differential pressure to the top of a balloon	L
y_s	vertical distance measured from the top of a spherical balloon to a point on the balloon skin. This distance may be given approximately by a quadratic equation	L

π	3.14159
θ	angle balloon skin makes with the vertical

List of Figures

Fig. 1	Spherical balloon shapes under full and partially full (slack) conditions. Note that the balloon is vented at the bottom so that air fills the slack balloon below the zero-pressure level . . .	6
Fig. 2	Some forms which a natural shape balloon may take	10
Fig. 3	Natural shape balloon fully inflated right and partially inflated left. There is no air inside the balloon.	12
Fig. 4	Distribution of stress on a spherical balloon and comparison of the spherical and natural shapes	26
Fig. 5	Comparison of meridional stress at the edge of the taut cap in a partially inflated spherical balloon with stress in the same balloon after it is fully inflated	29

Greek letters

ρ	air density	ML^{-3}
--------	-------------	-----------

EVOLUTION OF BALLOONING

A. HISTORICAL INTRODUCTION

Balloons, like all floating bodies, demonstrate the principle of Archimedes (see Chronology). He not only proved the principle experimentally but showed by sound reasoning that a statically floating body must displace its own weight of the fluid in which it floats. This principle in its original form is as valid in air as in water, yet for 2000 years thereafter, men watch smoke rising through the air without thinking how it could be put to practical use. This long period was broken by two flashes of inspiration--Roger Bacon's proposal in the middle of the 13th century of a (then hypothetical) lighter-than-air filling, and Father Lana's proposal in 1670 of a vacuum balloon. The latter device, which is theoretically sound, is still frequently reinvented by people unfamiliar with shell structures, available materials, and the realities of atmospheric pressure. Here, as usual, faith in an idea can be effective only when combined with knowledge of the difficulties to be faced and with realizable means of meeting them.

The practical breakthrough--the French Montgolfier brothers' hot-air balloon--was a tribute to the intelligent artisans' powers of observation and flair for feasible construction. Still, it was the noted scientist Charles, in collaboration with two artisans, the Robert brothers, who shortly afterward introduced the hydrogen-filled balloon, with features of construction that remained standard for over 150 years. Even the basic instruments have been retained for nearly as long as the general features developed in the early days.

The technological developments most effective in dictating modern balloon design and use are probably improved plastics, helium gas, and for sport use, a reversion to hot air. These developments are still far from complete. In general, however, flexible, high-strength film permits making the balloon a self-contained unit with no net to carry the load and with a weight saving that greatly extends the altitude capability. Gas-tight, high-strength material also makes feasible for the first time altitude stabilization by superpressure. Helium not only disposes of the fire risk but also significantly stabilizes the balloon with respect to altitude changes.

For special purposes older methods are still useful. The self-adjusting, load-carrying net might well be reconsidered for conditions varying from partial inflation to superpressure, and hydrogen is relatively inexpensive, readily available, and well suited to any demand for a fast-rising balloon or for one designed to float in a strongly stable layer of the atmosphere (1). The long and successful record in the use of flammable gas for free balloons seems to justify a re-evaluation of hydrogen for the more demanding of these conditions, with due consideration of the skin material's electrostatic properties, avoidance of flame in operation, and suitable precautions generally. Experience shows Mylar to be much more prone to static sparks than polyethylene.

A modern plastic balloon is essentially a shell structure of material incapable of carrying compression and having a small but appreciable weight. Each element of skin is in static balance from its own tangential tension and the normal pressure difference between inside and outside. This pressure difference, usually positive, can also be negative in gas below the level of zero-pressure difference.

A balloon's profile or axial section was formerly quite arbitrarily assumed, and common designed to be a circle. In fact, a free balloon was referred to as a spherical balloon to distinguish it from the elongated kite balloon or dirigible balloon (airship). Even the early netless balloons were close to spherical, with long footropes attached to loading points near the equator (1). The spherical concept had a further lingering death in the cone-on-sphere shape of the early plastic designs, but its structural limitations for high altitude use had already be recognized.

B. OPERATING CONDITIONS

We must here recall the status of balloon theory 40 years ago. In 1898 the term "scientific ballooning" was applied to physical and atmospheric research and was later applied to the use of scientific principles in balloon operation to replace the largely rule-of-thumb techniques in almost exclusive use up to 1913. These principles were at first applied mainly to the winning of balloon races with the objective of spanning the greatest distance from the starting point. As outlined in reference (1), the operational improvements introduced after 1913 included better instruments, precise navigation, a means of sounding for air currents, establish-

ment of quantitative balloon response to measured discharge of gas and ballast through the use of a stop watch with a calibrated gas valve; all of these were coupled with the best possible appraisal of the general weather conditions.

As shown by Fig. 1, two operational conditions of the balloon had long been recognized: full and partially full (slack or flabby). A rising, full balloon would discharge gas by automatic spillage; a slack balloon would not. Except for the final landing approach, this means of gas control remained the only one in practical use until the advent of the calibrated valve. Here it should be noted that vertical control was especially critical in the usual daytime unstable conditions dictated by the use of moist gas having two or more atoms per molecule. Such gas responded to altitude change with a temperature change numerically less than the average or standard lapse rate (negative gradient) in the troposphere.

It seemed to be tacitly assumed that the partially-filled balloon would necessarily be in a less critical condition structurally than a full one. The error in this assumption was not serious as long as operation was

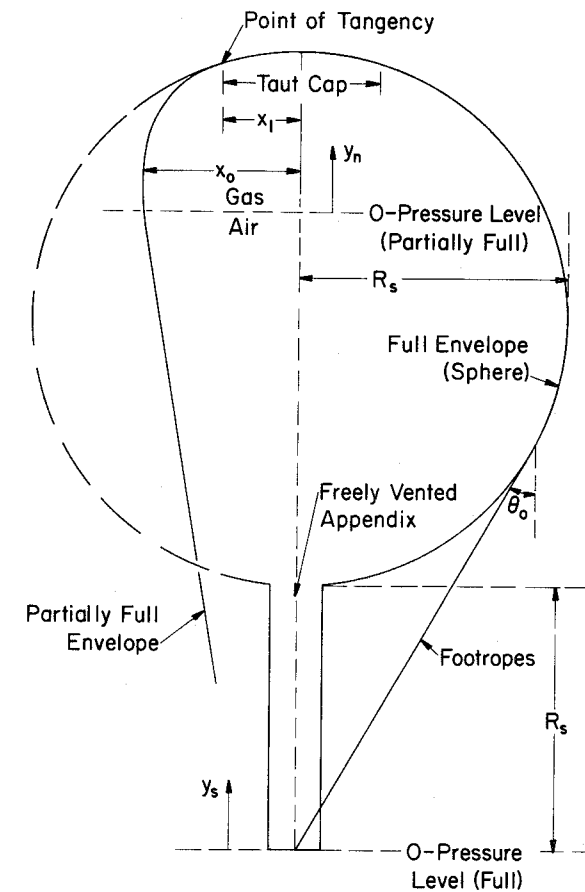


Fig. 1. Spherical balloon shapes under full and partially full (slack) conditions. Note that the balloon is vented at the bottom so that air fills the slack balloon below the zero-pressure level.

confined to the lower troposphere, but with stratosphere expeditions using netless balloons it was a different story (2).

An important property of the traditional balloon net is its distribution of load in two dimensions over a substantial range of shape and pressure variation, especially if similarly shaped meshes are retained toward the top. A similar property can theoretically be had by a suitable arrangements of threads and panels of woven fabric, but this property is practically destroyed in conventional two-ply rubberized fabric in which only one ply is laid on the bias. The same applies to any flexible but essentially inextensible membrane, for reasons that will now be apparent.

In a balloon carrying the usually concentrated payload, this gravity load must, of course, reappear in the axial component of circumferentially integrated (total) meridional tension adjacent to the load attachment level, where such stress must also be in normal balance with the local gas pressure. Since there must always be stress in the meridional direction, it is clear that any slack to accommodate a less-than-full condition must be in the circumferential direction. It is also clear that with gas pressure normal to the surface, only the skin weight, or other applied load, can

change the total tension within a slack portion of the balloon at a given altitude. Thus, in such a portion of the balloon, aside from skin weight, the stress or tension, t_m , per unit of horizontal circumference varies inversely as the circumference $t_m = G/(2\pi \times \cos \theta_o) = bV/(2\pi \times \cos \theta_o) = pR_m$, where G is the total weight carried at the concentration point. Also, the same stress is all that carries the pressure, which in this simplified case varies as the gas head measured from the level of zero gage pressure, or $p = by$. Then $t_m \propto 1/x$ and $p \propto y$, or

$$p/t_m = 1/R_m = Kxy = \frac{2\pi xy}{V} \cos \theta_o \quad (1)$$

where x and y are the coordinates of the profile curve, $1/R_m$ is the meridional curvature at the same point, and K is a constant applying to a particular slack portion of a balloon, which is quantitatively determined by the design and operational conditions. For finite skin weight the effective pressure p must include the normal weight component of unit skin weight and the integrated meridional component of skin weight t_m .

This is the basic equation of what has come to be known as the natural shape. Even in its elementary form for weightless skin carrying zero circumferential stress, the integrated curve of the profile can take an infinite

variety of shapes depending on the starting coordinates and slope and on the value of K . Several examples are qualitatively shown in Fig. 2. A particular shape studied in reference (2) was approximately the profile of a gas bubble in a partially-filled balloon designed as a sphere, as shown in Fig. 1. Here at the left the circumferential elements of the skin are slack below a certain critical level where the designed circle and the natural shape come tangent to each other. Above this level the envelope is free to fill out to its full designed shape in what has been called the taut cap, and the maximum stress is determined by the meridional stress at its edge.

The next step in design development came with the thought that the natural shape, prevailing over most of the surface during most of an ascent to high altitude, might logically be made the designed shape of the full balloon. In other words, for a balloon vented to the atmosphere the circumferential stress is of so little use that it may as well be assumed of no use and the balloon designed accordingly. This assumption also fitted well the commonly prevailing condition of meridional gores joined by relatively low-strength, unreliable seams carrying meridional reinforcing tapes.

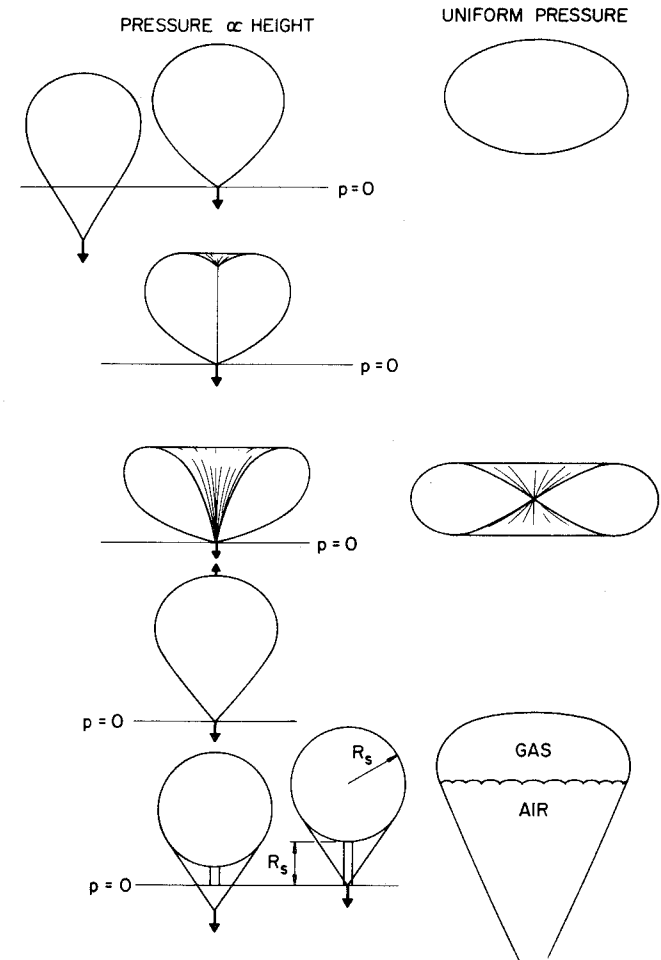


Fig. 2. Some forms which a natural shape balloon may take.

An idealized complete profile from the same equation is shown by the outer curve on the right in Fig. 3. It is based on the assumption that at the bottom $x = y = 0$ where θ_0 is 50.15° ; $K = 8.53$ throughout for balloon height = 1, reference (3). For comparison, the inner curve (right) in the same figure shows a full balloon with an appendix vent of length $a = 0.03$ ($K = 8.80$) on the same scale of $y_{\max} = 1$. Subsequent developments to date have been mainly refinements in balloons of this general shape, which, however, still present some problems of a rather basic nature.

C. ENVELOPE CONSTRUCTION

Beginning in 1910, the aspect of the aeronautical awakening of most interest to the management of the Goodyear Company was finding a new outlet for rubber products. After a brief and unsuccessful trial of rubberized fabric for wing covering, it was decided that a much better market for such fabric was balloons and airships. Also, since there was no fully established manufacturer of lighter-than-air (LTA) aircraft in this country, there appeared no alternative to the development of their own complete product in this field. As applied to free balloons, components of

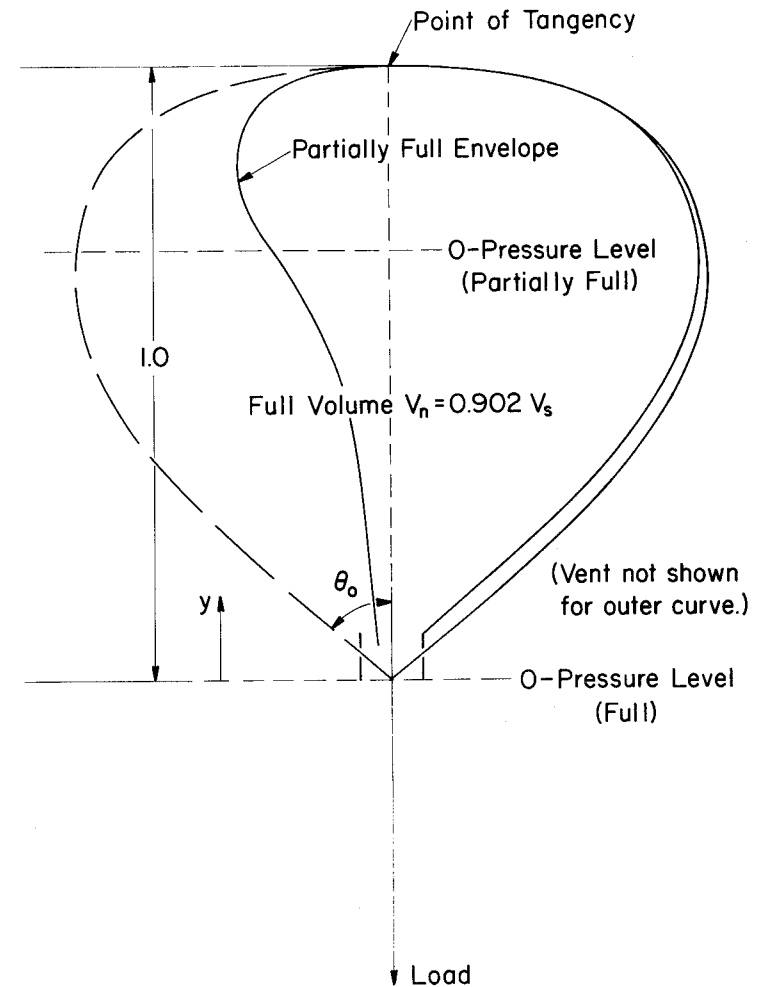


Fig. 3. Natural shape balloon fully inflated right and partially inflated left. There is no air inside the balloon.

the overall problem seemed to be as follows: material, general configuration, size and panel geometry, assembly, flight testing and operation.

Work proceeded at first with a relatively conventional shape and arrangement. With the type of fabric selected, it was obvious that its strength was not a critical factor, especially with a net to take the greater part of the load. Hence, the spherical shape was retained as having the maximum volume/weight ratio. This did not take into account at the time, however, the actual deformation of the shape in free flight with an open appendix of usual length and with a net proportioned to make its circumferential stress one-quarter of its meridional stress (width of each diamond mesh one-half of its height).

In approximating a sphere from initially flat panels, two arrangements were considered: 1) the commonly used meridional-gore system, and 2) conical rings. The latter was chosen for the first balloon, mainly for appearance and to facilitate arranging the panels brick fashion, thus avoiding four thicknesses of material at the corners. Each circumferential ring had the same number of identical panels except near the extreme top and bottom and allowed for seam overlap. The number of panels per circumference was

dictated by the need to economize labor and at the same time avoid excessive trim waste. Each pattern had typical dimensions tabulated as follows: chord length and off-set for convex side, same for concave side, width (end dimension). The chord length and off-set, setting up the required arc length and radius, were laid off by direct measurement on a simple double-bow device shaped to closely approximate a circular arc of any desired long radius, as determined by the setting of a central screw. The bias ply was run in the same helical direction (not herringbone) around the balloon, since the resultant slight twist about the center axis would be of no conceivable harm in a free balloon.

Seams were at first cemented, then sewed, and then taped, a procedure inherited from construction of the Vaniman airship envelope. The sewing was always a major headache, however, as the cement kept fouling the machines. Later, a properly made and aged seam was found to be adequate without the sewing. Some experimenting was done with small varnished balloons; one, built for an advertising contract, had an internal electric light. It was generally unsuccessful, however, because of the difficulty of tethering an

essentially spherical balloon. Sticking, cracking, and spontaneous combustion were other difficulties.

D. INSTRUMENTATION

Starting in 1910 there were several years of experiment and development for improving the sensitivity and utility of vertical-motion detectors. The European stratoscope, with a mechanical pointer, and the American Custer, a liquid type, were both good but lacked full quantitative significance. Tossing out a handful of fragmented tissue paper was about as informative. A more quantitative vertical airspeed meter consisted of a light counter-balanced vane, pivoted slightly above the center of gravity and free to swing over a calibrated scale. The utility of any aerodynamic indicator, however, depended largely on how closely a movement through the air correlated with a change in pressure altitude. This correlation was not always perfect and tended to break down completely with the much later introduction of dry helium.

A hypersensitive accelerometer was developed with the help of the Pioneer Instrument Company. It had a scale readable to 0.0001 of g, corresponding to less than 1.0 lb or 1/30 of a sandbag on an 80,000 ft³ balloon,

just the kind of accuracy wanted. It proved to be useless, however, because random creep, presumably due to elastic hysteresis, temperature change, and the passage of time, effectively destroyed any knowledge of the zero position. Present know-how would probably permit a satisfactory solution to this problem.

At the time the best solution was a sensitive change-of-altitude meter. This instrument was a long U tube containing two non-miscible liquids of slightly differing densities, one red, the other colorless. The line of separation was observed in a long glass tube of contracted section. One arm of the U vented directly to the atmosphere, the other through a chamber of finite volume whose atmospheric outlet could be closed off. The scale was calibrated so that when this outlet was closed, it read change of altitude. Watching and timing the change gave a fair idea of acceleration and vertical unbalance. The leak-type climb meter, subsequently developed for airplanes, was not too good because of its considerable lag and inadequate sensitivity.

E. FABRIC TESTING

A fabric testing program at Goodyear which was essential to the largely

parallel airship development gave results also of interest in ballooning. The mere handling of woven fabric shows the great difference in yield between the warp and web directions and the indefinitely large local yield in the diagonal direction of a single ply. Early tests showed that the strength of a sample tested rapidly in a standard tensile machine was deceptively large compared to strength of a sample under long-continued loading. The reduction of strength, although presumably asymptotic, seemed substantially complete after one or two days. With allowance for random variations, it was established that none of the fabrics tested could be expected to hold, for an indefinite time, more than about half of the machine-tested strength.

Another important material test was resistance to exposure. In this program, hundreds of samples were labeled, dated, and exposed to the elements on the roof and then strength-tested at specified intervals. In general, the rubberized fabrics were much more affected by sunlight than by any other agency. Almost all samples proved capable of going through a winter of cold, wet, ice, and snow, but many were almost ready to fall apart after a month of hot summer sun. Samples kept in the shade were much better

off. A fabric found most resistant to such deterioration was one heavily compounded with carbon black and externally aluminized. In 1919, this fabric was used in the construction of a racing balloon, Goodyear II, winner of the national race that year (Upson and Van Orman).

A series of tests on internal heating from radiation was also carried out. For this purpose, closed fabric envelopes containing thermometers were exposed to identical conditions of sun. From appearance the aluminized fabric already mentioned seemed a likely candidate for minimum heating but, to save time, was not actually tested prior to construction of the balloon. Its performance in flight was, in this respect, somewhat disappointing, and a subsequent comparative test showed it to heat more than the yellow fabric used in Goodyear I, possibly because of the carbon black under the thin aluminum surface since similar fabric without the aluminum heated most of all. A chalky white surface was the best, although not much better than yellow. No transparent material was tested since none then appeared suitable for balloon use. Considerable study was devoted to the relative importance of various fabric improvements (4).

F. INTERMEDIATE DEVELOPMENTS

In 1923 a balloon, designed by Upson but made by Goodyear, was tested with complete success. This balloon (1) is interesting as a transition between early and modern designs. It had a single thickness of white rubberized woven fabric laid herringbone fashion as in the old Upson parachute patent, and strengthened with meridional load-carrying tapes. These tapes were carried into a heavily reinforced conical cap at the top. The bias-laid fabric was self-adjusting to the effects of varying volumes and pressures. Rain was perfectly shed by the conical top, off-set valve, and an equatorial rim--the latter serving also to dampen the vertical motion, a feature not recommended for use with helium, however. The single, precise valve served all gas discharge purposes except quick deflation, for which a conventional rip panel was provided.

The following year (1924) the use of white, single-ply fabric was continued by W. T. Van Orman in Goodyear III with an envelope weighing 315 lbs as compared with 720 lbs for Goodyear II of the same size. In this and subsequent balloons up to Goodyear X in 1933, Van Orman set a phenomenal record by winning five national and three international distance races, three

times beating Belgium's Demuyter. A similar single-ply fabric was used in the record altitude Explorer II of Stevens and Anderson in 1935. Other improvements by Van Orman were the use of radio compass and celestial navigation, both later adopted by air transport and navigators.

Structural and aerodynamic experience with kite balloons and airships, particularly the metal-clad ZMC-2 (5), resulted in indirect benefits to all balloon development. Progress in airplanes and seemingly unrelated fields contributed its share. In the meantime, rubber and neoprene balloons had been improved to an extent permitting instrumented flights to altitudes previously unreachd by the more conventional, vented type. However, the usual bursting of the balloon at ceiling was an effective bar to prolonged flight. The time seemed ripe for new ideas.

Development of the modern plastic balloon started with a series of cellophane balloon flights by Jean Piccard with T. H. Johnson and John D. Ackerman, mainly at the University of Minnesota in 1936 (6). These flights were unmanned and were controlled by an automatic ballast dispenser based on aerodynamic vertical motion, like the vertical airspeed meter previously mentioned. These balloons and the succeeding ones of polyethylene built by

the General Mills Company had a rough approach to a natural shape approximated by a cone-on-sphere (6).

Studies at the University of Minnesota by Ney, Winckler, and others resulted in particularly valuable advances in launching techniques and in increased knowledge of the flight thermodynamics of helium-filled balloons.

Reference has already been made to the still impractical idea of a vacuum balloon, but the same type of equation, with modern materials, has definitely feasible application to superpressure balloons. A generally sound example of such application is in the mathematics of Zahm (7), which shows the relationship of stress and elastic yield required to maintain altitude in event of leakage. As may be noted in the Chronology, the superpressure idea was also proposed by Vaniman in 1912. The first structure capable of acting in this manner, however, was the metalclad ZMC-2 launched in 1929. Tested strength of the metal and seams, confirmed by water-model tests, showed that the hull could carry an ample reserve of pressure for altitude stabilization, although this was not a feature important in airship operation under power.

G. INTRODUCTION OF THE NATURAL SHAPE

The so-called natural shape of the freely vented balloon dates back to 1934 when the failure of the first Explorer balloon was the stimulus for a shape-and-stress analysis of a partially-inflated balloon in Upson's lecture to a lighter-than-air class at the University of Michigan. These lecture notes reappeared in an IAS paper published in 1939 (2). As a result of several studies for General Mills (3), a mathematically derived curve was applied to the designed profile of the entire balloon. In the meantime, Arnstein and Swan at Goodyear had simulated a form of the same curve by a system of weights and pulleys acting on a chain (8). Further development of this type of profile resulted in its becoming practically standard for vented plastic balloons. It is perhaps unfortunate that the natural shape has come to be so closely associated with the one general form typified by Fig. 3, with only minor variations in the design geometry due to skin weight, vent location, and load attachment. Experience continues to remind us that it is not the full balloon, envisioned by the design geometry, which usually poses the most critical problem. The really critical condition in any high-altitude operation almost invariably occurs as it did with the old Explorer,

when the balloon is inflated to a small fraction of the design volume.

Under these conditions any netless balloon of the type here considered takes a natural shape over a substantial portion of its surface, but this is a natural shape only in the mathematical sense, as defined by Eq. (1). It has little apparent resemblance to the full profile of Fig. 3 and is highly variable as changes of altitude change the volume ratio.

To summarize the physical conditions to which Eq. (1) applies: it is any portion of a pressure-and-load-balanced curve of polar symmetry, generated by weightless, flexible skin carrying zero circumferential stress with linear variation of pressure. In a preliminary analysis of this kind, simplifying assumptions serve the same purpose as those appropriate to slender struts, Newtonian orbits, and other inherently complicated concepts of science and engineering.

It is instructive now to compare the spherical design of Fig. 1 with the special form of the natural shape typified in Fig. 3. In the latter case, the partially inflated condition is shown with the gas filling below the same zero-pressure level. Broadly speaking, in each case for any less-than-full condition, the skin is circumferentially slack at all points up

to where the natural profile of the less-than-full shape comes tangent to the full designed shape. The most meaningful difference between the two cases is that for the spherical design the point of tangency rises gradually as the gas volume decreases, whereas for the natural-shape design the entire profile is circumferentially slack for anything less than full volume. Quantitative consideration of this difference in behavior should do much in answering the question as to whether a real improvement in design has been made, and if so, what potential it may hold for further improvement.

As shown in Fig. 1, the full spherical form is attained with an appendix venting one radius length below the balloon, on the assumption of 30° footropes and material of negligible weight. The same condition can, of course, be had by throttling the usually shorter appendix to a slight superpressure, a condition assumed equivalent to that at the pressure ceiling. For any predetermined shape, the meridional stresses are simply determined by a balance of forces on either the top or bottom portion of the balloon, cut on a horizontal plane at a given level.

If the design radius of the spherical balloon is R_s and the unit lift b_s , the maximum stress in the full balloon is found to be

$$t_s = 1.5 b_s R_s^2 \text{ force per unit of circumferential length.} \quad (2)$$

This value of the merional stress occurs at the top and also just above the suspension band. A balance of force on an increment of skin area normal to the surface makes the circumferential stress of equal magnitude at the top but zero just above the suspension band. The general distribution of stress is shown in Fig. 4.

The above stresses are for the full volume $V_s = (4/3)\pi R_s^3$. When filled to a small fraction of this design volume, far below pressure ceiling, where the unit lift is b_0 and the volume V_0 , the distorted profile approximates the form shown by the innermost curve, top left, in Fig. 4. Trial integration of this curve shows the volume to be approximately $V_0 = 0.77 \pi y_0^3$ with $K = 2.60/y_0^2$ in Eq. (1).

Inspection of Eq. (1) shows that the natural curve approaches a cubic parabola at the top (3), whereas the spherical profile there approaches an ordinary parabola. These curves are shown in Fig. 4. By equating their slopes at x_1 , where $x_1 \ll R_s$ and $y \approx y_0$, we get immediately $R_s = 2 R_m$. In other words, where the slack portion of the balloon merges into the taut

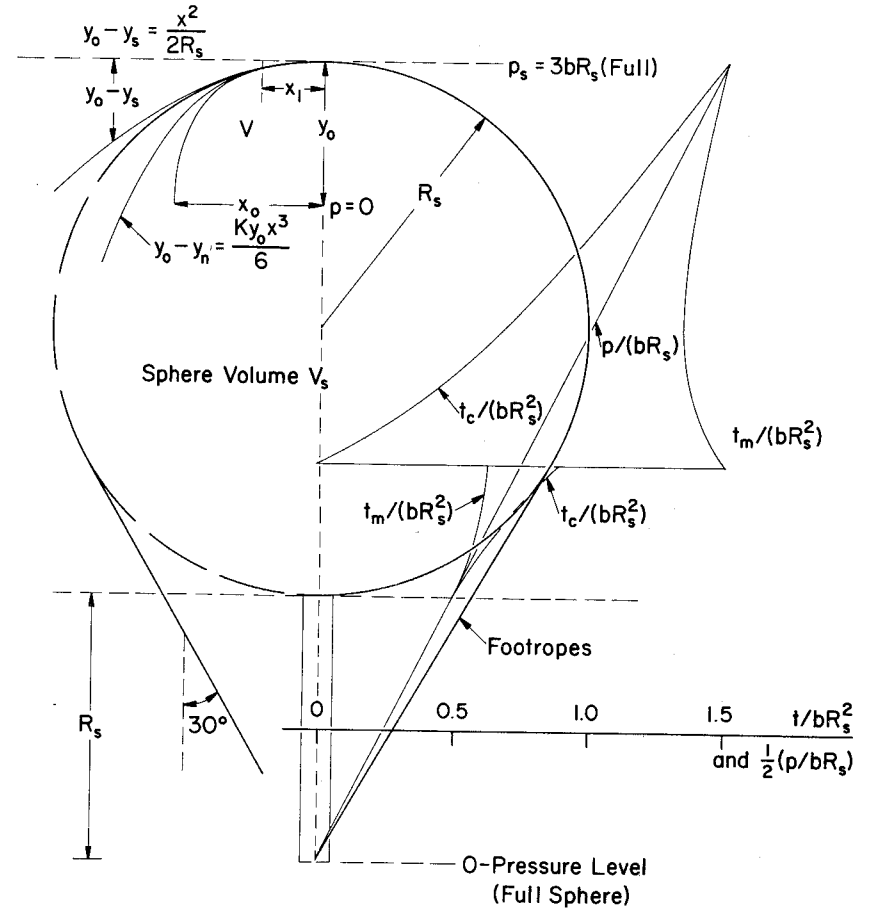


Fig. 4. Distribution of stress on a spherical balloon and comparison of the spherical and natural shapes.

portion, the meridional radius suddenly doubles. Just above this point, the normal force balance on an incremental area of fabric requires the meridional stress to remain unchanged, but now with a circumferential stress of equal magnitude, a condition which then prevails throughout the entire taut cap (if small).

Use of the above principles permits a simple comparison of stress between the full balloon and the same balloon with a small fraction of full inflation, but for constant gross lift and weightless fabric. As already noted, the maximum stress in the full spherical balloon is

$$t_s = 1.5bR_s^2 = 0.577bV_s^{2/3}$$

where b is the unit lift at ceiling. For partial inflation, at low altitude, where the unit lift is b_0 , the maximum stress at the edge of the taut cap of radius x_1 is given by

$$t_m = b_0 V_0 / (2\pi x_1)$$

where

$$V_0 / \pi = 0.77y_0^3$$

also

$$x_1 / R_s = 0.77 (y_0 / R_s)^2 = 1.11 (V_0 / V_s)^{2/3}$$

and

$$y_0 / R_s = 1.20 (V_0 / V_s)^{1/3}$$

The volume $V_s = (4/3)\pi R_s^3$ for the full sphere, $V_0 = 0.77\pi y_0^3 = \pi R_s x_1 y_0$ for variable inflation to a small fraction of V_s . Furthermore, $b/b_0 = V_0/V_s$ for expansion of the same mass of gas. Use of the above relationships now gives the stress ratio at partial inflation relative to full inflation as

$$t_m / t_s = \frac{(4/3\pi)^{1/3}}{2 \times 1.11 \times 0.577} (V_s/V_0)^{2/3} \approx 0.40 (V_s/V_0)^{2/3} = 0.40(\rho_0/\rho)^{2/3} \quad (3)$$

Results are plotted in Fig. 5 with the dashed curves corrected for the otherwise neglected volume difference of the spherical segment comprising the taut cap and the finite value of the meridional angle at the bottom of the gas-filled portion, as shown in Fig. 1.

It is clear from Eq. (3) that the stress tends rapidly to approach an infinite value as the design ratio V_s/V_0 increases. This theoretical value would actually be approximated were it not for the elastic and plastic yield of the material. The same condition is designed into the full natural shape of Fig. 3, since here the stress is concentrated at the top--the theoretical stress center--for all volume ratios, but the meridional force is finite per

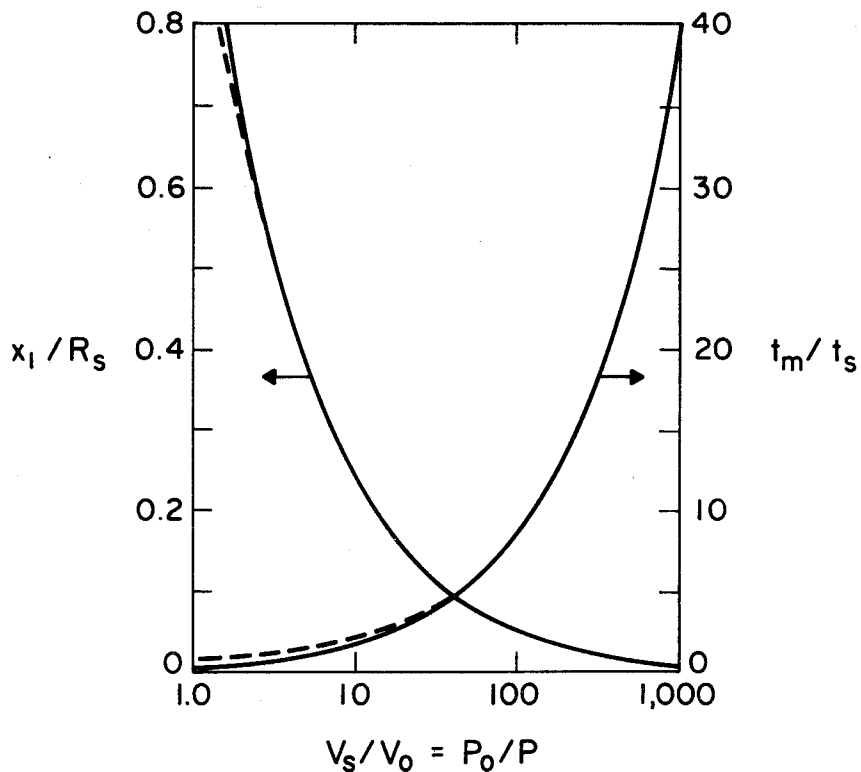


Fig. 5. Comparison of meridional stress at the edge of the taut cap in a partially inflated spherical balloon with stress in the same balloon after it is fully inflated.

meridian tape. On this basis, the load carried per tape actually increases as the volume expands, due to the increased cone angle at the bottom, but is constant along the meridian for any weightless natural shape. The area increment on which the pressure acts still varies with the circumference, making the mathematics basically the same as for any slack condition. The tape construction, however, seems no panacea for problems of the spherical shape, if any of it remains, since the stress in a small taut cap is theoretically the same in all directions, including the normally untaped circumferential direction. By the same theory, in the full natural shape we have reduced the dimensions of the taut cap to zero for all volume ratios. However, can we be sure of this actual result? A second look seems in order.

It is apparent, even from the rough sketches presented here, that practically all smooth curves become indistinguishable as we move close enough to the top. Specifically, we are interested in the difference of meridian or gore length in the taut cap between the spherical and natural shape ($s_s - s_n$), represented respectively by ordinary and cubic parabolas (3). Using the simplified integration of (9), we get for the "geometric strain" or relative difference between the two curve lengths out to a radius x

$$(s_s - s_n)/x = x^2/8R^2 \quad (4)$$

For example, if the cap has a radius one-tenth that of the full balloon, a material strain of 1/800 will make up the difference. Practically speaking, this means that the top of any balloon with a continuous curve and an unwrinkled surface is structurally indeterminate. The same point is brought out more fully in references (3) and (10).

Alleviation of this tendency toward over-stressing near the top may be approached in one or both of two ways: 1) insuring that the stress center--where the tapes cross--remains exactly in the designed position; for example, depressing the top by an axial suspension member or extending it by the lift of a smaller balloon above; 2) reinforcement of the top surface to an extent making the circumferential strength approach that of the meridian strength.

For reasons already brought out, need for the latter provision is not appreciably discounted by use of a spherical top. Return to the spherical upper portion is not ruled out, however, to make maximum use of the designed volume in the full condition, if kept within safe stresses for all conditions.

The concept of the natural shape can be readily applied to a super pressure balloon and deserves some attention here. The theory is the same as already explained, all forces being carried by meridional elements and none circumferentially. With uniform pressure (equivalent to an infinite head of lifting gas) and negligible weight in comparison, the curve is a true elastica, which can be solved by elliptic integrals. The mechanical analogue is a straight elastic rod bent into a hoop and then compressed by two diametric forces until the curvature just disappears on opposite sides. With equatorial radius $x_m = 1$, a closely approximate algebraic equation is: $y = 0.598 \sqrt{1 - (x)^2.9}$. The resulting surface of revolution has a half-gore length of $1.31 x_m$, an enclosed volume of $2.75 x_m^3$, and a meridional radius at the equator of $R_m = \frac{1}{2} x_m$. It is a relatively unfavorable application of the natural shape or meridian-tape construction.

For a given volume, the elastica must carry a tape stress-to-density ratio double that of the sphere's skin material to equal the same structural weight. Also, this natural shape has 15% more frontal area in vertical motion and roughly 50% more drag. This is but one example of how overall conditions affect design.

I have attempted in this section to show not only the development to date, but the great amount of work still to be done, as may be facilitated by the more detailed coverage in subsequent sections. With suitable interpretation, the principles brought out will be found applicable not only to balloons but to flexible fluid containers in general: fuel tanks, inflated satellites, decoys and targets, deceleration gear, underwater craft, air-supported roofs, pneumatic boats, airplanes, etc.

A CHRONOLOGY OF BALLOONING

- c. 240 BC: Archimedes discovered the principle of flotation.
- c. 1250 AD: Roger Bacon suggested that a light vessel filled with some (hypothetical) fluid lighter than air could use the same flotation principle in the atmosphere.
- c. 1600: Galileo determined the approximate density of low-level air.
- c. 1670: Francesco de Lana proposed a vacuum balloon to be driven by a sail--the latter, of course, a fallacy for free flight. He also confirmed the density of air and the effect of heat.
- c. 1766: Henry Cavendish discovered hydrogen and showed it to be at least seven times lighter than air.
- c. 1781: Tiberius Cavallo made hydrogen-filled soap bubbles that floated.
- 1782: Joseph and Jacques Montgolfier floated small paper balloons filled with smoke, called Montgolfier's gas.
- June 4, 1783: The Montgolfiers, in a public exhibition, sent up a paper-lined linen balloon about 10 m in diameter which floated about 3 km in 10 min. Although inflated with smoke from a straw fire, heat was not yet recognized as the dominant source of reduced density.
- Aug. 27, 1783: Under the auspices of the French Academy of Sciences, J. A. C. Charles sent up a hydrogen-filled balloon of rubber-coated silk, 4 m in diameter, made by the Robert brothers. It rose to about 1000 m and traveled 24 km

- in 45 min. Charles's name is also well-known for his work on gas expansion by heat.
- Sept. 19, 1783: A Montgolfier balloon successfully carried a sheep, a cock, and a duck about 3 km in 8 min.
- Nov. 21, 1783: First manned flight: Pilatre de Rozier and the Marquis d'Arlandes flew in a Montgolfier in which the heat was replenished in flight by a straw fire. The balloon, 15 m in diameter, ascended about 100 m and traveled 8 km in 20 min, during which time the balloon caught fire but was extinguished with water carried for that purpose.
- Dec. 1, 1783: J. A. C. Charles and M. N. Robert ascended from Paris to about 600 m and landed 43 km away after 2 hr in the air. Robert then alighted and Charles continued the flight briefly to 2700 m altitude as measured by a barometer. This hydrogen-filled balloon was substantially spherical and used a net, load ring, valve, open appendix, and sand ballast, all of which were later to be almost universally adopted.
- 1783: D. Rittenhouse and F. Hopkinson at Philadelphia experimented with a cluster of up to 47 small hydrogen-filled balloons with which James Wilcox was reportedly paid to make a flight of about 10 min, his downward control being effected by puncturing several of the balloons (the same in principle as Jean Piccard's control of a cluster a century and a half later). The evidence of Wilcox's flight seems not entirely convincing.

- Jan. 19, 1784: The largest hot-air balloon on record, over 30 m diameter, made one ascent (from Lyons), terminated in 15 min by a rent in the fabric--a seeming premonition of some modern failures. Although presumably netless like other Montgolfiers, its large area with whatever volume remained, was enough to land its seven passengers with no casualties.
- 1784: Dr. John Jeffries, with J-P. F. Blanchard as pilot, made observations of temperature and moisture and collected samples of air at various (moderate) altitudes over England, using a hydrogen-filled balloon of the usual varnished fabric.
- Jan. 7, 1785: Jeffries and Blanchard crossed the English Channel from England to France in an allegedly leaky, varnished balloon, sacrificing practically every available item of weight for ballast. Oars and a rudder proved ineffective.
- June 15, 1785: de Rozier and P. A. Romain attempted a reverse Channel crossing (France to England) in a tandem balloon consisting of an upper gas balloon 11.3 m diameter and a lower hot-air or fire balloon 3 m diameter, the latter intended for vertical control instead of ballast. (They may well have surmised that Jeffries and Blanchard's difficulties had been due more to instability than to leakage, not knowing, however, that whereas air over water is likely to be unstable in winter, it is the opposite in summer.) A chance was taken on the flammability

- of hydrogen in apparent confidence that its lightness would carry it up and away and that sparks could be contained. But less than a half-hour after the start, at about 1000 m, the craft was seen to burst into flame, with fatal results.
- Jan. 9, 1793: Blanchard made the first free flight in America (at least in a single balloon) under full control. He continued exhibitions over Europe but died from an unrecorded illness, impoverished by political complications. His widow continued successful exhibitions.
- Oct. 22, 1797: First successful parachute drop by Andre Garnerin over Paris, although Blanchard and others are credited with the original idea.
- 1804: The French Academy of Sciences, questioning the accuracy of previous upper-air data, commissioned physicists J. B. Biot and J. L. Gay-Lussac to make scientific observations. In flights together on Aug. 24 to 4000 m and by Gay-Lussac alone on Sept. 16 to 7000 m (hydrogen inflation) they established within this atmospheric layer substantial uniformity of gravitation, terrestrial magnetism, and air composition (except moisture content).
- 1819: Madam Blanchard, after about 60 other flights, died in attempting a fireworks display from a gas balloon. It seems such displays were fairly common, continuing even after her death.

- 1821: First balloon use of coal gas by the leading British balloonist Charles Green, at the coronation of George IV. Green is credited with first use of the drag rope (then termed 'guide rope').
- Nov. 7, 1836: Green, Monck Mason, R. Holland, M.P. set a distance record of 772 km from London to Weilburg, Germany, in flight of 18 hr with a balloon of about 2100 cu m.
- 1837: Dr. John Rae, a trader and surgeon for the Hudson's Bay Co., tried unsuccessfully to raise a balloon by sun heat alone. He attributed his failure to the weakness of sunlight in northern latitudes, but this could have been only a minor factor. The experiment has been done successfully with modern light plastic, blackened to absorb maximum heat.
- July 1-2, 1859: John Wise, leading American balloonist, made the first airmail flight and, incidentally, set a new world distance record of about 1300 km from St. Louis to Henderson, N.Y. (not shown on available maps). The first flight carrying official U.S. mail started from Lafayette, Ind., July 17, 1859, descending only a short distance away. To Wise is attributed first use of the rip panel. (Although the rip panel has virtually supplanted the anchor or grapnel in modern balloon operation, accounts indicate that Wise continued to use an anchor with continuing poor results.) Wise also demonstrated the ability of a collapsed balloon to spread out enough in the top of a net

- to parachute down. His monumental book, Through the Air, 1873, is a comprehensive collection of experiences, methods, and ideas from hundreds of flights.
- 1861-63: Tethered observation balloons used by both Union and Confederate armies. As with previous similar use in the French Revolutionary Wars, these balloons were of conventional spherical shape, prohibiting use in much wind.
- Sept. 5, 1862: Under auspices of the British Association for the Advancement of Science, Henry Coxwell and James Glaisher, meteorologist, made an apparent new altitude record (without oxygen) with various physical and physiological observations. The highest altitude reading--from a non-recording barometer--claimed to be 8800 m while still rising, but this observation is questionable due to the physical condition of the men. Both became unconscious as the altitude increased. Tragedy was averted by Coxwell, who, with his hands already paralyzed, pulled the valve rope with his teeth. Consciousness was regained and readings resumed about 13 min later with barometer at 293 mm of mercury or 7300 m altitude. Of two pigeons carried, one died.
- 1864: A hot-air balloon of about 11,000 cu m was built and flown by E. Godard in England. It had a straw-burning stove weighing about 450 kg. Except for the county-fair type with air heated only on the ground, used for exhibition parachutes drops, the hot-air type now seemed to disappear until its modern revival.

- 1870-71: A total of 66 balloons, carrying 164 people and miscellaneous cargo, left Paris during its siege by the Germans in the Franco-Prussian War; for 4 months balloons provided the only contact between the city and the outside world.
- April 15, 1875: First use of oxygen, and also first anoxia victims, in a flight from Paris. H. T. Sivel, Croce-Spinnelli, and G. Tissandier reached 8500 m, but only Tissandier survived. They didn't start using oxygen soon enough, not realizing the insidious approach of paralysis.
- 1878: Paul Bert published his classic work, La Pression Barometrique, on the physiological effects of altitude.
- 1885: Renard and Krebs in France made first fully successful application of power (electric motor) to an elongated balloon with a ballonet and steering organs. It was steered in a figure 8 at a speed of about 23 km/hr. (No further references to airship development will be given except as related to ballooning.)
- 1892: Hermite and Besancon developed instruments for unmanned high-altitude flight.
- 1895: Wm. Ramsay discovered helium in the atmosphere (previously observed by Janssen and Lockyer in the sun's spectrum in 1868).
- 1897: Andree and crew started from Spitsbergen on a projected balloon trip to the North Pole. Bodies found at White Island in 1930.
- 1898: Aero Club de France founded, primarily to promote ballooning

(parent organization of F.A.I. which sponsors international contests and controls official records).

1900: Comte de la Vaux set world distance record of 1920 km.

July 31, 1901: Suring and Berson set world altitude record of 10,800 m.

1901: Assman in Germany developed rubber sounding balloons.

1903: Cady and McFarland discovered helium in natural gas.

1904: First record of modern rubberized fabric used in Europe.

1906: First contest for the Gordon-Bennett Trophy, a distance race from Paris, won by Lt. Frank P. Lahm of U.S. Santos-Dumont unsuccessful with a balloon carrying powered propellers for vertical control.

1910: Based on previous European development, Goodyear Tire and Rubber Co. started making and improving single and multi-ply rubberized fabric suitable for LTA use. Previous American balloons were exclusively of varnished single-ply fabric.

1912: Melvin Vaniman proposed wire-bound balloon to be stabilized by superpressure. Apparently while experimenting with such pressure in his airship off Atlantic City, the fabric hull burst, causing death to himself and four crew members, a disaster erroneously attributed to fire in newspaper reports.

Dec. 13-17, 1913: Duration record of 87 hr set by H. Kaulen, Germany.

Feb. 8-10, 1914: Distance record of 3053 km set by H. Berliner, Germany.

1918: By Armistice Day 147,000 cu ft of helium was ready to ship to France for inflation of observation balloons.

1920: Post-war international balloon racing resumed. E. Demuyter of Belgium winner of the Gordon-Bennett race from Birmingham, Ala.

1921: U.S. Navy G-7 non-rigid was first LTA unit to be flown with helium.

1923: Radio used for first time in free flight by balloon in American National Race (R. H. Upson and C. G. Andrus).

1924: Demuyter took permanent possession of the G-B cup for Belgium, his fourth victory and third in succession.

Nov. 4, 1927: Capt. H. C. Gray of U.S. Army Air Corps died in altitude attempt; 12,950 m attained while still conscious, but record disallowed because pilot not in control throughout. His clock stopped on ascent and oxygen apparently ran out at about 9000 m on descent. Official inquiry made particular note of unprecedentedly slow ascent and descent, but said nothing about kind of gas used. Gray definitely used hydrogen in previous altitude flights.

1926-27-28: After three successive wins, W. T. Van Orman, E. J. Hill, and W. E. Kepner took permanent possession of the second G-B Cup for the U.S.

May 27, 1931: A. Piccard and P. Kipfer used sealed, pressurized gondola for first time in setting altitude record of 15,781 m (cabin pressure equivalent to 3000 m). Max. cabin temperature 41°C with top of gondola black and bottom white.

1932: A. Piccard and M. Cosyns reached 16,200 m. An attempt to reduce inside temperature with all-white gondola, apparently was too successful--minimum temperature -18°C .

Sept. 30, 1933: Russian crew of Prokief, Birnbaum, and Gudunow reached 18,500 m altitude.

Nov. 20, 1933: U.S. Navy crew of T. Settle and C. Fordney reached 18,665 m, 183,000-cu-m spherical balloon, Piccard gondola.

Jan. 30, 1934: Fedosienko, Wasienko, and Usyskin (all of Russia) reportedly reached 22,000 m (unofficial), but gondola broke loose at about 15,000 m on descent, fatal to all.

July 28, 1934: U.S. Army Air Corps and National Geographic Society balloon Explorer of 90,000 cu m (hydrogen) burst at about 18,000 m, but crew of W. Kepner, O. Anderson, and A. Stevens parachuted safely in gondola.

1933-34-35: F. Hynck and Z. Burzynski took permanent possession of third and last G-B Cup for Poland.

Nov. 11, 1935: Explorer II, 113,000-cu-m rubberized balloon (helium) made official record of 22,066 m in collecting atmospheric, cosmic-ray, and other data (crew, Anderson and Stevens).

1936: First successful plastic balloon flights. J. F. Piccard in collaboration with T. H. Johnson and J. D. Akerman launched a series of four cellophane balloons, 65 cu m each. A summer flight traveled 990 km in 10 hr. In cold weather, however, the material proved impractical due to cracking in the folds. The aerodynamic vertical stabilizer, working well with hydrogen, would be almost worthless with helium.

1937: J. Piccard made a successful flight to 3000 m with cluster of 98 small rubber balloons; proved that motion through air tends to separate the balloons.

1943-44: Several hundred Japanese paper balloons carried bombs across the Pacific Ocean but did little damage. These balloons were spherical of about 540-cu-m volume (hydrogen); ballast release was pressure-controlled. One balloon from a total of more than 9000 reached Kingston, Ontario; perhaps as many as 900, or 10%, reached North America.

1946: Development of large polyethylene balloons undertaken by General Mills. Subsequent study of plastic balloon operation, stresses, and shape sponsored by U.S. Navy at Univ. of Minnesota.

1947: Navy Skyhook balloon carried 32-kg load to 30,500 m.

May 6-7, 1958: A. Mikesell with M. Ross, pilot, made first astronomical observations from balloon at 12,000 m.

1953-54: Successful balloon-launched rockets.

Nov. 28-29, 1959: Water vapor first observed on Venus by C. M. Moore, Ross pilot, at 25,000 m with 406-mm telescope.

1960: Balloon of 28,300 cu m launched from carrier deck.

Aug. 12, 1960: First balloon-type satellite, Echo I, 30.5 m in diameter, made by G. T. Schjeldahl, Inc., launched by NASA.

April 28, 1961: World altitude record for manned aircraft of 34,700 m set by G. Mossolov, USSR, in E-66 jet airplane; first such record made by aircraft other than a balloon.

May 4, 1961: Manned balloon altitude record set by M. D. Ross, USNR, at 34,668 m over Gulf of Mexico, 28,300-cu-m balloon made

by Winzen Research, Inc. Copilot V. A. Prather drowned in an accident after landing.

Sept. 11, 1968: Polyethylene balloon of 813,300 cu m launched at White Sands Missile Range, N.M., reached 48.5 km altitude with a scientific payload of 26.8 kg. This was the largest balloon flown to that date and set an altitude record for balloons.

A SHORT BIBLIOGRAPHY OF BALLOON HISTORY

Encyclopedia Britannica, 1962-63 Edition, article on Ballooning by Jean and Jeannette Piccard.

Aeronautics II - Lighter-than-Air; M. J. B. Davy; Science Museum, London, Handbook of the Collections, 1934.

Through the Air; John Wise; dedicated to and with contribution by Prof. Joseph Henry, 1873.

Ballooning; G. May, London, 1885.

Navigating the Air; Aero Club of America, 1907.

Conquering the Air; Archibald Williams, 1926.

The First Century of Flight in America; Jeramia Milbank, 1943.

Files of the Wingfoot LTA Society Bulletin; Akron, Ohio.

A number of good articles in MD Medical News Magazine, April 1966.

La Pression Barometrique - Recherches de Physiologie Experimentale, (English translation by Mary and Fred Hitchcock); Paul Bert, 1878.

A Narrative of Two Aerial Voyages; John Jeffries MD, London, 1786.

Aeronautica; Monck Mason, London, 1838.

Aeronautics in the Civil War; J. D. Squires, American Historical Review, Vol. 42, 652.

The Air Arm of the Confederacy; J. K. Cornish III, Richmond Civil War Centennial Committee, Richmond, Virginia, 1963.

The Orion Book of Balloons; Charles Dollfus, (procurable from Wingfoot LTA Society).

Aircraft Year Book (yearly issue); includes various balloon events by year of occurrence.

Capt. H. C. Gray's Last Flight 1928; U.S. War Dept., Air Corps Official Report.

Ten Miles High; Alan Honour.

Exploring the Stratosphere; Gerald Heard, 1936.

Wonderful Balloon Ascents; F. Marion (Trans.), 1870.

Aeronautica Catalog of Aeronauts; Monck Mason, 1838.

Bag of Smoke; Zonzo Anderson, 1942.

A History of Aircraft; Magoun & Hodges, 1931.

Balloon & Airship Gases; Chandler, 1926 (contains good section on safety precautions against ignition).

Adventures in the Air; W. de Fonvielle (Trans.), 1877.

Aerial Navigation; C. C. Turner, 1910.

Trail Blazing in the Skies; F. Chase, 1943 (Goodyear Tire & Rubber Co.).

Ballooning; G. May, 1885.

Ballooning; Gibbs-Smith, 1948.

Scientific Ballooning; J. M. Bacon, Smithsonian Inst. Annual Report 1898 (scientific observations of atmosphere, optics, and acoustics).

Jambo; Anthony Smith, 1963 (African balloon safari).

The Flight of the Small World; Eiloart and Elstob, 1959 (attempted trans-Atlantic balloon flight).

Via Balloon Jupiter; Jerry Marlette, J. of American Aviation Historical Soc., Summer 1966. (John Wise's pioneer U.S. airmail flight)

Skyhooks; Kurt R. Stehling and William Beller, 1962.

REFERENCES

- (1) Upson, R. H. and Charles deForest Chandler, 1926: Free and Captive Balloons, Ronald Press, New York.
- (2) Upson, R. H., 1939: Stresses in a Partially Inflated Free Balloon. Journal of Aeronautical Sciences, Feb. 1939.
- (3) Upson, R. H. and James S. Holdhusen, 1952: Balloon Shapes--or Stress Analysis and Design of Thin, Axially Symmetric Fluid Containers. General Mills Report #1143, Sept. 1952.
- (4) Upson, R. H., 1915: Relative Worth of Improvements in Fabrics. Goodyear Tire & Rubber Co., NACA Report #5.
- (5) Upson, R. H., 1926: Metalclad Rigid Airship Development. SEA Journal, Feb. 1926, discussion Oct. 1926. Also May 1930.
- (6) Ackerman, John D. and J. Piccard, 1937: Upper Air Study by Means of Balloons, J. Aeronautical Sci., June 1937.
- (7) Zahm, A. F., 1950: Some Theorems in the Mechanics of High-Speed Balloons, International Aeronautic Congress 1900. Published In Vol. I of Zahm's collected papers, University of Notre Dame Press.
- (8) Arnstein, Karl, W.F.G. Swan, 1935-36: Stratosphere Series Nos. 1 & 2, Explorer I & II Balloons. National Geographic Soc. Contributed Technical Papers.
- (9) Upson, R. H., 1952: Simplified Mathematical Forms for Engineering Use. Aeronautical Eng. Review, Feb. 1952.
- (10) Upson, R. H., 1965: Clues to Balloon Failure. Scientific Ballooning, March 1965.

SECTION II

LIST OF SYMBOLS

THEORY OF BALLOON FLIGHT

by

Alvin L. Morris

List of Symbols ii

List of Figures vi

List of Tables vii

A. ARCHIMEDES' PRINCIPLE 1

B. DISTRIBUTION OF PRESSURE FORCES 1

C. COORDINATE AND UNITS SYSTEMS 8

D. BALLOON SYSTEM MASS 10

E. A BALLOON SYSTEM IN BUOYANT EQUILIBRIUM 12

F. VIRTUAL MASS 16

G. FORCES ACTING ON A BALLOON IN MOTION 18

H. EQUATIONS OF MOTION 23

I. ZERO PRESSURE BALLOON FLIGHT 31

1. Inflation and Release 31

2. Free Flight 40

a. Ascent in a windless atmosphere 41

3. Wind Effects on a Balloon in Free Flight 53

4. Behavior at Float Altitude 61

a. Ballasting and valving to maintain a float condition 71

5. Excursions from Float and Valved Descent 76

REFERENCES 99

<u>Symbol</u>	<u>Description</u>	<u>Dimensions</u>
a	subscript identifying its symbol with air	
A	area; subscripts may be used to make the area specific	L^2
b	angle relative wind makes with the vertical axis of a balloon	deg
b	subscript identifying its symbol with ballast	
B	buoyant force	MLT^{-2}
B	subscript identifying its symbol with the balloon	
C_B	added mass coefficient for a balloon undergoing acceleration through the air	
C_D	aerodynamic drag coefficient	
C_L	aerodynamic lift coefficient	
C_P	specific heat at constant pressure	$L^2 T^{-2} \theta^{-1}$
C_V	specific heat at constant volume	$L^2 T^{-2} \theta^{-1}$
\vec{D}	aerodynamic drag force exerted on a balloon system moving through the air	MLT^{-2}
D	subscript used to identify its symbol with aerodynamic drag	
e	subscript indicating that its symbol is an equilibrium value	
f	free lift ratio	

f'	fractional free lift	
$f\%$	percentage free lift; $f\% = 100 f'$	
\vec{F}	sum of all aerostatic and gravitational forces acting on a balloon	MLT^{-2}
g	acceleration due to gravity	LT^{-2}
g	subscript identifying its symbol with gas	
G	subscript identifying its symbol with gross mass, weight, or lift	
H	geopotential height	L
i	subscript used with V to indicate a fully inflated state	
\vec{i}	unit vector which is directed along the positive x coordinate	
\vec{j}	unit vector which is directed along the positive y coordinate	
\vec{k}	unit vector which is directed along the positive z coordinate (i.e., upward)	
ℓ	characteristic length used in Reynolds number	L
ℓ	subscript identifying its symbol with payload	
\vec{L}_a	aerodynamic lift force on a balloon	MLT^{-2}
L'	vertical temperature gradient; subscripts identify it with air or gas	θL^{-1}
m	mass; subscripts are used to make its identity specific	M
M	molecular weight; subscripts identify it with air or gas	$M(M\text{-mol})^{-1}$
o	subscript identifying its symbol with a base datum reference	

p	pressure; subscripts identify it with air or gas	$ML^{-1}T^{-2}$
r	radius	L
r	subscript indicating that its symbol is relative	
R	universal gas constant	$L^2 T^{-2} \theta^{-1}$
Re	Reynolds number	
S	surface area	L^2
t	time	T
T	temperature; subscripts identify it with air or gas	θ
v	speed; subscripts are used to make it specific and used with a vector symbol, e.g., \vec{v} , it is velocity	LT^{-1}
v	subscript used with m to indicate virtual mass	
V	volume; subscripts identify it with air, gas, or balloon	L^3
x	distance along the x coordinate	L
y	distance along the y coordinate	L
z	height or distance along the z coordinate	L
z	subscript identifying its symbol with height z	
<u>Greek letters</u>		
α	specific volume (V/m); subscripts identify it with air or gas	$L^3 M^{-1}$
\ominus	supertemperature	θ
μ	ratio of mass of gas in a balloon to gross mass of the balloon system	
μ	dynamic viscosity; subscripts identify it with air or gas	$ML^{-1}T^{-1}$

Π	superpressure	$ML^{-1}T^{-2}$
ρ_a	air density	ML^{-3}
σ	ratio of molecular weight of air to molecular weight of gas	
τ	ratio of absolute temperature of air to absolute temperature of gas	

List of Figures

Fig. 1	Pressure force vector distribution. The inflection points are identified by the dots below the z_0 line	7
Fig. 2	Coordinate system for balloon vector analysis	9
Fig. 3	Balloon system just after launch	11
Fig. 4	Drag and lift coefficients for a modified natural-shape balloon as a function of angle of attack. From Peters et al. (4)	21
Fig. 5	Vertical acceleration for a helium filled balloon	35
Fig. 6	Vertical acceleration for a hydrogen filled balloon	36
Fig. 7	Vertical velocity of a helium-filled balloon ascending at sea level where $\rho_a = 1.225 \text{ kg/m}^3$ and $g = 9.80665 \text{ m/sec}^2$. It is assumed that $\tau = 1.0$ and $C_D = 0.3$	44
Fig. 8	The variation of τ with air density required to maintain constant vertical motion (solid curves) and variation of τ with air density for an adiabatic ascent (dashed curves) in four atmospheric lapse rates. The lift gas is helium	46
Fig. 9	Diagram showing relationship between air density and balloon system density. Level numbers are used in the text. Vertical distances on the diagram are not proportional to vertical heights in the atmosphere	62

Fig. 10	Vertical oscillation of a balloon system on reaching float altitude. Not all balloon systems oscillate in this manner; many appear to approach float altitude in a nearly asymptotic manner.	66
Fig. 11	Graphical solution of the equation of buoyant equilibrium for a helium-filled balloon	72
Fig. 12	Diurnal excursions of a gas-tight, helium-inflated, polyethylene balloon in a typical summer, mid-latitude, continental atmosphere.	79
Fig. 13	Diurnal excursions of a slowly leaking, helium-inflated, polyethylene balloon in a typical summer, mid-latitude, continental atmosphere.	89
Fig. 14	Valved descent of a helium-inflated polyethylene balloon in a typical summer, mid-latitude, continental atmosphere	93
Fig. 15	Stepwise valved descent of a helium-inflated, polyethylene balloon in a typical summer, mid-latitude, continental atmosphere.	94

List of Tables

Table 1	Physical characteristics of a gas in a balloon	15
Table 2	Molecular weight, specific heat at constant pressure and dT_g/dz for an adiabatic ascent or descent for various lift gases.	51

THEORY OF BALLOON FLIGHT

A. ARCHIMEDES' PRINCIPLE

Archimedes' principle as usually applied to a balloon in the atmosphere states that a buoyant force equal to the difference in weight of the displaced air and the lifting gas will act on the balloon. Thus, if B is the buoyant force, m_a is the mass of displaced air, m_g is the mass of the lifting gas, and g is the acceleration of gravity, then

$$B = g(m_a - m_g) \quad (1)$$

B. DISTRIBUTION OF PRESSURE FORCES

Although Eq. (1) is general if the air displaced by the payload, etc. is negligible compared to the air displaced by the gas, it is instructive to look also at the distribution of pressure forces on a balloon surface.

The hydrostatic equation may be written

$$dp = -g \rho dz \quad (2)$$

where p is the fluid pressure, ρ is the density of fluid, and z is the vertical height above an arbitrary datum plane.

This may be integrated for the atmosphere to yield

$$p_{a,z} = p_{a,o} - \int_{z_o}^z g \rho_a dz \quad (3)$$

in which $p_{a,z}$ is the air pressure at level z . A similar equation may be written for the lifting gas

$$p_{g,z} = p_{g,o} - \int_{z_o}^z g \rho_g dz \quad (4)$$

Then the pressure difference across the balloon film at level z is

$$(p_{a,z} - p_{g,z}) = (p_{a,o} - p_{g,o}) - \left(\int_{z_o}^z g \rho_a dz - \int_{z_o}^z g \rho_g dz \right) \quad (5)$$

In a balloon which is not fully inflated there is a level at which $p_a = p_g$; let that level be z_o . Then

$$p_{a,z} - p_{g,z} = - \left(\int_{z_o}^z g \rho_a dz - \int_{z_o}^z g \rho_g dz \right) \quad (6)$$

If ρ and g are constant with height, Eq. (6) may be solved to yield

$$p_{a,z} - p_{g,z} = -g (\rho_a - \rho_g) (z - z_o) \quad (7)$$

Thus, for a lifting fluid having a density less than that of the ambient fluid, the pressure of the lifting fluid is greater than the pressure of the ambient air above $z = z_o$ and less below $z = z_o$.

It is known that neither ρ nor g is constant with height, but the variation of g over the height of a balloon may be ignored. Also, in spite of the known variation with height of ρ in both the lifting gas and the atmosphere, Eq. (7) is usually employed in ballooning work without reservation. It is not difficult, however, to show that the error incurred by assuming ρ constant with height is not large.

The equation of state for an ideal gas is

$$\rho = \frac{pM}{RT} \quad (8)$$

where M is the molecular weight [$\text{kg} (\text{kg} - \text{mol})^{-1}$], R is the universal gas constant [$8314.32 \text{ J } (^{\circ}\text{K})^{-1} (\text{kg} - \text{mol})^{-1}$], T is the temperature ($^{\circ}\text{K}$), p is the pressure [Nm^{-2}], and ρ is the density [kg m^{-3}].

The molecular weight for air at all altitudes of interest in scientific ballooning is 28.9644; the values of M for lifting gases are given in Table 1, Section IV. Both the air and common lift gases behave sufficiently like ideal gases at the temperatures and pressures encountered in ballooning that they may be treated as such. Substituting from Eq. (8) into Eq. (2) yields

$$dp = -g \frac{pM}{RT} dz \quad (9)$$

and

$$\ln \frac{p_z}{p_o} = - \frac{gM}{R} \int_{z_o}^z \frac{dz}{T} \quad (10)$$

Through most small vertical distances in the earth's atmosphere and probably within most balloons, the variation of temperature with height is approximately linear. If $L'_a = dT_a/dz$ and $L'_g = dT_g/dz$ are constants in the stratum $(z - z_o)$, then $T_{a,z} = T_{a,o} + L'_a (z - z_o)$ and $T_{g,z} = T_{g,o} + L'_g (z - z_o)$. Equation (10) may be written

$$\ln \frac{p_{a,z}}{p_{a,o}} = - \frac{gM_a}{RL'_a} \ln \left[\frac{T_{a,o} + L'_a (z - z_o)}{T_{a,o}} \right] \quad (11)$$

and

$$\ln \frac{p_{g,z}}{p_{g,o}} = - \frac{gM_g}{RL'_g} \ln \left[\frac{T_{g,o} + L'_g (z - z_o)}{T_{g,o}} \right] \quad (12)$$

for air and lift gas respectively. Also, since $p_{a,o} = p_{g,o} = p_o$,

$$p_{a,z} - p_{g,z} = p_o \left\{ \left[1 + \frac{L'_a (z - z_o)}{T_{a,o}} \right]^{\frac{gM_a}{RL'_a}} - \left[1 + \frac{L'_g (z - z_o)}{T_{g,o}} \right]^{\frac{gM_g}{RL'_g}} \right\} \quad (13)$$

Equation (13) may be compared with Eq. (7) by expanding the terms in brackets in Eq. (13) in a series, e.g., a binomial series. The first terms of the binomial series yield the expression on the right side of Eq. (7), and it can be shown that the sum of all other terms is small. A more straightforward way, however, is to compute and compare values of $(p_{a,z} - p_{g,z})$ for a given value of $(z - z_o)$ for both Eqs. (7) and (13). For this purpose, assume a very extreme case in which $(z - z_o) = 100$ m, $T_{a,o} = 250^\circ\text{K}$, $T_{g,o} = 270^\circ\text{K}$, $L'_a = -0.006^\circ\text{K m}^{-1}$, $L'_g = +0.006^\circ\text{K m}^{-1}$, $M_a = 28.9644$, and $M_g = 4.0026$. Then from Eq. (7)

$$p_{a,z} - p_{g,z} = \frac{g(z - z_o)}{R} \left(\frac{M_a}{T_{a,o}} - \frac{M_g}{T_{g,o}} \right) p_o = -0.01191 p_o$$

From Eq. (13)

$$p_{a,z} - p_{g,z} = -0.01184 p_o$$

The difference is less than 1% of the value calculated by means of Eq. (13).

Pressure is a force per unit of area which acts on the balloon fabric in a direction normal to the plane of the fabric. The orientation of the fabric then determines the direction of pressure forces on it. Therefore, if an infinitesimal area of balloon film is represented by the vector \vec{dA} ,

directed normal to the plane of the film from inside to outside, the pressure force on that area is $p d\vec{A}$. A closed, partially-inflated balloon takes approximately the shape of a solid of revolution about a vertical axis. Figure 1 depicts the intersection of the skin of such a balloon with a plane through its vertical axis and shows the distribution of the force vectors resulting from pressure difference across the balloon film. Note that the force vectors are directed outward above level z_0 and inward below z_0 . Note also that the balloon film is convex above z_0 and concave at most levels below z_0 . If the film were weightless, the inflection point in the film would occur at z_0 , but since all balloon film has weight, the inflection point occurs somewhere below z_0 .

The resultant, \vec{B} , of all pressure forces exerted on the balloon may be obtained by integrating $-(p_{a,z} - p_{g,z})d\vec{A}$ over the surface, S , of the balloon. Thus

$$-\iint_S (p_{a,z} - p_{g,z})d\vec{A} = \vec{B} \quad (14)$$

If $(p_{a,z} - p_{g,z})$ is substituted from either Eq. (7) or Eq. (13) and the integration is carried out \vec{B} is found to be a vector directed upward,

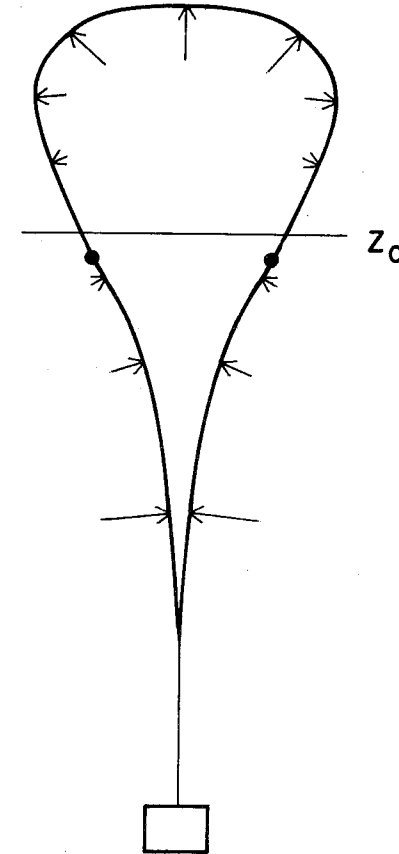


Fig. 1. Pressure force vector distribution. The inflection points are identified by the dots below the z_0 line.

and its magnitude is very nearly equal to the lift B given by Eq. (1).

This integration is easy to perform for some simple shapes, e.g., a cube, but Eq. (1) is much simpler and is more general.

C. COORDINATE AND UNITS SYSTEMS

The coordinate system used here is a rectangular system in which the z axis lies in the local vertical, and z increases upward. When the position of the x or y axis must be fixed relative to the earth, the orientation shown in Fig. 2 will be used. Figure 2 also shows the unit vectors \vec{i} , \vec{j} , and \vec{k} at point (x,y,z) in the coordinate system.

In this coordinate system $\vec{i}x$ denotes a vector of magnitude x pointing in the \vec{i} direction (i.e., east); $-\vec{i}x$ is a vector pointing west. Also the three dimensional vector, \vec{v}_B , which is used here to denote the velocity of the balloon system may be represented in either of the following forms:

$$\vec{v}_B = \vec{i}v_{B,x} + \vec{j}v_{B,y} + \vec{k}v_{B,z}$$

or

$$\vec{v}_B = \vec{i} \left(\frac{dx}{dt} \right)_B + \vec{j} \left(\frac{dy}{dt} \right)_B + \vec{k} \left(\frac{dz}{dt} \right)_B$$

where $v_{B,x}$, $v_{B,y}$, and $v_{B,z}$ are components of \vec{v}_B along the x , y , and z axes, respectively. Likewise $(dx/dt)_B$, $(dy/dt)_B$, and $(dz/dt)_B$ are compon-

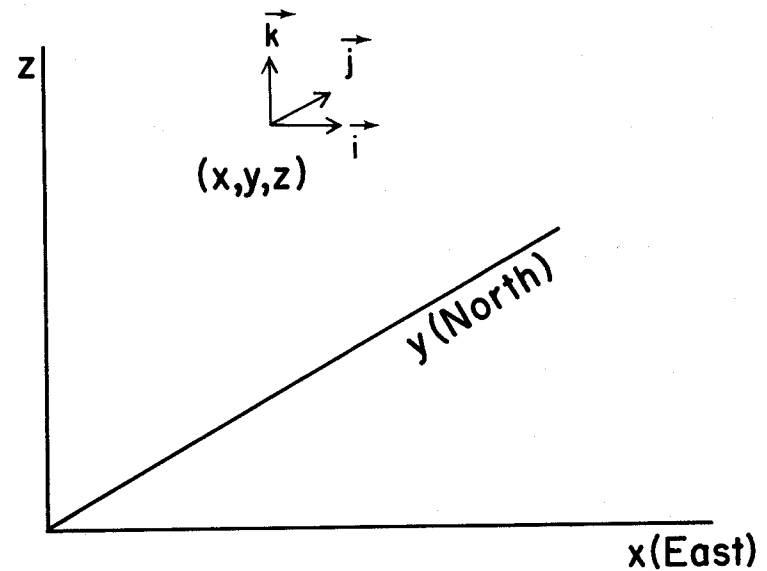


Fig. 2. Coordinate system for balloon vector analysis.

ents of \vec{v}_B shown as time derivatives of distance along the three coordinate axes.

The International System of Units (SI) will be used unless otherwise stated.

D. BALLOON SYSTEM MASS

A scientific balloon system consists of the balloon, a parachute, the scientific package, a control package, and miscellaneous control devices such as valves for valving gas from the balloon and ballast for decreasing the system mass. In the treatment here we shall consider the following masses separately: m_B --the mass of the balloon, including fabric, load tapes, fittings, valves, etc.; m_L --the mass of the payload, including scientific package, control package, parachute rigging, etc. but excluding ballast; m_b --the mass of the ballast; m_g --the mass of lifting gas; m_a --the mass of displaced air; and m_C --the gross mass of the system ($m_C = m_B + m_L + m_b$). Note that, as defined here, gross system mass does not include the mass of the lifting gas.

Figure 3 is a picture of a typical scientific balloon system on which the more significant components are marked.

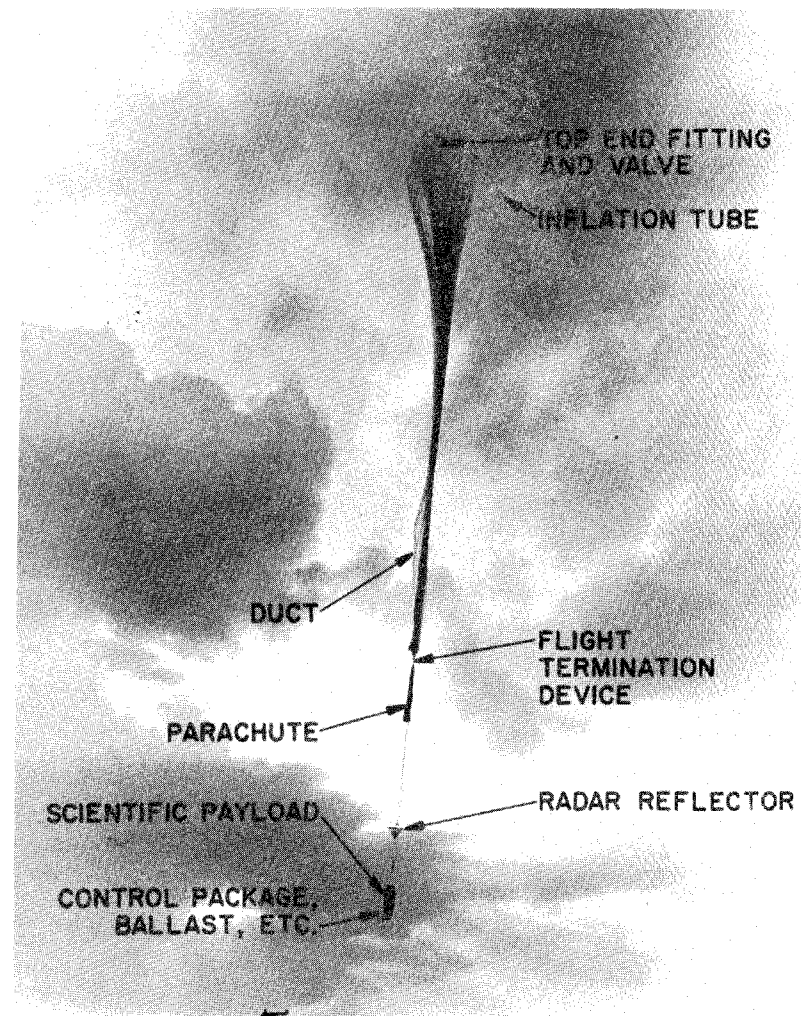


Fig. 3. Balloon system just after launch.

E. A BALLOON SYSTEM IN BUOYANT EQUILIBRIUM

A balloon system in a motionless atmosphere must displace a volume of air having a weight just equal to its own weight in order to be in buoyant equilibrium, according to Archimedes' principle. This may be written

$$g(m_G + m_g) = g(m_B + m_l + m_b + m_g) = gm_a \quad (15)$$

Equation (15) is identical with Eq. (1) if

$$B = g(m_B + m_l + m_b) = gm_G \quad (16)$$

that is, if the buoyant force is just equal to the total load to be supported. Recalling that $m_g = \rho_g V_g$ and substituting from Eq. (8) gives

$$m_g = \frac{M_g p_g V_g}{RT_g} \quad (17)$$

Also

$$m_a = \frac{M_a p_a V_a}{RT_a} \quad (18)$$

and

$$\frac{m_g}{m_a} = \frac{M_g p_g V_g T_a}{M_a p_a V_a T_g} \quad (19)$$

Substituting into Eq. (15) and rearranging gives

$$m_G + m_g \left(1 - \frac{M_a p_a V_a T_g}{M_g p_g V_g T_a} \right) = 0 \quad (20)$$

or

$$m_G + m_a \left(\frac{M_g p_g V_g T_a}{M_a p_a V_a T_g} - 1 \right) = 0 \quad (21)$$

In these equations, m_g and m_a are the masses of the entire volumes of gas in the balloon and of the air displaced, respectively. Therefore, p and T as used in Eqs. (17) through (21) must be values which are representative of the entire mass. This interpretation contrasts with the interpretation of p and T used in Section II.B, where their variability within the balloon was being discussed. Nonetheless, the interpretation adopted here is not particularly restrictive, and it is consistent with the practice generally followed in ballooning.

It should be noted also that the acceleration due to gravity has been factored out of Eqs. (20) and (21) for convenience, but if the weight or lift forces are desired, the terms of Eqs. (20) and (21) must be multiplied by g . Except for the small volume of air displaced by the balloon film and the suspended load, $V_a = V_g$. Also in ballooning superpressure and super-temperature (the latter often erroneously called superheat) are frequently used. Superpressure Π is given by

$$\Pi = p_g - p_a \quad (22)$$

and supertemperature Θ by

$$\Theta = T_g - T_a \quad (23)$$

Equation (21) may now be written

$$m_G + m_a \left[\frac{(p_a + \Pi) T_a M_g}{p_a (T_a + \Theta) M_a} - 1 \right] = 0 \quad (24)$$

This is a mathematical statement of the condition for buoyant equilibrium expressed in terms of the masses involved and the measurable characteristics of the lift gas and the ambient gas. Since all masses in m_G are positive and some are not zero, the term involving m_a must be negative to satisfy the equation. This can be accomplished by a judicious selection of values of Π , Θ , and M_g/M_a . All the combinations shown in Table 1 are valid in principle. Actually only combinations 5 through 8 are attainable in a non-rigid balloon, but Π is so small in one very important class of balloons that it can be ignored, thereby simplifying many computations. Therefore, combinations 1 through 4 are useful conceptually. In ballooning, when a gas has a molecular weight less than that of air, it is said to be lighter than air. It is feasible to use a gas that is heavier than air in a balloon and

Table 1

Physical Characteristics of a Gas in a Balloon

Combination Number	Π	Θ	M_g/M_a	Comments
1	0	>0	1	Balloon filled with warmed ambient gas
2	0	0	<1	Gas lighter than ambient
3	0	>0	<1	Gas lighter and warmer than ambient
4	0	<0	<1	Gas lighter and cooler than ambient
5	>0	0	<1	Gas lighter and gas pressure greater than ambient
6	>0	>0	<1	Gas lighter and warmer and gas pressure greater than ambient
7	>0	<0	<1	Gas lighter and cooler and gas pressure greater than ambient
8	>0	>0	1	Balloon filled with warmed ambient gas under pressure greater than ambient

make it buoyant by making Θ large enough, but except to lift the gas itself there would appear to be no practical reason for doing so.

Superpressure Π cannot be negative unless the walls of the balloon are rigid enough to prevent it from collapsing. Father Francesco de Lana suggested as early as 1670 that an evacuated sphere might fly, but no one has yet developed a sufficiently strong, light material from which to make such balloons which will fly in the atmosphere. Analogous vehicles have been used in the ocean, of course. The hot-air balloonist makes use of super-temperature, and because he can change it quickly by heating the gas inside the balloon or by venting hot gas and replacing it with cooler gas, he can change the buoyant lift rapidly. Scientific ballooning usually takes advantage of the low molecular weight of helium or hydrogen to make the ratio M_g/M_a small. Other lifting gases are less satisfactory because of their higher molecular weights.

F. VIRTUAL MASS

If the numerical value of the second term of Eq. (24) is not equal to the first term, the balloon system is said to have "free lift," and the resultant force on the system in the earth's gravitational field is no longer

zero. The system will be accelerated if it is not tethered.

The mass which will be accelerated will include the gross mass of the balloon system and the mass of the lift gas, but it will also include the mass of some of the environmental fluid. This is not surprising, but the precise mass of the environmental fluid involved and the resultant acceleration are difficult to determine. It is shown in fluid dynamics, e.g., Streeter (1), that for purposes of determining the acceleration of an immersed body due to an impressed force, the acceleration of the environment may sometimes be equated with that of the immersed body if the proper environmental mass is assumed to be accelerated. The immersed body mass and the "added" environmental mass are then combined into the "virtual" mass, i.e., the total mass which is assumed to be accelerated with the immersed body. For an immersed sphere, the added mass is equal to one-half the mass of the displaced fluid. For a circular cylinder being accelerated normal to its axis, the added mass is equal to the displaced mass. There are potential difficulties such as flow separation aft of the body, or for rapid accelerations, compressibility. Although no one has determined the appropriate added mass for a non-spherical balloon system, it is common practice to assume that it is the same

as the added mass of a sphere having the same volume as the enclosed gas.

Let m_v equal the virtual mass which must be accelerated. Then, if C_B is a coefficient which when multiplied by m_a gives the added mass,

$$m_B + m_\ell + m_b + m_g + C_B m_a = m_v \quad (25)$$

From Eqs. (19), (22), and (23) and recognizing that $V_a = V_g$, m_a may be expressed in terms of m_g as follows:

$$m_a = m_g \frac{M_a p_a (T_a + \Theta)}{M_g (p_a + \Pi) T_a}$$

Then Eq. (25) may be rewritten

$$m_v = m_B + m_\ell + m_b + m_g \left(1 + C_B \frac{M_a p_a (T_a + \Theta)}{M_g (p_a + \Pi) T_a} \right) \quad (26)$$

G. FORCES ACTING ON A BALLOON IN MOTION

A rigorous analysis of all the forces to which a balloon system is subjected during inflation, launch, and flight is beyond the scope of this book; however, those of greatest importance during flight are the gravitational forces, the buoyant forces, and the aerodynamic lift and drag forces which occur only when the balloon has motion relative to the ambient air.

Buoyant or aerostatic forces were discussed in sub-Sections A, B, and

E. Equation (20) which was derived for a balloon in a state of buoyant

equilibrium can be generalized to include free lift by equating the gravitational and aerostatic forces to \vec{F} . Thus from Eqs. (20), (22), and (23),

$$\vec{F} = -g\vec{k} \left\{ m_G + m_g \left[1 - \frac{M_a p_a (T_a + \Theta)}{M_g (p_a + \Pi) T_a} \right] \right\} \quad (27)$$

The negative sign of the term on the right is necessary to preserve the convention that positive free lift is an upward force and that the weight of the system is directed downward.

The drag D exerted by a fluid upon a submersed body which is in motion through the fluid is given by

$$\vec{D} = -\frac{1}{2} C_D \rho_a A_D |\vec{v}_B - \vec{v}_a| (\vec{v}_B - \vec{v}_a) \quad (28)$$

where C_D is a dimensionless drag coefficient, A_D is the effective cross sectional area of the body normal to its direction of motion relative to the fluid, \vec{v}_B is the velocity of the balloon, and \vec{v}_a is the velocity of the fluid (the ambient air). The drag coefficient is a function of both the shape of the balloon system and the Reynolds number referred to a characteristic dimension of the system. For a spherical balloon that dimension is the diameter of the balloon; also A_D is the area of a great circle. The Reynolds number Re is given for an object in air by

$$Re = \frac{\rho_a \ell |\vec{v}_B - \vec{v}_a|}{\mu_a} \quad (29)$$

where ℓ is the characteristic dimension and μ_a is the dynamic viscosity of the air.

For a sphere the variation of C_D with Re is not great for $Re > 5 \times 10^5$, and for most scientific balloon systems having measurable motion relative to the atmosphere, the Reynolds number exceeds 5×10^5 . It is pertinent to note, however, that for lower Reynolds numbers, the variation of C_D with Re cannot be ignored. Hoerner (2) shows graphically that for Reynolds numbers between 10^4 and 4×10^5 , C_D is nearly constant for a sphere and has a value of approximately 0.47. A sharp transition from laminar to turbulent flow occurs between $Re = 4 \times 10^5$ and $Re = 5 \times 10^5$, and at $Re \geq 5 \times 10^5$, C_D has a value of approximately 0.1. In a general way the drag coefficient of a natural shape balloon (see Section V) varies with Re in much the same way as a sphere at $Re \geq 4 \times 10^5$, Sherburne (3). It is sensitive to the shape, however, as shown by Fig. 4 from Peters, et al. (4). This figure was plotted from wind tunnel data obtained with a wooden, natural shape model. Tilting it to change the angle of attack changed the shape exposed to the air stream. The tests were run at $Re = 10^6$.

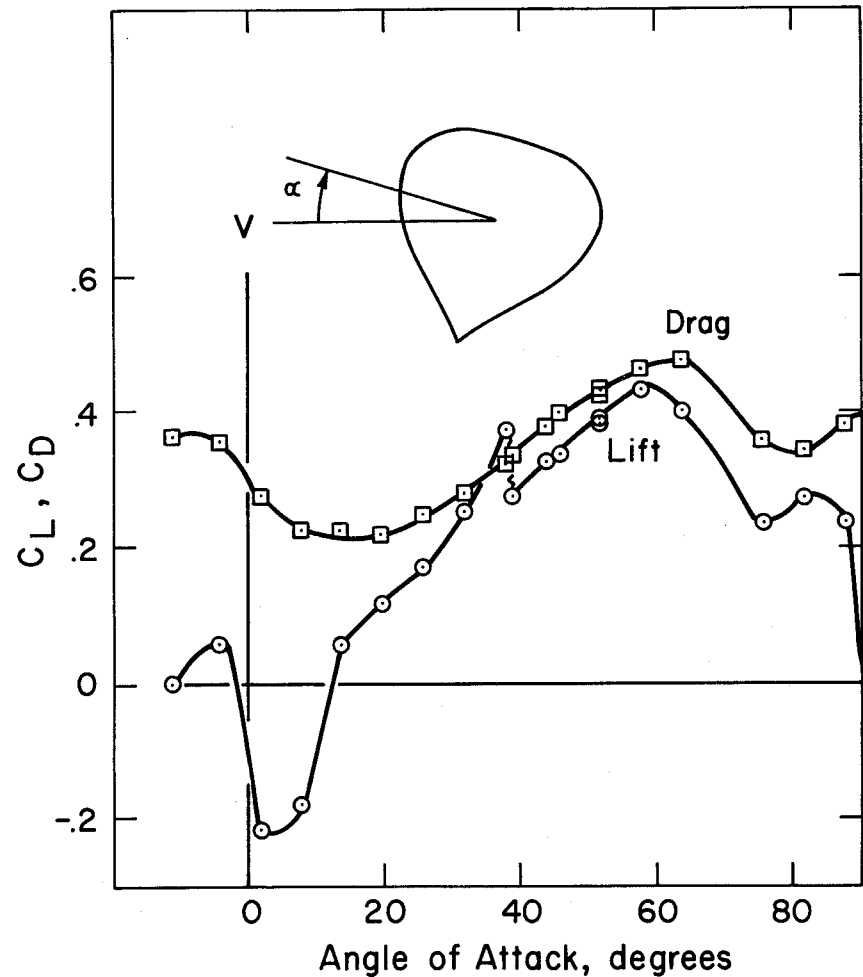


Fig. 4. Drag and lift coefficients for a modified natural shape balloon as a function of angle of attack. From Peters, et al. (4).

At best, estimates of C_D for a large balloon in flight will be coarse.

The following equations may be used to make such estimates:

$$\left. \begin{aligned} C_D &= 0.47 + \frac{24}{Re + 0.01} && \text{for } Re \leq 4.5 \times 10^5 \\ C_D &= 0.3 && \text{for } Re > 4.5 \times 10^5 \end{aligned} \right\} \quad (30)$$

The equations do not take into account change of shape, and they imply that the transition from laminar to turbulent flow is discontinuous at $Re = 4.5 \times 10^5$.

The lift on a tethered balloon, \vec{L}_a , due to horizontal motion of the atmosphere is

$$\vec{L}_a = \frac{1}{2} k C_L \rho_a A_L |\vec{v}_B - \vec{v}_a|^2 \quad (31)$$

where C_L is a dimensionless lift coefficient and A_L is the effective cross sectional area of the balloon normal to the direction of lift. The lift coefficient is even more sensitive to the shape of the balloon than C_D , and it may be greater than, equal to, or less than zero. The lift \vec{L}_a is usually small but it may be significant for a tethered balloon in a strong wind or for a partially inflated balloon in a stratum of the atmosphere in which the vertical wind shear is great.

The effect of the surface of the earth near a tethered balloon may also be important to the aerodynamic behavior of the balloon. It will be if it contributes to turbulence on a scale near or larger than the dimensions of the balloon. No attempt is made to account for the influence of the earth's surface here.

H. EQUATIONS OF MOTION

An equation of motion for the balloon system with free lift, embedded in a moving atmosphere, may now be written. It is

$$\vec{F} + \vec{D} + \vec{L}_a = m \frac{d\vec{v}_B}{dt} \quad (32)$$

or from Eqs. (26), (27), (28), and (31),

$$\begin{aligned} -k g \left\{ m_G + m_g \left[1 - \frac{M_a p_a (T_a + \Theta)}{M_g (p_a + \Pi) T_a} \right] \right\} - \frac{1}{2} \rho_a \left\{ C_D A_D |\vec{v}_B - \vec{v}_a| (\vec{v}_B - \vec{v}_a) \right. \\ \left. - k C_L A_L |\vec{v}_B - \vec{v}_a|^2 \right\} = \left\{ m_G + m_g \left[1 + C_B \frac{M_a p_a (T_a + \Theta)}{M_g (p_a + \Pi) T_a} \right] \right\} \frac{d\vec{v}_B}{dt} \quad (33) \end{aligned}$$

Equation (33) is a fairly general equation of motion which makes use of the concepts of superpressure and supertemperature in the classical manner. Because Θ , T_a , C_D , C_L , Π , p_a , A_D , and A_L are all functions of position and time, Eq. (33) cannot be readily solved. It can be solved numeri-

cally and such a solution is discussed in Section III. Some knowledge of the behavior of a balloon in flight can be gained by a qualitative evaluation of Eq. (33) however; furthermore, such an evaluation helps one to understand a numerical solution.

It is convenient to classify scientific balloons into three primary categories before undertaking further discussion of balloon motion. These are 1) zero-pressure and 2) superpressure, both made of inextensible material, and 3) extensible balloons. All three have a fully inflated volume, V_i . For the zero-pressure balloon this is the volume at which the balloon is completely inflated and the lifting gas starts to escape from the vent or duct which is open to the atmosphere at the balloon base.

The expression "zero-pressure" derives from the fact that the pressure difference between the atmosphere and the lift gas is essentially zero at some level in the gas throughout flight. The so-called zero-pressure level is high on the balloon, but is near the apparent bottom of the bubble of gas, when the balloon is only slightly inflated, i.e., when $V_g \ll V_i$. It moves down the balloon away from the top as the gas expands and reaches the base just as $V_g = V_i$. If the gas continues to expand and is vented to

the atmosphere, a slight superpressure must develop in the balloon to expel the gas. In fact, too small a vent could result in sufficient superpressure in a rising balloon to cause the balloon to burst.

A superpressure balloon is a sealed balloon which is designed to contain the lifting gas at pressures greater than that of the ambient atmosphere. Ideally, when fully inflated, it becomes a fixed volume containing a fixed mass of gas. Thus, when an ascending superpressure balloon becomes fully inflated, it will continue to rise until it reaches a level at which the volume of displaced air has a weight equal to that of the balloon system, including any suspended mass. It will then float at that atmospheric density level. The superpressure balloon is such an important balloon vehicle that Section VIII is devoted to it. Below the level at which $V_g = V_i$, a superpressure balloon is no different from a zero-pressure balloon except that it is likely to be made of different material; thus it may react differently to its radiation environment.

Extensible balloons are usually made of natural or synthetic rubber. These balloons are frequently, but not always, inflated sufficiently to subject the entire volume of lift gas to a slight superpressure, even at launch.

As the balloon ascends and the lift gas expands, the forces due to the differential pressure across the film just equal the elastic restoring forces of the film. Expansion continues until the film stretches to its limit and the balloon bursts. For present purposes, the fully inflated volume is the volume at which burst occurs.

The hot-air balloon is a special type of inextensible zero-pressure balloon. Its volume is kept essentially constant, and it is vented at the base so that $\Pi = 0$ there. Lift is achieved by making $\Theta > 0$. The hot-air balloon is discussed more completely in Section IX.

Since most balloons are essentially zero-pressure balloons until they become fully inflated, it is often assumed that Π is negligible. Equation

(33) can then be rewritten as follows:

$$\begin{aligned}
 & -\vec{k}_g \left[m_G + m_g \left(1 - \frac{M_a}{M_g} \right) \right] + \vec{k}_g m_g \frac{M_a}{M_g} \frac{\Theta}{T_a} - \frac{1}{2} \rho_a \left\{ C_{D^A} \left| \vec{v}_B - \vec{v}_a \right| \left(\vec{v}_B - \vec{v}_a \right) \right. \\
 & \left. - \vec{k}_{C_{L^A}} \left| \vec{v}_B - \vec{v}_a \right|^2 \right\} = \left[m_G + m_g \left[1 + C_B \frac{M_a (T_a + \Theta)}{M_g T_a} \right] \right] \frac{d}{dt} \left[\vec{i} \left(\frac{dx}{dt} \right)_B + \right. \\
 & \left. \vec{j} \left(\frac{dy}{dt} \right)_B + \vec{k} \left(\frac{dz}{dt} \right)_B \right] \quad (34)
 \end{aligned}$$

The term $-\vec{k}_g \left[m_G + m_g \left(1 - \frac{M_a}{M_g} \right) \right]$ alone is often called the free lift term. It is the true free lift only if $\Pi = \Theta = 0$; therefore, it is called

nominal free lift in this section. It is customary in scientific ballooning to inflate a balloon with a sufficient mass m_g of gas having a molecular weight M_g to get the desired nominal free lift. Since the molecular weight of air does not change significantly with altitude below 70 km (230,000 ft), the nominal free lift is invariant with altitude up to the altitude at which $V_g = V_i$ unless gas is lost or the mass of the system is changed. During ascent the gas in the balloon expands. When $V_g > V_i$, gas is vented to the atmosphere, thereby decreasing m_g and reducing the nominal free lift. In zero-pressure ballooning the nominal free lift is measured in terms of a percentage fraction. $f\%$ of gross system weight.

Thus

$$-g \left[m_G + m_g \left(1 - \frac{M_a}{M_g} \right) \right] = \frac{f\%}{100} g m_G \quad (35)$$

The mass of the lifting gas is then

$$m_g = \frac{m_G (1 + f')}{\left(\frac{M_a}{M_g} - 1 \right)} \quad (36)$$

where $f' = f\%/100$. The symbol $f\%$ is called the percentage free lift. The symbol f' is used here to designate the fractional free lift; it should be

carefully differentiated from the free lift ratio f used in superpressure ballooning practice. (See Section VIII.)

The term $k_{gm} M_a \Theta / M_g T_a$ in Eq. (34) is the thermal lift term to hot-air balloonists; it is most frequently known as the thermodynamic drag term to those who use helium to produce lift. If $\Theta > 0$, the term produces a force directed upward. If $\Theta < 0$, it produces a force directed downward. If a balloon is ascending and $\Theta < 0$, or if it is descending and $\Theta > 0$, the force opposes the motion.

A balloon system prior to launch is tethered to the earth so that its velocity is zero. The velocity of the atmosphere is essentially two dimensional, the vertical velocity being near zero. Therefore, $(\vec{v}_B - \vec{v}_a)$ in Eq. (34) is a horizontal vector prior to launch. The drag force of the wind on the balloon will tilt it about its tether point prior to release, and, upon release, will accelerate it in the direction of the wind. As its horizontal velocity approaches the horizontal velocity of the wind, the horizontal component of the relative wind vector $(\vec{v}_B - \vec{v}_a)$ approaches zero and the horizontal component of the drag also approaches zero. The remaining drag then is a vertical force which opposes the vertical motion of the balloon.

If the balloon rises or descends through a stratum in the atmosphere in which the vertical wind shear is significant, the horizontal component of $(\vec{v}_B - \vec{v}_a)$ will not be zero, and the balloon will be accelerated horizontally. Likewise, if \vec{v}_a changes in a stratum in which the balloon has been floating and in which $(\vec{v}_B - \vec{v}_a)$ was zero prior to the change of \vec{v}_a , the balloon will be accelerated.

Figure 4 suggests that a balloon may develop lift when the wind blows upon it, but the lift coefficient is quite sensitive to the shape of the airfoil. Therefore, the data of Fig. 4 cannot be applied directly to a real balloon which is distorted by the wind. In launch system design work, the designer usually assumes a small positive value for C_L to assure that his launch equipment is designed with adequate safety margins. The operations crew may assume a small negative value to assure that it has enough free lift in the balloon to guarantee lift-off. No use has been made of the concept of trying to predict the motion of a balloon system in flight.

At this point it is useful to introduce some additional symbols. Let $M_a/M_g = \sigma$, $m_g/m_G = \mu$, and $T_a/T_g = \tau$. Then Eq. (36) may be written

$$\frac{m_g}{m_G} = \frac{1 + f'}{\sigma - 1} = \mu \quad (37)$$

and

$$\frac{m_a}{m_G} = \mu \sigma \tau^{-1} \quad (37a)$$

These permit Eq. (33) to be written in the following form if $\Pi = 0$:

$$\left\{ -k g m_G \left[1 + \mu (1 - \sigma \tau^{-1}) \right] \right\}_1 - \left\{ \frac{1}{2} \rho_a C_D A_D \left| \vec{v}_B - \vec{v}_a \right| \left(\vec{v}_B - \vec{v}_a \right) \right\}_2 + \left\{ \frac{1}{2} \rho_a \vec{k} C_L A_L \left| \vec{v}_B - \vec{v}_a \right|^2 \right\}_3 = \left\{ m_G \left[1 + \mu (1 + C_B \sigma \tau^{-1}) \right] \frac{d\vec{v}_B}{dt} \right\}_4 \quad (38)$$

The number subscripts outside the braces are used to identify the terms.

For a balloon system in flight μ will change only if gas is gained or lost or the gross mass m_G of the system is changed. These changes are usually made deliberately and the amount of change is known. The values of σ and C_B may be considered constant, and for a balloon in steady state flight g , C_D , A_D , C_L , and A_L are all essentially constant. Air density ρ_a is an atmospheric variable which may be expressed in terms of p_a and T_a or, approximately, as a function of height.

The variable τ is important, but is difficult to measure during flight and equally difficult to estimate realistically. Experience in ballooning shows that it may take values ranging from 0.8 to 1.2. Balloonists usually consider it to have a value of 1.0 when they make calculations. They then make whatever qualitative corrections they feel are appropriate to account for deviations from 1.0. The relationship between τ and Θ is given by the equation, $\tau = T_a / (T_a + \Theta)$, so that for $\Theta > 0$, $\tau < 1$, and for $\Theta < 0$, $\tau > 1$.

Equation (38) is equivalent to Eq. (34). Neither is as general as Eq. (33) because in both the superpressure is assumed to be zero.

I. ZERO-PRESSURE BALLOON FLIGHT

1. Inflation and Release

A balloon is usually inflated rapidly to minimize the duration of exposure of the partially inflated shape to the elements prior to release. It is inflated sufficiently to provide the desired nominal free lift. During inflation the lift gas expands from cylinders, where it is under high pressure, into the balloon at essentially atmospheric pressure. It cools below atmospheric temperature in the process. Therefore, unless the balloon bubble is left standing in its atmospheric environment for some

time, $\tau > 1$, and the actual free lift is less than the nominal free lift.

At the instant a restrained balloon is released, it accelerates away from the release point. This is often of great concern because of the sensitivity of the payload to acceleration. Therefore, accelerations immediately after release will be reviewed in some detail.

If the aerodynamic lift on a balloon is negligible as suggested earlier, the only vertical forces on it at the time of release when $\vec{k}_{v_B} = 0$ are the buoyant and gravitational forces. The acceleration which a balloon system will experience if it is being acted upon only by buoyant and gravitational forces is, from Eq. (38)

$$\left(\frac{dv_B}{dt}\right)_1 = -\vec{k}_g \left[1 + \mu (1 - \sigma\tau^{-1})\right]_1 \left[1 + \mu (1 + C_B\sigma\tau^{-1})\right]_4^{-1} \quad (39)$$

where the number subscripts identify the terms which are used from Eq. (38).

The subscript used with $(d\vec{v}_B/dt)$, is intended to show that the acceleration is due only to the forces associated with the first term of Eq. (38).

If $\mu = 0$, indicating that there is no lift gas in the balloon, the system will have a free lift acceleration of $-\vec{k}_g$. It is then a freely falling body. On the other hand, if μ is positive and μ and τ^{-1} are both very

large, the system acceleration will approach $+\vec{k}_g/C_B$ as a limit. For a spherical balloon system this is 2 g upward, and that is the maximum acceleration a spherical balloon can have.

It is instructive to examine Eq. (39) for the special case when $\tau = 1$ and $f' > 0$ and also for the case when $f' = 0$ and $\tau \neq 1$. For $\tau = 1$ and $f' > 0$, one may write Eq. (39) in the following form:

$$\left(\frac{dv_B}{dt}\right) = \vec{k}_g f' [1 + \mu (1 + C_B\sigma)]^{-1} \quad (40)$$

Since μ , C_B , and σ are all greater than zero for all practical balloon systems, $[1 + \mu (1 + C_B\sigma)]^{-1} < 1.0$; therefore, the acceleration of a practical balloon system cannot exceed gf' . In fact, $[1 + \mu (1 + C_B\sigma)]^{-1}$ is maximum when $f' = 0$; it then has a value of approximately 0.57 for a helium inflated balloon in air and 0.62 for a hydrogen inflated balloon. It decreases with increasing value of f' , approaching $(\sigma - 1)/f'(1 + C_B\sigma)$ for very large values of f' .

An unenclosed gas bubble rising in the atmosphere may be compared to a balloon for which f' is very large. Therefore, a spherical gas bubble for which $\tau = 1$ would be expected to have an acceleration of $(\sigma - 1)g/(1 + C_B\sigma)$ which is approximately 1.35 g for helium in the atmosphere.

When $f' = 0$ and τ is not specified, Eq. (39) becomes

$$\left(\frac{d\vec{v}}{dt}\right)_1 = \vec{k}g \left(\frac{1-\tau}{C_B + \tau}\right) \quad (41)$$

For very small values of τ , i.e., for very hot lift gas in a cold atmosphere, this approaches $\vec{k}g/C_B$ the same limit as when μ was very large and τ very small. Note that Eq. (41) does not contain a term which is a function of the type of gas used in the balloon, but the condition that $f' = 0$ implies that the balloon system must be in a state of neutral equilibrium when $\tau = 1$. An unenclosed bubble of air would meet this criterion.

Incidentally, the acceleration of a massless body which nonetheless displaces a mass of air is also $\vec{k}g/C_B$. Therefore, a balloon could approach this limiting acceleration only if the lift gas were so hot that its density were negligible. The lift gas would then occupy an essentially infinite volume. No balloon system can be expected to approach the limit.

Figures 5 and 6 are graphs of Eq. (39) for a realistic range of values of f' and τ . It must be emphasized that all accelerations discussed thus far are those which a balloon system would experience if no aerodynamic drag or lift forces were acting on it. Further, the accelerations are those of the balloon system as a whole. The payload, because of the peculiarities

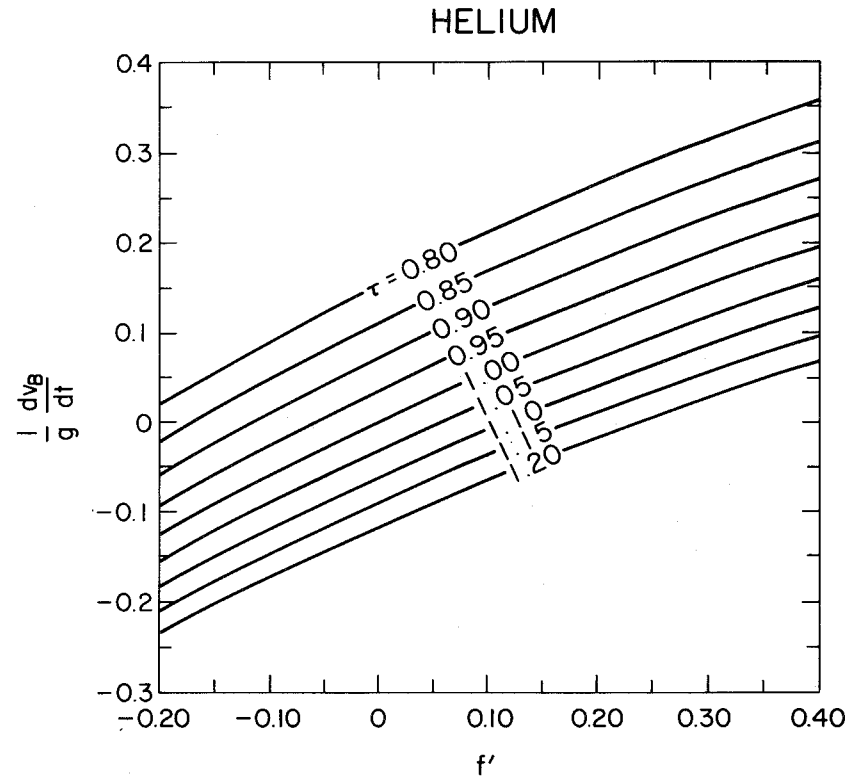


Fig. 5. Vertical acceleration for a helium filled balloon.

HYDROGEN

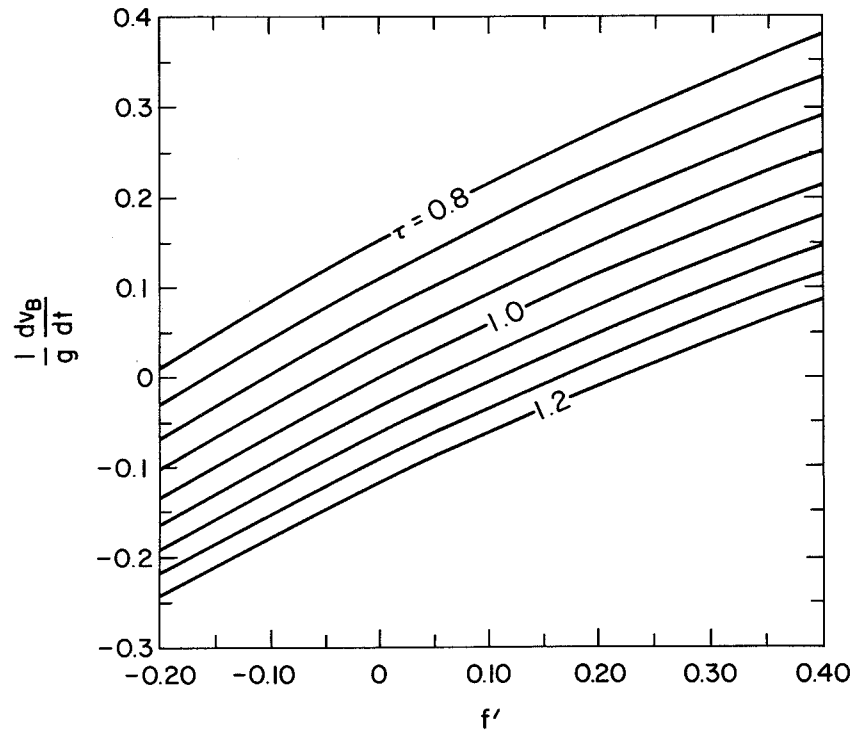


Fig. 6. Vertical acceleration for a hydrogen filled balloon.

of the suspension system, may experience transient or oscillatory accelerations which are quite different from the accelerations of the overall balloon system.

Aerodynamic drag contributes nothing to the vertical acceleration of the system at the moment of launch, because at that time $\vec{kv}_B = 0$ and \vec{v}_a has no vertical component. It does, however, contribute to the horizontal acceleration of the system if $\vec{v}_B \neq \vec{v}_a$, and its contribution is given by

$$\left[\frac{dv_B}{dt} \right]_2 = \left[\frac{1}{2} \rho_a C_D A_D \left| \vec{v}_B - \vec{v}_a \right| (\vec{v}_B - \vec{v}_a) \right]_2 \div m_G \left[1 + \mu (1 + C_B \sigma \tau^{-1}) \right]_4 \quad (42)$$

Now using the approximation $A_D = 4.66 r^2$ (see Section XII.B, Fig. B-1 for $b = 90^\circ$ and $\theta = 20^\circ$) and $V_g = v_a = m_a / \rho_a = m_G \mu \sigma / \rho_a \tau$, and letting the coordinate system be oriented so that the x-axis is parallel to the wind permits us to write this in the form

$$\frac{dv_{B,x}}{dt} = \frac{0.56 C_D (v_{B,x} - v_{a,x})^2 \mu \sigma}{[1 + \mu (1 + C_B \sigma \tau^{-1})] r \tau} \quad (43)$$

For $C_D = 0.4$, $f' = 0.1$, $C_B = 0.5$, $\tau = 1.0$, and $\sigma = 7.24$, this becomes

$dv_{B,x}/dt \approx 0.16 (v_{B,x} - v_{a,x})^2 / r$. During a short period following launch,

r may be considered constant, and if $v_{a,x}$ is constant along the balloon's trajectory, integration between the limits $v_{B,x} = 0$ at time t_0 and $v_{B,x} = v_{a,x} - v_r$ at time t_1 yields $(t_1 - t_0) \approx 6.2 r (v_{a,x} - v_r) / v_{a,x} v_r$. Thus, the time required for the balloon to reach a speed which differs by an amount v_r from the wind speed is, subject to the simplifications assumed in this analysis, a linear function of the radius of the gas bubble. Also, according to this analysis, a balloon will accelerate rapidly to a speed near that of the wind, but it will require a very long time to reach wind speed. For example, a balloon system having a gas bubble radius of 5 m launched from rest in a 10 m sec^{-1} wind will reach a speed of 9 m sec^{-1} in about 28 sec, 9.5 m sec^{-1} in 59 sec, and 9.9 m sec^{-1} in 310 sec. Since v_r is the relative, horizontal wind blowing against the balloon, another way to view this analysis is that the relative, horizontal wind blowing on the balloon decreases rapidly when the balloon is freed to fly with the wind, but requires a long time to reach zero.

The maximum horizontal acceleration occurs when $\vec{v}_{B,x} - \vec{v}_{a,x}$ is greatest, i.e., at the moment of launch. For the rather extreme example given above in which at launch $v_B = 0$, $v_a = 10 \text{ m sec}^{-1}$ and $r = 5 \text{ m}$, the horizontal ac-

celeration immediately after release is 3.2 m sec^{-2} or $\sim 0.33 \text{ g}$. A 5 m sec^{-1} wind would be a more realistic wind in which to launch a balloon. In such a wind, a balloon with a radius of 5 m would accelerate horizontally at 0.8 m sec^{-2} or 0.08 g . From Eq. (40) or Fig.5, it can be determined that if $\tau = 1$ and $f' = 0.1$, a helium filled balloon system would accelerate vertically at 0.055 g . The initial vector acceleration would, therefore, have a magnitude $g \sqrt{0.08^2 + 0.055^2} \approx 0.1 \text{ g}$ and be directed at an angle of $\tan^{-1} (0.055/0.08) \approx 35^\circ$ above the horizon.

The drag force is exerted almost wholly on the balloon bubble and the balloon fabric immediately below it. The horizontal acceleration of the payload must then be due to a horizontal component of force exerted on it by the balloon train. To exert such a force the train must be tilted away from the vertical, and the amount of tilt is a function of the acceleration. The angle the train makes with the vertical is $\tan^{-1} (dv_{B,x}/dt)/g$. For the example used above with launch in a 10 m sec^{-1} wind, the maximum angle is $\sim \tan^{-1} 0.33$ or 18° . Because a 10 m sec^{-1} wind is too strong for normal launches, most balloon systems will undergo less than 18° tilt at launch; the tilt is nevertheless often quite discernible.

A flight as described thus far can be summarized by saying that sufficient gas is placed in the balloon to provide an upward acceleration upon release. At release, the lift due to the gas accelerates the balloon system upward. The temperature of the gas in the balloon at release is generally lower than that of the ambient atmosphere, and when it is, the balloon experiences a smaller vertical acceleration than if the gas and air temperatures were equal. The balloon is accelerated in the direction of the wind at release and rapidly reaches very nearly the horizontal velocity of the wind. Thus, a few minutes after release, the balloon is moving upward at a velocity such that the sum of the weight, the aerodynamic drag force, and the lift force is near zero, and it is moving horizontally with essentially the speed of the wind.

2. Free Flight

Equation (34) was developed in such a way as to make use of atmospheric properties which are normally measured directly, i.e., temperature and pressure. The distribution of these and other properties in the atmosphere is discussed in Section XI.

a. Ascent in a windless atmosphere. When a balloon is released, the free lift causes it to accelerate upward. Experience shows, however, that after a short time the upward acceleration ends and the balloon rises, at least for a time, at a nearly uniform rate. Then, except for unusual circumstances, the vector $(\vec{v}_B - \vec{v}_a) = k\vec{v}_{B,z}$ and $d\vec{v}_B/dt = 0$, and the vertical component of Eq. (38) may be written

$$|v_{B,z}| v_{B,z} = \frac{-2 g m_G [1 + \mu (1 - \sigma\tau^{-1})]}{C_D \rho_a A_D} \quad (44)$$

Note that the aerodynamic lift term is not included because $C_L = 0$ when the relative wind on the balloon is a vertical wind.

Both ρ_a and A_D will change appreciably as a balloon ascends, and by comparison all other terms may be considered constant. For vertical motion, A_D is usually expressed as the area of a great circle of a sphere whose volume is that of the displaced air, and $\rho_a = m_a/V_a = m_G \mu \sigma / \tau V_a$. It follows that $\rho_a A_D = 3 m_G \mu \sigma / 4 \tau r$.

Substituting in Eq. (44) yields

$$|v_{B,z}| v_{B,z} = \frac{8 g r}{3 C_D} \left(1 - \frac{\tau \sigma + f'}{\sigma (1 + f')} \right) \quad (45)$$

The magnitude of $v_{B,z}$ is the positive square root of the absolute value

of the right side of Eq. (45), and $v_{B,z}$ takes the algebraic sign of the term in parenthesis on the right side of the equation. From Eq. (45) it is apparent that if $\tau = \sigma(1 + f')/(\sigma + f')$, the supertemperature just counteracts the nominal free lift and $v_{B,z} = 0$. This is also the necessary condition for $dv_{B,z}/dt = 0$, and the relationship is shown graphically in Fig. 6. From Eq. (45) it is also evident that for $f' = 0$, the motion will be upward (positive) when $\tau < 1.0$ and downward (negative) when $\tau > 1.0$. If f' is very large compared to σ or if $\sigma = 1.0$, the motion will be upward when $\tau < \sigma$ and downward when $\tau > \sigma$. This is the basis for controlling a hot-air balloon for which $\sigma \approx 1.0$.

It should also be noted that for a given value of $\tau(\sigma + f')/\sigma(1 + f')$, the vertical speed of the balloon is a function of the radius of the balloon and is apparently independent of the air density. Therefore, a balloon at 20 km will rise at the same rate as a balloon at sea level if they both have the same radius and if the value of $\tau(\sigma + f')/\sigma(1 + f')$ is the same for both. On the other hand, as a zero-pressure balloon rises, the pressure decreases, causing the radius to increase. Therefore, if the balloon is to maintain a constant upward speed, as was assumed in deriving Eq. (45),

the value of $\tau(\sigma + f')/\sigma(1 + f')$ must increase to compensate for the increase in r .

The radius of a spherical balloon may be expressed in terms of the gross mass of the balloon system and the air density as follows:

$$r = \left(\frac{3 m_a}{4 \pi \rho_a} \right)^{1/3} = \left(\frac{3 m_a \mu \sigma}{4 \pi \rho_a \tau} \right)^{1/3}$$

Substituted in Eq. (45), this yields

$$|v_{B,z}| \quad v_{B,z} = - \frac{8 g}{3 C_D} \left(\frac{3 m_a \mu \sigma}{4 \pi \rho_a \tau} \right)^{1/3} \left[1 - \frac{\tau \sigma + f'}{\sigma(1 + f')} \right] \quad (46)$$

or

$$|v_{B,z}| \quad v_{B,z} = \frac{1.66 g}{C_D} \left(\frac{m_a}{\rho_a} \right)^{1/3} \left[\frac{\sigma(1 + f') - \tau(\sigma + f')}{(1 + f')\sigma^{2/3} \tau^{1/3}} \right] \quad (47)$$

These equations show a dependence of upward speed on air density. Figure 7 is a graphical representation of Eq. (46) for $\rho_a = 1.225 \text{ kg/m}^3$ and $\tau = 1.0$, conditions usually assumed for a sea level launch.

Equation (47) shows that if m_a , τ , f' , and C_D were to remain unchanged during the ascent of a balloon system, the balance between buoyancy and aerodynamic drag could not be maintained unless the upward speed increased as the balloon gained height. Such an increase is not observed; therefore,

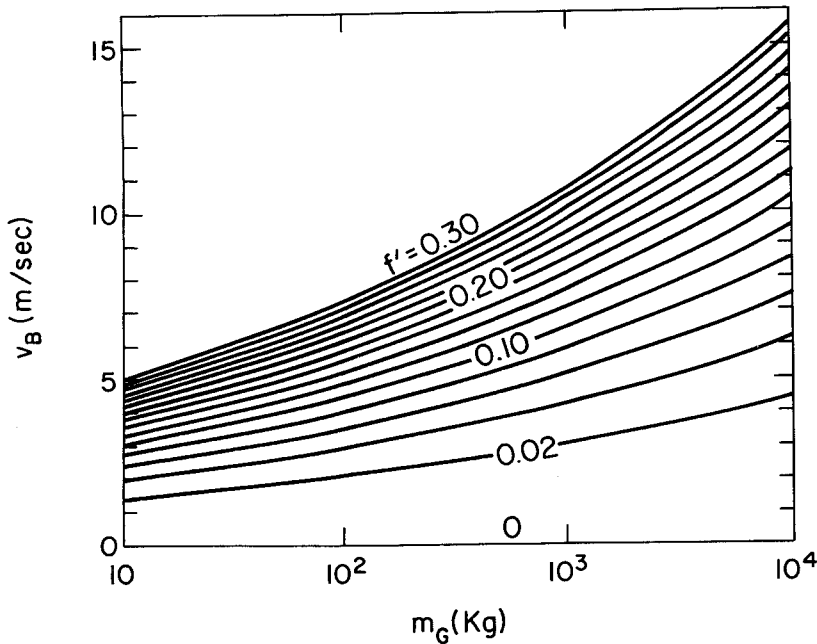


Fig. 7. Vertical velocity of a helium filled balloon ascending at sea level where $\rho_a = 1.225 \text{ kg/m}^3$ and $g = 9.80665 \text{ m/sec}^2$. It is assumed that $\tau = 1.0$ and $C_D = 0.3$.

compensatory changes in τ of C_D must occur during a normal ascent. The drag coefficient, C_D , is not believed to change significantly during ascent, but it will be shown that cooling by expansion of the gas in a balloon can readily cause adequate compensatory changes in τ .

A relationship may be expressed between τ , ρ_a , and f' which will maintain balance between aerodynamic drag and buoyancy during uniform vertical motion. Let Eq. (47) be written as follows for the level at which $\rho_a = \rho_{a,o}$ and $\tau = \tau_o$:

$$|v_{B,o}| v_{B,o} = \frac{1.66 g}{C_{D,o}} \left(\frac{m_{g,o}}{\rho_{a,o}} \right)^{1/3} \left[\frac{\sigma(1 + f'_o) - \tau_o(\sigma + f'_o)}{(1 + f'_o)\sigma^{2/3} \tau_o^{1/3}} \right]$$

Also, for all vertical motion, let $v_{B,z} = v_{B,o}$, $m_g = m_{g,o}$, $C_D = C_{D,o}$ and

$f' = f'_o$. Then dividing this equation into Eq. (47) and rearranging gives

$$\frac{\rho_a}{\rho_{a,o}} = \frac{\tau_o \left[\frac{\sigma(1 + f'_o) - \tau_o(\sigma + f'_o)}{(1 + f'_o)\sigma^{2/3} \tau_o^{1/3}} \right]^3}{\tau \left[\frac{\sigma(1 + f') - \tau(\sigma + f')}{(1 + f)\sigma^{2/3} \tau^{1/3}} \right]^3} \quad (48)$$

Equation (48) is plotted in Fig. 8 (solid curves) for helium for select values of f' and τ_o . Note that τ must increase (i.e., the gas in the balloon must cool relative to the ambient air) for the motion to remain constant whether that motion be upward or downward. In motion toward lower density,

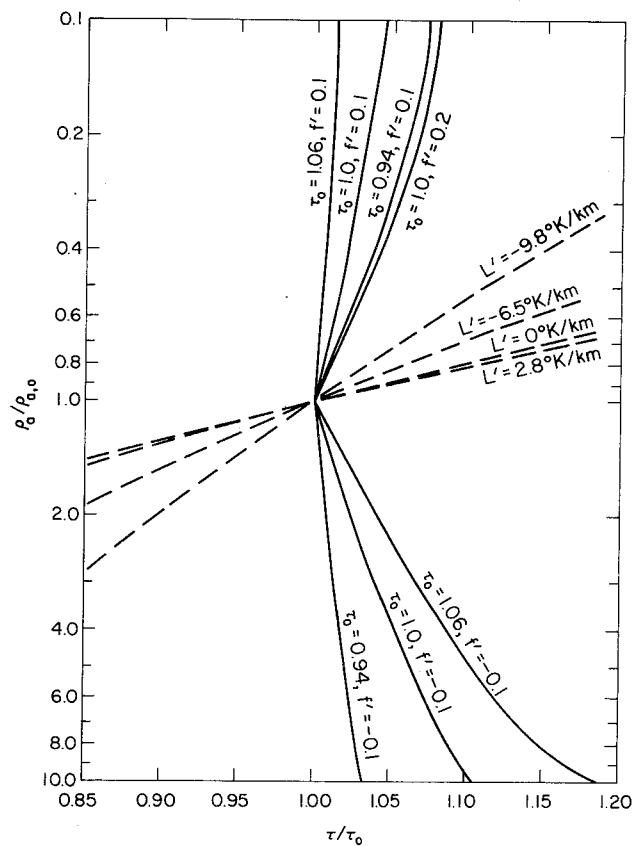


Fig. 8. The variation of τ with air density required to maintain constant vertical motion (solid curves) and variation of τ with air density for an adiabatic ascent (dashed curves) in four atmospheric lapse rates. The lift gas is helium.

the speed will increase unless τ increases. In motion toward higher density, the speed will decrease unless τ increases. Although each of the solid curves in Fig. 8 is an isoline of constant speed, the speed cannot be determined unless $\rho_{a,0}$ is assigned a value. The vertical line $\tau/\tau_0 = 1.0$ is an isoline along which $v_{B,z} = 0$.

Cooling of the gas in a balloon because of expansion during ascent will be adiabatic unless the gas can exchange heat with its environment. Most standard texts on thermodynamics show that the pressure-volume relationship of an ideal gas undergoing an adiabatic volume change may be expressed as $p_g \alpha_g^{(C_p/C_v)} = \text{const}$ where α_g is the specific volume of the gas, and C_p and C_v are the specific heats of the gas at constant pressure and volume, respectively. By differentiating the pressure-volume relationship and making use of the equation of state, Eq. (8), and the fact that $R/M_g = C_p - C_v$, it can be shown that

$$\frac{dT_g}{T_g} = \frac{R}{M_g C_p} \frac{dp_g}{p_g} \quad (49)$$

The gas pressure in a zero-pressure balloon is very nearly equal to the pressure of the ambient atmosphere at all times so that

$$\frac{dp_g}{p_g} = \frac{dp_a}{p_a}$$

From the hydrostatic equation and the equation of state

$$\frac{dp_a}{p_a} = -\frac{gM_a}{RT_a} dz$$

Combining this with Eq. (49) and solving for dT_g/dz gives

$$\frac{dT_g}{dz} = -\frac{g}{C_p} \frac{M_a}{M_g} \frac{T_g}{T_a} = -\frac{g\sigma}{C_p \tau} \quad (50)$$

Differentiating $\tau = T_a/T_g$ with respect to z yields

$$\frac{d\tau}{dz} = \frac{T_g \frac{dT_a}{dz} - T_a \frac{dT_g}{dz}}{T_g^2} \quad (51)$$

Let $dT_a/dz = L'$; this is the negative (additive inverse) of the lapse rate of the atmosphere. It is constant within each of the strata of the Standard Atmosphere, and it is often nearly constant through deep layers in the real atmosphere. It will be considered constant here. By combining Eqs. (50) and (51), substituting L' and rearranging, one may write

$$\frac{d\tau}{\tau} = \left(\frac{C_p L' + g\sigma}{C_p} \right) \frac{dz}{T_a} \quad (52)$$

Similarly, if the equation of state for air is differentiated with respect to z , the result may be written

$$\frac{M_a}{R} \frac{dp_a}{dz} = \rho_a \frac{dT_a}{dz} + T_a \frac{d\rho_a}{dz}$$

Substituting $-g\rho_a$ for dp_a/dz from the hydrostatic equation and L' for dT_a/dz and rearranging gives

$$\frac{dz}{T_a} = -\frac{R}{RL' + gM_a} \frac{d\rho_a}{\rho_a} \quad (53)$$

Combining Eqs. (52) and (53) yields

$$\frac{d\tau}{\tau} = -\frac{R(C_p L' + g\sigma)}{C_p (RL' + gM_a)} \frac{d\rho_a}{\rho_a} \quad (54)$$

which becomes

$$\frac{\tau}{\tau_0} \text{ (adiabatic)} = \left(\frac{\rho_{a,0}}{\rho_a} \right)^{\frac{R(C_p L' + g\sigma)}{C_p (RL' + gM_a)}} \quad (55)$$

upon integration. This relationship is shown graphically by the dashed lines in Fig. 8 for helium for three Standard Atmosphere lapse rates and for $L' = -9.8^\circ\text{K/km}$, the adiabatic lapse rate for air.

If $L' = -g\sigma/C_p$, the exponent in Eq. (55) will be zero and τ will not change with density although density will vary with height. The combination

$g\sigma/C_p$ is the adiabatic lapse rate of the gas in the atmosphere. Thus, if a gas is ascending or descending adiabatically through the atmosphere, Eq. (56) shows that:

- 1) if $L' > -g\sigma/C_p$, τ will increase with movement toward lower density (ascent) and decrease during descent.
- 2) if $L' = -g\sigma/C_p$, τ will not change during ascent or descent.
- 3) if $L' < -g\sigma/C_p$, τ will decrease during ascent and increase during descent unless $L' \leq -g M_a/R$.

When $L' = -gM_a/R$, it is apparent from Eq. (53) that ρ_a is independent of height. If $L' < -gM_a/R$, more dense air overlies less dense air and overturning can be expected. Overturning will tend to restore the lapse rate to adiabatic. In fact, $-L'$ is rarely more than the adiabatic lapse rate for air except in thin strata or very near the ground; therefore, the case when $L' = -gM_a/R$ is of theoretical interest only. Incidentally, meteorologists call the lapse rate gM_a/R an autoconvective lapse rate because it is so unstable.

The numerical values of dT/dz for several gases undergoing adiabatic ascent or descent are shown in Table 2. When these are compared with the

Table 2

Molecular Weight, Specific Heat at Constant Pressure and

dT_g/dz for an Adiabatic Ascent or Descent for Various Lift Gases

Gas	M_g	C_p (joule/kg ^o K)	dT_g/dz (adiabatic) (^o K/km)
H ₂	2.016	14,200	- 9.95
He	4.003	5,240	-13.5
NH ₃	17.031	2,190	- 7.63
Air	28.964	1,003	- 9.8

In the U.S. Standard Atmosphere, 1962, $L' = 06.5^{\circ}\text{K/km}$ in the troposphere and 0°K/km in the lowest stratum of the stratosphere. See Section XI, Table 1 for other values.

temperature gradients of Table 1 of Section XI, two of which are given below Table 2, it is clear that in all strata in the Standard Atmosphere listed in Section XI, τ will increase during ascent and decrease during descent for the gases listed in Table 2 if the motion is adiabatic. Thus, when these gases are used in a balloon flown in an atmosphere like the Standard Atmosphere, vertical motion causes τ to change in such a way as to oppose the motion. The effect is more significant with helium than hydrogen and least significant with ammonia. Lapse rates in the troposphere of the real atmosphere will on occasion be greater than the adiabatic lapse rate of ammonia, but very rarely will they be greater than the adiabatic lapse rates of hydrogen or helium.

Comparison of the adiabatic curves in Fig. 8 with the curves plotted from Eq. (48) reveals that for helium an adiabatic change of τ is greater than is needed to compensate for the change of air density during uniform upward motion. During descent an adiabatic change of τ would augment the slowing due to the increase of density. Thus, for both ascent and descent the change of temperature of the gas in a helium inflated balloon caused by the change of pressure and volume serves as a brake, but if the motion were

adiabatic, the braking action would be too severe. The same statement applies to a balloon inflated with hydrogen. It also applies to a balloon inflated with ammonia in most atmospheric strata, but occasionally an atmospheric stratum may exist in which the brake would fail. Thus, in most instances transfer of heat between the environment and the gas in a balloon is seen to be a requisite condition for uniform vertical motion.

Heat transfer processes include: radiation, convective exchange with the ambient air, and heat deliberately added to or subtracted from the lift gas by some means, such as chemical combustion. These are discussed more completely in Section III.

3. Wind Effects on a Balloon in Free Flight

A balloon in free flight moves with the air in which it is embedded, and, as was pointed out in I.1 of this section, it accelerates rapidly to nearly the speed of the wind immediately after it is released. It is common practice in calculating balloon trajectories to assume that throughout flight the horizontal velocity of the balloon is equal to the velocity of the air in which it is embedded. Interpreted strictly, this implies instant adjustment of the balloon's horizontal velocity as it moves from one stratum to another

where the air velocity is different. In fact, the accuracy with which the wind velocity is known as a function of time and place is not great enough to warrant more precise treatment for estimating trajectories.

For other reasons the difference between balloon and air velocities may be important. For example, it was shown earlier that the difference may cause the balloon system to tilt significantly from the vertical. Also, the uninflated portion of balloons have occasionally been observed to develop into huge spinnaker-like sails during ascent, and some observers have surmised that the wind forces on such sails may play a part in balloon bursts. Therefore, it is worthwhile to explore the possible magnitude of $(\vec{v}_B - \vec{v}_a)$ as a balloon ascends through atmospheric wind shear strata.

Consider a balloon system with the balloon envelope only partially inflated and rising at a constant rate through a deep stratum in the troposphere. Assume that the wind is blowing horizontally from the west at all levels and that its speed increases linearly with height. Assume also that the wind is invariant with time at all levels. Then the horizontal component of acceleration caused by aerodynamic drag in the stratum may be written

$$\frac{dv_{B,x}}{dt} = \frac{1}{2} \rho_a C_D A_D |\vec{v}_B - \vec{v}_a| (v_{B,x} - v_{a,x}) \div m_v \quad (56)$$

where $(v_{B,x} - v_{a,x})$ is the horizontal component of the relative wind on the balloon. If, for the time being, interest is restricted to a shallow layer which will be penetrated in a short time, ρ_a , C_D , A_D , and m_v may all be considered constant. The drag coefficient and area, C_D and A_D , must take those values which will give the proper response of the balloon system to the overall vector wind acting on it. Therefore, A_D is not a vertical cross sectional area through the balloon system; on the contrary, if the vertical component of the relative wind is large compared with the horizontal component, A_D will be a nearly horizontal area.

Now, the successful practice of using the horizontal components of \vec{v}_a as the horizontal components of \vec{v}_B in calculating balloon trajectories suggests that the difference $(v_{B,x} - v_{a,x})$ must be small. On the other hand, there must be a difference. If at some level there were no difference, then as soon as the balloon had risen a short distance into the stronger winds above, a difference would develop. One reasonable solution to Eq. (56) is $v_{B,x} = v_{a,x} + v_{r,x}$, where $v_{r,x}$ is the constant horizontal relative wind on the bal-

loon. Then also $|\vec{v}_B - \vec{v}_a| = v_{r,x} / \sin b$ where b is the angle the vector relative wind makes with the vertical axis of the balloon. Differentiating $v_{B,x}$ with respect to time yields

$$\frac{dv_{B,x}}{dt} = \frac{dv_{a,x}}{dt} = \frac{dv_{a,x}}{dz} \frac{dz}{dt}$$

where $dv_{a,x}/dz$ is the vertical wind gradient and dz/dt is the rate of rise of the balloon. Substituting into Eq. (56) and rearranging gives

$$v_{r,x} = \left(\frac{2 \frac{dv_{a,x}}{dz} \frac{dz}{dt} m_v \sin b}{\rho_a C_D A_D} \right)^{\frac{1}{2}} \quad (57)$$

This suggests that the relative horizontal wind on the balloon system would be significantly decreased if the uninflated portion of the balloon formed a spinnaker sail, because such a sail would increase C_D and A_D and decrease dz/dt without causing comparable changes in the other variables. It is not clear how b may change, but an example can provide some insight.

Data for the following example have been chosen to give larger values of $v_{r,x}$ than can be expected in the atmosphere during a flight except under an unusual combination of circumstances. Assume that a balloon at 8.0 km above sea level is ascending in an atmosphere which has the same density as

the Standard Atmosphere and that the wind shear is $40 \text{ m sec}^{-1} \text{ km}^{-1}$ or $4.0 \times 10^{-2} \text{ sec}^{-1}$, a more extreme value than is likely to be encountered in the real atmosphere except in very thin strata. (See Section XI.D.4 or pages 5-41 of The Handbook of Geophysics (5).) Assume also that the balloon is ascending at a speed of 10 m sec^{-1} , a rate two or more times the desired rate for most flights. A balloon having a nominal volume of $3 \times 10^5 \text{ m}^3$ could be expected to have a mass of 500 kg, and a gross mass for the system of 1500 kg is reasonable. At 8 km in the Standard Atmosphere, the air density is 0.525 kg m^{-3} , and if $f' = 0.2$ and $\tau = 1.03$, the balloon system would displace a volume of 3860 m^3 . Let $b = 45^\circ$ as a first guess. Also, as a first estimate, let $A_D = 1.21 v_g^{2/3} = 297 \text{ m}^2$, and $C_D = 0.35$.

Since the balloon is not accelerating relative to the fluid, the virtual mass is 1789 kg, the gross mass plus the mass of the gas. With these data $v_{r,x} \approx 4.3 \text{ m sec}^{-1}$, and the estimated magnitude of the vector relative wind is 10.9 m sec^{-1} . A new estimate of b is $\sin^{-1}(4.3/10.9)$ which is $\approx 23^\circ$. Using the sphere-on-cone model (Section XII.B), one can make new estimates of A_D and C_D . After several iterations, using a half-cone-angle of 15° for the balloon and 0.35 for C_D , the values of $v_{r,x}$ and b converge on 2.6 m sec^{-1}

and 15° , respectively.

When a balloon forms a spinnaker-like sail, the sail is shaped much like a hemispherical cup with the concave side facing into the wind (see Section XII.B). Assume for the present example that $C_D = 0.75$, and as a first estimate, that $b = 0$. Because a comparison is desired between the relative wind before and after the sail has formed, it will be necessary to estimate the value of dz/dt after sailing has occurred. By treating the vertical component of drag as if it were independent and assuming that the only essential differences between the system before and after the sail forms are the values of C_D and A_D , one can calculate the value of dz/dt after the sail has formed and the system has reached steady state. The following equation is used:

$$\left(\frac{dz}{dt}\right)_{\text{after}} = \left(\frac{dz}{dt}\right)_{\text{before}} \left[\frac{(C_D A_D)_{\text{before}}}{(C_D A_D)_{\text{after}}} \right]^{\frac{1}{2}}$$

It gives $(dz/dt)_{\text{after}} \approx 2.3 \text{ m sec}^{-1}$ for this example, and by an iterative solution of Eq.(57), $v_{r,x}$ and b are found to be 0.5 m sec^{-1} and 13° , respectively.

A relative, horizontal wind of 2.6 m sec^{-1} is not strong enough to create difficulty for a balloon, but it may be adequate to cause one to form a sail if other conditions are right. The magnitude of the relative wind vector is 10.3 m sec^{-1} under the conditions assumed for the ascending balloon before it sailed and 2.4 m sec^{-1} after the sail formed; consequently, the stresses during the transition period might conceivably be excessive.

The average aerodynamic pressure, \bar{p}_r , on the cross sectional area of a balloon normal to the relative wind on the balloon is

$$\bar{p}_r = \frac{m}{A_D} \frac{dv_B}{dt} = \frac{1}{2} \rho_a C_D v_r^2$$

The greatest pressure which might exist during the transition would occur immediately after the sail had formed and caused C_D to increase, but before v_r could be reduced by the increased drag. Thus, the maximum value which the mean aerodynamic pressure could have, using the data of the foregoing example, would be

$$\bar{p}_r \approx 0.5 \times 0.525 \times 0.75 \times 10.3^2 \approx 21 \text{ Nm}^{-2} \approx 3 \times 10^{-3} \text{ psi}$$

This pressure is not as large as the excess of gas pressure over atmospheric pressure at the top of the balloon, but the two may be additive, and it is

possible that local film stresses accompanying the transition might be great enough to cause damage.

In view of the rarity of situations in which a balloon will encounter relative winds as strong as the computed wind in the first part of this example and of the low aerodynamic pressures caused by such a wind, vertical wind shear does not loom as a very serious threat to balloons in flight.

A balloon in flight has an appreciable vertical dimension, and if the vertical wind shear is strong, the relative wind at the top may differ significantly from that at the bottom. The difference between the relative wind from top to bottom of a balloon system is the product of the length of the system and the vertical wind gradient.

If a balloon system 200 m long were ascending through a stratum in which the wind shear were $4 \times 10^{-2} \text{ sec}^{-1}$, the relative wind at the top would be 8 m sec^{-1} greater than at the bottom. Thus, the top of the ascending balloon system in the foregoing example will be subject to a relative horizontal wind greater than the 2.6 m sec^{-1} estimated for the system as a whole. If the balloon system were long enough, the payload might experience a relative wind from the opposite direction to that experienced by the top of the bal-

loon. This distribution of relative wind will cause the balloon system to tilt. This tilt has led to the suggestion that balloon systems in a stratum where wind shear exists may derive some aerodynamic lift from the relative winds. No quantitative measurements or estimates of the magnitude of lift are known to have been made.

4. Behavior at Float Altitude

In the following discussion frequent reference will be made to Fig. 9. Particular use will be made of the level numbers shown in the figure, often without otherwise referring to the figure.

As a balloon ascends into strata of lower pressure, the lift gas expands and the gas density decreases. The density of the balloon system, ρ_B , at any level is $(m_G + m_g)/V_g$ if the volume of the gondola, rigging, etc. are very small compared with V_g . This may also be written $m_G(1 + \mu)/V_g$. The density of the displaced air is m_a/V_g , which may be expressed as $m_G\mu\sigma/\tau V_g$. Thus the ratio of the density of the balloon system to that of the air is $\rho_B/\rho_a = \tau(1 + \mu)/\mu\sigma = \tau(\sigma + f')/\sigma(1 + f')$. But $\tau(\sigma + f')/\sigma(1 + f') = 1$ is the condition from Eq. (39) that the sum of buoyant and gravitational forces on the balloon be zero. Therefore, if ρ_B/ρ_a should become one during ascent or des-

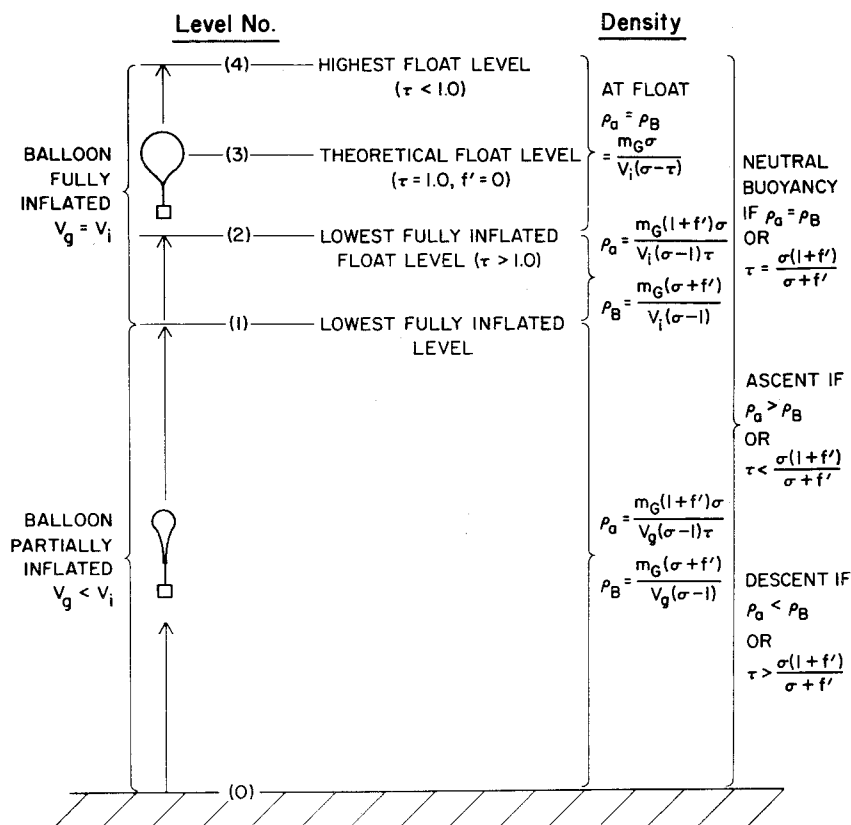


Fig. 9. Diagram showing relationship between air density and balloon system density. Level numbers are used in the text. Vertical distances on the diagram are not proportional to vertical heights in the atmosphere.

cent, aerodynamic drag would soon reduce the motion of the balloon to near zero.

The combination of f' and τ required to make $\rho_B/\rho_a = 1.0$ may be realized at any level during ascent or descent, but one combination has special significance. Clearly if $f' = 0$ and $\tau = 1.0$, $\rho_B/\rho_a = 1.0$. Under these circumstances, $\rho_B = \rho_a = m_G \sigma / V_g (\sigma - 1)$. Now if $V_g = V_i$ where V_i is the fully inflated volume of the balloon, ρ_a is the air density at which a fully inflated balloon should just be in hydrostatic equilibrium. The level (level 3) at which $\rho_a = m_G \sigma / V_i (\sigma - 1)$ is therefore called the "theoretical float altitude" of the balloon.

As f' is defined by Eq. (37), it is possible to change it during flight by changing m_G , m_g , or σ . The gross mass may be decreased by dropping ballast; such a change would increase f' . Gas may be exhausted from the balloon, thereby decreasing m_g ; this would decrease f' . Also it is possible to change σ , and in fact when balloons were open at the lower end so that air could enter while a balloon was ascending, σ usually decreased rapidly near the end of ascent, accompanied by an increase in m_g . In modern scientific ballooning σ is kept constant throughout flight, but the possibility of changing it

should not be overlooked if special requirements occur.

Typically, when a balloon reaches level 1 (i.e., when the gas in an ascending balloon has expanded to just fill the balloon) $f' > 0$ and $\tau > 1.0$. It is usual also that $\rho_B/\rho_a < 1$ at level 1. Consequently, the balloon will continue to rise past level 1 and become superpressured or expel gas through its ducts or both. If the balloon is a closed vessel, its behavior above level 1 will be quite different from that of a balloon which can freely lose gas to avoid excessive overpressure. Only the latter, the zero-pressure balloon, will be discussed here at levels above level 1. The superpressure balloon is discussed in Section VIII.

A loss of gas will decrease m_g , thereby decreasing f' . Unless this change in f' is compensated by a change in τ , the buoyant force on the balloon will decrease and the vertical speed of the balloon system will dwindle. Since expansion of the gas results from vertical motion and is a cause for τ remaining above its equilibrium value (i.e., the value it would reach if its vertical motion were restrained long enough for it to come into thermal equilibrium with its environment) during ascent, reduced upward speed usually allows τ to decrease. Nonetheless, when an ascending balloon reaches level 2,

the lowest level at which $V_g = V_i$ and $\rho_B/\rho_a = 1.0$, $\tau > 1.0$ normally, and $f' > 0$. If $\tau = 1.0$ at level 2, levels 2 and 3 will coincide.

An ascending balloon will not usually have lost all of its vertical motion when it reaches level 2, and its inertia will cause it to overshoot. At this time the pressure of the gas must exceed ambient air pressure slightly because gas is being forced into the atmosphere from the balloon at its base. With such overpressure and continued cooling due to the decrease in pressure, the rising balloon system will soon become more dense than the ambient air and so be subject to a downward force, which will increase with distance above level 2. This force will ultimately stop the upward motion and initiate downward motion. It is not unusual for balloons with small ducts to oscillate up and down through several cycles before the motion is damped out (see Fig. 10). The equation of motion of the cycle is complicated since f' , τ , and p_g are all simultaneously adjusting to the new environment and undergoing changes which are dependent on the phase of the cycle of oscillation. A numerical solution of the equation of motion (see Section III) can take all of these into account realistically. In a very simplified model which assumes the vertical motion of the gas to be adiabatic and $df'/dt = 0$, the period in

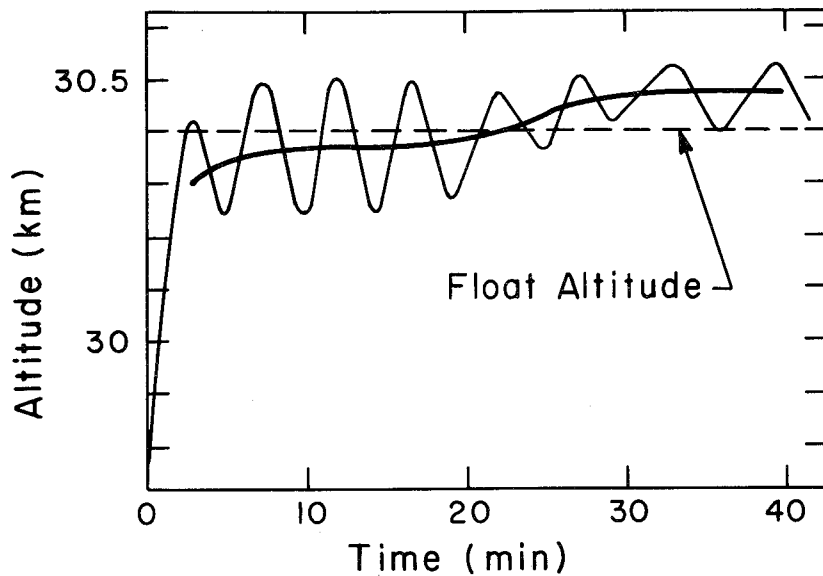


Fig. 10. Vertical oscillation of a balloon system on reaching float altitude. Not all balloon systems oscillate in this manner; many appear to approach float altitude in a nearly asymptotic manner.

seconds of the oscillation, $t(\text{osc})$, is given by

$$t(\text{osc}) = 2 \sqrt{\frac{T_a}{\frac{gC}{C_p} + L'}} \quad (59)$$

for a zero-pressure balloon. A derivation of a similar equation applicable to superpressure balloons is given in Section VIII. Equation (59) suggests that if $L' = -gC/C_p$, i.e., if the lapse rate of the atmosphere is equal to the adiabatic lapse rate of the gas in the atmosphere, the period will be infinitely long. In the isothermal stratum of the Standard Atmosphere where $T_a \approx 217^\circ$ and $L' = 0$, a helium filled balloon becoming fully inflated would be expected from Eq. (59) to have a period of 253 sec (4.2 min). The record plotted in Fig. 10 shows that the average period of the first three cycles was 4.5 min and that the period increased with elapsed time.

Figure 10 shows another characteristic of many flights. The heavy curve is a hand-smoothed average of the oscillating curve. The dashed curve represents the theoretical float altitude. The balloon appears to have oscillated about a float level which gained height as time passed. It can be shown that the ratio of the density of a balloon system floating in the stratum above level 2 to the density of the air at the theoretical float altitude

is $\rho_{B,2} / \rho_{a,3} = (\sigma - 1) / (\sigma - \tau_2) = (\sigma + f'_2) / \sigma$. If $\tau_2 > 1.0$, the density of the balloon system will be greater than air density at the theoretical float level, and the balloon will float at a level lower than the theoretical float level. Similarly, if $\tau < 1.0$ at the actual float level, balloon system density will be less than air density at the theoretical float level, and hence the actual float level will be higher than the theoretical. It is normal for a balloon to start floating at a level below the theoretical float level and to ascend slowly to a level above the theoretical level as the gas in the balloon warms.

In the stratosphere where most scientific balloon systems float, the temperature is nearly independent of height. Therefore, Eq. (10) may be integrated to yield the following relationship between the geopotential height (see Section XI.C.1) of two pressure levels:

$$H_2 - H_1 = \frac{RT_a}{M_a g_0} \ln \frac{p_{a,1}}{p_{a,2}} \quad (60)$$

Also, if temperature is independent of height and thus of pressure,

$\rho_{a,1} / \rho_{a,2} = p_1 / p_2$; therefore,

$$H_2 - H_1 = \frac{RT_a}{M_a g_0} \ln \frac{\rho_{a,1}}{\rho_{a,2}} \quad (61)$$

and

$$H_3 - H_2 = \frac{RT_a}{M_a g_0} \ln \left(\frac{\sigma - 1}{\sigma - \tau_2} \right) = \frac{RT_a}{M_a g_0} \ln \left(\frac{\sigma + f'_2}{\sigma} \right) \quad (62)$$

Equations (60) and (61) are applicable in any stratum in the atmosphere in which $L' = 0$ or the stratum is thin enough that the variation of T_a is not significant. Subject to these restrictions, the numerical subscripts may take any values. Equation (62) is valid only when level 3 is the theoretical float level and level 2 is any other float level at which $\rho_{B,2} = \rho_{a,2}$.

An example is useful. The value of $R/M_a g_0$ is $29.27 \text{ m}^2/\text{K}$. At 40 km in the Standard Atmosphere $T_a = 251^\circ\text{K}$, $\rho_a = 3.85 \times 10^{-3} \text{ kg/m}^3$ and $p_a = 277.5 \text{ N/m}^2$. Assume that a fully inflated balloon system first reaches float at that level (now designated level 2) and that $\tau_2 = 1.08$. Substituting τ_2 in the relationship $p_{a,2} / p_{a,3} = \rho_{a,2} / \rho_{a,3} = (\sigma - 1) / (\sigma - \tau_2)$ yields $p_{a,2} / p_{a,3} = 1.013$; therefore, $p_{a,3} = 274 \text{ N/m}^2$ and $\rho_{a,3} = 3.80 \times 10^{-3} \text{ kg/m}^3$. Also, from Eq. (62), $(H_3 - H_2) = 95 \text{ m}$. The initial float level is not far from the theoretical in this example.

It should be noted that the theoretical float level as used here is that level at which the density of the air is equal to the density of the balloon system when $\tau = 1.0$, $f' = 0$, and the balloon is fully inflated. To calculate

that density, one must know the mass of the system and the volume of the fully inflated balloon under existing conditions. If they are not known precisely, the calculated theoretical float level density will probably be in error, and deviations of the actual float level from the calculated theoretical float level may greatly exceed the deviation of the example above. The distinction between the actual theoretical float level and the calculated theoretical float level is not always kept in mind in the practice of ballooning.

If a balloon system reaches initial float altitude below the theoretical float level and the gas starts to warm relative to ambient air temperature, gas will continue to be lost through the ducts, and f' will decrease. A sound balloon system will then gain height slowly as long as warming continues. If a gas leak should develop which removes gas faster than is necessary just to compensate for the warming, f' will become less than $\sigma(1 - \tau)/(\tau - \sigma)$, and the balloon will start to descend. Similarly, if for any reason the gas in a floating balloon should cool relative to the air, τ will increase and unless f' can be increased to maintain the condition for no acceleration, the balloon will descend. Thus a balloon at float altitude is in a rather precarious state of equilibrium. The only satisfactory way that has

been found to maintain that equilibrium is to control f' , and that is done by dropping ballast and hence by decreasing m_G .

a. Ballasting and valving to maintain a float condition. It has been pointed out that dropping ballast and valving gas are the primary means of controlling the action of a balloon in flight. Theoretically, if the time rate of change of τ and f' are known, control can be precise.

The condition for zero acceleration of a balloon which is floating is that $1 + \mu(1 - \sigma\tau^{-1}) = 0$. Because T_a is nearly constant when a balloon is floating and because controls change m_G and m_g directly, the condition of zero acceleration for a floating balloon system is more convenient if written as

$$m_G = m_g(\sigma\tau^{-1} - 1) = m_g\left(\frac{\sigma T_g}{T_a} - 1\right) \quad (63)$$

A graphical solution of Eq. (63) is shown in Fig. 11 for helium. This graph and one similar to it for hydrogen are both given in Section XII in a more useful size. On the graphs, the numerical values on the ordinate may be multiplied by any constant and the validity of the chart will be preserved if the m_g values on the slanting lines are also multiplied by the same con-

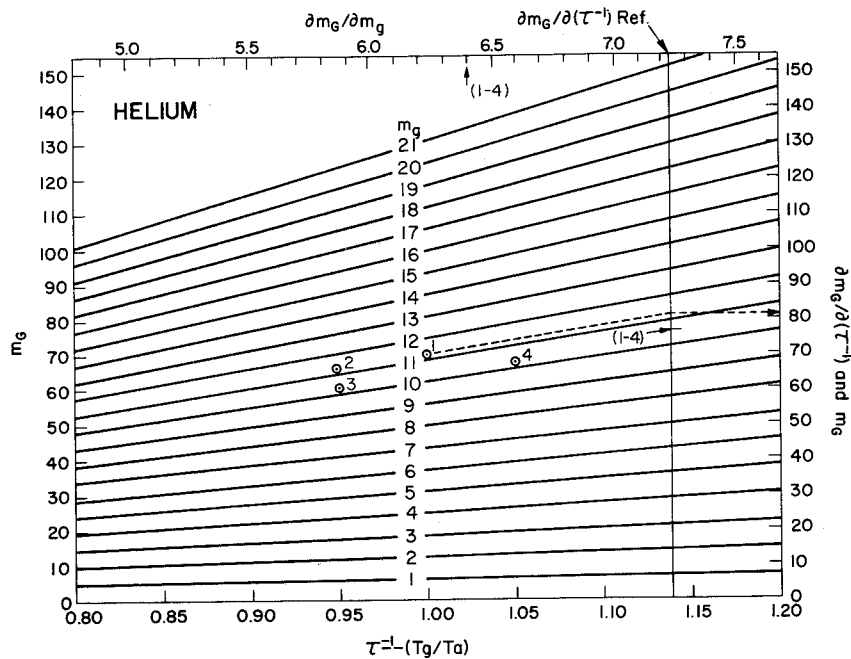


Fig. 11. Graphical solution of the equation of buoyant equilibrium for a helium-filled balloon.

stant, e.g., a multiple of 10. The values on the abscissa should not be changed. The chart thus serves for any range of values of m_G and m_g . With it, solving for any one of the three variables is simple if the other two are known. For example, point 1 on Fig. 11 may be interpreted as meaning that if $T_g/T_a = 1.0$, it will require 11.2 (or 112) units of mass of helium to support 70 (or 700) units of mass of balloon, scientific equipment, rigging ballast, etc. Any unit of mass may be used, but the gross mass and the mass of the gas must be measured in the same units.

The m_g lines are straight and their slope is

$$\frac{\partial m_G}{\partial (\tau^{-1})} = m_g \sigma = m_G \left(\frac{\sigma}{\sigma \tau^{-1} - 1} \right)$$

Therefore, when $\sigma/[\sigma \tau^{-1} - 1] = 1$, $\partial m_G / \partial (\tau^{-1}) = m_G$. This occurs for helium when $\tau^{-1} = 1.138$, and so by erecting a vertical reference line on the right side of the chart at $\tau^{-1} = 1.138$, one can read the slope of each of the m_g lines directly from the m_G coordinate at the point where the m_g lines cross the reference line. A scale of $\partial m_G / \partial m_g$ for constant values of τ^{-1} has been added along the abscissa at the top of the chart.

The following examples will illustrate the use of the chart: Assume that a stably floating balloon system has a gross mass of 700 kg and that $T_g = T_a = 250^{\circ}\text{K}$. Then $\tau^{-1} = T_g/T_a = 1.0$, and point 1 on the graph is a plot of m_G vs T_g/T_a . Note that the ordinate must be multiplied by 10. The mass of helium in the balloon as read from the slanting m_g lines is 11.2, and this must also be multiplied by 10, giving 112 kg. Following up the m_g line through point 1 to the reference line on the right shows the $\partial m_G/\partial(\tau^{-1})$ value to be 810 kg. Along the top scale $\partial m_G/\partial m_g$ is seen to have a value of 6.24 where T_g/T_a has a value of 1.0.

Assume further that the gas in the balloon is cooling uniformly at a rate of 12.5°K/hr and that the air temperature is not changing. Then $\partial(\tau^{-1})/\partial t = (1/T_a)(\partial T_g/\partial t) = -0.05 \text{ hr}^{-1}$. At what rate should ballast be dropped to maintain the balloon system at float altitude without loss of gas, i.e., what should be the value of $\partial m_G/\partial t$? It is

$$\frac{\partial m_G}{\partial t} = \frac{\partial m_G}{\partial(\tau^{-1})} \frac{\partial(\tau^{-1})}{\partial t} = -810 \times 0.05 = -40.5 \text{ kg/hr}$$

The same result can be obtained in another way. By noting that a change of -0.05 in the value of T_g/T_a would reduce it to 0.95 in an hour

and then plotting point 2 at $T_g/T_a = 0.95$ and $m_g = 112$, one finds the value of m_G to be 660 kg. The difference (700 - 660) is 40. Since this change will have occurred in an hour, the average rate is 40 kg/hr.

Using the same data, assume that 100 kg of ballast (an excess of 60 kg) was dropped at a uniform rate during the hour. How much gas was lost due to the excessive ballasting? Point 3, plotted at $m_G = 600$, and $T_g/T_a = 0.95$, shows the status of the balloon system at the end of the hour. The value of m_g is 102. Therefore, 10 kg (112 - 102) of gas and 60 kg of ballast will have been wasted.

Again using the same initial conditions for the balloon system and assuming that gas is leaking at a rate of 10^{-4} kg/sec , and that the air and gas temperatures are not changing, at what rate should ballast be dropped to maintain constant float altitude? The value of $\partial m_G/\partial t$ is desired when $\partial m_g/\partial t = -10^{-4}$ and $T_g/T_a = 1.0 = \text{const}$. Then

$$\frac{\partial m_G}{\partial t} = \frac{\partial m_G}{\partial m_g} \frac{\partial m_g}{\partial t} = -6.24 \times 10^{-4} \text{ kg/sec} = -2.25 \text{ kg/hr}$$

As a final example, starting with the initial conditions represented by point 1 and assuming that the balloon is leaking at a rate of 10 kg/hr

while the gas temperature is warming at a rate of 12.5°K/hr and the air temperature is remaining constant, what must the ballast rate be to maintain float? In an hour the mass of the gas will be 102 kg; the value of T_g/T_a will be 1.05. Using these, point 4 may be plotted. At point 4, m_G is 675 kg; therefore, during the hour ballast must have been dropped at the rate of 25 kg/hr to maintain float. Within the accuracy of the chart the same result may be obtained by using the rates of change in the total derivative as follows:

$$\frac{dm_G}{dt} = \frac{\partial m_G}{\partial m_g} \frac{dm_g}{dt} + \frac{\partial m_G}{\partial (\tau^{-1})} \frac{d(\tau^{-1})}{dt}$$

$$\frac{dm_G}{dt} = 6.4 \times (-10) + 770 \times 0.05 = -25.5 \text{ kg/hr}$$

The values of $\partial m_G / \partial m_g$ and $\partial m_G / \partial (\tau^{-1})$ must be mean values for the process through which the balloon system is going as its state changes from that of point 1 to that of point 4. They are identified by arrows and the notation (1-4) along the $\partial m_G / \partial m_g$ scale at the top of the chart and on the $\partial m_G / \partial (\tau^{-1})$ reference line.

5. Excursions from Float and Valved Descent

A balloon system may depart from its theoretical float altitude for a

number of reasons. If a flight is to be terminated by bringing the balloon system down intact, gas may be valved from the balloon. Also, unplanned departures from the theoretical float altitude may occur because of a leak which decreases f' without producing compensatory decreases of τ or because of warming or cooling of the gas relative to the air, which changes τ but leaves f' unchanged. Large excursions from the theoretical float altitude are always downward, and it is these which are the principal topic of discussion in the remainder of this section.

Balloon system descent, either planned or unplanned, can be controlled if f' can be controlled through the necessary range. In general, the discussion of I.2 of this section is applicable. Ballast can be dropped to increase f' , and gas can be valved to decrease it. The rate at which ballast or gas should be released is a complicated function of the desired rate of descent, the atmospheric lapse rate, the radiation environment of the balloon, the absorptivity and emissivity of the balloon, and a host of other things. The most important of these can be considered quantitatively in a numerical model (see Section III). It is possible, however, to gain a qualitative understanding of many of the reactions of a balloon system to the en-

vironment and to controls by studying them in reference to the equilibrium value of τ , called τ_e here.

The equilibrium value of τ is defined as that value which τ would ultimately reach in a balloon system floating stably for a long enough period to enable it to come into thermal equilibrium with its environment. Thus, it is the ratio of the thermal equilibrium temperature of the ambient air to the thermal equilibrium temperature of the gas in a balloon, and it is determined by the thermal characteristics of the balloon and its gas as well as by the environment (6, 7). Typical day and night curves of τ_e as a function of altitude for a helium-filled, polyethylene balloon in the middle latitude, summer atmosphere are shown in Fig. 12. Although τ_e is a function of many variables, the gross shape of the τ_e vs altitude curves may be explained by a greatly simplified model of the balloon-environment system.

The equilibrium temperature of a stably floating balloon is controlled essentially by convective heat exchange between the balloon and the ambient air and by radiative exchange between the balloon and its environment. The radiation environment of a balloon floating in the stratosphere at night consists of the relatively warm earth and atmosphere on one side and cold

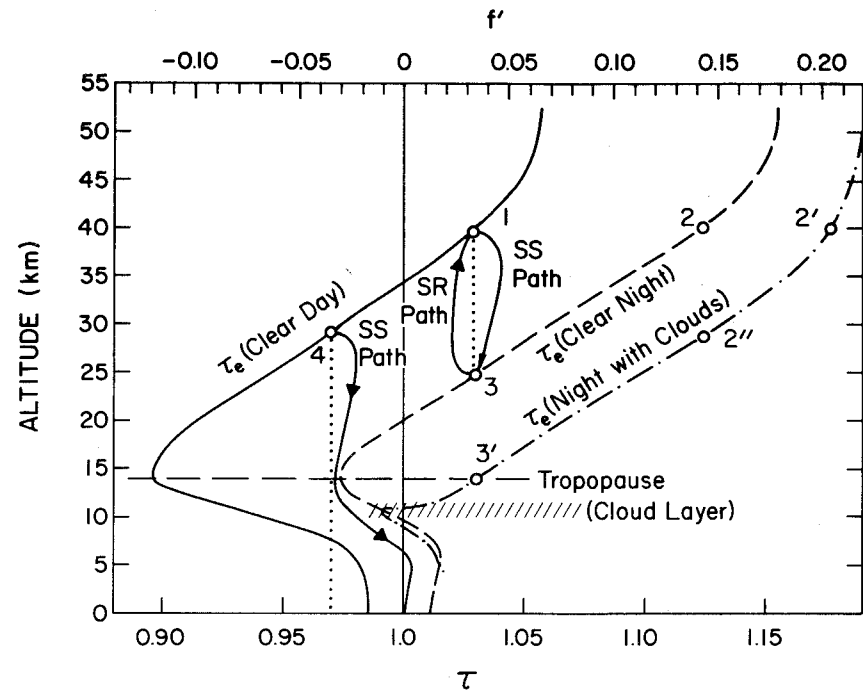


Fig. 12. Diurnal excursions of a gas-tight, helium-inflated, polyethylene balloon in a typical summer, mid-latitude, continental atmosphere.

space on the other. Convective exchange between the balloon and the air is normally small because of the low density of the air, but it can be significant if the air and balloon temperatures differ greatly. The temperature which the balloon gas would assume if it could come into thermal equilibrium with its radiation environment alone is colder than the air temperature in the stratosphere. Therefore, the actual equilibrium temperature of the lift gas will be below the air temperature, and τ_e will be greater than one.

A balloon in the lower troposphere will have a warmer radiation environment than a balloon in the stratosphere principally because it will be embedded in warmer air which is richer in water vapor and so can radiate well in certain bands of the infrared. Convective heat exchange will also be more important in the denser, tropospheric air. Even near the earth's surface at night, however, the radiation equilibrium temperature will be lower than air temperature in most instances, and the value of τ_e will be greater than one.

In the vicinity of the tropopause, a balloon will feel the influence of cold space slightly less and the warm earth and lower tropospheric air slightly more than in the high stratosphere. Consequently, the radiation equilibrium temperature of the gas in the balloon will be greater than at

higher levels, though not as large as near the earth's surface. Air temperature at the tropopause is lower than in either the stratosphere or the troposphere, and it is not unusual even at night for the radiation equilibrium temperature of a balloon to exceed the air temperature. When it does, equilibrium temperature of the balloon gas will be greater than air temperature and τ_e will be less than one.

During the day when the sun is shining, a balloon at any level will receive heat from the sun; hence its radiation equilibrium temperature will be greater than it would be under otherwise comparable conditions at night. The air may also be warmed by the sun, but air is much more transparent to the sun's radiation than a balloon and does not warm nearly as much as the balloon gas. Thus, the τ_e curve for daytime is shifted toward lower values of τ_e but retains much the same shape as the nighttime curve. During the sunrise and sunset periods, τ_e undergoes a marked change at all levels. A much slower change must occur throughout both the day and night periods with the minimum value at each level being reached sometime after noon and the maximum value occurring after midnight. Except for the changes brought about by clouds, however, it will be assumed here that all changes in τ_e occur in a

period of a few hours near sunrise and sunset.

A cloud layer in the atmosphere will change τ_e at all levels, but the most marked change will occur above a cloud which is much colder than the earth. The value of τ_e above a cloud will be greater with the cloud than without it, and the change will be greater at night than in daytime. Below a cloud at night τ_e will have a slightly lower value than if the cloud were not present. A cirrus cloud layer which is so thin that it cannot be seen at night can produce a drastic change in τ_e above the layer. This change, which is illustrated by the difference in the τ_e curves in Fig. 12 for a clear night and a night with clouds, can occur rapidly.

From the definition of τ_e it is apparent that if τ for a balloon in flight differs from τ_e for any reason, the heat exchange between the balloon and its environment will be in the direction which will move τ toward τ_e . Warming or cooling due to pressure changes during ascent or descent may prevent τ from reaching τ_e , however.

An f' scale has been plotted across the top of the chart. This scale has been arranged so that for any point on the chart $f' = \sigma(1 - \tau)/(\tau - \sigma)$. Since this is the condition relating f' and τ when the sum of the gravitational

and buoyant forces is zero, both the f' and τ values of a stably floating balloon system can be represented by a single point on the chart. If the f' and τ values for a balloon system do not plot as a single point on the chart, the balloon system will have a non-zero free lift. That free lift will be upward (+) if the τ, H point lies to the left of the f', H point and downward (-) if the τ, H point lies to the right of the f', H point. Further, its magnitude will vary as the distance between the two points.

An excursion from a stable float level must be expected each evening as the sunset effect increases τ_e unless compensatory ballast is dropped. For example, a balloon floating stably during the day at 45 km can be represented by point 1 in Fig. 12. At that point τ_e is 1.029 and f' is +0.033. As the sun approaches the horizon at sunset, the τ_e curve will start to migrate to the right, and as it does, τ for the balloon will increase. If ballast is dropped at precisely the right rate during the sunset transition, the points representing both the τ, H and f', H status of the balloon system can be made to move horizontally together from point 1 to point 2 on Fig. 12. Since at point 2, $f' = +0.145$, enough ballast must have been dropped to change f' from 0.033 to 0.145; any less ballast will not let the balloon reach its nighttime

value of τ_e without losing altitude. The following morning as sunrise causes the τ_e curve to migrate back toward its day value, the τ, H point representing the balloon will move leftward also, lagging the τ_e curve slightly. As the gas warms, it will be expelled through the ducts, thereby automatically causing the f', H point to move coincidentally with the τ, H point. The balloon system will be less massive than it was the previous day due to the loss of ballast and gas; consequently, it will climb slowly as it warms and occupy a slightly higher position on the day τ_e curve than it had occupied the previous day.

If no ballast is dropped at sunset, the τ, H point representing the balloon will move toward the right in an effort to follow the τ_e curve as it migrates. As soon as τ changes, however, without a compensating change of f' , the balance of hydrostatic and gravitational forces will be disturbed and the balloon will start descending. Descent will be accompanied by an increase in pressure and warming of the gas, which will tend to move τ to the left on the chart. The point representing the τ, H state of the balloon cannot cross the vertical dotted line below point 1, however, because if it did so the combination of τ and f' would cause an upward resultant force on the balloon

system. This would stop the downward motion until the gas could cool enough to initiate it again. The nighttime τ_e curve and the f', H curve of the balloon then serve as boundaries which the τ, H point, moving along its sunset (SS) path, cannot cross. Ultimately, the τ, H point of the balloon will reach point 3 and since it cannot cross the τ_e and f', H curves, the balloon will have again reached a stable float condition, where it will remain until sunrise causes the τ_e curve to start migrating leftward. The balloon will then rise and the τ, H point will follow the sunrise (SR) path back to point 1. The maximum nighttime excursion, if no ballast is used and no gas is lost, is just the vertical distance between the day and night τ_e curves.

A balloon floating stably at point 4 during the day would have a lower f' value than the lowest possible f' value of any point on the night τ_e curve. Therefore, the τ, H curve of such a balloon descending at sunset might reach all the way to the surface, as shown by the trace marked SS path below point 4, without encountering an intersection of the nighttime τ_e and the balloon's f', H curves. Only if the balloon were to descend so slowly during the sunset and night that it were caught by the τ_e curve as that curve migrates leftward at sunrise would it not descend all the way to the surface. Any balloon

floating lower during the day than the level represented by point 4 should be expected to descend to the surface at night under conditions such as those depicted by Fig. 12.

The τ_e curve for a cloudy night can be used in conjunction with the other τ_e curves to illustrate the effect of a cold cloud layer. Assume that a balloon at point 1 has been maintained at 40 km through sunset by ballasting and is floating stably at night at point 2 when a cloud layer forms under it. More ballast, dropped at the right rate, will force it to maintain its altitude and move its τ, H point to point 2'. If no additional ballast is dropped, the balloon will descend and its τ, H point will move to point 2''. In either event, sunrise the following day will cause it to move back to a point slightly above point 1 on the clear day τ_e curve if the cloud layer has disappeared or to an equivalent point on a cloudy day τ_e curve (not shown).

If a balloon is floating stably at point 3 at night when a cloud layer forms under it, it will immediately start moving downward, its τ, H point moving along a path similar to that followed from point 1 to point 3 at sunset. Unless ballast is dropped, the balloon will descend to the level marked 3' and float there until further adjustment of the τ_e curve occurs. If the

cloud remains unchanged, no adjustment will occur before sunrise the following day, but if the cloud should disappear before sunrise, the τ_e curve will lift up to the clear night τ_e curve and the balloon will rise toward level 3 again. Thus, it is quite conceivable that with variable cloudiness, a balloon may descend and ascend through short distances several times during a day or night period.

Another possible effect of a cold cloud layer is to open wider the "trap door" through which the balloon may descend all the way to earth at night. In Fig. 12, for example, any balloon floating stably on a clear day below an altitude of 30 km would have a good chance of descending all the way to earth on the following clear night. If a cloud should appear at night as shown in the figure, any balloon floating during the day below 33 km could conceivably descend all the way to earth.

It is often not necessary to maintain an unvarying float level throughout a flight; yet the magnitude of the excursions which would occur from day to night without ballast may be too large to be tolerated. In a situation like that depicted by Fig. 12, any ballasting which results in an increase in f' will decrease the magnitude of the excursion. A balloon at point 1 prior

to sunset can, for example, be ballasted at such a rate that it will maintain level float until f' reaches +0.10. If ballasting is then stopped, the balloon system will start descending, but it can descend only to the point where the night τ_e curve crosses the $f' = +0.10$ line. Since that occurs at about 34 km, the nighttime excursion will be 6 km instead of the 15 km which would occur without any ballasting. It does not matter when the ballast is dropped as long as the drop occurs far enough about the 34 km level to enable the balloon system to stop there and provided that the drop does not occur so early that it forces the balloon above its fully-inflated float level and causes it to vent gas. If gas is vented, f' will be decreased by the gas loss and the ballast will not have been fully effective. It is also pertinent to note that at the following sunrise, a balloon from which ballast has been dropped at night to limit its excursion will vent gas. Then the excursion the following night will again be the vertical distance between the day and night τ_e curves unless additional ballast is dropped to limit it.

Figure 13 is a τ, H diagram showing the same clear day and night τ_e curves as Fig. 12. The dotted line segment leading from point 1 to point 2 represents the path followed by the f', H point of a slowly leaking balloon.

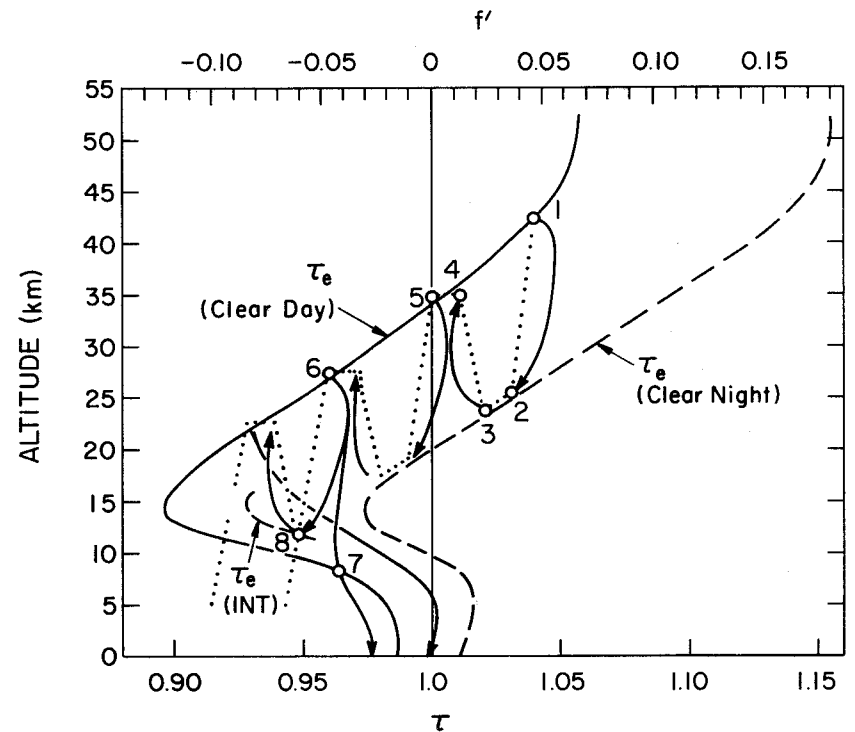


Fig. 13. Diurnal excursions of a slowly leaking, helium-inflated, polyethylene balloon in a typical summer, mid-latitude, continental atmosphere.

The τ, H point of the balloon will follow the solid curve from point 1 to point 2. Both curves are approximate; the important thing to bear in mind is that the f', H curve should show a decreasing value of f' and that during descent the τ, H curve should be to the right of the f', H curve. This assures negative buoyancy, which is essential to continued downward motion.

When the balloon reaches point 2, downward motion would cease if there were no leak. Because there is a leak, the downward motion must continue and the compressive heating will cause τ to be slightly lower than τ_e . Thus, the balloon will continue to descend along characteristic f', H and τ, H curves which are nearly identical and a little to the left of the night τ_e curve on the graph. As sunrise starts to influence the balloon at point 3, it will rise, eventually reaching its highest level at point 4, a point near the day τ_e curve. Because of the leak it will then start to descend, warming because of the increase in pressure so that its τ, H curve will cross the day τ_e curve. As the f', H and τ, H curves reach point 5, the effects of sunset overtake the balloon and start it on a second descent.

If the diurnal cycle of τ_e does not change at any level while the leaking balloon is flying, the balloon will descend further each night than it will

ascend on the following day. Its τ, H and f', H paths will progress leftward and downward on the chart in a series of up and down motions until one night the balloon's f', H curve will not intersect the τ_e curve during descent and the balloon will descend all the way to the surface. In Fig. 13, two possibilities are shown. One possibility is that after the balloon leaves point 6 it will descend past the day position of the τ_e curve at point 7 before the following sunrise can influence it. If it does, it will descend to the surface, even though it may not reach ground until well after sunrise. The second possibility is that sunrise will influence the balloon in its descent from point 6 before it has reached the position of the day τ_e curve. If the τ_e curve as it is migrating leftward at sunrise catches the balloon as shown by the τ_e (int) curve segment at point 8, the balloon will go through another ascent before it starts its final descent.

In the example of a leaking balloon discussed above, it was assumed that the leak was slow and continuous. A larger leak would have permitted the balloon to undergo fewer diurnal oscillations before bringing it to the surface. A leak large enough to decrease f' faster than compensatory changes in τ can be produced by sunrise will prevent the balloon from ascending, though

the descent rate will vary from day to night. Gas may leak or be valved rapidly enough to produce descent in a few hours. Figures 14 and 15 show the approximate form of some possible valved descent curves.

The A and A' curves of Fig. 14 are the f',H and τ,H curves respectively of a balloon which has descended to the surface during the daytime from level 1, where it was floating stably. The A curve shows that gas was valved rapidly for a short time to initiate descent and then subsequently left unchanged. Initially, since the vertical velocity of the balloon was zero, the loss of lift caused rapid downward acceleration. As the balloon moved downward, the increasing pressure warmed the gas above its equilibrium temperature, causing the balloon's τ,H curve to shift away from the τ_e curve toward lower values of τ . Also, as the downward velocity increased, aerodynamic drag built up. As descent continued above level 2, the τ,H curve moved closer to the f',H curve and downward velocity decreased until at level 2 the balloon was barely descending. Only a little less gas loss due to valving would have caused the balloon to reach a state of stable, level flight just above level 2. As the balloon descended below level 2, however, it entered an environment in which the value of τ_e increased rapidly as height decreased. Its own τ adjusted

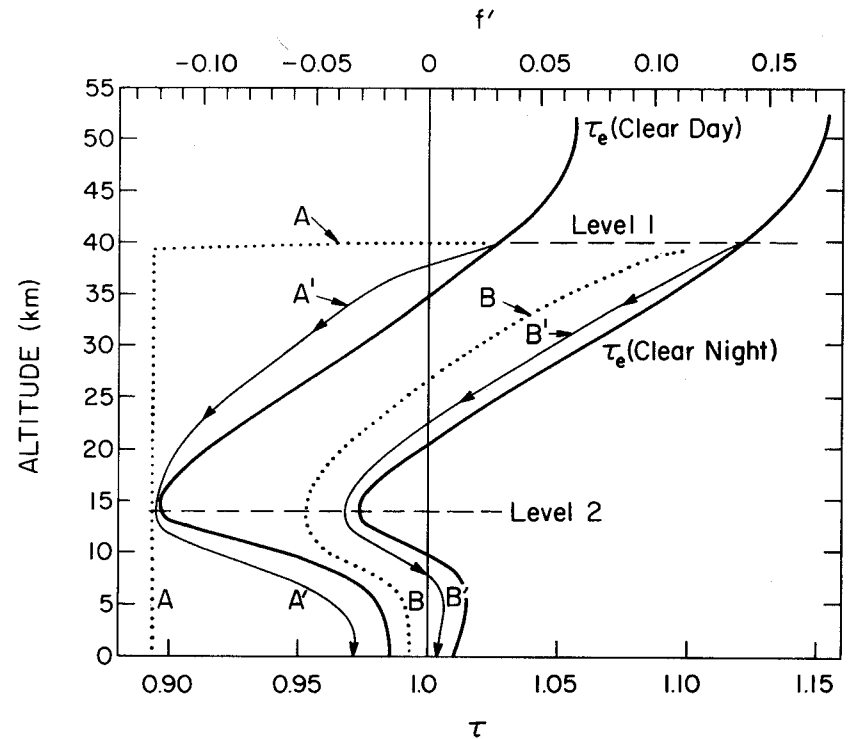


Fig. 14. Valved descent of a helium-inflated polyethylene balloon in a typical summer, mid-latitude, continental atmosphere.

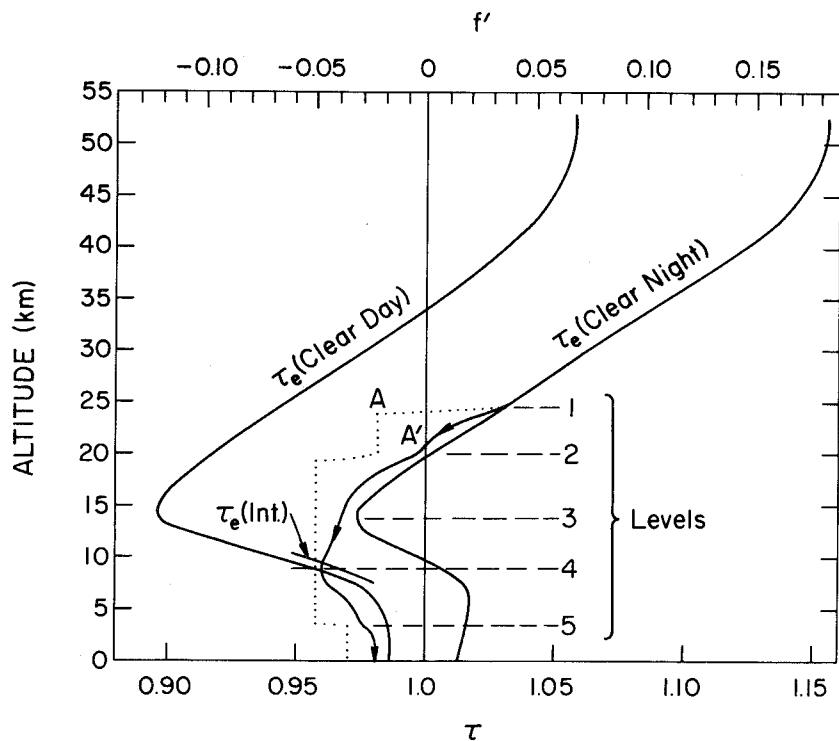


Fig. 15. Stepwise valved descent of a helium-inflated, polyethylene balloon in a typical summer, mid-latitude, continental atmosphere.

upward in response to the higher τ_e , and as its f',H and τ,H curves moved apart it accelerated downward again, reaching a high but nearly constant speed just a little way above the surface.

A nighttime descent is shown by the B and B' curves in Fig. 14. In this case continuous control was exercised during descent. As shown by the curves, gas was valved at a rate which kept the B and B' curves separated by a nearly constant distance down to level 2, and ballast was dropped at the proper rate to maintain the constant separation below level 2. This resulted in an approximately constant descent rate, and because of the constant descent, the displacement of the B' curve from the night τ_e curve was also approximately constant.

The simple broad brush treatment of a day and night descent given in the last two paragraphs is not meant to imply that one valving technique is a daytime technique while the other is a nighttime technique. Either can be applied at any time, in principle, but in practice neither is used. In one, only initial valving is used; in the other, either valving or ballasting is being used continuously. Practical limitations in a real flight, including limited knowledge about how a balloon system will react to a change in f' ,

prompts most flight directors to valve or ballast in what amounts to small increments. In Fig. 15 and the next paragraphs, steps are outlined by which a more complicated descent may be accomplished using stepwise valving or ballasting. The purpose is to illustrate the behavior of a balloon system in a relatively complex situation, without getting caught up in attempts to answer quantitative questions of timing, etc.; therefore, the treatment is again highly simplified.

The problem is to bring a balloon system which is floating stably at level 1 at night to the surface intact using a minimum of ballast. Gas is valved rapidly for a short time to start the descent from level 1 as shown by the f',H trace, curve A. As the downward speed increases the τ,H trace of the balloon, curve A' , separates from the night τ_e curve, but as the τ,H trace approaches the first constant portion of the f',H trace, vertical velocity slows and the τ,H curve swings back toward the τ_e curve. At level 2, gas is valved again in a short burst causing the τ,H curve to increase its distance from the τ_e curve again.

The valving which was done at level 2 was enough to cause the balloon to descend past level 3, and indeed all the way to the surface if it does not get

caught by the migrating τ_e curve at sunrise. Thus the minimum gas which must be ejected is that will cause the τ,H curve to cross the daytime position of the τ_e curve just short of the intersection of that curve with the f',H curve just before the τ_e curve reaches that position. A short section of an interim τ_e curve as it is approaching the day position of the τ_e curve is shown as $\tau_e(\text{int})$ in Fig. 15. Incidentally, the τ,H point representative of the balloon will stay ahead of the migrating τ_e curve as long as the balloon is descending and the atmospheric lapse rate is less than the adiabatic lapse rate of the gas in the atmosphere. Thus, the τ,H point as it traces out curve A' from level 3 to level 4 does not move away from the τ_e curve; it actually moves nearer the interim τ_e curve as it approaches the f',H curve. If the τ,H point should intercept the f',H curve as it moves leftward and downward ahead of the migrating τ_e curve, the balloon's downward motion will stop; it will be overtaken by the τ_e curve and, unless additional gas is valved, it will start ascending again.

Once the balloon system has descended below the day position of the τ_e curve, it will gain speed as it descends, if left to its own devices, until it reaches approximately the 3 km level. From there down the speed will be

nearly constant. If that speed is too great for a proper landing, ballast can be dropped as shown at level 5 to slow the descent. The key to making a descent such as this with minimum ballast is to have the balloon system penetrate the position of the day τ_e curve position with near zero speed just before the τ_e curve reaches that position.

REFERENCES

- (1) Streeter, V. L., 1961: Handbook of Fluid Dynamics, McGraw-Hill, New York, Sections 4 and 13.
- (2) Hoerner, S. F., 1965: Fluid-Dynamic Drag, published by author, 148 Busteed Drive, Midland Park, N. J. 07432.
- (3) Sherburne, Paul A., 1968: Wind Tunnel Tests of a Natural Shape Balloon Model, AD 667563, Goodyear Aerospace Corp.
- (4) Peters, Penn A., Shojiro Shindo, Hilton H. Lysons, 1972: personal communication with Mr. Peters. Forest Engineering Research, U.S. Forest Service, Seattle.
- (5) Anonymous, 1961: Handbook of Geophysics, Rev. Ed., The MacMillan Co., New York, 5-41.
- (6) Staff, Dept. of Physics, Univ. of Minnesota, 1953: Progress Report on High Altitude Balloons, Vol. IX, Office of Naval Research Contract NONR-710(01).
- (7) Gergen, John L., 1957: Atmospheric Infrared Radiation over Minneapolis to 30 Millibars, Journal of Meteorology, Vol. 14, December 1957, 495-504.

SECTION III

LIST OF SYMBOLS

ENERGY BALANCE AND A FLIGHT MODEL

by

Frank Kreith

List of Symbols ii

List of Figures vii

List of Tables viii

A. INTRODUCTION 1

B. THE ENERGY EQUATIONS 2

C. CONVECTION BETWEEN THE ATMOSPHERE AND THE BALLOON SYSTEM 7

D. CONVECTION INSIDE THE BALLOON 22

E. RADIATION HEAT TRANSFER 27

F. EMITTED RADIATION 38

G. DIRECT SOLAR RADIATION 42

H. REFLECTED SOLAR RADIATION 51

I. INFRARED RADIATION FROM THE EARTH AND THE ATMOSPHERE. 68

J. GAS EXPANSION AND LIFT AND LOAD ADJUSTMENTS 88

K. A VERTICAL MOTION MODEL 89

L. EXPERIMENTAL RESULTS 95

REFERENCES. 101

<u>Symbol</u>	<u>Description</u>	<u>Dimensions</u>
a	absorptance	
a	subscript identifying its symbol with air or atmosphere	
a _z	the angle measured from the south meridian of the projection on the earth's surface of the normal to a tilted surface	deg
A	area	L ²
A _z	azimuth of the sun from the south meridian	deg
b	film thickness	L
b	subscript identifying its symbol with ballast	
B	subscript identifying its symbol with the balloon	
c	subscript identifying its symbol with convection	
c _f	specific heat of film	L ² T ⁻² σ ⁻¹
c _v	specific heat at constant volume	L ² T ⁻² σ ⁻¹
C _D	drag coefficient	
C _M	virtual displacement coefficient	
d	subscript identifying its symbol with ducting	
D	diameter, used as a primary symbol and as a subscript	L
e	emittance	
e	subscript identifying its symbol with earth	
\dot{E}_d	volumetric gas flow rate through the ducts	L ³ T ⁻¹
\dot{E}_v	volumetric gas flow rate through valves	L ³ T ⁻¹

f	subscript identifying its symbol with the balloon film or fabric		L	length dimension	L
f'	fractional, nominal free lift		L'	lapse rate (-dT/dz) of a stratum in the atmosphere	ΘL^{-1}
F	force	MLT^{-2}	L_F	free lift	MLT^{-2}
F	subscript identifying its symbol with free lift		L_G	gross lift	MLT^{-2}
g	acceleration due to gravity	LT^{-2}	m	mass	M
g	subscript identifying its symbol with the lift gas		m	optical air mass; also used as a subscript	
G	radiation incident on a unit surface in unit time (W/m^2)	MT^{-3}	M	molecular weight	$M(M\text{-mol})^{-1}$
G	subscript identifying its symbol with gross lift		o	subscript identifying its symbol with a base state, e.g., z_o is zero height	
G_s	solar constant ($1395 W/m^2$)	MT^{-3}	p_a	pressure of ambient air	$ML^{-1}T^{-2}$
GHA	Greenwich hour angle	deg	p_g	pressure of lift gas	$ML^{-1}T^{-2}$
h	local hour angle	deg	\dot{p}	power dissipation	ML^2T^{-4}
h_c	heat transfer coefficient	$MT^{-3}\Theta^{-1}$	q	rate of heat transfer	ML^2T^{-3}
i	the plane angle which measures the dihedral angle between a tilted plane and a horizontal plane	deg	r	radial distance	L
i	subscript identifying its symbol with infrared		r	reflectance	
I	intensity of radiation ($W/steradian$)	ML^2T^{-3}	R	universal gas constant ($8314.32 J/Kg\text{-mol}^\circ K$ or $1.9859 BTU/lb\text{-mol}^\circ R$)	$L^2T^{-2}\Theta^{-1}$
J	joule	ML^2T^{-2}	s	subscript identifying its symbol with the sun	
k_a	thermal conductivity of air	$MLT^{-3}\Theta^{-1}$	S	surface area	L^2
k_g	thermal conductivity of lift gas	$MLT^{-3}\Theta^{-1}$	t	time	T
l	length dimension	L	t	thickness of cloud; also used as a subscript to indicate that its symbol is a function of thickness	L
l	subscript identifying its symbol with the payload		T	temperature	Θ
l'	equivalent length dimension selected by B6rner to correlate free convection for several shapes with one equation; also used as a subscript	L	v	subscript identifying its symbol with a valve or valving	

v	specific volume	$L^3 M^{-1}$	ϕ	angle between the normal to a tilted surface and the bearing of the sun	deg
V	volume	L^3			
V_a	volume of air	L^3	ϕ_1	longitude	deg
V_g	volume of gas	L^3	ψ	azimuth angle (see Fig. 9)	deg
x	ratio of a horizontal and vertical distance (Fig. 8)				
y	see x above				
z	altitude (frequently given as a geopotential height)	L			
z	subscript identifying its symbol with height				

Greek letters

α	absorptance				
β	temperature coefficient of volume expansion [$1/T(^{\circ}K)$] for an ideal gas	σ^{-1}			
δ_s	solar declination				deg
ζ	zenith angle of the sun				deg
θ	polar angle (see Fig. 9)				deg
λ	wave length of radiation	L			
λ_1	latitude				deg
μ	micron (standard abbreviation for $10^{-6}m$)	L			
ρ	mass density	ML^{-3}			
ρ	bidirectional reflectance				
σ	Stefan-Boltzman constant	$MT^{-3}\sigma^{-4}$			
σ_s	solar declination				deg
τ	transmittance				
τ	angle between a tilted surface and the horizontal				deg

List of Figures

Fig. 1	Schematic illustrating energy balance for lifting gas and balloon skin	3
Fig. 2	Average Nusselt number for sphere in combined free and forced convective flow	17
Fig. 3	Temperature field about a heated horizontal flat plate at a Rayleigh number of 50	21
Fig. 4	Emission of radiation from a balloon skin--the effective emittance.	40
Fig. 5	Spectral distribution of solar radiation in space and at sea level.	44
Fig. 6	Spectral distribution of solar radiation incident at sea level for air masses 1.0 to 8.0	47
Fig. 7	Albedo as a function of latitude under various sky conditions	55
Fig. 8	Shape factor for a small sphere and rectangular area	60
Fig. 9	Satellite- or balloon-to-earth geometric configuration.	64
Fig. 10	Variation of directional solar reflectance with zenith angle ($60^\circ < \zeta \leq 80^\circ$).	66
Fig. 11	Albedo map for the Northern Hemisphere during the period 16-28 July 1966.	67
Fig. 12	Variation of directional hemispherical reflectance with zenith angle.	69
Fig. 13	Infrared radiation map for the Northern Hemisphere during the period 16-28 July 1966. Multiply radiation values by 697.35 to obtain radiation in W/m^2	71

Fig. 14	Upward and downward radiation flux as a function of altitude	74
Fig. 15	Suomi-Kuhn flat plate radiometer	78
Fig. 16	Radiation environment at Green Bay, Wisconsin, in the summer	80
Fig. 17	Radiation environment at Green Bay, Wisconsin, in the winter. To obtain W/m^2 multiply $\lambda y/min$ by 697.35.	81
Fig. 18	Radiation environment at a desert island, $2^\circ S$	82
Fig. 19	Gergen "Black-Ball" radiometer	85
Fig. 20	Experimental results of balloon flight, October 1966; comparison of predicted and measured gas temperatures.	98

List of Tables

Table 1	Equivalent length dimensions of convection correlation	14
Table 2	Average Nusselt numbers for a horizontal plate in free convection	19
Table 3	Constants for the free convection equation (Eq. 14).	23
Table 4	Free convection in a sphere.	25
Table 5	Radiation characteristics of surfaces.	36
Table 6	Energy storage capabilities of water and batteries	37
Table 7	Relative spectral distribution of solar radiation under various sky conditions	56
Table 8	Mean values of thickness, reflectance, and absorptance as well as constants b_1 and b_2 for various cloud types.	62
Table 9	Radiation environment for superpressure balloons	77

ENERGY BALANCE AND A FLIGHT MODEL

A. INTRODUCTION

The vertical motion of balloon systems depends critically on the heat transfer to and from the gas inside, because the temperature and the pressure of the gas determine the lift of the balloon. In the past the thermal design of high altitude balloons has largely been based on a combination of experience, empirical data, and approximate calculations (1, 2). Recent advances in heat transfer research make it feasible, however, to calculate the temperature of the lifting gas as a function of altitude and to predict the vertical motion of the balloon system with the aid of high speed computers (3, 4).

There are three general problem areas in which thermal design can improve balloon operation. The first involves rapid variations in internal energy, which occur when clouds cause sudden changes in the radiation incident on the balloon. This type of change in the heat transfer rate is usually sensed only after the altimeter registers a change. After an altitude change is registered, altitude is maintained by dropping ballast or

exhausting gas. If one could control altitude by reacting rapidly and precisely to a change in radiation, the loss of ballast or gas could be reduced. The second area of thermal design is concerned with changes in heat loss during a complete day. More accurate predictions of heat loss and the use of appropriate materials or surface coatings could increase the payload or the float altitude for a given balloon system. The third area of thermal design involves long-range planning for balloon flights, such as those currently envisioned in the equatorial zone over new routes.

This section reviews recent advances in heat transfer experimentation and theory pertinent to the processes which affect the calculation of balloon performance and the thermal design of balloon instrument packages. Finally, the pertinent equations of fluid mechanics, heat transfer, and thermodynamics are combined to predict analytically the vertical motion of balloons.

B. THE ENERGY EQUATIONS

The conservation equation for the gas inside the skin of a balloon can be obtained by applying the First Law of Thermodynamics (Fig. 1). The rate of change of the internal energy of the gas equals the rate at which heat is

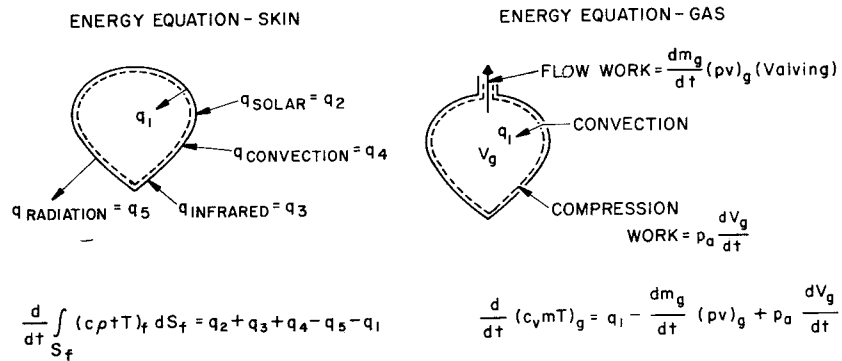


Fig. 1. Schematic illustrating energy balance for lifting gas and balloon

skin.

transferred to the gas (q_1) minus both the rate at which net work is done

by the gas and the rate at which internal energy is lost by valving.

Assuming that the equation of state of the gas can be approximated by the ideal gas law and that the temperature and pressure of the gas inside the balloon are uniform, one obtains

$$\frac{d}{dt} (c_v m T)_g = q_1 + \frac{RT_g}{M_g} \frac{dm_g}{dt} - p_a \frac{dV_g}{dt} + (c_v T)_g \frac{dm_g}{dt} \quad (1)$$

where the term on the left-hand side of Eq. (1) is the rate of change in internal energy of the balloon gas; the first term on the right-hand represents the rate of heat transfer by free convection from the interior surface of the balloon skin to the gas; the second term, the flow work done during gas release; the third term, the work done on the external pressure when the balloon volume changes because of a change in gas temperature or because of valving; and the last term the loss of internal energy by valving. If the pressure inside the balloon is uniform and equal to the atmospheric pressure, the flow work done during valving in the absence of heat transfer equals the work done by the atmosphere on the balloon, and the second and third terms cancel.

The assumption that the temperature of the gas inside the balloon is uniform may lead to serious error when short-term transients occur, and the gas adjacent to the balloon skin undergoes temperature variations while the gas in the interior does not. When this situation prevails, the term on the left-hand side of the energy equation should be replaced by

$$\frac{d}{dt} \iiint_V C_{vg} \rho_g T_g dv_g$$

A similar analysis can be performed on the balloon skin. The internal energy of the skin will change only because of heat transfer to and from its surfaces. The skin is so thin that one can neglect the temperature drop across it at any location, but since the heat transfer over the skin is not uniform, its temperature will vary. This variation cannot, however, be expressed analytically, and when it becomes important, only a numerical analysis can yield a satisfactory approximation of the physical reality.

To simplify the thermodynamic analysis, it will be assumed that an averaged skin temperature can be used. A First Law analysis (Fig. 1) then gives

$$\frac{d}{dt} \iint_{S_f} C_f \rho_f t_f T_f dS_f = C_f m_f \frac{d\bar{T}_f}{dt} = q_2 + q_3 + q_4 - q_5 - q_1 \quad (2)$$

where C_f is specific heat of skin, m_f is mass of skin, \bar{T}_f is average skin temperature, ρ_f is density of the balloon skin, q_2 is rate of absorption of solar radiation = ($q_{2, \text{direct}}$ + $q_{2, \text{reflected}}$), q_3 is rate of absorption of infrared radiation, q_4 is rate of heat transfer by convection from the atmosphere to the skin, q_5 is rate of radiant heat transfer from the skin, t_f is thickness of film, S_f is surface area of balloon, and q_1 is rate of heat transfer by convection from the skin to the lift gas.

The energy equations for the balloon gas and the skin fabric can be treated analytically if one assumes that all of the gas is at one temperature and the entire skin is at one temperature (these two temperatures may or may not be identical). This assumption is quite good at night, but can introduce appreciable errors during the day when solar energy heats the skin unevenly. Modifications for non-uniform heating could be made in the analysis (5) for the exterior of the fabric skin by numerical means, but the convection process inside a non-uniformly heated, balloon-shaped container is very complex. At this time the process is not well enough understood to be modeled analytically; thus, an accurate calculation of the heat transfer in the interior is not possible. Fortunately, during normal flight, balloons

rotate so all parts of their skins are exposed equally (on the average) to the sun and the balloon gas is mixed. This makes the assumption of uniform gas and skin temperatures valid for thermal analyses performed for times ranging from hours to days.

In the following three sub-sections, the heat transfer phenomena in balloon systems will be examined in the light of recent advances in heat transfer research. Sub-sections C and D will deal with convection and Sub-section E with radiation phenomena. The final objective will be the evaluation of the five heat transfer terms in Eq. (2).

C. CONVECTION BETWEEN THE ATMOSPHERE AND THE BALLOON SYSTEM [q_4 in Eq. (2)]

Convective heat transfer between balloon systems and the atmosphere occurs over wide ranges of the convectional parameters used to describe the process. Heat is transferred between the atmosphere and the balloon by forced convection or free convection, or both, at Reynolds numbers from 0 to 10^7 and Grashof numbers from 0 to 10^{11} . Depending on the circumstances, the flow can be laminar or turbulent. The shapes of superpressure balloons resemble a sphere, those of zero-pressure balloons resemble an onion, but instrument packages come in a variety of shapes, such as cubes,

cylinders, and plates. Balloon diameters may range from one to 100 m (3 to 330 ft), ascent velocities from near zero to 12 m/sec (0 to 40 ft/sec), and temperature differences (between the skin and gas) from zero to $30C^{\circ}$ (0 to $55F^{\circ}$).

Although convective heat transfer to and from an object in air has been studied extensively, few investigations extend into the extreme Reynolds- and Grashof-number ranges encountered by balloons and none have specifically treated the onion shape typical of zero-pressure balloons. Therefore, approximations and extrapolations of existing data are unavoidable.

Heat transfer from spherical shapes in forced convection has recently been investigated experimentally by Yuge (6) and Vliet and Leppert (7). Local values of the heat transfer coefficient in flow over a sphere in the neighborhood of the stagnation point have been calculated by Merk (8). The pressure distribution for flow over spheres has been investigated by Fage(9), who also measured the separation point. He found that at a Reynolds number of 1.6×10^6 , separation occurred at a polar angle ϕ of 70° and moved toward the rear with increasing Reynolds number. At the highest Reynolds number of his tests, $Re_D = 4.2 \times 10^6$, separation occurred at a polar angle

of 100° . The subscript D indicates that the diameter of the sphere was used in calculating the Reynolds number.

Extensive correlations of experimental data indicate that in forced convection the average Nusselt number, Nu, of the entire surface of a sphere of diameter D in air can be obtained from the relation

$$\text{Nu}_{D,m} = \frac{\bar{h}_c D}{k_a} = 2 + 0.30 \text{Re}_{D,m}^{0.57} \quad (3)$$

for Reynolds numbers between 1.8×10^3 and 1.4×10^5 (6) or from the relation

$$\text{Nu}_{D,m} = \frac{\bar{h}_c D}{k_a} = 2 + 0.41 \text{Re}_{D,m}^{0.55} \quad (4)$$

for Reynolds numbers between 0.4 and 2×10^5 (7). In both of the above equations, the subscript m indicates that all physical properties should be evaluated at the mean temperature between the skin and the atmospheric temperatures.

Using Eq. (4), the rate of heat transfer by convection to or from the surface of the balloon skin during ascent or descent can be written in the form

$$q_c = 3.9 \frac{V^{1/3}}{g} k_a (T_a - \bar{T}_f) \left(2 + 0.472 \frac{V^{0.188}}{g} \left[\rho_a \frac{dz/dt}{\mu_a} \right]^{0.55} \right) \quad (5)$$

Krause and Schenk (10) investigated thermal free convection from a warmer surrounding fluid to a cooler spherical body at uniform surface temperature in the range of Rayleigh numbers ($\text{Gr}_D \times \text{Pr}$) between 6×10^3 and 5×10^6 . The experimental results for the local heat transfer coefficient agree reasonably well with a theoretical analysis of Merk (11) up to the hydrodynamic separation point, which for the narrow Grashof-number range of this investigation occurred at a polar angle of about 145° from the vertical axis. Since Merk's theory applies equally well for laminar free convection from a heated sphere, it also seems reasonable to use it to calculate heat transfer from the upper hemispherical surface of heated balloons. No theory or data exist at present, however, to predict the influence of the non-uniform azimuthal temperature distribution, which is always present when the balloon is heated by the sun.

Experimental evidence is contradictory regarding the influence of the Grashof number on the separation point in laminar free convection to or from a sphere. Garner, et al. (12, 13) found a shift in separation point from 155 to 100° between mass transfer Rayleigh numbers ($\text{Gr}_D \times \text{Sc}$) from 1.5×10^3 to 5.5×10^3 for different fluids with $800 < \text{Sc} < 2,200$, whereas

Schütz (14) found a much weaker dependency in the region $2 \times 10^8 < Gr_D \times Sc < 2 \times 10^{10}$ (170 to 135°) for a fluid with $Sc = 1,800$. According to conventional boundary layer theory, the separation point should shift toward the stagnation point with increasing Grashof numbers and the heat transfer coefficient in the region of the free convection plume, where the flow is turbulent, will be larger than in the laminar flow regions. The results agree qualitatively with observations of free convection about a horizontal cylinder.

The point of transition from laminar to turbulent flow in the free convection regime is not presently known. Schlieren patterns (10) show that purely laminar flow prevails over a sphere between the stagnation point and the equator at Grashof numbers as high as 6×10^8 and that some disturbances exist between 100° and separation (190 to 150°), but real turbulence was observed only in the plume at a Grashof number of about 10^9 . Perhaps the stability analysis of Gebhart (15) could be applied to natural convection over a balloon-shaped body (idealized as a sphere) to analytically predict the point of transition. Gebhart's analysis for a flat plate predicts that

turbulent instabilities could amplify at local Grashof numbers of the same order of magnitude as have been observed on balloons.

If the designer can use averaged values of the heat transfer coefficient over the entire surface of the sphere, available data can be correlated (10) by a relation of the type

$$\overline{Nu}_{D,m} = \frac{\overline{h}_c D}{k_a} = 2 + 0.6 (Gr_D \times Pr)_m^{\frac{1}{4}} \quad (6)$$

for Rayleigh numbers between 10^5 and 2×10^{10} . The constant value of 2 applies in the limit as the Grashof number approaches zero and the heat transfer mechanism approaches pure conduction. The theoretical convergence of the Nusselt number at small Grashof numbers has recently been elegantly verified by Fendell (16).

The influence of vibration on the heat transfer from spheres has been investigated in free and forced convection (17), and the influence of rotation about a vertical axis has been studied experimentally for free convection (18, 19). The results of these investigations indicate that under flight conditions neither vibration nor rotation will influence balloon heat transfer characteristics.

Using Eq. (6), the rate of heat transfer by free convection to or from a balloon at float altitude can be written in the form

$$q_d = 7.79 \frac{V^{1/3}}{g} k_a (T_a - \bar{T}_f) \left[1 + 0.322 \left(\frac{\rho_a^2 g |T_a - \bar{T}_f| V^{1/3}}{T_a \mu_a} \right) \right] \quad (7)$$

For computational purposes a very convenient correlation of averaged experimental convection data has recently been provided by Börner (20), who reviewed 70 previous investigations of heat and mass transfer by free convection or forced convection, or both, in flow over single bodies, and who also conducted additional tests. One convenience of Börner's correlation is that data for bodies of different shapes can be handled (21) by choosing a pertinent length dimension, l' , defined in Table 1 for several shapes.

Reference (20) presents correlations of free convection data for horizontal and vertical plates, spheres, and horizontal and vertical cylinders as plots of $\overline{Nu}_{l'} = \bar{h}_c l' / k$ vs $(Gr_{l'} \times Pr) = (g \rho_a^2 \beta \Delta T l'^3 / \mu_a^2) \times (C_p \mu_a / k)$ and of forced convection data in the form $\overline{Nu}_{l'}$ vs $Re_{l'}$. A combined free and forced convection correlation was obtained by defining an equivalent Reynolds number for free convection $Re_{l'}^*$

$$Re_{l'}^* = f(Pr) (Gr_{l'})^{1/2} \quad (8)$$

Table 1

Equivalent Length Dimensions of Convection Correlation

Shape of Body	Equivalent Length l'
Very wide plate with surface parallel to the flow in forced convection with length l in direction of flow	$l' = l$
Sphere or long cylinder of diameter D with axis perpendicular to the flow in forced and free convection	$l' = (\pi/2)D$
Long rectangular bar of width a^* and height b^* with its long axis perpendicular to the flow in forced convection	$l' = a^* + b^*$
Vertical plate (surface parallel to gravity) of height l in free convection	$l' = l$
Long horizontal plate (surface perpendicular to gravity) of width l in free convection	$l' = l/2$

where the function $f(\text{Pr})$ for air, which is dependent upon the Prandtl number, should be taken equal to $\sqrt{\frac{1}{2}}$ for a "best fit correlation," compared to 0.64 predicted by analysis. With the definition of an equivalent Reynolds number for free convection given in Eq. (8), free convection dominates when $\text{Re}'_l < 2.4 \text{Re}'_{l,*}$ and forced convection dominates when $\text{Re}'_{l,*} < 2.4 \text{Re}'_l$. A transition region, where both free and forced convection are appreciable, exists between these limits. It has been shown that in this transition region free convection aids the forced convection transfer when the motion caused by buoyance is in the same direction as the forced flow and retards it (22, 23) when buoyancy opposed the flow. In order to bridge the gap between forced and free convection Börner (20) defines a third Reynolds number, $\text{Re}'_{l'}$, as

$$\text{Re}'_{l'} = \sqrt{\text{Re}'_{l'}{}^2 + (\text{Gr}'_l/2)} \quad (9)$$

and then plots Nu'_l vs $\text{Re}'_{l'}$. Figure 2 shows the results of this correlation for a sphere with downward forced convection. Under these circumstances free convection will oppose the forced convection flow, but visualization studies for this condition (20) have shown that the existence of a

free convection field will produce turbulence at low velocities and will also cause separation of the boundary layer. These effects tend to offset any decrease in the heat transfer, as predicted for purely laminar flow (22). The correlation function shown in Fig. 2 was also found to be applicable for upward flow. Sharma and Sukhatme (24) have recently published experimental results concerning the interaction between free and forced convection in flow over a horizontal cylinder for Reynolds numbers from 10 to 5,000 and Grashof numbers from 3×10^3 to 7×10^6 . These results indicate that the Reynolds number exponent n in the parameter Gr/Re^n is affected by turbulence and separation phenomena and that a value of 3.25 is most suitable when free convection dominates, whereas a value of 1.8 is more suitable at the forced convection end. An average value of 2.5 was found to give a reasonably good correlation in the transition region.

Börner's correlation does not give insight into local variations of the heat transfer coefficient, but it is convenient. By computing Re'_l and $\text{Re}'_{l,*}$ simultaneously and continuously from the time of launch until the balloon has reached the float altitude, a smooth transition between the

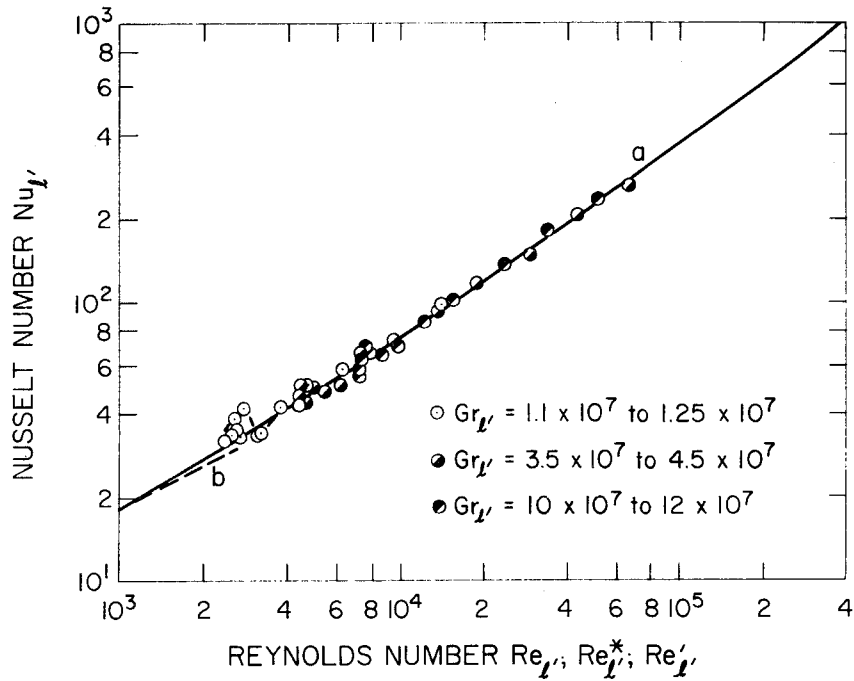


Fig. 2. Average Nusselt number for sphere in combined free and forced convective flow.

forced and free convection regions can be made and the influence of radiation can be superimposed directly.

In general, only the equilibrium temperature at float altitude is important to the thermal design of balloon instrument packages. During ascent forced convective heat transfer is quite effective (25) in maintaining a small instrument package at a temperature close to that of the ambient air, but when the balloon has reached its float altitude only free convection can transfer heat directly between the package and the surrounding air. The relative magnitude of the radiation to and from the surfaces of the package dominates the thermal transfer during the day, but convection enters prominently at night.

In certain specialized instrument packages, in addition to the averaged heat transfer coefficient, local values at the top and bottom surfaces are also sometimes of interest. The numerical study of Suriano and Yang (26) provides some insight into the flow and temperature field in the vicinity of a heated horizontal square plate at small Rayleigh numbers. Table 2 shows averaged Nusselt numbers obtained by their calculations for both the top and bottom surfaces. The temperature field over a horizontal plate at

Table 2

Average Nusselt Numbers for a Horizontal Plate in Free Convection

Ra	Pr = 0.72			Buznik and Bezloomtsev ¹
	x = 0-	x = 0+	Average	
0.	1.049	1.047	1.048	1.00
0.10	1.052	1.045	1.048	1.28
5.0	1.201	0.946	1.074	1.77
10.0	1.406	0.932	1.169	1.91
50.0	2.879	1.259	2.069	2.38
100.0	4.041	1.330	2.685	2.64
200.0	6.166	1.492	3.829	2.96
250.0	7.194	1.594	4.394	3.00
300.0	7.620	1.678	4.469	3.03

¹Buznik, V. M. and K. A. Bezloomtsev, 1960: A generalized equation for the heat exchange of natural and forced convection during external flow about bodies. Izv. Uyssh. Ucheb. Zaved. 2, 68-74; 1961: Ref. Zh. Mechl. 6, Rev. 6V506.

a Rayleigh number of 50 (Fig. 3) suggests boundary layer behavior on the lower surface but not on the upper. However, the analysis of Stewartson (27), as modified by Gill et al. (28), indicates that a boundary layer also forms over the upper surface of a heated horizontal strip and that the average Nusselt number for a strip of width L in air can be predicted from the relation

$$\overline{Nu}_L = \frac{\overline{h}_c L}{k_a} = 0.79 Gr_L^{1/5} \quad (10)$$

in the laminar flow region. This result is not in complete agreement with experimental data for the upper surface of a heated square plate of side L in air (29). These data give larger heat transfer coefficients that are correlated empirically by the relations

$$\overline{Nu}_L = 0.50 Gr_L^{1/4} \quad (10^5 < Gr_L < 2 \times 10^7, \text{ laminar}) \quad (11)$$

$$\overline{Nu}_L = 0.125 Gr_L^{1/3} \quad (2 \times 10^7 < Gr_L < 3 \times 10^9, \text{ turbulent}) \quad (12)$$

Heat transfer by free convection from the lower surface of finite heated plates (or to the upper surface of cooled plates) has recently been studied by Singh et al. (30) and Kimbadi et al. (31) for square and circular plates and a long strip. Local heat transfer coefficients are lowest in the

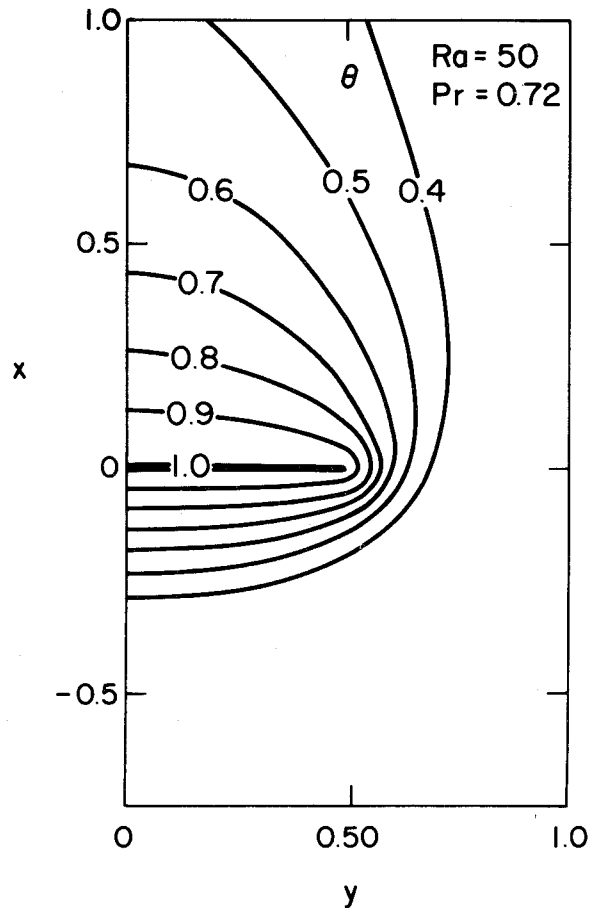


Fig. 3. Temperature field about a heated horizontal flat plate at a Rayleigh number of 50.

center and increase toward the edges. For a square plate of side L the local Nusselt number at a distance x from the center is

$$\frac{h(x)L}{k_a} = 0.58 \text{ Ra}_L^{1/4} \left\{ \left[1 - \left(\frac{2x}{L} \right)^2 \right] + 0.271 \left[1 - \left(\frac{2x}{L} \right)^2 \right]^4 + \dots \right\}^{1/4} \quad (13)$$

The average Nusselt number for square plates, as well as for circular plates and long strips, is given by the relation

$$\overline{\text{Nu}}_L = \frac{\bar{h} L}{k_a} = C \text{ Gr}_L^n \quad (14)$$

where constants C and n are given in Table 3.

Flow-visualization experiments with a number of other shapes, with heated surface facing upward, have been reported by Husar and Sparrow (32), but information regarding the interaction between the boundary layer flow over vertical surfaces and the flow developing over horizontal surfaces (i.e., the top and bottom of boxes or vertical cylinders) is still lacking.

D. CONVECTION INSIDE THE BALLOON [q in Eqs. (1) and (2)]

The convection process inside the balloon is important because it determines the temperature, the pressure, and the volume of the lift gas (usually helium). Little research has been done on convection inside a

Table 3

Constants for the Free Convection Equation (Eq. 14).

Reference Numbers		Constants	
		C	n
35 (analytical)	Square Plate ¹ (L is length of side)	0.89	0.2
34 (experimental)		1.00	0.2
35 (analytical)	Circular Plate ¹ (L is the diameter)	0.79	0.2
36 (experimental)		1.0	0.2
32 and 33 (analytical)	Long Strip ¹ (L is the width)	0.80	0.2

¹Heated surface facing downward, influence of side walls neglected.

sphere (33, 34) and none has been done on convection inside cavities resembling the shapes of high altitude balloons.

The heat transfer process is free convection. Hellums and Churchill showed as early as 1961 (35, 36) that the partial differential equations for the conservation of mass, momentum, and energy can be solved for laminar natural convection under many different conditions, but so far no solution for the heat transfer inside a balloon has been obtained. Investigations of natural convection in annuli (37) suggest that several types of flow patterns will exist as the temperature difference between the surface and the gas varies during a 24-hr period. It seems likely that in the daytime, when the balloon skin is warmer than the gas inside, there would be an upward flow near the balloon skin and downward flow in the interior. The reverse would be expected at night. But there could also be situations during the day when gas ascends on the side heated by the sun and descends on the cooler side. As a first approximation, one could use existing solutions for flow in a rectangular cavity heated on two sides as long as the flow is laminar. But the tremendous size of a balloon makes

it very likely that the flow will be turbulent, except for very small temperature differences.

A semi-empirical analysis (38) suggests that for turbulent free convection over a vertical plate the Nusselt number fits the relationship

$$\frac{\bar{h}_c L}{k_g} = 0.021 (Gr_L \times Pr)^{2/5} \quad (15)$$

at Grashof numbers of the order of 10^{12} , but Clark (39) suggests using a relationship of the type

$$\frac{\bar{h}_c D}{k_g} = C \left[\frac{\rho_g^2 g (\bar{T}_f - \bar{T}_g) D^3}{T_g \mu_g^2} \times Pr_g \right]^n \quad (16)$$

with the constants C and n selected from Table 4, and with all physical properties of the gas evaluated at the skin temperature.

Table 4

Free Convection in a Sphere
(Constant C and Exponent n for Eq. 16)

Gr x Pr	C	n	Type of Flow
$10^4 - 10^9$	0.59	1/4	Laminar
$10^9 - 10^{12}$	0.13	1/3	Turbulent

In the absence of more concrete information, Dingwell et al. (40)

used Eq. (16) for their balloon study, with C and n equal to 0.13 and 1/3, respectively. Equation (16) can then be used to write the rate of heat transfer from the skin to the gas in the form

$$\begin{aligned} \dot{q} &= \iint_{A_i} \bar{h}_c (T_f - T_g) dA_i = h_c \pi D_g^2 (T_f - T_g)_{ave} \\ &= 4.83 \bar{h}_c V_g^{2/3} (T_f - T_g)_{ave} \\ &= 0.628 V_g^{2/3} k_g (\bar{T}_f - \bar{T}_g) \left[\frac{\rho_g^2 g (\bar{T}_f - \bar{T}_g)}{\mu_g^2 T_g} Pr_g \right]^{1/3} \end{aligned} \quad (17)$$

Experimental data supporting the form of Eq. (16) have recently been reported by Ulrich et al. (41) for the transient condition encountered in filling a cylindrical tank with air at Grashof numbers between 10^8 and 10^{13} . The length-to-diameter ratio of their tanks varied between 0.5 and 2.0, so their results should indicate what might occur inside a sphere. The experiments showed that during the initial stages of the process the heat transfer coefficients were significantly higher than those predicted by turbulent free convection, but agreement with the heat transfer rate predicted by Eq. (17) was achieved after a few seconds. Available information

on the transient free convection heat transfer characteristics of vertical surfaces in the laminar region is extensive and has been summarized by Gebhart et al. (42); little information is available for the turbulent flow region (41).

E. RADIATION HEAT TRANSFER

The radiation heat transfer to and from balloons strongly influences their performance and determines their short-term stability. Balloon skins absorb direct and reflected solar radiation and radiation emitted by the earth and the atmosphere. Over 99% of the solar radiation is in the wavelength range between 0.2 and 4.0 μ , whereas the earth and atmospheric radiation is in the infrared range between 6 and 100 μ , with about 70% below 20 μ . Balloon skins are usually at temperatures of about 210-260^oK (380-470^oR) and thus emit infrared radiation. For approximate calculations the sun and earth can be considered to be blackbodies at 5550 and 300^oK (10,000 and 540^oR), respectively. The direct radiation from the earth and the clouds can be as high as 475 W/m² (150 BTU/ft² hr) (3). However, the direct solar radiation is collimated and, therefore, the effective receiving area is the projected area, which in the case of a

30,000 m³ (1.06 million ft³) spherical balloon is about 1170 m² (12,600 ft²). Reflected solar radiation, on the other hand, impinges on the lower half of the total surface area of the balloon, which is about 2340 m². Earth and atmosphere radiation impinges on the total area of the balloon (about 4670 m²) during ascent through the atmosphere, but only on the lower half of the balloon surface after it has risen to an altitude of 21 km, where less than 5% of the total air mass remains above. Thus, the total direct solar radiation is about 1.58 x 10⁶ W (5.4 x 10⁵ BTU/hr), and the reflected radiation is about 1.06 x 10⁶ W. Infrared radiation from the earth and the atmosphere can amount to as much as 2.11 x 10⁶ W, but at float altitude will be of the order of 0.59 x 10⁶ W. The balloon emits radiation at a rate of 1.41 x \bar{e}_f x 10⁶ W, where the effective emissivity \bar{e}_f may vary between 0.2 and 0.7 for different skin materials. In comparison, convection contributes only about 0.59 x 10⁶ W to the heat transfer over the exterior balloon surface, but it is the only heat transfer mechanism in the interior because helium is transparent to radiation.

Since the actual amount of radiation absorbed depends critically on the radiation properties of the receiving and emitting surfaces, a know-

ledge of these properties is very important to the designer. The two most common materials for balloon skins are polyethylene and Mylar, which have--according to available data (43)--an effective absorptance to solar radiation of about 0.12 and 0.17, respectively. The absorptance to infrared earth radiation, which is also approximately the emittance of the skin, is 0.21 for polyethylene and 0.63 for scrim Mylar (0.5 mil Mylar on dacron scrim). A Mylar balloon absorbs, therefore, a much smaller percentage of its total radiation load from the sun than does a polyethylene balloon, and since it also emits more radiation by virtue of its higher emittance, a Mylar balloon will be cooler than a polyethylene balloon. At the same time, however, because of its high emittance a change in environmental conditions (e.g., setting of the sun) will reduce the gas temperature in a Mylar balloon more quickly than in a polyethylene balloon. A Mylar balloon, therefore, has less altitude stability than a polyethylene balloon.

In the evaluation of the radiant contribution to the total heat load on balloons and their instrument packages, engineers are faced with a lack of experimental data for the pertinent surface radiation characteristics of balloon materials. To calculate accurately the percentage of direct

solar incident radiation absorbed by a surface, one must know its monochromatic absorptance for radiation of wavelengths between 0.2 and 4.0 μ at various angles of incident radiation (44). The absorptance of thin films has a strong angular variation; radiation perpendicular to the surface passes through more readily than does radiation at a grazing angle. This angle variation can become particularly important in a balloon system where the radiation incidence angle is zero at sunrise, rises to a maximum at noon, and then decreases again to zero at sunset. For passive temperature control, i.e., the use of surfaces with very different solar absorptances and infrared emittances, the influence of the average incident angle of radiation cannot be ignored.

The difficulty of determining radiation properties for balloon skins is exacerbated by the transparency of these skins, and the transmittance has to be considered (45). As will be shown, to calculate accurately the radiation heat load on a balloon, one needs to know the total hemispherical emittance of the skin at its temperature, the directional and the angular hemispherical absorptance in the solar spectrum (since surfaces are irradiated directly and indirectly by the sun), the directional reflectances of

clouds and terrestrial surfaces in the solar spectrum, and the hemispherical absorptance in the infrared (for the surfaces exposed to the earth or clouds).

In 1969 Edwards (46) summarized our knowledge of the radiative transfer characteristics of materials and surveyed techniques available to measure surface properties (47). It does not seem feasible to measure spectral-angular surface properties for all potentially useful materials. The amount of data would be unmanageable, and the cost with present equipment would be unreasonably high. It would, therefore, be desirable to classify materials according to their physical surface properties and to develop working relationships to estimate "effective" angular properties from measurements of a few select properties. One should also know the influence on the radiation surface properties of launch procedures, aging, solar radiation, and atmospheric phenomena so thermal predictions can be made not only for idealized laboratory samples but also for actual operational systems.

The flight lifetime of a balloon depends critically on the relationship between the amount of radiant energy absorbed during the day and the amount of radiant energy lost at night. In the morning the balloon is

usually at the lowest float altitude because the gas is at its lowest temperature. After sunrise the gas is warmed by transient free convection from the skin after the skin has been warmed by the absorption of solar radiation. The part of the skin exposed to the sun transfers heat by transmission and internal emission to the rest of the skin. As the temperature of the gas increases, the buoyancy of the balloon also increases and the system begins to rise. This rise will continue until shortly after sunset, whereupon the net loss of energy exceeds the net input of energy, and the balloon begins to sink. At present the total balloon heat balance over a 24-hr period shows a small loss in internal energy. One of the long-range objectives of balloon designers is a system which will passively maintain its average float altitude, i.e., the altitude for which the net change in lift-gas energy over a 24-hr period is zero.

Various schemes to achieve a zero net change have been tried without success. But even if a "permanent balloon" is not possible, increased balloon lifetime and altitude stability would materially contribute to programs aimed at permitting long-term weather prediction and eventual weather control.

At altitudes below 21 km the radiation incident on a balloon is subject to considerable variation, and quantitative estimates are uncertain. The amounts of infrared radiation from below and above will differ and will both depend on the weather and cloud cover. The incident solar radiation will also depend on the altitude and the clouds. At altitudes over 21 km a balloon is above the weather and receives nearly all of its infrared radiation from below. Under these conditions the infrared radiation heat load can be estimated with considerably more confidence. Fortunately, large balloons are generally launched in good weather so that changes in cloud cover during ascent are minimized.

Although measurements of upward and downward radiation in the atmosphere have been made for many years, accurate evaluation of rapid changes in radiation flux are unreliable because it is not possible to predict the critical local weather changes in advance. One could, however, modify the radiation heat flux calculations to include observed weather data, such as the types of clouds and their altitudes. Calculations based on recent observations made at NOAA by Kuhn (48) clearly correlate changes in the radiation flux with cloud cover. Application of available knowledge of

atmospheric radiation to balloon performance will, however, require the close cooperation of meteorologists, cloud physicists, and ballooning engineers.

For small packages used on superpressure balloons at intermediate altitudes, an engineering analysis of the thermal control problem and a summary of the experience gained in several flights by NCAR have been presented by Lichfield and Carlson (25). The basic problems of temperature control at float altitude are quite similar to those encountered in spacecraft. In space, where only radiation can transfer heat, the equilibrium temperature T developed by an opaque body subjected only to direct solar radiation at the rate G_s over a projected surface area S_s normal to the sun, having an averaged directional absorptance per unit projected area $\bar{a}_{s,ave}$ and a surface area S with an average hemispherical emittance in the infrared $\bar{e}_{H,i}$ is

$$T = \left(\frac{\bar{a}_{s,ave} G_s S_s}{\sigma \bar{e}_{H,i} S} \right)^{\frac{1}{4}} \quad (18)$$

Equation (18) shows that in this case the ratio of the absorptance in the solar spectrum to the emittance in the infrared controls the equilibrium temperature.

In the balloon packages the heat transfer problem is more complicated because of the addition of reflected solar radiation, convection, and the influence of the atmospheric radiation, all of which depend strongly on the cloud cover and weather. In daytime flights, the temperature can be controlled by proper treatment of the surface of the package. The properties of a number of materials and surface coatings for such use are presented in references (49-52); Table 5 presents a typical selection. Silver sulfide, which has an average infrared emittance of only 0.03 and an average solar absorptance of 0.60, has been used successfully in balloon packages for which a temperature between 7 and 16°C was desirable. A further increase in temperature during the day was achieved by covering the package with a thin film of material such as Mylar, which is transparent to radiation only in the solar spectrum between 0.2 and 3.0 μ , but has a large reflectance for infrared radiation. This method of trapping the

Table 5

Radiation Characteristics of Surfaces

Material	IR Emissivity	Solar Absorption	Ratio
Silver (polished)	0.02	0.07	3.50
Platinum	0.05	0.10	2.00
Aluminum	0.08	0.15	1.88
Nickel	0.12	0.15	1.25
Stellite	0.18	0.30	1.67
Aluminum paint	0.55	0.55	1.00
White lead paint	0.95	0.25	0.26
Zinc oxide paint	0.95	0.30	0.32
Gray paint	0.95	0.75	0.79
Black paint	0.95	0.95	1.00
Lamp black	0.95	0.97	1.02
Silver sulfide ¹	0.03	0.60	20.00
Nickel black ^{1,2}	0.10	0.90	9.00
Cupric oxide ^{1,2}	0.15	0.90	6.00

¹These are special surfaces where a metal is covered with a very thin layer of absorbing material. The layer is so thin that it is a fraction of a wavelength thick in the infrared and is, therefore, almost transparent to IR. The result is that the IR emissivity is nearly that of the underlying metal. However, the thickness is large compared to the wavelength of the maximum solar spectrum so the absorptivity is large for solar radiation.

²H. Tabor, 1961: Solar Energy.

radiation, using the so-called greenhouse effect, should be used cautiously to avoid an excessive temperature rise during the middle of the day.

For nighttime balloon flights, energy must be stored to maintain the internal temperature of the flight package. A simple heat reservoir is water. When a kilogram of water freezes, 3.34×10^5 J of energy are released. In addition, 4184 J of energy are released for each kg of water cooled 1C° . Table 6 compares the energy storage capacity of water with that of various batteries. The zinc-air and silver-zinc batteries have greater energy storage capacity than water, but zinc-air batteries require a supply of oxygen at balloon float altitude, and water is cheaper and easier to handle.

Table 6

Energy Storage Capabilities of Water and Batteries

	W-hr/lb	W-hr/kg	W-hr/in. ³
Water (heat of fusion)	42.0	92.6	1.52
Water (per $^{\circ}\text{C}$)	0.528	1.16	0.019
Zinc-air	80.0	176.	5.0
Lead-acid	11.0	24.2	1.2
Nickel-cadmium	8.0	17.6	0.4
Silver-cadmium	35.0	77.0	3.5
Silver-zinc	55.0	121.0	4.5

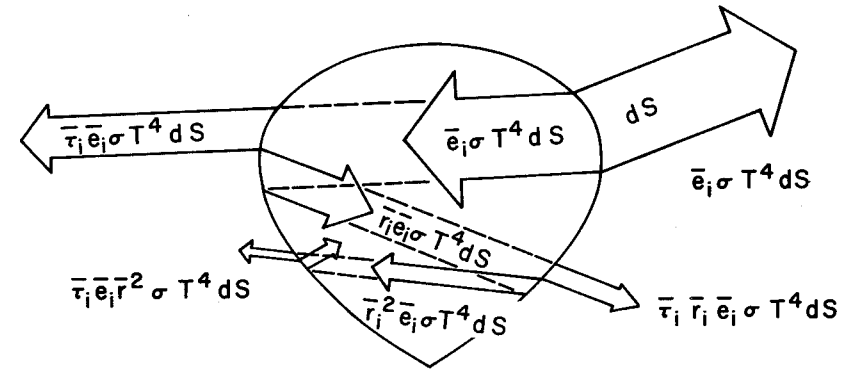
For flights lasting several days, the package must be able to absorb as much heat during the day as it loses during the night. With suitable black paint, daytime surface temperatures of -15 to -12°C can be attained, but since a typical nighttime surface temperature is -55°C , it is necessary to achieve a daytime surface temperature of about 55°C (131°F) to maintain temperature equilibrium in the water. This requires the use of special coatings, such as silver sulfide, or the use of one or more greenhouse covers. One can also use solar cells to generate energy within the package during the day, but this adds weight and complicates the system.

F. EMITTED RADIATION [q_g in Eq. (2)]

The balloon fabric, polyethylene or Mylar, transfers heat to the atmosphere by infrared radiation. A typical Mylar balloon fabric (9μ thick Mylar with dacron scrim, 160×240 strands per meter) has at its operating temperature an average transmittance of about 0.55, an average reflectance of about 0.20, and an average absorptance of 0.25. A typical poly-

ethylene film has an average transmittance of 0.75, an average reflectance of only 0.05, and an average absorptance of 0.20. However, the monochromatic properties of fabric materials vary considerably. Mylar, for example, has radiation windows with transmittances as high as 0.80 for wavelengths between 3 and 6 μ and opaque ranges with transmittances as low as 0.10 for wavelengths between 13 and 15 μ (53).

To calculate the emitted radiation it is necessary to know the spectrally averaged hemispherical emittance in the infrared region. The evaluation of an average hemispherical emittance for a given wavelength range or a given temperature offers no difficulties for an opaque surface (46, 50, 54). As shown in Fig. 4, however, a surface element of a balloon skin dS radiates not only directly into space, but also into the interior where radiation can pass through the fabric into space, can be reflected from the interior surface of the balloon fabric, or can be absorbed by the fabric. To calculate accurately the "effective emittance" of a balloon from data on the surface radiation properties of its fabric skin, bidirectional values of the monochromatic emittance, absorptivity, and reflectivity of the interior surface would have to be known for the infrared wavelengths between



$$E_f = \int_0^{\infty} \int_s e_i(\lambda) \sigma T_f^4 dS d\lambda \approx \bar{e}_i \pi D_g^2 \sigma T_f^4$$

$$Q_{\text{total}} \approx \bar{e}_i \pi D_g \sigma T_f^4 [1 + \bar{r}_i (1 + \bar{r}_i + \bar{r}_i^2 + \dots)]$$

Fig. 4. Emission of radiation from a balloon skin--the effective emittance.

6 and 100 μ (46). Such measurements are difficult and are generally too expensive. For balloon design it would actually be much more desirable to measure the actual emittance of a spherical sample of the fabric material filled with helium. However, no such data have as yet been taken, and calculations have been based on a model proposed by Germeles (55). This model assumes that the inner fabric surface obeys Lambert's law, i.e., it emits and reflects diffusely. It also assumes that average values can replace the spectrum of values for the emittance, absorptivity, and reflectivity of the inner surface over the wavelength range (between 6 and 20 μ) for which data are available (48). The net rate of emission from the entire balloon is then equal to the radiation directly emitted from the outer surface, $\bar{e}_i \pi D_g^2 \sigma T_f^4$, plus that portion of the radiation emitted by the interior surface which eventually passes through the fabric, $\bar{e}_i \bar{r}_i \pi D_g^2 \sigma T_f^4 (1 + \bar{r}_i + \bar{r}_i^2 + \dots)$. By summing the series, one obtains the effective emissivity of the fabric

$$\begin{aligned} \bar{e}_{\text{eff}} &= \bar{e}_i \left[1 + \bar{r}_i (1 + \bar{r}_i + \bar{r}_i^2 + \dots) \right] \\ &= \bar{e}_i \left(1 + \frac{\bar{r}_i}{1 - \bar{r}_i} \right) = \bar{e}_i \left(2 - \frac{\bar{a}_i}{1 - \bar{r}_i} \right) \end{aligned} \quad (19)$$

where

$$\bar{a}_i = \frac{\int_6^{100} a(\lambda) I(\lambda) d\lambda}{\int_6^{100} I(\lambda) d\lambda} \quad (20)$$

$$\bar{r}_i = \frac{\int_6^{100} r(\lambda) I(\lambda) d\lambda}{\int_6^{100} I(\lambda) d\lambda} \quad (21)$$

$$\bar{r}_i = 1 - \bar{r}_i - \bar{a}_i \quad (22)$$

$$\bar{e}_i(T_f) = \bar{a}_i(T_f) \quad (23)$$

Use of the effective emissivity gives the rate of heat transfer from the balloon fabric in the form

$$q_g = 4.83 \bar{e}_{\text{eff}} V_g^{2/3} \sigma T_f^4 \quad (24)$$

where \bar{T}_f^4 is the average of the fourth power of the absolute temperature of the balloon fabric.

The infrared hemispherical emittance of the surface of an opaque body can be measured easily, so the determination of radiation emitted by the surface of a balloon instrument package generally offers no problem.

G. DIRECT SOLAR RADIATION [q_2 , direct in Eq. (2)]

The solar radiation spectrum has been investigated in great detail, and summaries of the current state of knowledge are presented in references

(49) and (57). Figure 5 shows the solar spectrum at the outer fringes of the atmosphere and at the surface of the earth after attenuation and absorption by the atmosphere. Over 99% of the solar energy is contained within a narrow wavelength band between 0.2 and 4 μ , and for most engineering heat transfer calculations the sun's spectrum can be approximated by that of a blackbody at 5550°K (10,000°R). The solar constant, i.e., the radiation received by a surface placed perpendicular to the rays of the sun outside the earth's atmosphere, is 1395 W/m² (2.0 g cal/cm² min or 442 BTU/ft² hr). The solar radiation per unit area on a horizontal surface outside the earth's atmosphere depends only on the solar constant and zenith angle, i.e., the angle between a line normal to the surface and the rays of the sun. This angle, ζ , can be determined from the relationship

$$\cos \zeta = \sin \lambda_1 \sin \delta_s + \cos \lambda_1 \cos \delta_s \cos h \quad (25)$$

As shown in detail in references (54) and (56), the radiation per unit area on a surface tilted at an angle i to the horizontal is

$$\bar{G} = \bar{G}_s \cos \phi \quad (26)$$

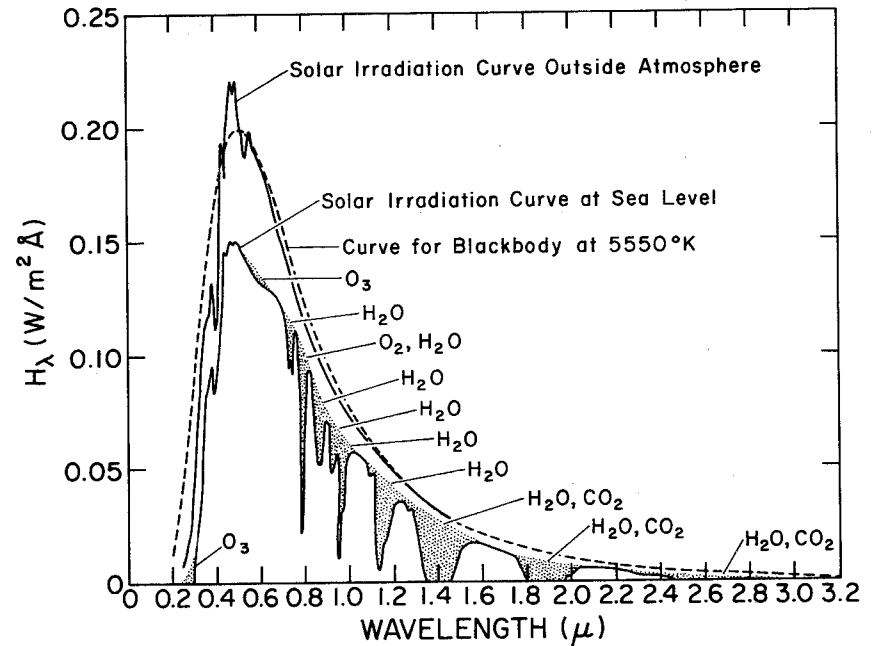


Fig. 5. Spectral distribution of solar radiation in space and at sea level.

where λ_1 is latitude, δ_s is solar declination, h is local hour angle, i is angle between the local vertical and the normal to the tilted surface, \bar{G}_s is average incident solar radiation, ϕ is angle between the normal to the tilted surface and the bearing of the sun, A_z is azimuth of the sun measured westward from the south meridian, a_z is the angle measured from the south meridian of the projection on the earth's surface of the normal to the tilted surface, and $\cos \phi = \cos (A_z - a_z) \sin \zeta \sin i + \cos \zeta \times \cos i$.

The zenith angle can be defined in a time coordinate system related to the flight of the balloon. If the Greenwich hour angle at the time of launch is GHA, then at any subsequent time t , the local hour angle at the balloon is

$$h = \text{GHA} - \varphi_1 + \frac{t}{240} \quad (27)$$

where GHA and the longitude φ_1 of the balloon are in degrees and t is in seconds.

Once ϕ is known the solar radiation absorbed by a surface outside the atmosphere is simply $\bar{a}_s(\phi)\bar{G}_s$, where $\bar{a}_s(\phi)$ is the effective directional absorptance for that angle.

In passing through the atmosphere, the intensity and spectrum of the solar energy are altered by absorption and scattering (58). Therefore, the radiation on an object is strongly dependent on the atmospheric path length of the solar rays, usually expressed in terms of the "optical air mass." Exact calculations of the attenuated spectrum are quite cumbersome (58, 59), and for engineering purposes such calculations are only useful when the directional absorptances of the receiving surfaces are known (60, 61). Figure 6 shows the distribution of direct solar radiation incident at sea level on a horizontal surface, as a function of wavelength, for several short paths corresponding to optical air masses between 1.0 and 8.0. The optical air mass, m , is unity when the sun is directly overhead and the body receiving radiation is on the earth's surface. When $m = 1.0$ the fraction of the solar constant received at sea level ranges from 0.62 to 0.81. A mean value of 0.7 is generally considered acceptable for most purposes. For other values of m , the fraction of solar radiation received may be expressed (55) by the empirical relation

$$\frac{\bar{G}_{s,m}}{\bar{G}_s} = 0.5 (e^{-0.65m} + e^{-0.095m}) \quad (28)$$

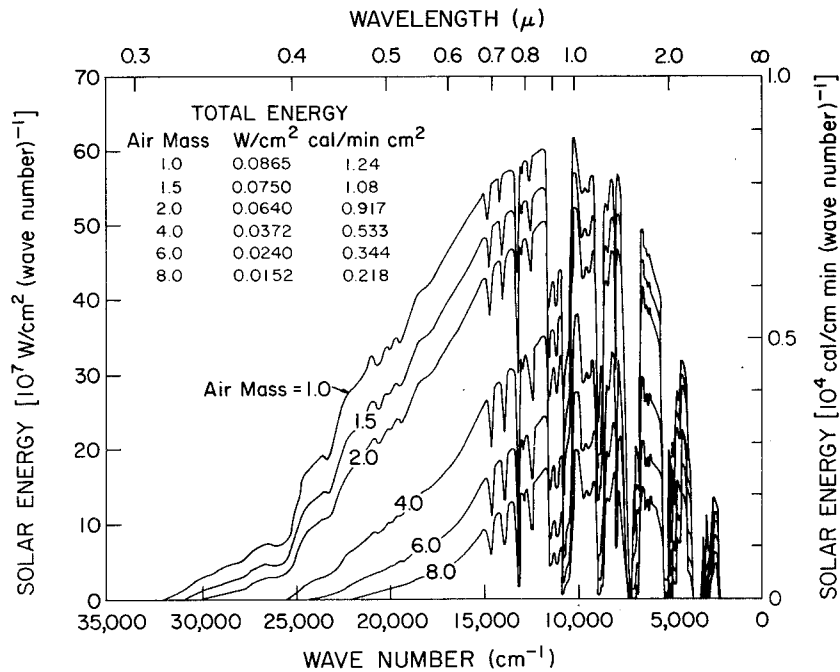


Fig. 6. Spectral distribution of solar radiation incident at sea

level for air masses 1.0 to 8.0.

where optical air mass depends on the altitude and the sun's zenith

angle, ζ . The variation of the optical air mass at sea level with

zenith angle, $m(o, \zeta)$, is given in Tables 16-18 of reference (57) and can

be closely approximated (55) by the relationship

$$m(o, \zeta) = [1229 + (614 \cos \zeta)^2]^{\frac{1}{2}} - 614 \cos \zeta \quad (29)$$

for $0 < \zeta < 90^\circ$. Since the attenuation is proportional to the number

of air molecules in the path, for a given zenith angle the optical air

mass at altitude z can be related approximately to the air mass at sea

level by the relationship

$$m(z, \zeta) = m(o, \zeta) [p(z)/p(o)] \quad (30)$$

Using Eqs. (25)-(30) one can determine radiation on a surface at any

altitude, geographical location, and time between sunset and sunrise.

There are two short periods

$$90^\circ < \zeta \leq 90^\circ + \cos^{-1} \left(\frac{D_{\text{earth}}}{D_{\text{earth}} + 2z} \right)$$

before sea-level sunrise and after sea-level sunset during which a bal-

loon also receives solar radiation. A method for determining the air mass

during these periods is presented in reference (5), but for most purposes

it is sufficiently accurate to double the value of the air mass calculated at sea-level sunrise or sunset.

The portion of the solar radiation absorbed at the surface of an opaque body, such as an instrument package, can be calculated once the orientation of the surface relative to the sun is known. The amount of incident radiation absorbed per unit area is

$$q_{\text{absorbed}} = \int_{0.2}^4 a(\phi, \lambda) \bar{G}(\lambda, m) d\lambda = \bar{a}_s(\phi) \bar{G}(z) \quad (31)$$

However, as mentioned previously, the problem is more complicated for the balloon because the skin is transparent, and a portion of the incident solar radiation is absorbed, a portion reflected, and the rest transmitted into the interior where some of the radiation transmitted on the first pass will be absorbed as a result of internal reflection and absorption.

Except for occasional measurements in connection with basic investigation of radiation (46, 60), only Dingwell (43) has attempted to make systematic measurements of the radiation properties of balloon fabrics. Since balloon skins are transparent, absorptances are difficult to measure

directly. Therefore, Dingwell measured the monochromatic transmittance of solar radiation using a Beckman D.K. spectrophotometer. The reflectance was then estimated by observing interference fringes caused by internal reflections and applying Fresnel's formula for normal incidence. Finally, the monochromatic absorptance for incident radiation, presumably normal to the surface, was calculated from the relationship

$$a(\lambda) = 1 - r(\lambda) - t(\lambda) \quad (32)$$

and the integrated normal absorptance of the fabric over the solar spectrum was determined by numerical integration of the relationship

$$\bar{a}_s(\text{normal}) = \int_{0.2}^{4.0} a(\lambda) I(\lambda) d\lambda / \int_{0.2}^{4.0} I(\lambda) d\lambda \quad (33)$$

No measurements have yet been made of the effect on the radiation properties of balloon films of the solar radiation angle of incidence.

Edwards (61) has shown, however, that predicted equilibrium temperatures can be as much as 22C° (40F°) in error if the angular dependence of radiation characteristics is neglected, and it would be desirable to measure the directional absorptance for some typical materials.

To estimate from available information the percentage of the solar radiation actually absorbed by the skin of a balloon, it will be assumed that the absorptance of the skin is independent of the angle of incidence and that radiation transmitted through the skin emerges diffusely from the interior surface. Furthermore, the shape of the balloon will be idealized as a sphere so that the projected area is $\pi D_g^2/4$. The fraction of the incident solar energy absorbed on the first pass is $\bar{\alpha}_s G(m) \pi D_g^2/4$, and the fraction transmitted is $\bar{\tau}_s G(m) \pi D_g^2/4$. Of the fraction transmitted, $\bar{\alpha}_s$ will be absorbed by the fabric and $\bar{\tau}_s$ will again be reflected. The total amount of the incident solar radiation eventually absorbed, obtained by summing this series of interreflections, will be

$$q_{s,d} = G(m) \left(\pi D_g^2/4 \right) \bar{a}_s \left(1 + \frac{\bar{\tau}_s}{1 - \bar{\tau}_s} \right) \quad (34)$$

or in terms of the gas volume in the balloon

$$q_{s,d} = G(m) 1.21 V_g^{2/3} \bar{a}_s \left(1 + \frac{\bar{\tau}_s}{1 - \bar{\tau}_s} \right) \quad (35)$$

H. REFLECTED SOLAR RADIATION [q_s , reflected in Eq. (2)]

Until recently, the heat load of greatest uncertainty in Eq. (2)

was the reflected solar radiation. It was known from an overall heat balance that the portion of the solar radiation reflected by the earth and its atmosphere (the albedo), when averaged over time and space, was about 34% (62). It was also known from balloon and aircraft observations that the albedo can vary widely, but no accurate long-term measurements could be made without an observation station outside the atmosphere. The early measurements of Explorer VII and several Tiros satellites resulted in data for only part of the globe because these satellites were not in polar orbits. In 1967 and 1968, however, the meteorological satellite Nimbus II measured the incoming and outgoing radiation over the entire globe for several weeks, and Raschke of the Goddard Space Flight Center correlated the results and presented them in convenient graphs (62). These results are very useful for estimates of the reflected solar radiation above the atmosphere at the geographic locations scanned by Nimbus II, but they cover only a limited period and do not indicate variations with weather or direction.

The works of Houghton (63) and Fritz (64) are, therefore, still very useful for engineering design. Houghton established a convenient graph

for the approximate albedo as a function of latitude for clear, partially overcast, and completely overcast skies (Fig. 7). Although these curves were designed for conditions above the atmosphere, they also will give approximate results for balloons in the atmosphere as long as the sky above is not completely overcast. The accuracy of the method, which is very good for altitudes above 18 km (60,000 ft), depends upon the altitude and the amount of cloud cover. From the work of Fritz (64) and Coulson (65) an estimate of the spectrum of the reflected solar radiation can be made. Table 7 presents the results (49) as the ratio of the solar radiation received from below at a wavelength λ to the radiation at the wavelength of maximum intensity for three sky conditions. The reflected solar radiation incident on a satellite or a balloon from a surface element of the earth-atmosphere dS_e is

$$dG_s = (\pi D_g^2 / 4) G_s r_s(\theta, \zeta) \cos \theta \cos \zeta (dS_e / l_{s-B}^2) \quad (36)$$

where $r_s(\theta, \zeta)$ is the bidirectional reflectance of dS_e for a solar zenith angle ζ in the direction of the balloon, θ (see Fig. 9); and l_{s-B} is the distance between the balloon and dS_e . For a known geographical distribution of $r_s(\theta, \zeta)$, the reflected radiation can be calculated numerically.

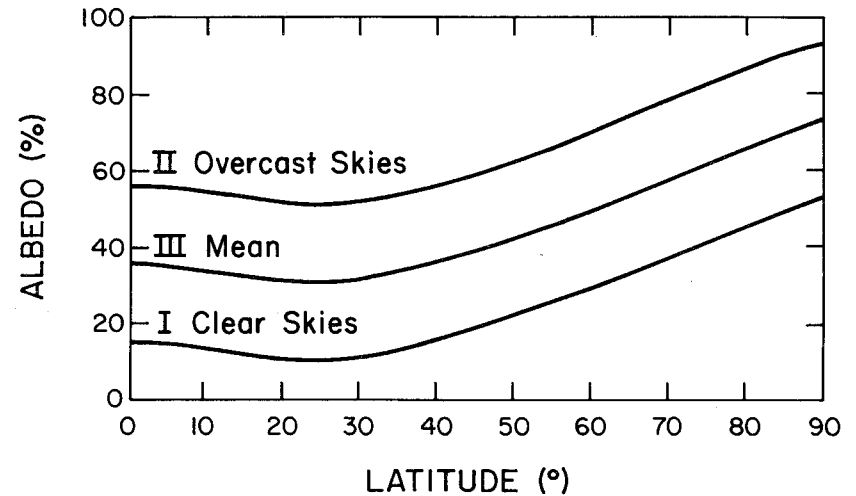


Fig. 7. Albedo as a function of latitude under various sky conditions.

Table 7

Relative Spectral Distribution of Solar Radiation under Various Sky Conditions

R_{λ}^1				R_{λ}^1			
λ (μ)	Clear Skies	Mean	Overcast Skies	λ (μ)	Clear Skies	Mean	Overcast Skies
0.29	0.	0.	0.	0.55	0.333	0.637	0.795
0.30	0.882	0.721	0.477	0.56	0.312	0.615	0.770
0.31	0.892	0.761	0.534	0.57	0.288	0.590	0.752
0.32	0.848	0.749	0.553	0.58	0.276	0.581	0.748
0.33	1.000	0.920	0.705	0.59	0.262	0.563	0.734
0.34	0.858	0.813	0.648				
0.35	0.815	0.802	0.661	0.60	0.241	0.541	0.717
0.36	0.744	0.746	0.634	0.70	0.134	0.396	0.554
0.37	0.768	0.796	0.700	0.80	0.084	0.293	0.425
0.38	0.671	0.714	0.632	0.90	0.057	0.224	0.331
0.39	0.575	0.624	0.570				
0.40	0.758	0.840	0.772	1.00	0.042	0.179	0.266
0.41	0.781	1.000	0.950	1.10	0.028	0.149	0.219
0.42	0.790	0.937	0.925	1.20	0.019	0.118	0.181
0.43	0.675	0.835	0.835	1.30	0.017	0.095	0.145
0.44	0.708	0.908	0.934	1.40	0.015	0.076	0.115
0.45	0.734	0.958	1.000	1.50	0.013	0.063	0.093
0.46	0.649	0.892	0.960	1.60	0.010	0.051	0.078
0.47	0.713	0.864	0.954	1.70	0.008	0.042	0.063
0.48	0.563	0.834	0.935	1.80	0.006	0.034	0.052
0.49	0.487	0.749	0.853	1.90	0.005	0.029	0.045
0.50	0.524	0.727	0.840	2.00	0.005	0.025	0.037
0.51	0.422	0.697	0.825	4.00	0.000	0.002	0.028
0.52	0.378	0.650	0.780				
0.53	0.378	0.668	0.807				
0.54	0.252	0.663	0.812				

¹ R_{λ} = the ratio of the solar radiation at wavelength λ to the solar radiation at the wavelength of maximum intensity.

If one assumes that the earth-atmosphere system reflects uniformly and diffusely, Eq. (36) can be approximately integrated (66) over the portion of the earth visible from the balloon, and the radiation heat load resulting from albedo reflection $q_{z,r}$ becomes

$$q_{z,r} = 1.21 \bar{V}_g^{2/3} \bar{a}_s G_s \left[2 \bar{r}_{s,a} \left(1 - \sqrt{z/D_e} \right) \cos \zeta \right] \quad (37)$$

where G_s is solar constant (1395 W/m² or 442 BTU/ft² hr), \bar{a}_s is average effective absorptance of the skin in the solar spectrum, $\bar{r}_{s,a}$ is average hemispherical albedo of the earth-atmosphere for a given zenith angle, z is altitude of the balloon, D_e is earth diameter (12,756 km), and ζ is zenith angle of the sun at the balloon.

When the atmosphere below a balloon is partially covered by clouds, the reflection from below will not be uniform. In such a situation one can improve the accuracy of the calculations by dividing the visible earth-atmosphere system into areas of uniform, but not equal, reflection. Assuming that each area reflects diffusely, one can approach this problem by means of shape-factor algebra (54, 66, 67, 68) just as in calculations of radiation between two diffuse surfaces.

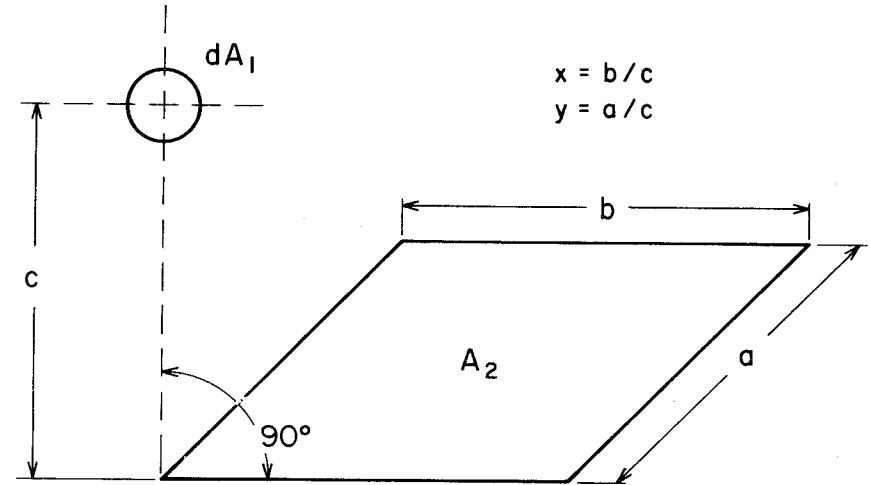
Although the atmospheric layers are curved, one can approximate the atmosphere below the balloon by a flat surface without introducing an appreciable error. The shape factor between a small sphere dA_1 and a plane rectangle A_2 when the sphere is located at one corner of a second rectangle having a common side with A_2 (Fig. 8) is

$$F_{dA_1 - A_2} = \frac{1}{4\pi} \tan^{-1} \frac{xy}{\sqrt{1 + x^2 + y^2}} \quad (38)$$

where $x = b/c$ and $y = a/c$.

An approximate method, sufficiently accurate for most purposes, is to assume that: (a) the atmosphere ends at the intersection of a straight line between the balloon and the horizon, and (b) the atmospheric surface below the balloon is flat.

As x and y approach infinity, the shape factor for radiation between a sphere and an infinitely large plane approaches $\pi D_g^2/2$, which is larger by a factor of $(1 - \sqrt{4z/D_{\text{earth}}})$ than the correct value between a small and a large sphere. At an altitude of 32 km (20 mi), the error would be about 10%. A calculation taking the curvature into account is presented by Cunningham (69).



$$F_{dA_1 - A_2} = \frac{1}{4\pi} \tan^{-1} \left(\frac{xy}{\sqrt{1 + x^2 + y^2}} \right)$$

Fig. 8. Shape factor for a small sphere and rectangular area.

The reflectance of various types of clouds can be estimated from

Table 8 in conjunction with the relationship (70)

$$r_t = r_\infty \left(1 - e^{-b_1 t} \right) \quad (39)$$

where r_t is reflectance of cloud of thickness t , r_∞ is reflectance of cloud of infinite depth, t is cloud thickness in meters, and b_1 is constant whose value depends on liquid water content or cloud type.

Data from which the geographic distribution of reflected solar radiation above the atmosphere can be calculated were gathered by the Nimbus II meteorological satellite, which was launched 16 May 1966 and remained in a polar, synchronous, circular orbit at a mean altitude of 1140 km (707 mi) until 28 July 1966. Its orbital period was 108.6 min, and during its 13 daily orbits the entire globe could be observed day and night. Reflected solar radiation in the wavelength range between 0.2 and 4μ and the earth-emitted long-wave radiation between 5 and 30μ were measured with a radiometer. Details of the data reduction and instrumentation are presented by Raschke (62). In the following, only the application of the averaged data to the evaluation of the reflected solar radiation will be discussed.

Table 8¹

Mean Values of Thickness, Reflectance, and Absorptance as Well as Constants b_1 and b_2 for Various Cloud Types

	Mean Reflectance \bar{r}_t ²	Mean Absorptance \bar{a}_t ³	Mean Thickness t (m)	$b_1 \times 10^4$ (m^{-1})	$b_2 \times 10^4$ (m^{-1})
Low cloud	0.60	0.07	450	21.9	4.5
Middle cloud	0.48	0.04	600	10.5	1.8
High cloud	0.21	0.01	1700	1.2	0.15
Nimbostratus	0.70	0.10	4000	4.2	0.78
Cumulonimbus	0.70	0.10	6000	2.8	0.52
Stratus	0.69	0.06	100	155.0	16.8

¹ Adopted from Yamamoto (70).

² $\bar{r}_t = r_\infty \left(1 - e^{-b_1 t} \right)$; value of \bar{r}_t corresponds to mean thickness.

³ $\bar{a}_t = a_\infty \left(1 - e^{-b_2 t} \right)$; value of \bar{a}_t corresponds to mean thickness.

Using the parameters defined in Fig. 9, the solar radiation reflected from a surface element dS_e depends on the location of dS_e on the globe, the time of year, the weather conditions (primarily the cloud cover), and the zenith angle of the sun. The total hemispherical radiation reflected from dS_e will be

$$q_{\text{reflected}} = \int_0^{2\pi} \int_0^{\pi/2} \bar{I}_s(\psi, \theta) \sin \theta \cos \theta \, d\theta d\psi \quad (40)$$

where \bar{I}_s is the intensity of the reflected solar radiation and θ and ψ are the zenith and azimuth angles of measurement, respectively. Since the intensity of radiation reflected from the earth-atmosphere system depends on θ , ψ , and ζ (the instantaneous zenith angle of the sun), ρ^1 , the instantaneous bidirectional reflectance of the area element dS_e at longitude λ_1 and latitude ϕ_1 can be defined as

$$\rho^1(\theta, \psi, \zeta^1, \lambda_1, \phi_1) = \frac{\bar{I}_s(\lambda_1, \phi_1)}{\cos \zeta^1 I_s^+} \quad (41)$$

where I_s^+ is the instantaneous direct intensity of the direct solar radiation incident on dS_e .

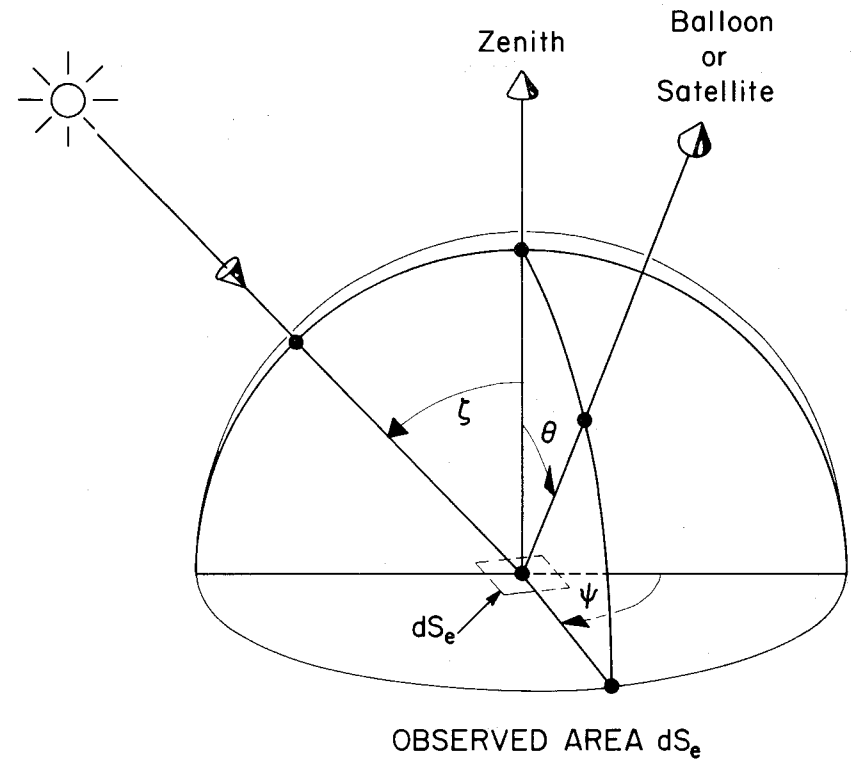


Fig. 9. Satellite- or balloon-to-earth geometric configuration.

The hemispherical directional reflectance $r(\zeta)$ is the ratio of the total reflected solar radiation (as would be received by a black hemisphere placed over dS_e) to the incoming solar radiation. It depends only on the zenith angle ζ and the time of year. From airplane and balloon measurements Raschke prepared diagrams relating the ratio between the directional hemispherical reflectance $r(\zeta)$ and the bidirectional reflectance ($\rho^1 = \rho/\pi$) at various azimuth angles within relatively narrow ranges of the zenith angle. Figure 10 shows one of these diagrams in which isolines of $x = r/\rho$ are drawn as functions of θ and ψ for a range of solar zenith angles between 60° and 80° . With the aid of these intermediate approximations, Raschke calculated the hemispherical directional reflectance from the Nimbus II data and presented his results as maps of the average albedo of the earth-atmosphere system during a two-week period (62). Figure 11 shows such a map for the northern hemisphere during the period 16-28 July 1966. The albedo varies from 20 to 30% over coastal parts of the North American continent to 80% over Greenland.

In addition to the albedo maps, Raschke also presented a correlation of available data showing the variation of the directional hemispherical

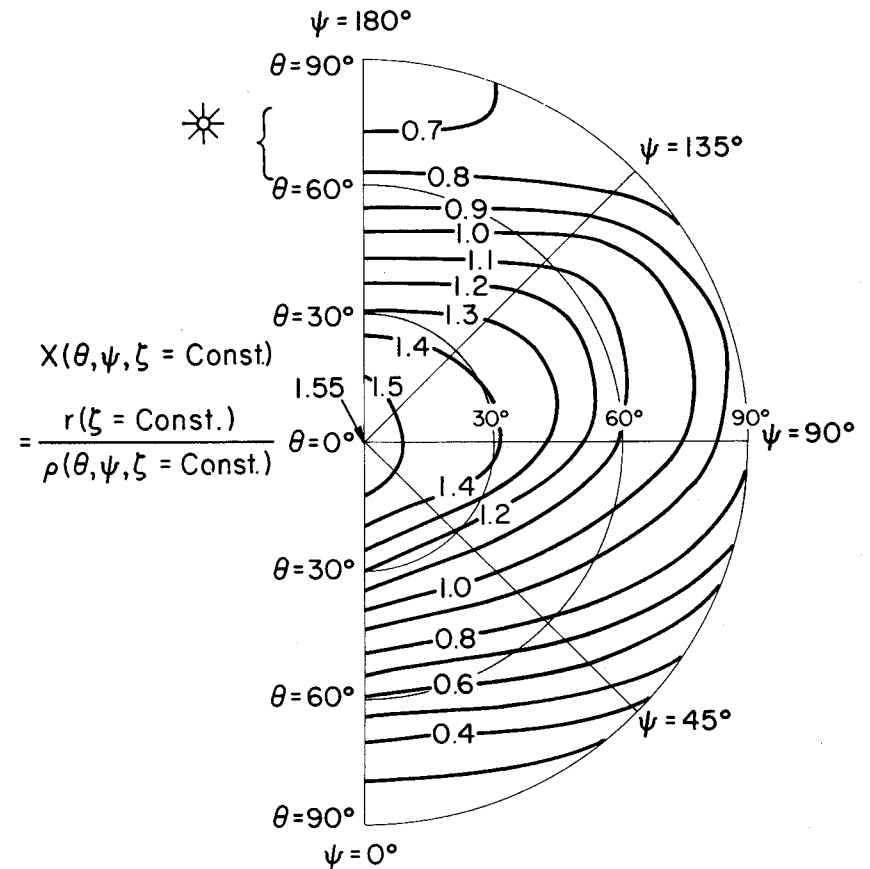


Fig. 10. Variation of directional solar reflectance with zenith angle ($60^\circ < \zeta \leq 80^\circ$).

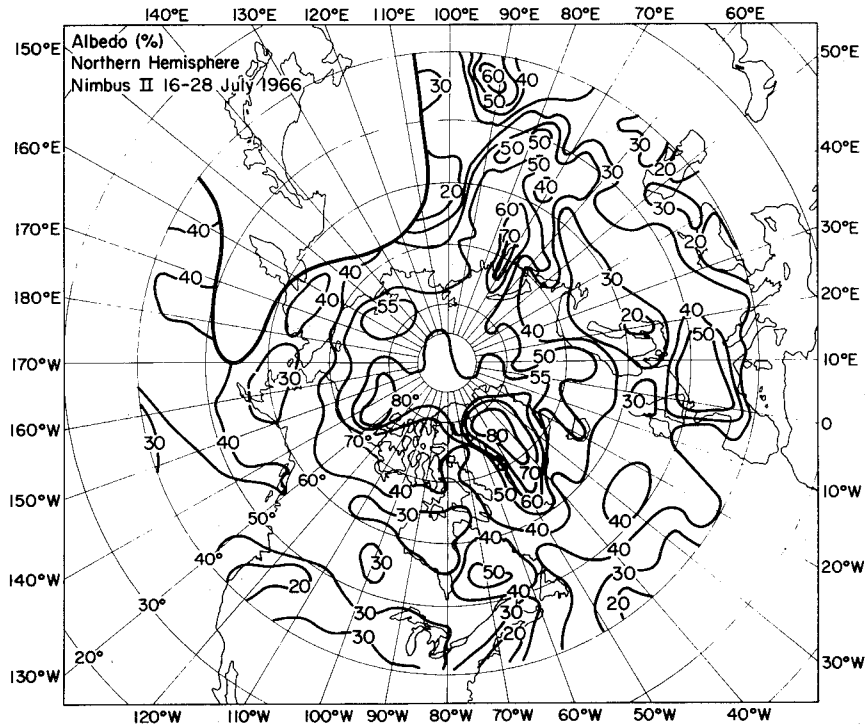


Fig. 11. Albedo map for the northern hemisphere during the period 16-28 July 1966.

reflectance with zenith angle (Fig. 12) and the ratio between the directional hemispherical reflectance and the bidirectional reflectance at various azimuth angles for snow, stratocumulus clouds, and cloudless ocean areas. With the aid of these diagrams one can make predictions of the reflection at altitudes above 18 km (60,000 ft). Such predictions are quite accurate except when there are changes in cloud cover. For engineering design it is usually satisfactory, however, to use Eq. (37) in combination with the graph in Fig. 12 relating the average hemispherical reflectance to the zenith angle, which can be calculated, using Eqs. (25) and (27) in a time-coordinate system related to a balloon flight.

I. INFRARED RADIATION FROM THE EARTH AND THE ATMOSPHERE [q_b in Eq. (2)]

The contribution to the total heat load on a balloon by the radiation from the earth and the atmosphere is an important variable in the energy balance formulated by Eq. (2). Unfortunately, the quantitative prediction of this portion of the total heat load is subject to some uncertainty because it depends on several factors difficult to specify.

The infrared radiation from the earth and the atmosphere varies as the balloon ascends. Immediately after its launch, the balloon receives

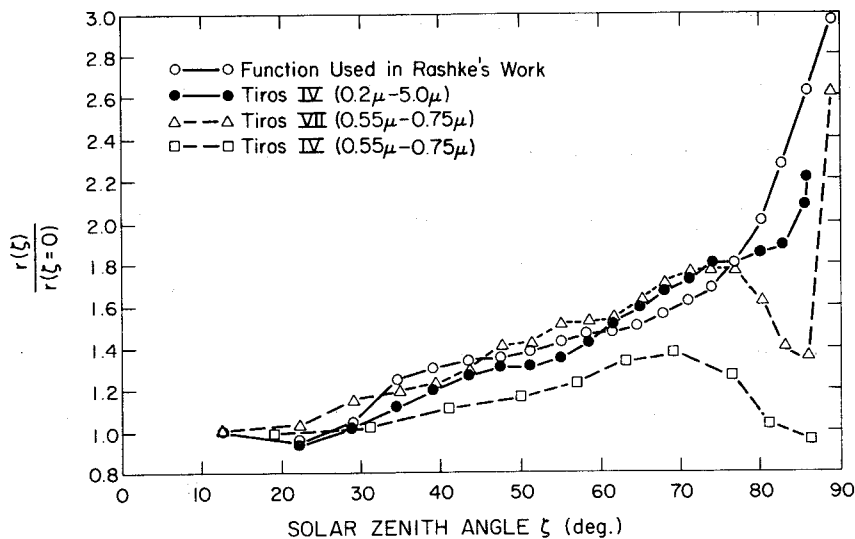


Fig. 12. Variation of directional hemispherical reflectance with zenith angle.

radiation from the atmosphere over its entire surface, but as it ascends the amount of air above the balloon continuously decreases. Eventually, only the lower part of the balloon receives radiation from the atmosphere. This infrared radiation is dependent on the altitude and cloud cover, and since the cloud cover often changes rapidly, a balloon can experience unexpected and unpredictable fluctuations in the radiation from the earth-atmosphere. The situation improves considerably, however, as the balloon ascends; once it has risen above the clouds and the weather to an altitude of about 18 km, the contribution of radiation from the earth and the atmosphere can be predicted with a considerable degree of accuracy.

Radiation from the earth and the atmosphere is of considerable interest to meteorologists. Comprehensive treatises on the radiation characteristics of the atmosphere have been published during the past decade by outstanding meteorologists such as Goody (71), Feigelson (59), Budyko (72), and Kondratyev (73). The radiation characteristics have been investigated and reduced to convenient graphs and charts by Simpson (74), Yamamoto (70), and Elsasser and Culbertson (75). Using Nimbus II data Raschke also prepared infrared radiation maps. Figure 13 shows the infrared radiation

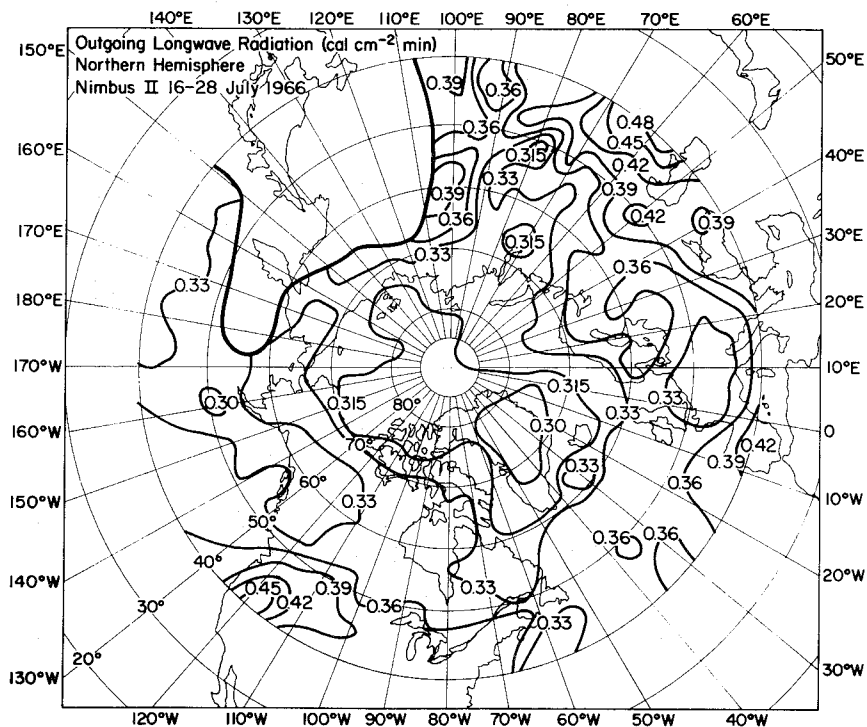


Fig. 13. Infrared radiation map for the Northern Hemisphere during the period 16-28 July 1966. Multiply radiation values by 697.35 to obtain radiation in W/m^2 .

emitted by the earth and the atmosphere into space over the northern hemisphere during the period 16-28 July 1966.

In connection with efforts to construct a general circulation model of the atmosphere, several researchers including Houghton (63), London (76), Manabe and Möller (77), and Davis (78) have studied theoretical aspects of atmospheric radiation, but most of them calculated the meridional distribution and seasonal variation of the radiation balance and not its global distribution. From a practical point of view, Simpson's simple model (74, 79) is still very useful for estimating radiation heat loads, although Budyko (72) presents more accurate heat balance calculations at the earth's surface. Neither of them, however, considers the radiation within the atmosphere. Recently, Katayama (80) has made valuable calculations of the radiation budget of the troposphere over the northern hemisphere, and Sasamori (81) has developed a method for calculating the upward and downward radiation flux in a cloudless atmosphere. Sasamori's calculations are based on empirical formulas for the spectral variations of the absorptances of water vapor, carbon dioxide, and ozone (the constituents of the atmosphere with absorption bands in the infrared range) and on the assumption

that the surface of the earth is perfectly black. A summary of his results is shown for various latitudes in Fig. 14, in which the upward and downward radiation fluxes are plotted as a function of altitude. The spectral characteristics of the radiation are not shown but can be calculated from the empirical relations in reference (81).

It should be noted that the atmosphere is almost transparent to wavelengths between 8 and 12 μ . Consequently, a balloon will receive such radiation directly from the earth. At longer and shorter wavelengths the atmospheric water vapor and carbon dioxide have strong absorption bands, and in those parts of the spectrum the infrared radiation received by a balloon is emitted by the atmosphere, usually at a temperature lower than that of the earth. Some balloon materials exhibit considerable variations in the monochromatic absorptance in the infrared, and to estimate reliably the infrared radiation absorbed by the skin, integrations over the spectrum between 6 and 100 μ , as shown by Eq. (20), are necessary (54, 82). For these integrations, simplified models of the variations in the monochromatic radiation of the atmosphere, such as those given in references (83) or (54), are quite satisfactory.

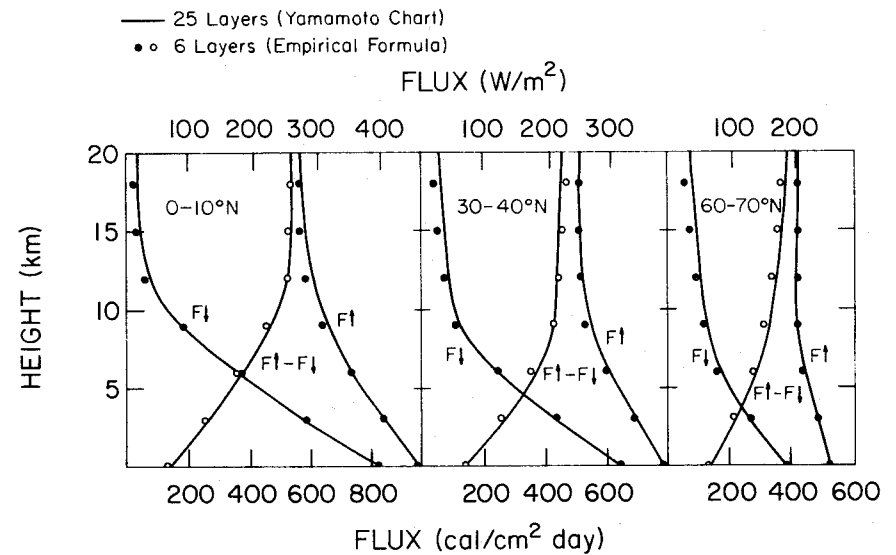


Fig. 14. Upward and downward radiation flux as a function of altitude.

In view of these complicated conditions it is not surprising that several approaches have been taken to calculate the radiation from the earth and its atmosphere which is absorbed by a balloon. Lally (3), dealing only with superpressure balloons, divided the incoming infrared radiation into four parts: from below, from above, and from two sides, each illuminating an area of $\pi D_g^2/4$. The radiation environment is then estimated using the following simplified assumptions:

1. Downward radiation.

- a. If clouds above: downward flux equals blackbody radiation from a source at the temperature of the cloud base.
- b. If clear above: balloon above 15 km (9 mi)-- 10 W/m^2 ($3.2 \text{ BTU/ft}^2 \text{ hr}$); balloon between 10-15 km (6-9 mi)-- 20 W/m^2 ($6.3 \text{ BTU/ft}^2 \text{ hr}$); balloon below 10 km (6 mi)-- 40 W/m^2 ($12.7 \text{ BTU/ft}^2 \text{ hr}$).

2. Upward radiation.

- a. If clouds below: upward flux equals blackbody radiation from a source at the temperature of the cloud tops.

- b. If clear below: upward radiation will vary from 150 W/m^2 to 450 W/m^2 (48 to $144 \text{ BTU/ft}^2 \text{ hr}$) depending on altitude and air mass. Table 9 provides estimates of the effect of upward flux for several altitudes and air masses.

3. The radiation from the sides can be estimated as equal to blackbody radiation from a source at the temperature of the air at balloon altitude.

London (82) considered only the upward and downward fluxes. The advantage of this approach is that theoretical analyses and measurements of atmospheric radiation usually provide the upward and downward, but not horizontal, radiation fluxes. An instrument which has been widely used at NOAA to obtain measurements of the upward and downward atmospheric radiation was developed by Suomi and Kuhn (84). This instrument (Fig. 15) is basically a double-faced, hemispherical bolometer with broad-response, blackened sensing surfaces shielded from convection currents by thin membranes of polyethylene. The upward and downward radiation flux can be calculated from the temperatures, measured with tiny thermistors, of the sensor surfaces and the air. A flight test of this instrument, also called an "economical

Table 9
Radiation Environment for Superpressure Balloons¹

Altitude	Season ²	Air temperature (°C)	Av. nighttime clear sky balloon super temperature		Mylar balloon (α ₀ = 0.05)		
			Mylar balloon (°C)	Metallized top balloon (°C)	Temperature increase per W/m ² increment (°C)	Maximum added solar flux (W/m ²)	Maximum daytime temperature increase (°C)
3 km (700 mb)	Winter	-10	0	5	0.24	35	8
	Summer	5	-3	2	0.21	35	8
	Tropic	10	-5	0	0.20	35	8
6 km (500 mb)	Winter	-30	0	8	0.30	35	10
	Summer	-15	-5	5	0.27	35	9
	Tropic	-5	-10	2	0.25	35	9
9 km (300 mb)	Winter	-50	5	15	0.36	40	14
	Summer	-35	-5	7	0.34	40	13
	Tropic	-30	-10	2	0.34	40	13
12 km (200 mb)	Winter	-55	10	20	0.36	45	16
	Summer	-55	10	20	0.36	45	16
	Tropic	-50	5	15	0.36	45	17
16 km (100 mb)	Winter	-60	5	5	0.42	45	19
	Summer	-65	10	10	0.42	45	21
	Tropic	-80	15	15	0.47	45	21
24 km (30 mb)	Winter	-55	-5	-5	0.45	45	20
	Summer	-55	-5	-5	0.45	45	20
	Tropic	-55	-5	-5	0.45	45	20

¹ Adapted from Lally (3).

² Winter and summer seasons in temperate latitudes and all seasons in the tropics.

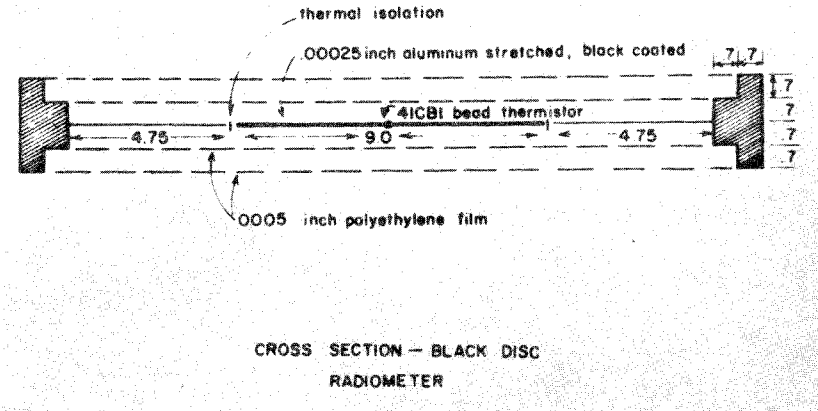
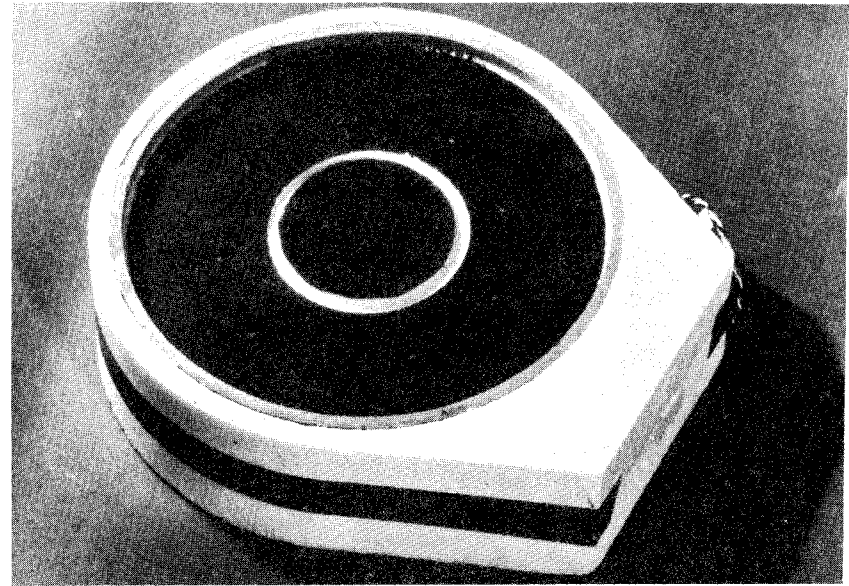


Fig. 15. Suomi-Kuhn flat plate radiometer.

net-radiometer," is reported in reference (85). Data taken during several balloon flights have been published [e.g., (85-89)], but data from other flights are still being processed at NOAA (48). Whenever the spectra of the upward and downward infrared radiation are known, the rate at which infrared radiation is transferred to the balloon skin can be calculated from the relationship

$$q_B = (\pi D_g^2/2) \int_4^{100} [\bar{a}_{\text{eff}}(\lambda) G_{i,\text{up}}(\lambda) + \bar{a}_{\text{eff}}(\lambda) G_{i,\text{down}}(\lambda)] d\lambda \quad (42)$$

where $\bar{a}_{\text{eff}}(\lambda)$ is the effective monochromatic absorptance of the balloon film, which can be approximated from Eq. (34) by

$$a(\lambda) \left[1 + \frac{1 - a(\lambda) - r(\lambda)}{1 - r(\lambda)} \right]$$

and where $G_{i,\text{up}}(\lambda)$ is the upward monochromatic radiation as measured by a hemispherical flat surface radiometer, and $G_{i,\text{down}}(\lambda)$ is the downward monochromatic radiation, measured likewise.

Unfortunately, only the total average radiation over all wavelengths is usually measured. Typical data from meteorological measurements are illustrated in the graphs of Figs. 16, 17, and 18. In all three figures

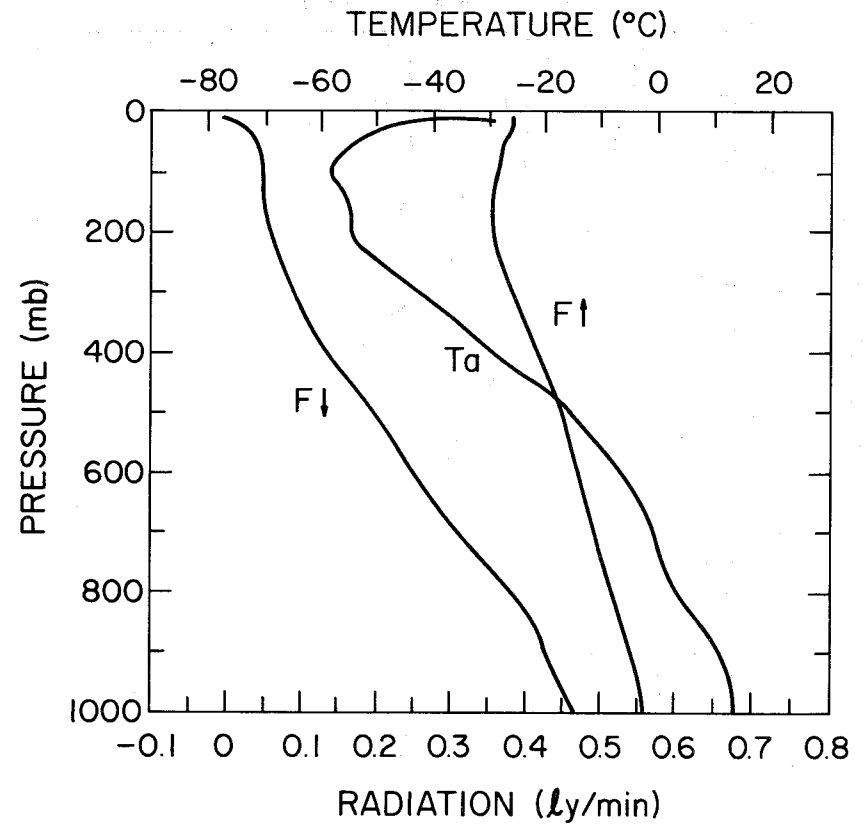


Fig. 16. Radiation environment at Green Bay, Wisconsin, in the summer.

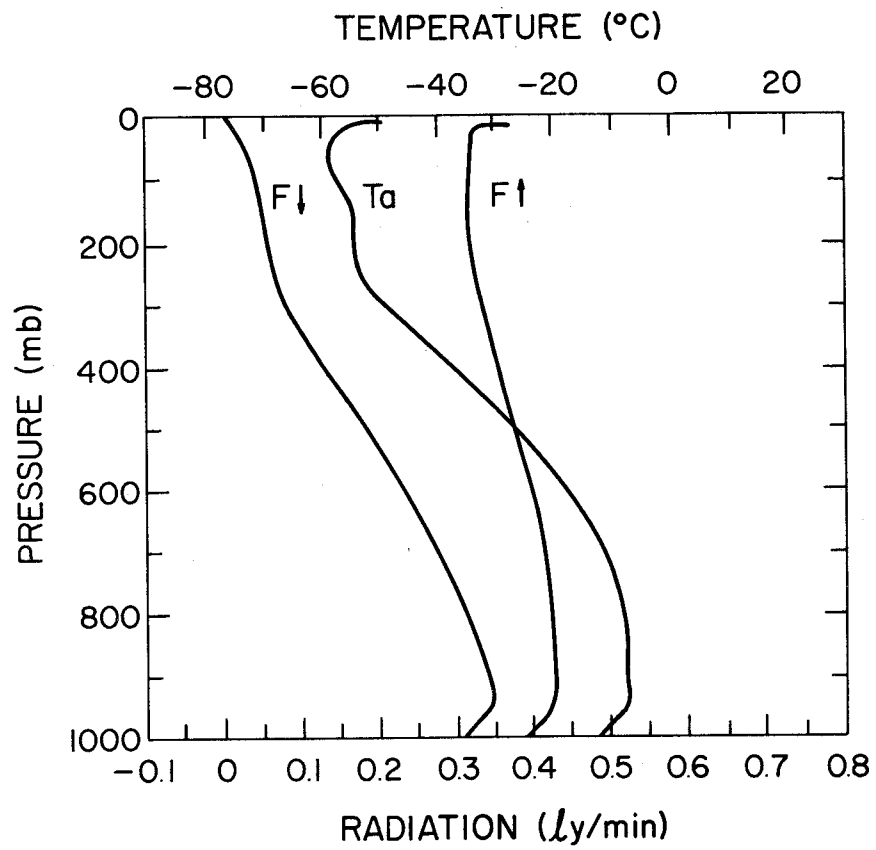


Fig. 17. Radiation environment at Green Bay, Wisconsin, in the winter.

To obtain W/m^2 multiply ly/min by 697.35.

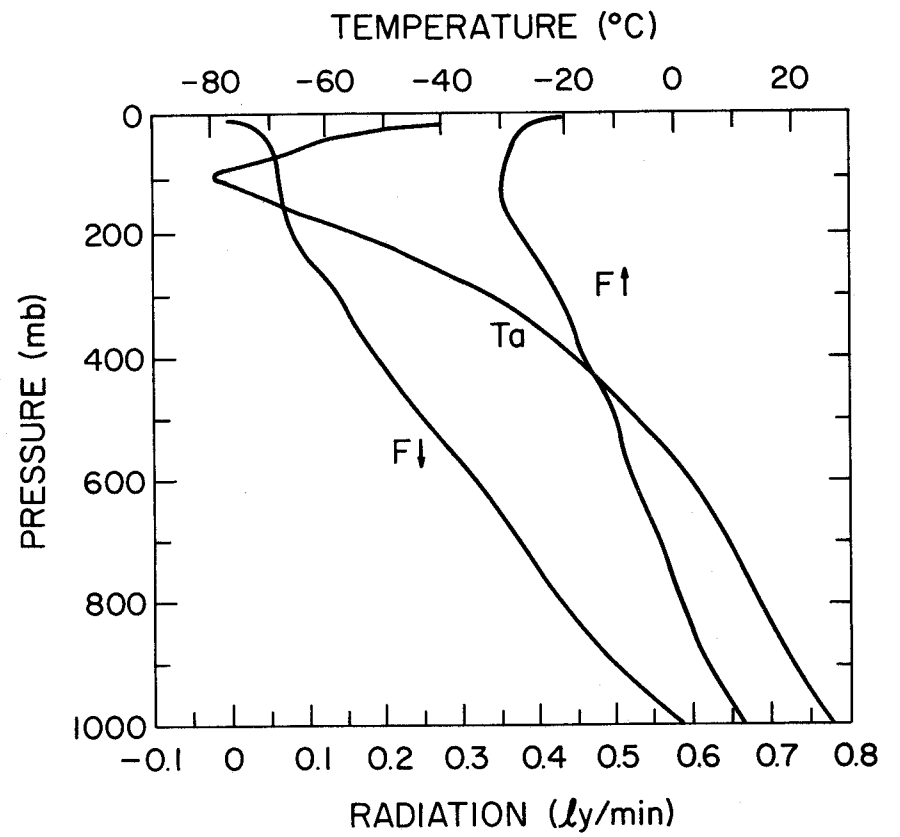


Fig. 18. Radiation environment at a desert island, $2^{\circ}S$.

the air temperature and the total radiation on a horizontal surface from above and below are plotted as a function of altitude. Also shown are the net radiation flux (i.e., the difference between the radiation from above and from below) and the atmospheric cooling rate--quantities which are of meteorological interest only.

Figures 16 and 17 show the average radiation environment at Green Bay, Wisconsin, during summer and winter, and Fig. 18 shows the radiation environment of a desert island at 2°S. The downward radiation increases markedly with decreasing altitude, whereas the upward radiation decreases slowly with increase in altitude. In winter, when the atmospheric temperature variation with altitude is less than in summer, the changes in radiation are also smaller. Near the equator where variation in the atmospheric temperature with altitude is even larger than at Green Bay during the summer, the changes in the infrared radiation environment are also more pronounced. It should be noted that the infrared radiation graphs in Figs. 16, 17, and 18 represent averages of the total hemispherical radiation over all wavelengths. When the spectrum is not known, an average absorptance must be estimated to calculate the rate of absorption of infrared radiation from

Eq. (42). There will, of course, always be variations with changes in weather conditions, and the amount of radiation absorbed by a balloon skin or an instrument package will depend not only on the spectrum of the incoming radiation but also on the variation with wavelength, as yet not known, of the directional hemispherical absorptance of the receiving surface.

A third method of estimating the infrared heat load has been proposed by Germeles (13). It uses the measurements obtained by a "black-ball" radiometer (Fig. 19), an instrument widely used by meteorologists to measure the radiation in the atmosphere. The instrument, developed by Gergen (90), consists essentially of a small balsa dodecahedron painted black and surrounded by a convection shield. A thermistor imbedded in the center is used to measure T_r , the "equilibrium radiation temperature" of the device. From this measurement, the radiation is then calculated from the relationship (90)

$$G_i = \sigma T_r^4 \quad (43)$$

Measurements with this device are carried out during the night so the detector is not affected by the sun. It is claimed that the temperature recorded by the black ball is representative of the total radiation field

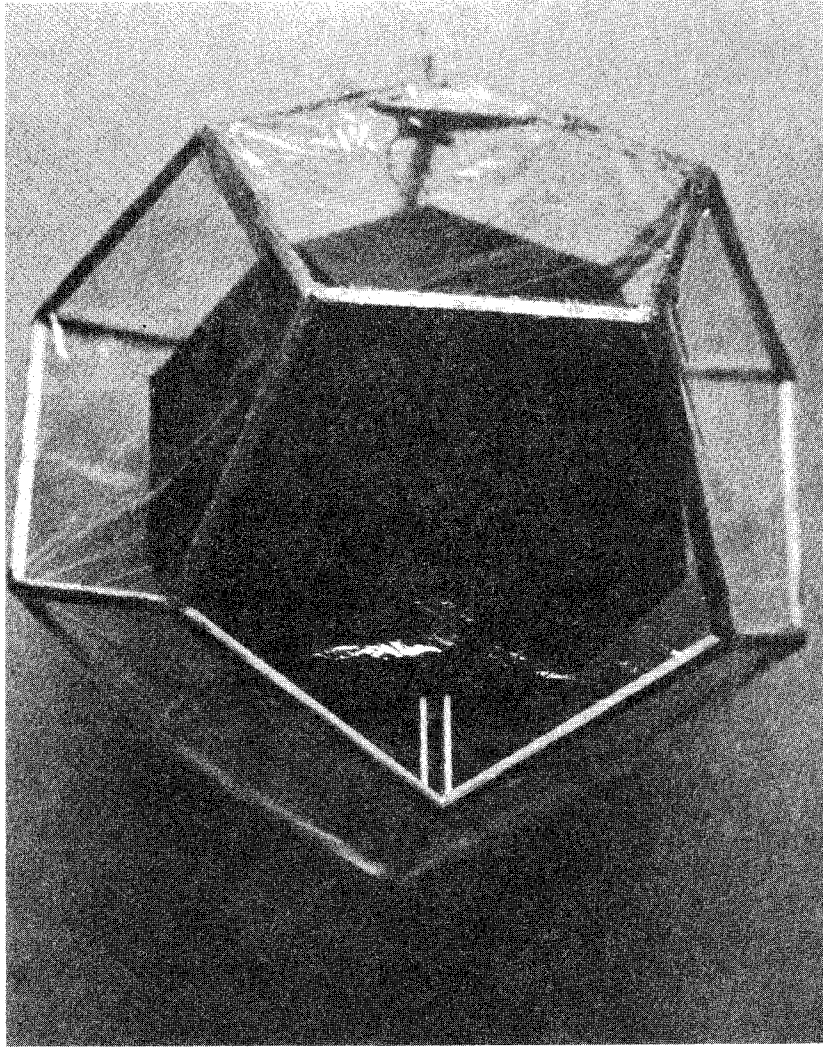


Fig. 19. Gergen "Black-Ball" radiometer.

to which it is exposed. Black-ball equilibrium temperatures have been recorded as a function of altitude at different geographic locations, and it has been observed that large changes in the black-ball temperature profile occur within days at the same location. The results of these measurements support the following approximate, simple, general rule. At ground level, the radiation temperature is usually less than the air temperature, and the deviation is about 5°C (10°F). The equivalent radiation temperature decreases almost linearly with altitude up to the tropopause, where it becomes about 75% of its ground value. From there to higher altitudes the radiation temperature remains approximately constant, indicating that most of the radiation is received from below.

Germeles (13) used data obtained by means of a black-ball radiometer to calculate the infrared radiation on a balloon. He assumed that the black-ball temperature profile is known. Since the black ball has a shape similar to that of a balloon, the radiation absorbed by the balloon can be obtained from the relationship

$$q_b = 4.83 \bar{a}_{\text{eff}} \sigma \frac{V^{2/3}}{g} T_r^4 \quad (44)$$

It is apparent that the estimates of radiation emitted by the atmosphere and the earth require considerable improvement and elaboration. It may well be that such improvement has not been made because the properties of balloon fabrics are not precisely known, so that even if the heat load could be calculated with considerably higher accuracy, the uncertainty in the absorption load would remain.

At this juncture, the following is recommended: (a) use black-ball radiometer data, when available, or (b) calculate the heat load from above and below, making use of measurements obtained with an instrument such as the Suomi-Kuhn radiometer, and calculate the actual amount of radiation with a simple model of the atmosphere such as that proposed by Simpson (74), which considers only water and carbon dioxide absorption. This approach, described in reference (53) for use in spacecraft design, is also directly applicable to calculations on balloon and instrument packages. For calculations of heat loads in areas where the Suomi-Kuhn instrument has not been flown, the Nimbus II data may be used. They are similar to albedo data in that they include the total radiation flux emitted by the earth's atmosphere. This approach, of course, will only be useful for altitudes

above 18 km since satellite data are taken far outside the atmosphere.

An aid to further improvement of the calculation of the heat load would be to fly several balloons instrumented to measure gas temperature, the radiation heat load, and air temperature simultaneously. Although such measurements have not been made, they are feasible with existing instrumentation.

J. GAS EXPANSION AND LIFT AND LOAD ADJUSTMENTS

The variation of the gas volume in the balloon with time is

$$\frac{dV}{dt} = \frac{d}{dt} \left(\frac{Rm T}{M P} \right) = \frac{Rm}{M P} \frac{dT}{dt} + \frac{RT}{M P} \frac{dm}{dt} - \frac{Rm T}{M P^2} \frac{dP}{dt} \quad (45)$$

If the relation between atmospheric pressure and altitude from Eq. (5), Section XI, is used and superpressure is neglected, the above equation can be written in the form

$$\frac{dV}{dt} = \frac{R}{M P a} \left(m \frac{dT}{dt} + T \frac{dm}{dt} - \frac{gm T M}{RT a} \frac{dz}{dt} \right) \quad (46)$$

As mentioned in Section II, the lift of a balloon system can be reduced by exhausting helium automatically through the gas expulsion duct when float altitude is reached, or by valving to maintain float altitude, to

reduce the rate of ascent, or to cause the balloon to descend. If \dot{E}_d is the volumetric gas flow rate through the expulsion duct (required to stabilize the balloon at ceiling) and \dot{E}_v is the flow rate through the exhaust valve, the net change in balloon mass due to loss of gas is

$$\frac{dm}{dt} = \rho_g \dot{E}_d + \rho_{gv} \dot{E}_v \quad (47)$$

The mass of the balloon system can be reduced by dropping ballast or part of the payload. This change in mass of the balloon system during a time increment $\Delta t = t_2 - t_1$ is

$$\int_{t_1}^{t_2} \frac{dm_G}{dt} = \int_{t_1}^{t_2} \frac{dm_b}{dt} + \Delta m_\ell \quad (48)$$

where Δm_ℓ represents the amount of payload mass or increments of ballast which may be dropped during the time interval $(t_2 - t_1)$.

K. A VERTICAL MOTION MODEL

The vertical component of Eq. (33) of Section II, the energy balance equations of this section, equations from Section XI which describe the atmosphere, and miscellaneous equations for calculating parameters such as Reynolds numbers may be combined into a set of equations which constitute

a mathematical model of the vertical motion of a balloon in the atmosphere.

One such set is listed here with a minimum of explanatory material, but a reference to the source of each equation is given.

$$-g \left[m_G + m_g \left(1 - \frac{M_a p_a T_g}{M_g p_g T_a} \right) \right] - \frac{1}{2} \rho_a C_D A_D \left| \frac{dz}{dt} \right| \frac{dz}{dt} = \quad \text{II, Eq. (33)}$$

$$\left[m_G + m_g \left(1 + C_B \frac{M_a p_a T_g}{M_g p_g T_a} \right) \right] \frac{d^2 z}{dt^2}$$

$$\frac{d}{dt} (C_V \bar{T})_g = q_1 + \frac{RT_g}{M_g} \frac{dm_g}{dt} - p_a \frac{dV_g}{dt} + (C_V T)_g \frac{dm_g}{dt} \quad \text{III, Eq. (1)}$$

$$\frac{d}{dt} \iint_{S_f} C_f \rho_f t_f T_f dS_f = C_f m_f \frac{dT_f}{dt} = q_2 + q_3 + q_4 - q_5 - q_1 \quad \text{III, Eq. (2)}$$

$$q_1 = 0.628 V_g^{2/3} k_g (\bar{T}_f - \bar{T}_g) \left[\frac{\rho_g^2 g (\bar{T}_f - \bar{T}_g)}{\mu_g^2 T_g} \text{Pr}_g \right]^{1/3} \quad \text{III, Eq. (17)}$$

$$q_2 = q_{2,direct} + q_{2,reflected}$$

$$q_{2,direct} = 1.21 G(m) V_g^{2/3} \bar{a}_s \left(1 + \frac{\bar{T}_s}{1 - \bar{T}_s} \right) \quad \text{III, Eq. (35)}$$

$$q_{2,reflected} = 1.21 V_g^{2/3} \bar{a}_s G_s \left[2\bar{r}_{s,a} \left(1 - \sqrt{z/D_e} \right) \cos \zeta \right] \quad \text{III, Eq. (37)}$$

$$q_3 = 4.83 \bar{a}_{eff} \sigma V_g^{2/3} T_r^4 \quad \text{III, Eq. (44)}$$

$$q_4 = 7.79 V_g^{1/3} k_a (T_a - \bar{T}_f) \left[1 + 0.322 \left(\frac{\rho_a^2 g (|T_a - \bar{T}_f|) V_g}{T_a \mu_a^2} \right)^{1/2} \right] \quad \text{III, Eq. (7)}$$

$$\text{if } Re_{\ell}' \leq 1.697 (Gr_{\ell}')^{\frac{1}{2}} \quad \text{III.C.}$$

$$\text{or } q_4 = 3.9 V_g^{1/3} k_a (T_a - \bar{T}_f) \left[2 + 0.472 V_g^{0.183} \left(\rho_a \frac{dz/dt}{\mu_a} \right)^{0.55} \right]$$

III,Eq. (5)

$$\text{if } Re_{\ell}' > 1.697 (Gr_{\ell}')^{\frac{1}{2}} \quad \text{III.C.}$$

$$q_5 = 4.83 \bar{e}_{\text{eff}} V_g^{2/3} \sigma \bar{T}_f^2$$

III,Eq. (24)

$$m_G = m_B + m_{\ell} + m_b$$

II.D.

$$\int_{t_1}^t \frac{dm_G}{dt} = \int_{t_1}^t \frac{dm_b}{dt} + \Delta m_{\ell}$$

III,Eq. (48)

$$m_g = \frac{m_G (1 + f')}{\left(\frac{M_a}{M_g} - 1 \right)}$$

II,Eq. (36)

$$\frac{dm_g}{dt} = \rho_{g,d} \left(\frac{dv_g}{dt} \right)_d + \rho_{g,v} \left(\frac{dv_g}{dt} \right)_v$$

III,Eq. (47)

$$V_g = M_g / \rho_g$$

$$\rho = \frac{PM}{RT} \text{ for either gas or air}$$

II,Eq. (8)

Gas will flow from a valve at the top of a balloon at a rate

$$\left(\frac{dv_g}{dt} \right)_v = -1.58 CA \sqrt{\frac{g \rho_a - \rho_g}{\rho_g} \left(\frac{m_g}{\rho_g} \right)^{1/3}}$$

XII,Eq. (E-5)

where C is a dimensionless coefficient which must be determined empirically

for each valve and A is the nominal area of the valve.

$$\frac{dv_g}{dt} = \frac{R}{M_g p_a} m_g \frac{dT}{dt} + T_g \frac{dm_g}{dt} + \frac{gm_g T M}{RT_a} \frac{dz}{dt} \quad \text{III,Eq. (46)}$$

If $V_g \geq V_B$ (the nominal volume of the loaded balloon at float),

$$\left(\frac{dv_g}{dt} \right)_d = \frac{dv_g}{dt} - \left(\frac{dv_g}{dt} \right)_v$$

where the subscripts d and v indicate loss of gas through the ducts and

valves, respectively.

$$\bar{G} = \bar{G}_{s,m} [\cos (A_2 - a_2) \sin \zeta \sin i + \cos \zeta \cos i] \quad \text{III,Eq. (26)}$$

$$\zeta = \cos^{-1} [\sin \lambda_1 \sin \delta_s + \cos \lambda_1 \cos \delta_s \cos h] \quad \text{III,Eq. (25)}$$

$$h = \text{CHA (at launch)} - \varphi_1 + [t(\text{sec})/240] \quad \text{III.G.}$$

$$\bar{G}_{s,m} = 0.5 \bar{G}_s (e^{-0.55m} + e^{-0.095m}) \quad \text{III,Eq. (28)}$$

$$m(o, \zeta) = [1229 + (614 \cos \zeta)^2]^{\frac{1}{2}} - 614 \cos \zeta \quad \text{III,Eq. (29)}$$

and

$$m(z, \zeta) = m(o, \zeta) [p_a(z)/p_a(o)] \quad \text{III,Eq. (30)}$$

for $0 < \zeta < 90^\circ$

$$m(z, \zeta) \approx 70$$

$$\text{for } z > 20 \text{ km and } 90^\circ < \zeta \leq 90^\circ + \cos^{-1} \left(\frac{D_{\text{earth}}}{D_{\text{earth}} + 2z} \right)$$

$$G_s = 1395 \text{ W/m}^2 = 442 \text{ BTU/ft}^2 \text{ hr}$$

$$\frac{dz}{dt} = - \frac{1}{g \rho_a} \frac{dp_a}{dt} \quad \text{XI, Eq. (1)}$$

$$\ln \frac{p_{a,2}}{p_{a,1}} = - \frac{gM_a}{R} \int_{z_1}^{z_2} \frac{dz}{T_a} \quad \text{XI, Eq. (5)}$$

In a stratum in which the lapse rate $L' (= -dT_a/dz)$ is constant but not zero

$$T_{a,2} = T_{a,1} + L' (z_2 - z_1) \quad \text{XI, Eq. (6)}$$

$$\text{and } \frac{p_{a,1}}{p_{a,2}} = \left(\frac{T_{a,2}}{T_{a,1}} \right)^{\frac{gM_a}{RL'}} \quad \text{and } \frac{\rho_{a,1}}{\rho_{a,2}} = \left(\frac{T_{a,2}}{T_{a,1}} \right)^{\frac{gM_a + RL'}{RL'}} \quad \text{XI, Eqs. (15) and (16)}$$

if $L' = 0$

$$\frac{p_{a,1}}{p_{a,2}} = \frac{\rho_{a,1}}{\rho_{a,2}} = e^{\frac{gM_a}{RT_{a,1}} (z_2 - z_1)} \quad \text{XI, Eqs. (9) and (18)}$$

$$A_D = 1.209 \sqrt[3]{\frac{V}{g}} \quad (\text{Area of great circle of a sphere})$$

$$C_D = 0.47 + \frac{24}{\text{Re} + 0.01} \quad \text{for } \text{Re} \leq 4.5 \times 10^5 \quad \text{II, Eq. (30)}$$

$$\text{or } C_D = 0.3 \quad \text{for } \text{Re} > 4.5 \times 10^5$$

III.G.

are simple approximations for drag coefficient.

$$\text{Re} = \frac{\rho_a D_B |dz/dt|}{\mu_a} \quad \text{II, Eq. (29)}$$

$$\mu_a = \frac{1.458 \times 10^{-6} T_a^{1.5}}{T_a + 110.4} \quad \text{kg/m sec; } T_a \text{ in } ^\circ\text{K} \quad \text{XII, (Eq. J-4)}$$

$$\text{or } \mu_a = \frac{7.30248 \times 10^{-7} T_a^{1.5}}{T_a + 198.72} \quad \text{lbm/ft sec; } T_a \text{ in } ^\circ\text{R} \quad \text{XII, (Eq. J-4)}$$

$$\mu (\text{helium}) = 1.895 \times 10^{-5} \left(\frac{T_g}{273.15} \right)^{0.647} \quad \text{kg/m sec; } T_g \text{ in } ^\circ\text{K} \quad \text{XII, (Eq. J-7)}$$

$$\mu (\text{helium}) = 1.273 \times 10^{-5} \left(\frac{T_g}{491.67} \right)^{0.647} \quad \text{lbm/ft sec; } T_g \text{ in } ^\circ\text{R} \quad \text{XII, (Eq. J-7)}$$

$$\mu (\text{hydrogen}) = 386.9 \times 10^{-5} \left(\frac{T_g}{273.15} \right)^{1.5} \frac{T_g + 650.4}{(T_g + 19.6)(T_g + 1176)}$$

$$\text{kg/m sec; } T_g \text{ in } ^\circ\text{K} \quad \text{XII, (Eq. J-6)}$$

$$\mu (\text{hydrogen}) = 467.2 \times 10^{-5} \left(\frac{T_g}{491.67} \right)^{1.5} \frac{T_g + 1170.7}{(T_g + 35.3)(T_g + 2116.8)}$$

$$\text{lbm/ft sec; } T_g \text{ in } ^\circ\text{R} \quad \text{XII, (Eq. J-6)}$$

$$\text{Gr}_L = \frac{\rho^3 g (T_f - T) L^3}{T \mu^2} \quad \text{Kreith (5)}$$

where T is the temperature of the air or gas at a distance sufficiently far from the film surface that it is not directly influenced by the surface. The length L must be a length appropriate to the correlating equation in which Gr is used; e.g., in Eq. (8), Section III.C. $L = \ell' = \pi D_g/2$ for a sphere or long cylinder while in Eq. (15), $L = D_g$.

$$Pr = \frac{C_p \mu}{k} \quad \text{XII, (Eq. J-8)}$$

Also Pr may be approximated by

$$Pr = a + b \times 10^{-4} T \quad \text{XII, (Eq. J-9)}$$

where a and b are functions of the gas and T is gas temperature in $^{\circ}K$.

See Section XII for values of a and b .

$$k = k_0 \left(\frac{T}{T_0} \right)^n \quad \text{XII, (Eq. J-2)}$$

See Section XII for values of k_0 and n .

$$C_p = R [a + b \times 10^{-2} T + c \times 10^{-6} T^2] \quad \text{XII, (Eq. J-1)}$$

See Section XII for values of R , a , b , and c .

L. EXPERIMENTAL RESULTS

Coordinated measurements of the thermal and aerodynamic characteristics of large balloons have been published for two flights conducted with

7000m³ (250,000 ft³) balloons designed to float at 24 km (80,000 ft)

(91, 92). The skins of both balloons were 1.5 mil polyethylene. During both flights the air temperature, the altitude, and the balloon helium temperature were measured continuously. During one flight the temperature of the balloon fabric was also measured at two locations, and the black-ball radiation temperature 90 m (300 ft) below the balloon was determined. These flights were conducted by NCAR from its launch site in Page, Arizona, in October 1966 and January 1968. During the first flight, two of the five thermistors inside the balloon failed during launch, and the system measuring the air temperature malfunctioned after the balloon reached its ceiling.

The thermistors used to measure the helium temperature inside the balloon have a diameter of 0.023 cm (9 mils), roughly 20 times the mean free path of helium at its pressure at 24 km. Such small thermistors were used to maximize the ratio q_c/q_r of heat loss by conduction or convection to heat loss by radiation (93). As shown by Ney et al. (94), for a spherical sensor this ratio is

$$q_c/q_r = 2 k_g / eD \sigma T^3$$

The error caused by incident radiation and self heating is given by the

equation

$$T - T_g = (D_a \bar{a}_i G/k_g) + (P/2\pi Dk_g)$$

where T is sensor temperature; T_g , the true gas temperature; D , the sensor diameter; k_g , the gas conductivity; \bar{a}_i , the absorptance for incident radiation; G , the incident radiation flux per unit surface area; and P , the internal power dissipation. The estimated temperature error in the tests is less than $0.1C^\circ$.

Uncertainties in the data reduction resulted from the difference between the value of the air temperature measured by a standard radiosonde and the value indicated by the thermistor suspended 90 m below the payload. Approximately 1.5 hr after launch, at an altitude of about 24 km (65,000 ft), the air temperature indicated by the radiosonde was $22^\circ C$ higher than the air temperature indicated by the thermistor.

The internal balloon temperatures measured during the flight were compared with the temperature computed using equations very similar to those representing the model presented in this section. The results of the comparison between the computed and measured temperatures are shown in Fig. 20 for the first flight. The relationship between the temperature of each

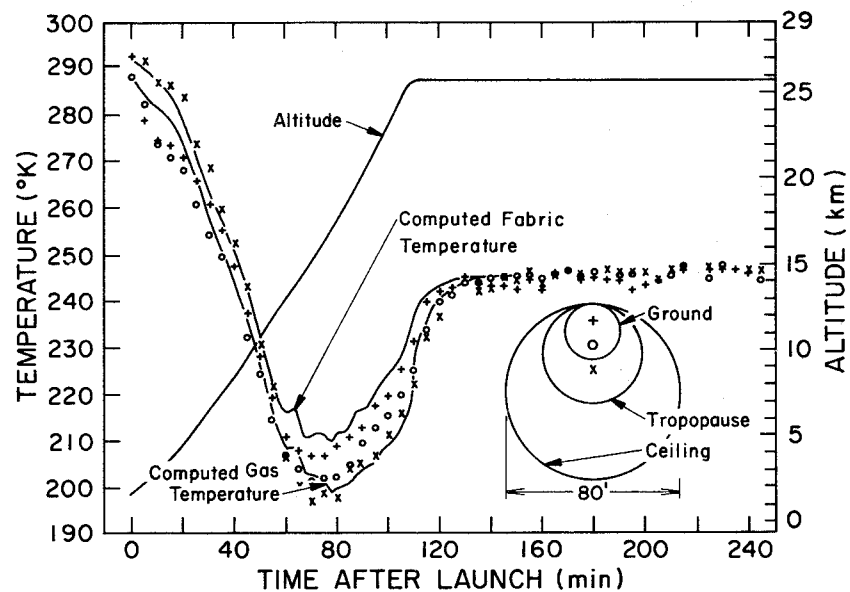


Fig. 20. Experimental results of balloon flight, October 1966; comparison of predicted and measured gas temperatures.

thermistor and the average temperature of the gas and fabric depends on the position of the thermistor in the balloon. In Fig. 20 the rough position of each thermistor during the flight is indicated on the sketch in the lower right-hand corner, in which the balloon is approximated by a sphere. The diameter of the balloon was about 8, 14, and 24 m at ground, tropopause, and ceiling, respectively. The lowest thermistor was buried in the loose fabric at ground level and became exposed to the helium only after the tropopause was reached.

An examination of the experimental data shows that there was considerable temperature stratification in the helium, but the averaged gas temperature followed closely the prediction of the idealized model. The computed gas temperature initially followed the upper thermistor, but just before reaching the tropopause it approached more closely the temperature record of the middle thermistor. At float altitude, the thermistor in the center of the balloon agreed most closely with the average temperature prediction. After about an hour, the temperature of the top thermistor followed closely the temperature predicted for the fabric of the balloon.

On the basis of the scant evidence available so far, it appears that the basic method outlined in this section can, with some additional measurements, be refined to the point where it can be used with confidence to predict the performance of high altitude balloons and to design instrument packages. The current rapid pace of research in heat transfer, meteorology, and atmospheric physics insures that those areas where knowledge is insufficient will be studied and the information needed for thermal design will become available in the near future. However, close cooperation between researcher and designer will be necessary to interpret and relate the results of research so they will be accessible to the people designing and operating scientific balloons.

REFERENCES

- (1) Gibbs-Smith, C. H., 1948: Ballooning. Penguin Books, London, 40 pp.
- (2) Dollfus, C., 1961: The Orion Book of Balloons. The Orion Press, New York, N.Y., 108 pp.
- (3) Lally, V. E., 1967: Superpressure Balloons for Horizontal Soundings of the Atmosphere. NCAR Technical Note TN-28, Boulder, Colo., 25 pp.
- (4) Kreith, F. and J. C. Warren, 1970) Thermal Analysis of Balloonborne Instrument Packages. NCAR Technical Note TN-45, Boulder, Colo., 25 pp.
- (5) Kreith, F., 1965: Principles of Heat Transfer, 2nd ed., International Textbook Co., Scranton, Pa., 620 pp.
- (6) Yuge, T., 1960: Experiments on heat transfer from spheres including combined natural and forced convection. J. Heat Trans. C-82, 214-220.
- (7) Vliet, G. C. and G. Leppert, 1961: Forced convection heat transfer from an isothermal sphere to water. J. Heat Trans. C-83, 163-175. (See also discussions by R. M. Drake, J. Kestin, and P. D. Richardson.)
- (8) Merk, H. J., 1959: Rapid calculations for boundary-layer transfer using wedge solutions and asymptotic expansions. J. Fluid Mech. 5, 460-480.
- (9) Fage, A., 1937: Pressure Distribution for Flow Past Spheres. Brit. Aeronaut. Res. Com. R. & M. No. 1766.
- (10) Krause, A. A. and J. Schenk, 1965-66: Thermal free convection from a

- solid sphere. Appl. Sci. Res. A-15, 397-403.
- (11) Merk, H. J. and J. A. Prins, 1954: Thermal convection in laminar boundary layers, Pts. I, II, and III. Appl. Sci. Res. A-4, 207-221.
 - (12) Garner, F. H. and R. B. Keey, 1958: Mass transfer from single solid spheres, Pt. I. Chem. Eng. Sci. 9(2 & 3), 119-129; also Garner, F. H. and R. B. Keey, 1959: Mass transfer from single solid spheres, Pt. II. Chem. Eng. Sci. 9(4), 218-224.
 - (13) Garner, F. H. and J. M. Hoffman, 1961: Mass transfer from single solid spheres by free convection. AIChE J. 7, 148-152.
 - (14) Schütz, G., 1963: Natural convection mass-transfer measurements on spheres and horizontal cylinders by an electrochemical method. Int. J. Heat Mass Trans. 6, 873-879.
 - (15) Gebhart, B., 1969: Natural convection flow, instability, and transition. J. Heat Trans. C-91, 293-309.
 - (16) Fendell, F. E., 1968: Laminar natural convection about an isothermally heated sphere at small Grashof number. J. Fluid Mech. 34, 163-176.
 - (17) Boxi, C. B. and A. Ramachandran, 1969: Effect of vibration on heat transfer from spheres. J. Heat Trans. C-91, 337-344.
 - (18) Kreith, F., L. G. Roberts, J. A. Sullivan, S. N. Singh, 1963: Convection heat transfer and flow phenomena of rotating spheres. Int. J. Heat Mass Trans. 6, 881-895.
 - (19) Nordlie, R. L. and F. Kreith, 1961: Convection from a rotating sphere. Int. Dev. in Heat Transfer, ASME, New York, N.Y., 461-467.
 - (20) Börner, H., 1965: Über den Wärme-und Stoffübergang an umspülten Einzelkörpern bei Überlagerung von freier und erzwungener Strömung. VDI-Forschungsheft 512, VDI-Verlag, Düsseldorf, West Germany.

- (21) Krischer, O. and G. Loos, 1958: Wärme und Stoffaustausch bei erzeugungener Strömung an Körpern verschiedener Form-Teilung. Chem. Ing. Techn. 30, 31-39.
- (22) Acrivos, A., 1958: Combined laminar free and forced convection heat transfer in external flows. AIChE J. 4, 285-289.
- (23) Mori, Y., 1961: Buoyance effects in forced laminar convection flow over a horizontal flat plate. J. Heat Trans. C-83, 479-482.
- (24) Sharma, G. K. and S. P. Sukhatme, 1969: Combined free and forced convection heat transfer from a heated tube to a transverse air stream. J. Heat Trans. C-91, 457-459.
- (25) Lichfield, E. W. and N. E. Carlson, 1967: Temperature Control of Balloon Packages. NCAR Technical Note TN-32, Boulder, Colo., 38 pp.
- (26) Suriano, F. J. and K.-T. Yang, 1968: Laminar free convection about vertical and horizontal plates at small and moderate Grashof numbers. Int. J. Heat Mass Trans. 11(3), 473-490.
- (27) Stewartson, K., 1958: On the free convection from a horizontal plate. Z. Angew. Math. Phys. 9, Ser. A, 276-282.
- (28) Gill, W. N., D. W. Zeh, and E. D. Casal, 1965: Free convection on a horizontal plate. Z. Angew. Math. Phys. 16(4), 539-541.
- (29) Saunders, O. and M. Fischenden, 1935: Some measurements of convection by an optical method. Engineering, 483-485.
- (30) Singh, S. N., R. C. Birkebak, and R. M. Drake, 1969: Laminar free convection heat transfer from downward facing horizontal surfaces of finite dimensions. In Progress in Heat and Mass Transfer, Vol. 2, Pergamon Press, Oxford.
- (31) Kimbadi, V. and R. M. Drake, 1960: Free surfaces for prescribed variations in surface temperature and mass flow through the surface.

- T. R. Mech. Eng. HT-1, Princeton University, 17 pp.
- (32) Husar, R. B. and E. M. Sparrow, 1968: Patterns of free convection flow adjacent to horizontal heated surfaces. Int. J. Heat Mass Trans. 11(7), 1206-1208.
- (33) Tyler, B. J. and A. F. Tuck, 1967: Heat transfer to a gas from a spherical enclosure: measurements and mechanisms. Int. J. Heat Mass Trans. 10(21), 251-253.
- (34) Sherman, M. and S. Ostrach, 1967: Lower bounds to the critical Rayleigh number in completely confined regions. J. Appl. Mech. 39(2), 308-312.
- (35) Hellums, J. D. and S. W. Churchill, 1961: Computation of natural convection by finite difference methods, Pt. I. Int. Dev. in Heat Transfer, ASME, New York, N.Y., 984-994.
- (36) _____ and _____, 1962: Transient and steady state, free and natural convection, numerical solutions, Pts. I and II. AIChE J. 8, 690-693, 719.
- (37) Powe, E. R., C. T. Carley, and E. H. Bishop, 1969: Free convective flow patterns in cylindrical annuli. J. Heat Trans. C-91, 310-314.
- (38) Eckert, E. R. G. and T. W. Jackson, 1950: Analysis of Free Convection Boundary Layer on a Flat Plate. NACA Rept. No. 1015, 7 pp.
- (39) Clark, A. J., 1968: Cryogenic heat transfer. Advances in Heat Transfer 5, Academic Press, Inc., New York, N.Y., 325-517.
- (40) Dingwell, I. W., W. K. Sepetoski, and R. M. Lucas, 1963: Vertical Motions of High Altitude Balloons. Tech. Rept. II, prepared for Office of Naval Research by A. D. Little, Inc., Cambridge, Mass., 119 pp.

- (41) Ulrich, R. D., D. P. Wirtz, and R. H. Nunn, 1969: Transient heat transfer in closed containers after gas injection. J. Heat Trans. C-91, 461-463.
- (42) Gebhart, B., R. P. Dring, C. E. Polymeropoulos, 1967: Natural convection from vertical surfaces, the convection transient regime. J. Heat Trans. C-89, 53-59.
- (43) Dingwell, I. W., 1967: Thermal Radiation Properties of Some Polymer Balloon Fabrics. Tech. Rept. VI, prepared for Office of Naval Research by A. D. Little, Inc., Cambridge, Mass., 43 pp.
- (44) Dunkle, R. V., 1963: Thermal radiation characteristics of surfaces. In Fundamental Research in Heat Transfer, J.A. Clark, Ed., MacMillan Co., New York, N.Y., 1-31.
- (45) Hartnett, J. P., E. R. G. Eckert, and R. Birkebak, 1959: The emissivity and absorptivity of parachute fabrics. J. Heat Trans. C-81, 195-201.
- (46) Edwards, D. K., 1969: Radiative characteristics of materials. J. Heat Trans. C-91, 1-15.
- (47) _____, 1969: Thermal Radiation Measurements. Measuring Techniques in Heat Transfer. E. R. G. Eckert and R. J. Goldstein, Eds., Advisory Group for Aeronautical Research and Development.
- (48) Kuhn, P. M., 1969: Environmental Science Services Administration, Boulder, Colo., private communication.
- (49) Goetzl, C. G., J. B. Rittenhouse, J. B. Singletary, Eds., 1965: Space Materials Handbook, 2nd ed., TORML 64-40 Air Force Materials Lab., Wright-Patterson Air Force Base, Ohio, 712 pp.
- (50) Camack, W. G. and D. K. Edwards, 1960: Effect of surface thermal radiation characteristics on the temperature control problem in satellites.

- In Surface Effects on Spacecraft Materials, F. J. Clauss, Ed. John Wiley and Sons, Inc., New York, N.Y., 3-54.
- (51) Gaumer, R. C. and L. A. McKellar, 1961: Thermal Radiative Control Surfaces for Spacecraft. Lockheed Tech. Rept. LMSD-704014, Lockheed Aircraft Corp., Sunnyvale, Calif., 198 pp.
- (52) Blau, H. H. and H. Fischer, Eds., 1962: Radiative Transfer from Solid Materials, MacMillan Co., New York, N.Y., 257 pp.
- (53) Wiebelt, John A., 1966: Engineering Radiation Heat Transfer. Holt, Rinehart and Winston, New York, N.Y., 278 pp.
- (54) Kreith, F., 1962: Radiation Heat Transfer for Spacecraft and Solar Power Plant Design, International Textbook Co., Scranton, Pa., 236 pp.
- (55) Germeles, A. E., 1966: Vertical Motion of High Altitude Balloons. Tech. Rept. No. 4 prepared for Office of Naval Research by A. D. Little, Inc., Cambridge, Mass., 88 pp.
- (56) Zarem, A. M. and D. D. Erway, Eds., 1963: Introduction to the Utilization of Solar Energy, McGraw-Hill, New York, N.Y., 398 pp.
- (57) Valley, S. L., Ed., 1965: Handbook of Geophysics and Space Environments, McGraw-Hill, New York, N.Y.
- (58) Gates, D. M., 1966: Spectral distribution of solar radiation at the Earth's surface. Science 151(3710), 523-529.
- (59) Feigelson, E. M., 1966: Light and Heat Radiation in Stratus Clouds, U.S. Dept. of Commerce, Springfield, Va., 245 pp.
- (60) Dunkle, R. V., D. K. Edwards, J. T. Gier, K. E. Nelson, and R. D. Roddick, 1961: Heated cavity reflectometer for angular reflectance measurements. In Proc. Int. Heat Trans. Conf., ASME-AIChE, New York, N.Y., 541-562.

- (61) Edwards, D. K., 1961: Directional solar reflectances in the space vehicle temperature control problem. ARS Journal, 1548-1553.
- (62) Raschke, E., 1968: The Radiation Balance of the Earth-Atmosphere System from Radiation Measurements of the Nimbus II Meteorological Satellite. NASA Tech. Note TN D-4589, Washington, D.C., 81 pp.
- (63) Houghton, H. G., 1954: On the annual heat balance of the northern hemisphere. J. Meteorol. 11(1), 1-9.
- (64) Fritz, S., 1949: The albedo of the planet Earth and of clouds. J. Meteorol. 6, 277-282.
- (65) Coulson, K. L., 1959: Characteristics of the radiation emerging from the top of a Rayleigh atmosphere: total upward flux and albedo. Planet, Space. Sci. 1(1), Pergamon Press, London, 277-284.
- (66) Hibbs, A. R., 1956: The Temperature of an Orbiting Missile. Progress Rept. No. 20-294, Jet Propulsion Laboratory, Pasadena, Calif., 20 pp.
- (67) Hottel, H. C. and A. F. Sarofim, 1967: Radiative Transfer, McGraw-Hill, New York, N.Y., 520 pp.
- (68) Sparrow, E. M. and R. D. Cess, 1966: Radiation Heat Transfer, Brooks Cole Publ. Co., Belmont, Calif., 322 pp.
- (69) Cunningham, F. E., 1961: Power Input to a Small Flat Plate from a Diffusely Radiating Sphere. NASA Tech. Note TN D-710, Washington, D.C., 15 pp.
- (70) Yamamoto, G., 1952: On a radiation chart. Sci. Rept. Tohoku Univ., Ser. 5, Geophys., 4, 9-23.
- (71) Goody, R. M., 1964: Atmospheric Radiation. Vol. I. Theoretical Basis. Oxford Monogr. on Meteorol., Clarendon Press, Oxford, 436 pp.

- (72) Budyko, M. I., 1956: The Heat Balance of the Earth's Surface. Hydrometeorological Publ. House, Leningrad (trans. by U.S. Weather Bureau, 1958), 259 pp.
- (73) Kondratyev, K. Y., 1965: Radiative Heat Exchange in the Atmosphere (trans. by O. Tedder). Pergamon Press, Oxford, 411 pp.
- (74) Simpson, G. C., 1928: Some studies in terrestrial radiation. Mem. Roy. Meteorol. Soc. 2.
- (75) Elsasser, W. M. and M. F. Culbertson, 1960: Atmospheric radiation tables. Meteorol. Monogr. 4(23), Amer. Meteorological Soc., Boston, Mass., 43 pp.
- (76) London, J., 1957: A Study of the Atmospheric Heat Balance. Final Rept. AF19, New York Univ., 122-165.
- (77) Manabe, F. and F. Möller, 1961: On the radiative equilibrium and heat balance of the atmosphere. Mon. Wea. Rev. 89, 503-532.
- (78) Davis, P. A., 1963: An analysis of the atmospheric heat budget. J. Atmos. Sci. 20(1), 5-22.
- (79) Simpson, G. C., 1929: The distribution of terrestrial radiation. Mem. Roy. Meteorol. Soc. 3.
- (80) Katayama, A., 1966: On the radiation budget of the troposphere over the northern hemisphere, Pt. I. J. Meteorol. Soc. Japan 44(6), 381-401; also Katayama, A., 1967: On the radiation budget of the troposphere over the northern hemisphere, Pts. II and III. J. Meteorol. Soc. Japan 44(1), 1-38.
- (81) Sasamori, T., 1968: The radiative cooling calculations for application to general circulation experiments. J. Appl. Meteorol. 7(5), 721-729.

- (82) London, J., 1965: The heat-load on a balloon. Unpublished notes, University of Colo., Boulder, Colo.
- (83) Valley, S. L., Ed., 1965: Handbook of Geophysics and Space Environments, McGraw-Hill, New York, N.Y.
- (84) Suomi, V. E. and P. M. Kuhn, 1958: An economical net radiometer. Tellus 10(1), 160-163.
- (85) Bushnell, R. H. and V. E. Suomi, 1961: Experimental flight verification of the economical net radiometer. J. Geophys. Res. 66(9), 2843-2848.
- (86) Suomi, V. E., D. O. Staley, and P. M. Kuhn, 1958: A direct measurement of infrared radiation divergence to 160 mb. Quart. J. Roy. Met. Soc. 84(360), 134-141.
- (87) Kuhn, P. M., 1963: Measured effective long-wave emissivity of clouds. Mon. Wea. Rev. 91, 635-640.
- (88) _____ and D. R. Johnson, 1966: Improved radiometer observations of atmospheric infrared irradiance. J. Geophys. Res. 71(2), 367-373.
- (89) Kuhn, P. M., L. P. Stearns, and J. R. Stremkis, 1967: Atmospheric Infrared Radiation Over the Antarctic. ESSA Tech. Rept. ER55-IAS2, Boulder, Colo.
- (90) Gergen, J. L., 1956: "Black ball": A device for measuring atmospheric infrared radiation. Rev. Sci. Instr. 27(7), 453-460.
- (91) Lucas, R. M. and G. H. Hall, 1960: The Measurement of High Altitude Balloon Gas Temperature. Tech. Rept. V, prepared for Office of Naval Research by A. D. Little, Inc., Cambridge, Mass., 30 pp.
- (92) Dingwell, I. W. and R. Lucas, 1968: Recent Theoretical and Experimental Studies of High Altitude Balloon Vertical Trajectories. AIAA

- Paper 68-940, presented at AIAA 2nd Aerodynamic Deceleration Systems Conference, El Centro, Calif., Sept. 1968.
- (93) Gabron, F., I. Dingwell, B. Allen, D. Comstock, 1968: A Study of Balloon-Borne Instrumentation (Radiometers) to Detect Thermal Radiation Transients. NCAR Subcontract 84-68, prepared by A. D. Little, Inc., Cambridge, Mass., 63 pp.
- (94) Ney, E. P., R. W. Maas, and W. F. Huch, 1961: The measurement of atmospheric temperature. J. Meteorol. 18, 60-80.

SECTION IV

LIST OF SYMBOLS

LIFT GASES

by

Alvin L. Morris

List of Symbols ii

List of Figures v

List of Tables v

A. EQUATION OF BUOYANCY 1

B. LIFT GAS CHARACTERISTICS 3

1. Hydrogen and Helium 5

2. Ammonia as a Lift Gas and Source of Hydrogen 6

3. Special Characteristics 8

C. GAS STORAGE AND MEASUREMENT 9

1. Pressure and Temperature Measurement 12

2. Stretched Volume of Steel Cylinders 14

3. Equations of Lift for Helium 19

4. Practical Helium Measurement During Balloon Inflation 22

5. Hydrogen Contained in Steel Cylinders 30

6. Determining Lift from STP Volume 32

D. PRECAUTIONS IN HANDLING GAS 35

1. High Pressure Containers 35

2. Cryogenic Containers 37

3. Helium Inflation 38

4. Inflation with Flammable Gases 39

REFERENCES 42

<u>Symbol</u>	<u>Description</u>	<u>Dimensions</u>
a	subscript identifying its symbol with air	
b	subscript indicating that its symbol has a base or standard value	
B	magnitude of buoyant force	MLT^{-2}
\vec{B}	buoyant force vector	MLT^{-2}
c	subscript used with pressure or temperature symbols to indicate that they are cutoff values, i.e., values at which gas flow from a container is stopped	
C_p	specific heat of a gas at constant pressure	$L^2 T^{-2} \theta^{-1}$
C_v	specific heat of a gas at constant volume	$L^2 T^{-2} \theta^{-1}$
e	linear coefficient of thermal expansion	θ^{-1}
E	Young's modulus	$ML^{-1} T^{-2}$
f	subscript used with pressure or temperature symbols to indicate that they are final values, i.e., values to which the gas in a container returns after some gas has been withdrawn and the remaining gas returns to thermal equilibrium with its environment	
F_t	factor to be multiplied by the base volume of a container to correct its volume for deviations of temperature from base temperature	
F_p	factor to be multiplied by the base volume of a container to correct its volume for deviations of pressure from base pressure	

F_v	factor which is a function of p and T which may be multiplied by the base volume (water volume) of a container to yield the volume of gas in the container reduced to a specified base temperature and pressure	
g	subscript identifying its symbol with a gas as contrasted to air	
g	acceleration due to gravity	LT^{-2}
g_o	standard sea level acceleration due to gravity at 45° N	LT^{-2}
i	subscript used with pressure or temperature symbols to indicate that they are initial values, i.e., values applicable to the gas in a container immediately prior to the withdrawal of gas	
k	exponent of pressure used to indicate the relation between pressure and temperature in a polytropic expansion of gas in a container, e.g., $T_1/T_2 = (P_1/P_2)^k$	
\vec{k}	unit vector directed upward	
L	internal length of a cylinder	L
m	mass; subscripts used with it make it specific, e.g., m_c is mass of a cylinder and m_g is mass of gas	M
M	molecular weight; subscripts used with it make it specific. Its dimensions are mass per mass mole, e.g., for air $M_a = 28.9644$ kilograms per kilogram mole	M/M-Mol
o	subscript indicating that its symbol is at the base datum level, e.g., V_o is the volume of a cylinder containing gas at the base temperature and pressure	

p	absolute pressure; subscripts used with it make specific, e.g., p_a is pressure of air	$ML^{-1}T^{-2}$
p^*	gage pressure; subscripts used with it make it specific, e.g., p_g^* is gage pressure of gas	$ML^{-1}T^{-2}$
R	universal gas constant	$L^2T^{-2}\theta^{-1}$
R_i	internal radius of a cylinder	L
R_e	external radius of a cylinder	L
s	subscript indicating that its symbol is associated with the stretched condition of a container, e.g., p_s is the pressure of a gas in a container whose dimensions are increased (stretched) by the excess of internal over external pressure or by a temperature different from the base temperature	
T	absolute temperature in °K or °R	θ
T^*	temperature in °F	θ
V	volume	L^3
V_o	volume of a gas container at base temperature and pressure. Also called water volume of a container	L^3
y	Poisson's ratio	
Z	gas compressibility = pM/R_pT	

Greek letters

γ	ratio of specific heats of gas ($\gamma = C_p/C_v$)	
β_v	mass which a unit volume of gas will lift in air when air and gas are both at the same base conditions of p and T	ML^{-3}

List of Figures

- Fig. 1 Lift gases for ballooning are usually transported in cylinders mounted on trailers as shown here. The cylinders are connected at the rear by a manifold in such a way that gas may be taken from any one or any combination of them simultaneously. Each tube normally has its water volume stamped on it. 14
- Fig. 2 Graph of Eq. (23) where $k/(1 - k)$ was determined from Eq. (24) 29

List of Tables

- Table 1 Lift gas comparison 4
- Table 2 Values of β_v and β_v^{-1} for helium and hydrogen for SI and English units 34

LIFT GASESA. EQUATION OF BUOYANCY

The buoyant force \vec{B} exerted on a volume of gas V_g displacing a volume of air V_a is (see Sect. II, Eq. [1])

$$\vec{B} = \vec{k} (\rho_a V_a - \rho_g V_g) g \quad (1)$$

where ρ_a and ρ_g are the density of air and lift gas, respectively, g is the acceleration due to gravity, and \vec{k} is a unit vector directed upward.

(For a description of the coordinate system used here, see Sec. II.C.)

Only the buoyant force will be considered in this section; therefore, the vector notation will be dropped. If $B > 0$, it is a force directed upward.

If $B < 0$ it is directed downward. Also, except for the small volume occupied by the balloon film, the rigging, and the payload, $V_a = V_g$. With these simplifications, Eq. (1) may be written

$$B = \rho_a V_a g \left(1 - \frac{\rho_g}{\rho_a} \right) \quad (2)$$

Although some potentially useful lift gases, such as ammonia, may be readily liquified, most gases will be used in balloons only under conditions of pressure and temperature which are enough above critical

to be considered to be ideal gases. Then

$$\rho_a = \frac{p_a M_a}{R T_a} \text{ and } \rho_g = \frac{p_g M_g}{R T_g} \quad (3)$$

and

$$\frac{\rho_g}{\rho_a} = \frac{p_g M_a T_a}{p_a M_g T_g}$$

where p , M , and T are pressure, molecular weight, and temperature, respectively; the subscripts a and g identify their symbols with air and gas, respectively; R is the universal gas constant.

Normally $p_g > p_a$. The difference is only slight in the so-called zero-pressure balloon, but it may be appreciable in a fully inflated super-pressure balloon. Also frequently $T_a \approx T_g$, although the difference may be quite significant at times. In fact, the hot air balloon relies on that difference to obtain lift. In searching for gases which may be used to provide lift, however, one may assume that $p_g T_a / p_a T_g \approx 1$ as a first approximation, so that

$$\frac{\rho_g}{\rho_a} = \frac{M_a}{M_g} \quad (4)$$

Then from Eq. (2)

$$\frac{B}{\rho_a V_a g} = \left(1 - \frac{M_g}{M_a}\right) = (1 - \sigma^{-1}) \quad (5)$$

where σ is substituted for the ratio M_a/M_g for convenience. Since $\rho_a V_a g$ is the weight of the displaced air, its algebraic sign is positive. Equation (5) then indicates that any gas having a molecular weight less than the molecular weight of air, so that $(1 - \sigma^{-1}) > 0$, is a potentially useful gas for ballooning. Also the term $(1 - \sigma^{-1})$ may be interpreted as the lift of the gas per unit weight of displaced air. Thus it serves as a useful index for selecting lift gases, although other characteristics, such as inflammability and toxicity, must also be considered.

B. LIFT GAS CHARACTERISTICS

Table 1 from Morris (1) lists several gases having molecular weights less than air and provides some other pertinent data about each. No effort is made to provide an exhaustive list of potentially useful lift gases. On the other hand most such gases are listed, and the table can be used to illustrate some useful information about gases for ballooning.

Table 1

Lift Gas Comparison

Gas	Chemical formula	Molecular weight	Lift index ($1 - M_g/M_a$)	Flammable limits in air (%)	Comments
Perfect lift gas		0.	1.000	Inert	Does not exist; vacuum is weightless, but difficult to contain
Hydrogen	H ₂	2.0159	0.930	4 - 75	Readily available, inexpensive
Helium	He	4.0032 ^(a)	0.862	Inert	Readily available in U.S., moderately expensive
Deuterium	D ₂	4.032	0.861	5 - 75	Very rare
Decomposed ammonia	N ₂ +3H ₂	8.515	0.706	7 - 73	Readily generated in small quantities
Methane	CH ₄	16.04	0.446	5.3-14	Major constituent of natural gas
Ammonia	NH ₃	17.03	0.412	15-28	Toxic only in high concentrations, liquifies readily
Water vapor	H ₂ O	18.01	0.378	Non-flammable	Liquifies too readily
Air	Mixture of N ₂ , O ₂ , etc.	28.96	0.000	--	Provides lift only if density of the air inside balloon is less than that outside

^(a)Molecular weight of helium supplied for ballooning in the U.S. in 1972.

1. Hydrogen and Helium

Hydrogen forms a molecule by combining two atoms; helium does not.

Therefore, the molecular weight of helium is only twice that of hydrogen,

and a given volume of hydrogen produces only 1.08 (0.930/0.862) times the

lift of a like volume of helium in the atmosphere. The value of $(1 - \sigma^{-1})$

is 0.930 for hydrogen and 0.862 for helium. A vacuum would produce the

maximum possible lift if it could be contained by the same balloon film

used for the gases. It cannot, of course, but hydrogen and helium both pro-

duce a very high fraction of the maximum possible lift.

The adiabatic lapse rate of hydrogen in the atmosphere is much nearer

the normal tropospheric lapse rate than is the lapse rate of helium (see

Sect. II, Table 3). Therefore, a hydrogen filled balloon is less stable,

i.e., its vertical movement is more difficult to control than that of a

helium filled balloon. Hydrogen is highly flammable in air; helium is

inert. Neither gas is toxic. If helium is available at reasonable cost,

it is preferred for ballooning. Hydrogen is satisfactory, however, if ade-

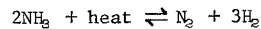
quate precautions are taken. Other gases are generally less satisfactory,

but some may have properties which make them useful under some circumstances.

2. Ammonia as a Lift Gas and Source of Hydrogen

Ammonia is an interesting gas. Its critical temperature is 132.9°C and it may readily be liquified at normal atmospheric temperatures. In fact, it is usually stored and transported as a liquid under its own vapor pressure, which equals $2.032 \times 10^6 \text{ N/m}^2$ (294.8 psia) at a temperature of 50°C (122°F). The liquid boils readily under normal atmospheric conditions, providing a gas. It is toxic in high concentrations, but it is so offensive that a person using it is not likely to suffer more than temporary discomfort if exposed to it unless he cannot escape. Its adiabatic lapse rate in the atmosphere is even closer to the normal tropospheric temperature lapse rate than that of hydrogen.

Ammonia can be decomposed into nitrogen and hydrogen according to the following formula:



The decomposition is endothermic, i.e., it requires heat. The reaction can proceed in either direction, but if nitrogen and hydrogen are mixed at normal atmospheric temperatures, the combination reaction is extremely slow. Further, at atmospheric pressures, the amount of ammonia in an

equilibrium mixture of ammonia, nitrogen, and hydrogen is very low. Therefore, if decomposition of ammonia can be accomplished, the hydrogen and nitrogen mixture can be used as a ballooning lift gas. Interestingly, because two volumes of ammonia when completely decomposed produce one volume of nitrogen and three volumes of hydrogen, the decomposed gas provides greater lift than the original ammonia. This can be demonstrated quantitatively by comparing molecular weights.

The molecular weight of this mixture of gases, M_m , may be calculated as follows:

$$M_m = \frac{(\text{Vol of N}_2)(M_{\text{N}_2}) + (\text{Vol of H}_2)(M_{\text{H}_2})}{(\text{Vol of N}_2) + (\text{Vol of H}_2)}$$

$$M_m = \frac{1 \times 28.013 + 3 \times 2.016}{4}$$

$$M_m = 8.515$$

A given volume of the decomposed mixture then provides 1.7 times the lift of a like volume of ammonia and 0.82 times the lift of a like volume of helium. At least one lift gas generator makes use of this property of ammonia, using a catalyst to aid in the decomposition. Unfortunately, the decomposition is not complete, and the mixture contains a small amount of

ammonia, which decreases its effectiveness somewhat. Using this method and present equipment, the rate at which lift gas can be generated at the launch site is great enough to provide gas for small meteorological sounding balloons but not for large scientific balloons. This same statement applies to most methods of generating hydrogen at the launch site. When hydrogen is needed in large quantities for ballooning, it is usually transported to the launch site in high pressure cylinders or as a cryogen in large dewars.

3. Special Characteristics

Several of the light gases are flammable, helium and neon are inert, and water vapor and nitrogen are nonflammable. Ammonia, hydrogen fluoride, diborane, and carbon monoxide are toxic. Methane, a major constituent of natural gas, is usually thought of as a toxic gas. However, while one will suffocate in a methane atmosphere, it is not toxic. Hydrogen fluoride and diborane are so corrosive or so unstable that they are not useful as lift gases.

Water vapor condenses so readily under atmospheric temperature and pressure conditions that it is not useful except perhaps for very special purposes.

C. GAS STORAGE AND MEASUREMENT

By following a series of steps like that used in deriving Eq. (5), one can derive the following equivalent form:

$$\frac{B}{g} = \rho_g V_g (\sigma - 1) \quad (6)$$

This form is more convenient as a starting point for measuring the buoyant lift of gas in a balloon. The product $\rho_g V_g$ is the mass of gas required to provide lift of magnitude B when the local acceleration due to gravity is g and the conditions assumed in deriving Eq. (5) are fulfilled. Thus, under these conditions, the mass which can be lifted is a function only of the mass of gas placed in the balloon and the ratio of the molecular weight of that gas to the molecular weight of air. Normally, at the time of inflation of either zero-pressure or superpressure balloons, conditions approximate the assumed conditions well enough that Eq. (6) may be used to determine the mass of gas required to lift the mass B/g.

The mass of gas may be measured directly by means of a set of balances or indirectly by measuring the volume and density and taking the product. It can be, and sometimes is, measured by measuring the lift of the balloon, but to measure the lift of very large balloon systems in the turbulent

atmosphere is difficult enough that it does not often serve as the primary means of determining how much gas to put into a balloon. Most often the volume and density of the gas are measured.

Lift gases are stored in either the gaseous state under high pressure or as cryogenics. A flowmeter has been described by Kubara (2) which can provide a sufficiently accurate measure of gas volume to serve the needs of scientific ballooning. Flowmeters can measure gas flow from any source, but if cryogenic storage is used, the gas must be warmed to a temperature which is within the operating limits of the meter. Their use is not yet commonplace, but cryogenic storage and transport are likely to increase in the future and to be accompanied by increased use of flowmeters.

Flowmeters must indicate both volume and density to be useful or they must provide volume reduced to some acceptable base temperature and pressure, often called standard temperature and pressure (STP). When volume is reduced to a given set of base conditions, the density is also determined for that set of conditions. That this is true when the base conditions permit the gas to be considered an ideal gas is apparent from Eq. (3), and base conditions are usually chosen so that Eq. (3) is applicable.

From Eq. (6) it is evident that if the product $\rho_g V_g$ of gas in a pressurized container can be ascertained, the mass which that gas will lift can also be determined. For conditions of temperature and pressure for which Eq. (3) serves as an acceptable equation of state, the product $\rho_g V_g$ is easily expressed in terms of the measurable quantities p_g , T_g , and V_g , where V_g is the nominal volume of the container, henceforth designated V_o . The nominal volume (also called water volume) of a container is usually determined by weighing the container empty and then when filled with water having a known temperature. The difference in weight divided by the known specific weight of the water yields the water volume of the container.

The actual (stretched) volume of a container is a function of the temperature of the container and the pressure exerted against its walls by the fluid it contains. Also the equation of state for a gas becomes much more complicated than Eq. (3) when the pressure is greater than a few atmospheres. Therefore, the product $\rho_g V_g$ of an actual gas contained under high pressure is not a simple function of p_g , T_g , and V_o .

1. Pressure and Temperature Measurement

Precision bourdon tube pressure gages which are carefully handled and checked are accurate to $\pm 0.5\%$, and gas pressure, measured when no gas is flowing from the container, is representative. To obtain a temperature which is representative of the gas in a container is more difficult. The practice of the U.S. Bureau of Mines and of most scientific ballooning crews is to place a mercury-in-glass thermometer in contact with the outside of the container and read it when it has come to equilibrium with the container. This is nothing more than the usual practice in measuring any temperature with a glass thermometer, but the temperature obtained is that of the container and not of the gas. Precautions must be taken, therefore, to assure that the temperature is representative of the gas inside the container. The best measurements are probably made at night when the temperature of the ambient air is at a minimum. Then air temperature does not change rapidly, and if air circulation is maintained about the container, the container and the gas in it are likely to be in thermal equilibrium with the air, and the temperature shown by the thermometer will be representative of the gas temperature. A temperature taken during the day when

ambient air temperature is at a maximum is likely to be all right also if the container is shaded from the sun and is well ventilated. Temperature measurements made when the temperature of the ambient air is changing rapidly or when the sun is shining on the container are not likely to be accurate.

In scientific ballooning a single tube rarely contains enough gas to inflate a balloon. Therefore, computations must be made of the lift of the gas in a number of individual tubes or several must be joined together by a manifold. The pressure of all tubes is then equal and may be read by a single gage. The temperature may also be determined by a single thermometer if the cylinders are close together and are in thermal equilibrium with the ambient air. The nominal volume of the entire container is the sum of the nominal volumes of the individual cylinders.

It is usually possible to exercise proper care in determining the lift in one or many cylinders before balloon inflation starts. A trailer such as the one shown in Fig. 1 is used to transport the gas to the launch site. The tubes on the trailer are interconnected at the rear by a manifold as shown in the picture, but each is usually sealed separately to minimize



Fig. 1. Lift gases for ballooning are usually transported in cylinders mounted on trailers as shown here. The cylinders are connected at the rear by a manifold in such a way that gas may be taken from any one or any combination of them simultaneously. Each tube normally has its water volume stamped on it.

leakage. Thus, the pressure and temperature of the gas in just those tubes needed for inflation may be determined under optimum conditions some time before inflation starts.

2. Stretched Volume of Steel Cylinders

It has been pointed out that the actual volume of a container is a function of its temperature and of the pressure of the fluid it contains. Equation (7), taken from Kalman (3), expresses the stretched volume of a cylindrical steel tube as a function of its nominal volume, its temperature, and the pressure of the gas it contains.

$$V_s = V_o \left[1 + 1.89 \times 10^{-5} (T^* - 70) \right] \left[1 + 7.4 \times 10^{-7} p_g^* \right] \quad (7)$$

where V_s is the stretched volume, T^* is the temperature of the tube in degrees Fahrenheit, and p_g^* is the gage pressure of the gas in pounds per square inch.

A number of assumptions were made in deriving Eq. (7). For example, since the coefficient of the temperature in the first bracket is actually three times the linear coefficient of thermal expansion of steel, it is clear that all products of small quantities of second and higher order have been neglected in accounting for thermal expansion. The pressure stretch

coefficient, given as 7.4×10^{-7} , is an unweighted average between a value obtained by testing helium tank-car cylinders hydrostatically and a value computed from the characteristics of the steel and the physical dimensions of the cylinders. The two values were in reasonable agreement and both were apparently believed to be equally well founded; therefore, their average was used as a "best" estimate of the coefficient. Another assumption which is made in applying Eq. (7) is that the temperature of the gas is equal to the temperature of the cylinder. Finally, if one expression is used for all steel cylinders, the assumption is made that all have essentially the same characteristics, in this case the characteristics of the helium tank-car cylinders used in the U.S. during and prior to 1968.

The assumptions made in deriving Eq. (7) have not caused problems in calculating lift for ballooning even when steel cylinders much smaller and much larger than tank-car cylinders were used. Nonetheless, if cylindrical containers are to be used which are significantly different from the helium tank-car cylinders used in the U.S. prior to 1968, new coefficients for Eq. (7) may be computed.

The first term in brackets in Eq. (7) may be expressed more generally

as

$$F_T = \left[1 + 3e(T - T_b) \right] \quad (8)$$

where F_T is a factor which can be multiplied by the volume of the cylinder at its base temperature T_b to correct the volume to temperature T , and e is the linear coefficient of thermal expansion of the material from which the cylinder is made. F_T is dimensionless; e must have the dimensions of T^{-1} . A more general expression for the second bracketed term of Eq. (7) is

$$F_p = \left[1 + \frac{2dR_i}{R_i} + \frac{dL}{L} \right]_p \quad (9)$$

where F_p is a dimensionless factor which may be multiplied by the volume of the cylinder at its base pressure to correct the volume to pressure p . R_i is the internal radius of the unstretched cylinder and L is its unstretched internal length. Also

$$\frac{dR_i}{R_i} = \frac{p}{E} \left[\frac{R_e^2 + R_i^2}{R_e^2 - R_i^2} - \nu \left(\frac{R_i^2}{R_e^2 - R_i^2} - 1 \right) \right] \quad (10)$$

$$\frac{dL}{L} = \frac{p}{E} \left[\frac{R_i^2}{R_e^2 - R_i^2} - \nu \left(\frac{R_e^2 + R_i^2}{R_e^2 - R_i^2} - 1 \right) \right] \quad (11)$$

In Eqs. (10) and (11) R_e is the unstretched external radius, E is Young's modulus, and ν is Poisson's ratio.

The external diameter and length of a cylinder may be measured, but the internal diameter and length cannot be determined directly. An average value of the internal radius of a tube may be approximated from its mass, length, and external radius by means of the formula

$$R_i = \left(R_e^2 - \frac{m_c}{\pi L \rho_c} \right)^{\frac{1}{2}} \quad (12)$$

or from its nominal volume and length by the formula

$$R_i = \left(\frac{V_0}{\pi L} \right)^{\frac{1}{2}} \quad (13)$$

where m_c is the mass of the cylinder and ρ_c is the density of the material from which it is made. In using Eq. (12) an average of several measurements of R_e taken along the tube should be employed. All measurements should be made when the tubes are in an unstretched condition and L should be measured so that the value obtained approximates as nearly as possible the internal length of the tube. This involves making allowance for the forming of the ends of the tubes.

3. Equations of Lift for Helium

Any of several equations of state might serve for measuring helium which is stored under high pressure. The form which has the best foundation in theory is the virial form, but the form most commonly used for engineering purposes is Eq. (3) with a compressibility factor Z included to account for deviations of the real gas from an ideal gas. The equation of state using Z is

$$\rho_g = \frac{P M}{Z R T} \quad (14)$$

The compressibility, Z_g , is a function of pressure and temperature; therefore, the very simple appearance of Eq. (14) is deceptive.

Generalized charts of Z can be found in most engineering handbooks (e.g., Eshbach [4]). Tables also exist, and a set taken from Lydersen et al. (5) is reproduced in readily usable form by Reid and Sherwood (6). These tables and charts provide values of Z which may be used for hand calculations, but for the machine calculation of lift tables, an equation relating Z , p , and T is preferable.

For computing the volume of helium in cylindrical steel containers,

Kalman (3) used the empirical expression

$$Z_g = 1 + \left[10.2297 \times 10^{-5} - 19.2998 \times 10^{-8} T_g + 1.1836 \times 10^{-10} T_g^2 \right] p_g - 2.217 \times 10^{-10} p_g^2 \quad (15)$$

which was developed by Miller et al. (7). Temperature must be entered

in degrees Rankine and pressure in pounds per square inch. Angevine (8),

who compared values given by several equations of state with available

experimental data, also elected to use an equation of the form of Eq. (14)

with Z_g given by Eq. (15) to compute lift tables for helium.

Equations (6) and (14) may be combined as follows:

$$\frac{B}{g} = \frac{M_g (\sigma - 1) p_{g,s} V_{g,s}}{R T_{g,s} Z_{g,s}} \quad (16)$$

where the subscript pair g,s indicates identification with the lift gas in

the stretched cylinder. Equation (16) is applicable to any gas. If it is

written specifically for the helium available in 1969 from the U.S. Bureau

of Mines ($M_g = 4.0032$), it and Eqs. (7) and (15) provide a set of equations

suitable for helium lift calculations. For convenience the equations are

given for direct calculations in Systeme International and English Engineering

Units (lb m, lb f, ft °R, sec).

$$\text{SI units } \left(\frac{B}{gV_o} \right)_{g,s} = \frac{3.0022 \times 10^{-3} p_{g,s} V_{g,s}}{T_{g,s} Z_{g,s}} \frac{V_{g,s}}{V_o} \text{ (kg/m}^3 \text{)} \quad (17)$$

$$\text{Eng units} = \frac{2.3260 p_{g,s} V_{g,s}}{T_{g,s} Z_{g,s}} \frac{V_{g,s}}{V_o} \text{ (lb m/ft}^3 \text{)} \quad (17a)$$

$$\text{SI units } \frac{V_{g,s}}{V_o} = \left[1 + 3.40 \times 10^{-5} (T_{g,s} - T_b) \right] \left[1 + 1.07 \times 10^{-10} (p_{g,s} - p_b) \right] \quad (18)$$

$$\text{Eng units} = \left[1 + 1.89 \times 10^{-5} (T_{g,s} - T_b) \right] \left[1 + 7.4 \times 10^{-7} (p_{g,s} - p_b) \right] \quad (18a)$$

$$\text{SI units } Z_{g,s} = 1 + (1.48369 - 5.03856 \times 10^{-3} T_{g,s} + 5.5620 \times 10^{-6} T_{g,s}^2) p_{g,s} \times 10^{-8} - 4.664 \times 10^{-18} p_{g,s}^2 \quad (19)$$

$$\text{Eng units} = 1 + (10.2297 - 19.2998 \times 10^{-3} T_{g,s} + 1.1836 \times 10^{-5} T_{g,s}^2) p_{g,s} \times 10^{-5} - 2.217 \times 10^{-10} p_{g,s}^2 \quad (19a)$$

Equation (17) gives the lift of each unit of nominal volume of helium in a cylinder at absolute temperature $T_{g,s}$ and absolute pressure $p_{g,s}$. Kalman (3) claims that volume factors based on Eqs. (7), (14), and (15) are accurate to within $\pm 0.05\%$ and that accuracy in measuring the volume of helium in cylindrical steel containers depends primarily on the accuracy of the pressure and temperature measurements. Tables I-1 and I-2 of Sect. XII are short helium lift tables in which linear interpolation is possible. More complete tables which avoid the need for interpolation can easily be generated from Eqs. (17)-(19) by anyone having access to a computer.

4. Practical Helium Measurement During Balloon Inflation

Unfortunately, one never finds precisely the amount of lift desired in any set of tubes, and some gas (enough to provide lift equal to the total initial lift in the set less the lift to be placed in the balloon) must be left in at least one of them when balloon inflation is completed. Also, removing all gas from a container is such a slow process that ballooning crews frequently prefer to maintain a high gas flow rate throughout inflation by withdrawing gas simultaneously from a container composed of enough cylinders so that when inflation is completed the pressure in the

container is still quite high. Neither gas pressure nor temperature can be measured accurately while gas is being withdrawn from the container. The pressure of the flowing gas will be lower than the static pressure of the gas in the container due to the Bernoulli effect, and the temperature of the gas is likely to be less than the temperature of the container because of the cooling of the expanding gas. It is a simple matter to close off the flow momentarily during inflation to check the static pressure, and this is what is normally done. (The usual precautions of waiting until transients have died out and tapping the gage prior to the reading must be taken.) There is no equally simple way, however, to measure the gas temperature during inflation and to be certain the measurement is representative. However, the container can be placed in a well ventilated, shady location and, when the ambient air temperature is steady, and air, container, and gas have all reached thermal equilibrium, both temperature and pressure can be read. This is not practical, but the concept is useful as an introduction to the reasoning behind the method which is developed here.

As stated before, when gas is being withdrawn from a container and withdrawal is stopped, the pressure can be readily determined but the

temperature cannot. Except under unusual circumstances, the temperature of the gas falls below the temperature of its container during withdrawal; therefore, gas temperatures may be expected to increase when the container is closed and withdrawal is ended. But the lift remaining in a closed container is constant, and any change in temperature of the enclosed gas must also be accompanied by a change in pressure. Any combination of temperature and pressure which satisfied Eqs. (17)-(19) when $(B/gV_o)_{g,s}$ is assigned the proper value and held constant is, in principle, an acceptable combination. Tables I-1 and I-2 of Sect. XII generated from these equations provide a means of solving for p, T, or $(B/gV_o)_{g,s}$ if any two of the three are known. $(B/gV_o)_{g,s}$ is constant for a closed container, and if the changes in p and T are small, then changes in $V_{g,s}/V_o$ and $Z_{g,s}$ are negligible, and approximately

$$\frac{P}{T} = \text{Const} \quad (20)$$

Thus, if one acceptable combination of p and T can be found for a closed container, other combinations may be readily determined from Eq. (20).

Let p_c and T_c be the cutoff pressure and temperature of gas in a container at the time immediately after withdrawal is stopped when the container retains precisely the desired amount of lift gas. T_c will be less than T_i , the temperature of the gas when inflation was begun. Assume also that $T_i = T_a = \text{Const}$ for the period of inflation and long enough after inflation is completed to let the gas "recover" its temperature--i.e., to let the gas temperature warm up to T_a , the temperature of the ambient air. Also let p_f be the "final" gas pressure, the pressure after the gas has recovered its initial temperature. Then if $(T_i - T_c)$ is not too large, Eq. (20) may be used to establish a relationship between p_c , T_c , p_f , and T_i . It is

$$\frac{P_c}{T_c} = \frac{P_f}{T_i} \quad (21)$$

The polytropic process is frequently assumed in gas compression and expansion work (e.g., Gill [9] or Streeter [10]). It is expressed in a form which relates the pressure and temperature of an expanding gas by Eq. (22)

$$\frac{T_c}{T_i} = \left(\frac{P_c}{P_i} \right)^k \quad (22)$$

For an adiabatic process, $k = (C_p - C_v)/C_p = (1 - \gamma^{-1})$ where C_p and C_v are the specific heats of the gas at a constant pressure and volume, respectively, and $\gamma = C_p/C_v$. For an isothermal process, $k = 0$.

During the withdrawal of gas, heat can readily flow from the container to the gas. Also the container is a good thermal conductor which will transfer heat from the ambient air to the gas if the gas temperature is lower than the air temperature. Therefore, the gas in the container cannot expand adiabatically as gas is withdrawn. Since it is observed to cool appreciably during balloon inflations, it clearly does not expand isothermally. For short periods it probably expands in such a way that Eq. (22) with $k = \text{Const}$ and $0 < k < (1 - \gamma^{-1})$ provides a good approximation to the expansion process. If withdrawal is rapid and $T_i = T_a$, little heat will flow into the gas during the first few seconds, and $k \approx (1 - \gamma^{-1})$. As withdrawal continues and $(T_a - T_g)$ increases, however, heat will flow more rapidly to the gas until, if withdrawal continues long enough, the process will become essentially isothermal.

This reasoning suggests that if Eq. (22) is to be used to relate T_i , T_c , p_i , and p_c , the value of k must vary during withdrawal. It is possible, nonetheless, to calculate a mean value of k for the entire withdrawal if T_i , T_c , p_i , and p_c are all known. Further, if gas is withdrawn at a constant, rapid rate, the mean value should be near $(1 - \gamma^{-1})$ for very small withdrawals and near zero for very large ones. This reasoning has been confirmed by test data reported by Gildenberg (11), which show k to correlate well with (p_f/p_i) .

Now Eqs. (21) and (22) can be combined to yield

$$\frac{p_c}{p_f} = \left(\frac{p_c}{p_i}\right)^k$$

from which

$$p_c = p_f \left(\frac{p_f}{p_i}\right)^{\frac{k}{1-k}} \quad (23)$$

Equation (23) makes use of p_f , p_i , and k to calculate p_c without making explicit use of the gas temperature, although T_i must be used to calculate p_f . The exponent $k/(1 - k)$ must be determined, and since k correlates with p_f/p_i , the ratio $k/(1 - k)$ might also be expected to do so. In fact, the data from 14 inflation tests reported by Gildenberg show that $k/(1 - k)$

correlates linearly with $(p_f/p_i)^3$ with a coefficient of correlation of 0.966, and $k/(1 - k)$ may be estimated by means of the regression equation

$$\left(\frac{k}{1 - k}\right) = 0.038 + 0.23 \left(\frac{p_f}{p_i}\right)^3 \quad (24)$$

Either Table I-1 or I-2 of Sect. XII may be used to determine p_f from p_i , T_i , and the residual lift. Then p_f and p_i may be entered into Eq. (24) to determine $k/(1 - k)$. Finally, Eq. (23) enables one to compute the pressure at which the gas in the container should be left immediately after withdrawal is ended to assure that the container retains the proper residual lift. Figure 2 is a graph of $(p_f/p_i)^{k/(1 - k)}$ (shown as p_c/p_f) as a function of p_f/p_i . The graph may be used to determine a factor p_c/p_f which can be multiplied by p_f to yield p_c .

The method developed here to calculate p_c gives values which are comparable to the values one may obtain from the much used General Mills Inflation Tables (General Mills, Inc. [12]). Unfortunately, the basis of the General Mills Tables was never published as far as can be determined, but their successful use over the years leaves little doubt that they give acceptable values. With both methods, the best measurements occur when p_f

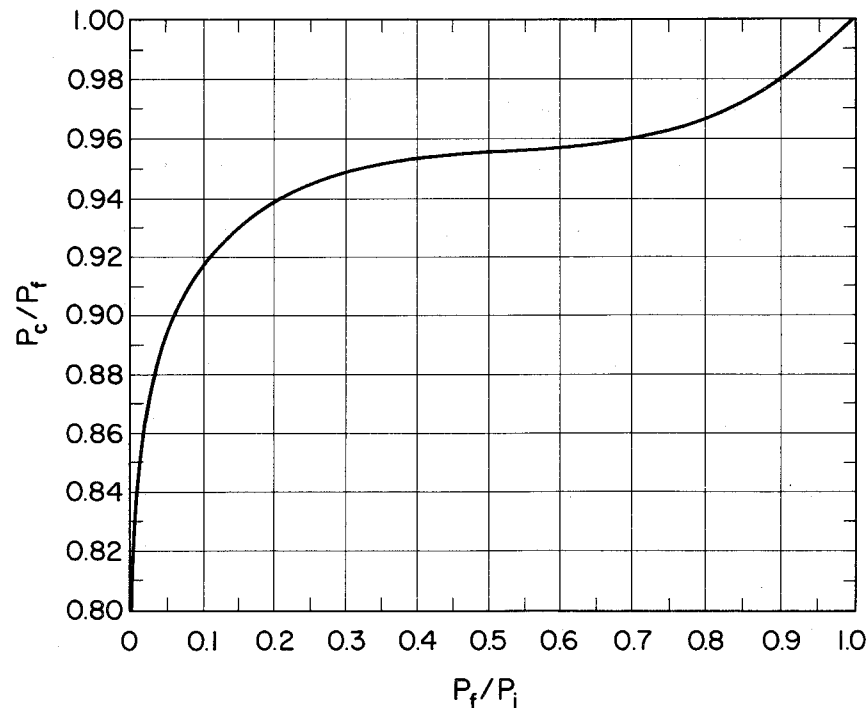


Fig. 2. Graph of Eq. (23) where $k/(1 - k)$ was determined from Eq. (24).

is very small, i.e., when essentially all the gas is removed from the container. Either method may result in a large percentage error when a very small fraction of the gas in a container is withdrawn. It is recommended that withdrawals resulting in $(p_f/p_i) > 0.75$ should be avoided if possible. This may be done by using fewer or smaller cylinders.

5. Hydrogen Contained in Steel Cylinders

The foregoing discussion has covered most of what can or needs to be said about measuring any gas for balloon inflation aside from the safety aspects and the need for an accurate equation of state for the gas if it is stored under high pressure.

The following set of equations is the counterpart for hydrogen of Eqs. (17) and (19) for helium. No counterparts of Eqs. (17a) and (19a) are given:

$$\left(\frac{B}{gV_o}\right)_{g,s} = \frac{3.2412 \times 10^{-3} p_{g,s}}{T_{g,s} Z_{g,s}} \frac{V_{g,s}}{V_o} \quad (\text{kg/m}^3) \quad (25)$$

$$Z_{g,s} = \exp \left[\frac{1}{T_{g,s}^{1.25}} \left(B_1 T_{g,s} - B_2 T_{g,s}^{\frac{1}{2}} - B_3 \right) \frac{\rho_{g,s}}{\rho_o} + \frac{1}{T_{g,s}^2} \left(C_1 T_{g,s}^{\frac{1}{2}} - C_2 \right) \left(\frac{\rho_{g,s}}{\rho_o} \right)^2 \right] \quad (26)$$

where $B_1 = 5.5478 \times 10^{-3}$, $B_2 = 3.6877 \times 10^{-2}$, $B_3 = 2.2004 \times 10^{-1}$,

$C_1 = 4.788 \times 10^{-3}$, $C_2 = 4.053 \times 10^{-2}$ and $\rho_o = 8.9886 \times 10^{-2} \text{ kg/m}^3$.

Equation (26) is a modified form of an equation by Wooley et al. (13).

Since Eq. (18) is a mathematical description of certain aspects of a steel cylindrical tube and is independent of the fluid the tube may contain, it applies also to hydrogen. Equations (18), (25), and (26) were used to generate Table I-3 of Sect. XII. They were also used with suitable conversion of units to generate Table I-4 of Sect. XII.

Equation (23) is essentially an empirical equation derived for helium withdrawals, but the reasoning leading to its form is as valid for hydrogen as for helium. The value of γ for hydrogen is 1.41 compared to 1.66 for helium, so that the limits for k are different, being 0 to 0.40 for helium and 0 to 0.29 for hydrogen. Further, the thermal conductivity for hydrogen is greater than for helium; the ratio of the two being approximately 1.2. These differences suggest that k is likely to be smaller for hydrogen than for helium when comparable withdrawals result in identical values of p_f/p_i ; consequently, $k/(1-k)$ will be smaller and $(p_f/p_i)^{k/(1-k)}$ will be larger. Using a value of $(p_f/p_i)^{k/(1-k)}$ for helium taken from Fig. 2

or Fig. I-1 of Sect. XII will result in a value of p_c which is slightly small for hydrogen, but a value which is too small will cause too much gas to be placed in a balloon rather than too little. Therefore, Fig. I-1 of Sect. XII is considered acceptable, but slightly conservative, for use with hydrogen.

6. Determining Lift from STP Volume

Gas used in commerce is usually measured in terms of volume reduced to a set of base conditions. Knowing the base conditions permits one to calculate the density corresponding to that volume also. Therefore, the product, $\rho_g V_g$, may be calculated, and from Eq. (6) lift may be determined. If Eq. (6) is written in the form

$$\frac{B}{g} = \rho_{g,b} (\sigma - 1) V_{g,b} \quad (27)$$

where the subscript b indicates that the variables ρ_g and V_g are both reduced to base conditions, it is apparent that

$$\rho_{g,b} (\sigma - 1) = \beta_v = \text{Const} \quad (28)$$

Table 2 lists values of β_v and β_v^{-1} for helium and hydrogen for some of the most frequently used base conditions. β_v may be viewed as the mass which a unit volume of gas under base conditions will lift in air under those same base conditions. It has the units of density. Its reciprocal is useful when one needs to calculate the volume of gas needed to lift a given mass. For example, the number 15.5 ($\sim \beta_v^{-1}$ for helium at $T_b = 70^\circ\text{F}$ and $p_b = 14.7$ psia) is often multiplied by the mass in pounds to be lifted to give the volume of helium in cubic feet required to lift that mass.

The volume under base conditions may be determined in many ways, but for scientific ballooning purposes gas is usually delivered in cylinders at high pressure, and tables are used to determine $V_{g,b}$ in the cylinders prior to and after withdrawal. The difference is the amount delivered. This is exactly parallel to the method of computing lift which was developed in C.4. of this section. Therefore, a volume table for the container in which a lift gas is delivered may be readily used to compute lift.

Kalman's (3) table for computing the volume of helium in cylindrical steel tubes gives tabulated values of what he calls a volume factor, F_v ,

Table 2

Values of β_v and β_v^{-1} for Helium and Hydrogen for SI and English Units

Units and Base Condition	Value of $\rho_{g,b}(\sigma - 1) = \beta_v$			
	Helium		Hydrogen	
	β_v	β_v^{-1}	β_v	β_v^{-1}
SI Units $T_b = 288.15^\circ\text{K} (15^\circ\text{C})$ $p_b = 101325 \text{ N/m}^2$	1.0557	0.9472	1.1397	0.8774
Mass - lbm Vol - ft ³ $T_b = 518.67^\circ\text{R} (59^\circ\text{F})$ $p_b = 14.6959 \text{ psia}$	0.06590	15.174	0.07115	14.055
Mass - lbm Vol - ft ³ $T_b = 529.67^\circ\text{R} (70^\circ\text{F})$ $p_b = 14.7 \text{ psia}$	0.06455	15.492	0.06969	14.349

which is a function of the temperature and pressure of the gas and which is defined by the following equation:

$$V_{g,b} = F_v V_o \quad (29)$$

Combining Eqs. (27), (28), and (29) yields

$$\left(\frac{B}{gV_o}\right) = \beta_v F_v \quad (30)$$

which shows that multiplying each of the entries of Kalman's table by β_v converts that table into a lift table comparable to Tables I-2 and I-4 of Sect. XII.

D. PRECAUTIONS IN HANDLING GAS

The individual characteristics of a gas must be considered when using it as a lift gas in a balloon, and anyone using toxic or flammable gas should acquaint himself with those characteristics. Only those precautions which are generally necessary when handling any gas stored under high pressure and those which are peculiar to ballooning are covered here.

1. High Pressure Containers

Any container filled with gas under high pressure constitutes a potential hazard; care should be taken to protect the container. It should not be struck violently or dropped. It should be stored in a dry area where

the temperatures are not excessively high; 125° F (~ 50° C) is usually stated as a maximum for compressed gas cylinders in the U.S. Flame should never be allowed to touch a cylinder, and a cylinder should never be allowed to become part of an electrical circuit. In particular, an electrical welding arc should never be struck against a cylinder containing pressurized gas. Cylinders should never be dragged or rolled. Small cylinders should be moved short distances on a hand cart, and when they are moved in a truck, care should be taken to assure that they do not strike each other violently. One should never tamper with safety devices in valves or cylinders, and the cap should be left in place until a cylinder has been securely fixed in place and is ready to be used.

Gas is frequently carried through high pressure hoses from the container to the balloon inflation tubes. Care should be taken to avoid kinking these hoses, because kinks may cause invisible weaknesses in them. All hoses, valves, gages, and other equipment used with the inflation system should be inspected regularly, and high pressure hoses should be replaced periodically, the period depending on the use and handling they receive, whether or not they show evidence of damage.

Some additional precautions should be taken with flammable or toxic gases. Flammable gases should not be stored with oxygen or other oxidizing materials, and special care should be taken to avoid open flames or sparks in an area where flammable gases are being stored or used. Only explosion-proof equipment and spark-proof tools should be used where such gases are being stored or used. All equipment should be grounded. People working with flammable gases should also keep themselves electrically grounded.

2. Cryogenic Containers

Gas is being transported increasingly as a cryogen because of the lower transport cost, and cryogenic hydrogen has been used to inflate balloons. The large dewars used to transport cryogenic gases must receive special care to avoid damage that will break the vacuum. They should be stored in an open, well-ventilated place, and all the precautions against flame, sparks, etc. which must be taken with compressed, flammable gas must also be taken with flammable cryogens. Even the best dewars leak heat to the cryogen, and eventually some gas will have to be removed to prevent excessive pressure buildup. Periodic use may take care of this buildup, but a safety valve will release gas if necessary. The gas may

be released at any hour of the day or night, and precautions must be adequate to assure that it does not create a hazard. Placing the dewar in an open field where it will not be molested is desirable. Lift gases, if expelled into the atmosphere, rise and so do not create a hazard at the surface for very long unless they are trapped. The very cold gases coming from a dewar may not rise immediately, however, so it is possible for them to flow along the surface and become trapped at some distance from the dewar.

Another danger associated with cryogens occurs when they are used in large quantities, as in scientific ballooning. As the cryogen is removed from the dewar, air condenses on the outside of the pipes and tubes carrying the cryogen. This liquid air drips off and may collect in sizeable quantities. The boiling point of nitrogen is lower than oxygen and as the nitrogen boils off, the liquid which remains becomes increasingly rich in oxygen. Then any material which will oxidize constitutes a danger if it comes in contact with this liquid. The usual precautions include catching the liquid air in an aluminum trough and being very careful to keep other materials away from it. This problem is associated with extreme cold and so any cryogenic gas, including the inert ones, will create it.

3. Helium Inflation

Helium, being an inert gas, is quite safe to handle during inflation. The hoses leading from the container to the balloon inflation tubes should be high pressure hoses which will not kink. If precautions are taken to assure that the helium containers are adequately protected and the pressure in the hoses is adequately provided for, no other special precautions are necessary.

4. Inflation with Flammable Gases

When a balloon is being inflated with a flammable gas, great care must be exercised by everyone in the vicinity. All possible preparations incident to the flight should be made away from the site of inflation or before inflation begins. In particular, no electrical testing should be done in the vicinity of the balloon or gas source during inflation. Also, all equipment should be grounded before any gas is released from its container. If it should be necessary to connect two pieces of equipment where there may be gas, they should first be connected by a wire either prior to the presence of the gas or outside of the area where gas may exist. No car or truck engine should be started or left running anywhere where gas

may reach it or where sparks from it may reach the gas. Even the handling of the balloon or work at the base of the bubble should be kept to an absolute minimum.

All who are handling inflation hoses or who must go near the sources of the gas should wear heavy flame-proof clothing and a conducting strip which makes contact with the leg and extends under the shoe. Anyone who must work under or near the gas bubble of the inflating balloon should also wear a hood--one with a small hole in the top to allow gas to escape. Each such person should also be in constant communication with someone who is well outside the area of danger and who is watching for fire. Because hydrogen burns with an invisible flame, the first warning anyone has of a fire may be the heat radiating from it, or the start of collapse of the balloon. The two events will occur nearly simultaneously, and a person working near the balloon will be in far more danger from the molten plastic of the balloon which may rain down under and downwind of the bubble than from the burning gas which will rise. Therefore, on receiving a warning, a man working near the balloon should retreat along the shortest path to a safe area. It is a good idea to have the danger area marked prior to the

start of inflation and to have each person constantly aware of his optimum route of retreat. In general, the area of danger may be visualized as an oval area oriented with its long dimension (major axis) parallel to the wind and with the balloon bubble near the upwind end. Anyone upwind of the balloon should move into the wind if he receives a warning; from all other locations it is usually best to move cross wind away from the major axis of the oval. Except in very unusual circumstances, one should never move toward or across the major axis if he perceives danger.

Any balloon which has contained a flammable gas and is lying on the ground constitutes a hazard. It may contain small pockets of gas which are nonetheless large enough to inflict serious burns if they are ignited. Consequently, it should not be left unattended until all pockets can be opened and the gas allowed to escape, and it should be handled with care by everyone working with it.

Anyone using flammable gases should study carefully the safety standards for handling hazardous gases, including local standards.

REFERENCES

- (1) Morris, Alvin L., 1969: Buoyancy of Gases in Air. Helium Symposia Proc. in 1968 -- A Hundred Years of Helium, U.S. Dept. of Interior, Bureau of Mines Information Circular 8417, 9-16.
- (2) Kubara, Robert S., 1968: A Liquid Hydrogen Inflation System. In Proc. Fifth ARCL Scientific Balloon Symposium, U.S. Air Force Cambridge Research Laboratories Special Report No. 85, 217-221.
- (3) Kalman, H.S., 1968: Computing Volume of Helium in Cylindrical Steel Containers at 10 to 10,000 PSIA. U.S. Dept. of Interior, Bureau of Mines Information Circular 8367.
- (4) Eshbach, Ovid W., 1952: Handbook of Engineering Fundamentals, 2nd ed., John Wiley and Sons, New York.
- (5) Lydersen, A. L., R. A. Greenkorn and O. A. Hougen, 1955: Generalized Thermodynamic Properties of Pure Liquids, Univ. of Wisconsin Coll. Eng. Rept.
- (6) Reid, Robert C. and Thomas K. Sherwood, 1966: The Properties of Gases and Liquids, 2nd ed., McGraw-Hill, New York.
- (7) Miller, J. E., L. W. Brandt and L. Stroud, 1961: Compressibility Factors for Helium and Helium-Nitrogen Mixtures, Bureau of Mines Report of Investigation 5845, p. 3.
- (8) Angevine, J. M., 1970: A Listing of Computer Programs Available at NCAR for Solving Recurring Problems in Ballooning. In Proc. Sixth AFCRL Scientific Balloon Symposium, U.S. Air Force Cambridge Research Laboratories Special Report No. 105, 198-203.

- (9) Gill, Thomas T., 1941: Air and Gas Compression, John Wiley and Sons, New York, 15-16.
- (10) Streeter, Victor L., 1962: Fluid Mechanics, 3rd ed., McGraw-Hill, New York, p. 249.
- (11) Gildenberg, Bernard D., 1954: Investigation of Inflation Techniques for Nonextensible Balloons, Holloman Air Force Base, New Mexico.
- (12) General Mills, Inc., Mechanical Division, Minneapolis, Minn., Helium Inflation Tables.
- (13) Wooley, Harold W., Russell B. Scott and F. G. Brickwedde, 1948: Compilation of Thermal Properties of Hydrogen in its Various Isotopic and Ortho-Para Modifications, U.S. Dept. of Commerce, NBS Research Paper R P 1932, Vol. 41, 426-427.

SECTION V

LIST OF SYMBOLS

BALLOON DESIGN CONSIDERATIONS

by

Justin H. Smalley

List of Symbols	ii
List of Figures	v
List of Tables	vi
A. DERIVATION OF EQUATIONS	1
B. NON-DIMENSIONAL EQUATIONS	8
C. PRELIMINARY DESIGN	10
D. CALCULATION OF MERIDIONAL STRESS	26
E. BALLOONS BELOW THEIR FLOAT ALTITUDE	27
<u>1. Cutting the Duct to Change Float Altitude</u>	28
F. BALLOONS WITH CIRCUMFERENTIAL STRESS	31
<u>1. The Ideal (i.e., Spherical) Balloon</u>	31
<u>2. Round-Top Balloons</u>	36
<u>3. Constant Circumferential Stress</u>	40
<u>4. Circumferential Stress Proportional to Meridional Stress</u>	40
G. COMPARISON OF BALLOON DESIGNS	42
REFERENCES	46

<u>Symbol</u>	<u>Description</u>	<u>Dimensions</u>
a	distance of zero-pressure level below the bottom of a balloon	L
\bar{a}	a/λ	
A	surface area of a balloon	L^2
b	specific buoyancy of a lifting gas	$ML^{-2}T^{-2}$
B	buoyant force	MLT^{-2}
c	dimensionless constant used to relate meridional and circumferential stresses	
c	subscript identifying its symbol with a circumference of a balloon which lies in a plane normal to the axis of symmetry	
C	circumference	
d	subscript identifying its symbol with the design condition	
es	subscript identifying its symbol with end section	
f	subscript identifying its symbol with the balloon film	
F	force; subscripts are used to make it specific	MLT^{-2}
G	gross weight of a balloon system exclusive of the lift gas; $G = W + P$	MLT^{-2}
GI	gross inflation force	MLT^{-2}
h	pressure head	L
k	dimensionless constant; $k = (2\pi)^{-1/3}$	
K	dimensionless parameter which is a function of ϕ	
L	load carried at the bottom of a balloon	MLT^{-2}

L	subscript identifying its symbol with lower	
m	subscript identifying its symbol with a meridian of a balloon; i.e., the circumference which lies in a plane that contains the axis of symmetry	
o	subscript identifying its symbol with a base value	
p	pressure	$ML^{-1}T^{-2}$
p	subscript identifying its symbol with pressure	
P	total payload carried on a balloon	MLT^{-2}
r	radius of the intersection of a balloon's skin with a plane which cuts the balloon normal to its axis of symmetry	L
\bar{r}	r/λ	
R	maximum radius of a balloon, i.e., the maximum value which r may have	L
s	distance measured along a gore	L
\bar{s}	s/λ	
S	gore length	L
t	subscript identifying its symbol with seams or load tapes	
T	force caused by film stress; subscripts c and m identify it with the circumferential and meridional directions, respectively	MLT^{-2}
U	subscript identifying its symbol with upper	
v	subscript identifying its symbol with vertical	
V	volume	L^3
w	weight of a unit area of balloon film	$ML^{-1}T^{-2}$
w	subscript identifying its symbol with weight	
W	balloon weight	MLT^{-2}

W_t	seam weight	MLT^{-2}
z	height	L
\bar{z}	z/λ	

Greek letters

θ	angle the balloon skin makes with the vertical in a plane which includes the vertical axis of symmetry	deg
λ	a length unit defined so that λ^3 is the volume of gas required to lift the payload alone	L
σ	film stress per unit of film width; subscripts c and m identify it with the circumferential and meridional directions, respectively	MT^{-2}
$\bar{\sigma}_c$	$\sigma_c/b \lambda^2$	
$\bar{\sigma}_m$	$\sigma_m/b \lambda^2$	
Σ	non-dimensional film weight parameter; $\Sigma = (2\pi)^{1/3} (w/b \lambda)$	
ϕ	angular coordinate (latitude) of points on a sphere-- positive above the equator	deg
ψ	dihedral angle between two planes, both of which contain the axis of symmetry of a balloon	deg

List of Figures

Fig. 1	Sketch showing relation of a surface element to a balloon	2	Fig. 10	Overall height of two extreme, zero-pressure, natural-shape flat-top balloon designs	20
Fig. 2	Sketch of surface element	3	Fig. 11	Graphical solution to the equation $G = bV$. The graph also shows the relationship between specific buoyancy for helium and altitude in the <u>U.S. Standard Atmosphere, 1962</u>	22
Fig. 3	Sketch illustrating various end sections and gore patterns.	11	Fig. 12	Pressure head at the top of various zero-pressure, natural shape, flat-top balloons	29
Fig. 4a	Effect of film weight on gross weight for zero-pressure, natural-shape, flat-top balloons with taper-tangent end sections. \bar{r}_e is the ratio of end section radius to maximum balloon radius	12	Fig. 13	Zero-pressure level in balloons below their design altitude as a basis for cutting the valving duct.	30
Fig. 4b	Effect of film weight on gross weight for zero-pressure, natural-shape, flat-top balloons with cylinder end sections. \bar{r}_e is the ratio of the end section radius to the maximum balloon radius	13	Fig. 14a	Meridional stress in an ideal, spherical, weightless, buoyant balloon	33
Fig. 5	Gore length of zero-pressure, natural-shape, flat-top balloons	14	Fig. 14b	Circumferential stress in an ideal, spherical, weightless buoyant balloon	34
Fig. 6	Maximum radius of zero-pressure, natural-shape, flat-top balloons	15	Fig. 15	Shapes of balloons with constant circumferential stress. The balloons are zero-pressure, and $\Sigma = 0.2$	41
Fig. 7	Total meridional film load at the top of the two extreme zero-pressure, natural-shape, flat-top balloons	16			
Fig. 8a	Surface area of zero-pressure, natural-shape, flat-top balloons with taper-tangent end sections; \bar{r}_e is the ratio of end-section radius to maximum balloon radius	17			
Fig. 8b	Surface area of zero-pressure, natural-shape, flat-top balloons with cylinder end sections; \bar{r}_e is the ratio of end-section radius to maximum balloon radius	18			
Fig. 9	Nadir angle of the two extreme zero-pressure, flat-top balloons	19			

List of Tables

Table 1	Non-dimensional physical parameters of ideal spherical balloons	37
Table 2	Non-dimensional physical characteristics of round-top balloons	39
Table 3	Non-dimensional physical characteristics of balloons with circumferential stress equal to net meridional stress	43
Table 4	Comparison of balloon designs on the basis of balloon weight	45

BALLOON DESIGN CONSIDERATIONS

A. DERIVATION OF EQUATIONS

The purpose of this section is to derive a set of differential equations which, with the proper boundary conditions, can be integrated to determine the characteristics of various balloon shapes.

The simplest development of the equations considers the balance of forces on an elemental surface area of the balloon. The top and bottom of this element are defined by two parallel planes normal to the axis of symmetry and located a distance Δz apart. The intersection of such planes with the balloon surface defines the circumferential direction. The sides of the element are defined by two planes containing the axis of symmetry and separated by an angle ψ . The intersection of such planes with the balloon surface defines the meridional direction. The tangents to the meridional and circumferential directions and the normal to the surface form an orthogonal set. The relationship of the surface element to the balloon is shown in Fig. 1. The element and the forces on it are shown in detail in Fig. 2.

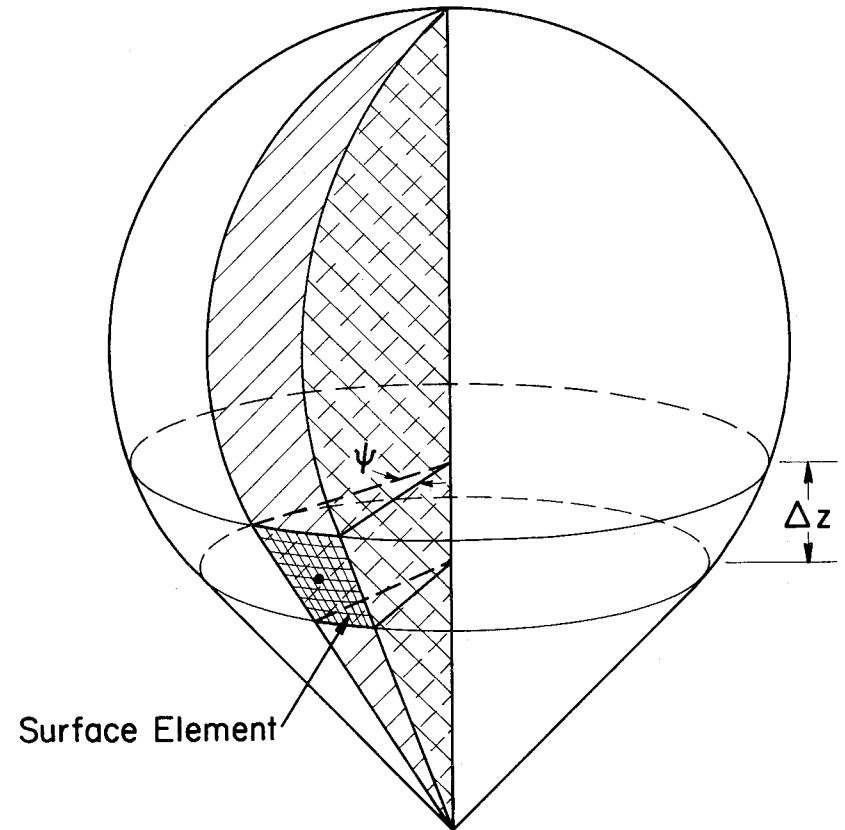


Fig. 1. Sketch showing relation of a surface element to a balloon.

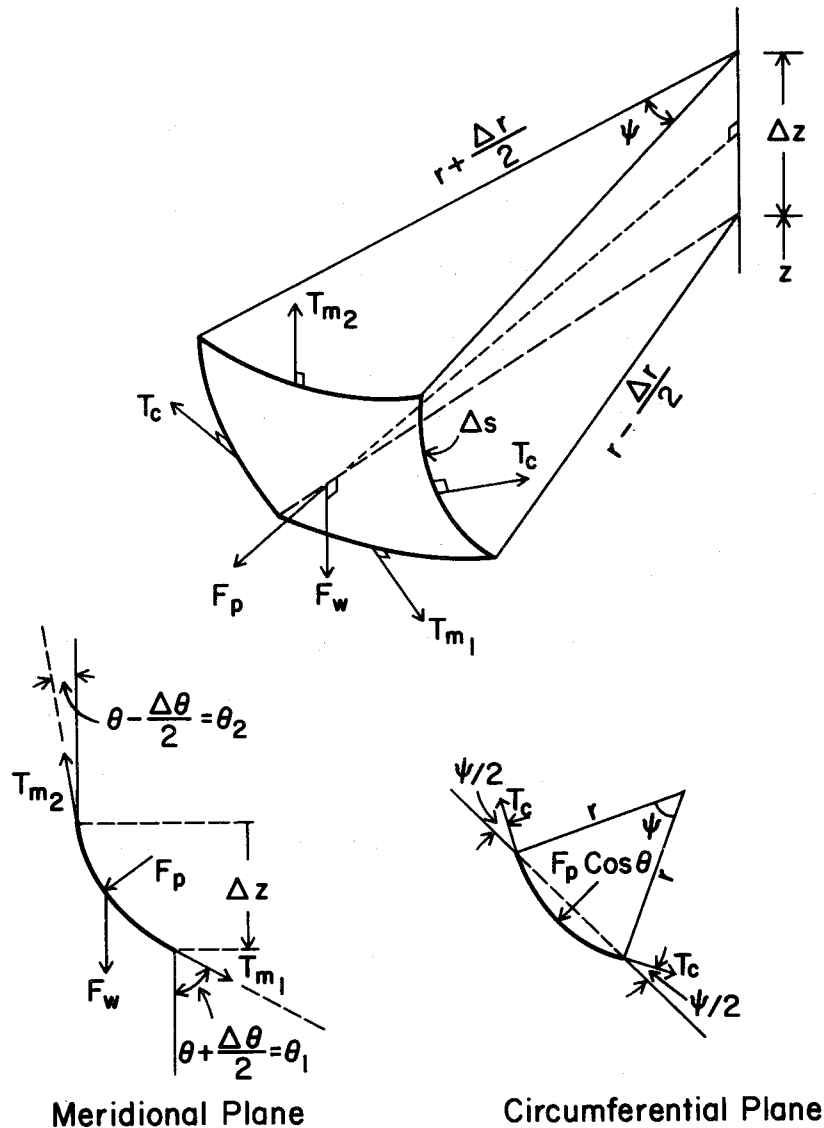


Fig. 2. Sketch of surface element.

The forces shown are: F_p , the pressure force on the element; F_w , the weight of the element; T_c , the circumferential force; and T_m , the meridional force. Using a very small element (i.e., $\Delta z \ll 1$ and $\psi \ll 1$) we can state to first-order accuracy

$$F_p = p (\psi r \Delta s)$$

$$F_w = w (\psi r \Delta s)$$

where p is the differential pressure across the balloon film, w is the weight of the balloon film per unit area, and $(\psi r \Delta s)$ is the area of the element.

Also,

$$T_c = \sigma_c \Delta s$$

$$T_{m_1} = \left(\sigma_m - \frac{\Delta \sigma_m}{2} \right) \psi \left(r - \frac{\Delta r}{2} \right)$$

$$T_{m_2} = \left(\sigma_m + \frac{\Delta \sigma_m}{2} \right) \psi \left(r + \frac{\Delta r}{2} \right)$$

where σ_c and σ_m are the film stresses per unit length in the circumferential and meridional directions, respectively. From Fig. 2,

$$\theta_1 = \theta + \Delta \theta / 2$$

$$\theta_2 = \theta - \Delta \theta / 2$$

Summing forces vertically and horizontally, respectively, in the meridional plane we obtain

$$T_{m_2} \cos \theta_2 - T_{m_1} \cos \theta_1 - F_p \sin \theta - F_w = 0$$

$$T_{m_2} \sin \theta_2 - T_{m_1} \sin \theta_1 + F_p \cos \theta - 2T_c \sin \frac{\psi}{2} = 0$$

It can be shown that when higher order infinitisimals are omitted,

$$T_{m_2} \cos \theta_2 - T_{m_1} \cos \theta_1 = \psi \Delta(r \sigma_m \cos \theta)$$

$$T_{m_2} \sin \theta_2 - T_{m_1} \sin \theta_1 = \psi \Delta(r \sigma_m \sin \theta)$$

and then, substituting further, assuming $\sin \psi/2 = \psi/2$, we obtain

$$\Delta(r \sigma_m \cos \theta) - rw \Delta s - pr \sin \theta \Delta s = 0$$

$$\Delta(r \sigma_m \sin \theta) - \sigma_c \Delta s + pr \cos \theta \Delta s = 0$$

Dividing by Δs and taking the limit as Δs approaches zero, we obtain

$$\frac{d}{ds} (r \sigma_m \cos \theta) - rw - pr \sin \theta = 0$$

$$\frac{d}{ds} (r \sigma_m \sin \theta) - \sigma_c + pr \cos \theta = 0$$

Another form of these equations is more convenient for integration. When

the indicated differentiation is carried out

$$\frac{d}{ds} (r \sigma_m) \cos \theta - (r \sigma_m) \sin \theta \frac{d\theta}{ds} - rw - pr \sin \theta = 0$$

$$\frac{d}{ds} (r \sigma_m) \sin \theta + (r \sigma_m) \cos \theta \frac{d\theta}{ds} - \sigma_c + pr \cos \theta = 0$$

Eliminating $d(r \sigma_m)/ds$ and substituting $p = b(z + a)$, where a is the distance the zero-pressure level is below the bottom of the balloon and b is the specific buoyancy of the lifting gas, gives

$$(r \sigma_m) \frac{d\theta}{ds} = \sigma_c \cos \theta - rw \sin \theta - br(z + a) \quad (1)$$

then eliminating p gives

$$\frac{d}{ds} (r \sigma_m) = \sigma_c \sin \theta + rw \cos \theta \quad (2)$$

These equations represent the balance of forces normal and parallel,

respectively, to the surface element. They could have been derived directly, but the geometry is not straightforward, particularly regarding the force T_c . To complete the set of equations necessary to define a balloon it is noted that

$$\frac{dr}{ds} = \sin \theta$$

$$\frac{dz}{ds} = \cos \theta$$

and by definition, where A and V are surface area and volume, respectively,

of the balloon

$$\frac{dA}{ds} = 2 \pi r$$

$$\frac{dV}{ds} = \pi r^2 \cos \theta$$

The total film load in the meridional direction is

$$T = 2 \pi (r \sigma_m)$$

Observe that there are three factors in the above which may be independently specified. They are σ_c , w , and a . When σ_c is set equal to zero everywhere, the very important natural-shape balloon results. If a is zero, the balloon is known as the zero-pressure type. If w is held constant, the resulting balloon will be fully tailored. If the term rw is constant, the balloon will be a cylinder type.

Various boundary conditions are of interest. In the usual case, $0 < \theta < \pi/2$ at the bottom of the balloon and $\theta = -\pi/2$ at the top (i.e., flat-topped). If $\theta = \pi/2$ at the bottom this means that there is no payload there and it must be carried elsewhere. If $\theta < -\pi/2$ at the top of the balloon, an additional lift force is being applied there.

If at either the top or the bottom of the balloon, rw is zero and $\sigma_c \neq \sigma_m$, then σ_m will be infinite. Although σ_m may diverge, the total film load will not. If there is a load L at the bottom of the balloon, the initial value of the total film load is $T = L/\cos \theta$.

B. NON-DIMENSIONAL EQUATIONS

In general it is convenient to work with a non-dimensional form of the equations. Equations (1) and (2) are repeated here in rearranged form

$$(r \sigma_m) \frac{d\theta}{ds} = \sigma_c \cos \theta - rw \sin \theta - br (z + a)$$

$$(r \sigma_m) = \int_0^s (\sigma_c \sin \theta + rw \cos \theta) ds + \frac{L}{2 \pi \cos \theta}$$

The non-dimensionalizing force and length are somewhat arbitrary. Certainly the payload L is a logical choice for the force. Dividing through by L yields the term b/L , which has the units of $(\text{length})^{-3}$. The cube root of L/b has been chosen as the length. These are not the only terms that could have been used, but are related to ones chosen by the University of Minnesota in their pioneering work and are continued here. Since it is not necessary that all the payload be at the bottom, it is convenient to use P rather than L in the length unit, where P is the total payload. Finally, $\lambda = (P/b)^{1/3}$,

which is a length. At float altitude, the equation of balloon equilibrium for a balloon of weight W and volume V is $bV = W + P = G$, or $V/\lambda^3 = (W/P) + 1 = G/P$. This simple expression shows the value of λ as the length unit. An interpretation of λ is that λ^3 is the volume of gas required to lift the payload alone. Another common and useful unit is the gore length. However, at the outset of a design, P and b and, therefore, λ are more apt to be known than the gore length.

The University of Minnesota defined the non-dimensional film weight parameter as

$$\Sigma = (2\pi/D)^{1/3} (V/G)^{2/3} w$$

This is identical to

$$\Sigma = (2\pi)^{1/3} (w/b\lambda)$$

which will be retained in the further work. With the following definitions:

$$\bar{a} = a/\lambda, \bar{r} = r/\lambda, \bar{s} = s/\lambda, \bar{z} = z/\lambda, k\Sigma = (2\pi)^{-1/3} \Sigma = w/b\lambda, \bar{\sigma}_c = \sigma_c/b\lambda^2,$$

and $\bar{\sigma}_m = \sigma_m/b\lambda^2$, the final non-dimensional differential equations of the

shape and stresses in the balloon are

$$(\bar{r}\bar{\sigma}_m)\theta' = \bar{\sigma}_c\bar{z}' - k\Sigma\bar{r}\bar{r}' - \bar{r}(\bar{z} + \bar{a}) \quad (3)$$

$$(\bar{r}\bar{\sigma}_m)' = \bar{\sigma}_c\bar{r}' + k\Sigma\bar{r}\bar{z}' \quad (4)$$

$$\bar{r}' = \sin\theta \quad (5)$$

$$\bar{z}' = \cos\theta \quad (6)$$

$$(A/\lambda^2)' = 2\pi\bar{r} \quad (7)$$

$$(V/\lambda^3)' = \pi\bar{r}^2\bar{z}' \quad (8)$$

where the prime denotes differentiation with respect to the gore length variable, \bar{s} . The independent variables are $\bar{\sigma}_c$, Σ , and \bar{a} . If two are fixed, the third then uniquely defines a family of balloon shapes. The famous Σ tables define a family of shapes for $\sigma_c = a = 0$. A version of these tables is presented as Table L-1 in Section XII.

From a practical standpoint, a real balloon is not tailored to zero gore width at the nadir and zenith as in the Σ tables. A sketch of a gore pattern illustrating cylinder-end, taper-tangent, and full-cylinder designs is presented in Fig. 3. Data for end-section radii of $\frac{1}{4}$, $\frac{1}{2}$, and $3/4$ times the maximum radius and for a full-cylinder design as well as portions of the data from Table L-1 of Section XII have been plotted in Figs. 4 through 10.

C. PRELIMINARY DESIGN

In the absence of a computer to solve Eqs. 3 through 8, a preliminary design using the data in Table L-1 of Section XII and Figs. 4 through 10 is as

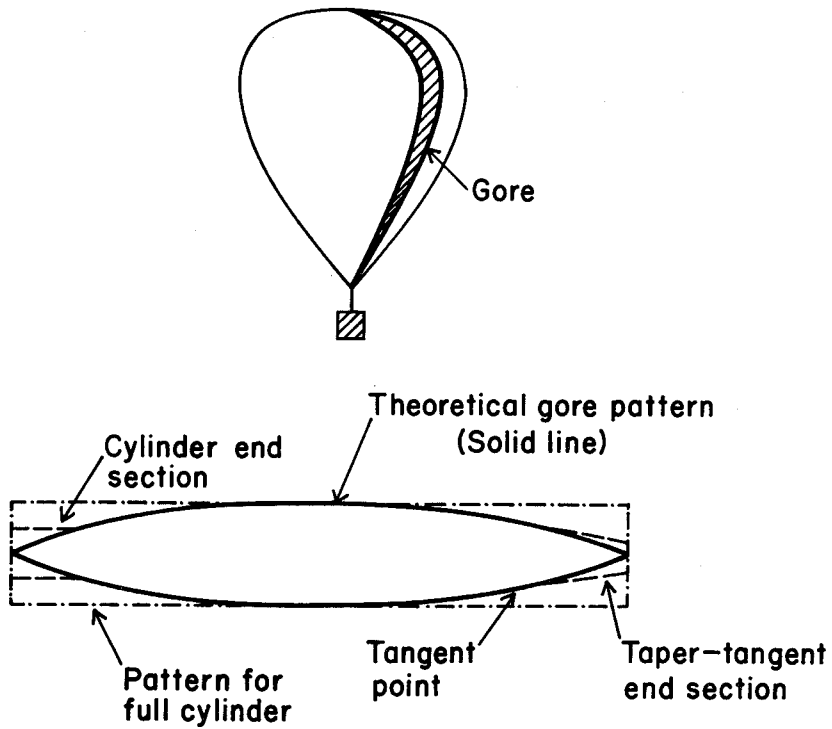


Fig. 3. Sketch illustrating various end sections and gore patterns.

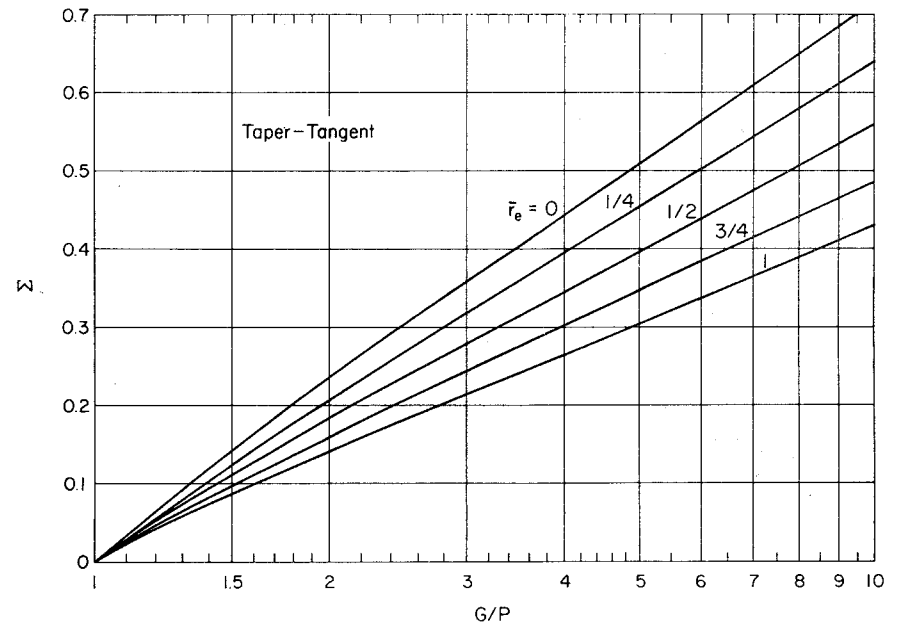


Fig. 4a. Effect of film weight on gross weight for zero-pressure, natural-shape, flat-top balloons with taper-tangent end sections. \bar{r}_e is the ratio of end section radius to maximum balloon radius.

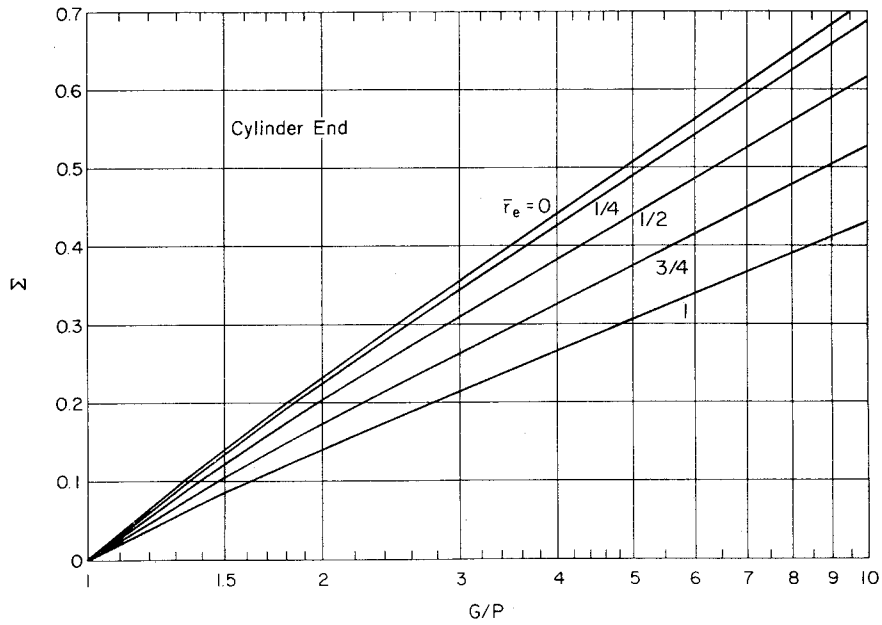


Fig. 4b. Effect of film weight on gross weight for zero-pressure, natural-shape, flat-top balloons with cylinder end sections. \bar{r}_e is the ratio of the end section radius to the maximum balloon radius.

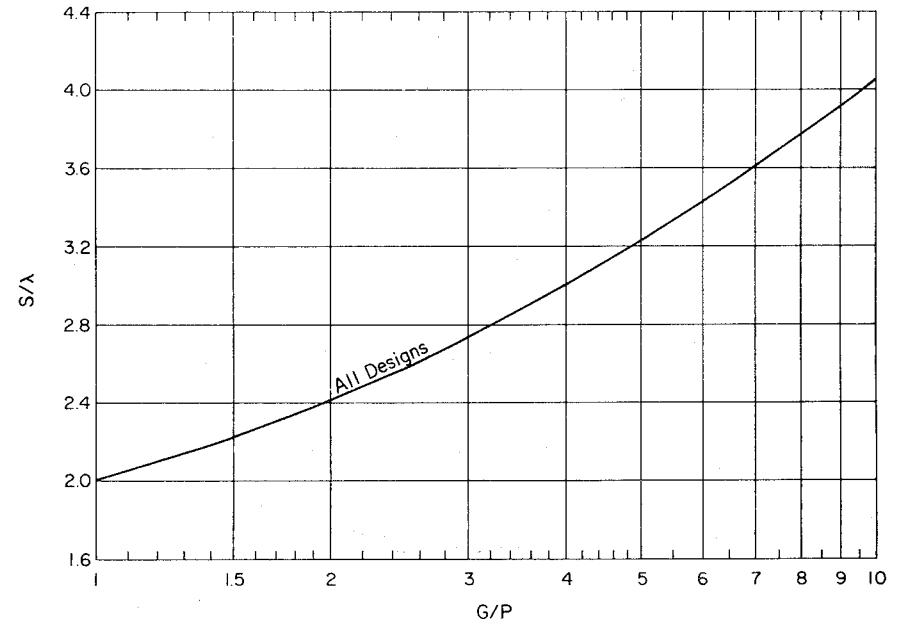


Fig. 5. Gore length of zero-pressure, natural-shape, flat-top balloons.

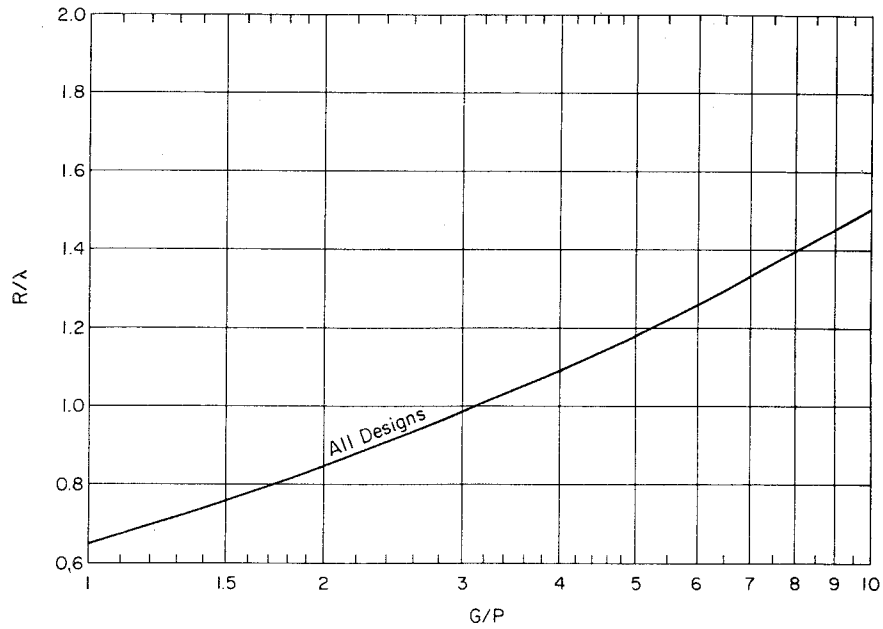


Fig. 6. Maximum radius of zero-pressure, natural-shape, flat-top balloons.

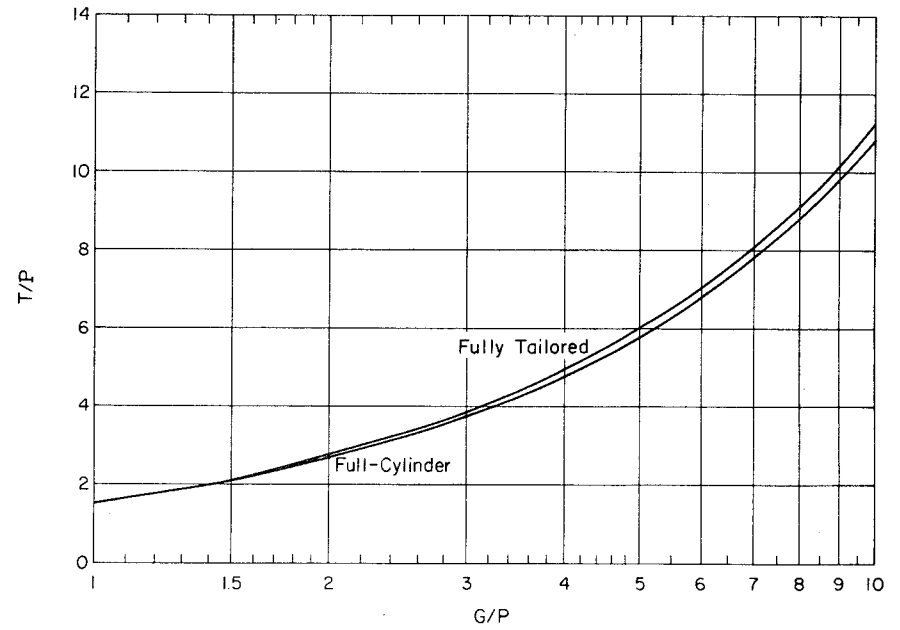


Fig. 7. Total meridional film load at the top of the two extreme zero-pressure, natural-shape, flat-top balloons.

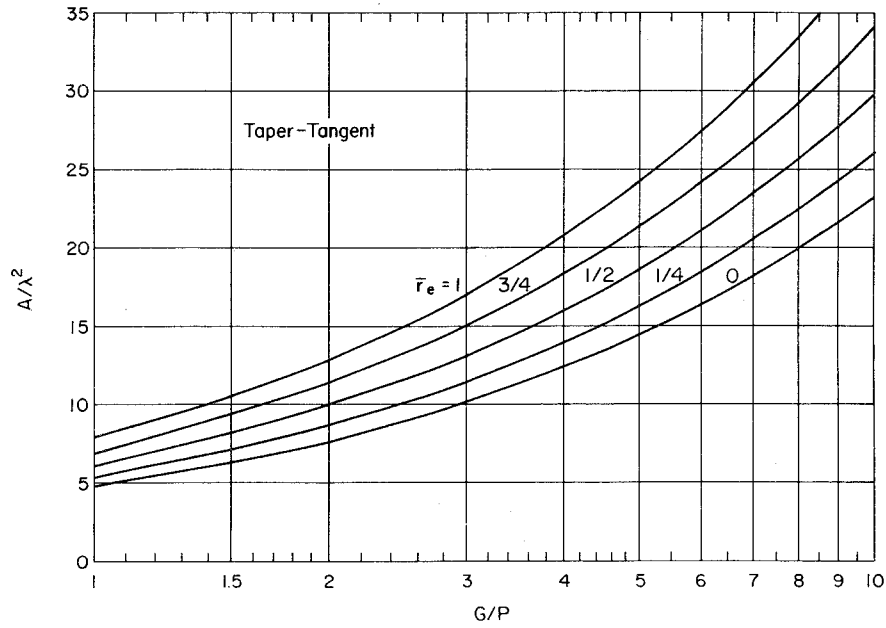


Fig. 8a. Surface area of zero-pressure, natural-shape, flat-top balloons with taper-tangent end sections; \bar{r}_e is the ratio of end-section radius to maximum balloon radius.

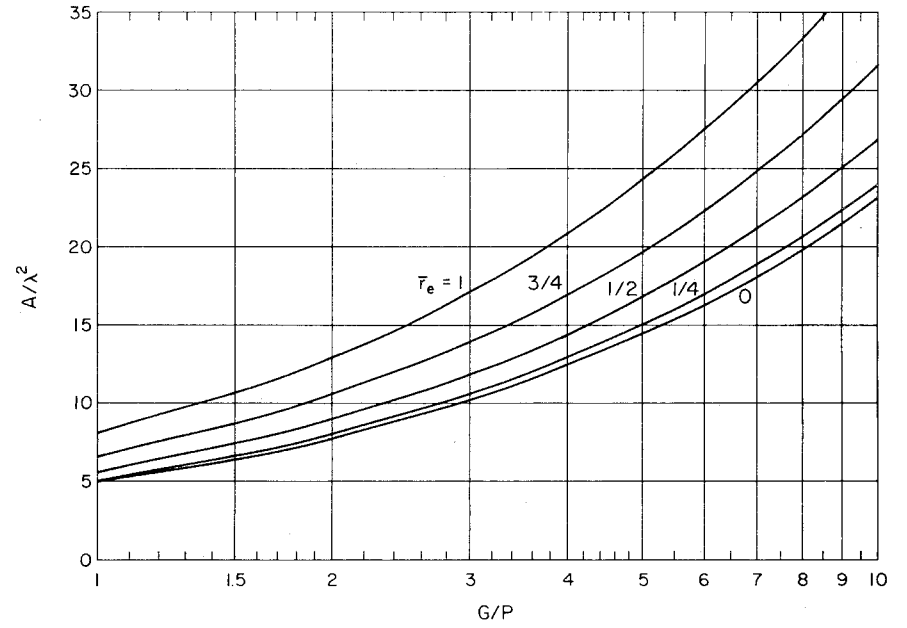


Fig. 8b. Surface area of zero-pressure, natural-shape, flat-top balloons with cylinder end sections; \bar{r}_e is the ratio of end-section radius to maximum balloon radius.

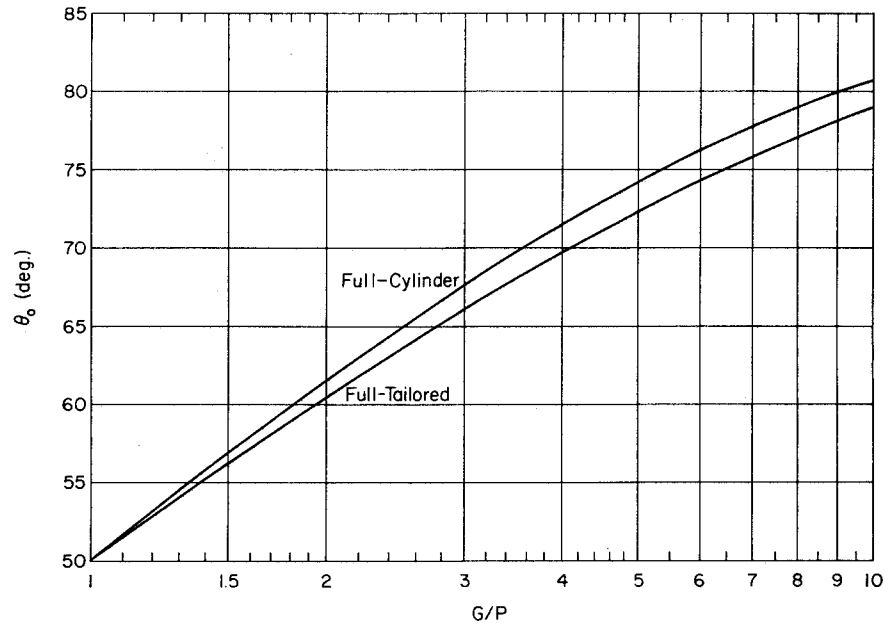


Fig. 9. Nadir angle of the two extreme zero-pressure, flat-top balloons.

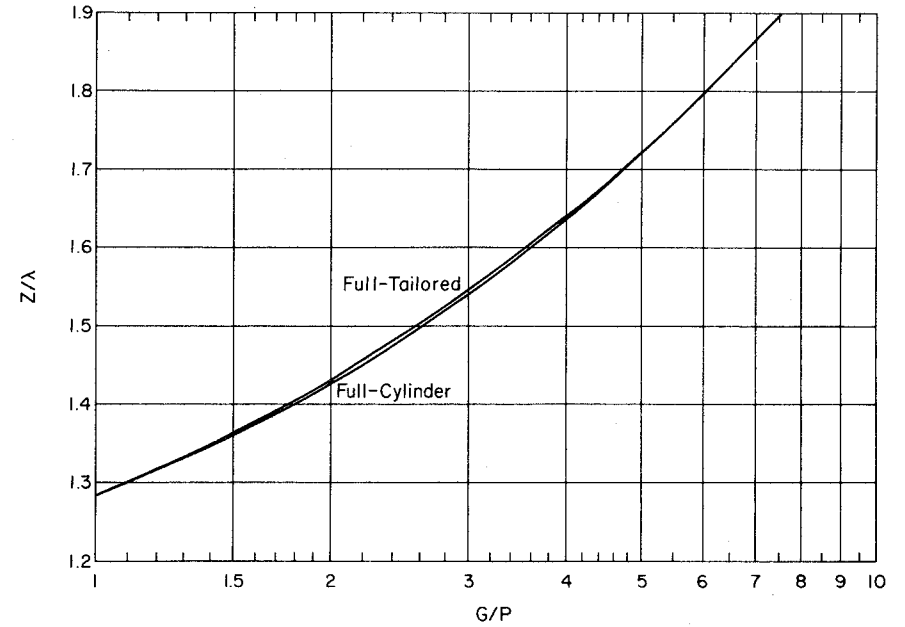


Fig. 10. Overall height of two extreme, zero-pressure, natural-shape, flat-top balloon designs.

follows:

1. Determine total payload P .
 - a. The payload includes: the experimental apparatus; support structure and rigging; shock absorbers; balloon command and control electronics telemetry and antennas; parachute and radar reflector; bottom end fitting; top end fitting; valves and other top loads; and miscellaneous items, e.g., ducts, destruct device, warning lights, pennants, inflation tubes, and electrical wires.

The method that follows determines the balloon size for payload P . If it is desired to accommodate a range of payloads, the P used should be the minimum value.

- b. Find the characteristic length, $\lambda = (P/b)^{1/3}$.

The value of b as a function of altitude in the U.S. Standard Atmosphere, 1962, is given by Fig. 11 of this section and by Table K-1 of Section XII.

For a range of altitudes, b should correspond to the highest altitude.

- c. Form the film weight parameter, $w/b\lambda$.
- d. Calculate Σ where $\Sigma = (2\pi)^{1/3}(w/b\lambda)$ and estimate G/P from

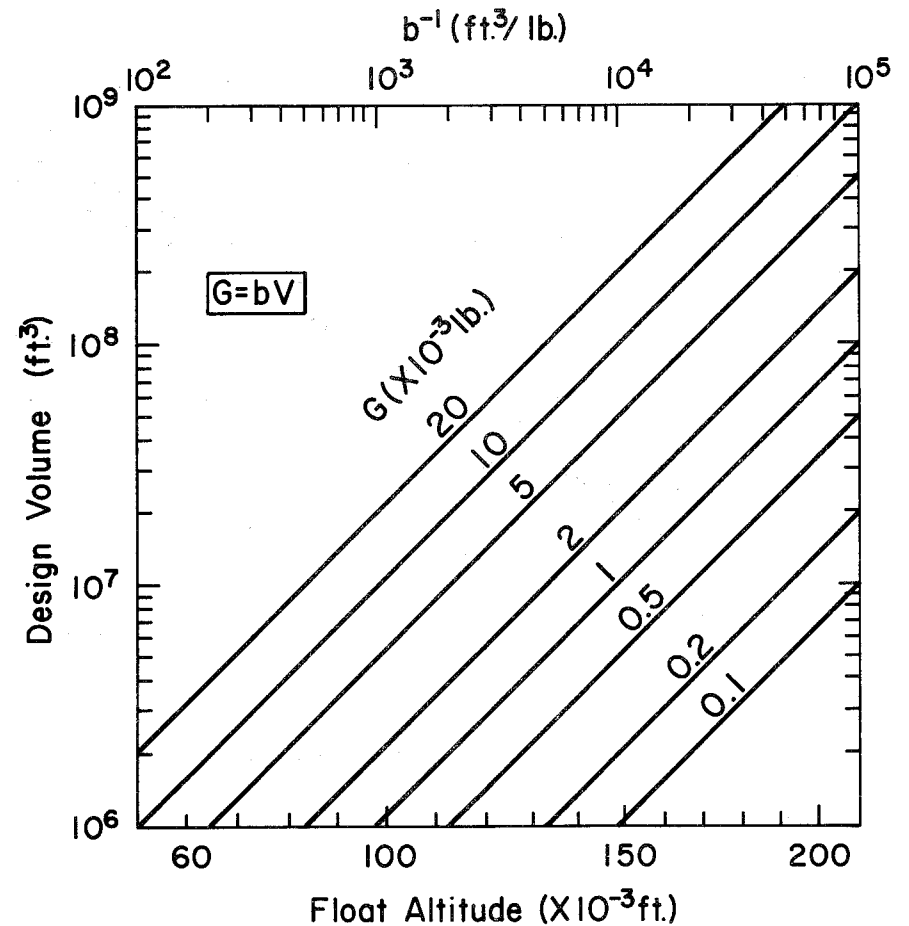


Fig. 11. Graphical solution to the equation $G = bV$. The graph also shows the relationship between specific buoyancy for helium and altitude in the U.S. Standard Atmosphere, 1962.

Fig. 4. Go to step 2b.

2. Determine balloon weight, W .

- a. Form the ratio, $G/P = (W + P)/P$.
- b. From Fig. 5, find the gore length (S/λ); from Fig. 6, find the radius (R/λ); from Fig. 7, find the total film load (T/P); and from Fig. 8, find the surface area (A/λ^2).
- c. Estimate the total film weight, $W_f/P = (A/\lambda^2) (w/b\lambda)$.
- d. Estimate the volume, $V/\lambda^3 = G/P$.
- e. Determine the total seam weight, W_t . The number of seams is $(2 \pi R)/(\text{usable material width})$.

The seam length is the gore length. The seam weight should include the weight of load tapes if used. The strength needed per load tape at float altitude is $(T/P) (\text{Payload}) (\text{Safety Factor})/(\text{Number of tapes})$.

A more critical condition is the load-tape tension at launch. The number of active load tapes is estimated to be $(2 \pi) (\text{radius of launch bubble})/(\text{local gore width at the radius})$. The strength needed in the load tapes at launch is $(GI) (\text{Safety Factor})/(\text{Number of active tapes})$, where GI is the gross inflation for the heaviest payload, including the free lift.

- f. If a balloon needs fullness in the end sections (for manufacturing reasons or because it does not have load tapes), this excess material must be included in the balloon weight. The end-section weight W_{es} is estimated from consideration of its geometry and the film weight. For the specific designs of Fig. 8, the area includes the excess material of the end sections. At the bottom, where θ_0 is the angle the film makes with the vertical (Fig. 9), the total load on the film is $L/\cos \theta_0$, and $(L/\cos \theta_0) (\text{Safety Factor})/(2 \pi r)$ must be less than the allowable film stress, where r is the radius of the bottom end section. At the top $(P) (\text{Safety Factor}) (T/P)/(2 \pi r)$ must be less than the allowable film stress, where r is the radius of the top end section.
- g. The balloon weight is $W = W_f + W_t$.
- h. Repeat 2a through 2g until $bV = G$.

Then the preliminary design is complete. It may be necessary to make slight adjustments to the payload value P if the size estimates vary significantly.

3. Determine the gore pattern. The gore pattern can be calculated from the appropriate Σ table. The height of the balloon is found in Fig. 10.

4. Determine the "Load-Altitude" curve for a range of payloads.

a. Using the value of W from the last iteration of 2g and a series of values of P , calculate corresponding values of G/P , where

$$G/P = (W + P)/P = V/\lambda^3.$$

b. From Fig. 5 determine S/λ for each value of G/P . Using these values of S/λ , the value of S from 2b, and the relationship

$$\lambda = S/(S/\lambda), \text{ calculate corresponding values of } \lambda.$$

c. From the definition of λ , the unit lift b is calculated,

$$b = P/(\lambda^3).$$

d. Finally, from Table K-1 of Section XII, or Fig. 11, the altitude is determined. A plot of these results will be the desired load-altitude curve.

The curve in Fig. 5 is based on the assumption of a perfectly deployed balloon with no weight at the top and bottom end fittings and the assumption that all balloon fabric is evenly deployed over the surface. In real balloons

the ducts are the biggest departure from this latter assumption. For engineering purposes, the manufacturer's stated weight and gore length should be adequate for W and S . A slight increase in the precision would result if the bottom end fitting and material in the end fitting were considered as part of the payload. This also circumvents the problem when $P = 0$.

Note: The data in Table L-1 of Section XII and Figs. 4 through 10 are only for zero-pressure, flat-top, natural-shape balloons. The user will need to modify the procedure if his balloon has a cap or caps, is a multi-cell system, or otherwise deviates significantly from the above designs.

D. CALCULATION OF MERIDIONAL STRESS

A convenient method for calculating meridional stress at any level in the balloon is to consider the balloon as a free body cut at the level in question. Either the part above or below the cut may be considered--which ever is easier. Let the vertical component of the meridional film load be T_v . Then, above the cut, $T_v = B_U + p \pi r^2 - W_U$, and below the cut, $T_v = W_L + p \pi r^2 - B_L$, where B is the buoyant force of gas; W is the weight of balloon, payload, etc.; p is the gas pressure at the cut; r is the radius of the balloon at the cut; L is a subscript referring to the part below the cut; and U

is a subscript referring to the part above the cut.

If z is the vertical distance from the zero-pressure level to the cut, $p = bz$. The total meridional film load T is $T = T_v / \cos \theta$, and the meridional stress is $\sigma_m = T/C$, where C is circumference of the balloon film at the cut. If the cut is in an end section where there is excess material, C will exceed the local balloon circumference.

The buoyant force and weight of a portion of a balloon can be determined from the partial area and partial volume data given in Table L-1, Section XII.

E. BALLOONS BELOW THEIR FLOAT ALTITUDES

The gas is not fully expanded in a balloon which is below its design altitude. As a result, some of the balloon material has large vertical folds in it, the bottom apex angle is reduced, and the position of the zero-pressure level is somewhat above the base of the balloon. These effects are most obvious just after launch. The shapes and stresses in such balloons have been calculated for the ideal case in which the excess material along the gore is uniformly distributed around the circumference, Smalley (1). This is known to be unrealistic for an ascending balloon. The vertical distribution of pressure determined by these same calculations is, however, representative

of the real balloon. From Fig. 12 the pressure at the top of a balloon may be calculated at any altitude below the design altitude for all styles of natural-shape balloons from fully tailored to full cylinder, for $\Sigma < 1$. The pressure is given in terms of the distance from the zero-pressure level to the top of the balloon. This head h is readily converted to pressure units if desired by the following equation:

$$\frac{p}{b_d \lambda_d} = \frac{h}{S} \frac{S}{\lambda_d} \frac{b}{b_d}$$

where the subscript denotes a value at the design condition.

1. Cutting the Duct to Change Float Altitude

The data in reference 1 can be used to determine where to cut a valving duct to cause a balloon to float below its design altitude. At design conditions, b_d is the specific lift and (G/P_d) is the ratio of gross weight to design payload weight. With the specific lift b at the new float altitude, Fig. 13 can be used to find the position of the zero-pressure level in gore length units. Cutting the duct at this position will cause the balloon to level off at the new altitude when carrying the design payload. For heavier payloads a new load-altitude curve should be constructed along the lines of the method of sub-Section C.4.

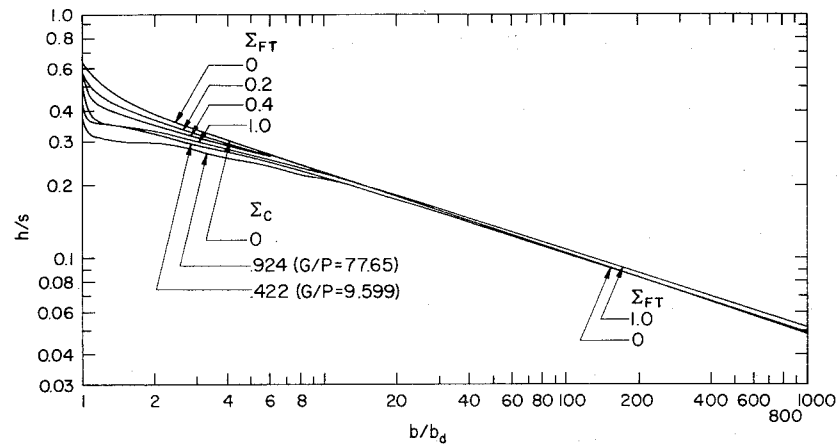


Fig. 12. Pressure heat at the top of various zero-pressure, natural-shape, flat-top balloons.

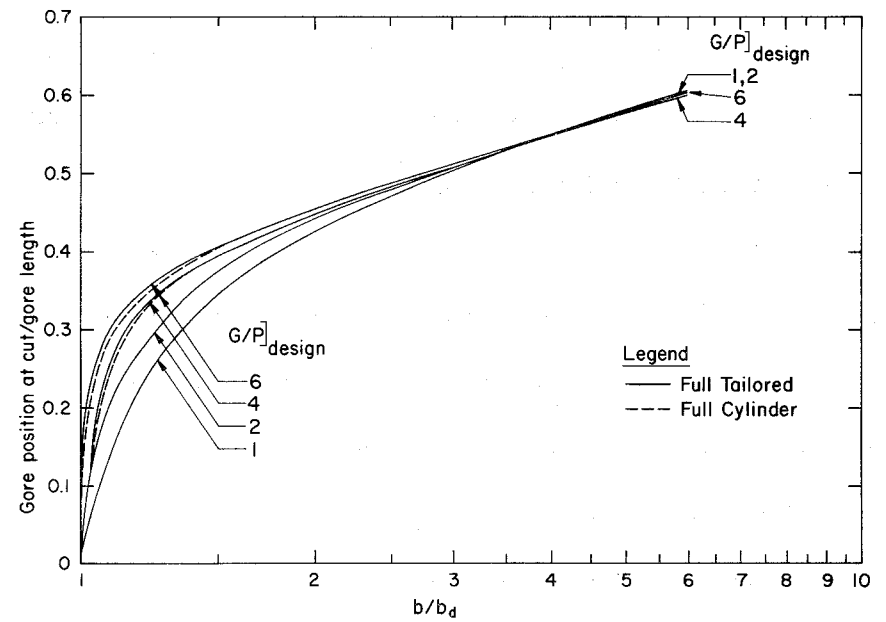


Fig. 13. Zero-pressure level in balloons below their design altitude as a basis for cutting the valving duct.

F. BALLOONS WITH CIRCUMFERENTIAL STRESS

A great amount of design work has been done (e.g., Table L-1 of Section XII and Figs. 4 through 10) and a great number of balloons have been built for which the circumferential stress was intentionally held zero. However, when considering balloons for very high altitudes, it is found that the natural shape pays a weight penalty when compared to the ideal spherical balloon. This penalty can be reduced if the balloon is designed to have circumferential stress. With today's materials and sealing methods, such a step is feasible. Various styles have been investigated and are discussed in the following sub-section.

1. The Ideal (i.e., Spherical) Balloon

As a basis for comparison, the weight and stresses for buoyant spheres are given first. The assumptions are made that: the shape is perfectly spherical (regardless of the magnitudes of the stresses) and the payload is attached along a circumferential ring with a force resultant which is tangent to the balloon surface at the ring.

Let p_o be the internal pressure at the center, R the radius, and ϕ the angular coordinate of points on the sphere--positive above the equator. Integrating the internal pressure over the surface of the sphere,

we find the film stresses to be

$$\frac{\sigma_m}{bR^2} = \frac{p_o}{2bR} + \frac{P}{3bV} K_m + \frac{\sin \phi}{3} \quad (9)$$

$$\frac{\sigma_c}{bR^2} = \frac{p_o}{2bR} + \frac{P}{3bV} K_c + \frac{\sin \phi}{3} \quad (10)$$

where, above the payload attachment,

$$K_m = \frac{1}{1 + \sin \phi}$$

$$K_c = \sin \phi - \frac{1}{1 + \sin \phi}$$

and, below the payload attachment,

$$K_m = \frac{1}{\sin \phi - 1}$$

$$K_c = \sin \phi - \frac{1}{\sin \phi - 1}$$

The stresses for a weightless sphere ($P/bV = 1$) are given in Fig. 14.

Several points should be noted. Meridional and circumferential stresses are equal only at the poles. There are discontinuities in both stresses where the payload is attached. The changes in stresses are

$$(\Delta\sigma_m/bR^2) = -(\Delta\sigma_c/bR^2) = \frac{2P}{3bV \cos^2 \phi}$$

These are minimum when $\phi = 0$. There is some value of p_o which will ensure

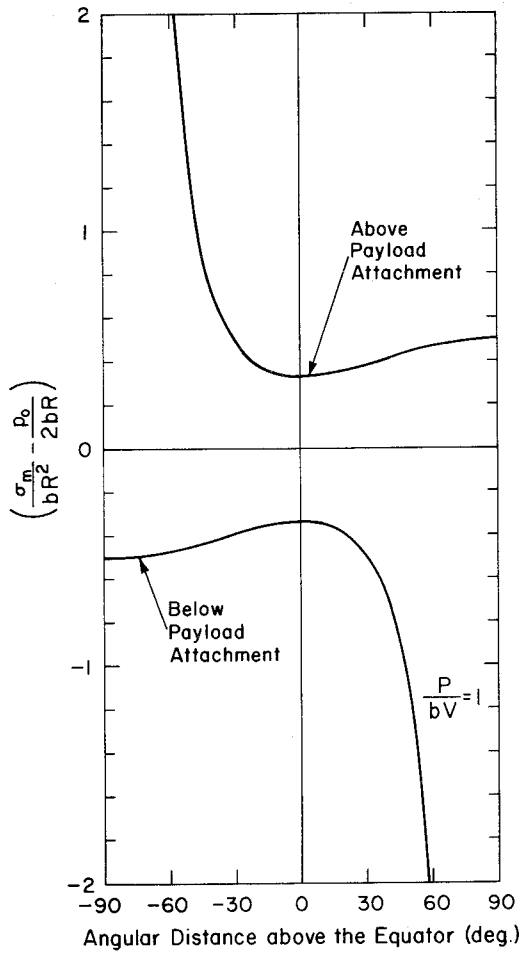


Fig. 14a. Meridional stress in an ideal, spherical, weightless, buoyant balloon.

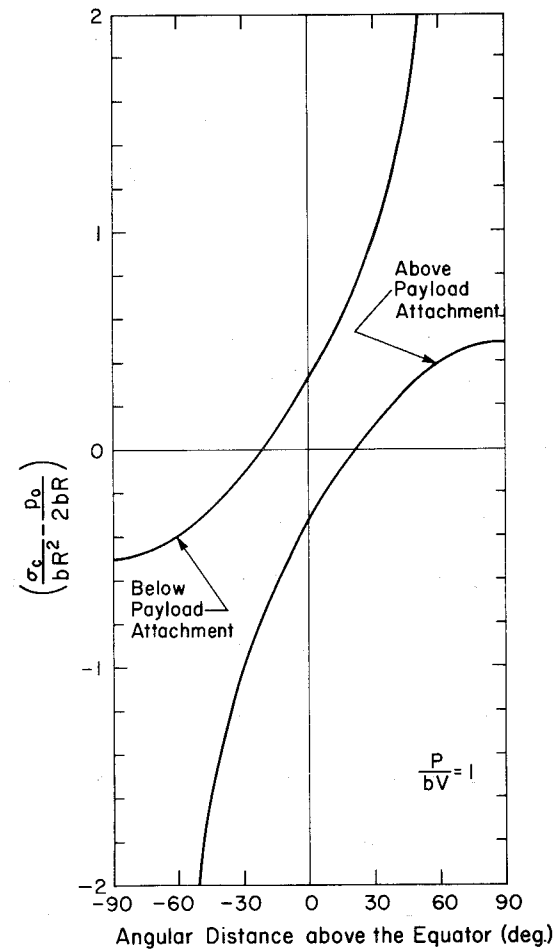


Fig. 14b. Circumferential stress in an ideal, spherical, weightless, buoyant balloon.

tension throughout the sphere no matter where the payload is attached (excepting the nadir). For example, if the payload is attached on the -30° latitude line, $p_o/2bR$ must be at least 1.0 to assure that $\sigma_c \geq 0$ above the payload attachment. It can be seen from Eqs. (9) and (10) that only when the payload is negligible ($P/bV = 0$) are the stresses equal to each other everywhere on the sphere. The minimum permissible pressure to maintain a spherical shape is determined by the stresses at the bottom. Here $\sigma_m = \sigma_c$ and the minimum pressure value is

$$\frac{p_o}{2bR} = \frac{P}{6bV} + \frac{1}{3}$$

If the pressure at the base of the sphere is exactly zero, then $p_o = bR$

and the location of zero circumferential stress is

$$\phi = \arcsin \left[\frac{\sqrt{\left(20 \frac{P}{bV} + 12\right) \frac{P}{bV} + 1} - 5 - 2 \frac{P}{bV}}{4 \left(\frac{P}{bV} + 1\right)} \right]$$

Example results are

$\frac{P}{bV}$	1	1/2	1/3	1/4	1/5
ϕ	-9.03	-25.00	-33.96	-39.92	-49.27

The payload attachment ring should not be lower on the balloon than these

angular positions.

For analysis purposes, it is desirable to know the volume of such ideal spheres as a function of film weight. If, as noted earlier,

$$\lambda^3 = P/b$$

$$\Sigma = (2\pi)^{1/3} (w/b\lambda)$$

$$V/\lambda^3 = bV/P = (W/P) - 1$$

then

$$V/\lambda^3 = 1 + 18^{1/3} (V/\lambda^3)^{2/3} \Sigma$$

This relationship has been solved in reference (2), and the results are presented in Table 1.

2. Round-Top Balloons

The ideal spherical balloons described in the sub-Section F.1 have the disadvantage that the payload must be applied at a circumferential ring. Such an attachment would be difficult to manufacture. Also, at this ring there are discontinuities in the stresses. From an efficiency standpoint, however, it would be desirable to approach closely the spherical shape. In the early days of plastic balloons a sphere-on-cone combination was used. This design suffered from the weak seam strength obtainable at that time.

Table 1

Non-dimensional Physical Parameters of Ideal Spherical Balloons

Σ	Radius	Gore Length	Area	Volume
0	0.62035	1.94889	4.83598	1.00000
0.1	0.67955	2.13487	5.80301	1.31448
0.2	0.74980	2.35556	7.06477	1.76572
0.3	0.83233	2.61485	8.70573	2.41536
0.4	0.92770	2.91446	10.81503	3.34438
0.5	1.03552	3.25319	13.47502	4.65123

It also had the disadvantage that there must be a discontinuity in circumferential stress at the juncture where the cone is tangent to the sphere.

It is possible, however, to match both the circumferential and meridional stresses by using a shape other than a cone. Figure 14b shows that, by proper choice of pressure, it is possible to obtain zero circumferential stress at any desired level on the sphere. It is probably simplest to match the stresses by using a natural shape below the zero stress level. The characteristics of such a design are given in Table 2. Table 2(a) gives results for round-top balloons with a fully tailored section. Table 2(b) gives results for full-cylinder bottom end sections. All other end-section designs fall between these two extremes.

As with all natural shapes, meridional stress is infinite at the nadir of the fully tailored bottom section. This must be accommodated by either tapes or fullness. No fullness is required at the top because the stresses are finite. However, caution should be exercised because stresses during inflation, launch, and ascent may exceed the design stresses at float. The results presented in Table 2 are only representative of the conditions at float.

Table 2

Non-Dimensional Physical Characteristics of Round-Top Balloons
(Zero superpressure, natural-shape bottom section, no load on top)

(a) Fully Tailored Bottom Section								
Σ	Base Angle	Radius	Height	Gore Length	Area	Volume	Sphere Size (deg)	Maximum Stress
0	47.778	0.61055	1.48344	2.05815	4.88155	1.00000	137.78	0.453
0.1	51.446	0.67249	1.57653	2.22657	5.84775	1.31691	141.45	0.512
0.2	55.262	0.74496	1.69084	2.43039	7.10691	1.77028	145.26	0.589
0.3	59.099	0.82917	1.83030	2.67420	8.74356	2.42151	149.10	0.691
0.4	62.809	0.92572	1.99683	2.96031	10.847	3.35138	152.81	0.824
0.5	66.253	1.03431	2.19055	3.28788	13.501	4.65835	156.25	0.993
(b) Full-Cylinder Bottom Section								
Σ	Base Angle	Radius	Height	Gore Length	Area	Volume	Sphere Size (deg)	Maximum Stress
0	47.778	0.61055	1.48344	2.05815	6.35400	1.00000	137.78	0.453
0.1	53.314	0.69008	1.60959	2.27996	7.80485	1.42297	143.31	0.537
0.2	58.864	0.78201	1.76167	2.54417	9.67403	2.04852	148.86	0.646
0.3	64.093	0.88609	1.94044	2.85074	12.0415	2.95769	154.09	0.788
0.4	68.739	1.00128	2.14470	3.19647	14.9738	4.24588	158.74	0.965
0.5	72.672	1.12597	2.37163	3.57585	18.5179	6.01766	162.67	1.183

3. Constant Circumferential Stress

The effect of a constant amount of circumferential stress along the entire gore is illustrated by an example in Fig. 15. The maximum possible circumferential stress is approximately 0.325 because at that value the bottom apex angle is essentially zero. It would be possible to use greater values of circumferential stress only if the initial pressure were positive. This design is not considered a practical one since it saves very little weight over the natural-shape design and would be difficult to manufacture in the areas near the end fittings. Examination of the defining equations and the figure shows that this style balloon has a negative meridional radius of curvature at the bottom.

4. Circumferential Stress Proportional to Meridional Stress

From the standpoint of reducing manufacturing tolerances, it is desirable to have zero circumferential stress at the end fittings. Circumferential stress may then exist for intervening points on the balloon. One such design uses circumferential stress as $\sigma_c = c(\sigma_m - \sigma_{mo})$, where σ_m is the local meridional stress, σ_{mo} is the meridional stress at nadir, and c is a constant.

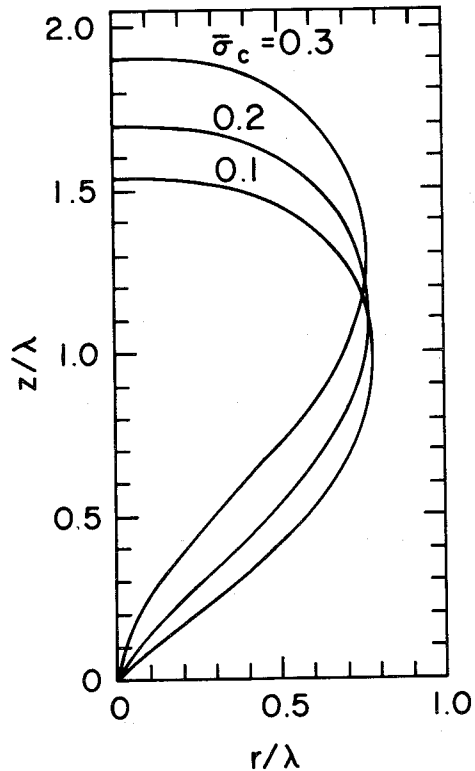


Fig. 15. Shapes of balloons with constant circumferential stress.

The balloons are zero-pressure, and $\Sigma = 0.2$.

Three cases arise. First, if $c < 1$, circumferential stress diverges at the zenith. Second, when $c = 1$, the circumferential stress rises asymptotically to a maximum at the zenith. Interestingly, this results in the total meridional film load being equal at the nadir and the zenith. Third, if $c > 1$, the circumferential stress tends to zero at the zenith. A value to use for the constant in this last case is somewhat arbitrary. Solutions to the equations do not exist if c is too large. Manufacturing tolerances would probably have to be tight to achieve the stress distribution predicted. Data for the case when $c = 1$ is presented in Table 3.

Another possibility for a design with zero circumferential stress at the nadir and zenith would be to use $\sigma_c = c$ (radius). The value of the constant to use would depend upon permissible stress level. No general data have been generated for this design.

G. COMPARISON OF BALLOON DESIGNS

Most large balloons have been and will continue to be made with the natural-shape design, i.e., with zero circumferential stress. Such balloons are quite efficient, and their simplicity and demonstrated reliability recommend them for normal use.

Table 3

Non-Dimensional Physical Characteristics of Balloons with Circumferential Stress
Equal to Net Meridional Stress
(Zero superpressure, fully-tailored, flat-top)

Σ	Base Angle	Radius	Height	Gore Length	Area	Volume	Maximum T/P*	Maximum $\frac{\sigma}{c}$
0	50.159	0.65219	1.28421	1.99441	4.91628	1.00000	1.56056	0.00000
0.1	52.615	0.71479	1.39793	2.17142	5.89795	1.31963	1.89687	0.07509
0.2	55.620	0.78945	1.50544	2.37943	7.17588	1.77776	2.36045	0.18650
0.3	59.129	0.87764	1.63751	2.62241	8.83555	2.43646	3.00122	0.26585
0.4	63.001	0.98014	1.78457	2.90297	10.9696	3.37789	3.88355	0.38634
0.5	66.993	1.09670	1.94666	3.22156	13.6673	4.70332	5.08494	0.52729

* Maximum T/P does not occur at the top of the balloon. In fact, in this design, T/P at the top equals the value at the bottom.

In the comparison to follow, the ideal buoyant sphere is used as a standard. For a given altitude, payload, and gas-barrier material, balloons should all be compared at the same Σ value. The designs presented in the foregoing sub-sections are compared in Table 4.

All weightless balloons ($\Sigma = 0$) are 100% efficient. As the film weight parameter increases ($\Sigma > 0$), efficiency decreases. The exceptions are those balloons with circumferential stress at the zenith, because they are more spherical. Balloons with circumferential stress are more efficient than natural-shape balloons. The exception is a round-top balloon with a cylinder end; however, this is an extreme design and would not be used. It can be seen that end sections quickly reduce efficiency.

The data in Tables 1 through 3 can be plotted as in Figs. 4 through 10, and a preliminary design made as outlined in sub-Section C.

Table 4

Comparison of Balloon Designs on the Basis of Balloon Weight

Designs	$\Sigma = 0.2$	$\Sigma = 0.4$
Ideal Sphere	1.	1.
Natural-Shape		
fully-tailored	0.9769	0.9615
cylinder end*	0.9246	0.8921
taper-tangent end*	0.8300	0.7686
Circumferential Stress Equal to Net Meridional Stress	0.9845	0.9859
Round-Top		
fully-tailored	0.9941	0.9970
full-cylinder end	0.7303	0.7223

* These designs are listed as being more representative of real balloons.
The ratio of end section radius to maximum radius is 0.25.

REFERENCES

- (1) Smalley, J. H., 1966: Balloon Shapes and Stresses Below the Design Altitude. NCAR-TN-25, December 1966.
- (2) Smalley, J. H., 1964: Determination of the Shape of a Free Balloon. AFCRL-65-68, Scientific Report No 4, November 1964.

SECTION VI

SCIENTIFIC BALLOON INSTRUMENTATION

by

Oscar L. Cooper

List of Symbols	iii	E. BALLOON CONTROL	74
List of Figures	v	<u>1. Ballasting</u>	75
List of Tables	vi	<u>2. Valving</u>	76
A. INTRODUCTION	1	<u>3. Flight Termination</u>	77
B. TELEMETRY AND DATA RECOVERY	1	<u>4. Timers</u>	78
<u>1. Basic Techniques</u>	3	F. TRAJECTORY DETERMINATION.	79
<u>a. FM/FM telemetry</u>	3	<u>1. Radar Tracking</u>	81
<u>b. Pulse-code-modulation telemetry</u>	17	<u>2. Rawin Set.</u>	83
(1) PCM data encoding	18	<u>3. Phase Shift Ranging</u>	84
(2) PCM data recovery	25	<u>4. Omega.</u>	86
<u>c. Pulse-amplitude-modulation telemetry</u>	29	<u>5. Tracking Aircraft.</u>	95
<u>d. Pulse duration modulation</u>	32	<u>6. FAA Transponder.</u>	96
<u>2. The Radio Frequency Link</u>	40	G. PRESSURE-ALTITUDE	97
<u>3. On-Board Data Recording</u>	53	<u>1. Barocoder.</u>	98
C. COMMAND-CONTROL	55	<u>2. Diaphragm Gages.</u>	100
<u>1. Tone Modulation</u>	57	<u>3. Thermoconductivity Gages</u>	103
<u>2. Tone-Digital Systems</u>	64	<u>4. Other Types of Pressure Transducers.</u>	104
<u>3. PCM Command</u>	68	<u>5. Altitude Measuring Devices</u>	108
<u>4. Verification</u>	71	REFERENCES	118
<u>5. Radio-Frequency Link</u>	72		
D. COMMUNICATION REPEATER	73		

LIST OF SYMBOLS

<u>Symbol</u>	<u>Description</u>	<u>Dimensions</u>			
a	subscript used to identify its symbol with antenna		R	range from balloon borne radio system to ground system	L
b	subscript used to identify its symbol with balloon		R	resistance	ohms
B	bandwidth	T^{-1}	T	temperature	θ
c	speed of light (3×10^8 m/sec)	LT^{-1}	<u>Greek Letters</u>		
C	capacitance		Δf	maximum frequency deviation of a subcarrier oscillator	T^{-1}
d	distance from a point on the ground below a balloon system to the radio horizon	L	λ	wave length	L
D	distance from an airborne balloon system to the radio horizon	L			
DR	deviation ratio				
f_r	pulse repetition rate of radar	T^{-1}			
F	noise factor				
F	maximum value of the data modulation frequency	T^{-1}			
G	gain				
h	height of an airborne balloon system	L			
k	Boltzmann constant ($1.38 \times 10^{-23} \text{ J K}^{-1}$)	$ML^2 T^{-2} \theta^{-1}$			
L	transmission loss				
n	integer				
n	subscript used to identify its symbol with noise				
N	total noise power				
NF	noise figure (NF = 10 log F)				
o	subscript used to identify its symbol with a base or reference level				

List of Figures

Fig. 1	Typical balloon instrumentation system	2
Fig. 2	FM/FM telemetry system block diagram	10
Fig. 3	Pre-emphasis curve for 3/2 power tapers.	14
Fig. 4	PCM data transmitting system	19
Fig. 5	PCM commutation and data formats using a simple commutator (a) and a commutator with subcommutators (b). Channel 8 in (a) and channels 15 and 16 in (b) are used for frame synchronization	22
Fig. 6	Waveforms of pulse code information.	24
Fig. 7	Block diagram of PCM data recovery system	27
Fig. 8	PCM data recovery equipment	30
Fig. 9	PAM pulse train waveform	31
Fig. 10	Block diagram of a typical PDM system	34
Fig. 11	PDM pulse train waveform	36
Fig. 12	Waveforms (a) used to create PDM bargraph display (b)	38
Fig. 13	L-Band telemetry receiving antenna	43
Fig. 14	Block diagram of two amplifiers in series	49
Fig. 15	Block diagram of UHF telemetry system	51
Fig. 16	Signal power-level diagram	52
Fig. 17	Block diagram of a tone modulated command system	59
Fig. 18	Latching relay circuit for single command channel operation	61
Fig. 19	Address-execute tone command structure	63
Fig. 20	Tone-digital command word structure and format	65
Fig. 21	Digital timer block diagram (a) and a photograph of the timer (b). Pulses from a crystal oscillator are divided to yield a 10 pulse/hr clock. Memory registers store counting bits for tenths of hours, hours, and tens of hours. The timer shown in (b) has two auxilliary sets of switches for additional timed functions, and more can be added if desired.	80
Fig. 22	Omega transmission format	89
Fig. 23	Omega land pattern between a pair of stations	91
Fig. 24	Block diagram of Omega system for balloon position determination	93
Fig. 25	Typical calibration curve for thermoconductivity pressure gage	105
Fig. 26	The NCAR integrated flight support package	114a

List of Tables

Table 1	Proportional subcarrier channels	6
Table 2	Constant bandwidth subcarrier channels	9
Table 3	Example of pre-emphasis scheduling	16
Table 4	Radio-horizon range for balloons at various altitudes	45

SCIENTIFIC BALLOON INSTRUMENTATION

A. INTRODUCTION

The free balloon has provided science with a very useful means of reaching the upper levels of the earth's atmosphere. To take full advantage of the balloon's capability as a scientific platform, methods for determining the balloon's trajectory, recovering the scientific data, and controlling the scientific equipment and balloon system are needed. Several radio linkages are necessary for complete instrumentation between the ground station and the balloon system, as illustrated in Fig. 1. Some of the systems and techniques required to accomplish the necessary communication and control are discussed in this section.

B. TELEMETRY AND DATA RECOVERY

All scientific balloon experiments must have a means of retrieving the data for real-time and post-flight analysis. Earlier experiments relied upon on-board recording such as tape recorders, photographic film, charts, and emulsion plates. Since telemetry has been introduced to scientific ballooning, most data are recovered in real time through radio transmission and are

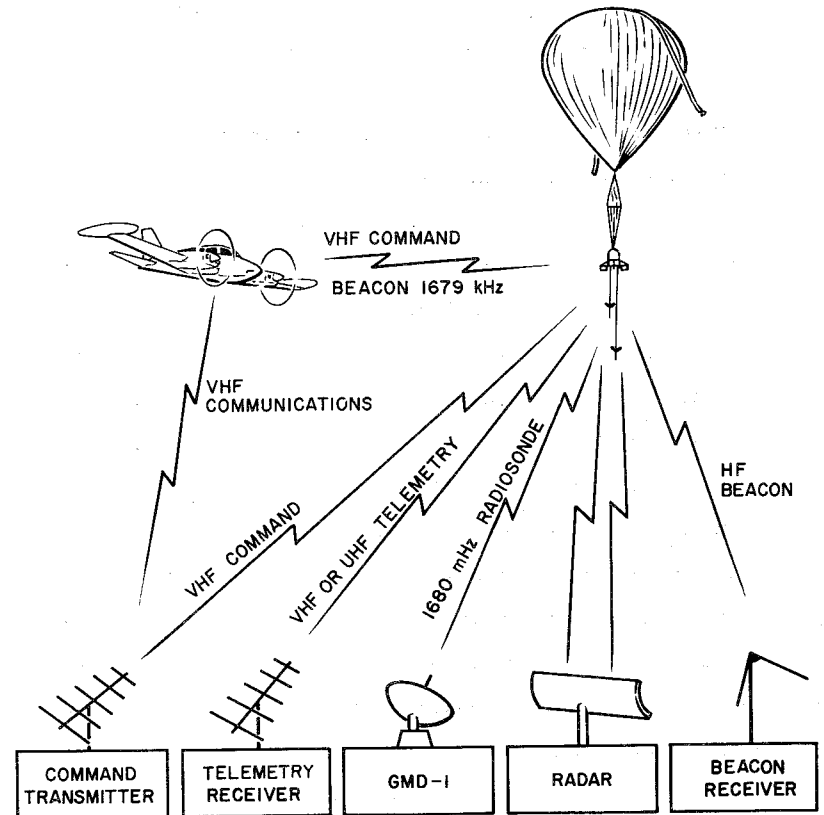


Fig. 1. Typical balloon instrumentation system.

recorded with graphic recorders, digital printers, or on magnetic tape for later computer analysis.

Telemetry may be defined as the science of transmitting data from inaccessible to accessible locations. Aerospace telemetry requires the transmitting of information from air and space vehicles to accessible (usually ground) locations. The source instruments of the system, sometimes called transducers, convert physical quantities, such as pressure, temperature, or strain into electrical signals, which can be transmitted to an accessible location, such as a balloon instrumentation ground station, where they are recorded for study, Stiltz (1).

1. Basic Techniques

The basic telemetry techniques in use today are FM/FM, PCM (pulse-code-modulation), PAM (pulse-amplitude-modulation), and PDM (pulse-duration-modulation). The first two are the most commonly used for general purpose data recovery from balloons and receive the most discussion here. Some balloon experiments include special purpose data encoders and use a coding technique which does not have a standard data format.

In order to establish standards for radio telemetry in the atmospheric

and space research fields, a standardization committee called the Inter-Range Instrumentation Group (IRIG) has established standards which are used by the telemetry industry to standardize telemetry techniques and equipment performance. The most recent compilation of the IRIG standards is found in IRIG Document 106-69 (2).

The subject of telemetry is extensive and is discussed only briefly in this section. A more complete discussion of the theory and application of telemetry may be found in Stiltz (1) and Gruenberg (3).

Radio telemetry systems are commonly classified in accordance with the methods employed to multiplex and modulate the RF carrier. The two basic methods for multiplexing are frequency division and time division. In frequency division the data signals from separate instruments are kept independent of each other by separate allocation of frequency channels, in time division separate periods of time are provided for each channel. The former is used in FM/FM telemetry, while the latter is used for pulse telemetry systems such as pulse-code-modulation (PCM).

a. FM/FM telemetry. The designation FM/FM refers to a frequency division technique of modulating a telemetry transmitter with the output of one

or more subcarrier oscillators which, in turn, are frequency modulated by data signals. One of the principal advantages of using FM/FM telemetry is the fact that a properly designed system will suppress noise caused by intermodulation, thermal agitation, and microphonics to a considerable degree. The ratio of the maximum deviation of a subcarrier oscillator Δf to the maximum value of the data modulation frequency F is called the deviation ratio.

$$DR = \frac{\Delta f}{F}$$

The greater this ratio the less noise the system will have. The same applies to the carrier deviation by the subcarriers. In practice, the system should be operated to make the best compromise between noise suppression and intelligence carrying capacity. The maximum data bandwidth of a channel has been defined by IRIG as that frequency which yields a deviation ratio of 5 when the subcarrier is deviated $\pm 7\frac{1}{2}\%$ (or 15% in some cases) of the center frequency, Bendix (4).

Table 1 lists the IRIG proportional bandwidth subcarrier channels and the data bandwidth of each channel. The designation proportional-bandwidth channel indicates that the width of each channel is proportional to its

Table 1

Proportional Subcarrier Channels

Channel	$\pm 7.5\%$ Channels						
	Center Frequencies (Hz)	Lower Deviation Limit* (Hz)	Upper Deviation Limit* (Hz)	Nominal Frequency Response (Hz)	Nominal Rise Time (ms)	Maximum Frequency Response*** (Hz)*	Minimum Rise Time*** (ms)
1	400	370	430	6	58	30	11.7
2	560	518	602	8	42	42	8.33
3	730	675	785	11	32	55	6.40
4	960	888	1,032	14	24	72	4.86
5	1,300	1,202	1,398	20	18	98	3.60
6	1,700	1,572	1,828	25	14	128	2.74
7	2,300	2,127	2,473	35	10	173	2.03
8	3,000	2,775	3,225	45	7.8	225	1.56
9	3,900	3,607	4,193	59	6.0	293	1.20
10	5,400	4,995	5,805	81	4.3	405	.864
11	7,350	6,799	7,901	110	3.2	551	.635
12	10,500	9,712	11,288	160	2.2	788	.444
13	14,500	13,412	15,588	220	1.6	1,088	.322
14	22,000	20,350	23,650	330	1.1	1,650	.212
15	30,000	27,750	32,250	450	.78	2,250	.156
16	40,000	37,000	43,000	600	.58	3,000	.117
17	52,500	48,562	56,438	790	.44	3,938	.089
18	70,000	64,750	75,250	1050	.33	5,250	.067
19	93,000	86,025	99,975	1395	.25	6,975	.050
20**	124,000	114,700	133,300	1860	.19	9,300	.038
21**	165,000	152,625	177,375	2475	.14	12,375	.029
	$\pm 15\%$ Channels****						
A	22,000	18,700	25,300	660	.53	3,300	.106
B	30,000	25,500	34,500	900	.39	4,500	.078
C	40,000	34,000	46,000	1200	.29	6,000	.058
D	52,500	44,625	60,375	1575	.22	7,875	.044
E	70,000	59,500	80,500	2100	.17	10,500	.033
F	93,000	79,050	106,950	2790	.13	13,950	.025
G**	124,000	105,400	142,600	3720	.09	18,600	.018
H**	165,000	140,250	189,750	4950	.07	24,750	.014

* Rounded off to nearest Hz.

** Recommended for use in UHF transmission systems only.

*** The indicated maximum data frequency response and minimum rise time is based upon the maximum theoretical response that can be obtained in a bandwidth between the upper and lower frequency limits specified for the channels.

**** Channels A through H may be used by omitting adjacent lettered and numbered channels. Channels 13 and A may be used together with some increase in adjacent channel interference.

center frequency. The channels were chosen to make the best use of present equipment and of the frequency spectrum. There is a ratio of approximately 1.33:1 between center frequencies of adjacent bands, except between 14.5 kHz and 22 kHz, where a larger gap was left for a compensation tone for magnetic tape recording. The deviation is kept at $\pm 7\frac{1}{2}\%$ for all bands, with the option of $\pm 15\%$ deviation on the eight highest bands to provide for transmission of higher data bandwidth information. The nominal frequency response listed for each band is computed on the basis of maximum deviation ($7\frac{1}{2}\%$ or 15%) and a deviation ratio of 5. While deviation ratios of 5 are recommended, ratios as low as 1 or less may be used for a higher data bandwidth, but in that case low signal-to-noise ratios, possibly increased harmonic distortion and cross talk must be expected, Stiltz (1). As a rule, the rms signal-to-noise ratio of a specific channel varies as the $3/2$ power of the subcarrier frequency employed.

As flexible and useful as the IRIG proportional bands are, there are many instances in which their progressive channel capacities do not provide a satisfactory distribution of channel bandwidths, particularly when a large number of data channels have the same data bandwidth requirements. A

system of IRIG constant bandwidth channels is listed in Table 2. The column headings state the deviation and frequency response for the three arrangements of subcarrier channels. The two frequency responses indicated in each column are based on deviation ratios of 5 and 1, Gruenberg (3).

Combinations of proportional and constant bandwidth subcarriers may be used, provided proper precautions are taken to avoid crosstalk.

Figure 2 is a simplified block diagram of an airborne FM/FM telemetry package containing several subcarrier oscillators. Physical phenomena within the scientific balloon experiment are converted to analog signals, usually ranging from 0 to 5 volts, to deviate the subcarrier oscillator. The frequency modulated outputs of all subcarrier oscillators are then mixed and amplified, thus providing a source of modulation energy which is used to frequency-modulate the transmitter. The transmitted RF signal is received at one or more ground stations where it is demodulated, Cooper (5).

Figure 2 includes a simplified block diagram of a telemetry receiving station capable of receiving, separating, and displaying signals which are proportional to the analog data or transducer outputs of the balloon-borne equipment. The received RF signal is demodulated by the receiver to produce

Table 2

Constant Bandwidth Subcarrier Channels

A Channels		B Channels		C Channels	
Deviation limits = ± 2 kHz		Deviation limits = ± 4 kHz		Deviation limits = ± 8 kHz	
Nominal frequency response = 0.4 kHz		Nominal frequency response = 0.8 kHz		Nominal frequency response = 1.6 kHz	
Maximum frequency response = 2 kHz**		Maximum frequency response = 4 kHz**		Maximum frequency response = 8 kHz	
Channel	Center Frequency (kHz)	Channel	Center Frequency (kHz)	Channel	Center Frequency (kHz)
1A	16				
2A	24				
3A	32	3B	32		
4A	40				
5A	48	5B	48		
6A	56				
7A	64	7B	64	7C	64
8A	72				
9A	80	9B	80		
10A	88				
11A	96	11B	96	11C	96
12A	104				
13A	112	13B	112		
14A	120				
15A	128	15B	128	15C	128
16A*	136				
17A*	144	17B*	144		
18A*	152				
19A*	160	19B*	160	19C*	160
20A*	168				
21A*	176	21B*	176		

* Recommended for use in UHF transmission systems only.

** The indicated maximum frequency response is based upon the maximum theoretical response that can be obtained in a bandwidth between deviation limits specified for the channel.

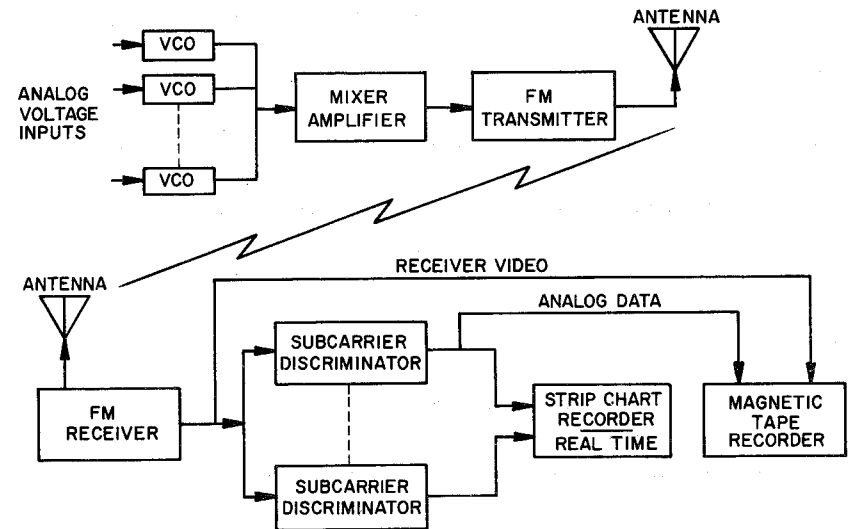


Fig. 2. FM/FM telemetry system block diagram.

the multiplexed signal which is equivalent to that at the output of the mixer-amplifier in the airborne package. The multiplexed signal is then routed to several subcarrier discriminators, corresponding to the subcarrier frequencies used, where the subcarrier signals are separated, and data signals proportional to the analog data are recovered. Separation of the subcarrier signals is accomplished by the use of bandpass input filters in the discriminators. Each filter is capable of passing a band of frequencies centered about the center frequency of the subcarrier channel. The filter bandwidth depends upon the percentage deviation of the channel.

In addition to the bandpass input filter, each discriminator contains a low-pass output filter. Cut-off frequencies of these filters are identical to the subcarrier response frequencies listed in Tables 1 and 2. This filter serves the dual purpose of passing the data frequencies and attenuating any higher undesired frequencies appearing at the discriminator output, Stiltz (1).

The outputs of the discriminators are used to drive graphic chart recorders, to display on meters or oscilloscopes, or to record on magnetic tape. The composite subcarrier signal which comes from the receiver output

may be recorded on magnetic tape for future playback through the discriminators. The response of the tape recorder must be great enough to accommodate the highest subcarrier frequency. If this is not the case, the analog data from the discriminator output may be recorded on a tape track through the use of an FM channel on the tape recorder. When signals are recorded on tape it is very desirable to record timing signals, such as WWV or another digital timing source. Voice annotation is also very desirable. Tape speed compensation or speed control should be used when recording the composite signal to eliminate any wow or flutter. A 17-kHz signal may be recorded with the subcarrier channels or on a separate track for speed control. Some subcarrier discriminators can be corrected for varying tape speed by using the output of a special discriminator tuned to a precision frequency recorded on the tape. The IRIG standards cover tape recording standards and should be referred to for specific detail.

When assembling an FM/FM telemetry system, one must consider the noise in the RF link when weak signals are being received. The receiver output noise spectrum concentrates the noise power in the higher subcarrier bands. The noise power at the subcarrier discriminator is proportional to the width

of the subcarrier bandpass filter. The subcarrier threshold is, therefore, proportional to the square root of the width of the band. It is also a linear function of the subcarrier frequency. For a proportional bandwidth system with a fixed percentage bandwidth, the noise thresholds of the subcarriers vary as the $3/2$ power of the subcarrier frequency. The greater the transmitter modulation from a given subcarrier, the lower will be the RF signal strength necessary to provide data with a favorable signal-to-noise ratio. In order to have a system with equal subcarrier thresholds, it is necessary to adjust the subcarriers so that the high channels deviate the transmitter signal more than the low channels. The theoretical pre-emphasis curve calls for the subcarrier amplitude to be adjusted in accordance with the frequency and the square root of the bandwidth. For the straight proportional bandwidth system this is the $3/2$ power taper as shown in Fig. 3. Generally, the channels below approximately 10 kHz are allowed to deviate the transmitter about 3 kHz in order to take into account microphonics in the equipment and intermodulation, (Bendix, (4).

The practical technique for assigning RF carrier deviations to the various subcarriers combines the theoretical noise susceptibility relation-

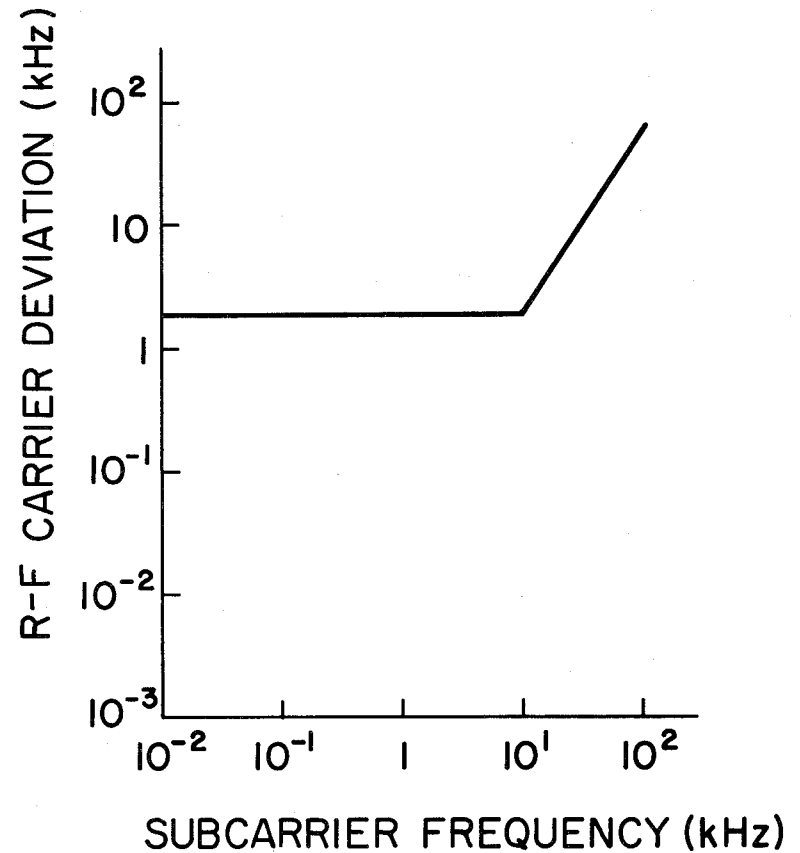


Fig. 3. Pre-emphasis curve for $3/2$ power tapers.

ship with considerations involving intermodulation distortion and microphonism, Gruenberg (3). Table 3 is an example of pre-emphasis scheduling involving seven 7½% and one 15% proportional bandwidth channels and two constant bandwidth channels in a VHF system. The channel numbers, center frequencies, and bandwidths are listed in the first three columns and the weighting factor in the next column. This factor is the product of the center frequency and the square root of the bandwidth of the channel normalized by dividing by the product of the center frequency and the square root of the bandwidth of the lowest channel, Gruenberg (3). In this example, 3 kHz is assigned to the lowest five channels, leaving 110 kHz of a total deviation of 125 kHz to be divided among the remaining channels on a pre-emphasis basis. Column 3 shows the deviation for each channel with all channels above channel 9 being deviated by an amount proportional to their weighting factor.

When establishing the deviation of the carrier by the individual sub-carrier frequencies, one must take care to avoid having sideband modulation components that exceed the limits established by IRIG, Gruenberg (3). Although normal operation of FM/FM multiplex systems does not create excessive

Table 3

Example of Pre-Emphasis Scheduling

Channel Number	Frequency (kHz)	Bandwidth (kHz)	$\frac{f\sqrt{BW}}{f_1\sqrt{BW_1}}$	RF Deviation (kHz)
1	0.400	0.060	1.00	3.00
3	0.730	0.110	2.47	3.00
5	1.300	0.196	5.88	3.00
7	2.300	0.346	13.80	3.00
9	3.900	0.586	30.47	3.00
12	10.500	1.576	134.38	3.15
14	22.000	3.300	407.85	9.56
B	30.000	9.000	918.36	21.52
5B	48.000	8.000	1385.70	32.47
7B	64.000	8.000	1848.14	43.30

sideband pairs, large deviations assigned to high frequency subcarriers can result in excessive sideband power output.

If the deviation sensitivity of the transmitter is known, the output voltage level of each subcarrier may be adjusted to give its proper transmitter deviation. A deviation meter, such as on a receiver, may also be used for adjusting individual subcarrier oscillators. When all are adjusted and operated simultaneously, the meter will not read the peak deviation, but will read the deviation corresponding to the rms value of the composite deviation voltage.

b. Pulse-code-modulation telemetry. Pulse-code-modulation (PCM) telemetry systems have come into wide usage in the last few years, particularly for space applications. For applications requiring high accuracy or the sampling of large numbers of channels of varying characteristics, PCM systems offer certain net advantages over competing modulating systems.

Basically, a PCM system is a time-multiplexed sampled-data system in which the values of the input channels sampled are expressed in digital, usually binary, form. The modulating signal in a binary PCM system is thus a sequence of ones and zeros which are grouped in binary "words" describing

the value of the particular channel sampled at the instant of sampling. The two-level signal corresponding to the ones and zeros may then be used to modulate a radio-frequency carrier signal in one of several ways: AM, FM, or PM. FM is generally used, and the system is then called PCM/FM modulation.

The primary advantages of PCM systems include the capability for handling both analog and digital signals, flexibility as to the number of channels and channel sampling rates, capability of transmitting data of high accuracy with little or no degradation in the RF link, and generally superior characteristics of information efficiency and noise immunity in the RF link. Offsetting these advantages is the fact that PCM systems are complex and the complexity varies little with the number of channels. PCM may be justifiable for a system with a large number of channels, but for a small number of channels and modest accuracy requirements, an analog system may be more desirable for reasons of simplicity.

(1) PCM data encoding. Figure 4 shows the basic elements of a typical PCM data encoder. Analog signals, after being conditioned, are fed into a multiplexer which is essentially a commutator that samples the analog signals

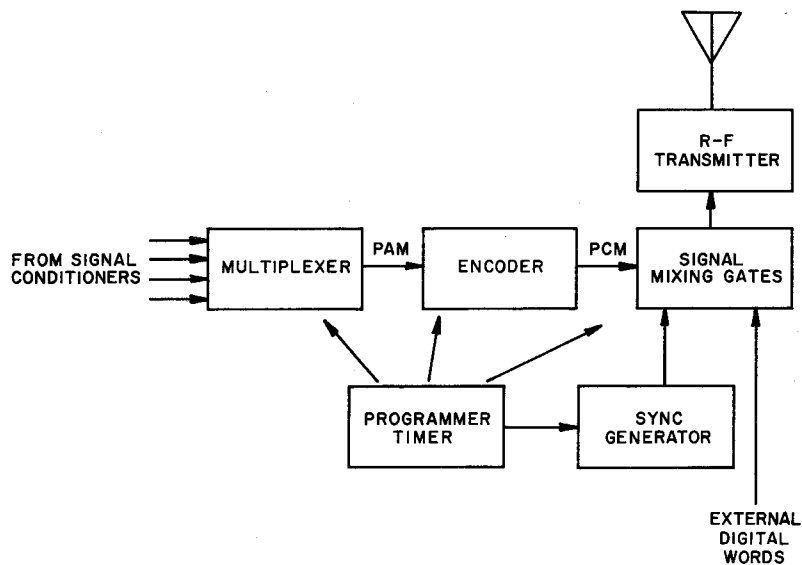


Fig. 4. PCM data transmitting system.

in a sequence and channels them to a common point. The signal at this point is a pulse-amplitude-modulated (PAM) signal, with the amplitudes corresponding to the analog voltages before multiplexing. The multiplexer is controlled by the programmer to sequence the input data in a manner that may be simple, but more often complex, allowing some channels to be sampled more frequently than others.

The PAM signal is fed to an encoder, which consists of an analog amplifier, a sample and hold circuit, and an analog-to-digital (A to D) converter. This converter is controlled by the programmer to make one analog-to-digital conversion per sampling interval. The output of the A to D converter is a sequence of binary digits represented by a two-level signal. The group of binary digits per sample is called a binary word and the number of bits per word determines the resolution. The number of bits per word may vary from 6 to 10. In many cases the resolution of an analog signal from a transducer is less than the resolution capability of the word as determined by the number of bits. The digital output of the encoder is fed to a set of digital gating circuits where they are sequentially mixed with digital data from other sources, such as off-on switches, digital registers and

transducer digital outputs.

The PCM system programmer controls all timing and control functions in the system. It also includes a synchronization generator which develops a pseudorandom binary sequence to synchronize the PCM frame, and in some cases the subframe and words. The largest amount of the programming involves sequencing the multiplexer. In the simple case each data channel is sampled once during the commutation cycle and may be represented by the circular diagram of Fig. 5a. The data format is shown in the adjacent tabulation.

In most applications it will be found that it is not desirable to sample all channels at the same rate. Some data, such as battery voltages and temperature, may be sampled at a much reduced rate. This may be done by attaching one or more subcommutators to the prime commutator in one or more word locations of the main frame. It is also possible to attach sub-subcommutators to the subcommutators. If the basic sampling rate is inadequate, several words in the main frame may duplicate a particular data channel for more frequent sampling called supercommutation. Many data formats may be devised. Modular construction of modern data encoders permits many varia-

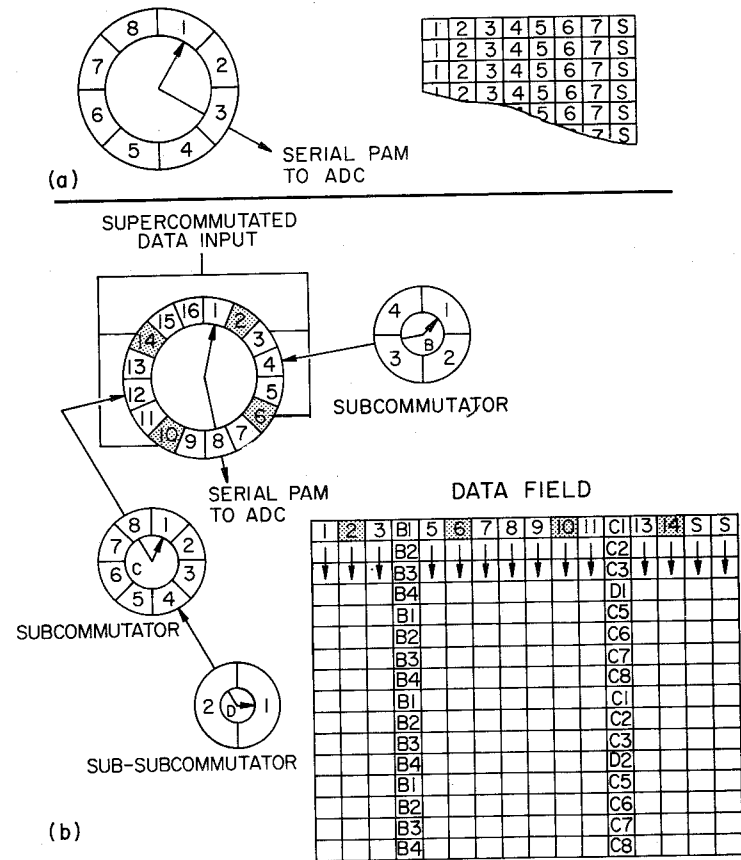


Fig. 5. PCM commutation and data formats using a simple commutator

(a) and a commutator with subcommutators (b). Channel 8 in (a) and channels 15 and 16 in (b) are used for frame synchronization.

tions. Figure 5b shows a multiplexer configuration, drawn like commutators, where a 16-word mainframe has two subframes of four and eight words. The eight-word subframe has a two-word sub-subframe. In addition to the subframes, four of the channels on the mainframe are tied together for supercommutation. Channels 15 and 16, in the time sequence, are used for the frame synchronizing pulse. The format diagram of the data field is also shown in Fig. 5b.

The serial bit stream output of the PCM data encoder is used to modulate the telemetry transmitter. There are a number of modulation techniques used to represent the logic levels one and zero. The IRIG standards give a complete description. The most commonly used ones are shown in Fig. 6. NRZL is a non-return-to-zero-level where a "1" bit is one signal level and an "0" bit is a different level. NRZM is a non-return-to-zero-mark. In this waveform the level is meaningless; "1" bits are represented by a change in level in either direction; "0" bits are represented by the absence of a change in level. RZ is return-to-zero. In this waveform, a finite width pulse, usually half-bit width is generated to mark a "1" bit, while "0" bits are not marked. There is an advantage for using NRZ over RZ in that the RF

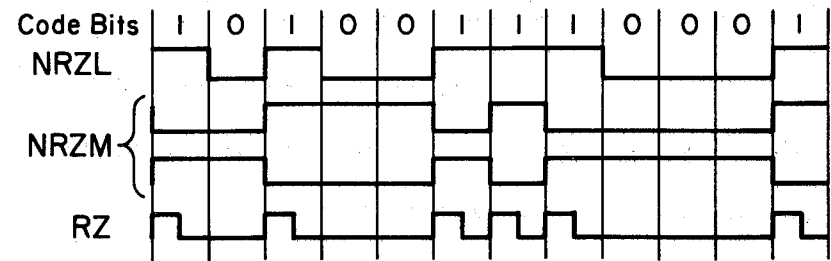


Fig. 6. Waveforms of pulse code information.

link need handle only frequency components of half the bit rate. NRZL is probably the most commonly used code. NRZM is a common form of digital saturation magnetic tape recording, since during tape playback, only the change in magnetic flux is detected, Stiltz (1).

Before the PCM output waveform is used to modulate the AM, FM, or PM transmitter, it is passed through a premodulation filter where the unnecessary high frequency components are removed. It is also possible to have a mixed system such as PCM/FM/FM where a subcarrier channel of an FM/FM system handles the PCM data. The band-width capabilities of the FM channel must be adequate to accommodate the bit rate in this case. In the case of direct frequency modulation of the carrier by the PCM signal, a higher bit rate can be accommodated with a wider deviation. With some balloon telemetry systems, rates as high as 100 kilobits per second are practical.

(2) PCM data recovery. In the PCM encoder, a fixed number of bits constitutes a data word (or sometimes a syllable), and a fixed number of words constitutes a data frame. Ordinarily a word would represent one digitized sample from a data channel and a data channel would occur at least once throughout a frame. The frame is repeated continuously at a fixed

rate. Some channels will provide a data sample once per frame, while others will appear several times in a frame. The subcommutated data samples may appear only once in a total data field.

The purpose of the PCM data recovery system is to detect the incoming data bits, determine the location of the first bit in the frame and then decommutate the data channels. For accurate decommutation, the bit frequency must be established. Also the frame synchronization pulses must be acquired so that the programmed counting pulses may be reset at the proper time. Figure 7 is a block diagram of a PCM data recovery system. The output of the receiver will contain the PCM data in a serial train of bits in NRZL or other data code. In the case of PCM/FM/FM the NRZL data will come from an FM subcarrier discriminator. The bit synchronizer extracts the bit synchronizing rate from the signal and converts the data format to one compatible to the frame and subframe synchronizer input. This unit, which has been preprogrammed to recognize the synchronization word generated by the data encoder, the word lengths, words per frame, and words per subframe, will demultiplex the output data according to the established format. In case some of the digital words are to be converted back to analog data, a digital-to-analog (D to A) converter is programmed to convert those par-

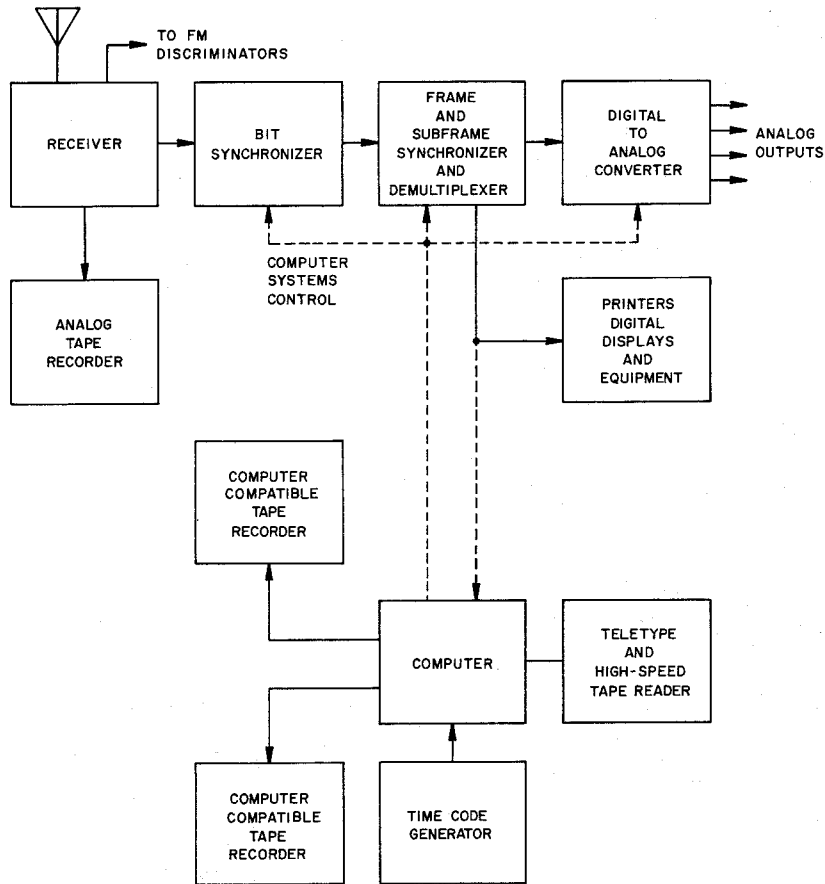


Fig. 7. Block diagram of PCM data recovery system.

ticular channels for graphic chart recorders or other instruments. If the data are to remain in digital form for display on alphanumeric devices, punched tape, magnetic tape, teletype, line printer, or digital voltmeters, then the digital data are taken from the demultiplexer.

It would be feasible to process data in real time if a central processing computer were available and could handle the information as fast as it can be retrieved. A more practical system is to record the data on computer-compatible tape along with a digital time code for future data reduction. This additional system is shown with dashed connections in Fig. 7. The computer here is a minicomputer with a teletype and a high-speed paper tape reader as input-output (I/O) devices. The magnetic tape may also be used for I/O in some cases. The computer is programmed to format the computer-compatible tape with the PCM data.

In some cases the demultiplexing equipment can be computer controlled for data format settings. This saves considerable time and reduces errors in set-up procedure. The system-control program could be stored on magnetic tape or punched tape and transferred to core storage for immediate system set-up.

A photograph of a ground station is shown in Fig. 8.

c. Pulse-amplitude-modulation telemetry. Pulse-amplitude-modulation (PAM) refers to a technique which is essentially the commutation of several sources of quasi-static data into a single telemetry channel, such as an FM/FM carrier or subcarrier. The data bandwidth of the telemetry subcarrier must be large enough to handle the data samples as determined by their duration and commutator speed. The data can be decommutated at the ground station or from a tape recording of the received signal. The IRIG telemetry standards have established standards for the PAM pulse train so that standardized decommutators can be used.

The duty cycle of the commutation pattern may be 50% (return-to-zero) or 100% (non-return-to-zero). An example of the 50% pattern is shown in Fig. 9. The information channels are allocated equal and constant time intervals within the PAM frame. Each interval T contains a sample pulse beginning at the start of the interval and having an amplitude determined by the amplitude of the data of the corresponding information channel accord-

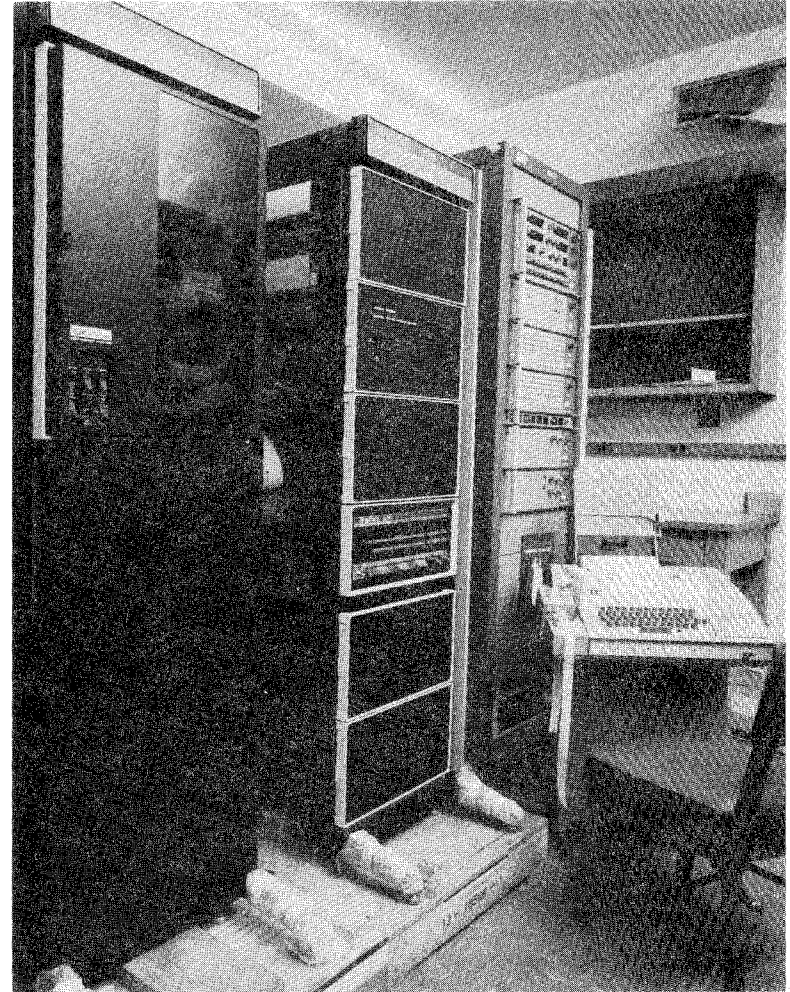


Fig. 8. PCM data recovery equipment.

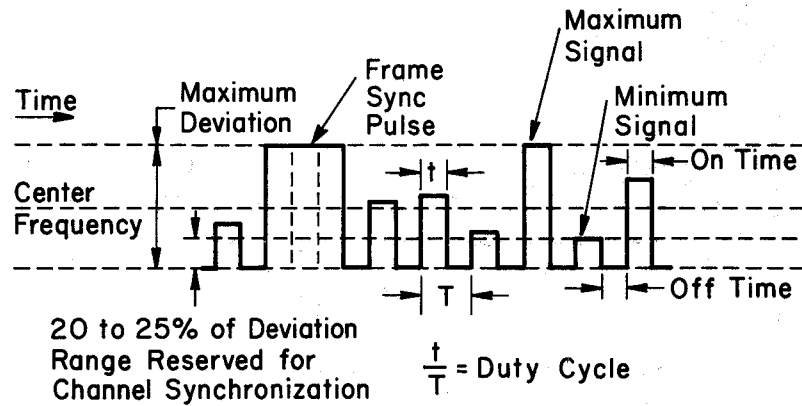


Fig. 9. PAM pulse train waveform.

ing to a fixed relationship, usually linear, between the minimum level (zero amplitude) and the maximum level (full scale amplitude). In this pattern the synchronization interval has a duration of $2T$ with full scale amplitude for $1.5T$ followed by the reference level for $0.5T$.

Decommutation of a PAM signal is the process whereby the individual channels of the time-division multiplexed sample data are separated. The composite signal, as shown in Fig. 9, is applied to a parallel bank of gates, each of which is closed for a short period, the closures occurring in cyclic order so that only one gate is closed at any instant. The gates are synchronized with the PAM pattern such that each gate will deliver output pulses representing only one channel of sampled data. The voltage levels of each channel are maintained until the next sample appears. With slowly varying data such as temperature or battery voltages there is little need for interpolation. The data can be recorded on individual graphic recorders for each channel, Stiltz (1).

d. Pulse-duration-modulation. Pulse-duration-modulation (PDM) is a time multiplexed system wherein the amplitude of each channel is converted to a pulse, whose duration is directly proportional to the amplitude. It

is sometimes referred to as pulse-width-modulation (PWM). PDM is perhaps a simpler system than PAM but, with modern telemetry components, it is probably less accurate than PAM. PDM was originally adopted because of the noise problems with early mechanical commutators and because the linearity of early FM/FM subcarriers, used with PAM, was not accurate, Stiltz (1).

In the PDM system a commutator is used to sample the analog data signals as with the PAM and PCM systems. To convert the constant width, variable amplitude pulses from the commutator to constant amplitude, variable width pulses, a keyer is inserted between the commutator and the subcarrier oscillator or the FM transmitter for PDM/FM/FM or PDM/FM telemetry. By converting the PAM pulses to PDM pulses a series of data pulses is obtained whose accuracy is not seriously impaired by amplitude fluctuation due to noise. Figure 10 is a diagram of a simple PDM system using a mechanical commutator. In addition to multiplexing the analog data, the commutator provides trigger pulses to the keyer. These trigger pulses are used to initiate the pulse-width data pulses at a fixed rate. The width or duration of these pulses is a direct function of the corresponding data amplitude. One method of accomplishing this is to start a square wave generator and a linear sawtooth

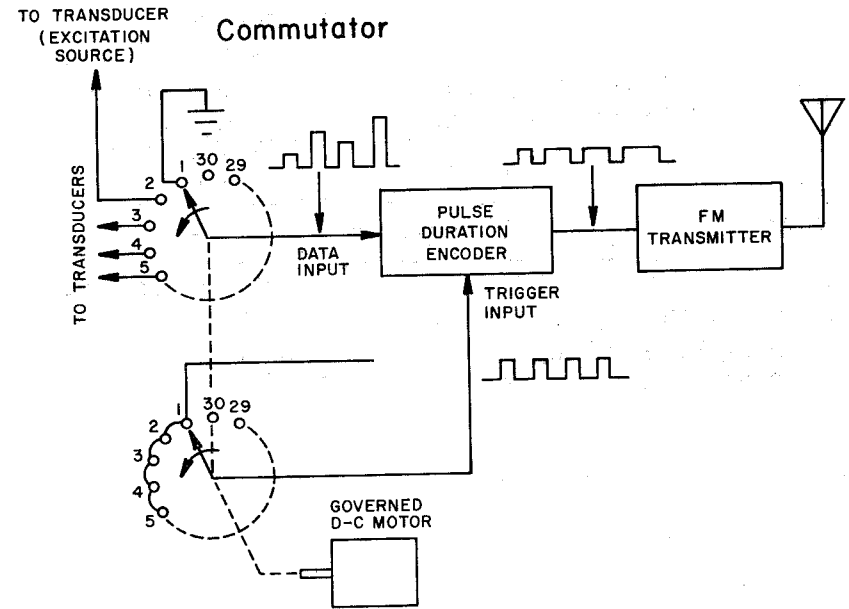


Fig. 10. Block diagram of a typical PDM system.

ramp voltage with the trigger pulse. When the ramp voltage equals the data voltage, a voltage comparator terminates the square wave generator. Since the trigger pulses occur at equal intervals, the data pulses occupy equal time intervals in the commutator sequence. Figure 11 illustrates the PDM pulse train.

As in the PAM technique, one channel is reserved for zero reference, one for full scale reference, such as zero and five volts, respectively, and two channels for decommutator synchronization. There are two types of synchronization formats. One is a full amplitude pulse with a duration of $1.5T$ where T is the channel interval. The other is the absence of any pulse for an interval of $2T$. The maximum frame length should be no greater than 128 intervals, including those used for calibration and synchronization. The IRIG telemetry standards include standards for the PDM pulse train so that standard decommutators can be used, IRIG (2).

The output voltage of the pulse duration encoder is generally applied to a high frequency channel of an FM/FM subcarrier system where the subcarrier frequency is shifted from near one band-edge to near the other band-edge in a manner of frequency-shift-keying. Accuracies of one percent of

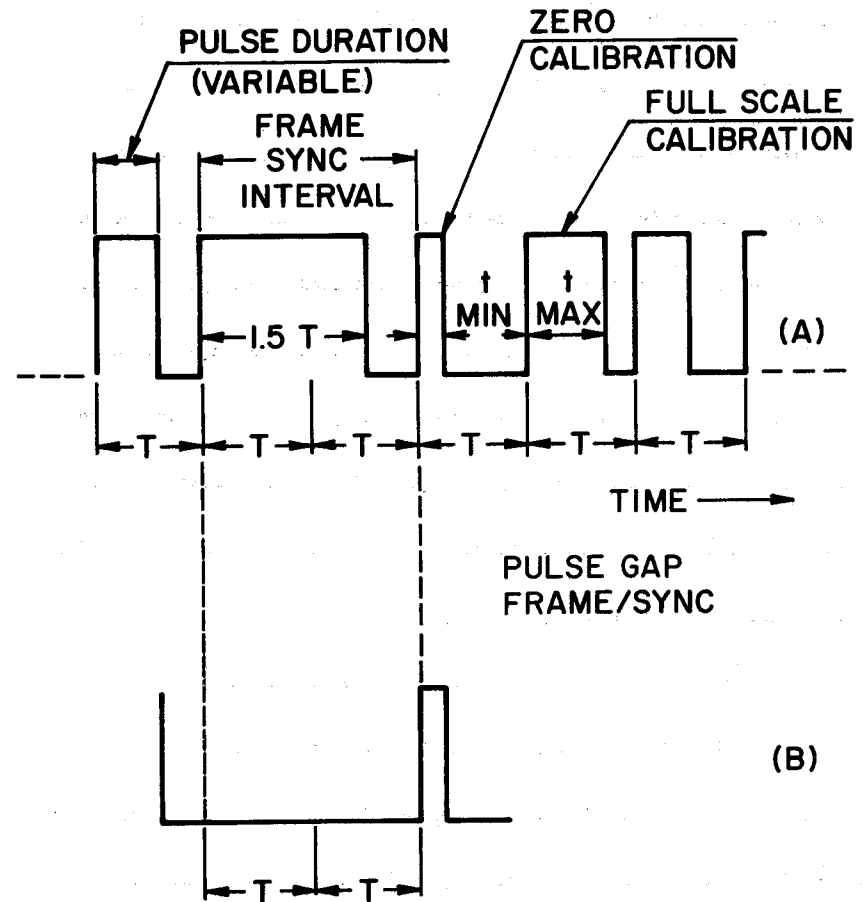
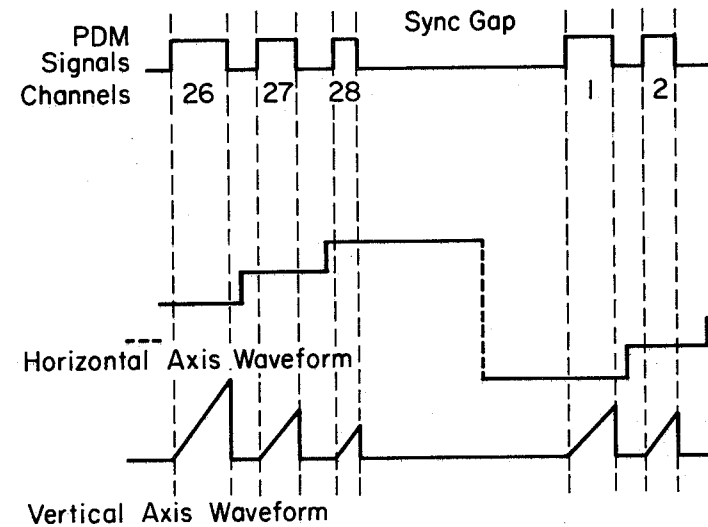


Fig. 11. PDM pulse train waveform.

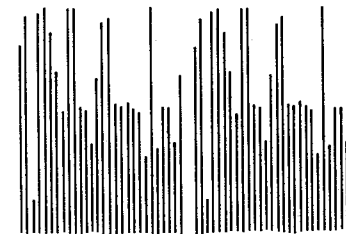
full scale are readily achieved with PDM systems. The accuracy of the system is primarily determined by the keyer. The output of the encoder may be used to drive the transmitter directly, especially for high commutation rates. When this is done, true FM transmitters should be used because of the large dc or low frequency components contained in the pulse train.

At the ground station the PDM data may be recorded on magnetic tape for future analysis, displayed by means of a bar graph presentation on an oscilloscope, or converted to analog voltages and recorded individually on graphic recorders. It is also possible to convert the information to a form suitable for digital computer processing.

The bar graph display and the waveforms used to generate the display are shown in Fig. 12. The length of the bars is representative of the PDM pulse duration or the amplitude of the analog data. These bars appear on the oscilloscope when it is unblanked by each channel pulse. The pulse durations are used to gate a sawtooth whose duration is the same as the channel data pulse duration. The amplitudes of the sawteeth are proportional to their duration and are used for vertical deflection. The horizontal sweep for the oscilloscope may be linear; however, a staircase generator, as shown,



(a)



(b)

Fig. 12. Waveforms (a) used to create PDM bargraph display (b).

makes a better sweep for this type of presentation, Stiltz (1).

A more satisfactory method of display consists of decommutating the data or separating the information from a serial train of pulses to a parallel configuration where each channel is available on a separate output. For this to be done, the data pulses must be converted from variation in duration to variation in amplitude. This can be accomplished by an integrating circuit, such as used for the bar graph display. The peak amplitude is sampled and held until the next corresponding data channel appears. This process is synchronized by the sampling rate pulses which are derived from the frame synchronization signal and the frame format information.

To convert the PDM data to digital information suitable for computer processing, it is necessary to convert the pulse duration to a digital form compatible to computer application. One method consists of gating a clock oscillator for the duration of the data pulses and counting the clock pulses during these intervals. Another method consists of converting the PDM pulses to PAM pulses, sampling the amplitude of the pulses at the proper time, and converting them to digital form with an analog-to-digital converter.

2. The Radio Frequency Link

It is the purpose of the radio frequency link to connect the inaccessible data to the accessible location. Since we are concerned with balloon telemetry, we are confined to RF links rather than wire links. The RF spectra used for telemetry are the UHF (1435-1535 MHz and 2200-2300 MHz) bands. The VHF (216-260 MHz) band for telemetry was to have been relinquished by January 1, 1970; however, some extensions were made to agencies which were not readily able to make the frequency changes. The UHF band which has been assigned to balloon telemetry is the L-Band (1435-1535 MHz).

The radio frequency link consists, essentially, of the transmitter and its antenna at the data source on the balloon, the receiver and its antenna at the ground station, and the propagation medium between.

The transmitter is generally a frequency modulated or phase modulated radio frequency energy source. The mixed output of the FM subcarrier channels or the direct modulation from the PCM digital data encoder is applied to the modulation input of the transmitter. Precautions are made to avoid the generation of undesired signals. It is the function of the transmitter

to apply this signal to a radio frequency carrier with the addition of as little distortion as possible. For most balloon telemetry the RF energy is nominally about two watts. The RF energy is radiated from the balloon system by means of an antenna with an omnidirectional horizontal pattern. A modified ground plane suspended below the balloon for vertical polarization is generally used.

The receiving system at the ground station consists of the antenna, preamplifier (if used), and the receiver with its detectors and amplifiers. The output of the receiver drives the appropriate demodulation equipment, discussed earlier. In some cases down-converters are used, especially when VHF equipment is available to use with UHF signals.

The receiving antenna may vary in size and configuration from simple ground planes or dipoles to parabolic dish antennas. For VHF telemetry a dipole array, yagi configuration, or an array of helical antennas may be used. Helical antennas are of broad bandwidth; they are simple to construct and accommodate circularly polarized signals. They are more popular for reception of signals from sources such as space vehicles or sounding rockets. For balloon work it is easier to transmit a linear, vertically polarized signal for omnidirectional coverage. Since there will be no Faraday rota-

tion in the course of a balloon flight, it is better to arrange for linear, vertical signal reception. In the case of VHF this dictates the use of dipole or parasitic (yagi) arrays, and for UHF a parabola with a vertical linear feed. Figure 13 is a photograph of a 1485 MHz receiving antenna.

Three important parameters describe a receiving antenna. These are directivity, gain, and effective aperture. Directivity is the ratio of the response of the antenna to signals in the direction of the maximum pattern lobe to its average response to signals in all directions. Gain is the power ratio of the response of the antenna to signals in the direction of its maximum lobe to the response of a reference antenna such as an isotropic antenna, expressed in decibels (dB). The effective aperture, or capture area, determines the amount of signal extracted.

Antennas may be entirely manually positioned, manually controlled but motor driven, or entirely operated by machinery with automatic tracking provisions. The choice of system depends on cost, antenna size and weight, beamwidth, wind loads, and flight path. Manual tracking, which usually relies on a simple indication of relative signal strength to guide the operator, is useful mainly with the simpler antennas.

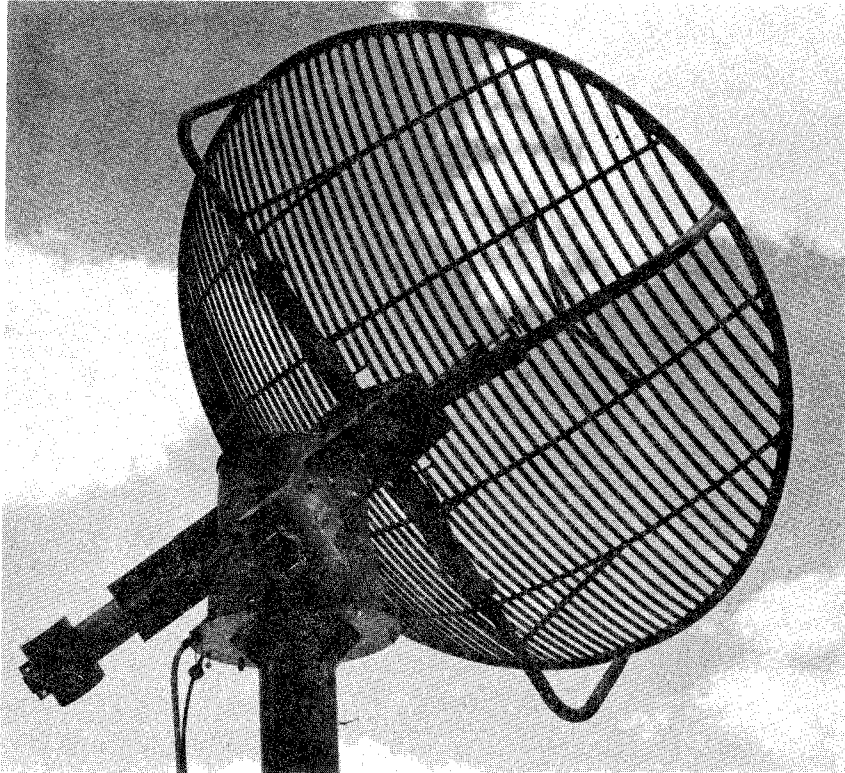


Fig. 13. L-Band telemetry receiving antenna.

The range of operation with UHF and VHF signals is limited to radio-horizon distances as determined by the heights of the balloon and the receiving antenna on the ground. The height of the receiving antenna has little significance for long range reception except that it should clear surrounding objects. The direct radio-horizon distance to a balloon from a ground station may be calculated approximately by the formula, $D = (3h/2)^{\frac{1}{2}}$, where h is in feet and D is in statute miles. The propagation range, which is greater than the tangential distance due to atmospheric refraction, may be approximated by considering the earth's radius to be $4/3$ its actual radius. The propagation distance is then approximated by $D = (2h)^{\frac{1}{2}}$. Table 4 gives the radio-horizon range for balloons at several altitudes.

When the balloon is approaching the radio horizon the elevation angle is small and multipath propagation due to reflection from the earth's surface or objects on it may occur. The effect of multipath propagation is the destructive or constructive interference in the RF signal and if the time difference of arrival of the two signals is very small compared to the period of the highest modulating frequency there is no effect on the FM modulation characteristics, Nichols (6). As the range of the balloon from the receiver

Table 4

Radio-horizon Range for Balloons at Various Altitudes

Balloon Altitude ($\times 10^{-3}$)		Maximum Range		
km	ft	km	Statute Miles	Nautical Miles
20	65.62	583	362	314
24.38	80	644	400	347
25	82.02	652	405	352
27.43	90	684	425	369
30	98.43	714	443	385
30.48	100	721	448	389
33.53	110	756	470	408
35	114.83	771	479	416
36.58	120	790	491	426
39.62	130	821	510	442
40	131.23	825	512	445
42.67	140	853	530	460
45	147.64	875	543	472
45.72	150	884	549	476
50	164.04	922	572	497
55	180.45	967	600	522
60	196.85	1010	627	545

increases, a predictable variation in the signal strength will occur. This might be avoided by adjusting the receiving antenna height during flight to insure constructive interference. The antenna height should be

$$h_a = n \frac{\lambda}{4} \frac{d}{h_b}$$

where d is the ground range and h_b is the balloon's height.

Without antenna height adjustments, the predictable signal strength variation with range is suggested as a method of estimating balloon range over a distance of 100-450 km, when other methods are unavailable, Clark (7).

It is very desirable to operate the RF link with a minimum of transmitter power at the signal source on the balloon. This is to reduce the battery ampere-hour requirement and hence the payload weight. VHF transmitters have approximately 40% dc to RF efficiency, while UHF transmitters at present are 10 to 15% efficient. Long duration flights require several ampere-hours of battery reserve, unless the telemetry is programmed, which adds much payload weight.

In order to assemble a system which uses a low power balloon-borne transmitter, emphasis must be placed on low-noise receiving equipment and an

antenna with reasonably high gain. This is necessary to cope with marginal signals which occur when the range approaches the radio-horizon.

The ability of a telemetry receiver to detect the presence of a signal is fundamentally limited by the presence of internally generated noise, such as thermal noise, shot noise, vacuum tube noise, and semiconductor noise. Since noise is always present, amplification in the receiver amplifies noise as well as the desired signal.

Thermal noise is a major contributor to the overall noise in a receiver. It is caused by the random motion of electrons in the circuit components and at absolute temperature T in $^{\circ}\text{K}$ the maximum available noise power is expressed by the Boltzmann expression kTB_n , where k is Boltzmann's constant ($1.38 \times 10^{-23} \text{ J}/^{\circ}\text{K}$) and B_n is the noise bandwidth.

An ideal receiver adds no noise to the signal being amplified; however, a practical receiver will generate noise to some extent. The measure of the noise generated by a practical receiver compared with that of an ideal receiver is called the noise factor F . The noise factor of the receiver may be considered to be the degradation of the signal-to-noise ratio of the receiver. When the noise factor F is expressed in dB, it is called the

noise figure NF, where $\text{NF} = 10 \log F$.

Figure 14 shows two amplifiers, such as a preamplifier and a receiver, connected in series. Each has the same noise bandwidth B_n , but different noise factors and gains; it can be shown that the overall noise factor

$$F_o = F_1 + \frac{F_2 - 1}{G_1}$$

where the gains and noise factors are ratios.

If the gain of the first amplifier is large, the contribution of the receiver to the overall noise factor is small; therefore, the system noise factor can be greatly improved with the addition of a preamplifier with a low noise factor, assuming it has a reasonably high gain such as 15 to 20 dB. It is better to place the preamplifier at the antenna where the signal-to-noise ratio is highest. After the signal has been amplified by the low-noise preamplifier, the attenuation and noise generated by long runs of coaxial cable and antenna rotary joints have little effect on the overall signal-to-noise ratio.

The total noise power in dBm (dB below one milliwatt) may be expressed

as

$$N = 10 \log \frac{kT_o B_n}{1 \times 10^{-3}} + \log F_o$$



Fig. 14. Block diagram of two amplifiers in series.

where T_o is a reference temperature (290°K) and B_n is the receiver noise bandwidth.

This equation is separated into two parts to show the effect of variations of the overall receiver noise factor. The noise contributed by the first term is due to the kTB_n noise term, Cooper (8).

An example of the power levels at different points in an L-Band UHF radio frequency link, such as illustrated in Fig. 15, are shown in Fig. 16. The power level is plotted in decibels relative to 1 mW (dBm). The transmitter power is 3 W or 35 dBm, which is shown on the upper right side of the diagram. The transmission line loss from the transmitter to the balloon antenna is 1 dB, while the antenna gain is 2 dB. The free space loss for a range of 400 n mi (radio-horizon) is 153 dB, based on the formula

$$L = 20 \log (4 \pi R/\lambda)$$

where λ is the wavelength and R is expressed in meters. The atmospheric loss, caused primarily by oxygen and water vapor is approximately 1 dB per 100 n mi. The signal level is increased by 29 dB with an 8-ft paraboloid antenna and 1 dB is lost in the antenna pedestal and associated cabling. The resultant -93 dBm represents the signal at the preamplifier input terminals.

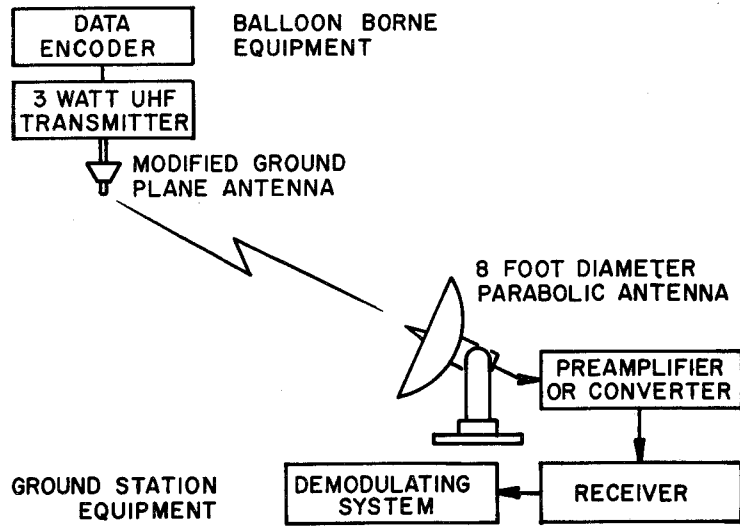


Fig. 15. Block diagram of UHF telemetry system.

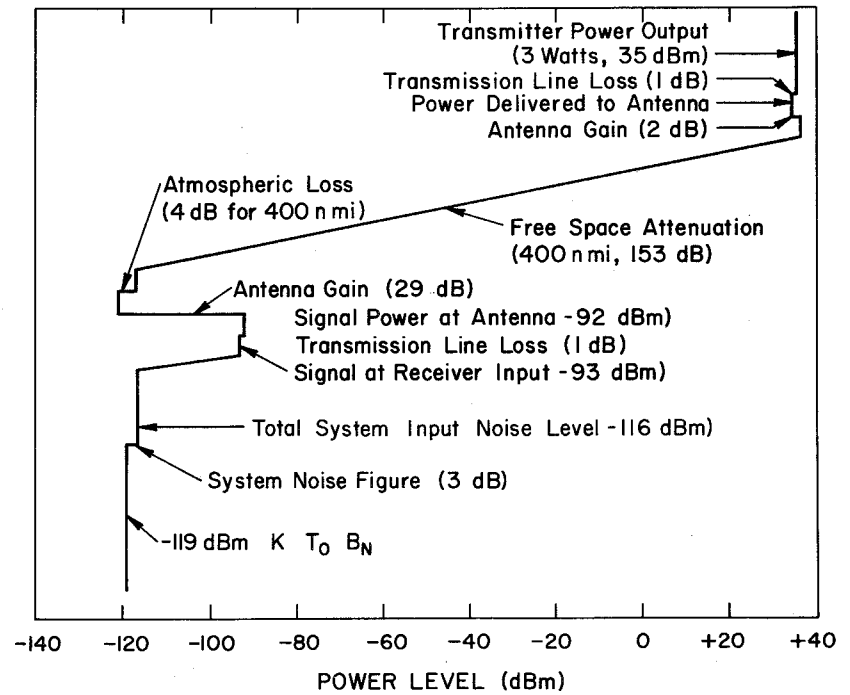


Fig. 16. Signal power-level diagram.

On the lower left side of the diagram, the receiver noise contributed by the kTB_n factors is represented by the -119 dBm level. This level plus the noise figure term represent the noise level of the receiving system. If the noise figure is 3 dB, then there is a -116 dB noise level. A larger noise figure will create a higher noise level and will require a greater signal for a margin of safety. In this case there is a 23 dB signal-to-noise ratio. This provides a margin of safety because 9 to 12 dB is considered adequate for FM/FM telemetry, and 13 dB is adequate for PCM/FM with an error probability of 1 bit in 10^5 bits, Cooper (8).

3. On-Board Data Recording

Scientific data that are not telemetered to ground stations and recorded there are recorded aboard the balloon. On-board recording is not as prevalent now as it was before reliable telemetry was available. It is sometimes used as a back-up for radio telemetry.

The method of recording depends on the type of experiment being performed. For example, if a scientist is counting the accumulation of high energy particles from a source outside the earth's atmosphere, he may use a system of scalar counters which may be displayed with a series of light

sources such as light emitting diodes (LED). These lights may be photographed on continuously moving film with periodic flashes of a clock and a photobarograph. The time and pressure-altitude may also be displayed with the other data in digital form. This technique permits the data, time, and altitude to be presented on the same film record.

Magnetic tape recorders are also used for on-board data recording. These may be analog or digital recorders. Incremental recorders can generate a computer-compatible format, useful for rapid data analysis. Digital time data from a time code generator is desirable for a complete data recording on the tape. Some tape recorders use cassette tapes which are useful for small amounts of data. The recorders may be programmed or commanded on and off as desired with the command-control systems.

Other miscellaneous types of on-board data recording include the measurement of radioactive particles by using photographic emulsion plates; particle collectors for micrometeorite detection; and cameras for photographing on-board phenomena such as the track of a high energy particle in a spark chamber.

C. COMMAND-CONTROL

Scientific balloon flights are practically always equipped with a command-control system for balloon control and scientific package control. Balloon control requires three or four command channels for ballasting, valving, and flight termination or cutdown. The number of channels required by the scientist for control of the experiment depends upon the complexity of the experiment. In some complex experiments the number of command channels may be one hundred or more.

There are several criteria for a reliable command-control system. First, the range over which it will operate successfully should be made as great as possible. With VHF or UHF as the radio link, a practical range is in the order of 400-450 n mi, limited by the radio-horizon. Ranges beyond this are generally unnecessary because the balloon trajectory can be covered by down-range stations or by tracking aircraft capable of command-control. The command system should have an extremely high reliability. The system must be designed to recognize all legitimate commands and to reject extraneous or inadvertent signals that are received. Locally generated noise, such as from dc motors, must not be decoded as commands nor

prevent true commands from being recognized. Finally, the balloon-borne equipment should be small, lightweight, and consume a small amount of power, especially when quiescent. As with all balloon-borne electronics, power consumption is a critical item because excessive power requirements create additional payload weight in the form of batteries.

The command-control technique resembles radio telemetry to a large extent. In the command system, the encoder and transmitter are located at a ground station while the radio receiver and decoder are aboard the balloon payload. The decoder output may be in the form of a voltage level, a closed circuit, a relay closure, or a digital word. The margin of signal-to-noise received at the balloon is much larger than a received telemetry signal primarily because the ground transmitter power is much greater. There are essentially three systems which may be used for balloon command-control. These systems are pure tone modulation of the RF carrier, tone-digital where a system of pulse modulated tones is used to set up a digital command word, and PCM where the digital bits are used to modulate an RF carrier or subcarrier. The modulation formats for any of these systems are limited only by the designer's imagination. The advent of medium scale and large scale integrated

(LSI) circuits have expanded the circuit possibilities tremendously.

1. Tone Modulation

The tone modulation system was the first developed for scientific ballooning and is used where relatively few commands are needed. There are various concepts that can be used with tone commands. Some use the simultaneous transmission of combinations of two or more standard Electronic Industries Association (EIA) tones to code a command channel. Others use a sequential series of tones to complete a command.

When the tone command system is used, the function of the tones is to modulate the command transmitter. On the balloon the RF signal is received, and the tones are detected and applied to the decoder where they are separated for their proper function. In the case of simultaneous multitone coding, each tone is decoded and used to establish the state of a circuit, such as a relay. The correct combination of tones will establish the proper combination of decoder circuit states to actuate the command. When tones are used simultaneously, precautions must be taken to prevent the generation of a sum or difference frequency of two tones which may actuate an undesired command channel.

A tone system, shown in the block diagram of Fig. 17, which has been used extensively for scientific ballooning, uses an RF link compatible with an existing VHF narrow band FM communication system. This minimizes the required ground station equipment and allows the transmission of commands from mobile stations, such as land vehicles or aircraft. Two tones are transmitted simultaneously. One tone (number 1), sometimes referred to as a squelch tone, is common to all command channels. It is used to enable the audio circuits at the receiver to allow the command tone to reach the tone decoders.

As many as twelve tone oscillators in the EIA audio frequency range are used to frequency modulate the command transmitter at the ground station. The tone oscillators may be any stable audio generator; however, circuits using resonant reeds are often used. Resonant reed circuits are also generally used as tone demodulators in the balloon-borne equipment, but other filters, such as active filters, could be used. The resonant reed is an electro-mechanical device that acts as an audio frequency filter with a bandwidth of about 1% of the design frequency. It has one or more steel reeds suspended in a magnetic circuit consisting of a permanent magnet and

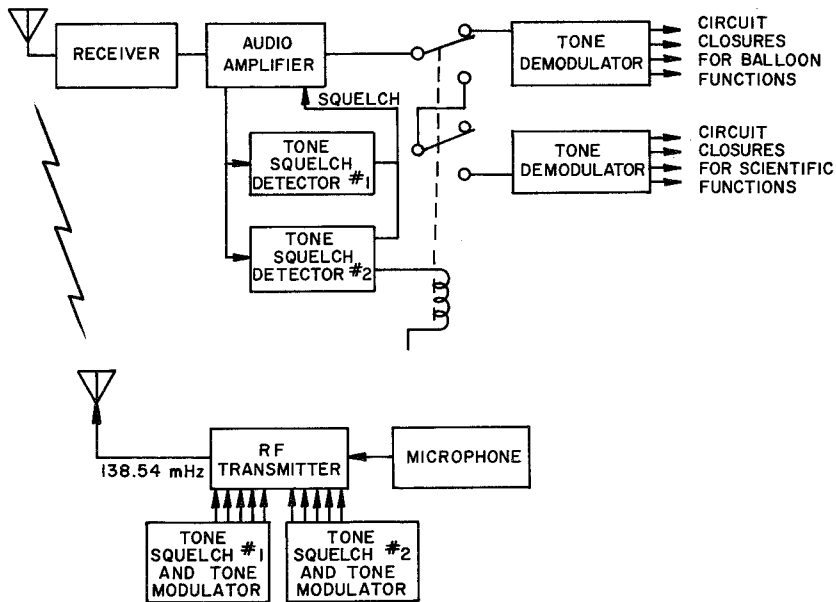


Fig. 17. Block diagram of a tone modulated command system.

a field coil. When operating at its resonant frequency each reed vibrates to make a circuit closure with a large duty cycle. This intermittent closure due to resonant vibration is integrated and used to actuate an amplifier and relay circuit. In all decoder channels, an adjustable delay of one to six seconds is designed into the circuits so that momentary or extraneous signals will not actuate a command function.

Sometimes it is desirable to use a single tone command channel to change the states of a latching relay rather than to use two channels for this purpose. This can be done with an additional miniature relay and an RC charging circuit as shown in the schematic diagram of Fig. 18. When a tone command is received, the decoder relay applies power to actuate the miniature relay and the latching relay to one state and begins to charge capacitor C through resistance R. If the command is transmitted for a time long enough to charge C with enough energy to actuate the latching relay to its other state, this will be done when the command transmission ceases and the decoder and miniature relays return to their de-energized state. For short duration commands the latching relay goes to one state without returning. It takes a short and a long duration command to transfer states se-

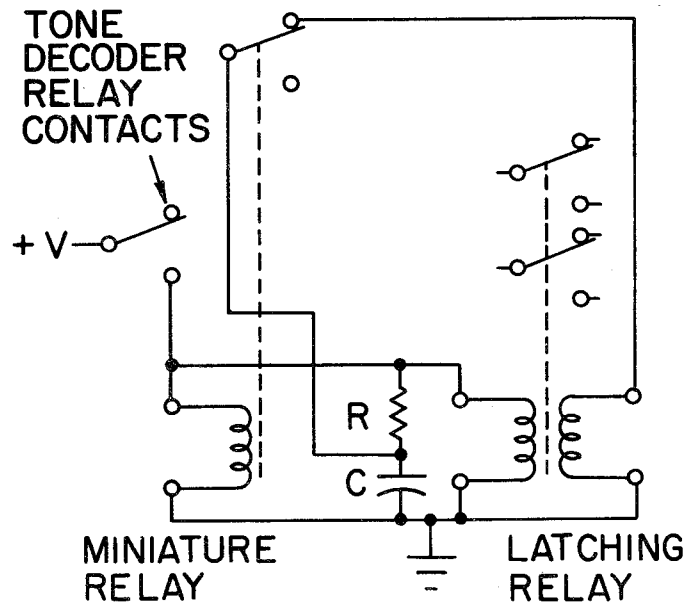
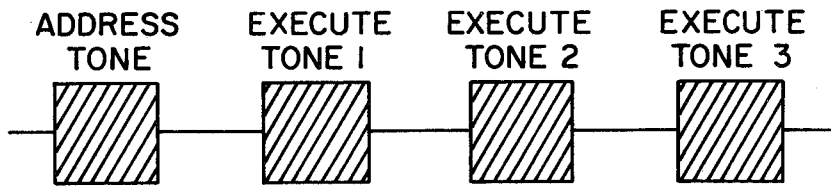


Fig. 18. Latching relay circuit for single command channel operation.

quentially. The RC time constant should be about 10 sec and the capacity of C should be adequate to store the charge necessary to actuate the latching relay.

If the transmitting system is capable of more than one tone squelch modulator, almost duplicate systems may be used on a balloon or two or more balloon systems may be commanded at a time. Figure 17 illustrates an example where two decoders are operating from the same receiver using two tone squelch frequencies. When transmitting a special command such as payload separation, it is necessary to have interlocking circuits on the encoder panel to prevent inadvertent transmission of that command.

A tone command system using sequential tones is the Address-Execute system used by The National Aeronautics and Space Administration on some of the earlier space flights, Coates (9). In this system the RF carrier of the ground command transmitter is modulated with a series of discrete single audio tones, as shown in Fig. 19. Sequential transmission is employed with an address tone sent first to "arm" the decoder. Each command receiving system is assigned to a unique address tone. The execute tones follow to accomplish the particular command function and may consist of up



Tone Duration:

0.5, 1.0, 1.5, 2.0, 2.5, 3.0, or 3.5 seconds
(Duration constant throughout sequence)

Interval Between Tones: 0.5 seconds

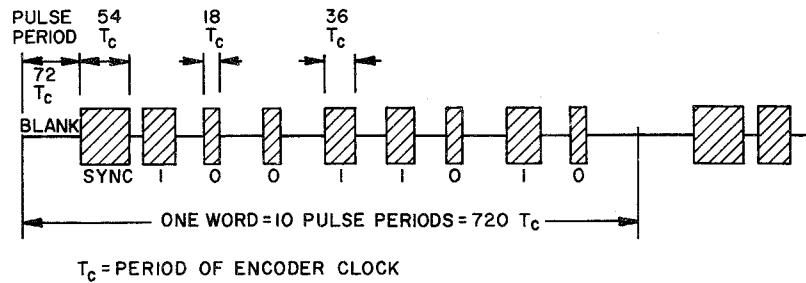
Fig. 19. Address-execute tone command structure.

to three different tones in sequence. The combined detection of these tones by the "armed" decoder causes initiation of the command actions. After a predetermined period of time, equal to the length of the longest execute sequence, the decoder is dearmed and cannot respond to an execute tone until it receives another valid address tone.

2. Tone-Digital Systems

The tone-digital command system was developed by NASA for spacecraft command-control, Coates (9). This particular coding format has not been used for balloon command, but illustrates possibilities for tone-digital systems. It consists of a pulse-duration-modulated (PDM) tone with constant bit ratio word coding and repetitive word formatting as shown in Fig. 20. A series of five words, each consisting of eight bits, one synchronization and one blank period, are sent for each command. The series consists of a unique address transmitted twice, followed by an execute word transmitted three times. The reception of one correct address word and one correct execute word will actuate a command. This redundancy increases the probability that the correct command will be received under weak signal and interference conditions.

Command Word Structure



Command Frame Structure

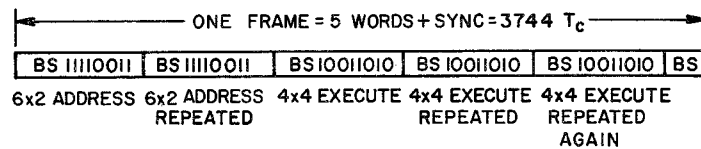


Fig. 20. Tone-digital command word structure and format.

The technique used for error detection and interference rejection consists of forming the code words from a fixed number of zeros and ones. The address code consists of a combination of two "ones" and six "zeros" while the execute code always contains a combination of four "ones" and four "zeros." This 4×4 combination provides 70 commands out of a possible 256 combinations of eight data bits. It provides a means of detecting all odd and 43% of all two-bit errors. To further reduce the possibility of spurious commands, the sync pulse must be detected before the words are detected, and once it is detected, a valid execute word must be read within a fixed period.

Pulse-duration-modulation of an audio oscillator is used, where the bit period is 72 audio cycles, the sync period is 54 cycles, and the "one" bit is 36 cycles and the "zero" bit is 18 cycles. The decoding logic is somewhat more complicated with this digital system than with the simultaneous or sequential tone systems described earlier.

Another form of the tone digital technique has been used for balloon command-control, Cooper (10). In this system the command words are digitally encoded into a train of pulse-duration-modulated 1600 Hz audio signals.

These signals modulate a narrow band FM transmitter. The coded pulses are transmitted in bit pairs (dibits) which represent "ones" and "zeros." An 18 msec pulse followed by an 8 msec pulse forms a one; a reverse sequence forms a zero. A complete command transmission consists of a 3-dibit address, a 28 msec sync pulse, and a 5-dibit command word. Each bit period requires 40 msec, and the complete command 640 msec. It is possible to transmit 8 different addresses and 32 command words; thus up to 256 commands are available to control a single balloon or several balloons simultaneously. A special interlocked command word is reserved for balloon flight termination.

On the balloon, the train of PDM signals is detected at the discriminator of the command receiver, then amplified with audio circuits and passed to the command decoder. An audio, phase-lock-loop, band-pass filter excludes undesired frequencies and noise before the audio signal is converted to dibit and sync pulses. The logic circuits of the decoder detect pulse width, dibit coding, and the presence of the sync pulse. The decoder produces momentary and latching relay closures to actuate the command functions. Six features of the decoder's operation act separately to prevent

inadvertent command activation; the dibit coding, the pulse-width modulation, the audio frequency, the 11-pulse word, the required sync pulse, and the three-dibit address word preceding the command word. When all of these coding features are performing properly, the command will be accepted by the decoders.

Command encoders for this system can be used both at the ground stations and in mobile vehicles. The radio frequency equipment is the same as is used for VHF-FM communications from the ground stations to the mobile vehicles.

3. PCM Command

A PCM command system may be a high capacity command transmission link. The message configuration is similar to a computer instruction, as partitioning is used to designate various functions, such as addressing, event timing, error checking, and system control. The modulation signal is similar to PCM telemetry such as PCM-NRZ where a voltage-controlled subcarrier oscillator is frequency-shift-keyed (FSK) from one frequency to another.

The word format may vary depending upon the requirements of the command

instruction and, for spacecraft, may be quite long. It may contain word synchronization bits, address bits, and instruction bits or memory load bits and their complements for error checking. In more exotic systems the command word may be transmitted back to the ground station for checking with the command word transmitted and if there is agreement, an execute command is transmitted from the ground.

A PCM command system that has been built for one scientific balloon experiment will transmit up to 32 discrete commands and a 16-bit instruction command to the balloon. The discrete commands can be increased to 64 with a small circuit change. The command word consists of 23 binary bits with the first six bits being the address. This address logic is permanently wired into the encoder; however, thumbwheel switch settings could be used for establishing the address of 00 through 31.

The binary discrete command words are determined by thumbwheel digital switch settings which determine the bit logic beginning with the eighth bit. If the command word is an instruction command, the digital switches are set to position 32 which changes the state of bit 7 and causes a 16-bit instruction command to be generated. The word format is established by the

settings of 16 toggle switches.

The encoder logic voltage levels are used to frequency-shift-key (FSK) a voltage-controlled-oscillator (VCO) such as is used with airborne FM/FM telemetry. For this particular system, a channel 1A VCO is used with 14 kHz being used for logic "zero," 16 kHz for a space, and 18 kHz for logic "one." The VCO output modulates an AM or FM transmitter. The bit rate is 30 bps. The six bit discrete commands are decoded on the balloon into voltage signals for actuating relays or whatever other purpose is desirable. Two channels are necessary for actuating a latching relay into two states.

The instruction commands, consisting of 16 binary bits, are decoded into an NRZ-L format on the balloon. In addition to the decoded binary word there is a clock-pulse, a "data-presence" signal and an end-of-message (EOM) pulse. All of these signals are desirable at the receiving end for handling the binary instruction words.

A recent development of data communication circuits has been made by the Larse Corp. of Palo Alto, California. These circuits are modular in form and are supplied in both transmitting and receiving modules. They can be configured with a large degree of versatility which makes them quite useful for many data transmission systems. These units have been utilized in a PCM command-control system by the National Scientific Balloon Facility.

The code format for this command system consists of 16 bits of data information grouped in eight coded groups. These groups consist of four consecutive bits, starting with a low clock bit followed by two data bits, which represent the status of two data inputs, and followed by one high clock bit. A sync pulse follows the entire group. The coded format is used to frequency-shift-key (FSK) an oscillator operating at $1620 \text{ Hz} \pm 180 \text{ Hz}$ at 360 bits per second. The low clock bit and a "zero" data bit are represented by one band edge while a high clock bit and "one" data bit are

represented by the other. This FSK signal is used to frequency modulate the command transmitter.

The 16-bit data word is used to transmit a 6-bit address and a 6-bit command word which can be coded into as many as 64 discrete command functions which appear as open collector transistor sources at the receiver on the balloon. The addresses and commands are established at the transmitter with thumbwheel switches in octal coding. The other switches are used when the system is used for instruction or data commands and for control. A 16-bit data word can be transmitted with the 6-bit address. The data format is established with 16 toggle switches and is transmitted in 2 successive groups of 8 bits.

The system provides several elements of security utilized by the system. No more than two negative transitions occur per code element; all clock bits must be in their proper position of proper polarity and duration; data bits must be in their proper position; and elements cannot have too few or too many transitions.

The 16-bit words are transmitted twice in immediate succession when a command is given. They are compared bit-by-bit by the receiving module to determine the validity of a command.

The binary instruction commands are useful on the balloon in many instances where binary information is desirable, such as setting up memory registers for positioning an instrument on the balloon payload. It is feasible to have an analog-to-digital converter at the ground station ahead of the digital code generator. This would allow one to dial in the desired data in analog form. If a real-time computer were available at the ground station, computer-controlled digital instruction commands with digital telemetry feedback could be used for instrument control. Techniques for using digital command and telemetry are almost unlimited.

4. Verification

There are various schemes for command verification for balloon commands. The obvious way is to use a telemetry channel where a signal is developed on the balloon when the command is decoded and is telemetered to the ground stations for visual observation. In some systems the telemetry signal may be used to turn on visual displays for command verification. In some instances a high-frequency tracking beacon signal frequency is shifted about 1 kHz when the command is actuated on the balloon.

It is more desirable, in some cases, to have verification that the ultimate operation being commanded has performed. This can be done, but because the command system is generally of independent design from the scientific experiment, the verification ends with command reception and decoding.

5. Radio-Frequency Link

For many command-control applications for scientific ballooning in the past, the voice-communications equipment used by launch, recovery and tracking crews has been used as the RF link to the balloon. This is narrow band VHF frequency-modulation equipment (± 5 kHz) using a 60-W transmitter with either a vertically polarized, horizontally omnidirectional or a directional antenna with about 8 dB gain at the ground station. The receivers are modules designed for portable VHF-FM gear which has been repackaged for noise suppression. They have a sensitivity of less than $1 \mu\text{V}$ for 20 dB quieting. The receiving antenna is a vertically polarized coaxial dipole.

By making signal strength calculations, as discussed in sub-Section B.2 for telemetry, it can be seen that there is adequate available signal for reliable operation.

Transmitted power 60 W	+ 48 dBm
Transmitting antenna gain	8 dB
Space loss (400 nmi)	-132 dB
Atmospheric and cable loss	- <u>2 dB</u>
Available signal	- 78 dBm

This signal is equivalent to 28 μ V across 50 ohms. Without the 8 dB antenna there would be -86 dBm or 11 μ V, where only a few microvolts are adequate.

Command-control functions are found in many frequency bands including the high frequency bands. The frequency used would depend upon the type of modulation system used, the range of operations, and the desired ground and airborne antenna configurations. The appropriate frequency management organization should be consulted for obtaining a frequency assignment.

When tone commands are used, a set of 20 IRIG tones (different from the EIA tones) are specified by the IRIG standards for radio command-control. These 20 tones range in frequency from 7.5 to 73.95 kHz, IRIG (11). Other tones and modulation formats can be used because the IRIG standards are not restrictive. They establish standards for commercial equipment as well as provide for efficient spectrum usage and reduction of interfering signals.

D. COMMUNICATION REPEATER

It is often desirable to have communication between two ground stations when the VHF-FM communication system will not function because they

are separated by a distance greater than the radio-horizon.

If the command-control system uses the communications RF links, it is a simple matter to create a radio repeater system using the FM/FM telemetry system. The audio output of the command receiver with proper dc offsets and amplitude limiting is applied to the input of a VCO. The VCO channel must have the frequency data capabilities to handle voice frequencies. Channel E with MI = 5 should be adequate. At the ground station the voice can be taken from the telemetry discriminator, amplified, and used to drive a speaker. This system will work between vehicles and aircraft as long as a telemetry receiver-discriminator is available. It is possible to modulate directly the telemetry transmitter by mixing the audio with other VCO signals. This eliminates the need for a discriminator at the receiving station, but may create intermodulation problems with the telemetry.

E. BALLOON CONTROL

Command-control is used for controlling the scientific balloon as well as the experiment. The experiment generally demands the most from the command system; however, the balloon control commands are very important. Command-control is used for dropping ballast, releasing lifting gas, and for

flight termination.

1. Ballasting

A ballast hopper is usually built in the form of a rectangular box with a pyramid shaped bottom opening into a round port. The port is open to ballast flow; however, the presence of a permanent magnet at the port causes the steel pellets to cluster together and prevent the flow. To allow the ballast to flow, an electromagnet is energized to oppose the permanent magnetic field. This action, called ballasting, may be done by command or by a timer.

The usual verification technique for ballast flow is to verify the reception of a command on the balloon. The actual ballast flow can be detected by means of a sensitive flap and switch in the ballast port. Another technique uses an oscillator as a VCO of the FM/FM telemetry system which has, as part of its frequency determining circuit, an inductance wound around a non-metallic part of the ballast port. When the ballast drops through the coil, the oscillator frequency is changed in proportion to the amount of flow.

Before a flight is terminated, it is usually desirable to remove all

ballast from the payload to relieve the load from the recovery parachutes.

This can be done by command-control, and a timer may be used as a back-up. As a last resort, the hoppers may be destroyed with pyrotechnic devices at the time of flight termination. Hoppers used this way are made of a fragile material such as cardboard.

2. Valving

For the purpose of releasing gas from a balloon, a valve is usually built into the apex of the balloon at manufacture. It is usually actuated by an electric motor which is controlled by timer or command-control. Limit switches stop the electric motor at the extremes of the valve travel and allow the motor to be reversed when desired.

It is desirable to have the receiver and command decoder located at the apex of the balloon with the valve. This eliminates a long wire run over the balloon. A repeater type command could be conceived with a radio link from the main payload to a simple receiver-decoder at the apex. If a telemetry transmitter can also be installed with the valve, the valve position may be monitored at the ground station. The ultimate verification of valving is in the response of the balloon.

3. Flight Termination

A flight is usually terminated by releasing the payload on a parachute. This action is initiated by command-control, generally by the pilot of the tracking aircraft who can better determine the recovery problems and impact hazards from his vantage point. The parachute is attached to the balloon with a coupling which is nearly always released with pyrotechnic devices. Reliability is assured by the use of redundant sub-systems in the coupling system. As a precaution against command failure, a timer-activated sub-system which is set at launch for a period longer than the maximum anticipated flight time is also included.

As in the case of the valve, it is desirable to have the command receiver-decoder at the location of the coupling system. This reduces long wire runs and other hook-up problems in the balloon train. If this cannot be done, wires can be run the length of the parachute to fire the pyrotechnic devices. The timer is always located with the coupling system.

When the parachute and its payload are separated from the balloon, a rip cord built into the balloon and attached to the parachute rips a hole in the balloon, allowing it to fall to earth.

4. Timers

Timers for balloons can have various configurations depending upon the complexity of the flight, the expense involved, and accuracy required, Cooper (12). Mechanical, chemical, and electronic timers have all been used for scientific ballooning. Some flights may use simple timers such as motor driven cams, conducting mixtures which are allowed to escape, and electrolytic cells. A precision tuning-fork driven time piece, called an Accutron, is useful for balloon timing. This timer is equipped with several switch contacts and is accurate to within a few seconds a day. A popular mechanical timer consists of a cam actuated switch driven by a chronometric motor and gear train. The motor has an accuracy of 1%. The desired elapsed time can be set by a dial on the cam. Several cams are available for effecting switch closures at different times. The predecessor to this timer was a long motor driven lead screw which drove a screw-follower to actuate a switch. The elapsed time was determined by the position of the follower on the screw.

Recent timer designs use crystal oscillators with binary and decimal dividers using integrated circuit components, such as RCA COS MOS logic

components. The elapsed time can be set with thumbwheel switches. When the states of the time storage registers in the decade divider chain agree with the decade switch settings, a circuit closure is made. If more than one set of switches is used, more than one circuit closure can be made. The circuit closure can be used to actuate a relay or thyrister circuit to handle large amounts of current. A block diagram and photograph of an electronic timer capable of three timed functions is shown in Fig. 21, Cooper (12). This timer can be updated during flight by command-control. It has status monitor circuits so that the elapsed time can be monitored through telemetry. This is useful when updating.

F. TRAJECTORY DETERMINATION

Balloon trajectory determination is necessary for several reasons. Since the scientific and balloon flight support equipment is seldom expended, it is necessary to know the balloon location for recovery purposes. To meet the requirements of the Federal Aviation Agency (FAA), the balloon position must be known to help prevent it from becoming a hazard to air traffic. In many instances it is important to the scientist to know accurately the geographical coordinates of the experiment. It is always important to the

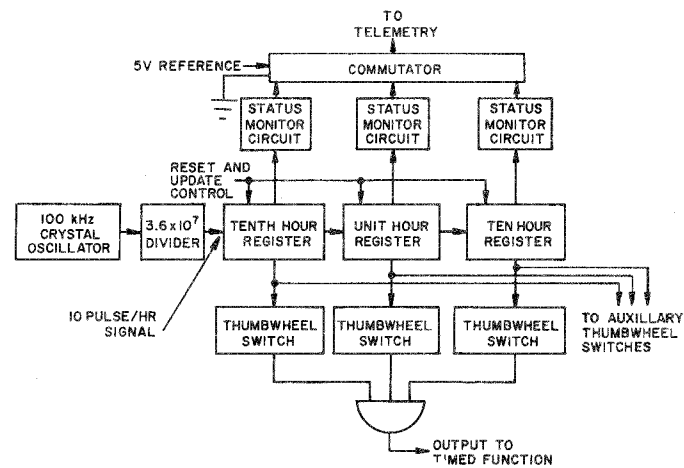


Fig. 21. Digital timer block diagram (a) and a photograph of the timer (b). Pulses from a crystal oscillator are divided to yield a 10 pulse/hr clock. Memory registers store counting bits for tenths of hours, hours, and tens of hours. The timer shown in (b) has two auxiliary sets of switches for additional timed functions, and more can be added if desired.

scientist to have an accurate measurement of the pressure-altitude of the balloon.

1. Radar Tracking

Radar is a contraction of the words, radio detection and ranging.

Radar provides a straight-forward method of tracking a balloon. A radar system used for balloon tracking must be capable of providing accurate position information. Its usefulness is limited by its range, which may extend to near the radio-horizon. Range measurements are a function of the elapsed time between the emission of a pulse of a radio-frequency signal and the reception of a reflected signal from the target. The rate at which successive pulses may be transmitted is usually determined by the longest range at which targets are expected. The range beyond which targets start to appear as second-time-around echoes is called the maximum unambiguous range and is $R = c/2f_r$, where f_r is the pulse repetition frequency (PRF) in Hz and c is the velocity of radio propagation, 3×10^8 m/sec.

When no transponder is used the signal is reflected from the balloon and its payload. Some payload configurations with their reflective surfaces provide excellent radar targets, but it is best to provide a corner

reflector target to insure a good reply signal.

If the radar antenna has a vertical fan beam, such as is used for target acquisition, the elevation accuracy will be poor. The more desirable radiation pattern is a narrow pencil beam. This provides more accuracy in azimuth and elevation. The antenna required to provide such a beam, generally a paraboloid, may be made to track the target with a servomechanism actuated by an error signal. The error signal may be generated by sequential lobing, conical scan, and simultaneous lobing or monopulse.

Any good tracking radar may be used for skin tracking a balloon for position determination. The surplus M33 fire control radar has been used for this purpose; however, these units are becoming difficult to maintain because of component aging and obsolescence. The X-band tracking system of this radar operates in the 8500-9600 MHz band with a peak RF power of 250 kW and a PRF of 1000 pps. A tracking antenna with a pencil beam with a half-power width of 2° is used for tracking. An integral computer, originally a part of the M33 fire control system, can provide a range reading on a counter. Typical accuracies for this radar are $\pm 0.1^\circ$ or better in azimuth and elevation and ± 10 yd at maximum range of 50 n mi (100,000 yd).

2. Rawin Set

Another straight-forward method of tracking a balloon within a limited range with a minimum of airborne equipment is the AN/GMD-1 Rawin set. This is a transportable, radio direction finder, designed for automatically tracking and recovering data from a balloon-borne radiosonde transmitter. A signal from the balloon-borne transmitter, such as radiosonde AN/AMT-12, containing meteorological information in the form of pulse modulation, is received, amplified, and detected by this equipment. The transmitted frequency is 1680 MHz at approximately 0.3 W. This is a continuous wave signal, pulse modulated with a cutoff pulse train ranging in rate between 5 and 200 Hz as determined by a transducer, such as a thermistor for temperature measurements.

The AN/GMD-1 equipment uses a 7-ft paraboloid antenna with a conical scan tracking system. The detected radiosonde signal is passed to separate equipment in the radiosonde system where it is recorded. By reference to calibration data for the airborne unit, the recorded information may be converted to values of temperature, humidity, and pressure. The AN/GMD-1 equipment was originally designed as a tool for sounding the atmosphere to

provide data for weather analysis and forecasting, and to prepare ballistic corrections for the effect of the atmosphere on the trajectory of projectiles.

When the radiosonde system is used with high altitude research balloons for parameters such as temperature and humidity, the measurements are reliable only at the lower altitudes. The temperature sensing system reaches a radiative balance in a rarefied atmosphere and is, therefore, not a reliable air temperature sensor at high altitudes.

Azimuth and elevation angles of the balloon are measured with the AN/GMD-1 antenna to an accuracy of $\pm 0.05^\circ$. These coordinates in conjunction with the altitude are useful in determining the balloon's trajectory. The radiosonde signal is generally accurate to about 150 mi where ground reflections begin to interfere.

3. Phase Shift Ranging

A simple ranging and direction finding system utilizing existing balloon electronic components can be used. This system adds practically no balloon-borne equipment to that normally required for scientific balloon flight support.

This technique utilizes the propagation delay characteristics of a

two-way radio signal from the ground station to the balloon. An audio signal with a convenient wavelength, such as 720 n mi (225 Hz), modulates a transmitter which is used for transmitting command signals to the balloon system. This audio signal is extracted from the command receiver on the balloon and used to modulate the telemetry transmitter, either directly or on an FM/FM subcarrier channel.

At the ground station the audio signal is extracted from the telemetry signal, and a phase comparison is made between the transmitted and received signal. A digital phase meter is used for phase measurements where one degree of phase shift represents one n mi of range, considering two-way propagation delay. More range resolution may be obtained by increasing the modulating frequency by an integral factor such as four, where 360° represents 90 n mi of balloon range. The lower frequency would then be used only for the coarse measurements to eliminate ambiguity.

The azimuth of the balloon from the transmitting station can be determined by using a highly directional telemetry receiving antenna. If the receiving antenna is inherently highly directional, such as a paraboloid used for UHF telemetry, its directional characteristics may be used. If a

signal in the VHF range of 216-260 MHz is used, a system using two receiving antennas may be used. The system consists of two high-gain vertically polarized yagi antennas, horizontally skewed so that the main pattern lobes intersect at the half-power points. The antennas are alternately switched into the telemetry receiver and a visual azimuth error is indicated on an oscilloscope. High resolution pointing accuracy is obtained by rotating the antenna system to null the pointing error. The azimuth readout is provided by a selsyn system and a mechanical counter.

With careful installation and calibration one might expect to get azimuth accuracies of one degree and 0.5 n mi or better in range.

The system could be automated with a servosystem for automatic azimuth tracking. With modern minicomputers, the azimuth and range could be converted to geographical coordinates and also used to drive an X-Y recorder for horizontal mapping.

4. Omega

The Omega navigation system has been used to some extent for following a scientific balloon in its trajectory. Its performance characteristics and the results of tracking experiments indicate that the one-standard-

deviation accuracy of the system is approximately 1 n mi during the day-time and 2 n mi at night, Pierce (13).

Omega navigation is based on the measurement of phase of the signals transmitted from each of several very low frequency (VLF) transmitting stations. Omega is best described as a time-shared CW type of radio navigation system in which the measurements are in terms of the relative phase of the received signals, rather than a comparison of the time of arrival of pulses.

One characteristic of VLF propagation is a low attenuation rate, making it possible to receive the signals at great distances. At the present time, only four Omega stations are in operation. It is anticipated that the system will comprise eight transmitters for global coverage. The existing four transmitters provide a navigation capability for many important geographical regions. The locations of the transmitters are shown below.

Omega Transmitter Locations

Station	Location	Latitude	Longitude
A	Aldra, Norway	66° 25.3'N	13° 09.2'E
B	Trinidad	10° 42.1'N	61° 38.3'W
C	Haiku, Hawaii	21° 24.3'N	157° 49.8'W
D	LaMoure, N. Dakota	46° 22.0'N	98° 20.1'W
E	Reunion Island	20° 58.4'S	55° 17.4'W
F	Argentina	43° 3.2'S	65° 11.5'W
G	Australia	No location established	
H	Japan	34° 36.9'N	129° 27.2'E

The first four stations are permanent stations and radiate from 1 to 3 kW of VLF power. The last four are new stations to begin operation

in the future to make the Omega system a world-wide system which will be useful for global ballooning operations. All except station G are presently under construction. The Trinidad station will eventually be replaced with a station in Liberia. Omega charts and other information may be obtained from the U.S. Naval Oceanographic Distribution Office, Philadelphia, PA or Clearfield, UT.

The frequencies presently being transmitted are 10.2, 13.6, and 11.333 kHz. These transmissions are on a sequential time-multiplexed basis as shown in Fig. 22. The frame repetition interval is 10 sec. Each 10-sec period is divided into eight time segments, A through H. (These letter designations are not to be confused with the station designations.) The time segments are not all equal. Omega navigation receivers, when tuned to one of the VLF frequencies, are synchronized with an internal commutator so that the station transmitting during any particular interval may be identified. The initial receiver commutation cycle may be established by synchronization with WWV or by considering the relative strength of the received

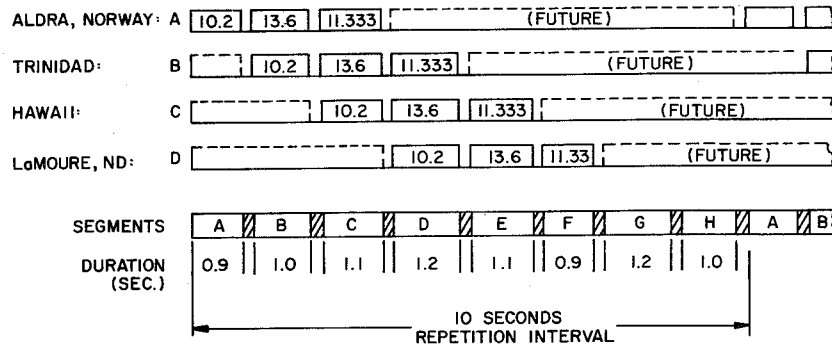


Fig. 22. Omega transmission format.

signals. Automatic segment synchronism may also be established by the unequal segment duration when using more complex receivers. Also, at present, one of the stations transmits a "phase signature" consisting of a 6μ sec phase advance. This creates a temporary 1 mi error, but identifies the station.

All Omega stations transmit on a phase-locked, synchronized basis.

Accurate frequency control is accomplished by employing ultrastable atomic frequency standards at each station. Phase synchronization is maintained by continual phase comparison of signals transmitted by individual transmitters using monitor receivers at the transmitters themselves and at central control locations.

The receiving equipment compares the phase difference of signals of the same frequency transmitted from two stations to determine the hyperbolic line of position (LOP) as shown in Fig. 23. Since the phase difference is repetitive at half wavelength intervals, ambiguous lanes will occur. This lane ambiguity must be accounted for by keeping precise records of the lanes the vehicle has traversed. By using a separate pair of transmitting stations, another set of intersecting lanes can be obtained to establish the position of the vehicle.

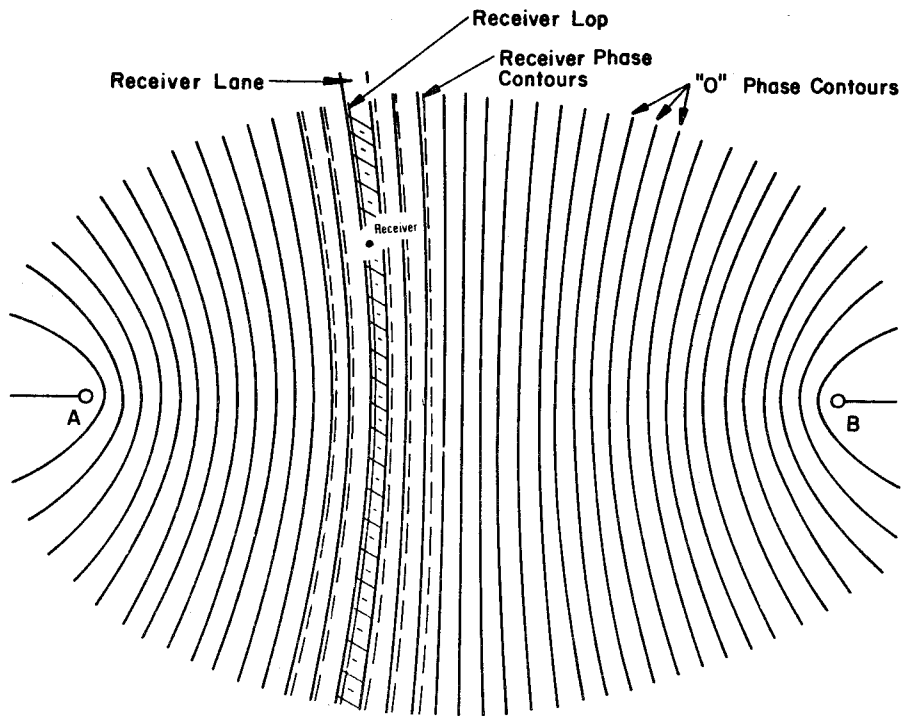


Fig. 23. Omega lane pattern between a pair of stations.

Lane ambiguity can be reduced by using two Omega frequencies. The difference between these two frequencies is used as a third frequency to establish a wider lane. For example, the width of four lanes at 13.6 kHz is equal to the width of three lanes at 10.2 kHz. Similarly, nine lanes at 10.2 kHz equals ten lanes at 11.333 kHz, the total width being the equivalent lane width of the frequency difference of 1.133 kHz, about 72 n mi.

Omega receivers normally present the lane data from pairs of transmitting stations in the form of a voltage on a strip chart recording. The information may be referred to a map or listing where geographical coordinates may be established. A more sophisticated system would use a mini-computer to convert the relative phase information from two pairs of stations (three stations) into geographical coordinates while automatically taking into account the varying skywave factors.

To implement the Omega system for balloon trajectory determination, it is necessary to receive the Omega signals at the balloon and retransmit them to one or more ground stations. A block diagram of a system is shown in Fig. 24. This shows a single frequency Omega signal amplifier on the balloon with its output used to modulate the telemetry transmitter. The

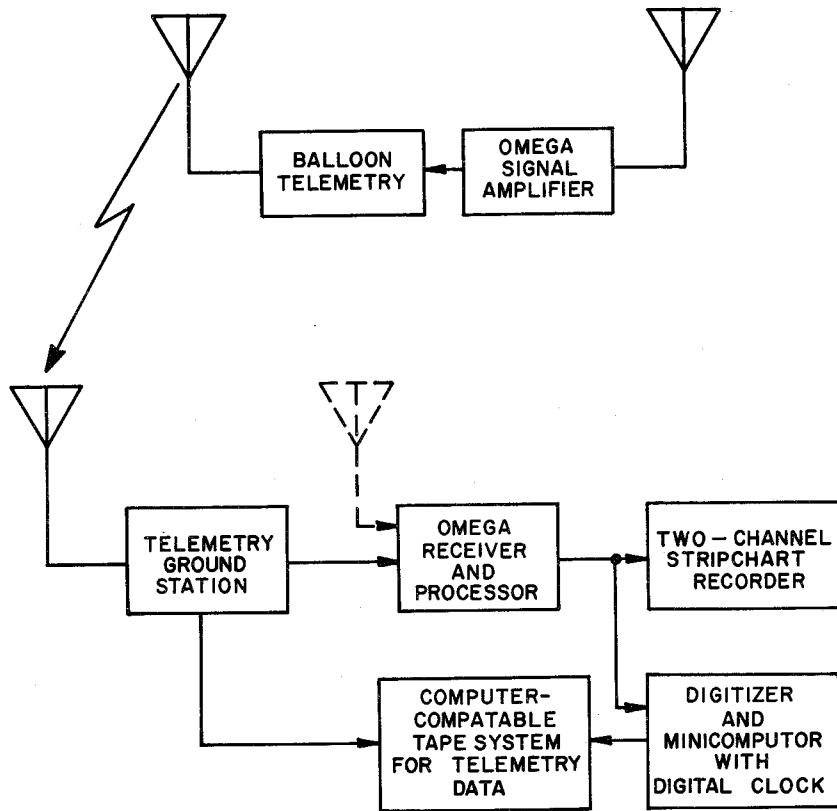


Fig. 24. Block diagram of Omega system for balloon position determination.

transmitter may be directly modulated or the Omega signal may modulate a subcarrier channel if FM/FM telemetry is used. The airborne equipment should be designed for minimum phase variation with Omega signal level variation.

At the ground station the telemetry signal is received and the telemetry information is processed in the usual manner. The Omega signals are extracted from the telemetry signal by demodulation of the carrier and subcarrier, and passed to the Omega receiving and processing equipment. The Omega equipment utilizes the Omega signals as though they were received directly. The fact that they are relayed by the balloon telemetry introduces delays that are determined by the balloon's position. The path from the balloon to the ground station is common to the Omega signals from all transmitters; therefore, the delay for all signals is equal and no relative phase variations occur.

The simplest approach to determining the balloon's ground position is by plotting lane information from the Omega processor onto an Omega map. It may be necessary to initialize the data based on system delays.

A more elaborate system employs digital techniques where appropriate lane tables are stored in a digital computer. These tables, which conform

to Omega maps, can be used to extract geographical coordinates of the balloon.

Another approach uses spherical hyperbolas and the geographical coordinates of the Omega transmitting stations to compute balloon lines of position.

The diurnal variations of propagation of the Omega signals must be considered when making calculations of balloon position using Omega. This variation may create errors of several nautical miles depending upon which transmitting stations are being used. Correction charts are available for these diurnal variations. A local approximation of the error may be determined at the ground station through periodic checks of the Omega position of the station, accomplished by direct reception of the Omega signals. The diurnal correction may be assumed to apply as well at the balloon location, when it is within close range of the ground station.

5. Tracking Aircraft

A method that has been used extensively for balloon trajectory determination is that of aircraft tracking. This method, though not capable of giving extremely accurate position, is necessary for general balloon sur-

veillance as well as for locating the payload impact at the earth's surface.

Most aircraft are equipped with high frequency, automatic direction finding (ADF) equipment for homing on signals such as those radiated from broadcast stations. If the scientific balloon has a signal such as the beacon signal commonly used with the barocoder, the aircraft can determine the location of the balloon by homing on that signal using the ADF equipment. If the geographical position of the balloon is not recognized by the aircraft pilot, he can take bearings to other signals or use the VOR system.

Another aircraft tracking system operates on a principle similar to the high frequency ADF system. It is designed to use the telemetry frequency to determine the bearing of the balloon from the heading of the aircraft. A servo controlled directional antenna locks onto the telemetry signal and a dial displays the bearing of the balloon.

6. FAA Transponder

ATC transponders, similar to those used by many aircraft, may be used on a scientific balloon. The FAA (Federal Aviation Administration) may then determine the balloon position and provide trajectory information. As

the FAA radar scans the horizon, it transmits a pulsed signal which is received by the balloon transponder. The received pulsed signal in turn causes the transponder transmitter to send a pulsed reply which is then received by the radar receiver. This reply signal consists of a digital code identifying the balloon, which has been assigned a special code. The distance is determined by the radar ranging circuits. A complex system of FAA radars provides a wide, though not complete, geographical range of coverage for vehicles carrying transponders, FAA (14).

To conserve power, the transponder may be time-pressure programmed or turned on by command. It is most useful to the FAA when the balloon is operating below 75,000 ft altitude. A programmer can be designed to allow operation constantly to this altitude, and for 5 min at 30-min intervals for the remainder of the flight.

G. PRESSURE-ALTITUDE

The altitude of a free balloon is one of the factors determining the trajectory. Also, scientists using high altitude balloons as vehicles are generally interested in knowing atmospheric pressure at the balloon or the

air mass above the balloon. When pressure and virtual temperature data are available from the balloon altitude to the surface, a pressure-to-altitude conversion can be made by integrating the hydrostatic equation (see Section XI). Atmospheric pressure measurements for scientific ballooning are generally made in millibars, a bar being 10^6 N/m² --slightly less than mean sea level atmospheric pressure. Gage pressure is referenced to atmospheric pressure, while absolute pressure is referenced to a vacuum.

Types of gages used to measure pressure include liquid manometers, Bourdon tubes, strain gages, piezo electric devices, capacity diaphragms, variable reluctance diaphragms, rare earth transducers, corona current devices, thermoconductivity measuring devices, radioactive density gages, and solid state pressure sensing devices. Many of these gages are applicable to on-board pressure measurements. The type used for a flight depends upon the accuracy desired, the type of data recovery, and other factors peculiar to the flight, Cooper (15).

1. Barocoder

One of the earliest types of instruments used for pressure measurements is the barocoder. This instrument has usually been used in conjunction with

a low-power transmitter operating at approximately 1680 kHz, and together they are commonly referred to as a beacon-barocoder. The beacon transmitter can be tracked by means of the automatic direction finding (ADF) equipment available on most aircraft; consequently, it provides a means of locating the balloon as well as providing the pilot with balloon altitude information.

When the beacon-barocoder was originally designed, it was used on balloon flights where radio telemetry for data recovery was not always available. This made the beacon-barocoder an independent instrumentation item. It is still widely used because of its accepted reliability, redundancy to other pressure systems, and for its compatibility with the tracking aircraft for balloon tracking and payload recovery after termination.

The barocoder consists of a system of aneroid bellows which are mechanically linked to a stylus which is allowed to move longitudinally across the surface of a code drum. The code drum is a motor-driven cylinder which has a systematic configuration of Morse code letter groups etched on its surface in the same fashion that electronic circuits are etched on copper-clad insulation board. As the pressure changes, different code letters are traversed by the stylus as the drum rotates and the circuit closures made by

the stylus on the etched drum key the transmitter on and off. The signal is radiated from a long wire antenna suspended below the balloon payload or attached to a load tape. Receivers are located in the tracking aircraft and at the ground stations.

2. Diaphragm Gages

There are two types of diaphragm gages that are applicable to pressure-altitude measurements. One is a capacitive device using a taut membrane stretched between two stationary capacitor plates. The space between the membrane and one stationary plate is evacuated, while the space between the membrane and the other stationary plate is connected to the gas whose pressure is to be measured. The displacement of the membrane with respect to the stationary plates is a measure of the pressure, and is determined by capacity measurements between the membrane and the stationary plates. An oscillator-detector circuit is used for capacity measurements, the dc output voltage being a direct representation of absolute pressure. The output voltage generally ranges between 0 and 5 V and varies linearly with pressure.

The other type of diaphragm gage is mechanically configured similar to

the capacity type, in that it consists of a taut membrane between two rigid blocks. This unit operates on the principle of variable reluctance rather than variable capacitance. An E-core and coil assembly is embedded in each block. A small gap between the diaphragm and the E-core in a symmetrical arrangement results in a condition of equal inductance with the membrane in an undeflected position. Diaphragm deflection results in an increase in the gap in the magnetic flux path of one core, with an equal decrease in the other. This increases the inductance of one coil while decreasing the inductance of the other. A simple bridge and detector circuit converts the inductance ratio to a dc output voltage of 0 to 5 V, which varies linearly with pressure. The output voltage from the diaphragm gages may be read at the ground station through the telemetry system.

Diaphragm gages have been used to a large degree on scientific balloons in recent years. Various pressure ranges are available, with the most sensitive ranges such as 0 to 0.1 psia (0 to 7 mb) being used for balloon float altitudes. With careful calibration, the accuracy of this most sensitive range should be within 0.1 mb. If the output voltage is digitized rather than being telemetered in analog form, readout accuracy can be improved.

An assembly of diaphragm type gages may be used to cover the complete pressure range traversed by balloons during ascent and descent, Cooper (16). If three gages are used in the assembly, good resolution may be obtained for float altitudes above 18 km. The three transducers cover the full ambient pressure range expected in balloon flights; each is engaged in the pressure interval to which it is most sensitive. Electronic circuits can be used to select the appropriate transducer for each pressure segment and supply calibration voltages for the telemetry system. Typical pressure ranges of transducers of this type are 0-1100 mb for low altitude pressure measurements (below 18 km), 0-70 mb for the range between 18 and 34 km, and 0-7 mb for flights above 34 km.

The dc analog voltage outputs of the transducers are individually applied to the input of a telemetry system. Calibration voltages for the telemetry system may also be supplied at intervals with the pressure analog from the transducer interface electronics. To conserve power, only the transducer required for a particular range need be functioning. They may be selected by command-control or by an electronic circuit which automatically selects the transducer which is most sensitive in the pressure range in

which the balloon is flying. The active transducer may be identified at the telemetry output by some identifying code, such as the manner in which the calibration pulses are applied to the telemetry encoder input.

Since taut diaphragm gages rely upon a reference vacuum for their operation as an absolute pressure gage, care must be taken to insure that the reference vacuum is not allowed to deteriorate. Manufactured gages have a reference as a part of their construction and are subject to leaks through glass seals, welds, or even through the thin metal material of the taut membrane. Careful manufacturing control must be maintained. A small leak may take months to detect. When one occurs, however, the gage suffers with a fixed shift in its output voltage and is more sensitive to ambient temperature changes.

3. Thermoconductivity Gages

A thermoconductivity pressure gage utilizes the change in the thermoconductivity of a gas to detect pressure changes. One transducer of this type uses a thermistor sensing element in a constant temperature environment. The thermistor is an element of a bridge circuit, whose output changes with pressure changes because the equilibrium temperature of the thermistor

changes inversely with the pressure being measured. The output voltage of the bridge is fed to an operational amplifier whose output is fed back to the bridge to bring it into balance. The output voltage of the operational amplifier is a function of the thermoconductivity of the gas surrounding the thermistor sensor, which makes it a pressure sensing device since T is constant. The voltage range can be designed to give an appropriate analog range, such as 0 to 5 V dc over the pressure range to be measured.

The thermoconductive transducer has good performance characteristics with good resolution in the very low pressure range under controlled conditions. The output voltage varies logarithmically with the absolute pressure, giving more resolution at the low pressure end of its range. A typical calibration curve is shown in Fig. 25. Since it measures thermal conductivity, its accuracy depends upon the chemical composition of the gas being measured. When used as a balloon pressure-altitude transducer, it may be exposed to helium or other gases which have a different thermal conductivity from that of air. This will change the calibration of the transducer and cause it to indicate an erroneous pressure.

4. Other Types of Pressure Transducers

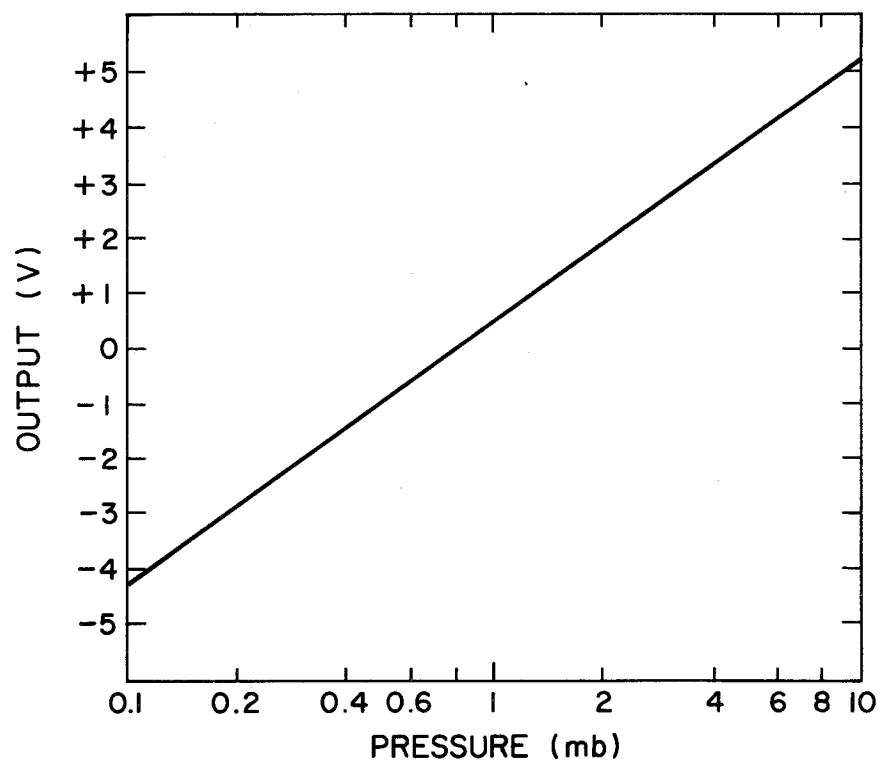


Fig. 25. Typical calibration curve for thermoconductivity pressure gage.

There are several other types of pressure transducers that have been used as balloon altimeters. Some of these transducers have special application and may not lend themselves to routine operational use because of their complexity, calibration problems, or their incompatibility with telemetry.

The hypsometer is an instrument which measures the pressure of a gas through the relationship of the vapor pressure of a liquid to its temperature. If a liquid is maintained at its boiling point, its vapor pressure is equal to the surrounding gas pressure. Thus the vapor temperature is a measure of this gas pressure. Some means, such as a thermistor, must be used to measure the temperature of the liquid. This temperature measurement must then be converted to an analog or digital signal, compatible with the telemetry, before transmission to the ground.

The hypsometer has a slow response and is tedious to prepare for flight. When it is working properly and has been carefully calibrated, it is an accurate pressure measuring device.

A transducer that has been used in scientific balloon flights is a corona transducer which operates on the density dependence of a corona dis-

charge in air. A positive ion flow is generated in a region of high electric field gradient in the immediate vicinity of a fine wire suspended axially within a conducting cylinder. The magnitude of the current flowing between the wire and the cylinder is a function of the gas density in the region between the electrodes. Since the unit is basically a density measuring device, the corona current is sensitive to temperature variations. The transducer has a temperature compensation circuit which makes it function as a pressure measuring system.

Radioactivity pressure transducers have also been used in scientific ballooning. These instruments have sensitive electrometers to measure the ionization currents produced by alpha-particles from a radioactive source. Voltage pulses are generated by a blocking oscillator at a rate determined by the ionization currents. At low pressures, the repetition interval is very long--on the order of 30 to 50 sec at 3 mb. In some cases the pulses are used to change the state of a flip-flop, making it easier to read on telemetry, Howard (17).

The radioactive type of transducer must be temperature controlled or temperature compensated since it is basically a density measuring device.

Some must be calibrated immediately prior to use because of the decay of the radioactive source. Like the thermoconductivity transducer, the radioactive transducer can be affected by the composition of the measured gas.

Early scientific balloon flights were equipped with an instrument called a photobarograph to provide redundancy in pressure measurements. This is a self-contained unit which operates independently from other electronic or telemetry equipment. It consists of an accurate aneroid pressure gage with a dial calibrated in millibars. The pressure dial and an accurate time piece are photographed at appropriate intervals during the balloon flight, and the camera film is processed after payload recovery.

5. Altitude Measuring Devices

A newly developed radio altimeter makes direct geometric altitude measurements of meteorological balloons up to altitudes of 35 km over water and 12 km over land. This radio altimeter is a pulse-radar system in which the elapsed time period between transmitted pulses is a measure of the altitude, Levanon (18), Stremmer (19). A single RF superregenerative stage serves as both the transmitter and the receiver. The transmitted pulse is

reflected from the water or earth surface and is received by the altimeter receiving circuits. The repetition frequency of the transmitted pulses is controlled by the round trip propagation time of the pulsed radio signals. At high balloon altitudes, the repetition interval may be less than the propagation time by one or more integral multiples. This creates an ambiguity in altitude but it can be overcome by extrapolating the balloon ascent data or by means of balloon-borne pressure gages.

The maximum altitude of operation is influenced by transmitter power, antenna gain, choice of operating frequency, terrain, etc. The upper limit for altimeters currently being used is 35 to 40 km over water and 12 to 15 km over land using 5-element yagi antennas at 403 MHz. These radio altimeters are obviously more practical to use over water than over land. Because of this, they find more use for meteorological or long duration global flights than for scientific balloon flights.

H. POWER

Solar cells, fuel cells, nuclear sources, and batteries have all been considered as power sources for balloon-borne electronic equipment. Solar cells have been used extensively only on small, long-duration balloon systems,

and batteries are used regularly to power both scientific and support equipment on large scientific flights. Other types of power sources have not been widely used.

Solar cells are p-n junctions, usually silicon, that develop electrical energy by the photovoltaic effect. When a junction is illuminated, photon energy creates electron-hole pairs, and a voltage is developed across the junction. The efficiency of modern solar cells is about 5-10%, and a 1-m² panel exposed perpendicularly to the direct rays of the sun at the top of the atmosphere will intercept 1395 W of solar power, see Section III.G. Thus a solar cell panel may be expected to provide a maximum of about 140 Wm⁻² during the day under ideal circumstances, and it will produce no power at night. In general, a large area of solar cells would be required to provide energy for a scientific flight, and stored energy would be needed to supplement the solar cells if power were required at night.

Mercury, lead-acid, nickel-cadmium, silver-zinc, and silver-cadmium batteries have all been used in scientific ballooning. No one type is clearly superior to all others; therefore, battery selection depends on the application and the type of service desired.

Mercury cells have a high energy density and are rugged and reliable. The terminal voltage during discharge is fairly constant; therefore, some models are useful as voltage references. Unfortunately, they have characteristics which render them incapable of providing power under the conditions generally required for balloon service. They are not rechargeable, they cannot be operated satisfactorily in parallel because circulating currents cause serious discharge of cell capacity, and they are not useful at temperatures below 5°C. They are useful, however, for low-power loads where current drain is well below the design maximum and the temperature can be controlled.

The lead-acid cell is probably the best known of the common storage cells. It has a relatively low energy density, but it has a high terminal voltage and a fairly level discharge plateau. When flown at high altitudes, it should be operated in a sealed container in which a pressure greater than the partial pressure of the electrolyte can be maintained. Also, in the case of liquid electrolyte types, it must be properly oriented to prevent spilling. Because of their low cost and universal availability, lead-acid batteries are sometimes used, but they are not generally recommended for balloon service.

Nickel-cadmium cells employ electrodes of nickel and cadmium in a potassium hydroxide electrolyte. There are two distinct cell forms--the Junger or pocket-plate and the Durac or impregnated, sintered-plate type. The sintered-plate type can sustain a higher current drain and it can be made thinner, and hence smaller, than the pocket-plate type. The principal advantages of the nickel-cadmium cell are that it can be hermetically sealed, it has a high cycle life, and it performs better than other cells at low temperatures. It has a higher energy density than the lead-acid cell.

The silver-zinc cell employs zinc and silver oxide as electrodes in a solution of potassium hydroxide. These cells, designed for high-energy applications cannot be hermetically sealed because of the evolution of oxygen. They may be operated in either series or parallel, provided they are all the same type and size. They have a high energy density and are especially suited for high current drains. The major disadvantages are the limited shelf life when activated and the limited recharge cycles as compared to nickel-cadmium and silver-cadmium. The energy density is good over a range of -30 to +50°C but is reduced at more extreme temperatures. The silver-zinc battery is well suited to balloon applications where the best

energy-to-mass ratio is desired and the recycle life is not important.

Silver-cadmium cells are similar in construction to silver-zinc cells except that the electrodes are silver and cadmium. The electrolyte is potassium hydroxide. The operating characteristics and watt-hour cost are also similar to those of silver-zinc cells. Silver-cadmium cells have better temperature stability and greater cycle life than silver-zinc cells but their energy to mass ratio is not quite as great. As with the silver-zinc cells, they cannot be hermetically sealed for high discharge rate applications. The main advantage over other types of storage cells is their increased cycle life for rechargeable application. This, together with their reasonably high energy density makes them desirable for use as power sources for repeated use where operating cost is a major factor, Garner (20).

I. EQUIPMENT PACKAGING

Equipment which is flown on a balloon must be protected against a rather severe environment during flight. Ambient air temperature may drop as low as -85°C . Air pressure is frequently less than 0.005 atmospheres and may reach values as low as 0.001 atmosphere (\sim one mb) on the highest flights. Also moisture may occasionally condense on equipment during ascent or descent even

in the absence of clouds. Finally, equipment which is to be recovered for post-flight evaluation or reuse must be protected against the accelerations associated with the flight. Landing shocks, in particular, can be severe. Experience has shown that equipment which is properly packaged can function satisfactorily in the adverse flight environment while improperly packaged equipment frequently fails.

Pressure and temperature in the atmosphere at balloon flight levels are discussed in Section XI. Heat exchange between a balloon-borne object and its environment is covered in Section III. Potentially damaging accelerations are most likely to occur during the parachute opening or upon landing. These are discussed in Sections X.C. and XII.G., respectively.

Equipment which is flown repetitively for routine flight support is usually packed in a self contained, serviceable configuration. Figure 26 shows one such support package. Its construction and protective covering (not shown in the figure) are the end result of extensive engineering analysis and flight experience. The packaging for scientific equipment, or special support equipment, being flown for the first time is often designed on the basis of engineering analysis alone. A preliminary flight for testing the

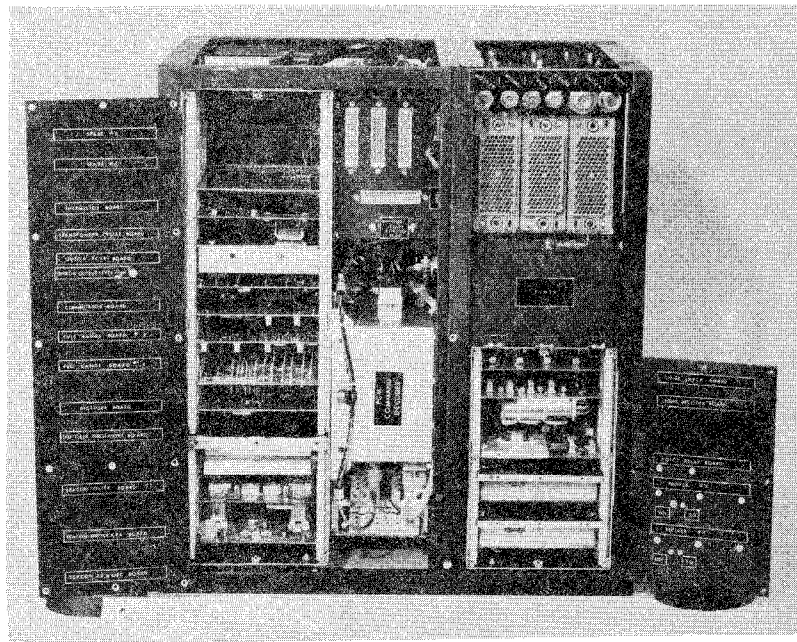


Fig. 26. The NCAR integrated flight support package.

packaging and other engineering features of new flight systems should always be considered. Tests in environmental chambers may also be useful.

The location of support instrumentation on a flight payload depends largely on the configuration of the scientific equipment. Large, bulky experiments may have adequate space within their structure to accommodate the support package without causing undue problems, e.g., center-of-gravity shifts. Smaller experiments may be placed above, below, or beside a self contained support package. Each such arrangement creates its own special problems in protective packaging.

The flight support package must be equipped with appropriate circuit connectors to connect the telemetry, command, pyrotechnic, and other circuits used with the scientific experiment and balloon control. Flight antennas should be placed on the payload with much care. Antennas are usually suspended well below the payload at distances and separations that will create a minimum radiation interference with each other. Some payload configurations require a long wire, high frequency antenna to be attached above the payload on a balloon load tape. The Omega tracking antenna whip may sometimes be located above the support package.

A flight package can be protected from low temperature environments with thermal insulation material, such as styrofoam sheets or similar molded material. It is seldom necessary to supply heat from an external source because high dissipation equipment such as telemetry transmitters provide enough heat to warm low dissipation equipment. Because of this, it is necessary to configure flight components within the package for uniform heat distribution and proper heat sinking. It may sometimes be necessary to release heat from highly dissipative components to the outside of the insulated housing by means of metal heat conductors. A part of the payload structure is often used as a heat sink. It is possible to use liquid thermal sinks and electrical or fluid heat exchangers as part of the package design. Liquid thermal sinks are often used with packages containing equipment with low internal heat release such as timers and command-receivers which are isolated from the main support package at the top of the parachute or balloon.

When configuring the flight package it is generally desirable to place the batteries in the lower portion of the package. This concentrates the weight at the bottom, utilizes the heat liberated by the batteries more ef-

fectively, and prevents stray electrolyte from damaging other circuit components.

REFERENCES

- (1) Stiltz, Harry L., 1961: Aerospace Telemetry, Vol. I. Prentice-Hall, Inc.
- (2) Telemetry Standards, Revised 1973. To be used in conjunction with document 118-73, Test Methods for Telemetry Systems and Sub-systems: Inter-Range Instrumentation Group, Published by Secretariat, Range Commanders Council, White Sands Missile Range, New Mexico, 88002.
- (3) Gruenberg, Elliot L., Ed., 1967: Handbook of Telemetry and Remote Control. McGraw-Hill Book Co.
- (4) Bendix-Pacific, 1958: The Theory and Application of FM/FM Telemetry, Revised 1958. Bendix Aviation Corp., North Hollywood Calif.
- (5) Cooper, Oscar L., 1967: Scientific Balloon Instrumentation, Proceedings of the Thirteenth I.S.A. Aerospace Instrumentation Symposium.
- (6) Nichols, Myron H. and Lawrence L. Rauch, 1956: Radio Telemetry, 2nd ed. John Wiley and Sons, Inc., New York.
- (7) Clark, T. A., 1969: Telemetry Signal-Strength Variations from Balloon-borne Equipment and a method for balloon range estimation. Journal of Scientific Instruments, Series 2, Vol. 2.
- (8) Cooper, Oscar L., 1970: Evaluation of UHF Radio Frequency Equipment for Balloon Telemetry, Proceedings, Sixth AFCRL Scientific Balloon Symposium. (AFCRL-70-0543)
- (9) Coates, Robert J., 1969: Tracking and Data Acquisition for Space Exploration. Goddard Space Flight Center, Greenbelt, Maryland. Publication X-520-69-200.
- (10) Cooper, Oscar L., 1970: PCM Command Control System, Facilities for Atmospheric Research, No. 12, Mar. 1970. National Center for Atmospheric Research, Boulder, Colo. 80302.

- (11) IRIG Standards for Radio Command Control, 406-550 Mcs Band, 1962: Inter-Range Instrumentation Group, published by Secretariat, Range Commanders Council, White Sands Missile Range, N. Mex., 88002.
- (12) Cooper, Oscar L., 1971: Timers for Balloons. Facilities for Atmospheric Research, No. 16, Mar. 1971. National Center for Atmospheric Research, Boulder, Colo. 80302.
- (13) Pierce, J. A., W. Palmer, A. D. Watt, R. H. Woodward, 1966: Omega, A World Wide Navigational System, 2nd Rev. U.S. Navy Dept. Bureau of Ships, submitted through Office of Naval Research P and B, publ. No. 886B, Project No. 347.
- (14) Federal Aviation Regulations, Vol. II, Part 37.180, July 1969: Supt. of Documents, Wash., D.C. 20402.
- (15) Cooper, Oscar L., 1968: Pressure Altitude Transducers, Facilities for Atmospheric Research, No. 7, Dec. 1968. National Center for Atmospheric Research, Boulder, Colo. 80302.
- (16) Cooper, Oscar L., 1970: Pressure Altitude Assembly for High-Altitude Balloons, Facilities for Atmospheric Research, No. 15, Dec. 1970. National Center for Atmospheric Research, Boulder, Colo. 80302.
- (17) Howard, R. L., S. W. Nelson, J. R. Winckler, 1968: An Alphanatron Pressure Gauge for High Altitude Constant Level Balloon Flights. School of Physics and Astronomy, Univ. of Minnesota, Minneapolis, Minn.
- (18) Levanon, N. and F. G. Stremmler, 1969: Accurate Pulse-Radar Altimeter for Meteorological Balloons, Proceedings of IEEE, Vol. 57, No. 9, Sept. 1969.
- (19) Stremmler, F. G., N. Levanon, V. E. Suomi, 1970: Applications of Radio Altimetry to Balloons, Proceedings, Sixth AFCRL Scientific Balloon Symposium. (AFCRL-70-054B)

- (20) Garner, Ruford V., 1964: Investigation of Electrical Power Sources
for Missile-Borne Applications, Report No. RE-TR-64-29, DA Proj. No.
IX27919D687, U.S. Army Missile Command, Redstone Arsenal, Ala.

SECTION VII

LIST OF SYMBOLS

STABILIZATION AND ORIENTATION OF BALLOON-BORNE INSTRUMENTS

by

Russell A. Nidey

List of Symbols ii

List of Figures v

List of Tables v

A. INTRODUCTION 1

B. AZIMUTH STABILIZATION 3

1. Reaction Wheel 4

2. Motors 7

3. Perturbations 13

C. GIMBAL CONSIDERATIONS 17

D. ERROR SENSORS 19

E. EXAMPLES OF VARIOUS BALLOON-BORNE CONTROL SYSTEMS 29

1. The Solar Azimuth Pointing Platform 30

2. The Bi-axial Pointing Control 30

3. Stratoscope I 32

4. Coronascope 35

5. StratoLab 36

6. BAL-AST 39

7. Star Gazer 41

8. BBSP-200 44

9. Skytop 46

10. Polariscope 49

11. Stratoscope II 50

F. CONCLUSIONS 53

REFERENCES 54

<u>Symbol</u>	<u>Description</u>	<u>Dimensions</u>
A	subscript denoting aximuthal axis	
A_o	area of the objective	L^2
A_p	area of a photo-element	L^2
B	function used in the form $B(\lambda, \theta, \varphi)$ to indicate the rate at which photons arrive at a position analyzer from the background	
B	subscript denoting background	
D	function used in the form $D(t)$ to describe the action of a signal demodulator	
D	subscript denoting dark current	
E	efficiency of a telescope; $E(\lambda)$ is the efficiency of a telescope including the spectral character of the optics and the photo-element	
F	focal ratio of a Fabry lens	
g	acceleration due to gravity	LT^{-2}
G	fractional gradient in the background illumination	
G	subscript used with I to denote moment of inertia of the aximuthal gimbal	
I	moment of inertia. Subscripts are used to specify the axis about which I is taken	ML^2
L	length of pendulum	L
L	subscript denoting longitudinal axis	

M	a function used in the form $M(\theta, \varphi, t)$ to indicate the transmission of an analyzer	
n	an integer, e.g., 1, 2, 3	
N	cycles of the analyzer over which the signal has been integrated	
R	radius of prismatic suspension system	L
S	signal	
S_D	minimum signal due to the dark current	
t	time	T
T	period	T
T	function used in the form $T(\lambda, \theta, \varphi)$ to indicate the rate at which photons arrive at a position analyzer from a target	
T	subscript used to denote the transverse axis	
T	subscript used to denote target	
$(TE)_\lambda$	function defined as $\int_\lambda T(\lambda) E(\lambda) d\lambda$	
V	magnitude of target	
X	angular error	

Greek Letters

β	angular elevation of objective above the local horizon
γ	half amplitude (angular displacement) of a gondola about the horizontal axis which the line of sight from the gondola to the object projects onto the horizontal plane
δ	angular diameter (relative to the objective) of the circle of illumination produced on the analyzer by the target
Δ	half amplitude (angular displacement) of a gondola about its own azimuth axis
ΔX_B	statistical limiting accuracy due to photon noise in the signal from the background
ΔX_T	statistical limiting accuracy due to photon noise in the signal from the target
ϵ	error due to gradient in the background illumination
η	dark current of a photo-element
θ	angular displacement about the vertical axis
Θ	position angle measured about the optical axis
λ	wave length of light
φ	position angle measured about an axis transverse to the optical axis
φ_0	position angle (see φ) used as radius of the field of view
ω	rate of rotation T^{-1}

List of Figures

Fig. 1	The prismoidal multipoint suspension system	6
Fig. 2	Cross-spin forcing of the azimuth control system	16
Fig. 3	The solar azimuth pointing platform (photograph courtesy of Ball Brothers Research Corp.)	31
Fig. 4	The solar biaxial pointing control (model 3-4M) (photograph courtesy of Hi-Altitude Instrument Company, Inc.)	33
Fig. 5	Coronascope II at Palestine, Texas, prior to the flight of June 6, 1970	37
Fig. 6	The Johns Hopkins University 12-in. telescope mounted on the StratoLab gondola (photograph courtesy of Librascope, Inc.)	38
Fig. 7	The BAL-AST unmanned telescope system (line drawing courtesy of Johns Hopkins University).	40
Fig. 8	The photoelectric tracker used on BAL-AST shown in a test fixture (photograph courtesy of Impro Corporation)	42
Fig. 9	The balloon-borne bi-axial solar pointer shown with simulated instrument and gondola (photograph courtesy of Ball Brothers Research Corp.)	45
Fig. 10	Stratoscope II, the largest of the current balloon-borne telescopes, shown at Huntsville, Alabama, prior to the flight of September 9, 1971	54

List of Tables

Table 1	Rating of selected azimuth motors	9
---------	---	---

STABILIZATION AND ORIENTATION OF BALLOON-BORNE INSTRUMENTSA. INTRODUCTION

In the context of this section stabilization is defined as the reduction of the angular velocity of the instrument about one (or more) of the axes to a value appropriately near zero; and orientation is defined as the directing of the instrument toward a specific target. Whether stabilization or orientation is required depends upon the measurement being made by the instrument and upon the extent of the degradation of the measurement due to the motion of the balloon.

The balloon can be expected to be rotating some tens of degrees per minute in azimuth. This motion is generated primarily during ascent and descent of the balloon by windmill action of the gores. In addition to the azimuth rotation of the balloon (and gondola) there is a pendulous motion of the gondola beneath the balloon, with the balloon participating to a degree in this motion. The motion can be that of a simple pendulum in a single vertical plane, or a combination of two such motions with the gondola describing an elliptical or more complex path beneath the balloon.

The amplitude and character of the pendulous motion depends very much on the portion of the trajectory under consideration. The motion may be very severe during the launch phase, but should be very small at float altitude. Characteristically, at float, the amplitude is of the order of a few minutes of arc, with one degree representing a reasonable design limit. The period of the pendulous motion is directly related to the length of the pendulum:

$$T = 2\pi(L/g)^{\frac{1}{2}}$$

where T is the period; L, the length of the pendulum; and g, the acceleration of gravity. Thus, if the length is 100 m the period is about 20 sec.

The gondola will also oscillate about its center of mass as a compound pendulum. The period of this motion is characteristically much shorter, and the amplitude much less; moreover, this motion is more readily damped by the ambient air.

Inasmuch as differential motion of the ambient air relative to the balloon system continually excites the natural frequencies of the system, it is essential that all mechanical resonances including that of the compound pendulum, be well outside the critical band pass of the control sys-

tem. Hence, the gondola must be constructed as a simple, rigid system to reduce the number of resonant frequencies and to assure that these frequencies are above those critical to the control system.

Uniaxial control suffices if it is necessary only to have one side of the instrument turned, say, toward the sun. Biaxial control is necessary if the instrument, such as telescope, must be pointed at a celestial target; and triaxial control is indicated if the image of the target is not to be allowed to rotate in the focal plane of the instrument, as for high resolution photography of the moon.

Though the choices of the number and order of the axes of the gimbals, the motors that drive the gimbals, and the sensors that command the motors are clearly based on the specific instrument to be controlled, a number of generalizations can be made. Since the azimuthal motion of the balloon constitutes the most severe of the motions to be countered by the control system, virtually all control systems will have an azimuth stabilization gimbal as the first gimbal.

B. AZIMUTH STABILIZATION

To control the instrument there must be a source of reaction torque.

A propeller on the end of a lever could be used to react against the ambient air. Though the accuracy of such a system would be limited severely by the lag of the torque behind the control signal, coarse stabilization could be obtained. Higher speed of response and hence greater accuracy would be obtained by ejecting a gas or pellets; however, not only would the duration of the mission be bounded by the quantity of "fuel" carried, but also the accuracy of control would be limited by the method of metering the ejecta. Greater accuracy can be obtained by driving a reaction wheel, the chief limitation being that the total impulse available is determined by the size and maximum speed of the wheel.

1. Reaction Wheel

For a top speed of 500 rpm in a wheel 0.5 m in diameter, the maximum total impulse available would be less than 200 N m/kg. Without active in-flight balancing of the gondola it would be very difficult to reduce the residual azimuthal gravitational moment to less than 0.1 N m. Thus, a reaction wheel of one kg mass could be expected to be saturated in less than one-half hour. In contrast, a 280 kg balloon 60 m in diameter subjected to the same secular bias would accrete speed at the rate of only 15° per

minute per hour. Furthermore, any rotational speed of the balloon in excess of a few degrees per minute would be aerodynamically dampened by the ambient atmosphere. Consequently, the balloon constitutes an excellent source of reaction torque for the azimuth gimbal. However, the balloon is not rigid; thus, to avoid undue velocity in the control motor, it is usually expedient to incorporate a wheel intermediate between the gondola and the balloon. This wheel is generally coupled to the balloon with a prismatic multipoint suspension system as illustrated in Fig. 1. The parachute risers may be used conveniently as the multiple load lines.

If the maximum torque that the suspension train can transmit to the balloon is less than can be developed by the azimuth motor, it is necessary to incorporate a torque limiter between the reaction wheel and the balloon to avoid winding the parachute into an ineffective rope. The torque limiter may be viscous or non-viscous, obtained by using a Teflon or a neoprene shoe, respectively, on a steel wheel in a classical prony brake. The latter maximizes the momentum transfer; the former strongly dampens the torsional oscillation of the wheel relative to the balloon.

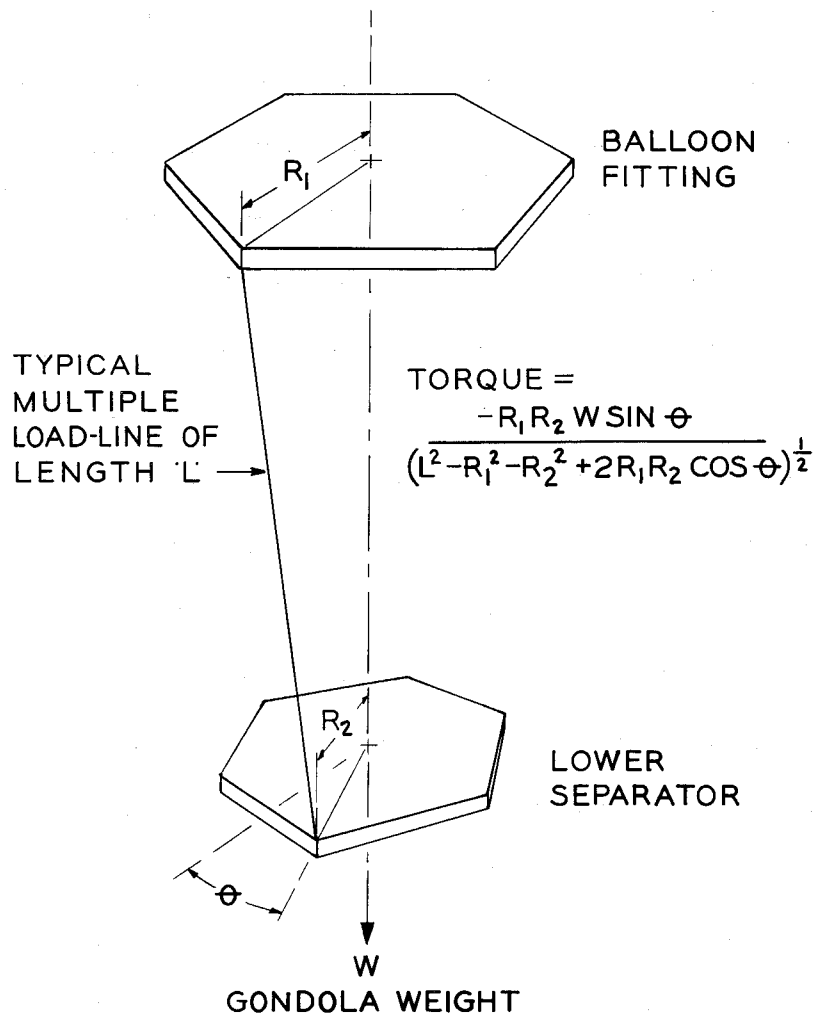


Fig. 1. The prismatic multipoint suspension system.

2. Motors

Consider now the selection of the motor. One can enumerate a number of ideal characteristics that this element should have:

- a. If the system is to be rather "tight," the torque produced by the motor must be proportional to the driving signal.
- b. The motor should also be non-viscous; i.e., the torque should be independent of the relative velocity between the reaction wheel and the gondola. Back emf (as well as any source of drag between the stator and the rotor) provides disadvantageous viscous reaction in the motor.
- c. To avoid inertial coupling of the wheel to the gondola, the motor should be directly coupled between the gondola and the wheel. Otherwise, oscillation of the wheel on the torsional suspension system will constitute a corresponding forcing function to the stabilization system.
- d. Since the balloon may make several revolutions during the flight, the motor must be able to accommodate a corresponding number of revolutions of the wheel relative to the gondola.

e. In addition, in some instances, power amplification may be required.

It may be necessary to derive relatively robust motion from a relatively weak power source.

f. Reliability of the motor is essential. The system must operate repeatedly in a predictable manner; the loop gain, adjusted on the ground for optimum performance, must not be grossly different at float altitude.

g. The motor should be easy to excite and to incorporate. A complex power output stage in the power amplifier, as a case in point, would be disadvantageous, as would a complex mounting involving many gears and bearings.

h. Finally, the motor must have a satisfactory frequency response; i.e., the torque output should be reasonably independent of the frequency of excitation (and without undue phase shift) to a suitably high frequency, the higher the better.

It is instructive to rate the three best suited motors (servomotors, torque motors, and electromagnetic clutches) on each of these factors

(Table 1).

Table 1

Rating of Selected Azimuth Motors

Characteristic	Servomotor	Clutches	Torque motor
Proportionality of torque to excitation	Excellent	Excellent	Excellent
Independence of torque with speed	Inferior	Superior	Mean
Adaptability to direct coupling	Inferior	Superior	Superior
Accommodation of multi-revolutions	Excellent	Excellent	Excellent
Power amplification	Mean	Superior	Inferior
Reliability	Superior	Inferior	Superior
Ease of excitation	Superior	Superior	Mean
Ease of incorporation	Mean	Mean	Superior
Frequency response	Superior	Inferior	Superior

The two-phase servomotor is perhaps the most highly developed of the three. A great deal of effort has been spent during the last three decades developing a servomotor exhibiting a high ratio of torque to moment of inertia. A large ratio is essential in control systems requiring high angular acceleration, but not particularly so in the balloon applications, where the angular acceleration required is relatively modest.

The servomotor exhibits excellent linearity, but is inferior in regard to viscous and inertial reaction. Further compromise is encountered with backlash between the bull gear and the drive pinion, usually necessitating anti-backlash gearing. The use of spring-loaded gears to eliminate the backlash introduces additional friction, as well as an asymmetry favoring one direction.

The servomotor is without peer in regard to reliability and exhibits a superior frequency response. It is more difficult to incorporate than the torque motor, but less difficult to excite.

The torque motor was initially developed for use on inertial navigation platforms, and has since been used to advantage on a number of balloon-borne instruments. The linearity of this motor is excellent. It exhibits

a more viscous response than the clutches, but less than the servomotor. It can be directly coupled, requiring no bull gear or bearings of its own. If it incorporates a commutator, it can be used without limit stops, but only at a moderate speed (less than 600 rpm). The commutator introduces some friction and limits the life of the motor, but neither is serious. Being a current device, it is wasteful of power, providing less than unity power gain. Hence, it is more difficult to excite than either the servomotor or the clutches; with transistors, however, a satisfactory output stage may be readily built.

Dual overrunning contra-rotating clutches have been used to avoid the viscous and inertial reactions and to obviate the difficulties pertaining to backlash in the gear train. By modulating the power from a separate prime mover, rather than converting electrical to mechanical energy directly, the electromagnetic clutch has a power amplification of about 50. By the same token, because the pair of clutches must be constantly overdriven by the prime mover (usually an electric motor), they are wasteful of power.

A single prime mover is usually used to drive the clutches in opposite directions, with the output shafts of the clutch pair coupled in opposition

directly to the bull gear. Because the pair is continuously opposed, the backlash is automatically removed. The output torque of a pair of clutches is proportional to the excitation independently of the speed of the output shaft. It is the absence of viscous, as well as inertial, reaction which makes the clutch particularly desirable as an azimuth motor. However, as far as reliability is concerned, the clutches are inferior. The output torque for a given excitation tends to decrease gradually with use.

The frequency response of the clutches is also inferior. The break frequency is about 2 cps; the mid-frequency attenuation, about 10 db per decade; the low frequency asymptotic phase shift, about 12 deg; and the high frequency asymptotic phase shift, about 60 deg, Stuart (1).

From a comparison of the ratings of these three motors, it is clear that no single one has all of the characteristics desired. A compromise on several factors must be made in each instance; the choice depends on the specific stabilization system. The choice will certainly be influenced by the magnitude of the perturbations encountered by the system during the flight.

3. Perturbations

Translational acceleration of the balloon gondola will result in perturbing torques if the center of mass of the gondola is not coincident with the axes of the stabilization system. During launch and ascent, this perturbation may be particularly severe, but should be of little consequence at float. At float, the gravitational bias resulting from an improperly balanced gondola or instrument may be significant. The bias in the azimuth degree of freedom may be conveniently alleviated by placing an aircraft universal joint at the base of the suspension train.

An asymmetric gondola will also be subject to aerodynamic perturbations. The aerodynamic moment is proportional to the square of the velocity of the air relative to the gondola and, save for gusts during ascent, is negligible, except for the excitation of mechanical oscillations.

Internal motion of components, such as the movement of a plateholder or the shifting of film from a supply spool to the take-up spool, may introduce inertial and gravitational perturbations of consequence depending upon the relative mass of the component and the gondola. On occasion, it may be necessary to provide counter-motion; i.e., if an object is moved, another

object would be moved in the opposite direction to compensate for the reaction.

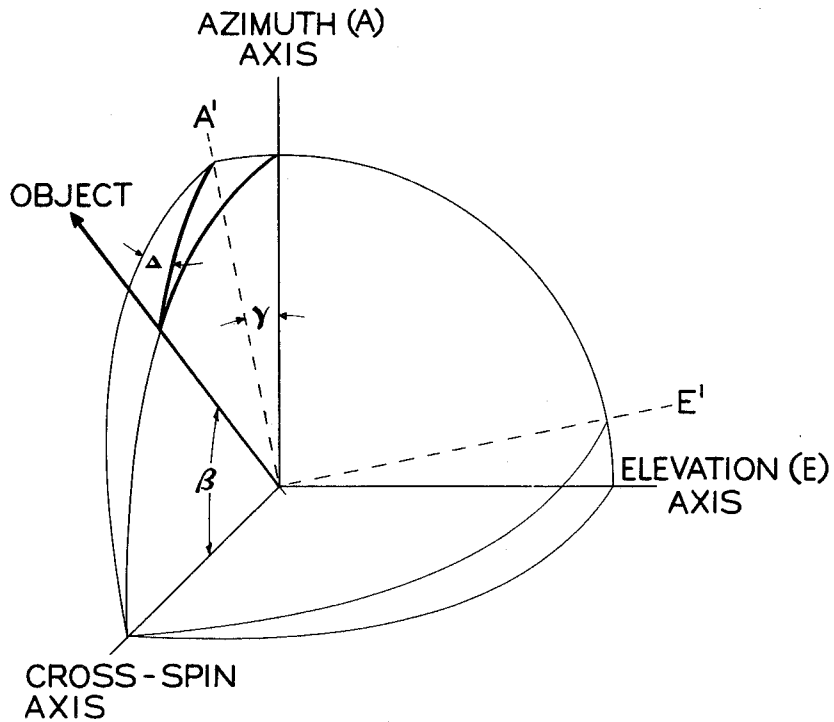
Friction in the gimbal bearings, both static and kinetic, constitutes a major perturbation. The static friction is the more troublesome, whereas the kinetic friction can be lumped with the viscous character of the motor. The friction noise, or stiction, characteristically contains frequencies higher than the bandpass of the stabilization system; hence, this noise must be attacked at the source by using floated bearings, by the use of dynamic bearings (in which an intermediate race is driven continually relative to both the outer and the inner race) or by the use of members that flex rather than slide. Because of the multi-revolution requirement, the flexure bearing is suitable only for gimbals other than azimuth (such as elevation) and then the design of the flexure member must be such that the suspension is virtually neutral.

Inertial and viscous reactions were mentioned earlier in connection with the discussion of the motor, but without explanation. The reaction wheel can be expected to be oscillating, whereas the stabilized instrument must not. Hence, if the motor is geared to the reaction wheel, the motor

must be accelerated in synchronism with the oscillation to avoid coupling the oscillation to the payload. The reflected inertia and the corresponding counter excitation of the motor is proportional to the square of the gear train ratio; consequently, the ratio should be selected to be the least possible consistent with the other considerations. This criterion is contrary to the usual practice of matching the reflected inertia to the load, as for maximum power transfer.

The viscous coupling is analogous to the inertial coupling and can likewise be lessened by the choice of the motor, by minimizing the gear train ratio, or by both.

The pendulous motion of the gondola introduces a gimbal restraint. Suppose the payload is to be oriented in azimuth relative to an object which has an elevation of β above the horizon, while the gondola is pendulously oscillating about the projection on the horizontal plane of the line of sight to the object (or cross-spin axis in Fig. 2) with a half amplitude of γ . Then the azimuth control system will be forced to cyclically drive the gondola about the azimuth axis with a half amplitude, Δ , given by the following expression:



$$\tan \Delta = \sin \gamma \tan \beta$$

$\beta = \text{ELEVATION ANGLE OF OBJECT}$

Fig. 2. Cross-spin forcing of the azimuth control system.

$$\Delta = \arctan (\sin \gamma \tan \beta)$$

for $\beta \approx 45^\circ$ and $\gamma < 1^\circ$, $\Delta \approx \gamma$.

Hence, the azimuth control system may suffer appreciable forcing due to the gimbal restraint. The restraint may be obviated by the use of at least three gimbals.

Virtually all that has been said about the azimuth control system also applies to the second and third control gimbals, except that in these gimbals, limited travel is required and the azimuth (or intermediate) gimbal, restrained by the gravitational field, constitutes sufficient reaction reference.

C. GIMBAL CONSIDERATIONS

The second gimbal to be added is logically an elevation gimbal since, to avoid inter-axis coupling, the second gimbal axis should be orthogonal to the first and, to point the instrument, the second axis should be transverse to the axis of the instrument. If, however, the azimuth error sensor is mounted on the instrument and senses the motion of the target relative to an axis transverse to the instrument, as is usually the case, the azimuthal sensor gain is proportional to the cosine of the elevation angle, β .

Moreover, if the longitudinal and transverse moments of inertia of the instrument (I_L and I_T , respectively) are unequal, the azimuthal moment of inertia, I_A , also varies with β .

Specifically,

$$I_A = I_T \cos^2 \beta + I_L \sin^2 \beta + I_G$$

where I_G is the moment of inertia of the azimuthal gimbal.

Hence, the loop-gain is proportional to

$$\cos \beta / (I_T \cos^2 \beta + I_L \sin^2 \beta + I_G)$$

and the azimuthal gain-margin may be minimum at an intermediate elevation angle requiring that the loop-gain be adjusted at the intermediate position to avoid oscillation of the control system during flight.

The third gimbal to be added may be either cross-elevation or cross-azimuth. If it is cross-elevation, the gain margin on two of the three gimbals, elevation and cross-elevation, will be constant; but, since the cross-elevation axis will not in general be orthogonal to the azimuth axis, inter-axis coupling will be obtained. On the other hand if the third gimbal is cross-azimuth, added between the azimuth and elevation gimbals, inter-axis coupling is obviated but the loop-gain on two of the three axes, azi-

imuth and cross-azimuth will not be constant. The choice between the two alternatives is not obvious. Thus, when the third gimbal is dictated (to avoid rotation of the image of the target, to obviate the gimbal restraint, or to accommodate offset guiding) a detailed study of the trade-offs should be made.

In some instances, redundant gimbals may be incorporated to avoid having one gimbal interfere with another, to maintain three independent degrees of freedom, or to utilize limited travel on one or more gimbals.

Moreover the gimbal system may be conventional, i.e., with the azimuth gimbal on the outside, or inside-out. The inside-out configuration is lighter, but affords less protection for the instrument. In addition, the counter-balances tend to be more complex and all testing must be done with the gondola suspended as during flight.

D. ERROR SENSORS

Any field sensing device can be used as the error sensor to excite the motor to control the gimbal. An example is a compass which senses the magnetic field. A compass is not a good choice for a precise control system, but may well serve as a coarse sensor to establish initial orientation.

The magnetic field also varies with geographic position as does the gravitational field. Hence, these fields are of primary value in conjunction with geophysical instruments and to control the third or fourth gimbal.

In addition, it is difficult to distinguish the gravitational field from the linear and angular accelerations of the gondola. In particular, a bubble level cannot be used to measure local vertical in the presence of pendulous motion, a point that has often been overlooked by balloonists.

Electromagnetic flux can also be used as a source of orientation signals. The emitted (or reflected) light from the sun, a planet, or a star can be detected by a photoelectric telescope to derive two control signals per celestial source. Though a third signal can, in principle, be derived from a source of finite angular size, which has surface features, such as the moon, it is expedient in general to use a second celestial source or another sensor, such as a gyroscope, to obtain the third signal.

A photoelectric guide telescope incorporates four elements to derive the control signals: An objective element, an image position analyzer, a field defining element, and the photo-element. The objective element collects the light from the celestial target and usually forms an image of the

target on the analyzer. The analyzer modulates the light energy as a function of the position of the image on the analyzer. The field element, by defining the field of view, rejects the stray light around the target enhancing the signal-to-noise ratio. Except in instances in which an extra-focal analyzer is used to increase the linear range of the telescope, it is advantageous to use a Fabry lens as the field element. The Fabry lens is used to form an image of the aperture of the objective element on the photo-element obviating local variations in the quantum efficiency of the photo-element. The photo-element may be a phototube, a photodiode, a photoconductor, a photomultiplier, or a photovoltaic device, depending on the intensity of the light and many other factors.

The "objective" element may range from a shadow casting aperture for a solar sensor to a large mirror for a stellar sensor with the error resolution ranging from a fraction of a degree to a millisecond of arc. The analyzer may be a fixed knife-edge, a prism, a split field polarizer, a mosaic of photodetectors or a rotating knife edge to name a few that have been used. Of these, the rotating knife-edge provides the greatest accuracy.

The accuracy of a guide-telescope is a function of the brightness and angular size of the image of the target, the efficiency of the telescope, the temperature and character of the photocathode, the time interval during which the signal is integrated, and the size and celestial position of the field of view of the telescope. The interplay of these factors can perhaps best be illustrated by considering a specific example. Let (1) θ and φ be the two position angles designating an element on the position analyzer (θ being measured about the optical axis and φ , transverse to the optical axis) where φ_0 is the radius of the field of view; (2) $A_0 T(\lambda, \theta, \varphi)$ and $A_0 B(\lambda, \theta, \varphi)$ be the rate at which photons of wave length λ arrive at the position analyzer from the target and from the background, respectively, where A_0 is the area of the objective; (3) $E(\lambda)$ be the efficiency of the telescope including the spectral character of the optics and of the photo-element; (4) $M(\theta, \varphi, t)$ be the transmission of the analyzer, a function not only of the position of the element on the analyzer, but also of time t ; (5) $D(t)$ be the function describing the action of the signal demodulator; and (6) η and A_p be the specific dark current and area of the photo-element,

respectively (the former, of course, depends upon the temperature at which the element is used). The signal from the telescope is then given by the expression:

$$dS = \int_0^{\varphi_0} \int_0^{2\pi} \int_{\lambda} \{ [T(\lambda, \theta, \varphi) + B(\lambda, \theta, \varphi)] [A_0 E(\lambda) M(\theta, \varphi, t) D(t) d\lambda d\theta d\varphi] + \eta A_p \} dt$$

For a rotating knife-edge and a synchronous demodulator $M(\theta, \varphi, t)$ and $D(t)$ are simple double-valued periodic functions: $M(\theta, \varphi, t) = 1$ for $\omega t - n\pi \leq \theta \leq \omega t - (n-1)\pi$ and $\varphi \leq \varphi_0$ and $M = 0$ for all other values of θ and φ , where n is an integer and ω is the rate of rotation of the knife-edge; and $D(t) = 1$ for $2n\pi \leq \omega t \leq 2\pi(n+1)$ and $D = -1$ for all other values of ωt . Thus, neglecting the background and dark current for the moment and considering a small angular error, X , where the image of the target is nearly bisected by the knife-edge, the target signal is sinusoidally modulated and full-wave rectified to give the following expression for the signal due to the target:

$$S_T = A_0 (TE)_{\lambda} N \left[\int_0^{\pi/\omega} \{ (4\delta X/\pi\delta^2) \sin \omega t + \frac{1}{2} \} dt \right]$$

$$- \int_{\pi/\omega}^{2\pi/\omega} \{ (4\delta X/\pi\delta^2) \sin \omega t + \frac{1}{2} \} dt]$$

$$= A_o (TE)_\lambda N [16X/\pi\delta\omega + \pi/2\omega - \pi/2\omega]$$

where $(TE)_\lambda \equiv \int_{\lambda} T(\lambda) E(\lambda) d\lambda$, δ is the angular diameter (relative to the objective) of the circle of illumination produced on the analyzer by the target (the circle is assumed here to be uniformly illuminated) and the signal has been integrated for N cycles of the analyzer (N must not be less than 20 for reasonably satisfactory demodulation). The latter two terms in the expression cancel in the absence of photon noise. With photon noise, the noise component may not cancel and the statistical limiting accuracy due to the photon noise in the signal from the target, ΔX_T , is given by the expression:

$$S_T = 0 = [16 A_o (TE)_\lambda N/\pi\delta\omega] \Delta X_T + \pi A_o (TE)_\lambda N/2\omega$$

$$+ [\pi A_o (TE)_\lambda N/2\omega]^{1/2} - \pi A_o (TE)_\lambda N/2\omega$$

$$+ [\pi A_o (TE)_\lambda N/2\omega]^{1/2}$$

or

$$\Delta X_T = [\pi^3 \delta^2 \omega / 128 A_o (TE)_\lambda N]^{1/2}$$

If $A_o (TE)_\lambda = 3.87 \times 10^5$ electrons sec^{-1} as for a target of magnitude $V = 0.00$ observed by a telescope with $A_o = 20 \text{ cm}^2$ ($\sim 3 \text{ in}^2$), an efficiency of 0.02 electrons photon^{-1} and an effective bandpass of 1,000 \AA (see Code 1962), and if $\delta = 12 \text{ sec of arc}$ and $\omega/N = 40\pi \text{ sec}^{-1}$ as for an integration time of (1/20) sec and a modulation frequency of 400 cps, the limiting accuracy due to photon noise in the target signal is 0.1 sec of arc. This limiting accuracy can be reduced by increasing the integration time (with attendant reduction of the speed of response of the control system), by increasing the area of the objective and by reducing the size of the image (with attendant increased difficulty in target acquisition). The size of the image cannot, however, be reduced to a value less than the larger of the diffraction limit of the objective or the angular diameter of the target.

If the background around the target produces a uniform gradient in the illumination of the analyzer, the signal due to the background is also sinusoidally modulated and rectified to give the following expression for the maximum signal from the background:

$$\begin{aligned}
S_B &= A_0 (BE)_\lambda N \left[\int_0^{\pi/\omega} \int_0^{\varphi_0} \{2GX(\varphi_0^2 - X^2)^{\frac{1}{2}} \sin \omega t \, dX + (\pi\varphi_0^2/2)\} dt \right. \\
&\quad \left. - \int_{\pi/\omega}^{2\pi/\omega} \int_0^{\varphi_0} \{2GX(\varphi_0^2 - X^2)^{\frac{1}{2}} \sin \omega t \, dX + (\pi\varphi_0^2/2)\} dt \right] \\
&= A_0 (BE)_\lambda N \left[8 \varphi_0^3 G/3\omega + \pi^2 \varphi_0^2/2\omega - \pi^2 \varphi_0^2/2\omega \right]
\end{aligned}$$

where $(BE)_\lambda \equiv \int_{\lambda} B(\lambda) E(\lambda) \, d\lambda$ and G is the fractional gradient in the background illumination. As before, the latter two terms in the expression cancel in the absence of photon noise. With photon noise the statistical limiting accuracy is given by the expression

$$\Delta X_B = [\pi^4 \varphi_0^2 A_0 (BE)_\lambda \delta^2 \omega / 128 A_0^2 (TE)_\lambda^2 N]^{\frac{1}{2}}$$

Assuming that $\varphi_0 = \tan^{-1}(0.1)$, $A_0 (BE)_\lambda = 1.04 \times 10^4$ electrons $\text{sec}^{-1} \text{deg}^{-2}$ as for the zodiacal light in the ecliptic some 80 deg from the sun, Allen (2), and the other parameters have the same values as before, the limiting accuracy due to the background photon noise will be 1.1 sec of arc. This error can be reduced by increasing the integration time and objective area, by reducing the field of view (with attendant increased difficulty in finding the target) and by observing a target in a less brightly illuminated portion of the sky.

The error due to the gradient in the background illumination is given by the expression

$$\epsilon = \pi \delta A_0 (BE)_\lambda \varphi_0^3 G / 6 A_0 (TE)_\lambda$$

If $A_0 (BE)_\lambda G = 2.32 \times 10^3$ electrons $\text{sec}^{-1} \text{deg}^{-3}$ again as for the zodiacal light in the ecliptic some 80 deg from the sun and the other parameters have the same values as before, the error is 0.7 sec of arc. This error can be reduced by observing a target in the region of the sky with a lesser gradient, by reducing the field of view, and by reducing the size of the image of the target.

If a Fabry lens is used, the minimum area of the photo-element is given by the expression

$$A_p = A_0 [2F \tan \varphi_0 / (1 - 2F \tan \varphi_0)]^2$$

where F is the focal ratio of the Fabry lens. Since $F \geq 1.5$, $A_p \geq 0.18 A_0$ (assuming $\varphi_0 = \tan^{-1} 0.1$ as before). The minimum signal due to the dark current is then given by the following expression

$$S_D = 0.18 A_0 \pi N [\pi/\omega - \pi/\omega]$$

As before, these two terms cancel in the absence of noise. The statistical limiting accuracy due to the noise in the dark current from a photo-element

of minimum size is then given by the expression

$$\Delta X_D = [0.18\pi^3 \eta A_o \delta^2 \omega / 64 A_o^2 (TE)_\lambda^2 N]^{1/2}$$

If $\eta = 4 \times 10^4$ electrons $\text{in.}^{-2} \text{ sec}^{-1}$ as for an S-11 photocathode used at room temperature and the other parameters have the same values as before, the limiting accuracy is 0.02 sec of arc. Though it would hardly be worthwhile in this example, this error can be reduced by cooling the photocathode, by reducing the size of the image, and by increasing the integration time and objective area.

It should be appreciated that in actual practice, the limiting accuracies, defined as in this example, can be approached only with difficulty. As a rule of thumb, it would be expedient to include a comfortable margin, say, an order of magnitude, between the design goal and the limiting accuracy due to each factor.

The photoelectric guide telescopes are used chiefly on orientation systems. For stabilization systems the floated rate integrating gyro is more appropriate, though equally expensive. This form of gyro, combining very low drift with high sensitivity (better than one deg per hr and 30 milli-

volts per milliradian, respectively), can be used for relatively long periods of time without assistance from an external reference. The low drift rate and the fact that the reference direction can be changed conveniently (as by remotely commanded torqueing) make this element particularly suited to multiple target missions.

Other gyroscopic elements may also be useful for providing coarse reference (such as the magnetically slaved free gyro) or for rate limiting (such as the spring restrained rate gyros).

E. EXAMPLES OF VARIOUS BALLOON-BORNE CONTROL SYSTEMS

There are as many different control systems for balloon-borne instruments as there are investigators that have seriously undertaken scientific measurements from balloons. This is true not only because of the individual preferences, but also because of the unique requirements of the various instruments. Most of the control systems have been designed to work automatically; of late, however, the tendency has been to invoke control by a radio system from the ground. Following the pattern of our previous discussions, I will first describe an automatic, single-axis stabilization system and progress to the more sophisticated multi-gimbaled and ground-commanded systems.

1. The Solar Azimuth Pointing Platform

Several single-axis orientation systems were built in 1959 for the Air Force Cambridge Research Laboratories by the Ball Brothers Research Corporation, Boulder, Colorado. These were intended to turn a variety of instruments mounted on the platform toward the sun with an accuracy of a fraction of a degree for several days. Special solar sensors, including one to activate the control system at sunrise and deactivate it at sunset, were incorporated. Two test flights were made in 1959, Dolder and Johnson (3).

A torque motor excited by a transistorized amplifier was used to drive the platform against the trapeze bar suspended below the platform. No torsional coupling to the balloon was used, windage on the trapeze bar and associated payload being deemed sufficient to prevent excessive speed of the torque motor. Universal joints on both ends of the azimuth shaft served to bound the gravitational bias on the control system. This system is shown in Fig. 3.

2. The Bi-axial Pointing Control

The first balloon-borne control system to be flown was developed at the

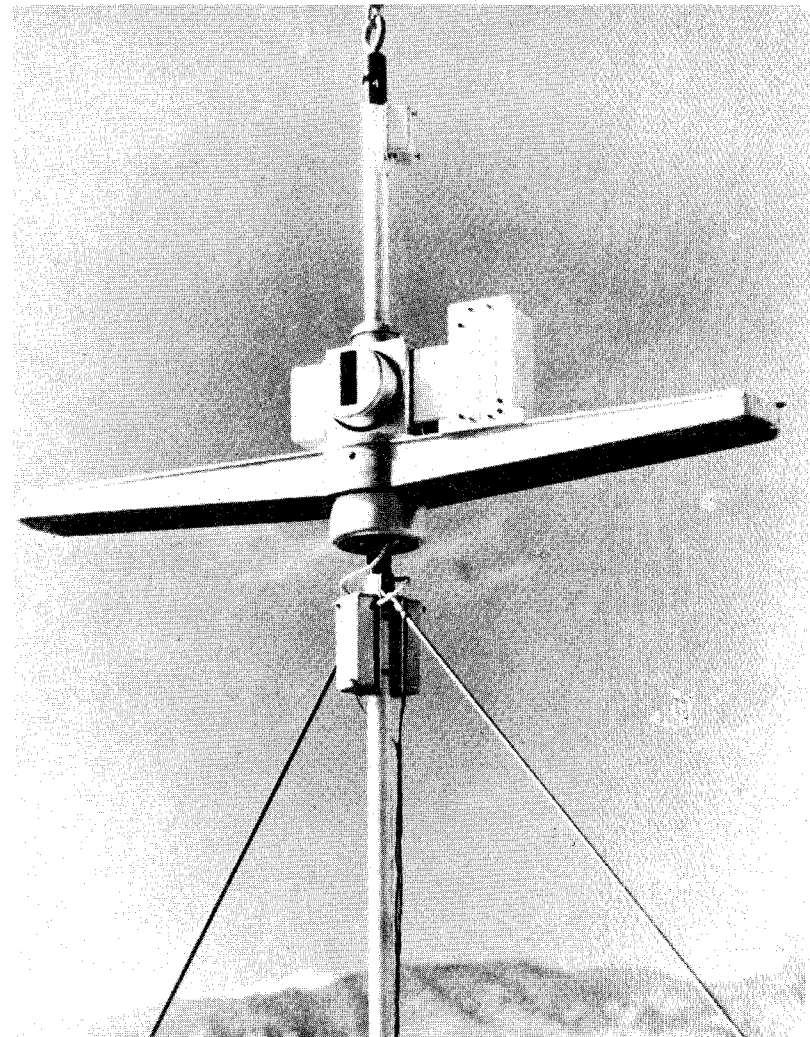


Fig. 3. The solar azimuth pointing platform (photograph courtesy of Ball Brothers Research Corp).

University of Denver, Edwards, et al. (4). It has since been improved and manufactured by the Hi-Altitude Instrument Company, Golden, Colorado.

Several designs are available, including lunar as well as solar versions.

One of these designs is shown in Fig. 4.

In general, counter-rotating clutches incorporating magnetically clamped disks have been used. Though these do not have the desired non-viscous character, they are much less wasteful of power than the magnetic particle clutches discussed earlier.

The accuracy is 0.1 deg or better in both azimuth and elevation. This system is relatively light in weight and low in cost. Several dozen flights have been made with it.

With the gondola suspended from the balloon by fine wires, complete freedom in azimuth has been obtained without undue occultation of the instrument and without use of the more complex reaction wheel system.

3. Stratoscope I

An explicit reaction wheel was first used on Stratoscope I in 1957.

Dr. Martin Schwarzschild of the Princeton University Observatory photographed the granulation of the solar photosphere with a very high resolu-

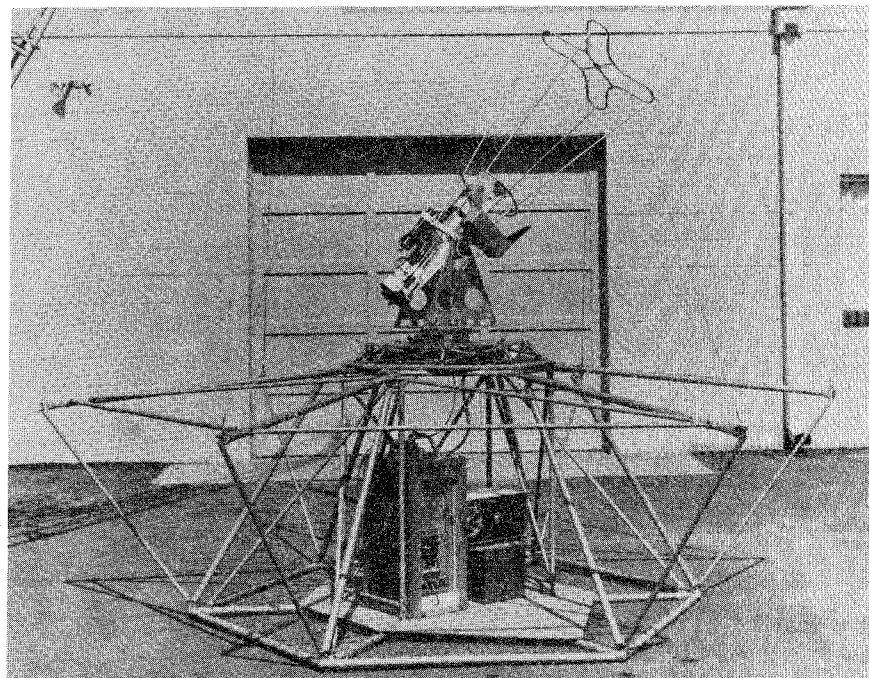


Fig. 4. The solar biaxial pointing control (model 3-4M) (photograph courtesy of Hi-Altitude Instrument Company, Inc.)

tion 12-in. telescope from above the stratosphere, Schwarzschild and Schwarzschild (5). Several sub-contractors were associated in the effort, including the University of Colorado, who developed the solar orientation system, borrowing heavily from the design of the earlier Aerobee-borne solar pointing control, Stacey, et al. (6). The azimuth and elevation drive units were constructed as rugged integral packages interconnected by welded tubular trusses; hence, remarkable longevity was obtained. Three flights were made in 1957, four in 1959, and many since as a part of "Coronascope." As originally built, both drive units used magnetic clutches. Inasmuch as the gears between the prime mover and the clutches generated undue high frequency vibrations of the telescope during flight, the clutches were replaced with geared servomotors prior to the second series of flights. In addition, a video-command link was incorporated in conjunction with an articulated guide-telescope assembly to permit selective observation of the solar photosphere, Danielson (7).

The accuracy obtained was a fraction of a minute of arc, though degradation of the accuracy was observed at higher elevation angles of the sun due to the gimbal restraint. Simple solar sensors, Nidey and Stacey (8),

were used with passive lead-lag networks for dampening.

4. Coronascope

The principal investigator with Coronascope has been Dr. Gordon Newkirk of the High-Altitude Observatory. Several flights have been made, Newkirk and Eddy (9) and Newkirk and Bohlen (10). Prior to a flight in 1964, a guide telescope sensing the limb of the sun was added to increase the absolute pointing accuracy to $\pm 1/3$ min of arc. Also, prior to a 1965 flight, the gear train in each of the servomotor drives was replaced with a steel-on-steel friction drive and the diameter of the objective of the guide telescope was increased from 1 cm to 5 cm to increase the accuracy to ± 5 sec of arc. At this accuracy, flexure of the instrument in the gravitational field of the earth became a problem. Thus, particular care was taken to assure that the guide telescope exhibited the same flexure as the coronagraph.

As the accuracy has increased, the difficulties with mechanical resonances have been compounded. In addition to the incorporation of an automatic gain control circuit to compensate for the loss of azimuth gain at high elevation angles of the sun, notched T filters in the compensation cir-

cuit and viscous dampeners on the servomotors have been tried with moderate success.

Coronascope is shown in Fig. 5.

5. StratoLab

With characteristic ingenuity Dr. John Strong of the Johns Hopkins University devised a novel optical system, Strong (11), to negate the majority of the motion of the manned StratoLab gondola. By use of his "monocentric" telescope design, using a servo-controlled secondary, the target image was stabilized to within ± 3 sec of arc in spite of motion of the telescope as large as ± 1 deg of arc. His 12-in. telescope was mounted on top of the gondola in an alt-azimuth mount (see Fig. 6). The elevation gimbal was controlled by an electrically powered Saginaw worm drive and the azimuth gimbal, by a variable-speed spur gearmotor. Both were operated by the observer located inside the gondola. The gondola was coupled to the balloon by a large diameter multipoint suspension system.

After many delays, due in main to failures of the balloons, the system was flown in 1959, Strong, et al. (12). Even with the monocentric telescope design, the gondola motion was sufficiently deleterious that the observer

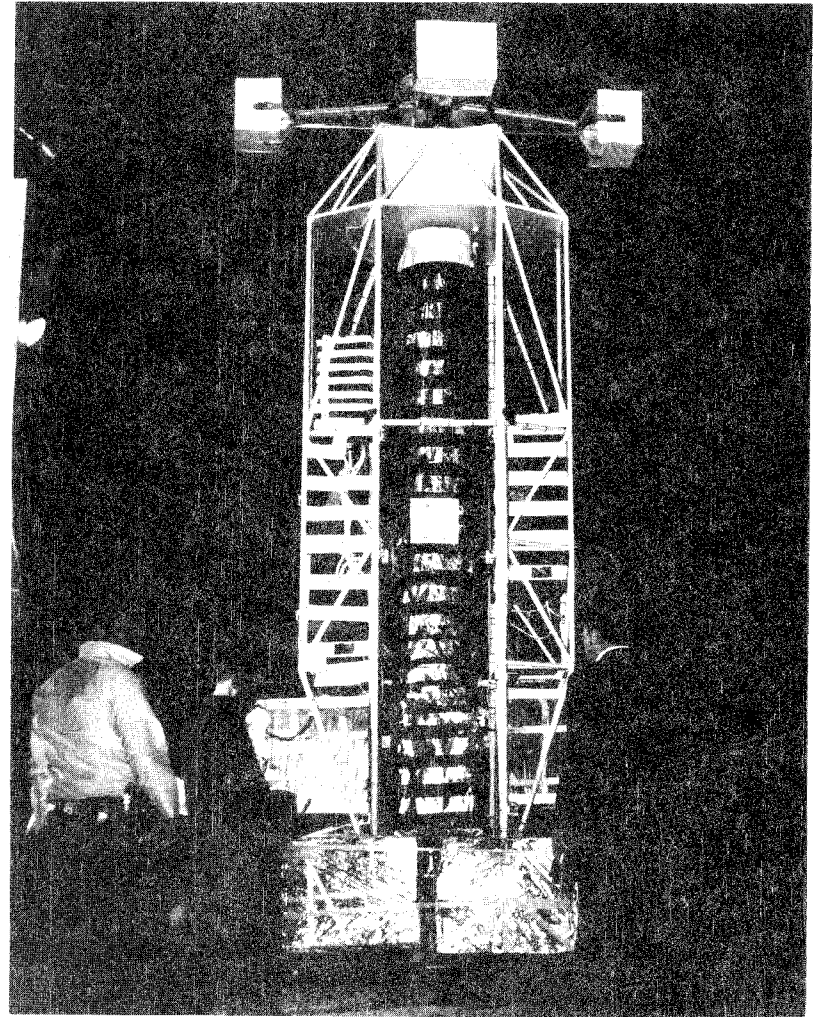


Fig. 5. Coronascope II at Palestine, Texas, prior to the flight of June 6, 1970.



Fig. 6. The Johns Hopkins University 12-in. telescope mounted on the StratoLab gondola (photograph courtesy of Librascope, Inc.).

was barely able to gather the scientific data.

6. BAL-AST

In the Johns Hopkins BAL-AST System the gondola has been replaced with a reaction wheel and the initial acquisition is accomplished automatically with a clock-driven, offset-guiding system, Strong and Bottema (13) and Strong (14), rather than by command. Torsional coupling of the reaction wheel to the balloon has been obtained by use of an off-axis mount for the telescope with a spectrometer serving as a counterbalance. Thus, the risers do not interfere with the light beam as on StratoLab nor is the heavy reaction wheel above the telescope as on Stratoscope. This system is shown in Fig. 7. Though the Saginaw elevation drive of the StratoLab design has been retained, the azimuth drive has been improved by the substitution of a torque motor for the gearmotor and solar sensors for the observer command. The accuracy of azimuth stabilization is now a few minutes of arc. The star-tracker has also been much improved. The current version, built by the Impro Corporation, Pasadena, California, uses an image dissector tube to obtain a large acquisition field of view with a small instantaneous field of view, the latter to achieve daytime tracking. In the acquisition mode the instantaneous

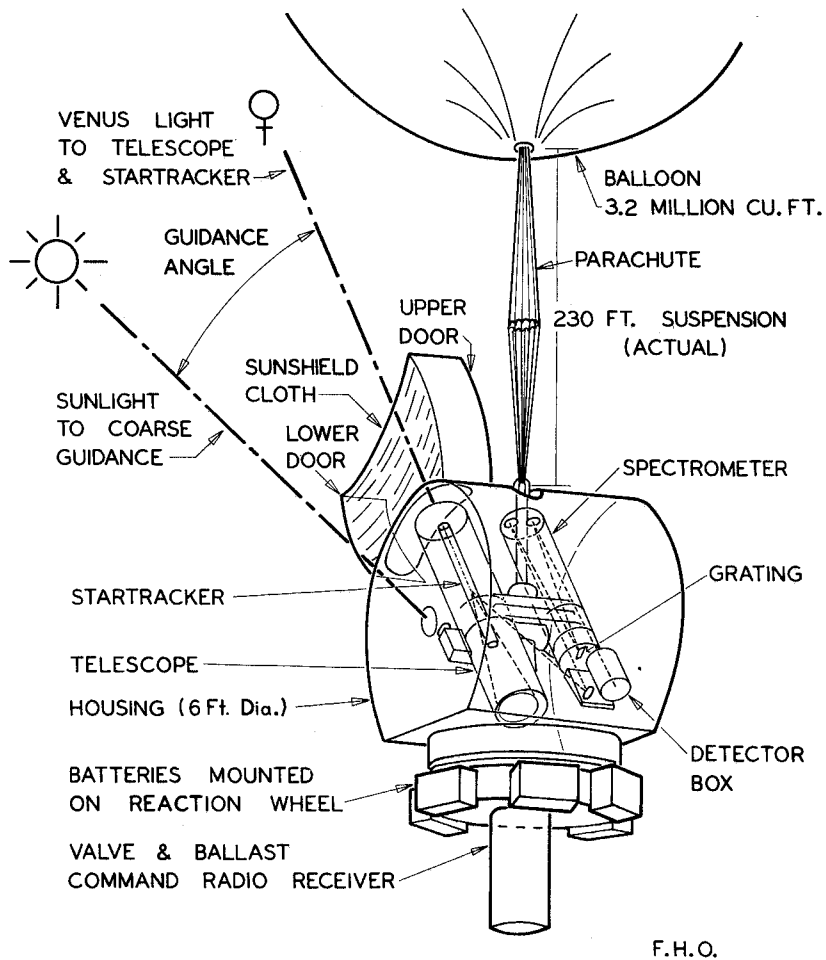


Fig. 7. The BAL-AST unmanned telescope system (line drawing courtesy of Johns Hopkins University).

field of view, some 10 min of arc in diameter, is electrically swept in a decaying spiral pattern from the circumference of the acquisition field of view, some 8 deg in diameter, to the center in about a second of time. After acquisition, the scan is switched to a cross pattern which generates the signals for the star-tracker actuators. These are two-phase 400 cps servomotors that tilt the star-tracker about elevation and cross-elevation axes. The gimballed tracker with a strap-down star-tracker is shown in a test fixture in Fig. 8. The test fixture simulates the azimuth and elevation drives of the primary telescope. The strap-down star-tracker in conjunction with a magnetometer can be used for nighttime acquisition of a bright target.

The BAL-AST System was flown twice in 1963: on the first flight the star-tracker malfunctioned because of high voltage arcing and on the second, the balloon burst at the tropopause, Strong (15). It was also flown successfully twice in 1964 and once in 1965.

7. Star Gazer

Under the guidance of Dr. J. Allen Hynek, then of the Smithsonian Astrophysical Observatory, the Massachusetts Institute of Technology built two balloon-borne control systems for a 12-in. telescope. The first of these,

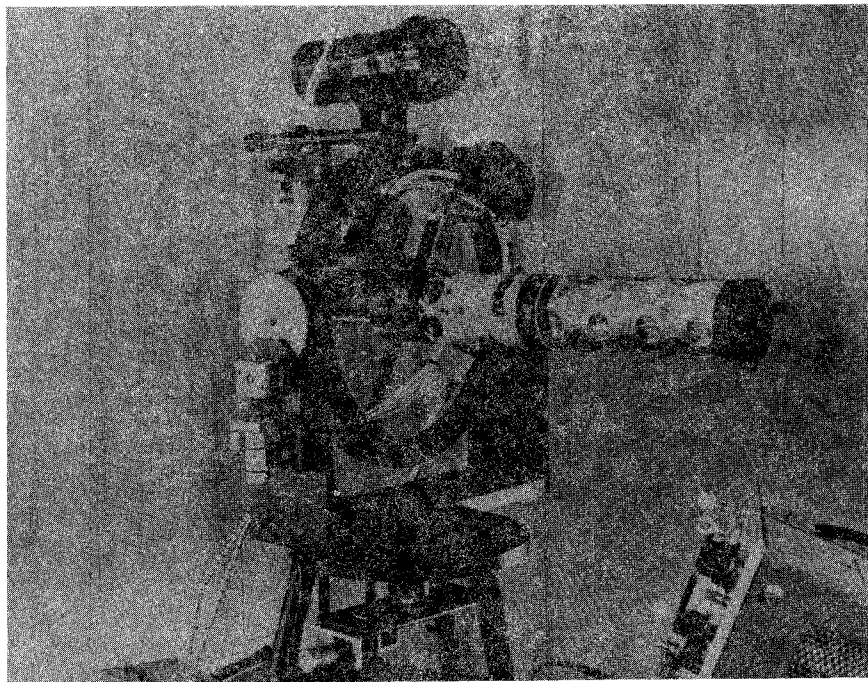


Fig. 8. The photoelectric tracker used on BAL-AST shown in a test fixture (photograph courtesy of Impro Corporation).

an unmanned tri-axial system, was wrecked at launch on its maiden flight. The second, a bi-axial system, was flown once in 1962, Markey, et al. (16). On this flight high-voltage arcing in the guide-telescope caused difficulties in tracking.

The manned system was superficially much like that used on StratoLab. Two gimbals were used, azimuth (or train) and elevation. Both were driven by torque motors. Though a guide telescope was used to trim the gyros, primary control of the telescope was vested in two floated rate integrating gyros. Initial acquisition was made by torquing the gyros from a console mounted inside the gondola.

The guide telescope used a 1P21 photomultiplier in conjunction with a rotating knife edge. The control accuracy obtained during pre-launch testing was ± 25 sec of arc with moderate gimbal motion and ± 2 min of arc with rolling and pitching motion of the order of 10 deg amplitude and 5 sec period. During flight, the stabilization accuracy was ± 30 sec of arc and some scientific data were obtained in spite of the tracker failure.

As on StratoLab, the Star Gazer gondola was coupled to the balloon with risers that occulted the telescope to a minor degree. The gondola served

as the azimuth reaction wheel. Initial acquisition of brighter objects was made by pre-setting the elevation angle of the telescope and then slewing the telescope in azimuth until the object to be observed appeared in the field of view of the telescope. Objects in the field of the telescope could be observed in the gondola by a mirror geared to the elevation gimbal which reflected light from the telescope through a window in the top of the gondola.

8. BBSP-200

Based on their earlier work on the Solar Azimuth Pointing Platform, the Ball Brothers Research Corporation has since developed a balloon-borne bi-axial solar pointer for the Air Force Cambridge Research Laboratories, Greeb (17). This system, shown in Fig. 9, an off-axis alt-azimuth system, has been built to point a 36-kg instrument up to 0.9 m in length to an accuracy of about ± 2 min of arc in both axes. Torque motors are used in both axes with fine and coarse solar sensors providing telemetry signals as well as control signals. Average power consumption is 17 watts from a 26-volt power source. The control system has a mass of 59 kg and is intended for use with a gondola having a mass of not more than 450 kg and a moment of inertia about the azimuth axis of not less than 70 kg m^2 .

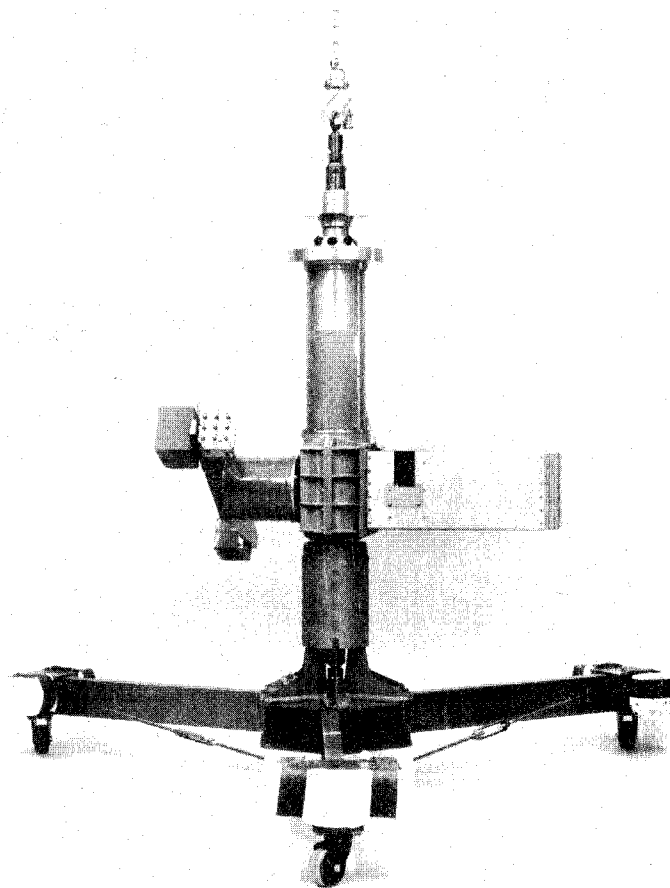


Fig. 9. The balloon-borne bi-axial solar pointer shown with simulated instrument and gondola (photograph courtesy of Ball Brothers Research Corporation).

The azimuth gimbal completely encloses the azimuth axle permitting electrical leads (as for load line severance) to be connected directly to the balloon from the gondola through the azimuth axle without the use of sliprings. Universal joints are used at the top and bottom of the azimuth axle to bound the gravitational bias.

9. Skytop

Dr. Alvin Howell's group at Tufts University has built and extensively used a unique orientation system for a 12-in. telescope. Three gimbals were used: coarse azimuth (initially controlled by a north-seeking gyro for target acquisition) and azimuth and elevation (controlled by a photoelectric guide telescope). The coarse azimuth motor was a simple gearmotor, whereas the azimuth and elevation gimbals each used a dual contra-rotating free gyroscope combining the reaction wheel and torquer in a single unit. The gyroscopes were constructed by Tufts expressly for the control system. At 12,000 rpm each gyro provided 3.0 SI units of angular momentum. The elevation and azimuth torques were derived by precessing the rotors; hence, the system had a relatively short operating time. This time was extended indefinitely, however, by appropriately off-setting a traveling weight

driven by an electric motor to trim the elevation gyroscope and by twisting the shroud lines of the parachute against the balloon with the coarse azimuth drive to trim the azimuth gyroscope.

The accuracy obtained was about ± 1 min of arc. Eleven flights were made. On the last, in March 1964, the system was expended in a freak fail.

10. Polariscope

Under the direction of Dr. T. Gehrels, a group at the University of Arizona has developed a 28-in. telescope system intended primarily for photoelectric photometry and polarization studies. A geared servomotor is used on each of the gimbals, azimuth, elevation, and cross-elevation. The latter two motors are controlled by floated rate integrating gyros. The gyros are torqued initially by signals from the command receiver for target acquisition and subsequently by signals from a photoelectric guide telescope for fine tracking. A television camera is used to identify the target. Multiple targets are to be observed on each flight. Control accuracy of ± 1 min of arc in elevation and cross-elevation was achieved during the maiden flight on May 27, 1966, from Palestine, Texas.

11. Stratoscope II

Since the completion of the 1959 series of flights with Stratoscope I, the balloon astronomy group at Princeton has developed the 36-in. (~ 0.91 m) Stratoscope II system. The telescope and gimbal system have been built by the Perkin-Elmer Corporation, Norwalk, Connecticut, and the television, telemetry, and ground command system by the RCA Corporation, Princeton, New Jersey. This system is by far the most sophisticated of all the systems yet built. It has seven control axes in an inside-out gimbal system: azimuth, fine cross-azimuth, fine elevation, coarse cross-azimuth, coarse elevation, ultrafine elevation, and ultrafine cross-elevation. Torque motors are used on three of the gimbals (azimuth, fine cross-azimuth, and fine elevation); spur-gear motors on two (coarse cross-azimuth and coarse elevation); and magnetic coil drivers on two (ultrafine elevation and ultrafine cross-elevation). The first five gimbals provide orientation of the telescope to an accuracy of about 1 sec of arc and the other two, stabilization of the image to about 0.03 sec of arc.

The azimuth gimbal is supported on a mercury bearing to bound the friction noise in the azimuth gimbal. As on Stratoscope I, a reaction wheel is

used to limit the speed of the azimuth motor.

Flexure bearings are used in the fine cross-azimuth and fine elevation gimbals. These bearings, designed to have virtually zero torsional constants while supporting the entire weight of the telescope, necessarily have very limited travel, ± 5 deg. Thus, as the target is tracked, these gimbals must be returned continually to the null position by driving the corresponding coarse gimbals. These gimbals are equipped with inertially compensated gearmotors. (The rotors in the motors rotate in directions opposing those of the gimbals and the gear train ratios are equal to the ratios of the moments of inertia of the gimbals to the moments of inertia of the rotors.) Thus, the telescope is scarcely disturbed during resetting of the flexure bearings. The coarse gimbals, as well as an elaborate set of counterbalances, are driven by ground command. The three fine gimbals are driven by signals derived from two stars in the field of the primary telescope. Inasmuch as the sensing axes are not collinear with the control axes, a rather complex coordinate transformation is required, Schlesinger (18).

The ultrafine control is accomplished by driving a spring-restrained wiggle lens transverse to the optical axis of the telescope by an orthogonal pair of magnetic coils. Signals for the coil drivers are derived from two pairs of photomultipliers mounted around the lens receiving light through the primary telescope from a guide star in the field (9th magnitude or brighter).

Guide stars in the field of view of the telescope for both the fine and ultrafine gimbals can be selected by ground commanded retrodividers driven on carriages by electric motors.

Six flights have been made. On the first two, the wiggle lens system was not used. The first flight, made early in 1963, was successful though fraught with harrowing malfunctions, Danielson, et al. (19). The second flight, made late in 1963, was somewhat more gratifying, Woolf, et al. (20). The third flight, made in July 1965, was unsuccessful because of excessive unbalance in the gimbal system caused by a malfunction in the cooling system for the primary mirror. The fourth flight in May 1966 was unsuccessful because of a malfunction in the latch mechanism for the tele-

scope occasioned by strain in the gondola due to unjetisoned ballast. Successful flights were made on 26 March 1970 and 9 September 1971. Figure 10 shows Stratoscope II at Huntsville, Alabama, prior to the flight of 9 September 1971.

F. CONCLUSIONS

It should be obvious to the reader that there is no pat solution to the problem of controlling a balloon-borne instrument. The solutions to the problem are legion. There is a wide variety of components, all far from ideal, from which to choose. Compromises must be made not only in the choice of the components, but also in the number and configuration of the gimbals. The compromises that best suit a given application must, of necessity, be determined by a careful evaluation of the trade-offs in the specific case.

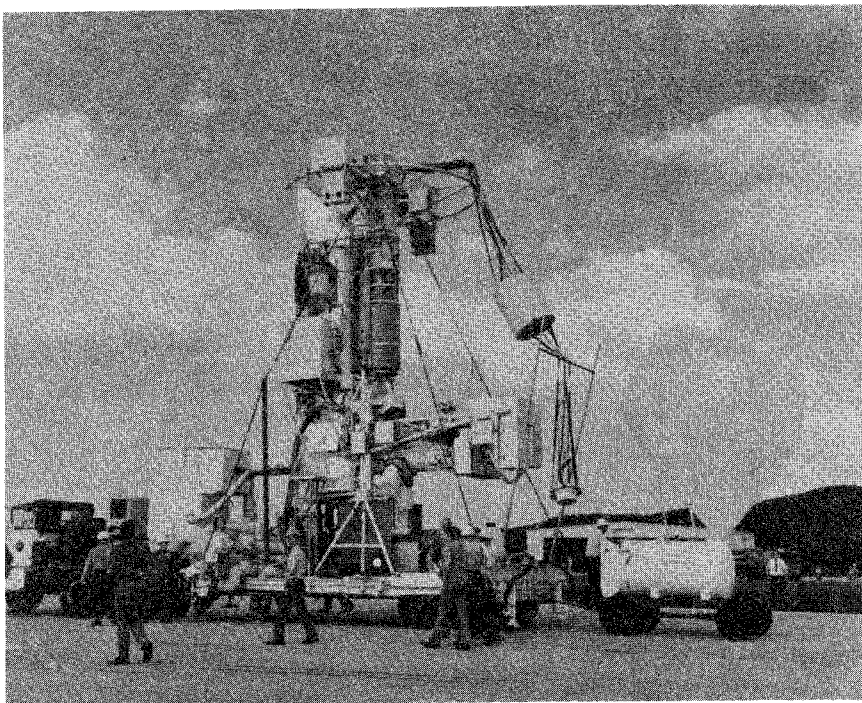


Fig. 10. Stratoscope II, the largest of the current balloon-borne telescopes, shown at Huntsville, Alabama, prior to the flight of 9 September, 1971.

REFERENCES

- (1) Stuart, F. E., 1965: Private communication.
- (2) Allen, C. W., 1955: Astrophysical Quantities, Athlone Press, London, p. 171
- (3) Dolder, F. P. and D. S. Johnson, 1960: Solar Azimuth Pointing Platform. Final Engineering Report by Ball Brothers Research Corp. under Contract No. AF19(604)-5543 from the Air Force Cambridge Research Center.
- (4) Edwards, Howard D., A. Goddard, Jr., M. Juza, T. Maher, F. Speck, 1956: Balloon-Borne Systems for Tracking the Sun, Review of Scientific Instruments, Vol. 27, No. 6, 381-385.
- (5) Schwarzschild, M. and B. Schwarzschild, 1959: Balloon Astronomy, Scientific American, Vol. 200, 52-59.
- (6) Stacey, D. S., G. A. Stith, R. A. Nidey, W. B. Pietenpol, 1954: Rocket-borne Servo Tracks the Sun, Electronics, Vol. 27, 149-151.
- (7) Danielson, R. E., 1961: The Structure of Sunspot Penumbrae I. Observations, J. Astrophys., Vol. 134, 275-288.
- (8) Nidey, R. A. and D. S. Stacey, 1956: Photoelectric Angular Error Sensors, Rev. Sci. Inst., Vol. 27, 216-218.
- (9) Newkirk, G. A., Jr. and J. A. Eddy, 1962: A Coronagraph Above the Atmosphere, Sky and Telescope, Vol. 24, 3-7.
- (10) Newkirk, G. A., Jr. and J. D. Bohlen, 1964: The First Flight of Corona-scope II, Sky and Telescope, Vol. 28, 1-4.

- (11) Strong, J. D., 1957: Interferometry for the Infrared, J. Opt. Soc. Am., Vol. 47, 354-357.
- (12) Strong, J. D. and associates, 1961: Astronomical Observations Using the ONR StratoLab. Technical report by the Johns Hopkins Univ. under Contract No. NONR 248(52) from the Office of Naval Research and Grants G-4880 and G-9262 from the National Science Foundation.
- (13) Strong, J. D. and M. Bottema, 1964: A Daytime Acquisition System for Balloon Astronomy, Mémoires Soc. R. Sc. Liège, Vol. 9, 528-532.
- (14) Strong, J. D., 1965: Infrared Astronomy by Balloon, Scientific American, Vol. 212, 28-37.
- (15) Strong, J. D., 1964: Balloon-Astronomy Program at the Johns Hopkins Univ. Final report by the Laboratory of Astrophysics and Physical Meteorology under Contract No. AF19(628)-202 from the Air Force Cambridge Research Laboratories.
- (16) Markey, W. R., J. B. Searcy, C. L. Lothrop, 1964: Final Report: Project Star Gazer, Experimental Astronomy Laboratory, Massachusetts Institute of Technology.
- (17) Greeb, M. E., 1965: Design and Development of the Balloon-Borne Solar Pointer BBSP-200. Final report by the Ball Brothers Research Corp. under Contract No. AF19(628)-4314 from the Air Force Cambridge Research Laboratories.
- (18) Schlesinger, E. R., 1963: Aiming a 3-Ton Telescope Hanging from a Balloon, Electronics, Vol. 36, 47-51.
- (19) Danielson, R. E., J. E. Gaustad, M. Schwarzschild, H. F. Weaver, N. J. Woolf, 1964: Mars Observations from Stratoscope II, Astronomical J., Vol. 69, 344-352.

- (20) Woolf, N. J., M. Schwarzschild, W. K. Rose, 1964: Infrared Spectra of Red-Giant Stars, J. Astrophys., Vol. 140, 833-852.

SECTION VIII.

SUPERPRESSURE BALLOONS

by

Vincent E. Lally

List of Symbols iii

List of Figures iv

List of Tables vi

A. INTRODUCTION 1

B. BALLOON SHAPES AND STRESSES 1

1. The Sphere 1

2. The Cylinder 3

3. The Tetroon 3

C. FREE LIFT AND SUPERTEMPERATURE STRESSES 4

1. Superpressure Due to Free Lift and Supertemperature 4

a. The free lift ratio 5

b. Superpressure 8

2. Stresses Produced by Superpressure 13

D. BALLOON LIFE 13

1. Diffusion 13

2. Leakage 19

E. BALLOON STABILITY 20

1. Diurnal Changes in Altitude Due to Supertemperature 20

2. Change in Altitude Resulting from Gas Loss 25

3. Creep 28

4. Altitude Variation Caused by Vertical Currents 30

F. NATURAL OSCILLATION PERIOD OF A SUPERPRESSURE BALLOON 32

G. BALLOON MATERIALS. 35

1. Desired Characteristics for Balloon Materials 35

2. Minimum Specifications for Balloon Materials 36

a. Modulus of elasticity 37

b. Strength of the balloon material 38

c. Transparency 38

d. Formability 40

e. Brittleness 41

f. Sealability 42

g. Permeability 43

REFERENCES 45

LIST OF SYMBOLS

<u>Symbol</u>	<u>Description</u>	<u>Dimensions</u>			
a	subscript indicating air		R	universal gas constant	$L^2 T^{-2} \theta^{-1}$
A	balloon surface area	L^2	s	subscript identifying values with level z_s	
A_D	balloon cross section	L^2	S	stress in psi	$ML^{-1} T^{-2}$
C_D	coefficient of drag		S*	Stress in Nm^{-2}	$ML^{-1} T^{-2}$
E	modulus of elasticity	$ML^{-1} T^{-2}$	t	thickness of balloon envelope in mils (0.001 in.)	L
f	free lift ratio		t*	thickness of balloon envelope in m	L
F	free lift	MLT^{-2}	T	temperature of enclosed gas or air. Subscripts identify the symbol with gas or air	θ
g	subscript indicating gas		T_o	temperature at z_o	θ
g	acceleration due to gravity	LT^{-2}	T_s	temperature at z_s	θ
G	mass of gross load (including mass of lifting gas)	M	V	volume of air or gas	L^3
l	cylinder length	L	V_i	nominal balloon volume	L^3
$\Delta l/l$	fractional change in length, strain		w	vertical wind velocity	LT^{-2}
m_f	mass of gas which provides free lift	M	$\Delta V/V$	fractional change in volume	
M_a	molecular weight of air	$M(M\text{-mol})^{-1}$	z_o	altitude at which balloon becomes fully inflated	L
M_g	molecular weight of lifting gas	$M(M\text{-mol})^{-1}$	z_s	altitude at which balloon is in static equilibrium, i.e., floating altitude	L
n	number of moles of gas		Δz	incremental change in altitude	L
p	pressure	$ML^{-1} T^{-2}$	<u>Greek letters</u>		
p'	partial pressure of gas	$ML^{-1} T^{-2}$	δ	permeability constant ($m^3 \text{ mil} / (m^2 \text{ mb day})$)	$L^3 TM^{-1}$
$P_{a,o}$	atmospheric pressure at z_o	$ML^{-1} T^{-2}$	Θ	supertemperature ($T_g - T_a$)	θ
$P_{a,s}$	atmospheric pressure at z_s	$ML^{-1} T^{-2}$	Π	superpressure in mb	$ML^{-1} T^{-2}$
$P_{g,s}$	gas pressure at z_s	$ML^{-1} T^{-2}$	Π_f	superpressure due to free lift	$ML^{-1} T^{-2}$
r	balloon radius	L	Π_T	superpressure due to supertemperature	$ML^{-1} T^{-2}$
			Π^*	superpressure in Nm^{-2}	$ML^{-1} T^{-2}$

$\rho_{a,o}$	air density at z_o
$\rho_{a,s}$	air density at z_s
$\rho_{\Delta z}$	air density at $z_s \pm \Delta z$
τ	period of oscillation, sec

ML^{-3}
 ML^{-3}
 ML^{-3}
 T

List of Figures

Fig. 1	Diffusion of helium through a Mylar balloon. Balloon life in days per mil thickness is based on the assumption that a 6% loss will cause failures	18
Fig. 2	Creep as a function of stress for 2-mil bilaminated Mylar at 20-25°C	29

List of Tables

Table 1	Permeability* (δ) of films to gases at 25°C	16
Table 2	Permeability of Mylar to helium	17
Table 3	Relative leakage rates of gases for three types of leaks . .	21
Table 4	Altitude displacement of superpressure balloons as a function of vertical wind	33

SUPERPRESSURE BALLOONS

A. INTRODUCTION

The superpressure balloon is a non-extensible balloon which is sealed to prevent gas release. By the time float level is reached, the free lift gas has been converted into superpressure, i.e., an internal pressure greater than the ambient atmospheric pressure. The variations in the radiation environment produce significant changes in the superpressure but, generally, negligible changes in the balloon volume. As long as the balloon is superpressured, it will continue to float at a constant-density level.

B. BALLOON SHAPES AND STRESSES

1. The Sphere

A balloon can be manufactured in almost any desired shape. When the balloon is superpressured, the stress distribution will vary over the surface, with the highest stresses in areas of maximum radii of curvature. Only a sphere provides uniform stress distribution over the entire surface. Intuitively, it would appear that the sphere is the most efficient shape for providing the largest enclosed volume at a given maximum stress and a

given mass of material. However, constructional difficulties arise which can offset much of the geometric efficiency of the sphere. In addition, the application may be one where factors other than efficiency are of prime importance. For example, the cylinder is a simple structure which is less affected by vertical currents at low altitudes; the tetraon (tetrahedral balloon) provides a compromise between ease of construction and design efficiency which makes it suitable for low-cost flight programs where maximum performance is not required.

The stress on the envelope of a spherical balloon is

$$S^* = \frac{r\Pi^*}{2t^*} \quad (1)$$

where S^* is stress (Nm^{-2}), r is balloon radius (m), Π^* is superpressure (Nm^{-2}), and t^* is film thickness (m).

Since American manufacturers usually express film characteristics in mils (10^{-3} in.) for film thickness and psi (lb/sq in.) for stress, it is necessary to deviate from the SI units of Eq. (1) and express the stress on a spherical balloon as

$$S = \frac{286 r\Pi}{t} \quad (1a)$$

where S is stress (psi), r is balloon radius (m), Π is superpressure (mb), and t is film thickness (mils).

2. The Cylinder

The cylinder is an inefficient shape for a superpressure balloon, but it is simple to manufacture and a cylindrical balloon which is long compared to its diameter provides a low drag relative to an equivalent sphere for motion normal to its circular cross section. It has application to low-altitude flight with light payloads. The circumferential stress on a long cylinder is

$$S^* = \frac{r\Pi^*}{t^*} \quad (2)$$

These factors are the same as those used in Eq. (1). The stress in manufacturers' units is

$$S = \frac{572 r\Pi}{t} \quad (2a)$$

where S is stress (psi), r is radius (m), Π is superpressure (mb) and t is film thickness (mils).

3. The Tetron

The tetron is made from a cylinder whose circumference is equal to

2.31 times the cylinder length. The ends are sealed with the straight seams orthogonal to each others. A complete description of the tetron is given by Grass (1). The basic advantage of the tetron is manufacturing simplicity. Stresses on the triangular faces are much higher than the stresses on a sphere. The tetron is not considered further in this section.

C. FREE LIFT AND SUPERTEMPERATURE STRESSES

1. Superpressure Due to Free Lift and Supertemperature

A superpressure balloon is normally launched as a sealed container. It can be lifted to the desired altitude by a tow balloon, or it can be inflated with an excess of lift gas over that required to give the desired superpressure. The excess is then expelled through a valve after the balloon has reached its float altitude. This second alternative is undesirable for long duration flights since it adds a complicated device which may cause leakage. Fortunately, a free lift (an excess of buoyancy over weight) of 8 to 10% is sufficient to carry small (1.5-2 m in diameter) spherical balloons aloft without assistance at an ascent rate of about 1.5 m per sec. When a balloon reaches float altitude, the free lift gas becomes the reservoir of excess gas which is drawn upon to sustain flight for extended periods.

As it rises, the gas fills out the balloon. A height is reached at which the balloon is completely inflated and begins to overpressure. The balloon continues to rise to a height about 1 km above the zero superpressure altitude, losing lift and gaining overpressure.

a. The free lift ratio. According to Archimedes' principle the buoyant force on a balloon system in the atmosphere is equal to the weight of the air displaced by the balloon system. The sum of the buoyant and gravitational forces acting on a balloon are then

$$F = gm_a - g(m_G + m_g) \quad (3)$$

where m_a is mass of the displaced air (kg), m_G is total mass of the balloon system (kg) exclusive of the mass of the lift gas, m_g is mass of the lift gas (kg), F is the resultant of the buoyant and gravitational forces (N) acting on the balloon, usually called free lift, and g is acceleration due to gravity ($m \text{ sec}^{-2}$).

Let the free lift ratio for superpressure balloons, f , be defined by Eq. (4)

$$f \equiv \frac{F'}{g(m_G' + m_{g,f})} \quad (4)$$

where F' is the free lift of a balloon system under the following conditions:

$V_{g,f} = V_{a,f}$, $p_{g,f} = p_{a,f}$, $T_{g,f} = T_{a,f}$, and m_G' is the total mass exclusive of the mass of the gas which the balloon system will have when it has achieved an equilibrium float condition. Note that this excludes any ballast dropped during ascent. The subscript f is used to denote the conditions associated with the definition of the free-lift ratio, and $m_{g,f}$ is mass (kg) of the lift gas, $V_{g,f}$ is volume (m^3) of the lift gas, $V_{a,f}$ is volume of the displaced air, $p_{g,f}$ is pressure (Nm^{-2}) of the lift gas, $p_{a,f}$ is pressure of the air, $T_{g,f}$ is temperature ($^{\circ}K$) of the lift gas, and $T_{a,f}$ is temperature of the ambient air.

If a superpressure balloon is inflated so the defining restrictions of the free lift-ratio are fulfilled and if the balloon remains a closed container from inflation until it reaches float altitude, z_s , and achieves hydrostatic equilibrium, the total mass of the system at float altitude, including the mass of the lift gas, will be $(m_G' + m_{g,f})$. Since a balloon in a state of hydrostatic equilibrium has no free lift, the mass of the system must then equal the mass of the displaced air at level z_s , i.e.,

$(m'_G + m_{g,f}) = m_{a,s}$. If this mass is substituted in Eq. (3), the free lift

upon completion of inflation is found to be

$$F' = gm_{a,f} - gm_{a,s} \quad (5)$$

Substituting into Eq. (4) yields

$$f = \frac{m_{a,f} - m_{a,s}}{m_{a,s}} \quad (6)$$

Now $m_{a,f} = n_{a,f}M_a$ and $m_{a,s} = n_{a,s}M_a$; $n_{a,f}$ is the number of moles of air having molecular weight M_a making up the gas mass $m_{a,f}$ and filling the volume $V_{a,f}$. For the conditions under which the free lift ratio was defined

$n_{a,f} = n_{g,f}$. Also in a closed balloon $n_{g,f} = n_{g,s}$. Therefore, Eq. (6) may also be written

$$f = \frac{n_{g,s} - n_{a,s}}{n_{a,s}} = \frac{\Delta n_s}{n_{a,s}} \quad (7)$$

where Δn is the difference in the number of moles of gas inside the balloon and the number of moles of air displaced by the balloon when it is in hydrostatic equilibrium with its environment. It was to achieve this convenient result, which will be used in the next sub-section, that f was defined as it was here.

In zero-pressure ballooning, a fractional free lift is defined by the equation

$$f' \equiv \frac{F'}{gm_G} \quad (8)$$

and by all of the conditions used in defining f , except that m_G in zero-pressure ballooning is normally the total mass of the balloon system at the time of launch, exclusive of the lift gas. Thus, m_G usually includes ballast and other masses which may be detached during ascent. It is convenient at times, however, to define f' by Eq. (9)

$$f' = \frac{F'}{gm_G} \quad (9)$$

and the conditions defining f . Then the following convenient relationship exists between f' and f :

$$f' = \frac{\frac{M_a}{M_g} f}{\left(\frac{M_a}{M_g} - 1\right) - f} \quad (10)$$

b. Superpressure. The superpressure of the balloon at z_s is defined as

$$p_{g,s} - p_{a,s} = \Pi_s \quad (11)$$

Then

$$\frac{\Pi_s}{P_{a,s}} = \frac{P_{g,s} - P_{a,s}}{P_{a,s}} \quad (12)$$

Both the air and the gas behave essentially like an ideal gas under all conditions in which a balloon might conceivably operate in the atmosphere.

One form of the gas law for an ideal gas is

$$pV = nRT \quad (13)$$

where R is the universal gas constant [$J (^\circ K)^{-1} (kg \cdot mol)^{-1}$]. The other variables (with appropriate subscripts) have already been introduced.

Remembering that $V_{a,s} = V_{g,s}$ and substituting from Eq. (13) in the right side of Eq. (12) and simplifying yields

$$\frac{\Pi_s}{P_{a,s}} = \frac{n_{g,s} T_{g,s} - n_{a,s} T_{a,s}}{n_{a,s} T_{a,s}} \quad (14)$$

Let the lift gas supertemperature be defined as follows:

$$\Theta_s = T_{g,s} - T_{a,s}$$

or

$$T_{g,s} = T_{a,s} + \Theta_s \quad (15)$$

Similarly, let

$$n_{g,s} = n_{a,s} + \Delta n_s \quad (16)$$

Substituting from Eqs. (16) and (17) into Eq. (14) permits one to write

$$\frac{\Pi_s}{P_{a,s}} = \frac{(n_{a,s} + \Delta n_s)(T_{a,s} + \Theta_s) - n_{a,s} T_{a,s}}{n_{a,s} T_{a,s}}$$

which may be simplified to

$$\frac{\Pi_s}{P_{a,s}} = \frac{T_{a,s} \Delta n_s + n_{a,s} \Theta_s + \Delta n_s \Theta_s}{n_{a,s} T_{a,s}}$$

or

$$\frac{\Pi_s}{P_{a,s}} = \frac{\Delta n_s}{n_{a,s}} + \frac{\Theta_s}{T_{a,s}} + \frac{\Delta n_s \Theta_s}{n_{a,s} T_{a,s}} \quad (17)$$

After substituting for $\Delta n_s/n_{a,s}$ from Eq. (7), one may state Eq. (17)

in any of the following equivalent forms:

$$\frac{\Pi_s}{P_{a,s}} = f + \frac{\Theta_s}{T_{a,s}} (1 + f) \quad (18)$$

$$\frac{\Pi_s}{P_{a,s}} = f \left(1 + \frac{\Theta_s}{T_{a,s}} \right) + \frac{\Theta_s}{T_{a,s}} \quad (18a)$$

$$\Pi_s = p_{a,s} \left[f + \frac{\Theta_s}{T_{a,s}} (1 + f) \right] \quad (18b)$$

If supertemperature is zero, it follows readily from Eq. (18) that

$$\left(\frac{\Pi_s}{p_{a,s}} \right)_{\Theta = 0} = f \quad (19)$$

That is, the fractional superpressure resulting from the free lift only is equal to the free-lift ratio. Also, if the free-lift ratio is zero, Eq.

(18a) shows clearly that

$$\left(\frac{\Pi_s}{p_{a,s}} \right)_{f = 0} = \frac{\Theta_s}{T_{a,s}} \quad (20)$$

There are then two causes of superpressure: the extra gas added to produce free lift and supertemperature.

If f and $\Theta_s/T_{a,s}$ are sufficiently small compared to 1, the two basic causes of superpressure act essentially independently and may be added to yield the total superpressure. Thus, when a free-lift ratio of 5% is added to a fractional supertemperature of 5% to yield a fractional superpressure of 10%, the error compared with the more nearly correct value of 10.25% is not large. It is not difficult to retain the more precise form, however, and for the stress analysis which follows, that is done.

Of course, the volume for any real balloon does not remain constant under conditions of superpressure and supertemperature, but we can ignore the change for stress analysis. Section VIII.E, in which balloon stability is analyzed, treats the change in volume and the consequent change in altitude resulting from changes of superpressure.

It should be clearly noted that changes in air temperature do not directly affect the superpressure. The balloon floats along a constant-density surface. If the air temperature decreases and that decrease is not accompanied by any change in supertemperature, the balloon floats at a lower pressure, but the superpressure does not change.

The supertemperature varies not only from night to day but also during the day as the radiation environment changes. The extremes for polyester (polyethylene terephthalate) balloons measured in flight range from -15% (tropics, 30 mb, nighttime) to +15% (tropics, 100 mb, daytime). The sunset effect on these balloons has been measured to be from 3 to 10%. A more detailed analysis of supertemperature variations is included in Section VIII.E.

2. Stresses Produced by Superpressure

The stress in a sphere caused by superpressure may be determined by Eqs. (1a) and (18b) as follows:

$$S \text{ (sphere)} = \frac{286 r p_{a,s}}{t} \left[f + (1 + f) \frac{p_s}{T_{a,s}} \right] \quad (21)$$

Similarly, the stress in a cylinder, obtained from Eqs. (2a) and (18b), is

$$S \text{ (cyl)} = \frac{572 r p_{a,s}}{t} \left[f + (1 + f) \frac{p_s}{T_{a,s}} \right] \quad (22)$$

D. BALLOON LIFE

1. Diffusion

For the purpose of this section, we shall distinguish between two methods of gas loss from a superpressure balloon: diffusion and leakage. We define diffusion as the gas loss through the wall of a balloon that is without defect in material or assembly.

Leakage is defined as gas loss through defects in the balloon, e.g., pinholes, defective seals, or abrasions, which permit a larger gas loss than through film without imperfection.

If a plastic film is used to contain a gas, the gas dissolves in the film and diffuses to the outside. The rate at which the gas passes through a barrier of area A varies directly with the permeability of the film to the gas, δ , and the difference in partial pressure, p' , of the gas across the film and inversely with the film thickness, t ,

$$\text{Rate of Loss} = \frac{\delta p' A}{t}$$

For a balloon, the percentage of loss of gas per day can be obtained by dividing the rate of loss by balloon volume

$$\% \text{ Volume Loss per Day} = \frac{100 \delta p' A}{tV} \quad (23)$$

For a spherical balloon, the percentage loss of gas per day is

$$\text{Sphere \% Volume Loss per Day} = \frac{300 \delta p'}{rt} \quad (24)$$

For a long cylindrical balloon, Eq. (23) becomes

$$\text{Cylinder \% Volume Loss per Day} = \frac{200 \delta p'}{rt} \quad (25)$$

The permeability of plastic films is a marked function of temperature. Permeability at low atmospheric temperatures (200°K) may be less than 1% of the value at high temperatures (300°K).

Table 1 shows permeability data for a number of gases and films at 25°C. Table 2 gives specific data on the permeability of the polyester Mylar to helium at various temperatures. The values used are derived from a number of sources. Since the permeability of Mylar to helium varies with the crystallinity of the Mylar film, the data available are not consistent. The data derived by Lally, Mellor, and Verstraete in extensive tests with inflated balloons indicate lower values than given by other sources with the exception of the General Mills, Inc. tests made in 1960. The values derived from balloon measurements are used in Table 2, since the combination of stressed film, bilamination, and taped areas appears to provide a lower overall diffusion than would be indicated from the other test results.

Figure 1 is a presentation of the expected life of balloons at several altitudes using permeability values from Table 2, Eqs. (24) and (25), and assuming 6% gas loss to failure.

Circled points on the 500-mb and 200-mb curves are the designs used in the initial GHOST (Global Horizontal Sounding Technique) test flights in the Southern Hemisphere. Life expectancies for balloons without defect are 120 days for a 2.5-mil balloon at 500 mb and over 600 days for a 1.5-mil

Table 1

Permeability* (δ) of Films to Gases at 25°C

Film	He	H ₂	O ₂	N ₂
Saran	7.5×10^{-7} (0.03)	2.5×10^{-7} (0.01)	1.2×10^{-8} (0.0005)	2.5×10^{-9} (0.0001)
Mylar	22×10^{-7} (0.088)	15×10^{-7} (0.06)	7.5×10^{-8} (0.003)	1.2×10^{-8} (0.0005)
Polyethylene	185×10^{-7} (0.74)	220×10^{-7} (0.86)	140×10^{-7} (0.55)	50×10^{-7} (0.20)

*First-line entries are δ in NCAR units; second-line entries are in "trade" units.

NCAR units: m³ mil/m² day mb.

Trade units: std cc cm 10⁻⁹/sec cm² cm Hg.

To convert Trade units to NCAR units multiply by 2.5×10^{-5} .

Table 2

Permeability of Mylar to Helium

T_{O_2} °K	NCAR units ($\times 10^7$)	Trade units	T_{O_2} °K	NCAR units ($\times 10^7$)	Trade units
300	22	0.090	250	3.8	0.015
295	19	0.076	245	3.0	0.012
290	16	0.067	240	2.4	0.0095
285	14	0.056	235	1.9	0.0076
280	12	0.047	230	1.5	0.0058
275	10	0.039	225	1.1	0.0044
270	8.2	0.033	220	0.87	0.0035
265	6.8	0.027	215	0.65	0.0026
260	5.5	0.022	210	0.50	0.0020
255	4.7	0.019			

See Table 1 for definition of units.

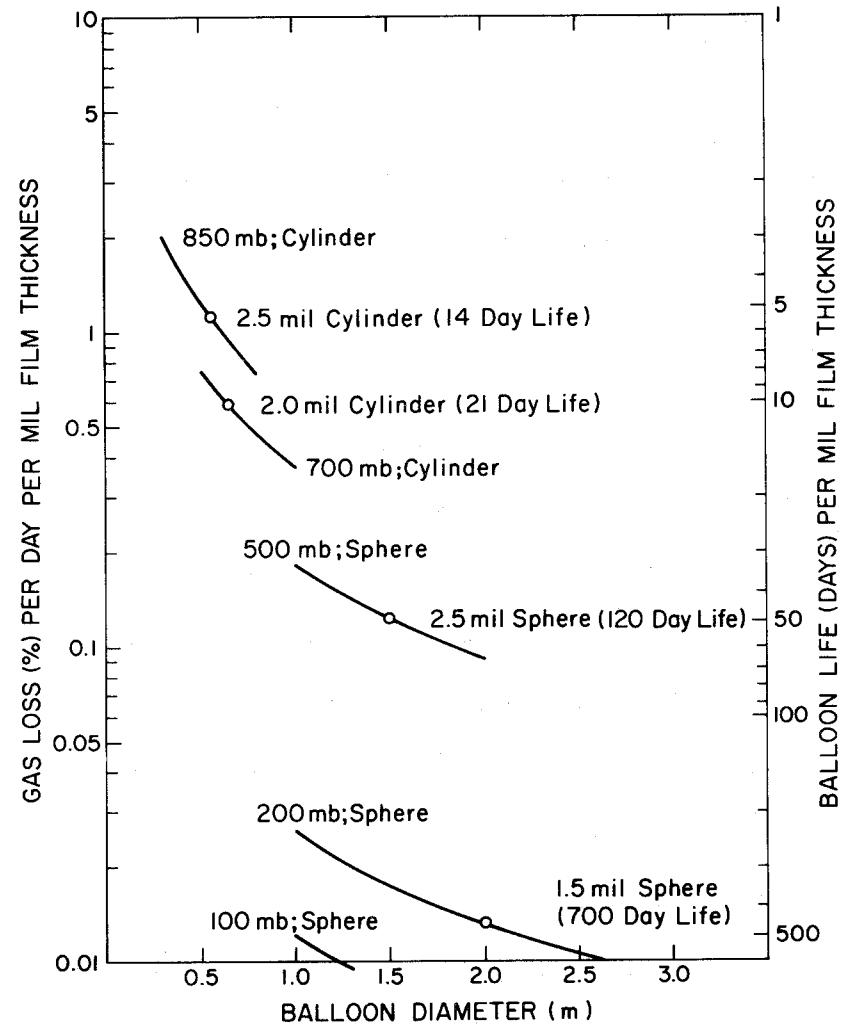


Fig. 1. Diffusion of helium through a Mylar balloon. Balloon life in days per mil thickness is based on the assumption that a 6% loss will cause failure.

balloon at 200 mb. Above 200 mb life expectancy is limited by ultra-violet deterioration, not by diffusion.

2. Leakage

Diffusion of gas through a plastic film is a function of the partial pressure of the gas contained within the film. Leakage is a function of the differential pressure, which we call either overpressure or superpressure, Π . For "small" leaks the flow through the orifice is molecular flow, and it is directly proportional to the overpressure. For "large" leaks the flow is turbulent, and flow rate is proportional to the square root of overpressure. Molecular flow occurs when the mean free path of the gas molecules exceeds the largest dimension of the hole. The mean free path for helium in the lower atmosphere is at all times less than $1 \mu\text{m}$. A $1\text{-}\mu\text{m}$ hole will not produce a significant gas loss in a superpressure balloon in a period of a year. It is possible for a plastic film to have many hundreds of microholes, which would cause serious gas loss, but the technique of laminating together two sheets of film should eliminate such imperfections. The bilaminated film can develop holes during manufacture, packing, and testing, but the number of holes that are introduced should be few.

The characteristics of leaks in plastic films have not yet been investigated. Extensive data have been taken on leaks through vacuum systems. Table 3 is derived in part from a paper by Nerken (2). Data are provided on hydrogen, helium, air, and Freon 12, since they all may be used to test for leaks or as lifting gases for flight.

Empirical tests must be made to determine the nature of hole defects in balloons. Measurements as a function of pressure and for dissimilar gases such as air and helium will permit analysis of the holes which are introduced in balloons.

E. BALLOON STABILITY

1. Diurnal Changes in Altitude Due to Superpressure

The volume of a superpressure balloon does not remain constant. As the internal pressure increases, the stress on the film increases; consequently, volume increases. The expression relating stress, S , to strain, $\Delta l/l$, is the modulus of elasticity, E ,

$$E \equiv \frac{S}{\frac{\Delta l}{l}} \quad (26)$$

For a spherical balloon, the fractional volume change (for small changes) is three times the fractional change in linear dimension

Table 3

Relative Leakage Rates of Gases for Three Types of Leaks

Gas	Viscosity at 25°C (Air = 1)	Molecular Weight (Air = 1)	Flow Rate Relative to Air		
			Leak: Flow: Turbulent	Very Large Large Viscous	Small Molecular
Hydrogen	0.48	0.070	3.9	2.7	3.6
Helium	1.08	0.139	2.7	1.4	2.7
Air	1.00	1.00	1.00	1.00	1.00
Freon 12	0.67	4.20	0.49	0.97	0.62

$$\frac{\Delta V}{V} = \frac{3\Delta \ell}{\ell} \quad (27)$$

(For a long cylinder balloon, the fractional volume change is twice the fractional linear change.) The volume change for a spherical balloon can be expressed by combining Eqs. (26) and (27)

$$\frac{\Delta V}{V} = \frac{3S}{E} \quad (28)$$

Since we are concerned with changes in volume resulting from changes in stress rather than the total volume change from no stress, the equation can be written as

$$\frac{\Delta(\Delta V)}{V} = \frac{3\Delta S}{E} \quad (28a)$$

By combining Eqs. (1a) and (18b) and substituting in Eq. (28a), we can derive an expression for the volume change resulting from a change in super-temperature

$$\frac{\Delta(\Delta V)}{V} = \frac{3}{E} \times \frac{286r}{t} \times \frac{P_{a,s} \Delta \Theta (1+f)}{T_{a,s}} \quad (29)$$

If we assume a spherical balloon design which produces 10,000 psi stress at 25% superpressure, we can obtain a rough estimate of the variation of volume with supertemperature change. Thus, for the typical design we are

considering here, an increase of 1% in the superpressure produces a 400-psi increase in stress. We can express this mathematically as

$$\Delta S \approx 400 \times 100 \frac{\Delta(\Delta P)}{P} \approx 400 \times 100 \frac{\Delta\Theta}{T} \quad (30)$$

Substituting this value into Eq. (28a)

$$\frac{\Delta(\Delta V)}{V} \approx \frac{3 \times 4 \times 10^4}{E} \frac{\Delta\Theta}{T} \quad (31)$$

Using the value of 1.2×10^6 psi for the biaxial modulus of elasticity of Mylar, we have

$$\frac{\Delta(\Delta V)}{V} \approx \frac{1.2 \times 10^5}{1.2 \times 10^6} \frac{\Delta\Theta}{T} = 0.10 \frac{\Delta\Theta}{T} \quad (32)$$

A fractional change in volume will produce an equal but negative fractional change in density at the level at which the balloon floats. A 1% change in density causes a change of approximately $0.3T$ m in altitude, where T is the air temperature in $^{\circ}\text{K}$.

The altitude variation resulting from a supertemperature change on a spherical balloon can be roughly written as

$$\Delta z \approx -0.3 T \frac{\Delta\rho}{\rho} 100 \approx 0.3 T \frac{\Delta(\Delta V)}{V} 100 = 30 T \frac{\Delta(\Delta V)}{V} \quad (33)$$

Substituting from Eq. (32), we obtain

$$\Delta z \approx 30T \times 0.10 \frac{\Delta\Theta}{T} \quad (34)$$

Thus

$$\Delta z \approx 3.0 \Delta\Theta \quad (35)$$

To summarize, Eq. (29) provides a precise expression for the volume change resulting from a change in supertemperature. From the volume change, the altitude change can be computed using Eq. (33). However, as a sweeping approximation, we can state that a 1.0C° change in supertemperature will produce a 3.0 m change in altitude for a typical spherical balloon designed to reach a stress of 10,000 psi with 25% superpressure.

The average day-night supertemperature difference observed on GHOST test flights has been 10C° in the troposphere and 15C° in the stratosphere. The variation in density altitude between day and night is 30 to 50 m.

The variation in temperature during the day may be as much or greater for a Mylar balloon than the day-night effect. Maximum differences observed to date have been 20C° .

The diurnal changes in altitude resulting from supertemperature may be summarized as:

- a. A predictable day-night altitude change of 30 to 50 m.
- b. An unpredictable variation in the radiation environment on the order of ± 60 m.

2. Change in Altitude Resulting from Gas Loss

During inflation more gas is placed in a superpressure balloon than is required to provide buoyant equilibrium. The mass of this gas is

$$m_f = \frac{f V_i \rho_{a,s}}{\left(\frac{M_a}{M_g} - 1\right)} \quad (36)$$

where m_f = mass(kg) of gas which provides free lift.

During the life of the balloon this excess gas diffuses through the balloon. If we assume the balloon descends at the time that all free-lift gas has been lost, the change in balloon system mass during its life is

$$\Delta m_B = m_f \quad (37)$$

The percentage mass loss is

$$\frac{100 \Delta m_B}{m_B} = \frac{100 f V_i \rho_{a,s}}{V_i \rho_{a,s} \left(\frac{M_a}{M_g} - 1\right)} = \frac{100f}{\left(\frac{M_a}{M_g} - 1\right)} \quad (38)$$

For a helium-filled balloon having 10% free lift, the percentage mass loss is

$$\% \text{ Mass Loss} = \frac{100f}{\left(\frac{M_a}{M_g} - 1\right)} \approx \frac{100 \times 0.1}{\left(\frac{28.96}{4} - 1\right)} \approx 1.6\%$$

This 1.6% mass loss would cause the balloon to float (near the end of its useful life) at a level 1.6% lower in density than its original float level. However, the overpressure resulting from free lift decreases as the free lift gas is lost. This decrease in overpressure causes a reduction in volume which tends to balance out the mass loss.

We can design the balloon so that the mass loss exactly balances the loss in free lift superpressure. Basically, the technique requires that the fractional volume loss caused by a percentage reduction in overpressure equals the fractional mass loss produced by the same percentage loss in free lift. Combining Eq. (28) with (1a) and (19) and assuming $\theta_s = 0$, we get

$$\frac{\Delta V}{V} = \frac{3S}{E} = \frac{3}{E} \frac{286}{t} r f p_{a,s}$$

Equation (38) established that

$$\frac{\Delta m_B}{m_B} = \frac{f}{\left(\frac{M_a}{M_g} - 1\right)}$$

As discussed above, we want

$$\frac{\Delta m_B}{m_B} = \frac{\Delta V}{V}$$

Thus

$$\frac{858 r f p_{a,s}}{Et} = \frac{f}{\left(\frac{M_a}{M_g} - 1\right)} \quad (39)$$

For a helium-filled sphere in air

$$\frac{r}{t} = \frac{E}{858 \times p_{a,s} \left(\frac{M_a}{M_g} - 1\right)}$$

If we assume $E = 1.2 \times 10^6$, then

$$\frac{r}{t} = \frac{224}{p_{a,s}}$$

For example, the value of r/t needed to provide an exact balance of gas loss against volume decrease for a balloon floating at 200 mb would be $224/200$, or 1.12. A balloon constructed of 2.5-mil polyester having a radius of 2.8 m will meet this criterion; it will not vary in density altitude as a result of gas loss during the useful life of the balloon.

3. Creep

All plastic materials exhibit some degree of creep under stress.

Creep is the permanent elongation of the plastic film when stressed. The relationship between stress and strain is defined by the modulus of elasticity, which is a function of temperature. The non-elastic creep is a function of stress and temperature as well, but it also depends strongly on the prior history of the material.

Plastics exhibit markedly different characteristics above and below the "glass-transition" temperature. At higher temperatures they have "plastic" characteristics, and at lower temperatures the plastic behaves more like a glass. The "glass-transition" temperature for polyesters is about 350°K --thus, the polyesters are "glassy" substances at all temperatures of importance in ballooning.

Tests have been conducted at room temperature on bilaminated Mylar strips to measure creep. Results are shown in Fig. 2. Creep will be less at the lower temperatures which balloons experience at float altitude.

Tentative results for Mylar can be summarized as:

- a. Creep under moderate stress reduces with time, becoming negligible

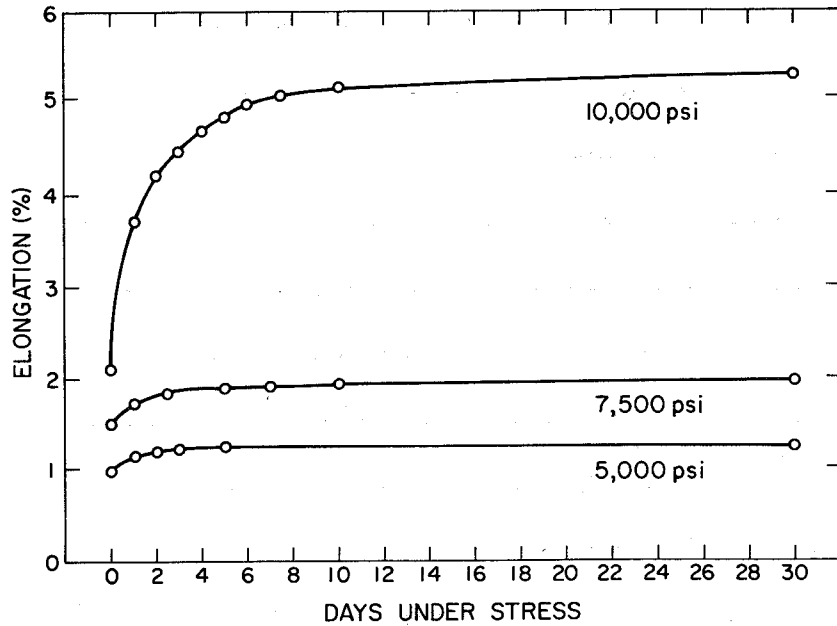


Fig. 2. Creep as a function of stress for 2-mil bilaminated Mylar at

20-25°C.

after two weeks. The time constant is about two days at room temperature for stresses between 5000 psi and 10,000 psi. Total creep is 3.3% at 10,000 psi and 0.25% at 5000 psi.

- b. A balloon may be prestressed to minimize creep. This procedure will also serve to relieve stresses produced in balloon manufacture.
- c. If a balloon is prestressed at 10,000 psi for one week at room temperature and is not stressed at float altitude beyond 7500 psi, creep will be negligible for one year.

The polyester material Cellanar has a higher modulus and a shorter time constant than Mylar.

4. Altitude Variation Caused by Vertical Currents

The drag on a balloon in a vertical current is

$$\text{Drag} = \frac{1}{2} C_D A_D \rho_{a,s} w^2 \quad (40)$$

where C_D is the coefficient of drag (dimensionless), A_D is the balloon cross section (m^2), and w is the vertical wind velocity (m/sec).

The restoring force can be expressed as

$$\text{Restoring Force} = V_i (\rho_{a,s} - \rho_{\Delta z}) g \quad (41)$$

where

$$\rho_{\Delta z} = \text{air density at } (z_s \pm \Delta z)$$

We can use the excellent approximation, derived from Eq. (33), that the

density difference at height Δz above or below the buoyant density $\rho_{a,s}$ is

$$\Delta\rho = \frac{\Delta z \rho_{a,s}}{30T_{a,s}}$$

Thus, we find that

$$\Delta\rho = (\rho_{a,s} - \rho_{\Delta z}) = \frac{\Delta z \rho_{a,s}}{30T_{a,s}} \quad (42)$$

Substituting Eq. (42) into (41) and equating Restoring Force to Drag,

we have

$$\frac{C_D A_D \rho_{a,s} w^2}{2} = \frac{V_i \Delta z \rho_{a,s} g}{30 T_{a,s}} \quad (43)$$

Solving for Δz , we obtain

$$\Delta z = \frac{15 C_D T_{a,s} w^2 A_D}{g V_i} \quad (44)$$

For a sphere this equation reduces to

$$\Delta z = \frac{1.15 C_D T_{a,s} w^2}{r} \quad (45)$$

For a cylinder balloon Eq. (44) becomes

$$\Delta z = \frac{1.53 C_D T_{a,s} w^2}{\ell} \quad (46)$$

where ℓ is cylinder length (m).

Table 4 provides data on the deviation from the buoyant altitude as a function of vertical wind velocity for typical spheres and cylinders.

The vertical excursion is negligible for vertical winds less than 0.5 m/sec (1 knot) but is quite serious for vertical winds greater than 1 m/sec (2 knots).

At the lower altitudes where convection may be severe, the balloon will move with the updrafts and downdrafts. The response of a cylinder-type superpressure balloon will, in general, be about 30% of the response of an equivalent spherical superpressure balloon. Because of this, the cylinder design is recommended for all altitudes up to 700 mb. Above 700 mb the cylinder design becomes too large and unwieldy.

F. NATURAL OSCILLATION PERIOD OF A SUPERPRESSURE BALLOON

If a superpressure balloon is displaced from its buoyant altitude, z_s , there is a restoring force which is proportional to the balloon volume and

Table 4

Altitude Displacement of Superpressure Balloons as a Function of Vertical Wind

Vertical Wind Speed (m/sec)	Δz (m)			
	700 mb sphere $C_D = 0.5$ $T_{a,s} = 269^\circ K$ $r = 0.75$ m	700 mb cylinder $C_D = 1.0$ $T_{a,s} = 269^\circ K$ $r = 0.3$ m $l = 7.0$ m	500 mb sphere $C_D = 0.5$ $T_{a,s} = 252^\circ K$ $r = 0.75$ m	200 mb sphere $C_D = 0.5$ $T_{a,s} = 217^\circ K$ $r = 1.0$ m
0.1	2	0.6	2	1.3
0.5	51	15	48	31
1.0	206	59	193	125
2.0	824	237	--	--
5.0	5150	1480	--	--

The value for $T_{a,s}$ is taken from the U.S. Standard Atmosphere, 1962.

and the density difference

$$G \frac{d^2 z}{dt^2} = -gV(\rho_{a,s} - \rho_a)$$

or

$$\frac{d^2 z}{dt^2} = -g \frac{(\rho_{a,s} - \rho_a)}{\rho_{a,s}}$$

Over a short vertical distance $d\rho/dz = \text{const}$, approximately, and

$$\frac{\rho_{a,s} - \rho_a}{\rho_{a,s}} = z \left[\frac{\left(p \frac{\partial T}{\partial z} - T \frac{\partial p}{\partial z} \right)}{pT} \right]_{a,s} = z \times \text{const}$$

$$\frac{d^2 z}{dt^2} = z \left[\frac{-g \left(\frac{\partial T}{\partial z} - \frac{T}{p} \frac{\partial p}{\partial z} \right)}{T} \right]_{a,s} = z \times \text{const}$$

This is the familiar equation for simple harmonic motion with the period

of oscillation, τ , equal to

$$\tau = 2\pi \sqrt{\left[\frac{T}{g \left(\frac{\partial T}{\partial z} - \frac{T}{p} \frac{\partial p}{\partial z} \right)} \right]_{a,s}}$$

or

$$\tau \approx 2 \sqrt{\left[\frac{T}{\frac{\partial T}{\partial z} + 3.42 \times 10^{-2}} \right]_{a,s}}$$

since

$$\frac{\partial P}{\partial z} = -3.48 \times 10^{-3} \frac{P}{T} \text{ g}$$

For an isothermal region ($\partial T/\partial z = 0$), the expression for period of oscillation simplifies to

$$\tau \approx 11\sqrt{T}$$

The natural oscillation period for a superpressure balloon in an isothermal atmosphere varies from 150 sec at -75°C to 180 sec at 0°C . An adiabatic lapse rate ($\partial T/\partial z = -10^{-2} \text{ }^{\circ}\text{C/m}$) will increase the period by approximately 15%.

G. BALLOON MATERIALS

1. Desired Characteristics for Balloon Materials

The ideal plastic film for balloon material would have a very large modulus of elasticity (10^7 psi) and would be transparent to the entire spectrum of radiation from infrared to ultraviolet. Such a material would not need to have a high ultimate strength since it would never be highly stressed. The material, in addition, should be easily formed so that a balloon could be manufactured out of few spherical sections. It should be readily sealed with seal strengths as high as the strength of the basic material. The

material should be impermeable to helium, oxygen, nitrogen, and water vapor.

In addition, it should be plastic in characteristics at room temperature so that it can be readily packed without damage. At the floating altitude of the balloon, the material could well have glassy characteristics so that it would shatter harmlessly into many pieces if struck by an aircraft.

No existing material comes close to meeting the above ideal specifications for balloon material. However, at least one material does come sufficiently close to providing an acceptable film for fabricating superpressure balloons. This is the polyester, polyethylene terephthalate.

2. Minimum Specifications for Balloon Materials

Most plastic materials fall short of the minimum specifications in some characteristic so that they cannot provide a long-lived, stable vehicle. The minimum specifications to permit flight are interrelated; for example, a material that has great strength but at the same time is highly absorbent of solar radiation, will be over-stressed by the pressure buildup caused by supertemperature. A weaker film may survive if it is sufficiently transparent.

The minimum specifications for a balloon material are indicated below.

a. Modulus of elasticity. A balloon with an insufficient modulus of elasticity will stretch as it superpressures, and if the volume increase due to stretch is sufficient to move the balloon to a higher altitude so that the stress is maintained, the balloon will continue to ascend until it bursts in the same fashion as neoprene and rubber balloons. The minimum modulus of elasticity for an acceptable balloon depends on the free lift introduced in the balloon and on the supertemperature which the balloon will realize at floating altitude. All materials with a modulus of elasticity less than 300,000 psi are unacceptable for superpressure use. This minimum modulus applies at the temperature at altitude. There are a number of film materials with too low a modulus at room temperature or at lower floating altitudes which are acceptable at higher altitudes where the film temperature is -30°C or lower. A realistic minimum modulus of elasticity for a plastic film with average transparency is 500,000 psi. The higher the modulus, the more stably the balloon will fly and the smaller the variation in altitude will be between night and day. A balloon with a modulus of 1.2×10^6 psi will undergo an altitude change of 30 to 50 m between day and

night. A modulus of 10^7 psi would reduce the altitude change between night and day to an insignificant amount.

b. Strength of the balloon material. The modulus of elasticity is a much more important characteristic of superpressure balloon film than the ultimate film strength, provided that the balloon is never stressed beyond its elastic limit. A lighter material may have a lower ultimate strength than a more dense material since a thicker film may be used. For example, polypropylene, which is 40% less dense than polyester, can provide a stronger material for balloon design than polyester, even though its strength is somewhat lower. An acceptable film strength for superpressure design depends on the altitude at which the balloon is to be flown, the payload weight, and the density of the film. As a general rule, the film material should be capable of stresses at 10,000 psi in its elastic range, while maintaining an acceptable modulus of elasticity.

c. Transparency. Balloon films vary markedly in their transparency to solar and infrared radiation. The ideal material should be transparent to the entire spectrum of solar and earth radiation. There are a number of plastic materials which approach this ideal. Polyethylene approaches this

ideal most closely, absorbing less than 6% of the radiation through the solar infrared band. Polyester film approaches polyethylene transparencies at the shorter solar wavelengths but is almost black in the infrared. As a result, a balloon made of this material shows larger variations in internal heating resulting from night and day differences.

It may be thought that a metalized balloon would have ideal characteristics. However, the best values of reflectivity achieved with metalized balloons have been on the order of 94% for solar radiation and 99% for infrared radiation. The infrared emissivity of the metalized film is 1%, so the balloon film becomes very hot in the region where the solar input is maximum. The metalized balloon, in general, is inferior in radiation characteristics to a clear balloon at the higher altitudes. For lower altitude flights, a metalized balloon will provide improved characteristics over a thick-walled semi-transparent balloon. In this case conduction is relied on as the basic mechanism to remove the excess heat caused by the inefficiency as an infrared emitter. Note that a metal capped balloon will increase both daytime and nighttime gas temperatures. A cap covering the upper third of the balloon has been used with dramatic success on flights near the tropopause

to overcome frost formation caused by nighttime cooling. The cap raises nighttime temperatures by 10 to 15 C° over those experienced by a clear balloon.

No complete theory has been worked out which will permit the theoretical computation of the amount of supertemperature experienced by a balloon in flight. The effectiveness of conduction and convection in removing heat from a balloon at float altitude can only be estimated at present. The simplest procedure for obtaining these data is to conduct flight tests of instrumented balloons with measurements of air temperature and lifting gas temperature.

d. Formability. The ideal film material should be readily formed into a hemisphere, or at least a large sector of a sphere, by heat or pressure in a die or mold. Most plastics can be so formed. However, the more readily they can be formed in this fashion the poorer they usually are as a balloon material in their characteristics. Polyethylene terephthalate film, a polyester, which is the best of the available balloon materials, is cast in sheet form and is drawn into other forms with great difficulty. As a result, the balloons used presently for superpressure flight are made from a large

number of flat gores to simulate a spherical form. The tapes required for sealing constitute a large increase in weight and an additional chance for leakage.

The optimum characteristic for formability would be a material which can be blown into a spherical shape in the same manner as rubber balloons or glass bulbs. However, attempts to blow large glass forms have failed because of the brittleness of the material. All the plastics which have been successfully formed by blowing have been completely inadequate in strength and modulus. It is not inconceivable that thin-walled glass balls may be blown using helium instead of air to provide a lighter-than-air sphere. We would need then only to enclose thousands of these balls in a netting to provide our superpressure balloon system.

e. Brittleness. Since superpressure balloons will be flown in the air lanes, it is essential that the material either shatter or tear easily. Actually, a number of plastic materials have a sufficiently high "glass transition temperature" that they exhibit glass-like characteristics at flight temperatures. Polyethylene terephthalate is one of these materials with a glass transition temperature above 70°C . Although this polyester

has ten times the strength of polyethylene, it has only about one-tenth the tear resistance. Since the balloon is never shocked during testing, inflation, launch, or flight there is no need for a high tear resistance. The glassy materials present a major problem in one general area, however. That is in the manufacture, packing, and unpacking. Creases in the material can cause holes. A double fold, one transverse to the other, in a glassy material makes a sharp point which can tear another section of the film or cause a pinhole at the point of intersection. To prevent such defects, the balloon can be assembled at the launch site. In most cases this does not provide a practical solution. The simplest procedure, which experience has proved to be adequate, is to ensure that the balloon is handled, packed and unpacked, and inflated at temperatures high enough ($\sim 30^{\circ}\text{C}$) so that the material has more plastic characteristics.

f. Sealability. Many of the plastics, such as polyethylene, can be heat-sealed using simple techniques. These seals have over 90% of the strength of the plastic material. Polyesters and polypropylene are materials which are not easily sealed to themselves and require tape seals with a thermal-setting adhesive. The tape seals are more difficult and costly, but they do provide additional strength to the balloon.

The desired specification for any seal is that it be gas tight and provide equivalent strength to the basic material.

g. Permeability. Most plastics serve as quite adequate gas barriers for a one-day flight. There are, however, few existing plastic materials which have low enough permeability to permit extended flight using either helium or hydrogen. It is not sufficient that the balloon film have low permeability for just helium and hydrogen. Its permeability for nitrogen, oxygen, and water vapor must also be sufficiently low so that there is no appreciable transfer of air into the balloon during flight. All of the materials under consideration as a balloon film do exhibit a much lower permeability to nitrogen and oxygen than to hydrogen and helium.

For extended flights of superpressure balloons, helium is the only acceptable filling gas. Too heavy a penalty is paid in balloon design if ammonia is used. Hydrogen is unacceptable because of the fire hazard not only during testing but after the balloon has finally returned to the ground at the end of its flight, when it becomes even a greater hazard with the possibility of an air mix with the hydrogen.

The best of the existing plastics for helium retention is cellophane. Saran ranks second, and polyethylene terephthalate ranks third. There are few other plastics with acceptable helium permeability characteristics at room temperature. However, because of the very great dependence of diffusion upon temperature among plastics, polyethylene and polypropylene become acceptable at temperatures below -30°C . As a rule of thumb, for long-duration flights, the rate of diffusion through a plastic material should be less than 10^{-6} m^3 mil per m^2 per day per mb (4×10^{-11} std cc cm per sec per cm^2 per cm Hg pressure).

REFERENCES

- (1) Grass, L. A., 1962: Superpressure Balloon for Constant Level Flight, AFCRL Res. Report 62-824 (Aug.), 9, 11, 12.
- (2) Nerkin, A., 1956: Experiments on Flows of Gases Through Leaks, 1956 National Symposium on Vacuum Technology Transactions, pp 4.
- (3) Lichfield, E. W. and R. W. Frykman, 1966: Ghost Balloons Riding the Skies Will Report the World's Weather, Electronics (Nov. 28), 98-106.
- (4) Anonymous, 1966: The Feasibility of a Global Observation and Analysis Experiment, Report of the Panel on International Meteorological Cooperation to the Committee on Atmospheric Sciences, NAS-NRC Publ. No. 1290, pp. 172.

SECTION IX

List of Figures

HOT-AIR BALLOONING

by

Richard G. McCarty

List of Figures ii

A. INTRODUCTION 1

B. PRINCIPLES OF HOT-AIR BALLOONING 2

C. FLIGHT LIMITATIONS AND CONTROLS 26

D. APPLICATIONS 32

Fig. 1. Specific lift vs balloon internal temperature for a balloon operating at sea level in the U.S. Standard Atmosphere, 1962 4

Fig. 2. Specific lift vs ambient temperature for a balloon with an internal gas temperature of 250°F (121°C) operating at a pressure of one atmosphere 5

Fig. 3. Specific lift vs altitude for a balloon operating in the U.S. Standard Atmosphere, 1962, with: 1) an average internal temperature of 250°F (121°C) and 2) an average internal temperature which differs by 191°F (88°C) from ambient air temperature 6

Fig. 4. Gas and skin temperatures as observed in static model hot-air experiment. Average temperature differential is 140°F 8

Fig. 5. Propane burner for a hot-air balloon 10

Fig. 6. Typical hot-air balloon in flight 14

Fig. 7. Payload vs diameter for hot-air balloons at sea level. It is assumed that the envelope is a metalized material, that specialized, light-weight, stainless steel tanks are used, that rigging weight is 10% of envelope weight, that fuel is carried for one-hour flight at sea level, and that 50% of the fuel will be used for ascent. Internal temperature is 250°F (121°C) 16

Fig. 8. Payload vs diameter for hot-air balloons at 20,000 ft (6 km) See caption of Fig. 7 for balloon system characteristics 17

Fig. 9	Volume vs diameter for a natural-shape hot-air balloon	18
Fig. 10	Surface area vs diameter for a natural-shape hot-air balloon .	19
Fig. 11	Gross lift vs diameter for balloon flying in the <u>Standard Atmosphere</u> with an internal temperature of 250°F	20
Fig. 12	Envelope weight vs diameter for a balloon made of available fabric. In flight at sea level in the <u>U.S. Standard Atmosphere, 1962</u> , with an internal temperature of 250°F; the safety factor is three	21
Fig. 13	Propane vapor pressure vs temperature	23
Fig. 14	Basic envelope heat loss rate vs gross lift for a balloon at sea level having an internal temperature of 250°F	25
Fig. 15	Double propane burner	28
Fig. 16	Inflated balloon with maneuvering vent open	29
Fig. 17	View of the removable cap inside a hot-air balloon	31
Fig. 18	An unmanned hot-air balloon. The white sectors are scoops which help the falling balloon to inflate before the burner is turned on. This balloon was dropped from an airplane . . .	36
Fig. 19	Performance of a hovering hot-air balloon.	38

HOT-AIR BALLOONING

A. INTRODUCTION

Any gas less dense than the surrounding atmosphere is capable of providing the buoyance necessary for balloon operation. Since the density of air diminishes as its temperature rises, "hot air" can serve as a pseudo lighter-than-air medium. Hot air, the most readily available buoyant gas, was used by the brothers Joseph and Etienne Montgolfier in the first demonstration of a balloon in November of 1782.

Within a year of the invention of the balloon, man was ready to fly. On the 21st of November, 1783, the Marquis d'Arlandes and Pilatre de Rozier went aloft carrying a fire with them. For fuel they used chopped wood and straw, which had the effect of quickly generating large amounts of heat and dense smoke, which was thought to be beneficial. At one point the upsurgent flame nearly turned their "globe volant" into a fiery bier.

Although hydrogen soon replaced hot air as the dominant balloon gas, hot-air balloons have been constructed and flown occasionally since 1782.

One well-publicized hot-air balloon was "L'Aigle" constructed by Eugene Godard in France in 1864. L'Aigle carried an 18-ft diameter stove which generated enough heat to fill its half-million-cu-ft envelope with hot air. A gondola, which surrounded the furnace, provided ample room for more than a half-dozen passengers. A series of flights was conducted between 1864 and 1866.

The current resurgence of interest in hot-air ballooning arises out of improvements in operational capabilities that are a direct result of gains in material technology. New materials mixed with modern engineering techniques are generally credited for the development of the modern hot-air balloon.

B. PRINCIPLES OF HOT-AIR BALLOONING

The average density of the heated air and associated combustion products is fairly close to the density of air alone at the equivalent temperatures. The air within the balloon is not uniformly hot, but is a circulating turbulent mixture of air in which strong temperature gradients exist. Nevertheless, considerable insight can be achieved by assuming an average value. It is possible, for example, to derive a specific lift as a func-

tion of temperature for any specified altitude. Whenever balloon performance is computed at a given altitude, it is generally assumed that environmental conditions at that altitude may be represented by the U.S. Standard Atmosphere, 1962. Figure 1 illustrates the variation of specific lift with temperature at sea level on a standard day with an ambient temperature of 59°F (15°C). The lifting force is quite sensitive to ambient temperature, and Fig. 2 illustrates the variation of specific lift with outside temperature, again at sea level, for a balloon hot-air temperature of 250°F (121°C). A temperature of 250°F ensures long envelope fabric life, and Fig. 1 shows that the specific lift is approximately 0.020 lb/ft³ (0.32 kg/m³) on a standard day at sea level. Specific lift is plotted as a function of altitude in Fig. 3, both for a constant balloon temperature of 250°F and for a constant temperature differential between balloon and air of 191°F (88°C).

Figure 3 shows one of the problems of achieving very high altitude flights for hot-air balloons--the specific lift decreases monotonically as altitude increases. It is reasonable to expect that hot-air systems will find utility in the upper reaches of the troposphere, but above the tropopause it seems unlikely that hot-air balloons will be used except as

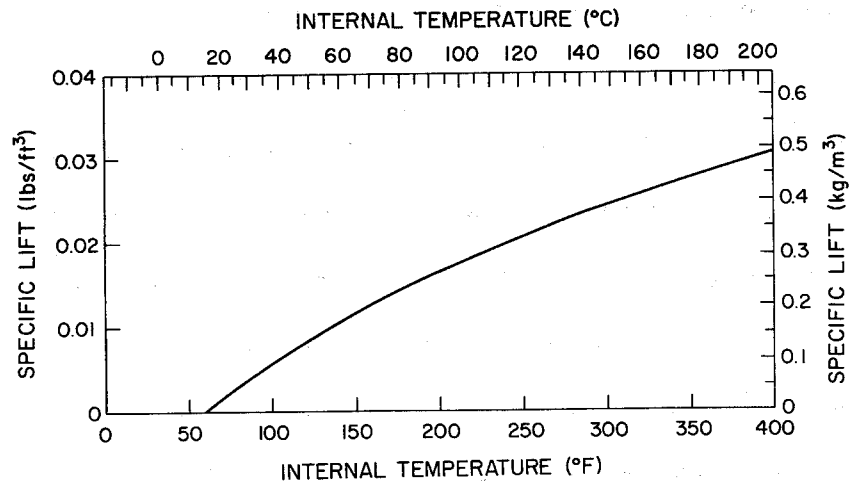


Fig. 1. Specific lift vs balloon internal temperature for a balloon operating at sea level in the U.S. Standard Atmosphere, 1962.

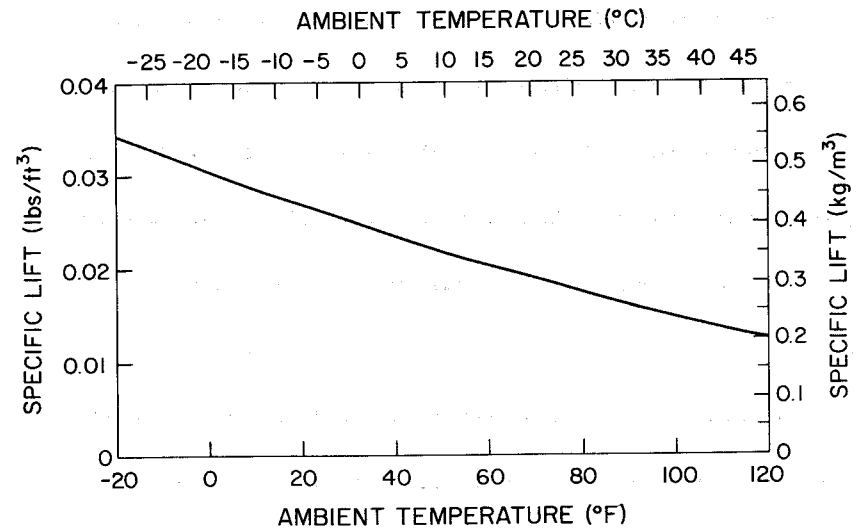


Fig. 2. Specific lift vs ambient temperature for a balloon with an internal gas temperature of 250°F (121°C) operating at a pressure of one atmosphere.

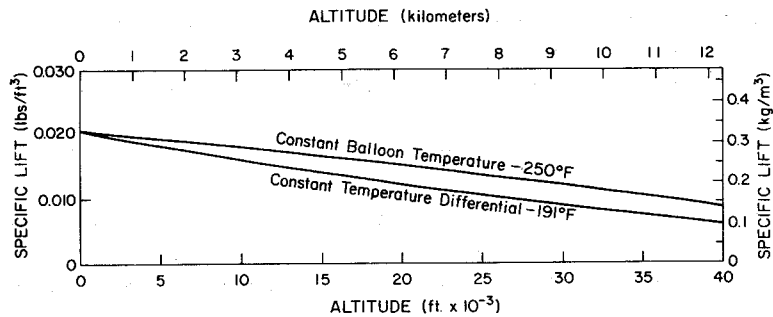


Fig. 3. Specific lift vs altitude for a balloon operating in the U.S.

Standard Atmosphere, 1962, with: 1) an average internal temperature of 250^oF (121^oC) and 2) an average internal temperature which differs by 191^oF (88^oC) from ambient air temperature.

decelerating devices that ultimately fall into the lower atmosphere.

The specific lift can be increased by operating at higher temperatures although the nature of the lift equation sets an upper limit even for infinite temperatures. Hot-air balloons normally operate in the neighborhood of 0.25 to 0.5 the theoretical maximum. Fabric durability at elevated temperatures is, of course, one of the paramount restraints on increasing lift by increasing temperature.

To determine the effects of flame temperature on fabric temperature, Raven Industries, Inc. instrumented a small balloon and obtained the results illustrated in Fig. 4. It can be seen that the temperature probe indicated a flow field that starts at the burner, rises to the crown of the balloon, and then descends down the sides. Along the streamlines the temperature gradually moderates, which is a fortuitous effect with regard to the fabric. In the experiment illustrated, the temperature near the flame was 240^oF (116^oC) above ambient, but at the crown it was only 140^oF (60^oC) above ambient.

An interesting outcome of the measurement was that the maximum skin temperature turned out to equal the temperature that would account for the

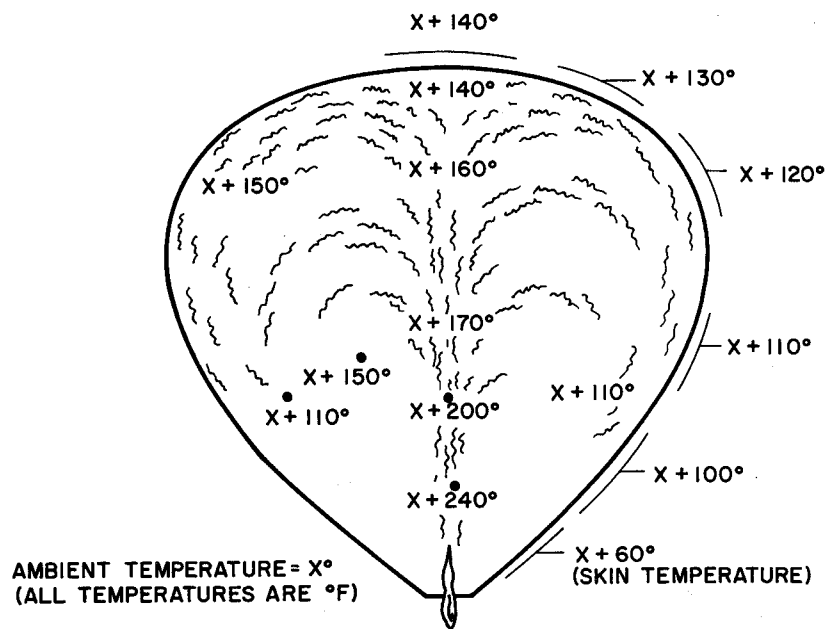


Fig. 4. Gas and skin temperatures as observed in static model hot-air experiment. Average temperature differential is 140°F .

measured lift. This immediately suggested that a temperature probe at the crown of the balloon be used to compute lift and also to warn if maximum temperatures approached unsafe values.

The use of a burner, as suggested by Fig. 4, causes ambient air to be entrained into the flow field. The air not only provides the oxygen for combustion of the fuel, but also serves to reduce the temperature. In addition to several other effects, the entrained air loosely couples the internal temperature to the outside temperature. There is, therefore, a tendency toward a constant temperature difference rather than a constant temperature.

At sea level a burner such as the one shown in Fig. 5 passes about 180% of the air required to sustain combustion. The excess air and the combustion products are ultimately exhausted by seepage through the fabric and the seams and by counterflow or ventilation through the base throat. A significant part of the thermal input can ultimately be lost in this fashion under some circumstances.

In practice a maximum operating temperature based upon the durability requirements of the envelope is established for a balloon. Then the sizes of balloon and the burner to accomplish the mission profile without exceed-

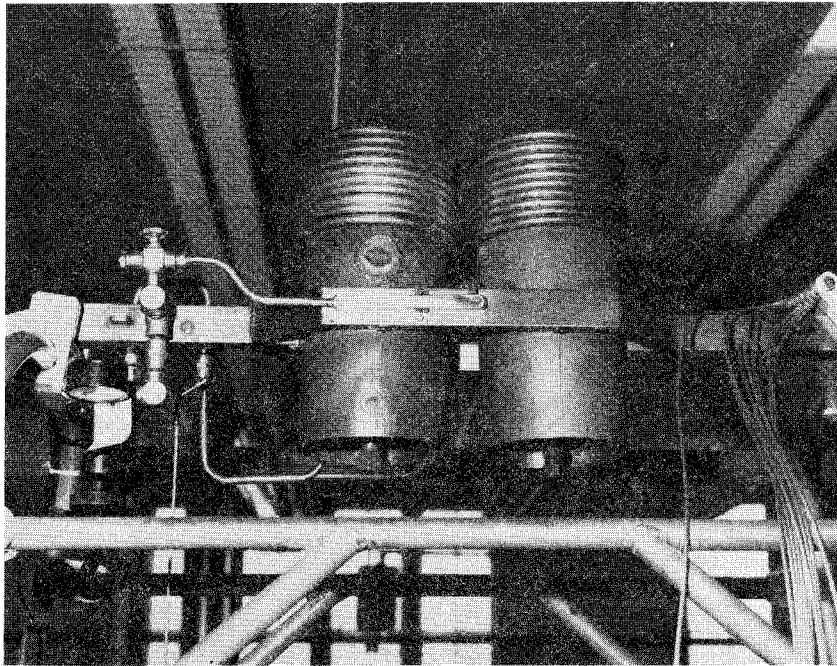


Fig. 5. Propane burner for a hot-air balloon.

ing that limit are established. For manned systems the limit is 250°F (121°C), and for short-lived unmanned systems it may be as high as about 350°F (177°C).

Nylon is the most frequently used fabric, although dacron is also used. Special high-temperature materials exist and are being considered for special applications as either full envelopes or as crown caps.

The polymeric fabrics, nylon and dacron, tend to soften with elevated temperatures. At the same time the percentage elongation under strain increases markedly and much of it is inelastic. At 484°F (251°C) these materials actually melt and, of course, their strength evaporates.

Recent improvements in the cross-linking of nylon and dacron molecules have resulted in the so-called high-tenacity forms which do not degrade in strength as rapidly as previous forms. High-tenacity nylon is most commonly used in hot-air balloons and some of its characteristics are included below.

Breaking tenacity	$1.5 - 1.9 (\times 10^{-2})$ lb/denier [6.7 - 8.4 ($\times 10^{-2}$) N/denier]
Breaking elongation	17-45%

The basic strength and temperature characteristics are not the only characteristics of interest. Other important factors include: 1) high strength-to-weight ratio at design temperature, 2) high strength-to-packed volume ratio, 3) minimal creep at elevated temperatures, 4) good crease resistance, 5) low thermal conduction, 6) low storage degradation, 7) moderate gas permeability, and 8) for repeated use, good scuff resistance.

Clearly the physical characteristics of the basic material are only part of the story. The way the fibers ultimately are formed into a fabric remains equally important. The choice of fabric or fabrics ultimately depends upon the mission to be accomplished. For medium-sized balloons (30 to 50 ft in diameter--9 to 15 m) the standard material is 1.6 oz/yd² (54 gr/m²) ripstop nylon which has been calendared (pressed with a hot roller to flatten the threads and reduce permeability). The physical properties of the fabric are:

Tensile strength	90 lb Warp and filling
Thread count	120/in.(47/cm) Warp and filling
Tear strength	6 lb (27 N) Warp and filling
Thread	30 denier High-tenacity nylon

A typical hot-air balloon is shown in Fig. 6. Since hot-air balloons tend to operate at low altitudes with large payload-to-balloon weight ratios, the design shape corresponds to a low sigma value.

Although the natural-shape balloon has no circumferential stresses when fully deployed, the manner in which hot-air balloons are used frequently introduces transient circumferential stresses. The balloon gores are sewn together in a simple lap seam that retains 75% of the parent fabric strength. Since the ventilation loss through the throat is comparatively large, it is not necessary to make the seams gas tight, which alleviates the production problem considerably.

The magnitude of the meridional loads normally exceeds the circumferential stresses considerably. For manned systems it is common practice to provide a design load factor of seven or more to ensure safe operation. Special care must be exercised in the way the load is introduced into the fabric and in the design of the balloon near the crown where stresses concentrate and the temperature is a maximum.

The rigging weight associated with the envelope accounts for some 10-20% increase over the bare envelope weight. The burner and fuel add additional



Fig. 6. Typical hot-air balloon in flight.

weight that subtracts from the lift available for carrying a payload.

Figure 7 illustrates the payload that can be carried by balloons of various diameters under one set of assumptions at sea level. Figure 8 shows the same information for a balloon operating at 20,000 ft (6 km).

The relationship between diameter, surface area, and volume is not simple for balloon shapes (see Section V). For the low altitude hot-air balloon, the following relationships apply: $\Sigma = -0.05$, $V = 0.125 \lambda^3$, $R = 0.3175 \lambda$, $A = 1.21 \lambda^2$, $H = 0.66 \lambda$, and $\theta = 95^\circ$, where V is volume, R is radius at the equator, H is height, A is area, θ is base cone angle, and λ is gore length.

To facilitate comparison, the relationships between diameter and volume, area, and gross lift are included in Figs. 9, 10, and 11. Figure 12 compares the envelope weight with balloon diameter. The envelope weight is purposely left somewhat indeterminate since for the larger balloons it depends upon design safety factors and the materials used.

The heat required to initiate and sustain flight may, in theory, be supplied from a wide variety of sources, including propane burners, modified liquid or solid fuel rocket motors, pyrotechnic devices, and nuclear power

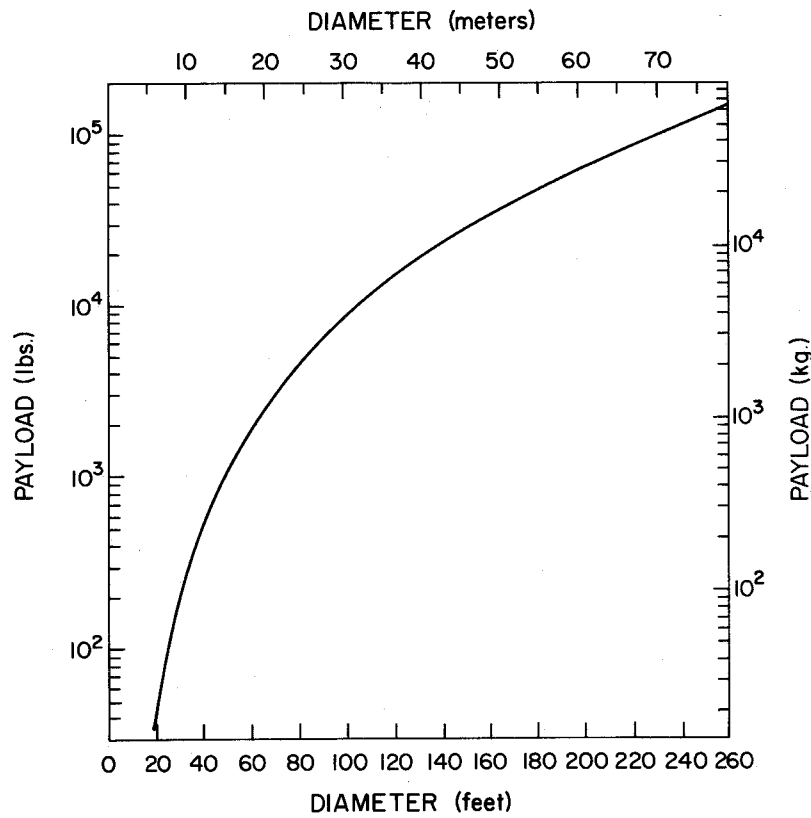


Fig. 7. Payload vs diameter for hot-air balloons at sea level. It is assumed that the envelope is a metalized material, that specialized, light-weight, stainless steel tanks are used, that rigging weight is 10% of envelope weight, that fuel is carried for one-hour flight at sea level, and that 50% of the fuel will be used for ascent. Internal temperature is 250°F (121°C).

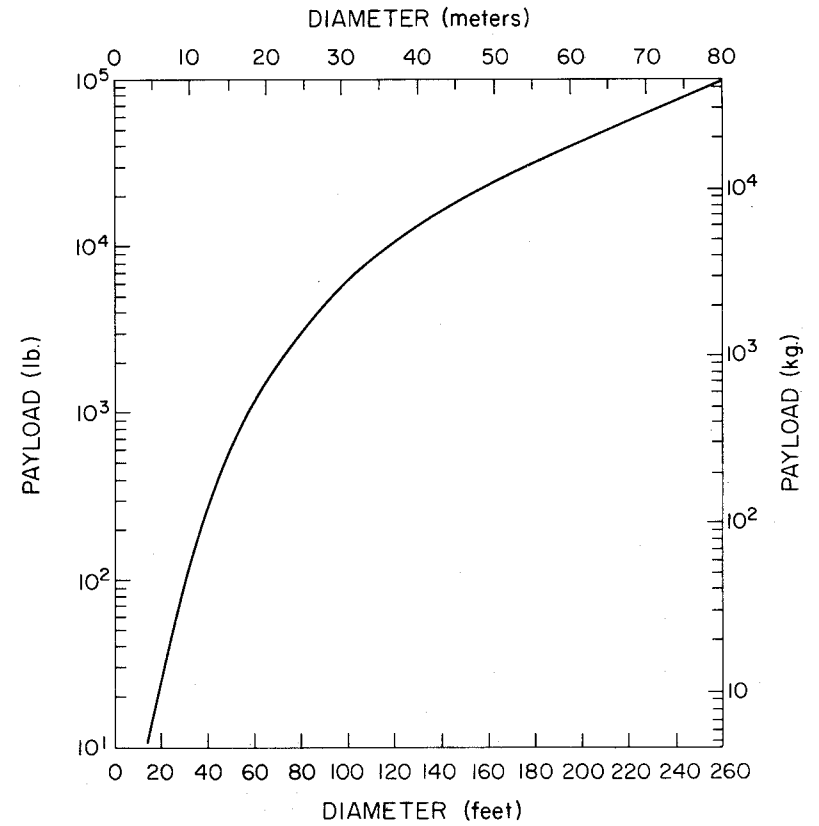


Fig. 8. Payload vs diameter for hot-air balloons at 20,000 ft (6 km).

See caption of Fig. 7 for balloon system characteristics.

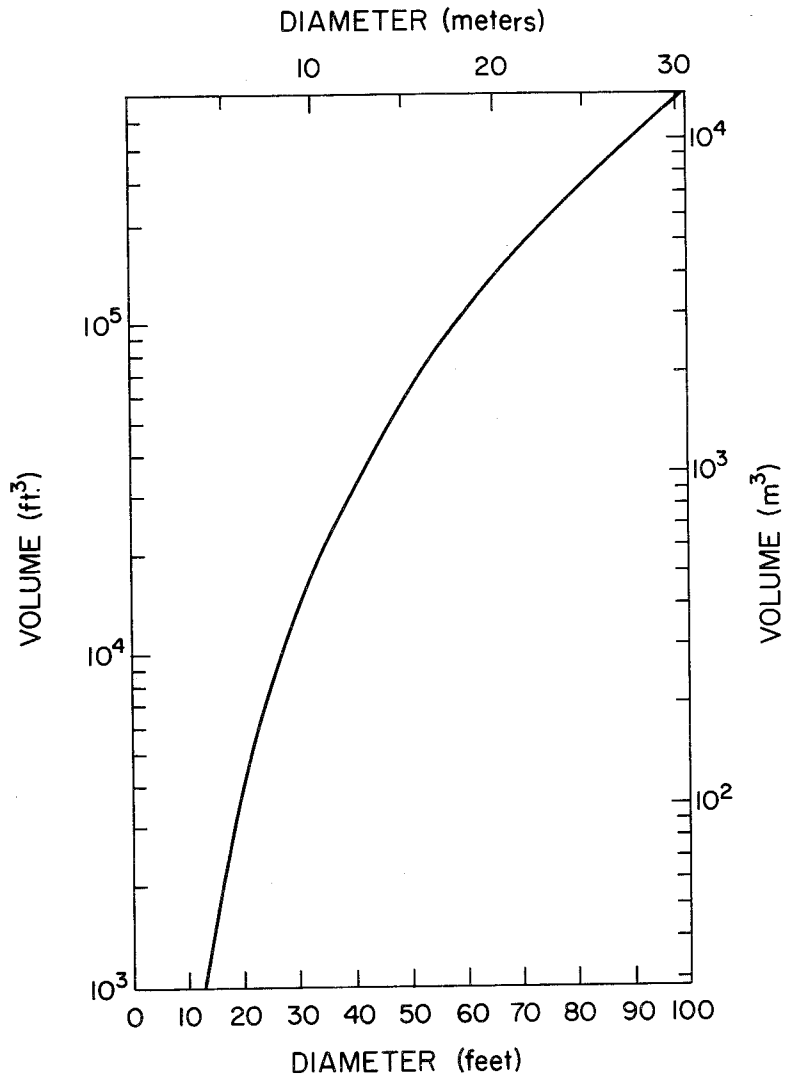


Fig. 9. Volume vs diameter for a natural shape hot-air balloon.

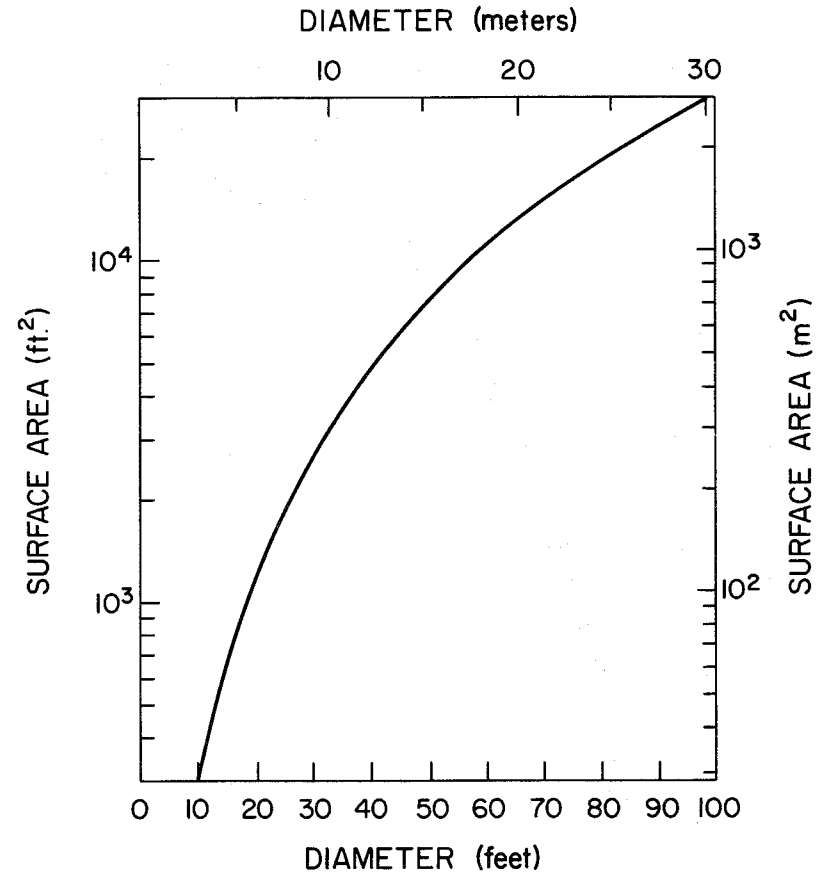


Fig. 10. Surface area vs diameter for a natural shape hot-air balloon.

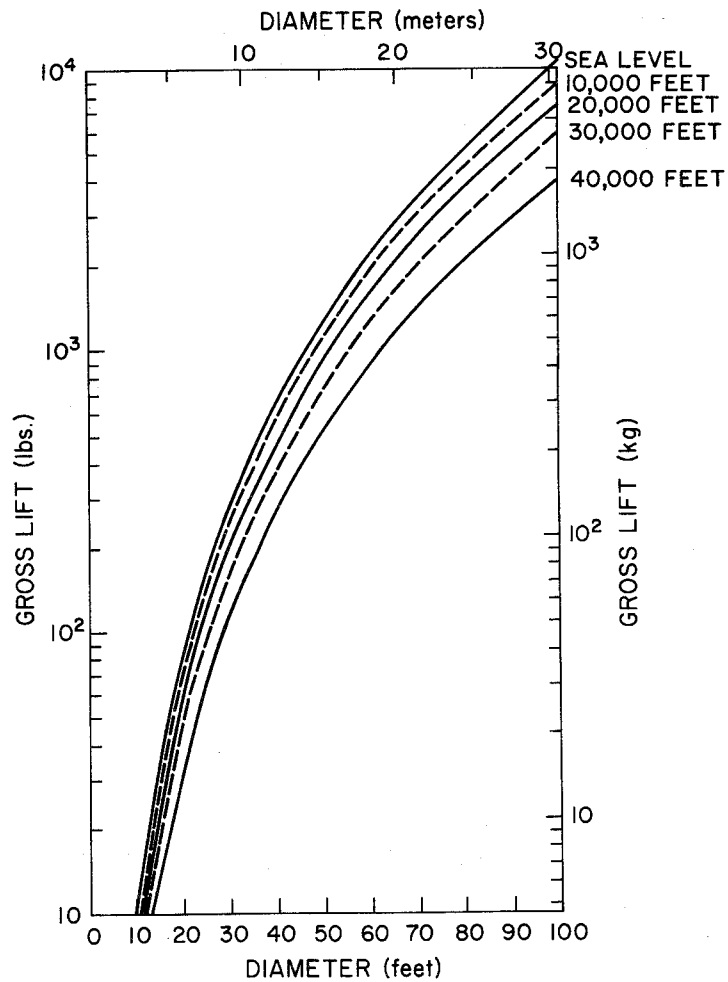


Fig. 11. Gross lift vs diameter for balloon flying in the Standard Atmosphere with an internal temperature of 250°F.

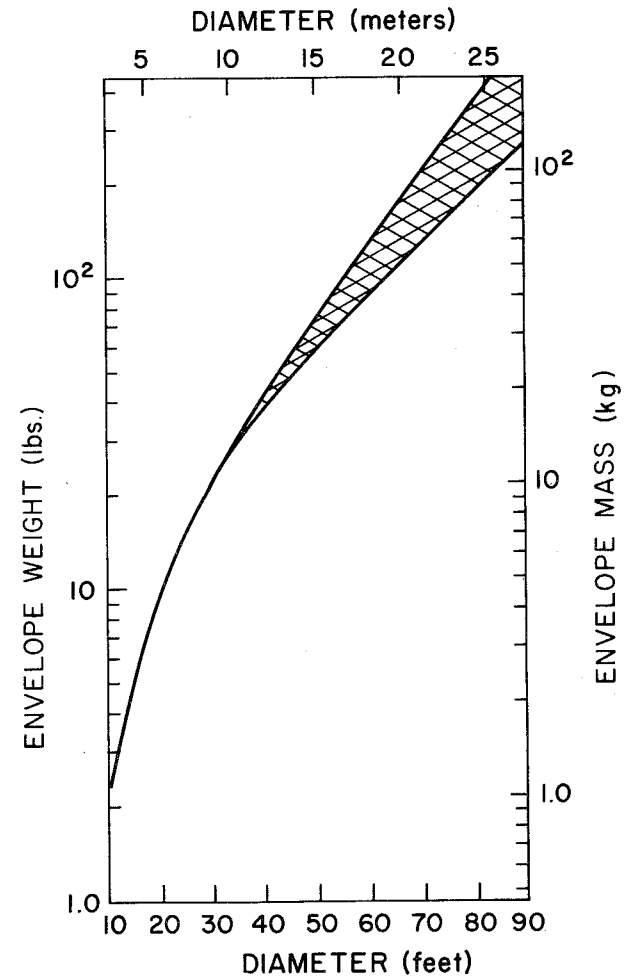


Fig. 12. Envelope weight vs diameter for a balloon made of available fabric. In flight at sea level in the U.S. Standard Atmosphere, 1962, with an internal temperature of 250°F; the safety factor is three.

supplies. Only propane burners and pyrotechnic devices have been extensively evaluated.

Propane has many desirable features. It is stored as a liquid but has a significant vapor pressure at normal temperatures, which alleviates the need for pumping mechanisms in many cases. At the same time the vapor pressure does not rise to excessive values in "hot" conditions. Figure 13 shows the vapor pressure of propane as a function of temperature. For normal usage, the U.S. Interstate Commerce Commission has established standards for propane tanks, which cause them to weigh approximately 75% as much as the propane in a full tank. Special purpose tanks can be made which achieve more nearly 45% of the full fuel weight. In all cases it is mandatory to provide a pressure relief valve to compensate for unanticipated thermal surges.

By far the most difficult aspect of hot-air balloon system design is the computation of fuel and burner requirements. Energy balance relationships of hot-air balloons are complex. They must account for thermal storage and compression of the air in the balloon, burner heat addition, heat transfer through the balloon fabric, ventilation heat losses, and variability of air temperature and pressure.

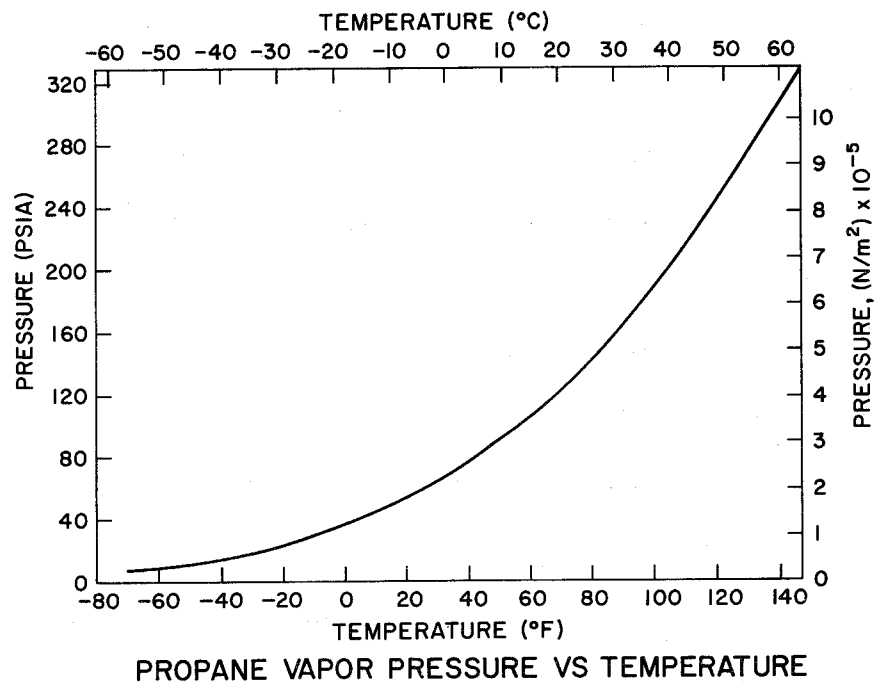


Fig. 13. Propane vapor pressure vs temperature.

Many of the effects--burner performance, for example--are further dependent upon altitude and velocities. The energy relationships may, however, be analyzed with a computer. By also solving the equations of motion, the entire flight performance of a hot-air system may be simulated with fair success. (See Section III.)

For many applications it is not necessary to determine performance with precision, since it will vary with atmospheric conditions, and the analysis may be simplified. Figure 14 serves as a guide for computing the hovering requirements for a balloon at sea level.

Considerably larger values may be needed for maneuvering or for initial heating. Rules of thumb indicate that initial heating may require 10 times as much heat as hovering. Maneuvering vertically requires about twice the heat rate of hovering.

Propane, with a density of 4.2 lb/gal (500 kg/m³), has a thermal output of approximately 20,000 BTU/lb (actually 21,560, but there are losses). A propane burner of the type shown in Fig. 6 is capable of producing 2 x 10⁶ BTU/hr (585 kw). The burners are designed to provide more than 1000 hr of service. The specific weight of burners (in lb of burner weight per

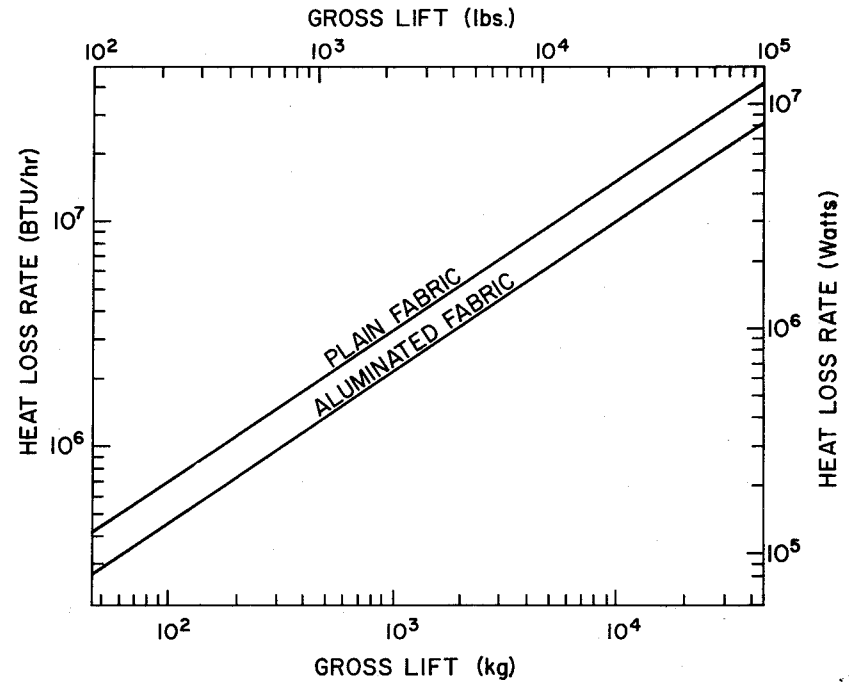


Fig. 14. Basic envelope heat loss rate vs gross lift for a balloon at sea level having an internal temperature of 250°F.

BTU/hr capacity) can be improved by cutting the life cycle, using more expensive materials, or using higher unit outputs.

C. FLIGHT LIMITATIONS AND CONTROLS

The modern hot-air balloon is an outgrowth of an effort to devise a manned flight vehicle that would be simple to operate, inexpensive, and capable of storage for long periods of time without degradation. Today most manned balloons are 50 ft (15 m) in diameter, although both smaller and larger versions do exist.

A balloon 50 ft in diameter having a volume of 61,000 ft³ (1700 m³) is a commonly used balloon. Though normally considered a two-man system, it is possible to carry three--a pilot and two passengers--at the lower altitudes. With conventional burners it has been flown to 24,000 ft (7.3 km), but this cannot be recommended.

The flight duration of a balloon depends heavily upon the amount of fuel carried. Typically, two 22-gal tanks of propane (83 kg) are enough for three to four hr of flight for a 50-ft balloon, depending upon the ambient temperature and the amount of maneuvering. As with aircraft, fuel reserve should always be maintained.

The propane burner is a relatively simple apparatus. As shown in Fig. 15 the fuel flows from the tanks through coils surrounding the burner barrel. The propane leaves the fuel tank as a liquid but is transformed to a gas as a result of heat passing from the barrel to the fuel line. Air is entrained through the lower opening in the burner barrel and serves to supply oxygen for combustion and to moderate the temperature of the combustion product.

The rate of flow of propane is governed by a needle valve that acts as a cruise control and is adjusted as needed during the flight. To provide maximum lift in emergencies, a by-pass valve and line permit the full burner capacity to be made available instantaneously.

A maneuvering vent in the envelope provides an additional means of controlling lift. The maneuvering vent illustrated in Fig. 16 is a feature available with hot-air balloons that is impractical for helium or hydrogen systems. Basically a controllable slit in the envelope, the maneuvering vent is possible as a result of the "zero circumferential stress" design. The vent is controlled by a line extending from the gondola and along the side of the balloon wall where it is split into a "Y" and then passed through a pulley and connected to each side of the vent. A simple pull from the

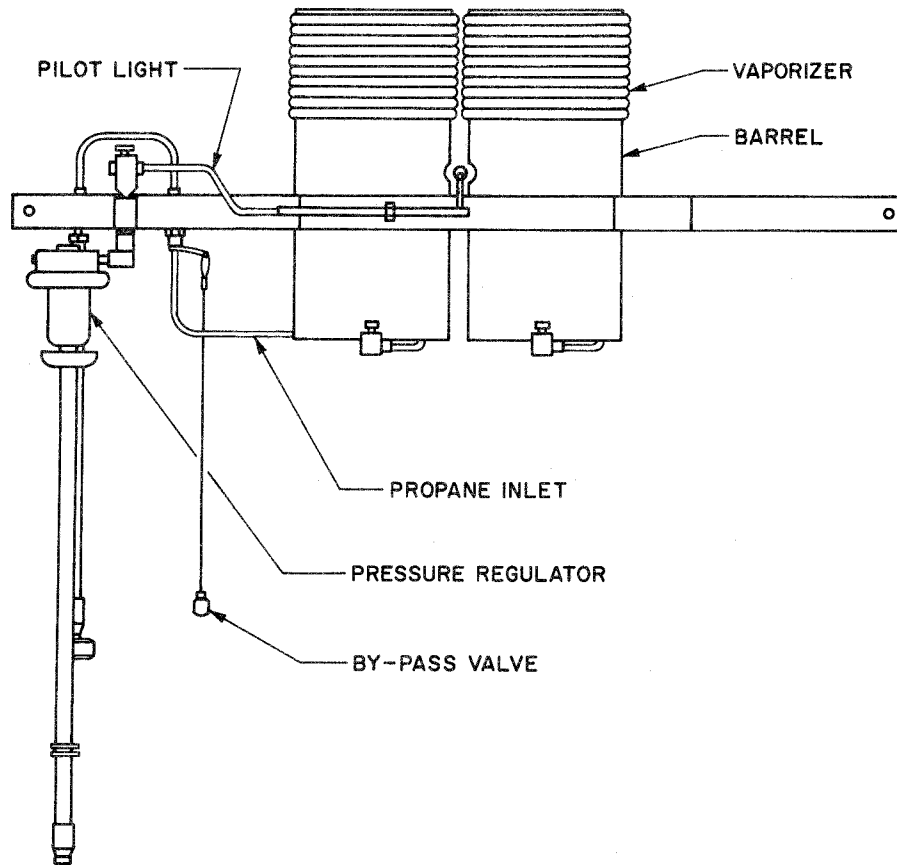


Fig. 15. Double propane burner.



Fig. 16. Inflated balloon with maneuvering vent open.

gondola opens the vent proportionally to the amount of line taken in.

A maneuvering vent in a balloon can be quite useful. Normally a balloon of the 50-ft class will take approximately a minute to respond sensibly to a change in thermal input. By spilling heated air through a maneuvering vent, almost instantaneous decrease in lift is possible. Precise altitude control, even at low levels, can be achieved by running the burner a little "high" while spilling the excess lift through a partially opened vent as needed for increasing or decreasing the effective lift.

Another interesting feature of the modern hot-air balloon is a cap which can be removed by a steady pull on a line (rip cord) from the gondola. In the Raven Industries, Inc. design, shown in Fig. 17, load tapes fastened along the gore lines cross over the top of the balloon where the top portion of the envelope has been eliminated. Then the cap is placed under the load tapes and secured at its edge with Velcro tape except for an 18-in. section, which is sewn. The Velcro keeps the cap in place; the load is taken up by the load tapes; and once on the ground, only a light steady tug with the rip cord is necessary to peel open the cap and spill the hot air. Reinstallation of the cap is made easy by the Velcro.

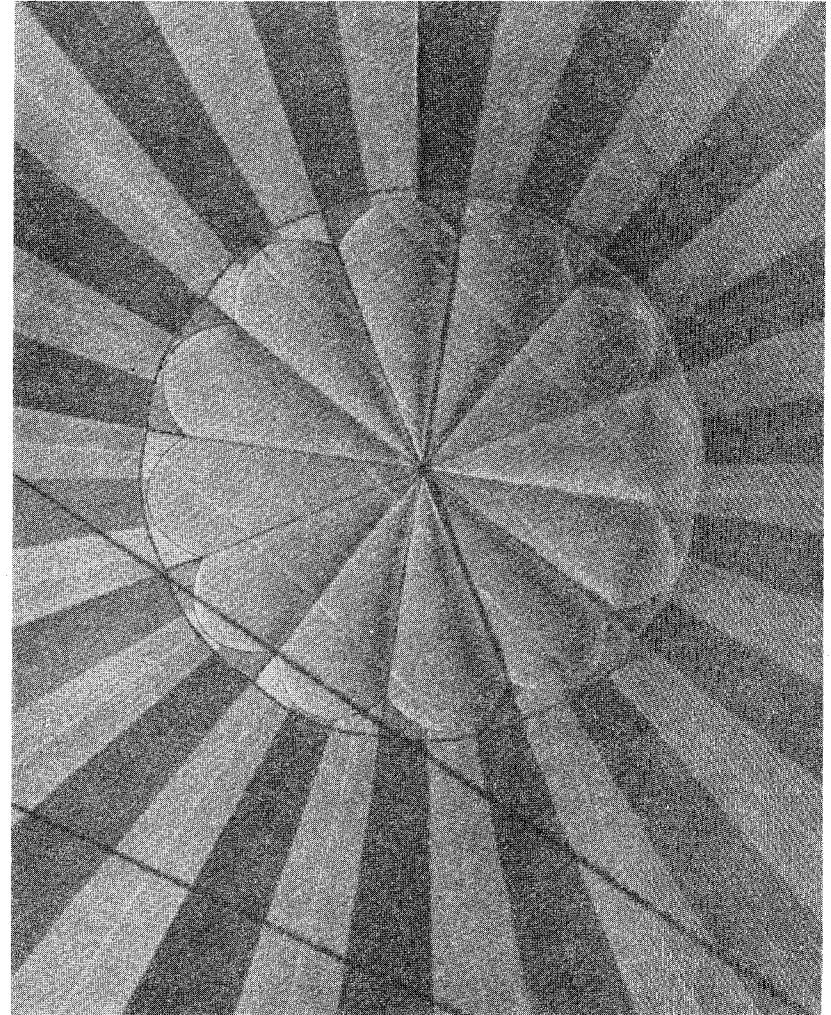


Fig. 17. View of the removable cap inside a hot-air balloon.

A cylindrical skirt is attached to the bottom of the balloon externally. At the attachment point this skirt has the same diameter as the balloon. The skirt is 6 ft long and 8 ft in diameter. The purpose of the skirt is to direct the hot gases into the interior of the balloon and divert horizontal wind gusts which might deflect the burner flame onto the main envelope. The skirt has a spring steel hoop at its base to maintain its circular shape.

Handling lines attached near the equator of the envelope are used to assist in inflation and launching of the balloon.

Instrumentation of hot-air balloons is relatively simple. An altimeter and a rate-of-climb meter are required. A fuel gage is indispensable. From a safety standpoint, the most important instrument is a thermocouple sewn near the crown of the balloon to indicate maximum envelope temperature.

D. APPLICATIONS

From a technical standpoint the upsurge in sport ballooning has provided a great deal of information on balloon performance that would not otherwise have become available at this time, and flight experience with hot-air balloons has led to a number of commercial and technical applications. For

example, pheasant populations have been checked in South Dakota by slowly and silently gliding low over fields. It has been possible to test and evaluate instrumentation for satellites on balloons in cases where the speed of airplanes and the vibration of helicopters have prohibited their use. Schools of fish have been studied from a hot-air balloon tethered above a ship.

More and more applications for tethered hot-air balloons are being found. A 60-ft (18 m) balloon is capable of carrying two or three technicians, plus oscilloscopes and auxiliary laboratory equipment for an hour. It is less expensive to use a balloon than to build a tower, and a tethered balloon may be moved from one site to another for subsequent tests without difficulty. Experience indicates that a 60-ft balloon is capable of such operations in winds up to 15mi/hr (~ 7 m/sec).

Both tethered balloons and ground launched free balloons have considerable historical precedence, and the movement of hot-air balloons into these fields is not surprising. What is somewhat startling is that the promise of air launched hot-air balloons is perhaps even greater. Air launched hot-air balloons offer the potential of causing a suitable payload to rise, to hover, or to descend slowly--more slowly than possible with a parachute or

other passive decelerators. With the addition of modest controls the hot-air balloon can accomplish all these modes on a programmed or adaptive basis.

The air launched hot-air balloon may be ejected from either aircraft or rockets. If the speed and altitude of injection are such as to provide an excessive dynamic pressure, it may be necessary to provide a primary decelerator, a drogue parachute, for example, to slow the system down. Below a specified dynamic pressure (30 lb/ft^2 [1450 N/m^2] in a system to be described) the balloon may be deployed. The balloon, when filled with air, serves as a secondary decelerator. Based upon cross sectional area, the cold balloon will have a drag coefficient of between 0.5 and 1.0 depending upon whether high drag is desired.* Thus, the cold balloon compares favorably with a standard parachute on area drag, although not on a weight basis. The important fact is that a cold balloon will provide a terminal descent rate comparable to that of a parachute in the event that the burner does not function or fuel should be exhausted.

*Experiments have shown that a "burble fence" on the balloon increases both stability and drag.

The balloon is somewhat more difficult to fill than a parachute--or rather takes a bit more sophistication. Common practice is to place a series of inflation scoops near the equator. The inflation scoops allow the top of the balloon to fill and stiffen the envelope to the point where the base throat may be opened (see Fig. 18). Then additional air is "rammed" into the balloon through the throat until the envelope is filled. Early air-launched balloons used throat inflation only, and problems were occasionally encountered. As the first air was ingested, a bubble developed at the throat of the envelope that tended to buffet and alternately open and close the throat as a result of instabilities in the air stream. The result was to permit the envelope to fall too far before inflation was complete and to burn the envelope if the burner was turned on.

In a normal sequence with inflation scoops, the inflation process is completed in a matter of seconds. When the cold inflation process has progressed sufficiently to hold the throat open, the burner may be turned on.

Computer studies have revealed considerable insight into the performance of air-filled balloons undergoing heating while falling. If, for example, the balloon is dropped at one altitude and the mission involves hovering

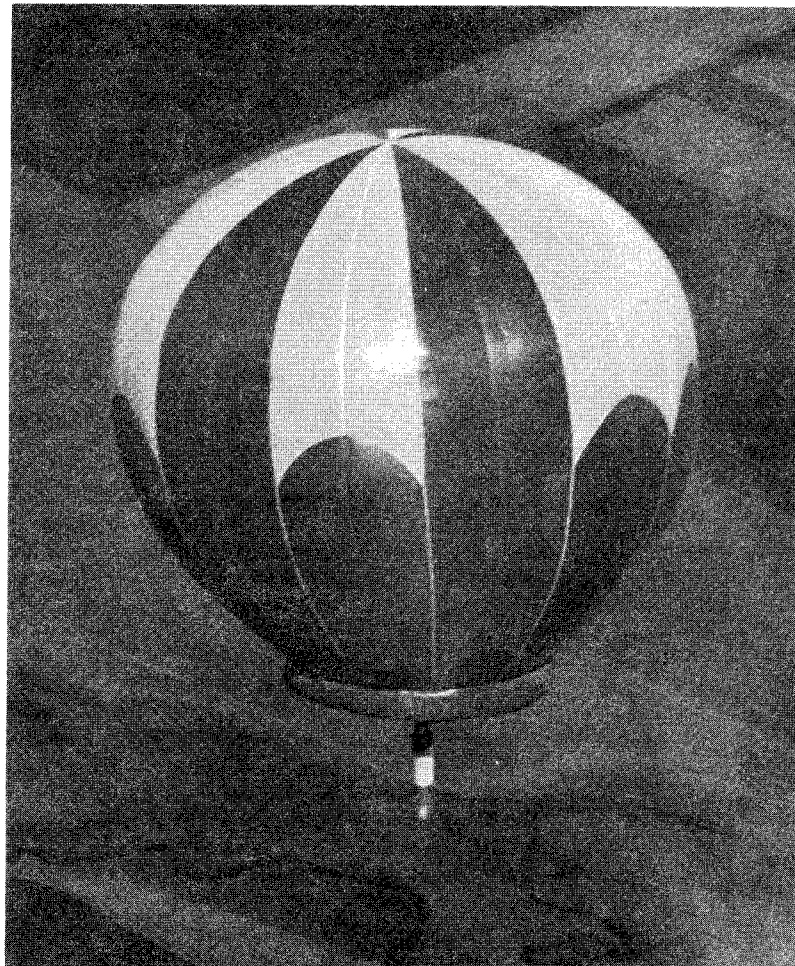


Fig. 18. An unmanned hot-air balloon. The white sectors are scoops which help the falling balloon to inflate before the burner is turned on. This balloon was dropped from an airplane.

at a lower altitude, there is an optimum heat generation profile. The optimum amount of heat at any instant is that which is just adequate to raise the volume of the balloon gas enough to compensate for the compression that occurs as a result of falling, plus heat losses due to conduction. In other words, the thermal input should be just that which results in no flow of air in or out of the balloon.

Since a variable heat generation profile is complex, a comparison has been made of the loss of efficiency that occurs for a fixed heat generation system. It turns out that there can be found an on-off fixed level heat generation profile that differs in fuel consumption from the optimum profile by a negligible amount. Analysis also shows that the distance that a balloon will fall during the heating period (assuming that the vertical motion just stops and the balloon hovers) will be one-third the distance that the balloon would free-fall in that same time. Finally, it has been determined that little is gained in beginning to heat a balloon at altitudes above 30,000 ft (9 km) since the percentage energy requirement is low at those altitudes.

Figure 19 illustrates the performance of a system which was designed to hover in the vicinity of 25,000 ft (7-8 km) regardless of the altitude de-

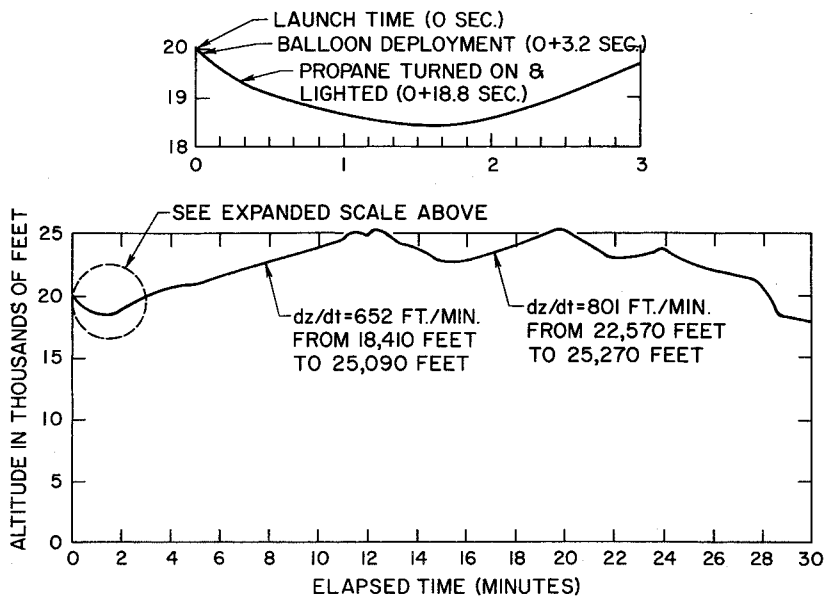


Fig. 19. Performance of a hovering hot-air balloon.

ployed. In this instance the balloon was deployed at 20,000 ft (6 km), descended to 18,600 ft (5.7 km) during initiation and then climbed to 25,000 ft (7.6 km). At that altitude the burner was turned off and the system settled to 22,500 ft (6.9 km), where reignition was accomplished.

In summary, the hot-air balloon provides an inexpensive way to carry a useful payload upward through as much as two-thirds of the atmosphere. It is easy to fly, capable of extended storage, and it can be moved from site to site in a small truck or trailer.

SECTION X

LIST OF SYMBOLS

PARACHUTES

by

Alvin L. Morris

List of Symbols. ii

List of Figures iv

A. INTRODUCTION 1

B. DESCRIPTION OF A PARACHUTE SYSTEM 1

C. PARACHUTE DESCENT. 5

1. A Simplified Descent Model 13

a. Phase 1 15

b. Phase 2 17

c. Phase 3 28

d. Phase 4 29

D. CONSIDERATIONS IN SELECTING A PARACHUTE 30

1. Parachute Size 32

2. Multiple Parachutes 40

3. Time of Descent 42

REFERENCES 44

<u>Symbol</u>	<u>Description</u>	<u>Dimensions</u>
A	cross-sectional area, usually the effective area of the inflated canopy	L^2
A'	nominal area, usually taken as the area of material in the canopy	L^2
B	subscript indentifying its symbol with the balloon system	
C	constant of integration	
C_D	drag coefficient (dimensionless)	
C'_D	pseudo drag coefficient, used with an area other than the effective area	
D	diameter of a canopy	L
D'	nominal diameter of a canopy, usually taken to be the diameter of a circle whose area is equal to the nominal area, A'	
d	symbol indicating differentiation of the variable following it	
g	acceleration due to gravity	LT^{-2}
H	height above sea level	L
m	mass of parachute system	M
m_v	virtual mass of an accelerating parachute system	M
N	number of parachutes used in a cluster	
n	exponent of 10 used to expand the scales of Figs. 6 and 7	

o	subscript identifying its symbol with the base or zero level
Re	Reynolds number
T	subscript used with v to indicate terminal or equilibrium velocity
t	time
v	vertical velocity. Algebraic sign identifies its direction, (+) upward and (-) downward
v_T	terminal or equilibrium velocity
v_w	horizontal speed of surface wind

Greek letters

ρ	air density
π	3.14159

T
 LT^{-2}
 LT^{-2}
 LT^{-2}

ML^{-3}

List of Figures

Fig. 1	Parachute nomenclature	3
Fig. 2	Acceleration versus time for a parachute system for which terminal velocity is constant. Acceleration is in effect plotted as multiples of the acceleration of gravity and time as multiples of $(-v_T/g)$	20
Fig. 3	Acceleration traces of quick-opening and delayed-opening parachutes	23
Fig. 4	Descent velocity versus time for a parachute system for which terminal velocity is constant. Velocity is plotted as a multiple of v_T and time as a multiple of $(-v_T/g)$	26
Fig. 5	Loss of altitude versus time for a parachute system for which terminal velocity is constant. Height difference is in effect plotted in multiples of (v_T^2/g) and time in multiples of $(-v_T/g)$	27
Fig. 6	Sea level terminal velocity of a parachute as a function of parachute system mass and the product of parachute area and drag coefficient. Numbers on the abscissa and ordinate may be multiplied concurrently by any factor 10^n to cover all non-zero values	34

Fig. 7 Nominal diameter of a parachute as a function of area and drag coefficient. Numbers on the ordinate may be multiplied by 10^n if numbers on the abscissa are concurrently multiplied by 10^{2n} to cover all non-zero values 36

Fig. 8 Terminal velocity and time of descent as functions of sea level terminal velocity and altitude in the U.S. Standard Atmosphere, 1962 39

PARACHUTES

A. INTRODUCTION

Parachutes are used on most scientific balloon flights to lower the scientific payload upon termination of the ballooning phase of the flight. A parachute is also used as a safety device on virtually every balloon flight even though the balloon system is to be brought down intact by valving gas from it. This section discusses a highly simplified theory of parachute behavior during descent and explains procedures for selecting a parachute. For a more complete discussion of parachute theory and practice the reader is referred to the U.S. Air Force Technical Report cited as reference (1).

B. DESCRIPTION OF A PARACHUTE SYSTEM

A parachute consists of a woven textile or plastic canopy which is attached to the load by means of suspension lines, frequently called shroud lines. The canopy may have various forms, but is usually axially symmetric about the vertical axis, and may be made with or without holes in it. For some special purposes the canopy is made of ribbons.

Figure 1 schematically illustrates a descending parachute with attached load. Most features of parachutes used in scientific ballooning are shown, though variations may be found. A parachute with its payload and ancillary equipment will be termed a parachute system.

The suspension lines join the canopy at its outer periphery, or skirt. They are normally fastened to the skirt at the seams between gores, and they may or may not continue upward over the canopy to the vent on the top. Not all parachutes have vents, but, although the theory of parachute behavior is far from complete, it is generally believed that parachutes having an axially symmetric canopy benefit from the vent.

The porosity of the canopy material affects the performance of a parachute in several important ways. A highly porous canopy fills more slowly, is more stable, and has a lower drag coefficient than a less porous canopy. The effective porosity of a cloth is defined as the ratio of the average speed of air through the porous sheet to the free stream speed. A canopy can be made more porous than the cloth from which it is made by leaving open areas in it. Geometric porosity is defined as the ratio of the open area of a canopy's drag-producing surface to the total area of the drag-producing surface.

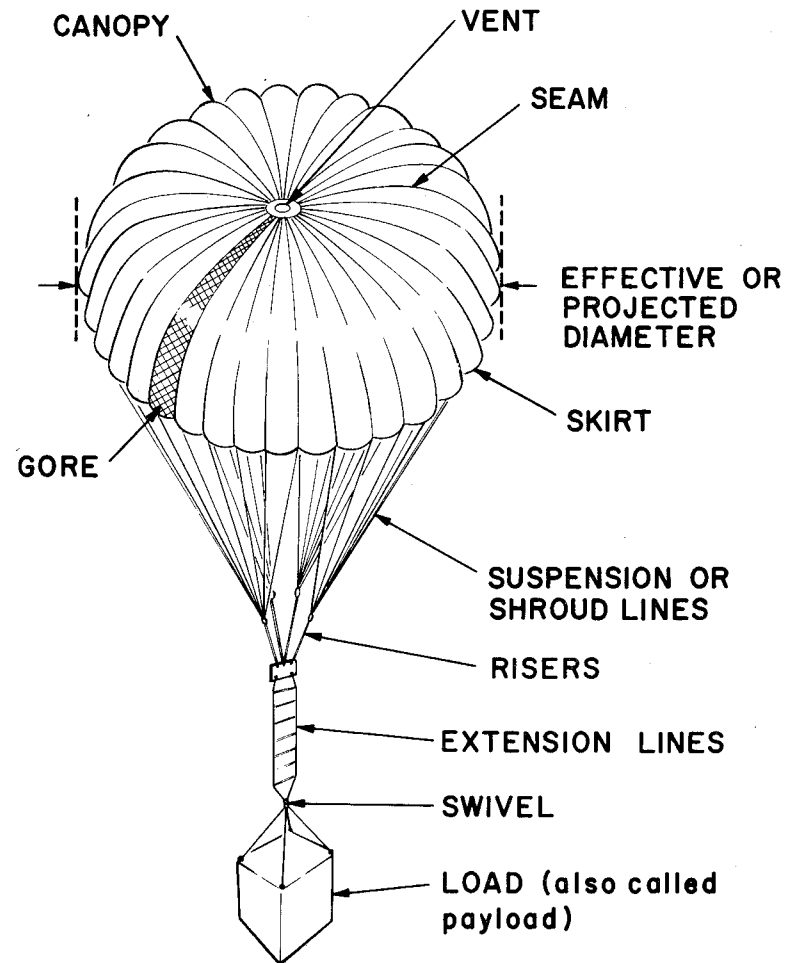


Fig. 1. Parachute nomenclature.

The payload may be fastened directly to the lower end of the risers, but if there is reason to suspend it lower, extension lines may be used. A prismatic, multipoint suspension system (see Fig. 1, Section VII) consisting of two or more cables is commonly used. If it is desirable that the payload be free to turn independently of the parachute, a swivel may be placed in the suspension system anywhere below the risers.

Parachutes are usually described by their nominal diameter, the diameter of a circle whose area is equal to the area of the drag-producing surface of the canopy. Thus the nominal diameter of a flat circular canopy is the diameter of the material in its flat form, whereas the effective diameter is the projected diameter of the inflated parachute as shown in Fig. 1. The latter is a function of the parachute's design and the load it is carrying.

Packed parachutes are used only occasionally in scientific ballooning. Instead, the parachute is fully deployed (extended) at all times, and inflation can start immediately upon separation from the balloon. The parachute frequently serves as a link in the suspension system between the

balloon and the payload. Or, it may be fully deployed throughout the flight but not carry the suspended load prior to flight termination. In the latter case, the parachute is carried parallel to the suspension system or up along the balloon, and is fastened at the top by a break-away device, frequently a light cord.

C. PARACHUTE DESCENT

Existing theory cannot describe the complete behavior of a parachute system in flight, but theory does give some insight into the behavior and provides the foundation for methods of selecting parachutes for given applications.

The equation of motion of a body through a still, fluid subject to the forces of gravity and fluid drag may be written

$$\frac{d(m_v v)}{dt} = -\frac{1}{2}C_D \rho A |v| v - mg \quad (1)$$

where m_v is the virtual mass of the moving body, v is its vertical velocity, C_D is a dimensionless drag coefficient, ρ is the density of the fluid, A is the cross-sectional area of the body normal to its direction of motion, m is the mass of the body, and g is the acceleration due to gravity.

Virtual mass is discussed in Section II.F. The virtual mass of a parachute system, when the canopy is filled, is approximately the mass of the system plus an added mass which is equal to 0.7 times the mass of a spherical volume of air having the density of the ambient air and a radius equal to the effective radius of a parachute canopy. The mass, m , of a descending parachute system is equal to the mass of the payload, the parachute, the suspension system, and all other attached objects. At the high altitudes (low densities) at which parachutes dropped from balloons are normally inflated, the added mass is small compared to the mass of the parachute system; therefore, the approximation $m = m_v$ will be used henceforth.

The coordinates and units discussed in Section II.C. will be used here. Thus, during descent, the vertical velocity causes a positive, or upward, acceleration, and the weight of the system (mg) causes it to accelerate negatively, or downward. Since the direction of the vector velocity is determined by its algebraic sign, vector notation is not used.

For a parachute, C_D is a function primarily of the shape and porosity of the canopy. It is weakly dependent on Reynolds number. If the fluid is

compressible and the motion causes appreciable compression, C_D is a function of Mach number also. However, unless a parachute system's descent velocity exceeds half the speed of sound, compressibility may be ignored. In practice, the drag coefficient is normally considered constant for a given parachute system throughout descent.

Air density is a function of altitude in the atmosphere. This functional relationship is discussed in detail in Section XI. It is necessary to consider the variation of ρ with time in a descending parachute system, but some phases of the descent are of such short duration that during those phases ρ can be considered constant.

The cross-sectional area of the parachute system during descent is essentially the effective cross-sectional area of the parachute canopy since, by comparison, the payload contributes a negligible area. The canopy's area is dependent on the design and size of the parachute and on the load it bears. Prior to the start of inflation, A is negligible; after the canopy is inflated and a steady state descent is reached, A can be calculated from known conditions. While inflation is occurring, A may momentarily have a value from nearly zero to the area of the flat canopy.

The vertical velocity of a parachute system only is considered here since a still or motionless fluid has been specified. Equation (1) is valid in a moving fluid if v is defined as the relative vector velocity of the body through the fluid, but the magnitude of vertical motion of the atmosphere is small enough compared to the magnitude of the descent velocity of a parachute system that vertical atmospheric motions are neglected. If parachute descents were made in convective cells such as thunderstorms, the theory developed here would differ markedly from practice. An equation similar to Eq. (1) may also be used to calculate the horizontal motion of a parachute system in a moving atmosphere, but it is usually assumed that the parachute system moves horizontally at the speed of the wind system in which it is embedded. Until wind velocity as a function of time and position is known much more accurately than it is now, any refinement in currently used methods of calculating parachute drift does not appear to be warranted unless it also offers a cost advantage.

For convenience of discussion, a parachute descent may be divided into four phases: 1) the initiation of descent and deployment of the parachute,

2) inflation of the canopy and acceleration to terminal velocity, 3) steady state descent at terminal velocity, and 4) landing.

A parachute descent is initiated when the parachute system is separated from the balloon. A parachute is deployed when it is fully extended just before or even during inflation. Packed parachutes usually deploy before starting to inflate. Parachutes which are serving as a link in the suspension system (see Fig. 3, Section II) usually contract like a stretched spring upon separation from the balloon and then deploy again as inflation is starting.

During inflation, air rams into the open lower side of the canopy and fills it under slightly greater pressure than ambient air pressure. The adjustment of the canopy to the incoming air is rapid, as disclosed by cameras on the payload, but the canopy does undergo several oscillations about its equilibrium shape before it assumes that shape. Drag force develops rapidly as the canopy inflates. Parachutes are often referred to as decelerators, implying that they decrease the speed of the parachute system. In scientific ballooning use, a system frequently continues to

gain speed after the parachute is inflated. This will be discussed in greater detail later.

Terminal velocity (also called equilibrium velocity) is the velocity which a parachute system would have if it were descending without acceleration, i.e. if $dv/dt = 0$ or $v = \text{const.}$ Under conditions of terminal velocity and constant virtual mass, Eq. (1) becomes

$$\frac{1}{2}C_D\rho A|v_T|v_T = -mg \quad (2)$$

or

$$v_T = -\sqrt{\frac{2mg}{C_D\rho A}} = \text{const.} \quad (3)$$

Now for a parachute system in phase 3 descending in the atmosphere, m , C_D , and A may all be expected to remain constant, and g varies quite slowly. Air density, however, increases from near $4 \times 10^{-3} \text{ kg/m}^3$ at 40km to near 1.2 kg/m^3 at sea level. Therefore, v_T at 40km cannot be the same as v_T at sea level. If not, a parachute system must accelerate as it descends, and thus the condition for terminal velocity is not fulfilled. Although terminal velocity may never be achieved by a descending parachute system, the concept is still useful if the limitations are kept in mind. For example,

the descent velocity of a parachute system may be quite adequately computed by Eq. (3) for a thin stratum in the atmosphere using for ρ the mean density of the stratum. Also, by using many thin strata, time of descent from any given level to any lower level may be satisfactorily calculated. Finally, the concept of terminal velocity simplifies theoretical examination of parachute descent.

As a parachute system nears the surface, motions other than the vertical motion may become important. The most critical of these are drift and oscillation. An ideal landing is one in which the parachute system descends at a known rate in a perfectly vertical position without horizontal motion onto a readily accessible, unoccupied, firm surface. Manned parachute systems have been developed to the point where this sort of landing can generally be made. The man must, of course, plan ahead, making his descent only at times and in places where the parachute system controls are used within their limitations. To a lesser extent a parachute system can be controlled remotely. Although some experimental remote-control descents have been made, such systems are neither common nor well developed. Anyone planning a parachute drop from a balloon must anticipate that the landing

site cannot be selected precisely, that the system will be drifting horizontally at the time of impact, and that an oscillation of the system probably will cause the payload to be tilted at touchdown.

Proper planning and execution can make parachute descents safe and effective despite difficulties. Carefully designed buffer systems, such as a framework which yields progressively or honeycomb crush pads can be used to absorb the kinetic energy that the system has at the moment of impact. Forecasts by a competent meteorologist can prevent flights from being undertaken when low level winds at the landing site are likely to be excessive, and can provide descent drift vectors in the flight termination area. A drift vector is based on the winds anticipated at all levels through which the parachute system must descend, and it lets the flight controller on the scene estimate the landing site from the known position of the balloon system at the time of flight termination. Stable parachutes, i.e., parachutes which do not oscillate during descent, may also be used to increase the probability that the payload will land upright so that the landing buffer system will have an opportunity to function properly. Unfortunately, choosing a stable parachute may lead to other compromises, such as slow

opening or less certain opening, which may be unacceptable. Available data are inadequate to answer this question definitively.

1. A Simplified Descent Model

Equation (1) and the concept of terminal velocity provide a starting point for a simplified theoretical model of a parachute system descending in the atmosphere which simulates many of the features of a real descent. For a given parachute system at a level in the atmosphere where ρ and g are known, a value of v_T can be calculated using Eq. (3). Unless the parachute system has reached the steady state phase of its descent, the terminal velocity will not constitute a good approximation to the actual velocity. It may, however, be viewed as a value toward which the actual velocity tends, and it is a convenient single variable which may be substituted for a combination of others.

Substituting from Eq. (2) into Eq. (1) and rearranging gives

$$\frac{dv}{dt} = \frac{g}{v_T^2} (v^2 - v_T^2) \quad (4)$$

if it is assumed that $m_v = m = \text{const.}$ Equation (4) may also be written

$$\frac{dv}{v^2 - v_T^2} = \frac{g}{v_T^2} dt \quad (5)$$

Now although both g and v_T are functions of time during descent, they both change slowly. Let it be assumed that over a short time interval they may be treated as constants.

In phase 1 of the descent, the canopy is not inflated. Consequently, the cross-sectional area of the system is quite small. Air density will also be small, and although the drag coefficient may be relatively large, the magnitude of v_T will be large during phase 1. Assume further that the change from phase 1 to phase 2 is instantaneous--that is, the canopy snaps instantly from its deployed but uninflated state to a state of full inflation. This is not entirely in keeping with the actual behavior of a parachute, but, as will be shown later, it leads to conservative results from the design and planning point of view.

Throughout phases 2 and 3 the parachute remains essentially unchanged; therefore, A may be considered constant. The drag coefficient is a function of Reynolds number, Re , and therefore of the actual speed and dimensions of the parachute system, the air density, and air viscosity. For Reynolds numbers associated with a parachute system in phases 2 and 3, however, the dependence of C_D on Re is weak and the assumption of constant C_D is realistic.

Density is then essentially the only variable in v_T ; therefore, any time interval in which ρ does not change significantly will be short enough to justify the assumption that v_T is constant.

Integrating Eq. (5) once yields

$$-\frac{1}{v_T} \tanh^{-1} \frac{v}{v_T} = \frac{gt}{v_T^2} + C \quad \text{for } \frac{v}{v_T} < 1 \quad (6)$$

$$\text{or } -\frac{1}{v_T} \coth^{-1} \frac{v}{v_T} = \frac{gt}{v_T^2} + C \quad \text{for } \frac{v}{v_T} > 1 \quad (7)$$

$$\text{or } v = \text{const} = v_T \quad \text{for } \frac{v}{v_T} = 1 \quad (8)$$

a. Phase 1. Let $t = t_0 = 0$ be the time at which the parachute is separated from the balloon. At that time $v = v_B$ (velocity of the balloon); consequently, the constant of integration, C , in Eq. (6) is $(-1/v_T) \tanh^{-1}(v_B/v_T)$. Because v_B is frequently zero and is always small compared to v_T , the integration constant may be ignored in most descents. It will be considered negligible here in further discussions of phase 1. In phase 1, $(v/v_T) < 1$; therefore Eqs. (7) and (8) are not applicable.

Equation (6) may now be written

$$v = v_T \tanh \left(-\frac{gt}{v_T} \right) \quad (9)$$

Note that in the coordinate system in use here, $v_T < 0$. Thus the argument of the hyperbolic tangent is positive and grows linearly with time. As time increases, $\tanh(-gt/v_T)$ also increases, approaching but never reaching one. Similarly, v will approach but never reach v_T . This tendency of v to approach v_T as a limiting value is characteristic of the descent model used here. For practical purposes, $v = v_T$ and Eq. (6) degenerates into Eq. (8) when $(-gt/v_T)$ grows larger than three.

Substituting dH/dt for v in Eq. (9) and integrating yields

$$H = -\frac{v_T^2}{g} \ln \cosh\left(-\frac{gt}{v_T}\right) + C \quad (10)$$

where H is height and C is the constant of integration. When $t = t_0$,

$H = H_0$; therefore, $C = H_0$ and

$$H = H_0 - \frac{v_T^2}{g} \ln \cosh\left(-\frac{gt}{v_T}\right) \quad (11)$$

Differentiating Eq. (9) yields acceleration in terms of t as follows:

$$\frac{dv}{dt} = g \left[\tanh^2\left(-\frac{gt}{v_T}\right) - 1 \right] \quad (12)$$

Examination of Eq. (12) shows the acceleration to be made up of two parts, one of which is downward (negative) and one upward, and the upward accelera-

tion grows with time. The growth term can never quite reach one, although for practical purposes it will have done so when $(-gt/v_T)$ has reached 3.0. At that time acceleration will have ceased, and the descending system will have reached terminal velocity.

Equations (9), (11), and (12) contain a description of the motion of a parachute system starting from rest and descending without change of shape in a homogeneous atmosphere. If interest is restricted to a short time interval so that the stratum through which the system falls in that interval is thin, the restriction on homogeneity may be relaxed.

b. Phase 2. Equations (7) and (8) as well as Eq. (6) must be considered in a discussion of phase 2 because the magnitude of the downward velocity may be less than, equal to, or greater than the magnitude of v_T . The initial velocity in phase 2 in the descent model being used is equal to the final velocity in phase 1. This permits evaluation of the constants of integration in Eqs. (6) and (7). Thus for $t = t_1$ (the time of inflation of the canopy and the initiation of phase 2) $v = v_1$, and from Eqs. (6) and (7) respectively

$$C = -\frac{1}{v_T} \tanh^{-1} \frac{v_1}{v_T} - \frac{gt_1}{v_T^2}$$

$$C = -\frac{1}{v_T} \coth^{-1} \frac{v_1}{v_T} - \frac{gt_1}{v_T^2}$$

Substituting these in Eqs. (6) and (7) and solving for v yields

$$v = v_T \tanh \left[\tanh^{-1} \frac{v_1}{v_T} - \frac{g(t-t_1)}{v_T} \right] \quad \text{for } \frac{v_1}{v_T} < 1 \quad (13)$$

$$\text{and } v = v_T \coth \left[\coth^{-1} \frac{v_1}{v_T} - \frac{g(t-t_1)}{v_T} \right] \quad \text{for } \frac{v_1}{v_T} > 1 \quad (14)$$

Integrating Eqs. (13) and (14) gives

$$H = H_1 + \frac{v_T^2}{g} \left\{ \ln \cosh \tanh^{-1} \frac{v_1}{v_T} - \ln \cosh \left[\tanh^{-1} \frac{v_1}{v_T} - \frac{g(t-t_1)}{v_T} \right] \right\} \quad \text{for } \frac{v_1}{v_T} < 1 \quad (15)$$

$$H = H_1 + \frac{v_T^2}{g} \left\{ \ln \sinh \coth^{-1} \frac{v_1}{v_T} - \ln \sinh \left[\coth^{-1} \frac{v_1}{v_T} - \frac{g(t-t_1)}{v_T} \right] \right\} \quad \text{for } \frac{v_1}{v_T} > 1 \quad (16)$$

Similarly Eq. (8) may be integrated to give

$$H = H_1 - v_T(t-t_1) \quad \text{for } \frac{v_1}{v_T} = 1 \quad (17)$$

Differentiating Eqs. (13) and (14) provides the following expressions

for acceleration as functions of t :

$$\frac{dv}{dt} = g \left\{ \tanh^2 \left[\tanh^{-1} \frac{v_1}{v_T} - \frac{g(t-t_1)}{v_T} \right] - 1 \right\} \quad \text{for } \frac{v_1}{v_T} < 1 \quad (18)$$

$$\frac{dv}{dt} = g \left\{ \coth^2 \left[\coth^{-1} \frac{v_1}{v_T} - \frac{g(t-t_1)}{v_T} \right] - 1 \right\} \quad \text{for } \frac{v_1}{v_T} > 1 \quad (19)$$

Also, from the definition of v_T

$$\frac{dv}{dt} = 0 \quad \text{for } \frac{v_1}{v_T} = 1 \quad (20)$$

Equations (18) through (20) are plotted in dimensionless form in Fig. 2. Two distinctive features of the descent model are immediately obvious. First, the acceleration at time $t = t_1$ is very sensitive to the value of the ratio (v_1/v_T) . Thus for low acceleration the parachute should inflate when this ratio is small. In fact, if inflation occurs before the velocity of the system has reached the inflated terminal velocity, downward acceleration will continue until $v = v_T$. If inflation should occur just as

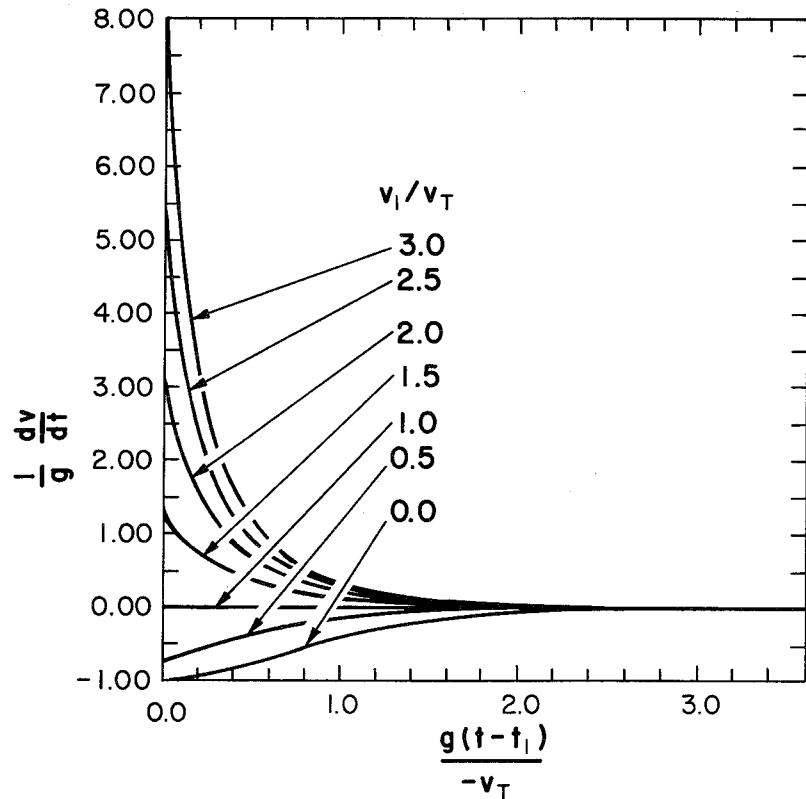


Fig. 2. Acceleration versus time for a parachute system for which terminal velocity is constant. Acceleration is in effect plotted as multiples of the acceleration of gravity and time as multiples of $(-v_T/g)$.

inflated terminal velocity is reached, acceleration will cease. If, on the other hand, inflation does not occur until the system velocity has exceeded the terminal velocity of the inflated system, an upward acceleration will immediately start to slow the descent. The magnitude of that acceleration is most easily determined from Eq. (4) written as follows:

$$\left(\frac{dv}{dt}\right)_1 = g \left[\left(\frac{v_1}{v_T}\right)^2 - 1 \right]$$

The subscript 1 is used to denote that the events are occurring at the instant of inflation, i.e., at $t = t_1$. If this equation is multiplied through by the mass of the system, it may be written

$$m \left(\frac{dv}{dt}\right)_1 = mg \left(\frac{v_1}{v_T}\right)^2 - mg$$

Thus the forces acting on the system are the upward drag and the downward weight. Since the drag is exerted almost wholly on the canopy of the parachute, the suspension system must be strong enough to withstand at least the force $mg(v_1/v_T)^2$. This force is called opening shock. In this model it is proportional to the square of the velocity at the time of inflation. Equation (9) shows that the system velocity increases in phase 1 as a func-

tion of time up to its uninflated terminal velocity, and since the uninflated terminal velocity can be several times as great as the inflated terminal velocity, early inflation will assure low opening shocks, while delayed inflation will cause large opening shocks. This is contrary to the experience of parachutists jumping from high-speed aircraft. Their initial speed through the air is generally greater than the magnitude of their terminal velocity without a parachute. Therefore, their speed starts to decrease immediately, and they realize a lower opening shock by waiting until they have reached the terminal velocity of their own body to "pop the chute."

The second distinctive feature of Fig. 2 is that regardless of the magnitude of the acceleration at the time of inflation, it has, for practical purposes, been reduced to zero after an elapsed time $(t-t_1) = -3v_T/g$.

Figure 3 shows time vs acceleration traces for two parachute systems descending according to this model. Since time is shown in the dimensionless form which involves v_T , the time scale changes at $t = t_1$. The symbols $v_{T,1}$ and $v_{T,2}$ are used for the terminal velocities in phases 1 and 2, respectively.

The curve for a system which does not open until $v = v_1 = 2v_{T,2}$ is the curve labeled 1,2,3,4,5,6. At point 1 the parachute is separated from

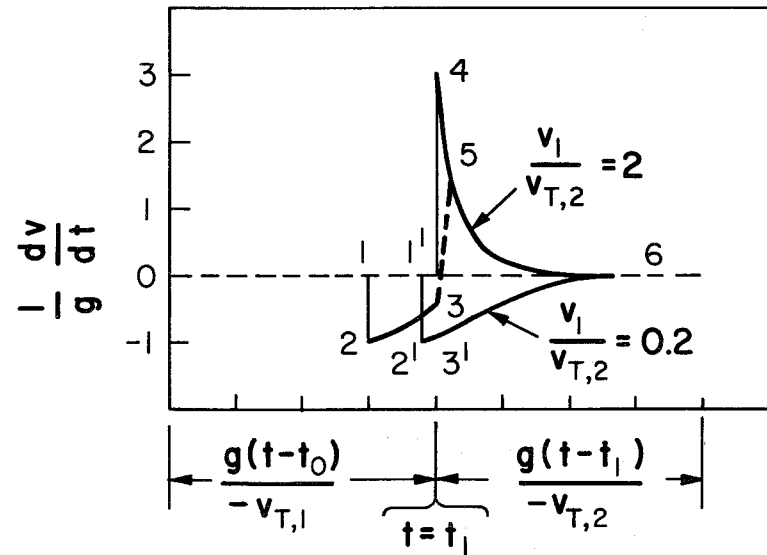


Fig. 3. Acceleration traces of quick-opening and delayed-opening parachutes.

the balloon. A downward acceleration of 1 g occurs immediately, as shown by point 2. The magnitude of that acceleration is then decreased slowly by the drag of the system with a deployed but uninflated parachute until at point 3 opening occurs instantaneously, and the acceleration changes to an upward acceleration of 3 g (point 4). This decays rapidly, reaching zero at point 6. More realistically, the parachute does not open instantaneously, and the change from a downward to an upward acceleration occurs over a small time increment along a path something like that shown from point 3 to point 5. This decreases the maximum acceleration the system will experience; therefore, the model used here is conservative from the design point of view. A more realistic model is discussed by Heinrich and Noreen (2), who have studied the forces on a parachute during the period of opening.

The curve labeled 1', 2', 3', 6 is representative of a parachute system whose parachute opens well before the system velocity has reached $v_{T,2}$. Its general characteristics have already been explained.

Opening accelerations as great as 16 g have been reported in parachute drops from balloons by Niccum and Aube (3), but 70% of the accelerations

they reported were under 4 g. The accelerometers used were mounted in such a way that they may have sensed large accelerations which were internal to the suspension system. Unfortunately, neither the time of opening nor the downward speed at the time of opening could be determined reliably from the data; therefore, attempts to check these data against other observations and against theory led to inconclusive results. These data point to the possibility of high opening accelerations, but the known areas of uncertainty in the measurements suggest that the values are too high so that they also are generally conservative for design purposes.

The graphs of Eqs. (8), (13), and (14) are shown in Fig. 4, also in dimensionless form. The curves of $(v_1/v_T) = \text{constant}$ on this graph resemble the curves in Fig. 2. The most significant feature is that regardless of the velocity at the time of inflation, within an elapsed time given by $(t-t_1) = -3v_T/g$, the descent velocity will have become very nearly equal to the terminal velocity.

Equations (15) through (17) are plotted in dimensionless form in Fig. 5. The curves show the rather obvious fact that a parachute system will

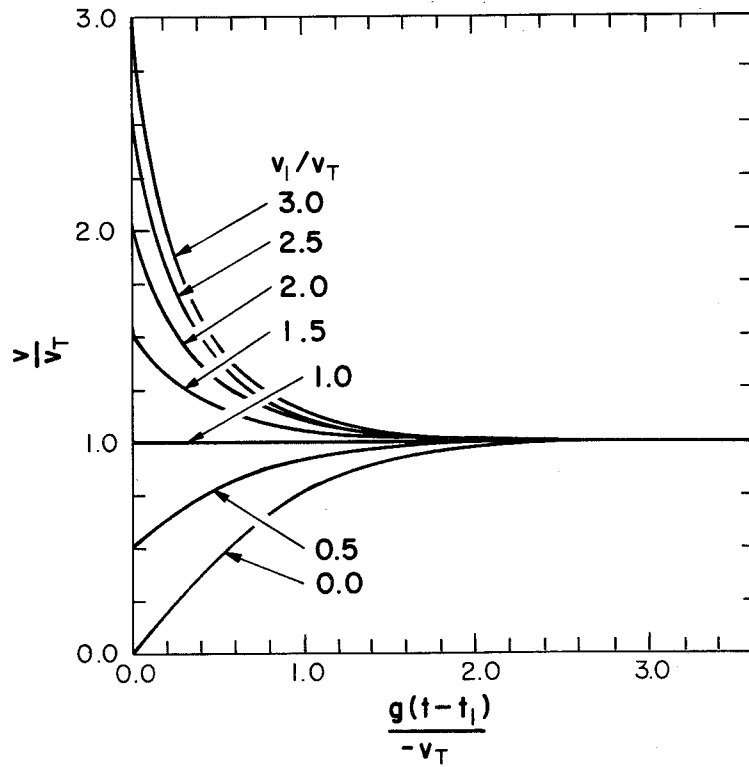


Fig. 4. Descent velocity vs time for a parachute system for which terminal velocity is constant. Velocity is plotted as a multiple of v_T and time as a multiple of $(-v_T/g)$.

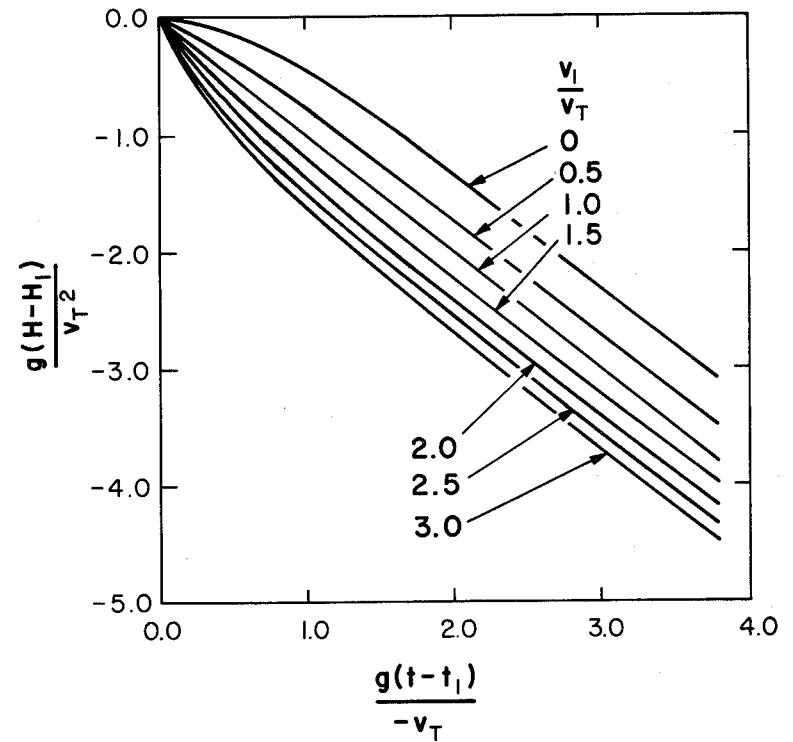


Fig. 5. Loss of altitude vs time for a parachute system for which terminal velocity is constant. Height difference is in effect plotted in multiples of (v_T^2/g) and time in multiples of $(-v_T/g)$.

have descended further in a given time if it had a high downward velocity at the time of inflation than if its velocity were low. After $-g(t-t_1)/v_T$ exceeds 3.0, however, the separation remains virtually constant.

The time period given by $(t_2-t_1) = -3v_T/g$ is the period required for a descending parachute system to accelerate from its opening velocity v_1 to its terminal velocity v_T . Time t_2 is then the time at which phase 2 ends and phase 3 begins. The change of v_T during phase 2, because of the change in air density, is large enough in descents from altitudes in excess of 30km that holding it constant may produce errors of up to 10% in the calculated distance traveled during phase 2. Such errors are rarely important, but they can be overcome by slicing the atmosphere into thin strata and using the mean value of the terminal velocity within each stratum to calculate descent data.

c. Phase 3. As soon as an inflated parachute system has reached terminal velocity, i.e. when $(t-t_1) = -3v_T/g$, it will enter phase 3. Equations (13) through (20) and Eq. (8) are valid for this phase of descent, but the smaller set consisting of Eqs. (8), (17), and (20) provides an

adequate description of the descent in phase 3 of this model. Because v_T is not constant throughout the deep atmospheric stratum through which a parachute system descends in phase 3, the equations must be applied through a number of thin strata with v_T calculated from Eq. (3) for each stratum.

d. Phase 4. The few seconds immediately preceding and following the actual landing of a parachute system are the most critical in the descent. Descent velocity is given adequately by Eq. (8) and hence by Eq. (3) if the system has passed through phase 2 before reaching the surface.

Any acceleration of the payload immediately prior to landing which is large enough to be important will be due to an oscillation of the system about the vertical. Such accelerations are internal to the parachute system; their principal consequence is to decrease the probability that the payload will land on its base, but motion of the payload because of them may cause the payload to have a velocity significantly different from the motion of the system as a whole.

Horizontal motion is quite important, and an appropriate balance between the horizontal and vertical velocity components is a consideration in selecting a parachute for a given job. From Eq. (3) it appears that large parachutes can be selected to produce a low vertical velocity and

assure a relatively soft landing. If winds exist near the surface, however, lower vertical velocities increase the probability that the system will drag on obstacles, such as power lines, trees, etc. during the final seconds of descent; this in turn increases the probability of damage to people and property, as well as to the payload. A large parachute also increases the likelihood that the payload will be dragged by the wind after landing. The drag force is given approximately by Eq. (2) written as

$$F = \frac{1}{2} C_D \rho A v_w^2, \text{ where } v_w \text{ is the speed of the surface wind.}$$

Separation of the parachute and payload upon landing would obviate the danger of dragging, but unless the separation mechanism were highly reliable, it could cause greater danger by causing premature separation.

D. CONSIDERATIONS IN SELECTING A PARACHUTE

To be satisfactory for scientific ballooning a parachute should be highly reliable, and it should prevent accelerations, including landing accelerations that are destructive to the payload. Choosing a parachute involves making compromises between conflicting demands, and because of incomplete knowledge of parachute behavior at high altitude, the selection of one type of parachute over another is often a matter of personal pref-

erence. This discussion is therefore limited to a brief summary of the questions usually considered in selecting a parachute and to aids which are general enough to be used with several types of parachutes.

The most important factors in selecting a parachute are those which are directly concerned with safety. At the very least, a parachute must open reliably and be strong enough to withstand any opening shocks and carry the weight of the payload in all conceivable situations; it must also be capable of slowing the entire system to an acceptable vertical velocity at landing. Other features may also be desirable, e.g., that the parachute not swing or spin during descent; but unless these can be provided without sacrificing the features which are essential to safety, they should not be considered.

Two types of parachutes have been used enough for scientific ballooning flights to be considered proven. One has a flat circular canopy with a vent in the center; the other has a canopy in the form of a cross with no vent. The flat circular canopy is known to open reliably and rapidly even at the high altitudes where it is used in scientific ballooning. It is commercially available in sizes up to 30 meters in diameter, and two or more

can be used together. Its terminal velocity can be predicted accurately when it is used within proper load limits. Its chief drawback is its tendency to oscillate more than is desirable during descent.

Parachutes with cross-shaped canopies have been used in scientific ballooning almost exclusively by the firm which manufactures them. Their use has been reported informally by a representative of the Office of Naval Research (4) for whom they have been flown. They have performed well in all respects and are less subject to oscillation than flat canopy parachutes. No load more massive than 365kg (800 lbs) has been flown on one, and no flight has been made which used two or more of them together. At present, anyone desiring parachute descent for a heavy load will find that the history of satisfactory descents with comparable loads is much more extensive for flat canopy parachutes than for any other type.

1. Parachute Size

To determine the parachute size required for a particular job, the mass of the payload and the permissible vertical velocity at impact must be known. The mass of the payload can usually be determined by simply weighing it, but the permissible vertical velocity at impact must normally

be based on a value judgment. If a payload is particularly sensitive to shock, a large parachute can be used. An oversized parachute is not likely to give greater protection than a smaller one, however, unless it is used when surface winds are lower. Therefore, using a larger parachute than is considered optimum for general safety will increase the time one must wait for satisfactory weather conditions. Added to the cost of waiting is the cost of purchasing and maintaining the larger parachute. Since most of the reasons underlying the determination of an acceptable vertical landing speed can only be stated qualitatively, no quantitative guide to choosing it is offered. Vertical speeds of 7 to 8 m/sec (~25 ft/sec) have been found to give results which are acceptable for most payloads.

A solution of Eq. (3) in SI units, using sea level values of g and ρ from the U.S. Standard Atmosphere, 1962, is shown in graphical form in Fig. 6. This graph is reproduced in a more usable size in Section XII, together with a similar graph in English units. On the first pass through this graph, the user does not ordinarily know parachute mass and must approximate it. The mass of the payload multiplied by 1.05 is an adequate first approximation of the total system mass. With values for the system mass and the

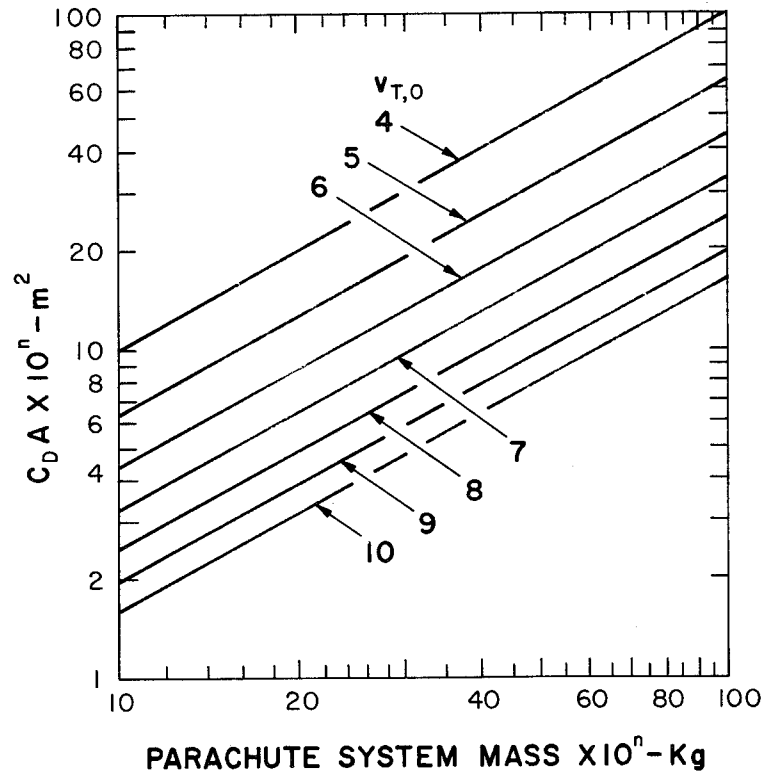


Fig. 6. Sea level terminal velocity of a parachute as a function of parachute system mass and the product of parachute area and drag coefficient. Numbers on the abscissa and ordinate may be multiplied concurrently by any factor 10^n to cover all non-zero values.

sea level terminal velocity, one may use the graph to determine a value of the product $C_D A$. Note that the numbers on the abscissa may be multiplied by a factor 10^n , where n may take any value, provided only that the numbers on the ordinate are also multiplied by the same factor. Thus, the graph can be used for any non-zero mass.

Having obtained a first approximation for $C_D A$ from Fig. 6, one may enter that value in Fig. 7 to obtain the diameter of a parachute if the value of C_D is known. Figure 7 is a graphical representation of the equation $C_D A = C_D' \pi (D/2)^2$; therefore, if the C_D for an inflated circular parachute is used, the value of D obtained from Fig. 7 will be the effective or projected diameter of the parachute (see Fig. 1). This value of D is not often of direct interest, however, because parachutes are described by the nominal diameter of the canopy. (See Section X.B.) To obtain the nominal diameter from Fig. 7, a pseudo drag coefficient must be used. Although the pseudo drag coefficient is usually determined experimentally, its significance can be readily explained.

Let C_D' and A' be the pseudo drag coefficient and the nominal area, respectively, of a parachute having an effective drag coefficient C_D and

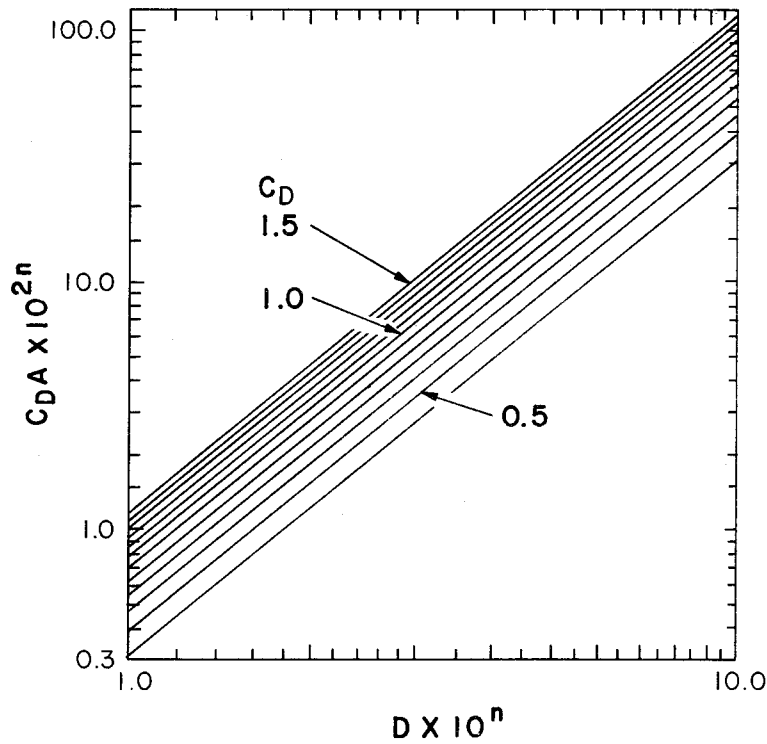


Fig. 7. Nominal diameter of a parachute as a function of area and drag coefficient. Numbers on the ordinate may be multiplied by 10^n if numbers on the abscissa are concurrently multiplied by 10^{2n} to cover all non-zero values.

effective area A so that $C_D' A' = C_D A$. Also let the nominal area be defined as the area of a circle of nominal diameter D' . Then if C_D' is defined so that $C_D A = C_D' \pi (D'/2)^2$ and its value is known, D' can be determined from Fig. 7. An excellent example of the use of the concept of pseudo drag coefficient is provided by the cross-shaped canopy. Rarely is its effective area or its drag coefficient known, but for one such parachute design, the product of the two is known to be given with acceptable accuracy by multiplying the area of a circle whose diameter is equal to the length of one of the cross members of the canopy by 0.55. Thus C_D' is 0.55 and D' is the length of the cross member for this particular parachute design.

Although parachutes can be manufactured in any size, it is more practical to manufacture them in certain discrete sizes, and it is rare that the size indicated by the selection process described thus far will agree precisely with one of the sizes commonly manufactured. Usually a scientific ballooning group will have parachutes of various sizes on hand, and a size can be selected which has a nominal diameter close to the first estimate of the required value. The known mass and the $C_D' A'$ of that parachute can then be used in conjunction with Fig. 6 to obtain the sea level terminal

velocity of the parachute system. If that velocity is too low or too high to be satisfactory, the data of the next smaller or the next larger parachute may be checked.

It is possible that the altitude of the anticipated landing site will be so far above sea level that the terminal velocity there will be significantly different from that at sea level. The curve in Fig. 8 labeled v_T provides a simple way to approximate the terminal velocity at any level up to 52km if the sea level terminal velocity is known. If $v_{T,0}$ is the sea level terminal velocity and v_T is the terminal velocity at any other level, then from Eq. (3)

$$v_T/v_{T,0} = \sqrt{\rho_0/\rho} \quad (21)$$

assuming that m , g , C_D , and A do not change with height. From Eq. (21) $v_T/v_{T,0}$ may readily be plotted as a function of ρ , and since ρ is a function of height in the atmosphere (see Section XI), $v_T/v_{T,0}$ may also be plotted as a function of height. That has been done in Fig. 8, using the relationship between ρ and H given in the U.S. Standard Atmosphere, 1962. Thus it is only approximate for the real atmosphere.

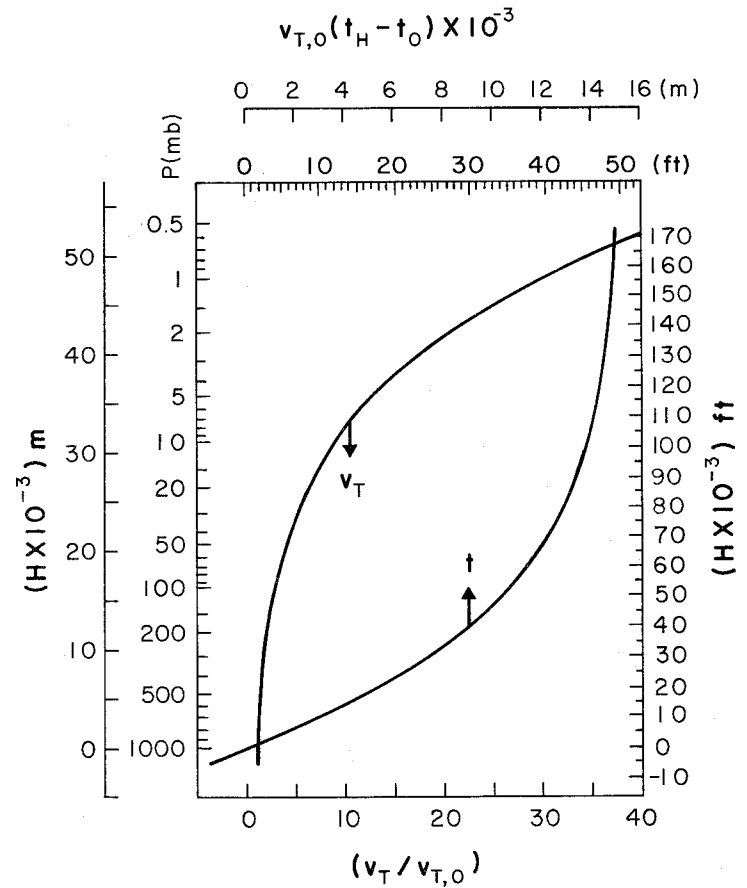


Fig. 8. Terminal velocity and time of descent as functions of sea level terminal velocity and altitude in the U.S. Standard Atmosphere, 1962.

It is apparent that the change of $v_T/v_{T,0}$ in the lowest 3km is not great enough to be resolved satisfactorily in Fig. 8. Yet it is that stratum in which almost all landings will occur. In it the linear relations $v_T/v_{T,0} = 1 + 5 \times 10^{-5}H$, where H is in meters above sea level, and $v_T/v_{T,0} = 1 + 1.52 \times 10^{-5}H$, where H is in feet, yield good approximations. Thus at 1 km (~3000 ft), v_T is 5% larger than at sea level, a difference which is nearly equal to the difference (error) which must be anticipated between the calculated and observed sea level terminal velocities. Nonetheless, the difference will occasionally justify using a larger parachute for a landing at a higher altitude than might be used at sea level.

2. Multiple Parachutes

It is sometimes convenient or necessary to use two or more parachutes to lower a load. Many low level, multiple parachute drops have been made; a few have been made successfully from balloon float altitudes. Thus it is known that drops using a cluster of parachutes are feasible, but the number of multiple parachutes flights on balloons to date has been too limited to warrant the degree of confidence that has been established for parachutes used singly.

The number and size of parachutes required to lower a load when more than one is needed may be determined by the procedure discussed above if 1) all parachutes used together are alike and the same size, 2) the drag coefficient of the cluster can be determined from the drag coefficient of one parachute used alone, and 3) the nominal area of a cluster of N parachutes is equal to the nominal area of a single one times N. Then one may enter Fig. 6 with 1.05 times the mass of the payload and the desired landing velocity (suitably corrected to sea level terminal velocity) to obtain $C_D A$. Dividing $C_D A$ by N and entering Fig. 7 with the quotient and C_D' for the cluster yields D' for one of the parachutes of the cluster. If there are N parachutes of nominal diameter D' available, the solution should be checked using the mass and C_D' data of the actual parachutes. If there are not N parachutes of diameter D' available, another value of N may be tried. When a satisfactory check is achieved using the data of available parachutes, the problem is solved.

The value of C_D' for a cluster of identical flat, circular, solid cloth canopy parachutes may be approximated by the equation $C_D'(\text{cluster}) = C_D'(\text{individual}) \times (0.95 - 0.3N)$ for $2 \leq N \leq 6$. Incidentally, a cluster of

flat canopy parachutes is more stable than a single one. The value of C_D' for a cluster of identical parachutes whose canopies have large geometric porosity (e.g. ribbon, ring slot, or cross-shaped parachutes) is nearly identical to the value of C_D' for one of the individual parachutes.

3. Time of Descent

Recalling that $v_T = (dH/dt)_T$, Eq. (21) may be written

$$\frac{dH}{dt} = v_{T,o} \sqrt{\frac{\rho_o}{\rho}} \quad (22)$$

where one of the T subscripts has been omitted for convenience. This may be integrated as follows:

$$v_{T,o}(t_H - t_o) = \rho_o^{-\frac{1}{2}} \int_0^H \rho^{\frac{1}{2}} dH \quad (23)$$

The integration indicated on the right side of Eq. (23) can be performed if ρ is a known function of H; integration in the Standard Atmosphere yields the curve labeled t in Fig. 8. A value of $v_{T,o}(t_H - t_o)$ may be determined from the curve if the altitude of a parachute system is known. That value divided by the sea level terminal velocity of the system is the time required for the system to descend to sea level. The time of descent between any two levels may also be determined; it is the difference between

the two $v_{T,o}(t_H - t_o)$ values divided by $v_{T,o}$. If the two levels are close together, however, a more accurate result may be obtained by dividing the thickness of the stratum by the mean velocity within the stratum as determined from the v_T curve.

A number of auxiliary scales have been placed on Fig. 8 to make it more versatile. The terminal velocity, v_T , obtained from the figure will be in the units in which $v_{T,o}$ is expressed. Since $v_{T,o}(t_H - t_o)$ is a length, scales are given in both meters and feet; the scale to be used must be compatible with the units in which $v_{T,o}$ is expressed. The resulting time units are easily determined: for example, if $v_{T,o}(t_H - t_o)$ is read in feet and $v_{T,o}$ is expressed in feet per minute, time will be determined in minutes.

REFERENCES

- (1) U.S. Air Force, 1963: Performance of and Design Criteria for Deployable Aerodynamic Decelerators, Technical Report No. ASD-TR-61-579 of the U.S. Air Force Flight Dynamics Laboratory, Research and Technology Div., Air Force Systems Command, Wright-Patterson AFB, Ohio.
- (2) Heinrich, H.G. and R. A. Noreen, 1969: Analysis of Parachute Opening Dynamics with Supporting Wind Tunnel Experiments. In Proc., Aerodynamic Decelerations Systems Conference of Sept. 23-25, 1968, Vol. I-- Technical Report No. 69-11, Defense Document Center, Cameron Station, Alexandria, Va.
- (3) Niccum, R. J. and A. E. Aube, 1968: Heavy Load Recovery from High Altitude Balloon Borne Platforms. In Proc., Aerodynamic Deceleration Systems Conference of Sept. 23-25, 1968, Vol II--Technical Report No. 69-11, Defense Document Center, Cameron Station, Alexandria, Va.
- (4) Cross, William F., CDR, USN, February 22, 1972: Personal communication.

THE ATMOSPHERE

by

Alvin L. Morris and Samuel B. Solot

List of Symbols	ii	a. <u>The quasi-biennial oscillation.</u>	49
List of Figures	v	b. <u>The semiannual oscillation.</u>	53
List of Tables	vii	4. <u>Middle Latitude Vertical Structure in the Free Atmosphere.</u>	56
A. INTRODUCTION	1	5. <u>Boundary Layer</u>	60
B. OPERATIONAL METEOROLOGICAL REQUIREMENTS	3	6. <u>Low-Level Jet</u>	64
1. <u>Inflation</u>	4	E. OTHER METEOROLOGICAL VARIABLES, DATA SOURCES.	69
2. <u>Launch</u>	6	F. FORECASTS	75
3. <u>Ascent</u>	13	G. OPERATIONAL PLANNING.	76
4. <u>Tracking and Float</u>	13	REFERENCES.	79
5. <u>Descent</u>	15		
6. <u>Landing and Recovery</u>	17		
C. THERMAL STRUCTURE OF THE ATMOSPHERE	18		
1. <u>Temperature and Density</u>	18		
a. <u>The hydrostatic relationship</u>	18		
b. <u>The U.S. Standard Atmosphere, 1962</u>	25		
c. <u>Supplementary atmospheres</u>	29		
d. <u>Mean thermal structure</u>	33		
2. <u>Thermal Radiation</u>	33		
D. CIRCULATION	35		
1. <u>Mean Zonal Structure</u>	35		
2. <u>Polar Wind Structure</u>	47		
3. <u>Equatorial Zonal Wind Structure</u>	48		

List of Figures

Fig. 1	Balloon during inflation. The gas bubble is restrained by a roller through which the balloon may move.	5	Fig. 11	Typical summer anticyclonic vortex in the upper stratosphere. See Fig. 10 for explanation of the isolines . . .	40
Fig. 2	Static launch	7	Fig. 12	Time-Height cross section of the mean monthly zonal winds in the southern U.S. stratosphere	42
Fig. 3	Dynamic launch	8	Fig. 13	Well developed wave in the winter westerlies. Note the variety of wind directions on each pressure surface and the differences which occur between the surfaces, i.e., essentially between 54 km (a) and 41 km (b). See Fig. 10 for explanation of the isolines	44
Fig. 4	Temperature as a function of geopotential height in the <u>U.S. Standard Atmosphere, 1962</u>	28	Fig. 14	Transition from a winter cyclonic circulation to a summer anticyclonic circulation. A small anticyclone has formed in the vicinity of the pole and is spreading equatorward. See Fig. 10 for an explanation of the isolines	46
Fig. 5	Temperature-Height profiles of the 30 ^o , 45 ^o , 60 ^o , and 75 ^o N January and mid-latitude spring/fall Supplementary Atmospheres	30	Fig. 15	Time-Height cross section of mean monthly zonal winds at Canton Island (1953--Aug. 1967) and at Gan/Maledive Islands (Sept. 1967--1970). From Kriester (11). Lines are isolines of wind speed in meters per second	50
Fig. 6	Temperature-Height profiles of the 30 ^o , 45 ^o , 60 ^o , and 75 ^o N July and 15 ^o N annual Supplementary Atmospheres.	31	Fig. 16	Amplitude of the quasi-biennial and semiannual, equatorial oscillations as functions of height. Also, time of occurrence of maximum west winds (phase) of the semiannual oscillation in months	51
Fig. 7	Percentage departure from standard of densities of certain supplemental atmospheres given in reference (2)	32	Fig. 17	Estimated variation of zonal wind with month and altitude at the equator. After Reed (9)	54
Fig. 8	Mean thermal structure of the atmosphere in summer and winter, after Palmén and Newton (5)	34	Fig. 18	Selected zonal wind profiles for the White Sands Missile Range, New Mexico	57
Fig. 9	Mean zonal wind in summer and winter, after Palmén and Newton (5)	36			
Fig. 10	Typical winter cyclonic vortex in the upper stratosphere. Winds flow along the height contours (solid lines). The speed is indicated by the feathers--each flag represents 50 knots, each bar 10 knots, and a half bar 5 knots. The dashed lines are isotherms of temperature in °C	39			

Fig. 19 Dimensionless wind profiles according to the power-law.
 The value of b may be estimated from the scale at the top if dT/dz is known add 0.1 to the value of b estimated from dT/dz if the terrain is rough or wooded 63

Fig. 20 Mean cross section of the wind associated with a low-level jet, from Bonner et al. (20). The solid lines are isotachs of the wind component parallel to the jet axis; dashed lines are isotachs of the normal component 65

Fig. 21 Average vertical wind shear (m/sec km) in a vertical cross section normal to the core of the jet, after Bonner et al. (20) 66

Fig. 22 Mean wind component along the jet axis at the 0.5-km level, after Bonner et al. (20). 67

List of Tables

Table 1 Defining temperature vs height relationships in the lowest 61 km of the U.S. Standard Atmosphere, 1962 . . . 27

THE ATMOSPHERE

A. INTRODUCTION

Balloon flight is possible only because the density of the atmosphere in which a balloon is embedded is equal to or greater than the density of the balloon system. Therefore, atmospheric density is vitally important to the success of ballooning. The engineer who must calculate lift tables is keenly aware of this (see Section IV). The engineer who must calculate heat exchange between the balloon system and the environment (Section III) is also interested in the density of the balloon's immediate environment. These people must consider the composition of the environment also, at least to the point of determining whether changes of composition are significant to them. To a large extent, however, scientific ballooning needs for density and composition data are adequately met by some sort of mean or standard atmosphere.

The U.S. Standard Atmosphere, 1962, (1) is a model atmosphere which has gained widespread acceptance. When the expression "Standard Atmosphere" is used in this section, it should be understood that the U.S. Standard Atmosphere, 1962, is being named. In the Standard Atmosphere temperature

and composition are defined as functions of height. A number of other useful properties can be derived from the defining properties.

To fulfill the need for atmospheric data at high and low latitudes and in the hot and cold seasons for which the Standard Atmosphere is not adequate, supplementary model atmospheres have been defined. The most generally accepted of these are described in U.S. Standard Atmosphere Supplements, 1966

(2). Each represents approximately the mean state of the real atmosphere at some season and latitude. Thus, they provide some information about the temporal and latitudinal variability of the real atmosphere.

Balloon flight personnel and meteorologists who must provide atmospheric information for balloon operations find that wind is the most critical atmospheric variable. There are others, e.g., cloudiness, which may affect operations, but most of them are not of such continuing concern as wind. Unfortunately, the range of variation of the wind is so great and wind data are so sparse at the high altitudes at which modern balloons are flown that reliable mean values are available only in a few locations. Idealized circulation models based on the wind data available must, therefore, be used with full appreciation of their limitations.

The task of forecasting the actual state of the atmosphere a few days or hours in advance of a balloon flight demands understanding of the behavior of the atmosphere and data from which to establish its state at some time before the forecast period. Large balloon systems fly higher than meteorological sounding balloons. Rocket soundings provide data at these levels in a few locations and on a quite limited schedule. Despite the difficulties, experienced forecasters can provide 24-hour wind forecasts which are accurate enough to be useful for flight operations, and they can provide planning data on winds weeks or months in advance.

In this section the most important properties of the atmosphere in its relationship to scientific ballooning are discussed. Also, forecast and planning problems are covered briefly to give the non-meteorologists an idea of the magnitude of the forecaster's task and to suggest to meteorologists who have not supported ballooning operations the requirements for this task. Equations and data which are useful to an engineer who needs information about the atmosphere for his work are also provided.

B. OPERATIONAL METEOROLOGICAL REQUIREMENTS

To simplify the discussion, a balloon flight will be arbitrarily divided

into the following stages: 1) inflation, 2) launch, 3) ascent, 4) tracking and float, 5) descent, and 6) landing and recovery.

1. Inflation

Figure 1 illustrates a balloon during inflation. Many variations of the technique shown in Fig. 1 are used. Most large balloons are now inflated through tubes leading into the balloon near the top. This permits the balloon to be restrained at some point near the top but below the entry point of the inflation tubes, so that not much of the balloon fabric is exposed to the wind as gas flows into the balloon.

Until enough gas has entered the balloon to lift the fabric enclosing it, the fabric-encased gas bubble is free to roll about on the ground in response to the slightest wind. Therefore, wind is a critical factor during the early minutes of inflation. Rapid inflation shortens the period of greatest danger, but no way has been found of eliminating it. The danger to a balloon during early inflation is a function of both wind speed and the toughness of the balloon fabric. Steady winds less than five m/sec are acceptable for inflations of thin polyethylene balloons used for high altitude flights. Light winds are rarely steady, and a strong gust a few

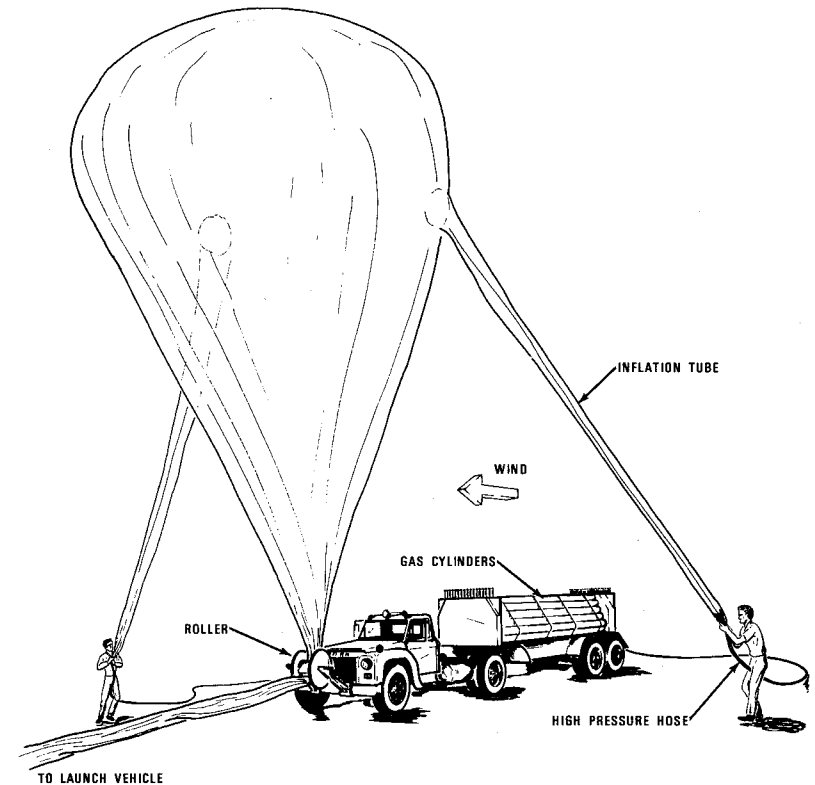


Fig. 1. Balloon during inflation. The gas bubble is restrained by a roller through which the balloon may move.

seconds in duration can destroy a balloon. Therefore, even lighter winds are preferred.

Occasionally balloons are inflated through a tube which enters the base. When this type of inflation is used, the balloon undergoes a much longer period during which it is not under control. Also, as the relatively small bubble rises and lifts the uninflated portion of the balloon, it is affected by the wind at levels up to 100 m. Therefore, the wind must be light (< 3 m/sec) through a deep stratum adjacent to the ground if this type of inflation is to be satisfactory.

Other factors are important during inflation, but none are as critical as the wind. Temperature extremes can cause discomfort to flight personnel, but they are not particularly limiting to the operation in other ways. Humidity is not a problem when the inflation gas is helium. If a flammable gas is used, however, low humidity may be more conducive to static discharges and so increase the hazard. Humidity can be controlled locally by sprinkling.

2. Launch

Two primary types of launch, static and dynamic, are used for large balloons. Figures 2 and 3 are illustrations of typical static and dynamic launches.

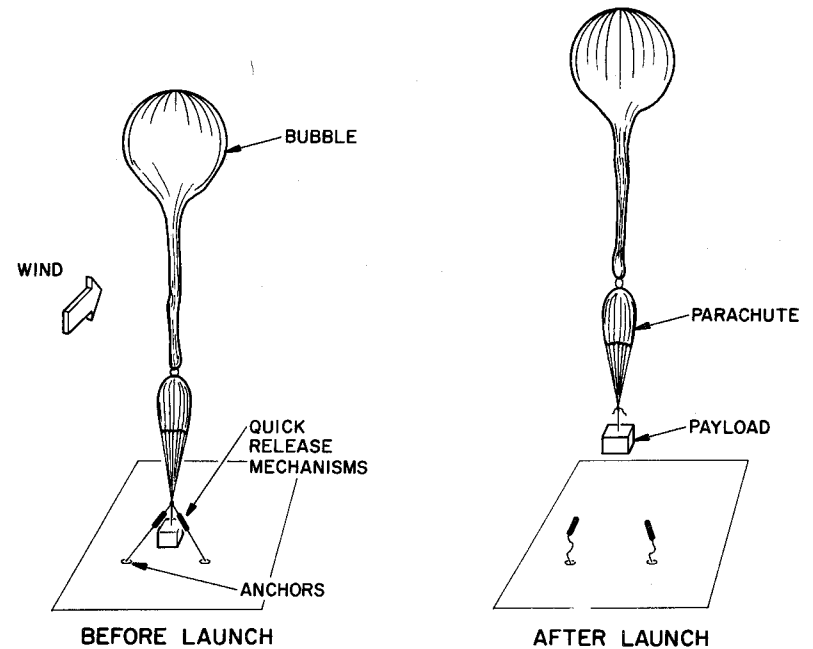


Fig. 2. Static launch.

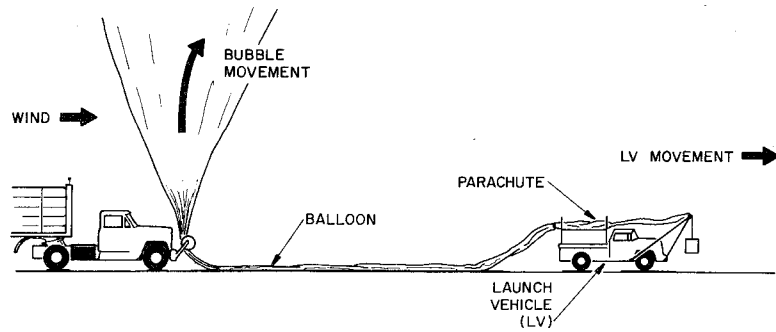


Fig. 3. Dynamic launch.

In the static launch, the balloon is allowed to stand erect over the payload immediately prior to launch. The payload is not moved until the balloon lifts it; then it moves in response to the free motion of the balloon. The meteorological factor that is most critical is the wind in the stratum immediately above the surface. Some of the larger balloon systems coming into use may stand 200 m (650 ft) high. Balloons standing erect in this manner have been known to form huge spinnaker-like sails. If this happens, the balloon will almost surely be destroyed, and the forces involved are quite sufficient to drag large vehicles or tear a payload apart. Thus, unless the winds are less than the design limits throughout a deep stratum adjacent to the surface, a static launch can rapidly change into a dynamic disaster. Design limits vary widely from system to system but few large systems have been designed to be launched in winds in excess of eight m/sec (~16 knots) at any level reached by the standing balloon system.

It is standard practice to choose a launch time when the diurnal winds are at their minimum. This consideration is especially important at tropical stations, subject to trade winds; at island and coastal stations, under the influence of land and sea breezes; and in deserts,

with intense diurnal heating and cooling. Instances may be found in all of the above cases where there is only a very short time span during the diurnal cycle when the surface wind speed has a significant probability of remaining below critical limits. As a general rule, unless the launch site is influenced by anomalous topographic effects, such as drainage winds from nearby slopes, the optimum time of launch is just before dawn, before the onset of diurnal heating.

A particularly damaging phenomenon known as the low-level jet is often widespread in the southern part of the United States during the summer months. The low-level jet is a nocturnal condition which usually begins near midnight and disappears near dawn. In a fully developed low-level jet, even a moderately small bubble may be difficult to launch. Thus, a paradox arises: if inflation is begun early enough for a safe launch, the balloon may be destroyed during inflation, but if inflation is delayed, it may be too late for a safe launch.

Dynamic launches are usually initiated while most of the balloon is lying on the ground, as shown in Fig. 3. Thus, before launch the balloon system is exposed only to the winds in a very shallow surface layer. The

first step in launch is to release the bubble at the launch spool. As soon as the balloon train is lifted off the ground by the rising bubble, the launch vehicle moves forward and to right or left, maneuvering the payload into a position which will be directly under the balloon bubble when the bubble has reached a height equal to the length of the balloon train. The payload is then released to be carried aloft. This type of launch can usually be accomplished if the maximum wind on the balloon at any level during launch does not exceed eight m/sec, but the actual limiting speed depends on the maneuverability of the launch vehicle, the space it has for maneuvering, and many other factors.

The launch depicted by Fig. 3 is called an upwind launch because the bubble is inflated and released from a position upwind of the launch vehicle. In another type, termed a downwind launch, the bubble is inflated and released downwind from the vehicle. After the bubble is released and has lifted the balloon train off the ground, the vehicle must move faster than the wind at the level of the bubble and overtake it. This type of launch requires that the vehicle be capable of greater speed than required during an upwind launch. It also requires more surface area in which to maneuver

the vehicle. In any dynamic launch, timing is important; it is perhaps less critical for a downwind than for an upwind launch. The wind on the balloon during this type of launch should normally not exceed eight m/sec.

Wind is the meteorological factor which is most restrictive in a physical sense at launch, and the wind through a stratum as deep as the length of the balloon train must be considered. Legal requirements may cause other meteorological variables to be restrictive also. For example, there may be a legal restriction against launching when the surface visibility is less than some specified value or when the balloon system must subsequently fly through a cloud layer. Falling rain or snow may create conditions which impose a legal restriction on launch, and either can make it more difficult. Snow on the ground or soft, muddy ground may also create a problem; therefore, a forecaster must be prepared to consider the possibility of precipitation as the flight date approaches. The possibility of lightning must be seriously considered also because many balloon systems have wires running from top to bottom. Usually, however, if lightning occurs, strong, gusty winds will also be probable.

3. Ascent

After launch, an ascending balloon system responds to its environment in a very complex way. Essentially, its horizontal speed is equal to the speed of the ambient air, but its rate of rise (ascent rate) is a function of the lapse rate of temperature in the atmosphere ($-dT/dH$) and the thermal environment (including radiation) of the balloon. The interaction of a balloon with its environment is described in some detail in Sections II and III.

As a balloon ascends through the tropopause it encounters extreme cold, and although most modern balloon materials can withstand quite low temperatures, a temperature below -80°C can cause problems. Cloud strata encountered during ascent may affect the radiation environment of the balloon enough to cause a dramatic change in its ascent rate. Cirrus clouds so thin that they are invisible, especially at night, may be significant. The distribution of moisture with height can give a clue to the existence of such clouds.

4. Tracking and Float

It may be desirable to track a balloon system for a variety of reasons.

Knowledge of the position of the system as a function of time may be essential to the scientist whose experiment is being flown. Legal restrictions may exist which require tracking, especially during ascent and descent while the balloon is moving vertically through space shared by airplanes.

During ascent, tracking may be done visually and electronically (radar, radio direction finding, etc.) from the launch site. Cloudiness and low visibility can severely limit visual tracking, but weather is not particularly restrictive to electronic tracking until the balloon nears the radio horizon. Then strata of differing reflective-index gradients may cause erratic radio transmission between the balloon system and the launch site.

As a balloon system moves away from the launch site, tracking may be done from a down-range station. Tracking away from the launch site is also frequently done by airplane. Automatic direction-finding equipment which is standard on many airplanes may be used to determine the location of a balloon system which includes a transmitter operating on an appropriate frequency. Visual fixes from an airplane are frequently possible even when visibility or cloudiness at low levels may prevent a balloon from being seen from the ground. An airplane thus constitutes an excellent, and nearly uni-

versal, tracking instrument for long balloon flights, and terminal and enroute flight weather for the airplane becomes more important to successful tracking than any meteorological element which may affect the balloon system directly, with the possible exception of the wind at balloon float level. In winter, in middle latitudes, balloon speed may exceed the speed of the tracking airplane.

5. Descent

A balloon-borne experiment may be returned to earth by the balloon itself or by parachute. A descending balloon system is affected by the atmosphere in much the same way as an ascending system. Therefore, the meteorological problems associated with descent are similar to those associated with ascent, except that they may be displaced many miles from the launch site and become critical many hours after launch. Thus, the forecaster must make a longer range (in time) forecast for descent than for ascent, for a site perhaps thousands of miles away from his base of operations.

Most balloon-borne payloads are returned to earth on a parachute. Section X describes the behavior of a descending parachute system. Its

descent rate depends on air density, and that is well enough defined in the Standard Atmosphere to enable one to calculate the descent rate quite accurately. Consequently, the descent vector, if it is assumed that the parachute system's horizontal velocity is equal to the velocity of the ambient air, can be calculated with an accuracy comparable to the accuracy with which the wind is known as a function of height. An accurate descent vector is particularly important in a parachute recovery, because operations personnel depend on it to enable them to start the descent when the balloon system is in an appropriate location to assure that the parachute will land in a safe, convenient spot.

Daytime parachute descents can often be followed to earth visually. Good visibility and clear skies enhance the probability of success. A payload containing a radio transmitter which can be tracked from an airplane can be followed to the ground even though it cannot be seen. This technique is used for night landings, and it may be used when low-level visibility is poor. A descent in the vicinity of a thunderstorm should be avoided if possible. Descending through any kind of convective cloud is also undesirable. Finally, it is important that winds near the surface

not be excessive. Designing and constructing a device to absorb the energy of horizontal motion safely and effectively is difficult, and if there is wind enough at the surface to drag a parachute system, a payload may be destroyed even after a satisfactory landing. Low-level winds in excess of eight m/sec are difficult to protect against in designing an energy absorber; also they are likely to drag a payload unless it is separated from the balloon or parachute upon landing. Winds less than three m/sec may be treated as zero wind in energy-absorber design, and such winds will not drag a payload after landing.

6. Landing and Recovery

One aspect of the landing was mentioned in the last paragraph, i.e., the dragging of the payload after landing. A balloon can form a much larger drag surface than a parachute. Therefore, immediately after a payload touches down with the balloon attached, the balloon should be deflated even if the surface winds are negligible.

The ideal landing area is a firm, unoccupied site which is readily accessible by truck. The immediate area should be free from trees, large bushes, etc. which might damage the payload or the parachute. The nearest

inhabitants should be close enough to provide assistance if needed, but far enough away that no question of danger to people or property will arise. The most important meteorological variables are surface and low-level winds; recent precipitation which may have left the surface soft, slick, or snow-covered; and precipitation anticipated during the few hours required to recover the payload. Low-level visibility and low clouds can also adversely affect recovery, because a ground crew must frequently be guided to a landing site by a low-flying airplane.

C. THERMAL STRUCTURE OF THE ATMOSPHERE

1. Temperature and Density

Taken together, the U.S. Standard Atmosphere, 1962, (1) and the Supplements (2) constitute a description of the whole atmosphere from which horizontal (latitudinal) and temporal variations may be coarsely determined. They are adequate for most scientific ballooning needs. The relationships between temperature, density, and height which are given in this section are applicable in the real and standard atmospheres unless otherwise noted.

a. The hydrostatic relationship. Although the atmosphere is in constant motion, the hydrostatic relationship is very nearly valid. A

more general relationship expressing the balance of vertical forces in a moving atmosphere is given by Haltiner and Martin (3). The hydrostatic equation may be stated

$$dp = -\rho g dz \quad (1)$$

where p is atmospheric pressure, g is the acceleration due to gravity, ρ is the air density, and z is height; p , g , and ρ are all functions of height, but the variation of g through the stratum in which balloons operate is not great. Equation (1) is, therefore, often written

$$dp = -g_0 \rho dH \quad (2)$$

where g_0 is a defined constant and H has the dimensions of height and is nearly equal to z . The acceleration of gravity at sea level at 45° is usually the value assigned to g_0 . If a height increment, ΔH , is determined by integrating Eq. (2) through an elevated atmospheric stratum bounded by pressure surfaces p_1 and p_2 where $g < g_0$, the value of ΔH will be less than the geometric distance between the pressure surfaces. To differentiate H from z , H is called geopotential height and is measured in geopotential meters or geopotential feet. At great height a geopotential meter is

longer than a physical meter; below sea level it may be shorter. Equation (2) is the hydrostatic equation which will be used for further development.

Air density under conditions found in the atmosphere may be expressed as a function of pressure and temperature by means of the equation of state for an ideal gas. Thus,

$$\rho = \frac{PM}{RT} \quad (3)$$

where M is the molecular weight of air, R is the universal gas constant, and T is the absolute temperature of the air. Since air is a mixture of gases, it has no single, true molecular weight, but for most purposes a molecular weight may be determined from Eq. (4)

$$M = \frac{m}{\sum (m_i/M_i)} \quad (4)$$

in which M_i is the molecular weight of the i th constituent which has a mass of m_i . The mass of the mixture is m . According to Glueckauf (4), the upper atmosphere, up to a height of at least 70 km, has the same composition as that of dry air found at the ground. Therefore, a single value of M for dry air suffices for almost all scientific ballooning needs. If a correction for water vapor, the most variable constituent, should be

deemed necessary, it may be made by multiplying the value of M for dry air by the factor $(1-0.379e/p)$ in which e is the vapor pressure of gaseous water in the atmosphere and p is atmospheric pressure.

Equations (2) and (3) may be combined to yield

$$\frac{dp}{p} = - \frac{Mg_0}{R} \frac{dH}{T} \quad (5)$$

This can be integrated if T can be expressed as a function of H. In the atmosphere T is often very nearly a linear function of height through deep layers, and it may not change with height through shallow layers. Both of these cases will be considered.

In a layer through which T varies linearly with H, one may write

$$T = T_b + L'(H - H_b) \quad (6)$$

where T_b is the temperature at the base of a stratum whose height is H_b and L' ($=dT/dH$) is the vertical gradient of temperature. The negative of L' is called the lapse rate by meteorologists. With Eq. (6) substituted into Eq. (5), the latter can be integrated as follows

$$\int_{p_b}^p \frac{dp}{p} = - \frac{Mg_0}{R} \int_{H_b}^H \frac{dH}{T_b + L'(H - H_b)}$$

to yield

$$p = p_b \left[1 + \frac{L'}{T_b} (H - H_b) \right]^{-\frac{Mg_o}{RL'}} \quad (7)$$

or

$$H = H_b + \frac{T_b}{L'} \left[\left(\frac{p_b}{p} \right)^{\frac{RL'}{Mg_o}} - 1 \right] \quad (8)$$

A layer through which T is constant may be integrated in the following

way

$$\int_{p_b}^p \frac{dp}{p} = - \frac{Mg_o}{RT_b} \int_{H_b}^H dH$$

to yield

$$p = p_b e^{-\frac{Mg_o}{RT_b} (H - H_b)} \quad (9)$$

or

$$H = H_b - \frac{RT_b}{Mg_o} \ln \frac{p}{p_b} \quad (10)$$

The notation employed in Eqs. (9) and (10) uses the temperature at the base of the layer. The mean temperature through a layer of thickness $(H - H_b)$ may be substituted for T_b in Eqs. (9) and (10) if it is known,

even though temperature changes with height in the layer. In thin layers, the mean temperature can readily be determined from a plot of T vs H, a practice which is widely used in meteorology. Similarly, a mean value of L' may be determined from a T vs H plot and used in Eqs. (7) and (8) although the actual T vs H curve may not be linear. Thus, Eqs. (7)-(10) are not as restricted in their application as the assumptions made in deriving them may suggest.

Starting from the equation of state and the hydrostatic equation, the relationship between density and height may also be derived. The derivation is shown here with a minimum of explanation. Taking the derivation of Eq. (3) yields

$$\frac{dp}{dH} = - \frac{M}{RT^2} \left(T \frac{dp}{dH} - p \frac{dT}{dH} \right)$$

In a layer in which $dT/dH (=L')$ is a constant not equal to zero, $T = T_b + L'(H - H_b)$, and

$$\frac{dp}{dH} = - \left(\frac{Mg_o}{RT} + \frac{pML'}{RT^2} \right) = - \frac{p}{T} \left(\frac{Mg_o}{R} + L' \right)$$

$$\int_b^p \frac{dp}{p} = - \left(\frac{Mg_o}{RL'} + 1 \right) \int_{H_b}^H \frac{d[T_b + L'(H - H_b)]}{T_b + L'(H - H_b)}$$

$$\rho = \rho_b \left[1 + \frac{L'}{T_b} (H - H_b) \right] - \left(\frac{Mg_o}{RL'} + 1 \right) \quad (11)$$

or

$$H = H_b + \frac{T_b}{L'} \left[\left(\frac{\rho}{\rho_b} \right)^{\frac{RL'}{Mg_o + RL'}} - 1 \right] \quad (12)$$

Similarly, in a layer in which $dT/dH = 0$,

$$\frac{d\rho}{dH} = - \frac{Mg_o \rho}{RT_b}$$

$$\int_{\rho_b}^{\rho} \frac{d\rho}{\rho} = - \frac{Mg_o}{RT_b} \int_{H_b}^H dH$$

$$\rho = \rho_b e^{- \frac{Mg_o}{RT_b} (H - H_b)} \quad (13)$$

or

$$H = H_b - \frac{RT_b}{Mg_o} \ln \frac{\rho}{\rho_b} \quad (14)$$

Note that the expression $[1 + (L'/T_b)(H - H_b)]$ is equal to T/T_b ;

therefore, it follows that Eq. (7) may be written

$$P = P_b \left(\frac{T}{T_b} \right)^{- \frac{Mg_o}{RL'}} \quad (15)$$

Also Eq. (11) may be written

$$\rho = \rho_b \left(\frac{T}{T_b} \right)^{- \left(\frac{Mg_o}{RL'} + 1 \right)} \quad (16)$$

Finally, Eqs. (15) and (16) may be combined to give

$$\rho = \rho_b \left(\frac{P}{P_b} \right)^{\frac{RL'}{Mg_o} + 1} \quad (17)$$

Equations (15) through (17) are useful relationships between pressure,

temperature, and density in an atmospheric layer in which L' is constant

but not zero. If L' is zero, the relationship between pressure and density

is

$$\frac{P}{P_b} = \frac{\rho}{\rho_b} \quad (18)$$

and neither pressure nor density are functions of temperature within the

layer.

b. The U.S. Standard Atmosphere, 1962. The U.S. Standard Atmosphere,

1962, is defined up to 61 km as follows:

(1) The air is a dry gas, devoid of liquid water, water vapor, and dust, and it obeys the ideal gas law.

(2) The following defined and physical constants are applicable:

Sea level temperature-- $T_0 = 15^\circ\text{C} = 59^\circ\text{F} = 288.15^\circ\text{K} = 518.67^\circ\text{R}$

Sea level pressure-- $p_0 = 1013.25 \text{ mb} = 101325.0 \text{ N/m}^2 = 2116.22 \text{ lbf/ft}^2$

Sea level acceleration due to gravity-- $g_0 = 9.80665 \text{ m/sec}^2 =$
 32.1741 ft/sec^2

Molecular weight-- $M = 28.9644 \text{ kg/(kg - mol)}$

Universal gas constant-- $R = 8314.32 \text{ J/}^\circ\text{K(Kg - mol)} =$
 $1545.31 \text{ ft lbf/}^\circ\text{R(lb - mol)}$

(3) Temperature varies with geopotential height as shown in Table 1.

Pressure and density are also given at the base of each of the layers for convenience, but of these only the sea level pressure is a defined value.

Figure 4 is a plot of T vs H for the lowest 61 km of the U.S. Standard Atmosphere, 1962. Note that the curve is made up of a series of straight line segments; therefore, Eqs. (6) through (18) and the definition of the atmosphere given in (1) through (3) above may be used as appropriate to determine T, p, and ρ at any height H. More generally, given a value of T, p, or H, it is possible to determine uniquely the values of the other

Table 1

Defining Temperature vs Height Relationships in the Lowest 61 km
of the U.S. Standard Atmosphere, 1962.

Layer Height, Base and Top (gpm)*	Temperature at Base of Layer °K	Temperature Grad. in Layer °C	Temperature Grad. in Layer (°K/gpm)	Pressure at Base of Layer (mb)**	Density at Base of Layer (kg/m ³)
0-11,000	288.15	15.00	-0.0065	1013.25	1.2250
11,000-20,000	216.65	-56.50	0.00	226.320	0.36392
20,000-32,000	216.65	-56.50	+0.0010	54.749	0.088035
32,000-47,000	228.65	-44.50	+0.0028	8.680	0.013225
47,000-52,000	270.65	- 2.50	0.00	1.109	0.0014275
52,000-61,000	270.65	- 2.50	-0.0020	0.590	0.0007594

*The symbol gpm is the abbreviation for geopotential meter.

**One millibar (mb) is equal to 100 N/m^2 .

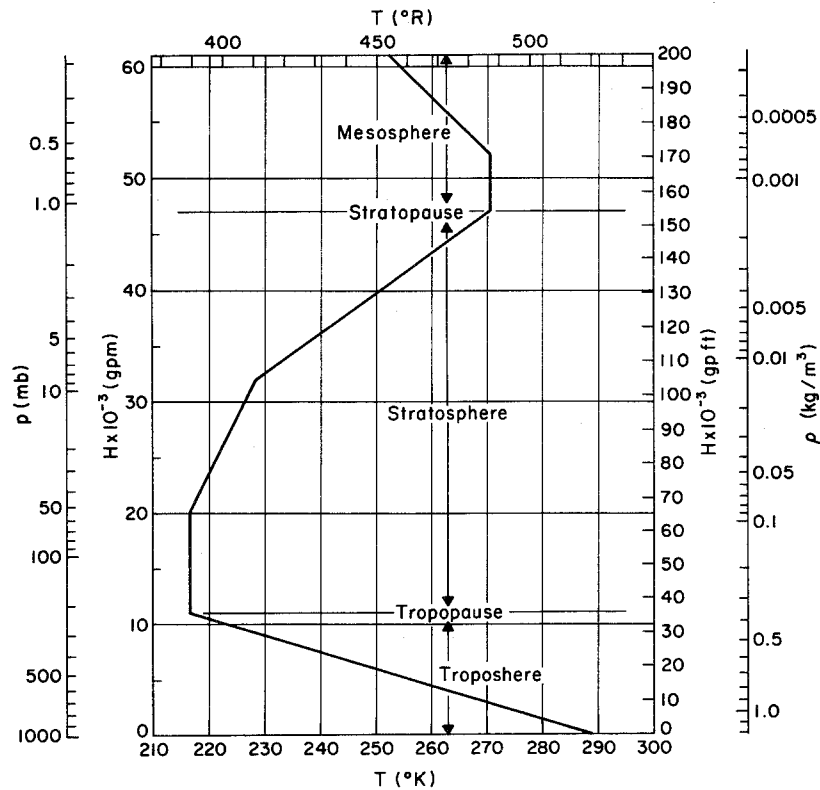


Fig. 4. Temperature as a function of geopotential height in the U.S.

Standard Atmosphere, 1962.

two and T, but it is not usually possible to determine a unique value for any of the other variables if T alone is known. Auxiliary scales of p and ρ are shown along the ordinate of Fig. 4.

c. Supplementary atmospheres. Supplementary atmosphere temperature-height curves for several latitudes for January are given in Fig. 5. Similar curves for July are shown in Fig. 6. An annual curve for 15°N is also given in Fig. 6. Because of the small temporal variation of temperature in the tropics, the one curve is valid at any season. Also, the U.S. Standard Atmosphere, 1962, has been found to be a good approximation for the middle-latitude curves of spring and fall below 69 km. Supplementary atmospheres are not often used in scientific ballooning; if one is needed its precise definition may be found in reference (2).

Data, especially for balloon flight planning, can sometimes be obtained with sufficient accuracy from Figs. 5 or 6. If density is needed, Fig. 7 may be more convenient. Adapted from reference (2), it shows the percentage departure of density from the standard atmosphere as a function of height, season, and latitude. The variability in winter at high latitudes is so great that curves are given for warm and cold atmospheres as well as for the mean.

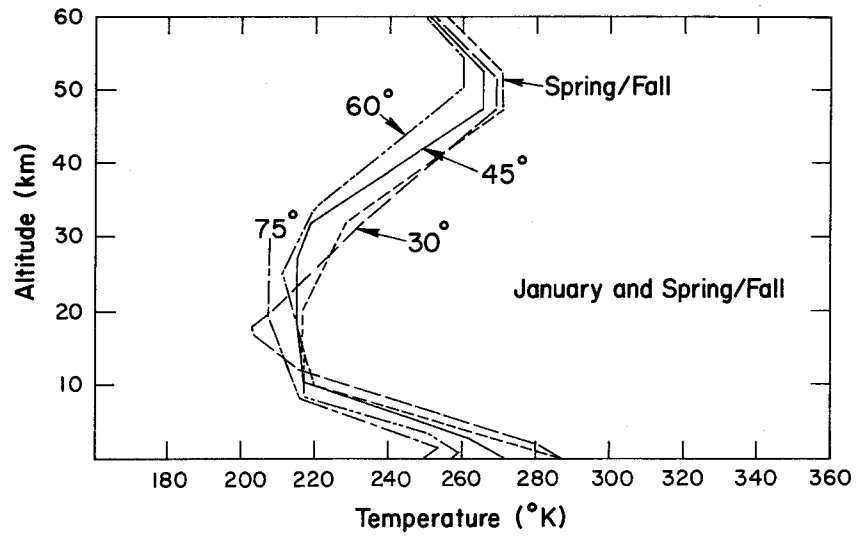


Fig. 5. Temperature-Height profiles of the 30°, 45°, 60°, and 75°N

January and mid-latitude spring/fall Supplementary Atmospheres.

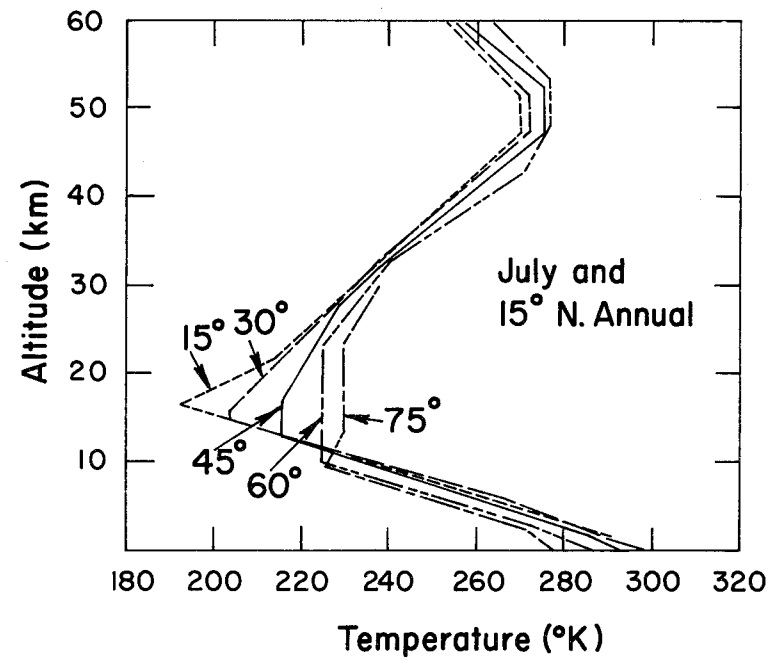


Fig. 6. Temperature-Height profiles of the 30°, 45°, 60°, and 75°N

July and 15°N annual Supplementary Atmospheres.

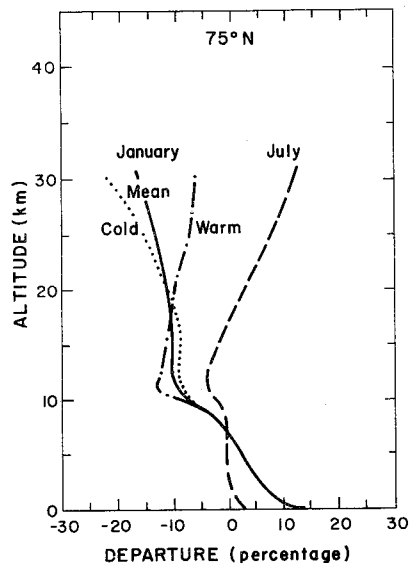
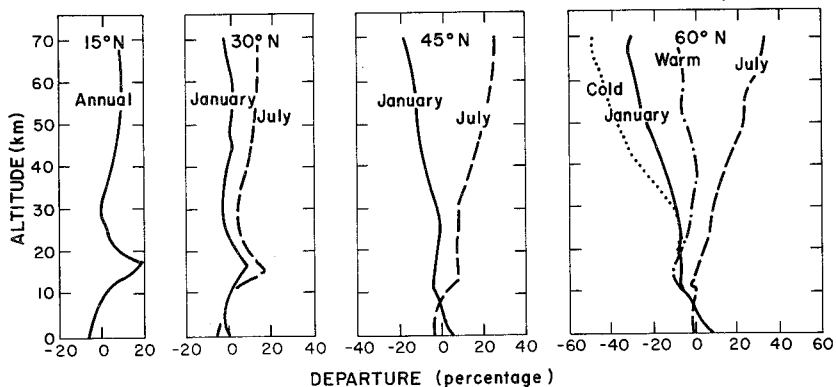


Fig. 7. Percentage departure from standard of densities of certain supplemental atmospheres given in reference (2).

d. Mean thermal structure. Mean temperature as a function of height and latitude for summer and winter is shown in Fig. 8 from Palmén and Newton (5). Because of the limited quantity and quality of high level data used to construct the figure, it will undoubtedly be found wrong in detail as additional, more reliable data become available. Nonetheless, the principal features of the temperature patterns depicted by the figure are believed to be essentially correct. Also, most of the data were observed in the Northern Hemisphere so that the chart shows the patterns of the Northern Hemisphere summer and winter. It may be interpreted, however, as a pattern of summer and winter hemisphere patterns shown concurrently.

2. Thermal Radiation

The atmosphere receives radiation from the sun and from earth, and it radiates to space. It is transparent to most of the solar radiation, but it absorbs enough radiant energy in several wave bands to affect its vertical temperature structure significantly. Much of Section III must necessarily be devoted to this subject; therefore, it is not discussed further here.

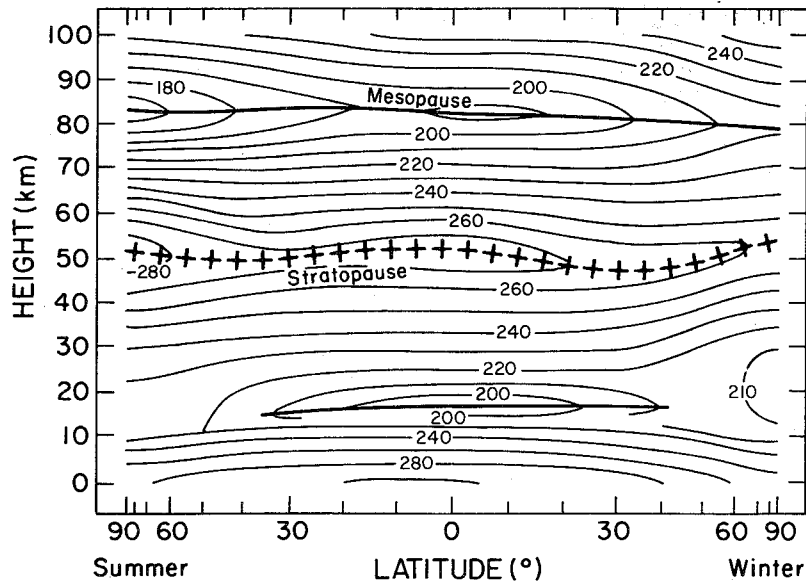


Fig. 8. Mean thermal structure of the atmosphere in summer and winter, after Palmen and Newton (5).

D. CIRCULATION

In the free atmosphere, especially at the high levels at which balloons fly, winds are nearly horizontal, and in the mean they are nearly zonal, i.e., they blow from either east or west. This makes it possible to describe the principal features of atmospheric circulation in terms of easterly (winds blowing from the east) and westerly winds only. However, for computing probable balloon trajectories, Solot and Darling (6), knowledge of the meridional (north-south) winds is also essential; therefore, although zonal winds receive most of the attention in this discussion of atmospheric circulation, it should be emphasized that meridional winds are highly important in balloon flight planning and operations.

1. Mean Zonal Structure

Figure 9 is a chart showing the mean zonal wind structure of the atmosphere as a function of height and latitude for the summer and winter seasons. It, like Fig. 8, is taken from Palmen and Newton (5), and it may also be interpreted as showing the winter and summer wind patterns in one hemisphere or the concurrent pattern in both hemispheres.

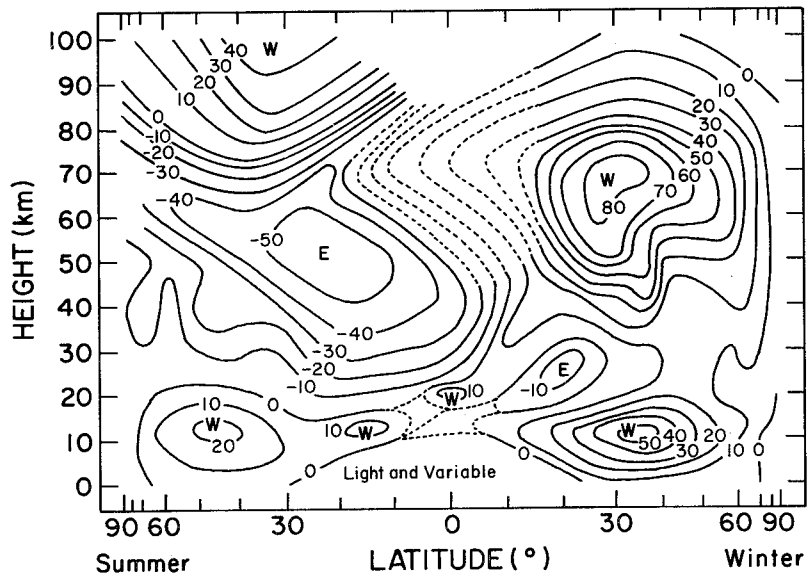


Fig. 9. Mean zonal wind in summer and winter, after Palmén and

Newton (5).

The patterns in Figs. 8 and 9 are not independent. Vertical wind shear is correlated closely with horizontal temperature gradient in the atmosphere. If the wind were geostrophic (horizontal, unaccelerated, frictionless flow) at all levels, the correlation between vertical wind shear and horizontal temperature gradient would be perfect. This correlation was kept in mind as the two charts were constructed so that the two patterns would be mutually consistent.

The most important features of Fig. 9 from the point of view of high altitude scientific ballooning are the stratum of low speed winds near 20 km, the strong westerlies which exist at higher levels in the winter hemisphere, and the easterlies which exist generally between 20 and 75 km in summer. It is also pertinent to note that westerlies exist at all levels below 20 km in the middle latitudes in both winter and summer. Neither polar nor tropical winds are explained well by Fig. 9. Both will be discussed separately later.

If west winds dominate the circulation of the middle latitude stratum between 20 and 75 km in winter and are replaced by east winds in the summer, there must be at least two transition periods when neither west nor east winds are strong.

It is useful, though vastly oversimplified, to view the winter stratospheric circulation as consisting of a cyclonic vortex centered near the pole. Figure 10, from reference (7), shows a typical winter flow pattern. There is no wind at the center of the vortex, and the wind at lower latitudes is westerly. Typically, the speed increases equatorward from the pole to a maximum at about 30° and then decreases from 30° to about 15° where it merges with an equatorial wind system.

Similarly, the summer circulation in the stratosphere may be viewed as an anticyclonic vortex centered near the pole (see Fig. 11). East winds increase in speed equatorward from the pole, reach a broad maximum in lower middle latitudes, and then decrease to $10 - 15^{\circ}$, where they merge with the equatorial system. The summer wind system in the stratosphere is perhaps the most stable current system in the atmosphere. After it becomes firmly established, it persists with remarkably little variation until the autumn transition, when it is replaced by the winter west wind system.

The autumn transition is one of the most predictable of the changes which the atmosphere undergoes. In the mean, it occurs at the time of the autumn equinox, usually starting at high altitude near the pole about a

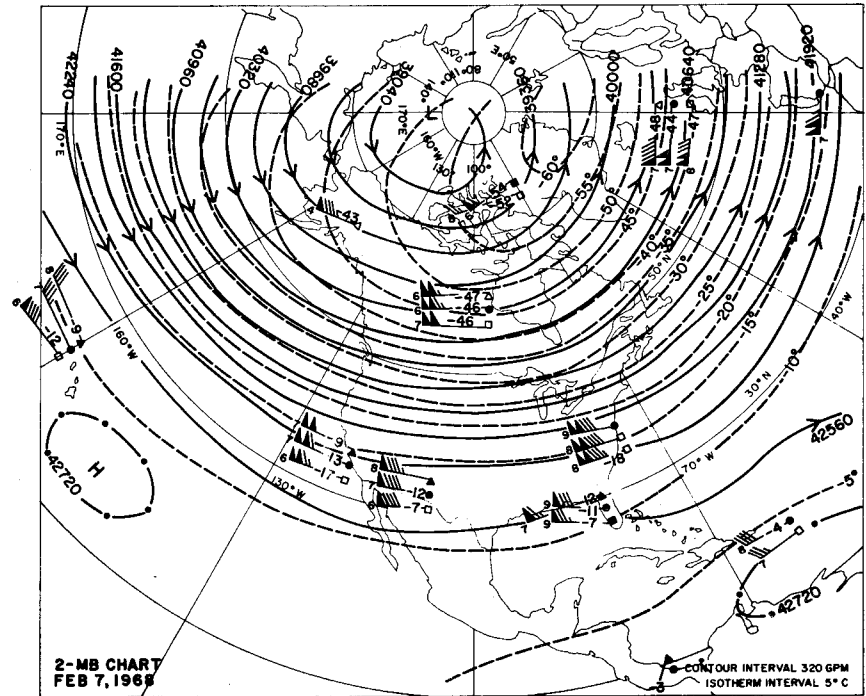


Fig. 10. Typical winter cyclonic vortex in the upper stratosphere.

Winds flow along the height contours (solid lines). The speed is indicated by the feathers--each flag represents 50 knots, each bar 10 knots, and a half bar 5 knots. The dashed lines are isotherms of temperature in $^{\circ}\text{C}$.

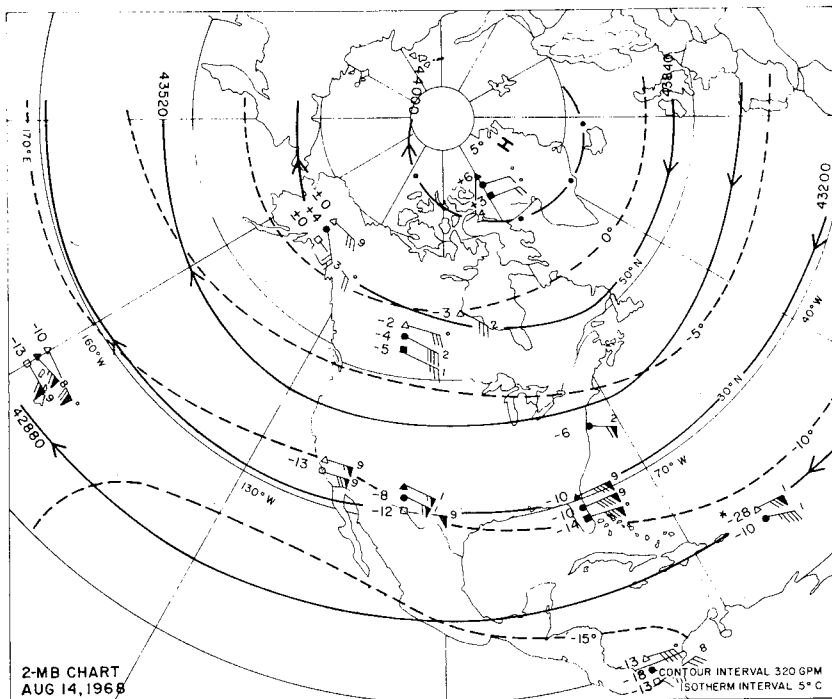


Fig. 11. Typical summer anticyclonic vortex in the upper stratosphere.

See Fig. 10 for explanation of the isolines.

month before the equinox. It then works its way downward and equatorward, and a month after the equinox, all winds poleward of 15° and above 30 km will be west winds. The downward and equatorward progression of the autumn transition is regular enough that its time of occurrence at one height and place is a good predictor of its time of occurrence at another. At any particular altitude and geographic location, light winds which are quite variable in direction may be expected to last about two weeks during the transition.

Figure 12 is a time cross section of stratospheric winds over the southern United States. It was derived from high level rawinsonde and rocket data from the southern United States, but it is believed to be representative of winds generally at 30° N. Mean zonal wind speed and the standard deviation of the zonal wind are given as functions of height and time of year. The isoline of zero wind speed may be interpreted as the wind reversal line. The zone on either side of the zero speed line in which the speed is less than one standard deviation gives a clue to the duration of light variable winds accompanying the transition.

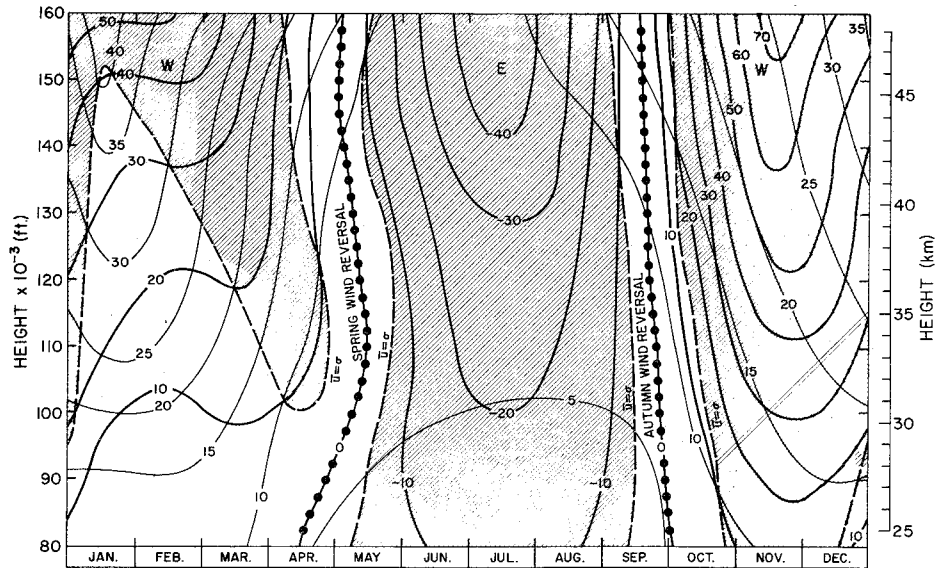


Fig. 12. Time-Height cross section of the mean monthly zonal winds in the southern U.S. stratosphere.

Winter winds in the stratosphere are much more variable than summer winds. After the autumn transition, the westerly flow becomes quite strong, usually reaching maximum speed in about two months. During the third month after transition, the mean zonal speed decreases but the variability increases. By the beginning of winter, a distinct wave pattern is likely to have formed on the westerly current, and during the winter these waves will occasionally grow so large that they dominate the circulation over a large part of the hemisphere. When this happens strong north, south, or even east winds may temporarily replace the usual west winds over large areas. Figure 13 shows how a typical well developed wave may distort the zonal winter wind system. Note that the only westerly winds over North America at 2 mb (~ 41 km) are found in the southwestern United States. Higher, at 0.4 mb (~ 54 km), the southern United States is experiencing west to southwest flow, but at Point Mugu, California, strong northeast winds are directly opposed to the southwest winds at 2 mb.

Occasionally, the polar cyclonic vortex will be almost entirely replaced in winter by an anticyclonic vortex. This occurs with dramatic suddenness, accompanied by a large increase in the high latitude, strato-

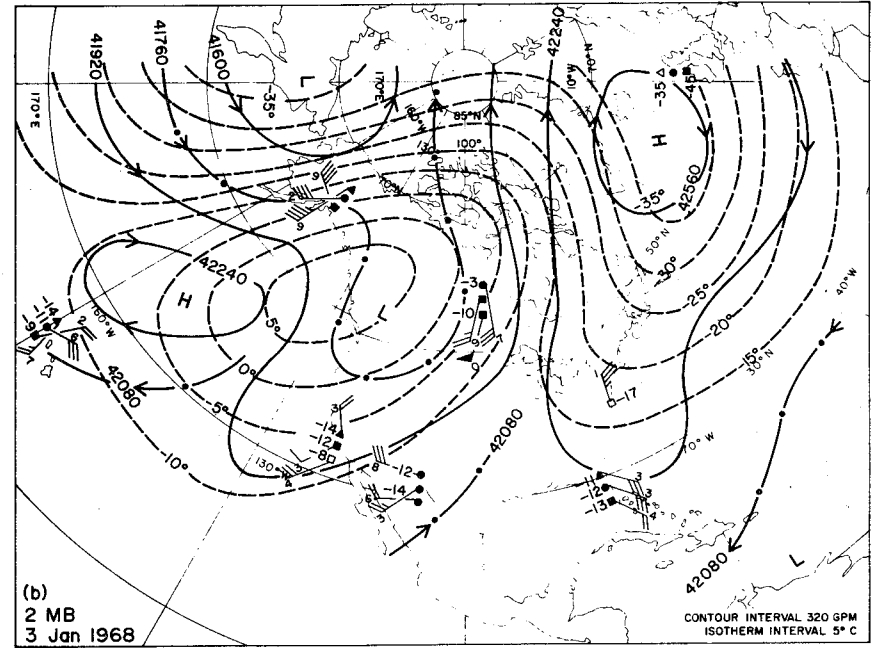
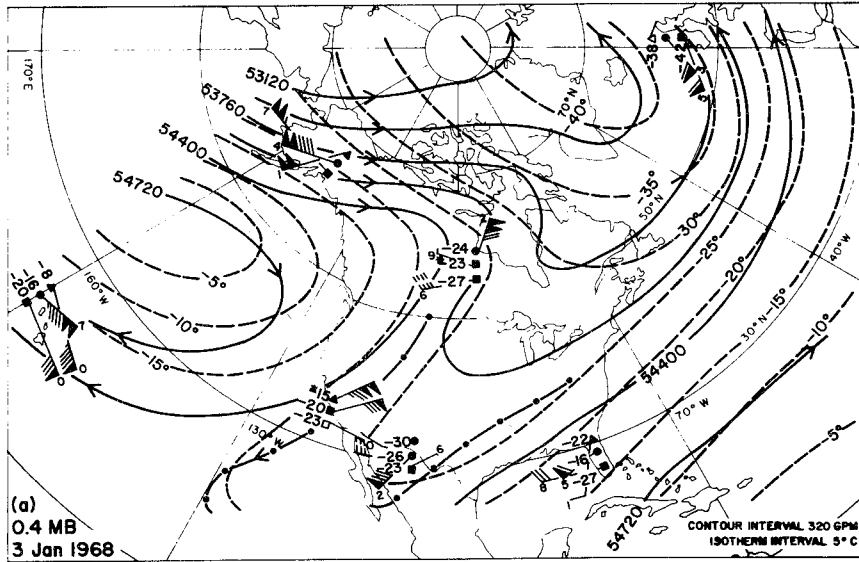


Fig. 13a. Well developed wave in the winter westerlies. Note the variety of wind directions on each pressure surface and the differences which occur between the surfaces, i.e., essentially between 54 km (a) and 41 km (b). See Fig. 10 for explanation of the isolines.

Figure 13b

spheric temperature; therefore, meteorologists often refer to the phenomenon as a sudden, stratospheric warming. Meteorologists who are forecasting for scientific balloon flights are more likely to think of it as a temporary wind reversal.

As winter wanes, the mean speed of the stratospheric wind system decreases. Temporary reversals often make it difficult to know when the summer easterlies have indeed begun. The true transition from the winter to the summer circulation pattern follows much the same pattern as the autumn transition. Westerlies give way to easterlies first at high altitude in polar latitudes. The northern hemisphere spring transition of 1968 at 43 km is shown by Fig. 14 shortly after it had started. A small vortex has already formed near the pole and is spreading southward. Westerly winds are still being observed in most of the United States. Nearly all observed winds are light, although the easterlies over Alaska are rapidly gaining speed.

The transition progresses downward and equatorward, requiring up to two months for completion. This transition occurs in middle latitudes roughly a month after the spring equinox. Neither its time of occurrence

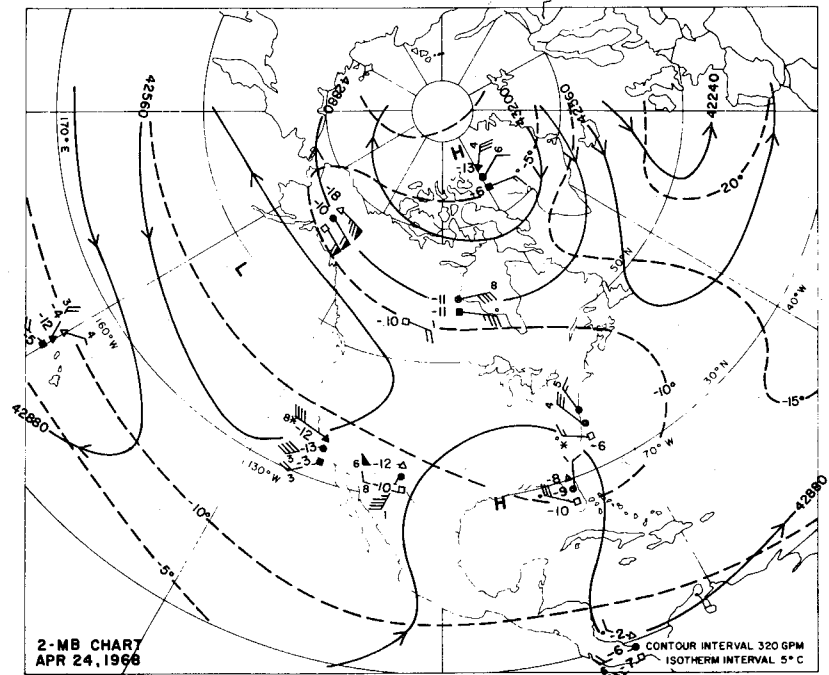


Fig. 14. Transition from a winter cyclonic circulation to a summer anticyclonic circulation. A small anticyclone has formed in the vicinity of the pole and is spreading equatorward. See Fig. 10 for an explanation of the isolines.

nor its rate of progression is as regular as the autumn reversal. Therefore, it is not as predictable.

The true wind reversals are highly important to scientific ballooning. Because of the light wind speeds in the stratosphere during the transition periods, balloons can fly for long periods without violating forbidden territory, e.g., over an ocean where recovery would be difficult or impossible. Often a balloon can fly up to 24 hours and remain above the radio horizon of the launch site. The temporary reversals of winter are sometimes accompanied by light winds over large areas. However, the winds associated with a well-developed wave in the stratospheric westerlies are likely to be strong. Except for flights of a few hours duration or flights which do not require payload recovery, attempts to take advantage of the light winds during temporary winter reversals of the normal stratospheric westerly circulation are not recommended. At such times the circulation is very unsteady and notoriously unpredictable.

2. Polar Wind Structure

The discussion of the mean zonal wind structure above included the polar regions, but some additional discussion is warranted. If the vortices

always remained centered at the poles, the winds there would always be zero. Further, the wind would never be strong in the vicinity of either pole. Note, however, that in none of the analyses shown (Figs. 10, 11, 13, and 14) is the center of the vortex at the pole. Winds at or near the poles are on the average lighter than at lower latitudes, but they can be strong, and they are highly variable in direction.

3. Equatorial Zonal Wind Structure

In the lower equatorial stratosphere, the principal wind system is a zonal current that alternates between east and west in an irregular fashion with a period which is usually a little more than two years. The oscillation is referred to as a 26-month or quasi-biennial oscillation by Reed (8). Higher in the stratosphere and in the lower mesosphere, equatorial winds oscillate from east to west in a semiannual cycle, Reed (9). In the middle stratosphere, where neither the quasi-biennial nor the semiannual cycle dominates, the variation of the wind with time is quite disorderly. Also, at a distance of $\sim 15^\circ$ from the equator in the lower stratosphere, the quasi-biennial oscillation has an amplitude about equal to the annual oscillation so evident in middle latitudes; therefore, the variation with time

of the wind structure there appears generally chaotic, Belmont and Dartt (10).

a. The quasi-biennial oscillation. Figure 15 from Kriester (11) shows the march of the quasi-biennial oscillation in the lower equatorial stratosphere from 1953 through 1970. Clearly, throughout most of the stratum from 20 to 30 km, west winds have alternated with east winds. Also, a directional regime (west or east) appears first at the top of the stratum and then progresses downward with the passage of time. Reed (8) has found that the downward speed of propagation is about 2 km per month above 30 km and 1 km per month below 30 km. By treating the oscillation at each level as a wave (making west wind speeds positive and east wind negative), Reed also found that the wave has its greatest amplitude at 24 km. Figure 16 shows the mean amplitude as a function of height.

At a given level in this stratum the wind appears to flow from the east for approximately a year and then from the west for a year. If one views the entire stratum from 18 to 35 km, however, both easterlies and westerlies will usually be flowing simultaneously, one above the other. When, roughly, the upper half of the stratum is dominated by west winds,

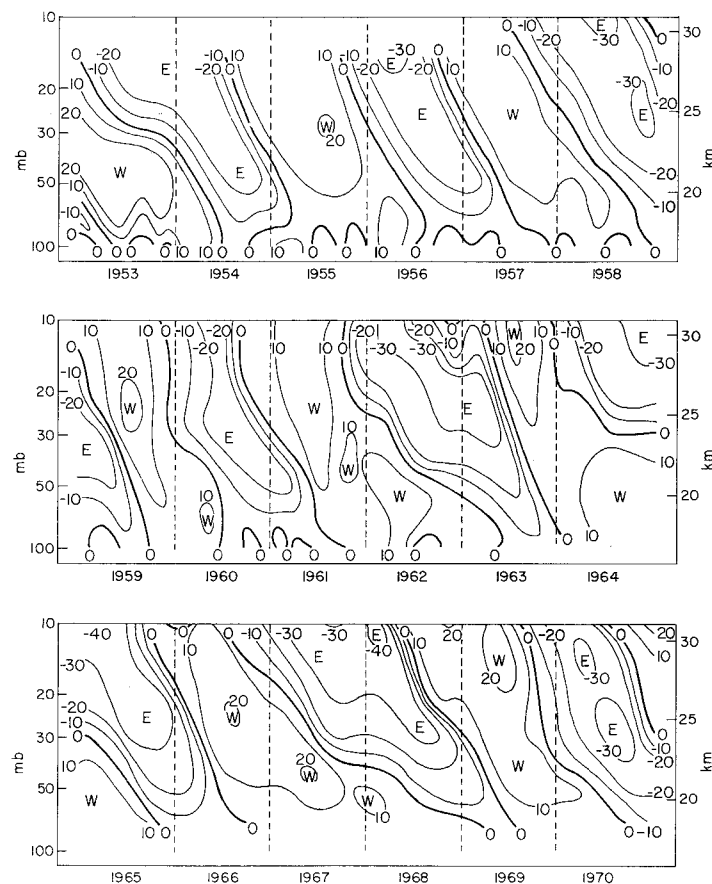


Fig. 15. Time-Height cross section of mean monthly zonal winds at Canton Island (1953--Aug. 1967) and at Gan/Malediv Islands (Sept. 1967--1970). From Kriester (11). Lines are isolines of wind speed in meters per second.

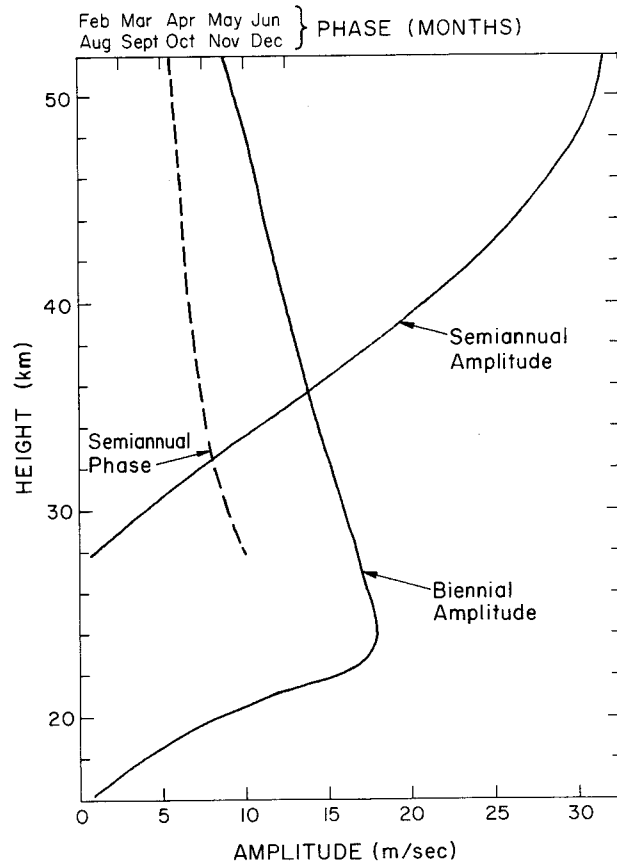


Fig. 16. Amplitude of the quasi-biennial and semiannual, equatorial oscillations as functions of height. Also, time of occurrence of maximum west winds (phase) of the semiannual oscillation in months.

weak east winds will appear at the top. These east winds will grow downward and gain strength in their lower reaches as they do so. When they have occupied about half of the stratum, weak west winds will appear above them. The east wind stratum, now sandwiched between two layers of westerlies, will continue to move downward, gaining strength until it reaches the vicinity of 24 km. Then it will lose strength as it moves on to lower levels until it disappears just above the tropopause. The westerly current which had formed above it will have a similar life cycle. Between the east and west currents is a thin stratum of light, variable winds.

One who wishes to fly a superpressure balloon on the surface of constant density (essentially constant height), will find that the wind can carry his balloon around the earth many times in one direction before it reverses. On the other hand, one who is flying large zero-pressure balloons may choose to take advantage of either an easterly or westerly current, or he may use controlled or uncontrolled (diurnal) height changes of the balloon system to fly alternately east and west. He may also attempt to fly in the low speed stratum between the east and west winds.

b. The semiannual oscillation. As shown by Fig. 16, the amplitude of the semiannual oscillation grows rapidly with increasing altitude above 28 km, reaching a maximum at about 52 km. The amplitude of the quasi-biennial oscillation decreases with height in this altitude range, and the two are equal in the vicinity of 35 km. From 30 to 40 km, the interference pattern of the two oscillations makes it difficult to identify either. Above 40 km the semiannual dominates.

Figure 17 shows Reed's (9) estimate of the variation of the equatorial zonal wind with month and height in the stratum in which the semiannual oscillation prevails. The quasi-biennial oscillation was filtered out of the data used to construct Fig. 17 so that the semiannual oscillation is apparent down to 30 km. The figure also suggests that above 64 km westerlies may prevail throughout the year; observation seems to confirm this.

Within the stratum from 35 to 64 km, the fully developed easterly flow in January and July is maximum in the layer between 45 and 50 km. However, the fully developed westerly flow maximum occurs somewhere above 64 km. In general, both east and west winds reach their maximum value at high altitudes sooner than at low altitudes. This is shown by both Figs.

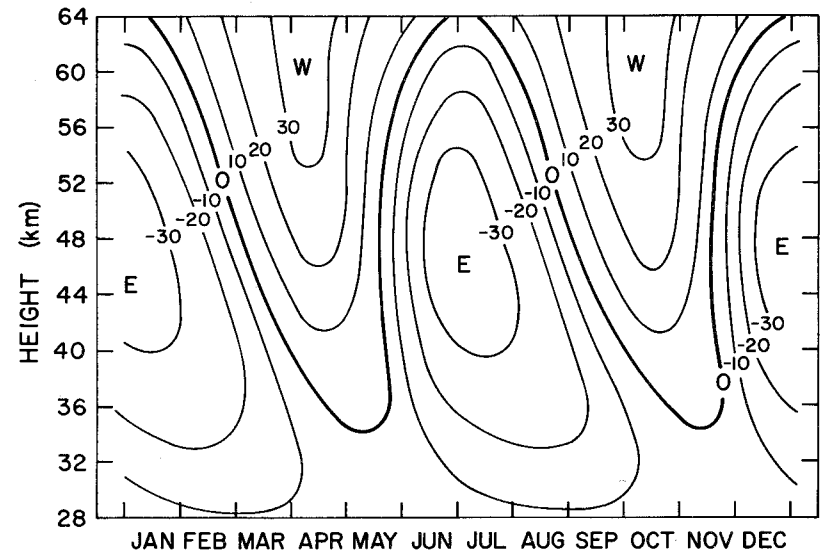


Fig. 17. Estimated variation of zonal wind with month and altitude at the equator. After Reed (9).

16 and 17. The semiannual phase curve in Fig. 16 shows that the time of maximum westerly flow occurs about two weeks after the equinoxes at 50 km and about a month after the equinoxes at 35 km.

Unlike the quasi-biennial oscillation below it, the semiannual oscillation fits into the annual oscillation to poleward in both the summer and winter hemispheres in a predictable way. Viewed most simply, the westerlies are an extension of the winter hemisphere west winds over the equator. Thus, following the spring equinox in the northern hemisphere, the equatorial, semiannual westerlies are part of the southern hemisphere, mesospheric, west wind system. Similarly, following the northern hemisphere fall equinox, the equatorial, semiannual westerlies are part of the northern hemisphere, mesospheric, west wind system.

The equatorial, semiannual easterlies may also be viewed as an extension of the summer hemisphere easterlies into equatorial regions. Indeed, Fig. 9 shows equatorial easterly winds from about 35 to 60 km as an extension of the summer hemisphere, high level easterlies. Reed (9) has some evidence to support the existence of a small easterly jet stream near 15° of latitude in the summer hemisphere, however. The existence of

such a jet will cause the easterly winds to increase in strength toward the pole on the summer hemisphere side of the equator, reach a maximum at about 15° , decrease to perhaps 20° , and then increase again as the summer, middle-latitude easterly wind maximum is approached.

4. Middle Latitude Vertical Structure in the Free Atmosphere

Some typical wind soundings for White Sands, New Mexico, are shown in Fig. 18. All of them show a stratum of relatively strong west winds in the vicinity of the tropopause, between 12 and 16 km. They also show a stratum of minimum wind speed near 20 km, but there the similarity ends. At higher levels the strong stratospheric westerlies are quite evident in the winter (Nov.) sounding, the summer easterlies are clearly shown in the summer (Aug.) sounding, and the light variable stratospheric winds so typical of the transition period are shown by the Sept. sounding. Note that the westerlies are established at high levels on 25 Sept.

The wind profiles shown in Fig. 18 are smoothed curves which show only the major features of the vertical profile. There are many perturbations having vertical dimensions of the order of one kilometer or less which are not measured by most sounding techniques. The profiles of Fig. 18

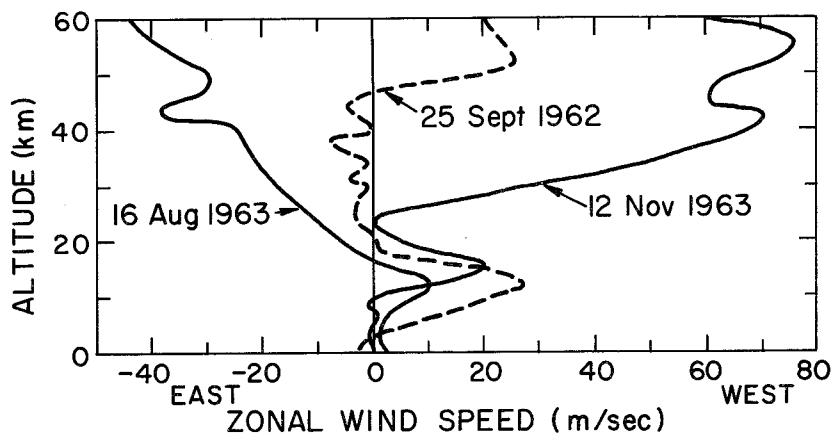


Fig. 18. Selected zonal wind profiles for the White Sands Missile

Range, New Mexico.

show that relatively strong vertical wind shear exists through deep layers above and below the wind maximum at 12 to 16 km. The shear is strongest just below and above the jet stream core where the speed is also greatest, and according to Endlich, et al. (12) in the mean the speed decays nearly linearly above and below the level of maximum speed, reaching a speed equal to one-half the maximum speed in a distance of about 5 km. Thus, the shear through a deep layer near the jet core is proportional to the wind speed at the jet core.

Both wind speed and shear are important in scientific ballooning.

Strong winds cause rapid movement of a balloon during ascent and may carry it beyond effective control from the launch site much sooner than is desirable. Strong wind shear has been suspected of causing balloon failure during ascent. (See Section II for a discussion of wind shear on an ascending balloon.) The flight of large balloon systems through strong jet streams should be avoided.

Shear in the free atmosphere has also been studied by Essenwanger (13) and (14), Weinstein, et al. (15), and Adelfang (16). Their studies included shear through thin layers and showed that very strong shear may

occur in thin strata. Essenwanger (13) proposed that the magnitude of the mean vector wind shear \bar{w} , may be expressed as a function of the height increment, ΔH , through which the shear occurs by means of an equation of the form

$$\bar{w} = a_0 (\Delta H)^{a_1} \quad (19)$$

where a_0 and a_1 are arbitrary constants. He also proposed that the standard deviation of the shear vector, σ_w , may be expressed in the following way

$$\sigma_w = a_2 (\Delta H)^{a_3} + D \quad (20)$$

where a_2 , a_3 , and D are all arbitrary constants.

Adelfang (16), using accurate wind data from the test ranges at Cape Kennedy, Florida, and Point Mugu, California, found that D may be considered negligible and that a_0 , a_1 , a_2 , and a_3 all vary with height and perhaps with season. Nonetheless, $a_0 = a_2$ and $a_1 = a_3$, approximately. This essential equality of the mean and the standard deviation is convenient because the extreme may then be taken as four times the mean, i.e., $(\bar{w} + 3\sigma_w)$. Doing so implies that the shear is normally distributed about the mean.

It is not, but estimates made in this way using Eq. (22) are well outside of the envelope of the data presented by Weinstein, et al. (15), and they are comparable in layers 200-1000 m thick with values estimated by a formula for extreme values given by Essenwanger (14).

The constants in Eqs. (21) and (22) are estimated from the 12-14 km region of Adelfang's (16) graphs. Equation (21) fits the mean data of Weinstein, et al. (15) relatively well. Equations (21) and (22) are believed to provide mean and extreme shear data, respectively, which are suitable for planning purposes for flights in middle latitudes.

$$\frac{\bar{w}}{\Delta H} = 0.12 (\Delta H)^{-0.4} \quad (21)$$

$$\frac{w_e}{\Delta H} = 0.48 (\Delta H)^{-0.4} \quad (22)$$

As written, Eqs. (21) and (22) yield values having the dimension of sec^{-1} , but it is more meaningful to think of shear in terms of (m/sec)/m or (ft/sec)/ft. As long as the length units in velocity are consistent with the length units in height, the equations are valid.

5. Boundary Layer

The wind structure in the lowest 200 meters above the surface is of great interest during inflation and launch. Discussions of the theory of the variation of wind with height near the surface may be found in Priestly (17) and Lumley and Panofsky(18). In general, the shape of the wind profile is a function of the roughness of the surface, the mean wind speed, and the change of temperature with height.

The wind speed profile that has the best theoretical foundation is a generalized profile which is logarithmic in height. A profile which fits observed data relatively well and is simple to use is called a power-law profile. It may be expressed by an equation of the form

$$\left(\frac{\bar{v}}{\bar{v}_1}\right) = \left(\frac{z}{z_1}\right)^b \quad (23)$$

in which \bar{v} and \bar{v}_1 are the mean winds (averaged over a short time from a few minutes to an hour) at heights z and z_1 above the surface, respectively;

b is a constant for each profile which may take values from 0 to 1.0

depending on the lapse rate of temperature through the stratum from the surface to level z and the roughness of the surface. If z_1 is the height above the surface of an anemometer at which \bar{v}_1 is measured, and if b is

known or can be estimated, the speed of the wind at any level z may be approximated from Eq. (23). Figure 19 is a graphical solution of Eq. (23). The scale at the top of the graph shows a relationship between b and dT/dz which is adapted from Frost (19). It is valid when the terrain is relatively level and vegetation is short. The value of b should be increased by about 0.1 to correct for wooded or rough terrain.

It must be emphasized that the power-law profile can provide only a rough approximation to the real wind profile. Ideally, the anemometer level z_1 should be as near as possible to the level of greatest interest. If winds are measured at two levels, b may be determined directly from Fig. 19, or it may be calculated since $b = \log(v_2/v_1)/\log(z_2/z_1)$. Normally, with one measurement near or above 10 m, the power-law approximation is useful through a stratum up to 200 m deep.

The value of b undergoes a readily discernible diurnal variation. This is associated with the static stability of the air in the boundary layer; hence, it is associated with changes in the value of dT/dz . Large values of dT/dz occur on clear nights when the mean wind speed is low. Low values occur at the time of maximum heating, usually in the early after-

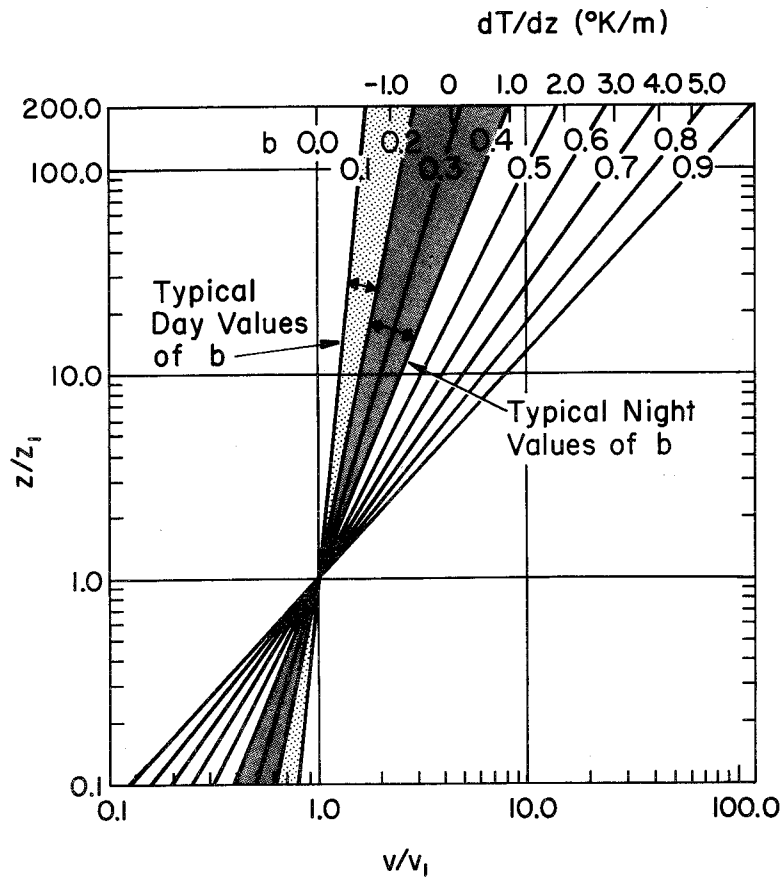


Fig. 19. Dimensionless wind profiles according to the power-law. The value of b may be estimated from the scale at the top if dT/dz is known; add 0.1 to the value of b estimated from dT/dz if the terrain is rough or wooded.

noon. The ranges of typical day and night values of b are indicated on

Fig. 19.

6. Low-Level Jet

A phenomenon which occurs commonly in the Great Plains area of the United States is called a low-level jet or nocturnal jet. Figure 20, from Bonner, et al. (20), is a mean cross section of the winds through the core of a well developed low-level jet. The section, taken normal to the axis of the jet, shows isotachs of wind along the axis and normal to it. Clearly, the wind vector is directed nearly parallel to the jet axis. The most remarkable feature of the jet is its diurnal variation. It appears at night and disappears early the following day.

Other features of the low-level jet which are shown by Fig. 20 are its very small vertical extent, the proximity of the core to the surface, and the strong vertical wind shear under the jet. The vertical wind shear about the jet core is shown more directly by Fig. 21. An important feature which is not obvious from Fig. 20 is the wafer-like character of the jet. Note that the 12 m/sec isotach encloses an area which is about 1.7 km thick and 650 km wide. Figure 22 shows it to be well over 1600 km long.

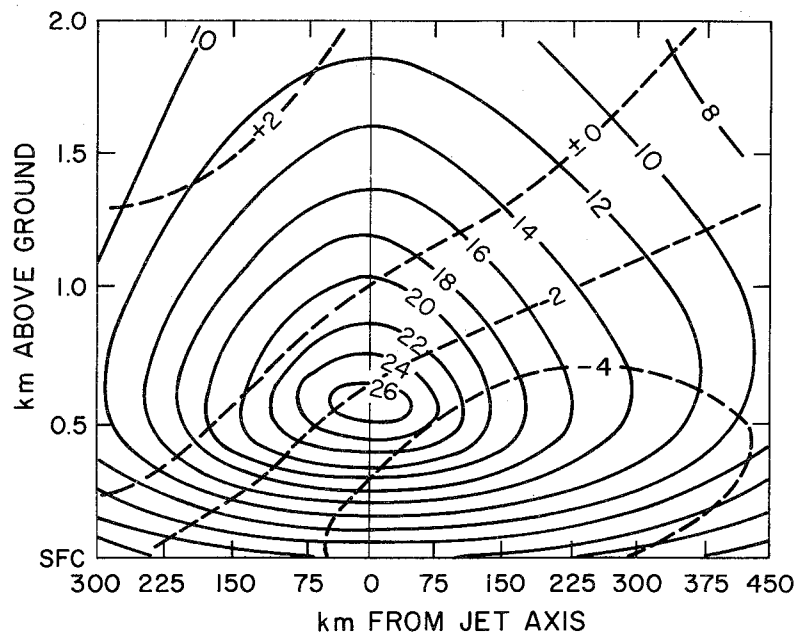


Fig. 20. Mean cross section of the wind associated with a low-level jet, from Bonner et al. (20). The solid lines are isotachs of the wind component parallel to the jet axis; dashed lines are isotachs of the normal component.

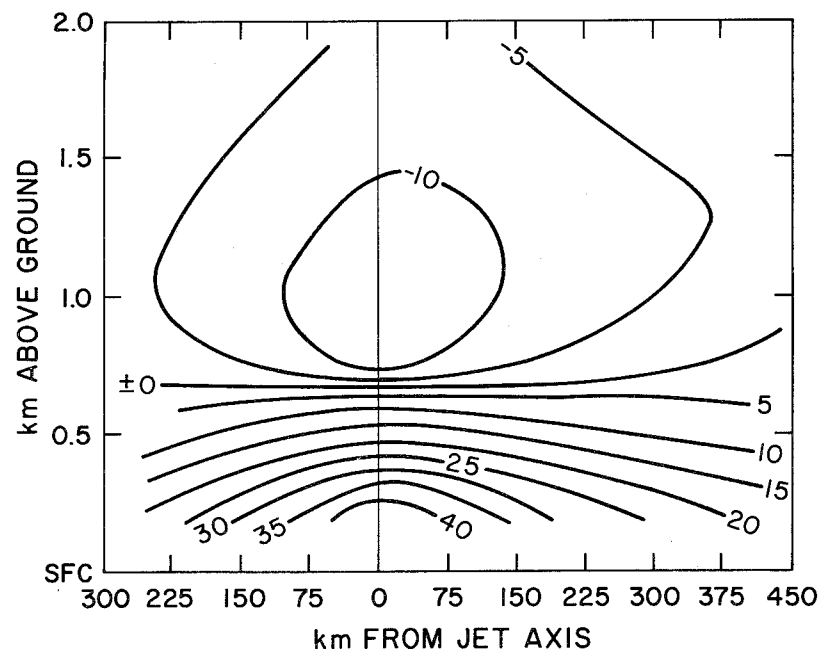


Fig. 21. Average vertical wind shear (m/sec km) in a vertical cross section normal to the core of the jet, after Bonner et al. (20).

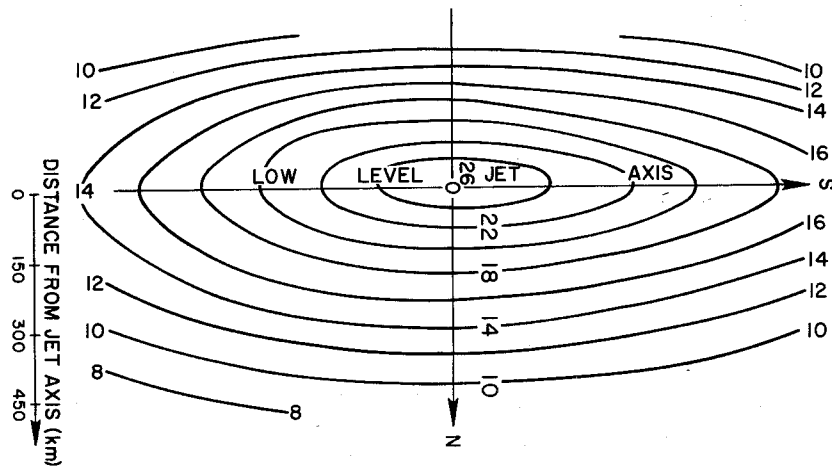


Fig. 22. Mean wind component along the jet axis at the 0.5-km level, after Bonner et al. (20).

The diurnal oscillation of the low-level jet is nearly opposite in phase to the surface wind oscillation. Winds at the level of the jet core reach maximum speed early in the morning (0000-0600 local standard time) and minimum speed in the afternoon. At the time of maximum development, the wind profile under the jet core is approximated satisfactorily for balloon flight planning by Eq. (23) if a value of 0.35 is used for b . The maximum wind shear under the jet core also falls within the values given by Eq. (22) for extreme shear in the free atmosphere.

The low-level jet appears to reach a high state of development in summer in the central Great Plains area of the United States, but diurnal wind variations at low levels which shared most of the features associated with the low-level jet were observed throughout most of the United States in July 1958 by Hering and Borden (21). Also, Rider and Armendariz (22) have reported many well-developed low-level jets in the valley between the Organ and San Andres mountains on one side and the Sacramento mountains on the other in New Mexico. Theory (which is inadequate to explain many features of the jet) and observation suggest that if the mean circulation in the lower troposphere is changing little from day to day in middle latitudes

in summer and if the hydrostatic stability of the boundary layer is undergoing marked diurnal changes, a phenomenon akin to the low-level jet should be expected.

E. OTHER METEOROLOGICAL VARIABLES, DATA SOURCES

The thermal structure of the whole atmosphere and its circulation have been described briefly in C and D of this section. To attempt to describe global cloudiness or visibility in a meaningful way is not feasible here. The same is true of most of the other atmospheric properties which may affect a scientific ballooning operation. However, once the proposed site for a balloon flight has been localized to a few areas, a competent meteorologist can usually find climatological data for those areas, from which he can answer most planning needs. Studying the climate of an area also gives a meteorologist a better perspective of day-to-day weather in the area and is helpful in making an operational forecast.

The following list of sources of data is not complete, but the sources listed do provide much valuable, summarized data useful to a meteorologist. Others may also find much of value in them, but they can be misleading if

they are not properly interpreted. General data summaries are listed first, and more specialized summaries are listed later.

Handbook of Geophysics, Rev. Edition. Published initially by the U.S. Air Force in 1957 and in revised form by The Macmillan Company in 1961, this volume is an excellent source of geophysical data. It also contains much explanatory material which helps the reader to understand and interpret the data.

U.S. Naval Weather Service World Wide Airfield Summaries. Most meteorological data in recent decades have been observed at airfields. These summaries provide that data in highly usable form. Volume I covers Southeast Asia; Vol. II--Part 1 and Part 2--the Middle East; Vol. III, the Far East; Vol. IV, Canada, Greenland, and Iceland; Vol. V, Australia and Antarctica; Vol. VI--Part 1 and 2--South America; Vol. VII, Central America; Vol. VIII--Parts 1 through 8--the United States. These summaries are available from the Federal Clearinghouse for Scientific and Technical Information, Springfield, Va. 22151.

U.S. Navy Marine Climatic Atlas of the World. This atlas in seven volumes provides highly useful summaries of weather information for all

the world's oceans. The volumes and the area covered by each are:

Vol. I, North Atlantic; Vol. II, North Pacific; Vol. III, Indian Ocean;

Vol. IV, South Atlantic; Vol. V, South Pacific; Vol. VI, Arctic; Vol.

VII, Antarctic. These may be obtained from the U.S. Navy Weather

Service Command MOIA, Washington Navy Yard, Bldg. 200, Washington,

D.C. 20390.

Climatic Atlas of the United States. This atlas, published by the U.S. Department of Commerce, contains many useful climatic charts of the United States. It is available from the U.S. Government Printing Office, Washington, D.C. 20401.

Selected Level Temperatures and Dew Points for the Northern Hemisphere. This is a collection of monthly mean Northern Hemisphere temperature and dew point charts for selected levels up to and including the 100-mb level. It is available from the U.S. Naval Weather Service Command MOIA, Washington Navy Yard, Bldg. 200, Washington, D.C. 20390.

Climate of the Upper Air, Part 1--Southern Hemisphere. Planned as a four-volume series, the first volume was published in September 1969. It contains monthly mean temperatures, dew points, and heights

at selected pressure levels up to and including the 100-mb level for some variables. Later volumes are to contain geostrophic wind data and meridional cross sections of temperature, dew point, and isobaric height.

Volume I may be obtained from U.S. Naval Weather Service Command MOIA, Washington Navy Yard, Bldg. 200, Washington, D.C. 20390.

Upper Wind Statistics Charts of the Northern Hemisphere.

Vol. I (850-, 700-, and 500-mb levels)

Vol. II (300-, 200-, and 100-mb levels)

These volumes show charts of wind vectors and vector standard deviations. This method of presentation concentrates information tremendously, but to recover the information, the user must have a good understanding of the basis and limitations of the data presentation technique. Instructions are provided.

These volumes may be obtained from U.S. Naval Weather Service Command MOIA, Washington Navy Yard, Bldg. 200, Washington, D.C. 20390.

Data Report Meteorological Rocket Network Firings. These reports contain data from the U.S. meteorological rocket network. Data are

shown in both graphical and tabular form. The reports, covering data for the fall of 1959 through December 1963, were prepared by the U.S. Army Electronics Research and Development Activity, White Sands Missile Range, New Mexico. The data of January 1964 through December 1968 were prepared by the World Data Center A for Meteorology, which is located at the National Climatic Center of the National Oceanic and Atmospheric Administration, Asheville, North Carolina 28801.

High Altitude Meteorological Data. Beginning with the January 1969 data, the World Data Center A for Meteorology started publishing monthly reports of all types of high altitude meteorological data, including U.S. and other rocket data. These reports are available from the Superintendent of Documents, Government Printing Office, Washington, D.C. 20402.

Exametnet Data Report Series Annual Reports. These annual reports contain data from the Experimental Inter-American Meteorological Rocket Network. Published by The National Aeronautics and Space Administration, they are available from the Clearinghouse for Federal Scientific and Technical Information, Springfield, Va. 22151.

Weekly Synoptic Analyses, 5-, 2-, and 0.4 Millibar Surfaces.

The Upper Air Branch of the U.S. National Meteorological Center, using data from the rocket network and rawinsonde data with elaborate extrapolation techniques, prepares weekly analyses at high levels which are a valuable source of information to a meteorologist who must support scientific ballooning operations. Unfortunately, the analyses are not available until months after the data are observed; therefore, they serve as a tool for learning about the behavior of the high atmosphere, but not as a forecasting tool. Inquiries about these reports may be addressed to The Upper Air Branch, National Meteorological Center, National Oceanic and Atmospheric Administration, Washington, D.C.

Special Data Summaries. The National Climatic Center of the National Oceanic and Atmospheric Administration at Asheville, North Carolina 28801, can provide special data summaries upon request. The cost of such a summary can be high, and a careful review of requirements with personnel at the Center is well worthwhile before a summary is ordered.

F. FORECASTS

A meteorologist can make a completely successful forecast for an operation only if he understands the operation well enough to know how it is sensitive to the weather, has adequate current meteorological data, and has a thorough understanding of the atmosphere and its behavior.

In B of this section an attempt has been made to show how balloon operations are affected by the weather. It can serve as a starting point for both the meteorologist and operations personnel when a balloon flight is being planned, but as flight techniques and requirements change, meteorological and support requirements will also change. Therefore, they should be reviewed before each flight. Having the meteorologist serve as an active member of the operations team throughout the flight planning and execution is one way to assure that he or she understands support requirements.

Most experienced airways forecasters who have been briefed on balloon flight requirements will be able to make adequate forecasts for launch and recovery operations. They will also be able to forecast for the operation of a tracking aircraft. These aspects of balloon flight operations occur in the lower troposphere where data are most available and where data analyses

are most carefully performed.

Only one who has devoted much study to the middle and upper stratosphere can analyze the extremely limited data at those levels and make an acceptable forecast from them. A local forecast office may be able to provide some high level data, but often it can do that only if special arrangements are made in advance. Also, the computation of ascent and descent vectors, although conceptually simple, is not a part of the service normally offered by a local forecast office. Furthermore, high level wind forecasts must be made before ascent and descent vectors can be computed. Consequently, this computation must be done by a specialist if it is to be done well.

G. OPERATIONAL PLANNING

It is important that an experienced balloon meteorologist be consulted before deciding on an operational plan for any but the most routine balloon flights. By fitting the requirements of the operation into the optimum atmospheric environment, a knowledgeable operations analyst can reduce the probability of failure and, indeed, make a close estimate of the feasibility of an operation. He can often suggest minor modifications of the original requirements which will improve the cost-effectiveness of the operation.

Because most scientific balloon flights are conducted in middle latitudes and a successful flight depends so much on the winds, the following rather specific thoughts are offered.

The stratospheric easterlies in summer are the scientific balloonists' best friend. They are the steadiest winds known, and during the season in which they blow, one can launch a balloon a considerable distance upwind from a target area (~ 120 km) with reasonable confidence that it will cross the target meridian in a given time and that the crossing will be practically over the target. The optimum months for such flights are July and August at latitude 35°N, somewhat earlier farther north, and later farther south, at any altitude above 25 km. Long-range flights, even round-the-world flights, can be planned with the aid of these winds with excellent prospects of recovery.

In the stratospheric westerlies in winter, transcontinental flights of up to three days' duration from United States west-coast sites, and one-or two-day-duration flights from sites farther east can be achieved. Winter ballooning in temperate latitudes is severely limited, however, by unfavorable surface weather. Also, west-coast sites, in particular, are inoperative

for several weeks during periods of circulation reversal. These winds, unlike the easterlies, are often characterized by waves of great amplitude so that tracking and recovery facilities must be very flexible.

The stratum of minimum winds found at about 20 km may be used to good advantage, especially in the spring and fall, for long duration flights of limited horizontal displacement. Experience has shown that although the vector mean wind may be zero, the scalar winds at these levels are never really zero, and they meander with a minimum speed of about 6 m/sec.

Hovering flights are also feasible in the early summer. In these flights, the balloon rises during the daytime to the edge of the easterlies and descends at night into the light westerlies below. Such flights require careful planning and coordination.

REFERENCES

- (1) U.S. Standard Atmosphere, 1962: U.S. Government Printing Office, Washington, D. C., pp. 278.
- (2) U.S. Standard Atmosphere Supplements, 1966: U.S. Government Printing Office, Washington, D. C., pp. 289.
- (3) Haltiner, George J. and Frank L. Martin, 1957: Dynamic and Physical Meteorology, McGraw-Hill, New York, p. 164.
- (4) Glueckauf, E., 1951: The Composition of Atmospheric Air, Compendium of Meteorology, edited by Thomas F. Malone, American Meteorological Society, Boston, Mass., p. 3.
- (5) Palmén, E. and C. W. Newton, 1969: Atmospheric Circulation Systems, Academic Press, New York and London, pp. 603.
- (6) Solot, Samuel B. and Eugene M. Darling, Jr., 1958: Theory of Large Scale Atmospheric Diffusion and its Application to Air Trajectories, Vols. I and II. Geophysical Research Paper No. 58, U.S. Air Force Cambridge Research Laboratory, Bedford, Mass.
- (7) Anonymous, 1971: Weekly Synoptic Analyses 5-, 2-, and 0.4-Millibar Surfaces for 1968, NOAA Technical Report NWS 14.
- (8) Reed, Richard J., 1965: The Present Status of the 26-Month Cycle, Bulletin of the American Meteorology Society, Vol. 46, No. 7, 374-387.
- (9) Reed, Richard J., 1966: Zonal Wind Behavior in the Equatorial Stratosphere and Lower Mesosphere, Journal of Geophysical Research, Vol. 71, No. 18, 4223-4233.

- (10) Belmont, A. D. and D. G. Dartt, 1966: The Non-Repeating Variations of the Observed Wind in the Equatorial Stratosphere, Tellus XVIII, 2, 381-390.
- (11) Kriester, Barbara, 1971: Large Scale Circulation Patterns of the Stratosphere. A paper presented at the SPARMO Colloquium on The Technology and Utilization of Stratospheric Balloons, Seattle, Wash., June 1971.
- (12) Endlich, R. M., S. B. Solot and H. A. Thur, 1955: The Mean Vertical Structure of the Jet Stream, Tellus 7, 308-313.
- (13) Essenwanger, O., 1963: On the Derivation of Frequency Distributions of Vector Wind Shear Values for Small Shear Intervals, Geofis. Pura. Appl. 56, 216-224.
- (14) Essenwanger, O., 1967: Comments on "Mesoscale Structure of 11-20 km Winds," Journal of Applied Meteorology, Vol. 6, No. 3, 591-593.
- (15) Weinstein, A. I., E. R. Reiter and J. R. Scoggins, 1966: Mesoscale Structure of 11-20 km Winds, Journal of Applied Meteorology, Vol. 5, No. 1, 49-57.
- (16) Adelfang, Stanley I., 1971: On the Relations Between Wind Shears over Various Altitude Intervals, Journal of Applied Meteorology, Vol. 10, No. 1, 156-159.
- (17) Priestly, C. H. B., 1959: Turbulent Transfer in the Lower Atmosphere, University of Chicago Press, Chicago, Ill.
- (18) Lumley, John L. and Hans A. Panofsky, 1964: The Structure of Atmospheric Turbulence, Interscience Publishers, New York, 99-118.
- (19) Frost, R., 1948: Atmospheric Turbulence, Quarterly Journal, Royal Meteorological Society, Vol. 74, 316-338.

- (20) Bonner, W. D., S. Esbensen and R. Greenberg, 1968: Kinematics of the Low-Level Jet, Journal of Applied Meteorology, Vol. 7, No. 3, 339-347.
- (21) Hering, Wayne S. and Thomas R. Borden, Jr., 1962: Diurnal Variations In the Summer Wind Field over the Central United States, Journal of the Atmospheric Sciences, Vol. 19, No. 1, 81-86.
- (22) Rider, Laurence J. and Manuel Armendariz, 1970: Nocturnal Maximum Winds in the Planetary Boundary Layer at WSMR, Tech. Report ECOM 5321, U.S. Army Electronics Command, Fort Monmouth, N.J.

SECTION XII

TABLES, GRAPHS, AND MISCELLANEOUS INFORMATION

by

Alvin L. Morris

List of Figures iii

List of Tables v

A. INTRODUCTION 1

B. CROSS SECTIONAL AREA OF A BALLOON 2

C. BALLOON ROTATION 6

D. BALLOON SYSTEM PENDULATION 9

1. Simple Pendulum 9

2. Compound Pendulum 14

3. Torsional Pendulum 16

 REFERENCES 21

E. GAS FLOW THROUGH AN ORIFICE 22

F. VERTICAL CUTOFF RIGIDITY 24

 REFERENCES. 26

G. LANDING ENERGY ABSORBERS 27

1. Landing Energy 27

2. Energy and Acceleration 27

3. Energy Absorbers 29

4. Horizontal Motion 40

 REFERENCES. 45

H. PARACHUTE COMPUTATIONAL AIDS 46

1. Selecting a Parachute 46

2. Terminal Velocity and Time of Descent 50

I. GAS MEASUREMENT AND INFLATION PROCEDURES 58

J. GAS DATA 78

1. Miscellaneous Gas Data 79

 REFERENCES 80

2. Gas Constant and Specific Heat Data for Selected Gases 81

 REFERENCES 89

3. Thermal Conductivity of Selected Gases 90

 REFERENCES 96

4. Viscosity of Selected Gases 97

 REFERENCES 103

5. Prandtl Number of Selected Gases 104

 REFERENCES 108

K. SPECIFIC LIFT OF HELIUM AND HYDROGEN AND PROPERTIES OF THE
 U.S. STANDARD ATMOSPHERE, 1962 109

 REFERENCES 119

L. BASIC NATURAL-SHAPE BALLOON PARAMETERS 120

M. BUOYANT EQUILIBRIUM DIAGRAMS 128

N. SUNRISE AND SUNSET 131

O. STAR CHARTS. 133

List of Figures

Fig. B-1	Area of a sphere-on-cone figure projected on a plane normal to the vector \vec{v}_r	3	Fig. H-1a	Sea level terminal velocity of a parachute system as a function of system mass and the product of parachute area and drag coefficient.	54
Fig. B-2	Sketch of a partially inflated balloon which has formed a spinnaker-like sail in a relative wind represented by the vector \vec{v}_r	5	Fig. H-1b	Sea level terminal velocity of a parachute system as a function of system weight and the product of parachute area and drag coefficient.	55
Fig. C-1	Rotation data for large balloon systems. For any point on a curve, rotation rates less than or equal to the abscissa value of the point were observed to occur with the percentage frequency of the ordinate value of the point	7	Fig. H-2	Diameter of a parachute as a function of area and drag coefficient. Diameter is nominal diameter if the pseudo drag coefficient is used. The following are typical pseudo drag coefficients: $C_D' = 0.75$ (design value often quoted for a flat, circular canopy), $C_D' = 0.85$ (empirical value used by NCAR for large flat, circular canopies), and $C_D' = 0.55$ (value quoted by Raven Industries, Inc. for their RAVEN PLUS $\text{\textcircled{R}}$ shape).	56
Fig. D-1	A sketch of a balloon system showing the nomenclature used in considering the system as a pendulum	10	Fig. H-3	Terminal velocity and time of descent as functions of sea level terminal velocity and altitude in the <u>U.S. Standard Atmosphere, 1962</u>	57
Fig. D-2	A balloon payload acting as a compound pendulum	15	Fig. I-1	Relationship between p_c , p_l , and p_f	65
Fig. D-3	Torsional pendulum model of a balloon system	17	Fig. M-1	Buoyant equilibrium diagram for helium	129
Fig. F-1	Vertical cutoff rigidity. The curves are isolines of vertical cutoff rigidity in gigavolts.	25	Fig. M-2	Buoyant equilibrium diagram for hydrogen	130
Fig. G-1	Typical stress-strain curve for paper honeycomb.	30	Fig. O-1	Northern Hemisphere star chart	135
Fig. G-2	Rod and die energy absorber	32	Fig. O-2	Southern Hemisphere star chart	136
Fig. G-3	Plan view (upper) and side view of a single layer of a crush pad made of sections of honeycomb between light, rigid plates.	39			
Fig. G-4	A multilayer honeycomb crush pad bound by vertical cables-- before and after landing	42			

List of Tables

Table G-1 Paper honeycomb strength data	38
Table I-1 Lift (kg/m^3) of gas contained in steel cylinders--helium . . .	66
Table I-2 Lift (lb/ft^3) of gas contained in steel cylinders--helium . . .	68
Table I-3 Lift (kg/m^3) of gas contained in steel cylinders--hydrogen . . .	72
Table I-4 Lift (lb/ft^3) of gas contained in steel cylinders--hydrogen . . .	74
Table J-1 Miscellaneous gas data.	85
Table J-2 Constants for the specific heat-temperature correlating equation.	86
Table J-3 Gas constant R in various systems of units	87
Table J-4 Value of C_p/R for select gases as a function of temperature . . .	88
Table J-5 Values of C_p/C_v for select gases as a function of temperature . . .	89
Table J-6 Values of n for select gases.	93
Table J-7 Values of k_o for selected gases	93
Table J-8 Thermal conductivity ratios for selected gases as a function of temperature.	95
Table J-9 Values of S for selected gases	99
Table J-10 Values of μ_o for selected gases	101
Table J-11 Values of μ/μ_o for selected gases as a function of temperature. . .	102
Table J-12 Constants for the Prandtl number-temperature correlating equation	106
Table J-13 Prandtl number for selected gases as a function of temperature. . .	107
Table K-1 Specific lift of helium and hydrogen and properties of the <u>U.S. Standard Atmosphere, 1962</u>	113
Table L-1 Balloon design parameters	122

TABLES, GRAPHS, AND MISCELLANEOUS INFORMATIONA. INTRODUCTION

This section contains information which is useful in the practice of scientific ballooning but was not deemed appropriate for inclusion in any of the other sections. Each topic is essentially complete and unrelated to the others in the section; the topics are arranged arbitrarily. Tables, figures, and equations are number sequentially within each principal sub-section with letter prefixes corresponding to the sub-section. Each sub-section lists its own literature references.

B. CROSS SECTIONAL AREA OF A BALLOON

The form of a tethered balloon and of a balloon in normal flight may be approximated by the sphere-on-cone shape shown in Fig. B-1. The radius r is the radius of a sphere whose volume is equal to the volume of the gas. The value of θ is controlled in a tethered balloon and is known. For a balloon in flight, θ may take a value as low as 15° when the balloon is only slightly inflated; when the balloon is fully inflated, it will be the nadir (base) angle of the balloon (see Sections V and XII.L).

The area A_D of a sphere-on-cone figure projected on a plane normal to the relative wind is

$$A_D/r^2 = \pi + \left[\sin \cos^{-1} \left(\frac{\sin \theta}{\sin b} \right) \right] \left[\left(\cot^2 \theta - 1 + \frac{\sin^2 \theta}{\sin^2 b} \right)^{\frac{1}{2}} \right. \\ \left. \sin \left(b - \tan^{-1} \frac{\tan^2 \theta}{\tan b} \right) + \frac{\sin \theta}{\sin b} \right] - \cos^{-1} \left(\frac{\sin \theta}{\sin b} \right) \quad (B-1)$$

where b is defined by Fig. B-1. When $b < \theta$, let $\sin \theta / \sin b = 1.0$.

A graph of this equation is also presented in Fig. B-1.

The equation

$$\frac{A_D}{r^2} = \pi + \left(\theta - \frac{\pi}{2} + \cot \theta \right) \sin b \quad (B-2)$$

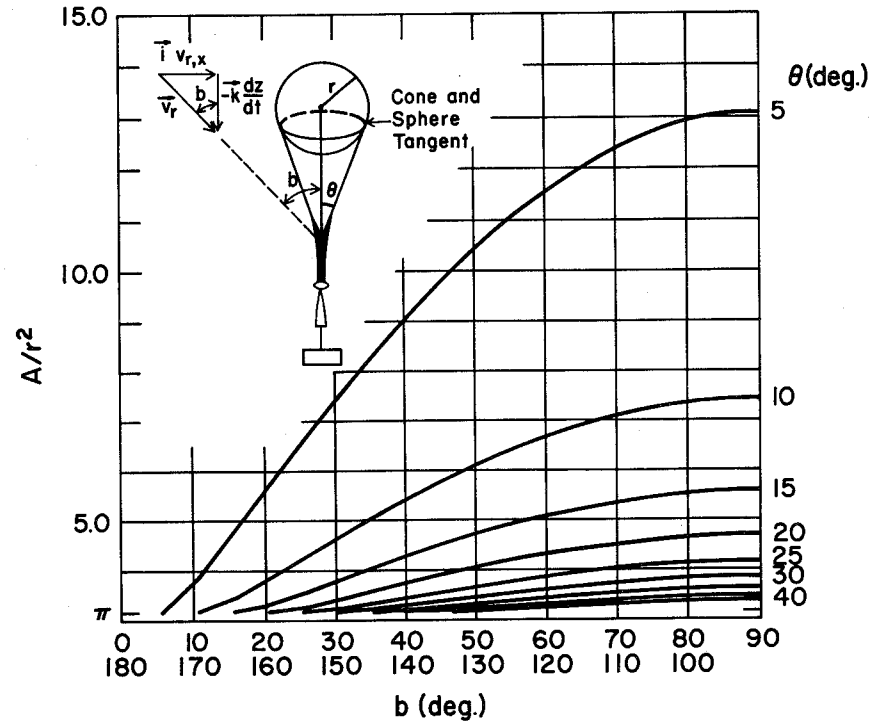


Fig. B-1. Area of a sphere-on-cone figure projected on a plane normal to the vector \vec{v}_r .

is much simpler, and for most ballooning calculations it provides an adequate means of approximating A_D .

A balloon which has formed a sail is shaped much like a hemispherical cup with the concave side facing into the wind. Figure B-2 depicts a balloon which has "sailed." The equation

$$A_D = 1.21 V_i^{2/3} \left(\frac{1 + \sin b}{2} \right) \quad (\text{B-3})$$

may be used to approximate A_D for such a balloon. In this case V_i is the nominal, fully-inflated volume of the balloon.

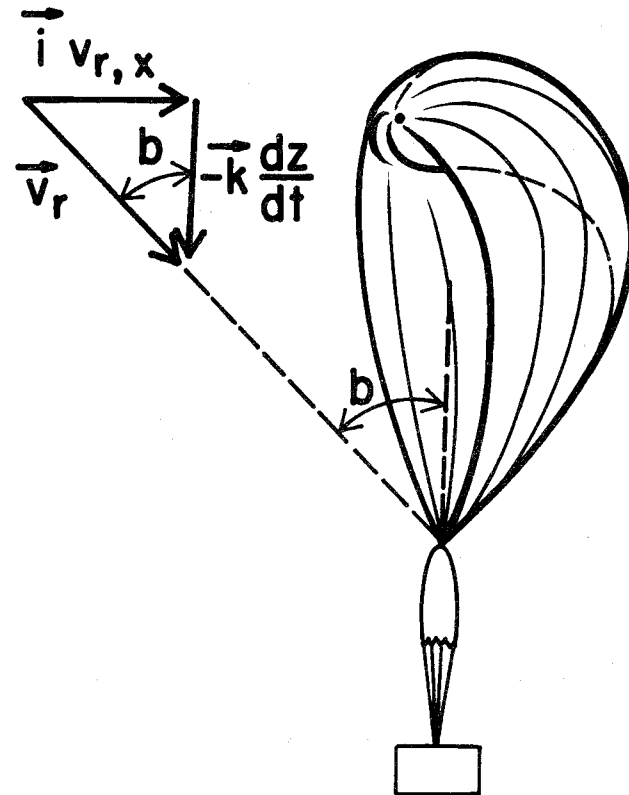


Fig. B-2. Sketch of a partially inflated balloon which has formed a spinnaker-like sail in a relative wind represented by the vector \vec{v}_r .

C. BALLOON ROTATION

A balloon is set in rotation about its vertical axis during ascent by the relative downward motion of the air past it. Even when a balloon is floating, it often oscillates up and down with a period of a few minutes (see Section II.I.4), and either this motion or the turbulent motion of the ambient air is enough to cause rotation.

Rotational data from five flights are summarized by the curve marked "FLOAT" in Fig. C-1. One balloon floated at 22 km, two at 37 km, one at 39 km, and one at 40 km. The data are not adequate to permit the rotation rate to be related quantitatively to float altitude, but they do suggest that balloons floating at greater heights rotate less than balloons at lower heights. The curve for floating balloons can be fitted quite well by the empirical equation

$$y = 100 \left(\tanh \frac{x}{22} \right)^{\frac{1}{2}} \quad (C-1)$$

where y is the percentage frequency of occurrence of rotation rates of x deg/min or less.

The curve marked "ASCENT" summarizes ascent rotational data up to 150 deg/min for three flights. All of the balloon systems rose to heights of 37

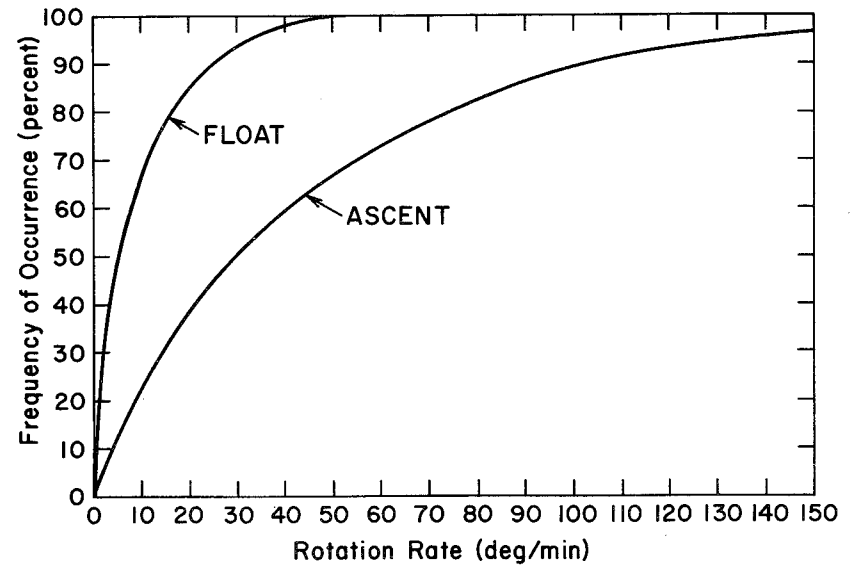


Fig. C-1. Rotation data for large balloon systems. For any point on a curve, rotation rates less than or equal to the abscissa value of the point were observed to occur with the percentage frequency of the ordinate value of the point.

km or more, and no systematic variation from flight to flight was noted.

The data are fitted well for all rotation rates by the empirical equation

$$y = 100 \left[\tanh \frac{x^2}{94(x+8)} \right]^{\frac{1}{2}} \quad (C-2)$$

The maximum angular acceleration observed on any of the flights was 2.5×10^{-2} deg/sec², averaged over a two-minute period. This occurred during ascent when the vertical speed of the balloon was large and the moment of inertia of the system was relatively small.

D. BALLOON SYSTEM PENDULATION

1. Simple Pendulum

The longitudinal (vertical) axis of a large, fully-inflated balloon with a payload suspended from it is known to deviate very little from the vertical during flight. The balloon system is embedded in the air and moves with it; therefore, unless there is wind shear, turbulence, or wind acceleration in the atmosphere, there are no perturbing forces external to the balloon to act upon it. Internal forces which may be created in an effort to change the aspect of all or part of the payload may perturb the system.

Figure D-1 is a sketch of a balloon system which shows the nomenclature used here.

Perhaps the simplest pendulum model is one which treats the payload as a point mass at the end of a massless suspension system and the balloon as a rigid platform. This is the simple pendulum. Its period is $2\pi\sqrt{l/g}$; its angular frequency is $\sqrt{g/l}$.

A more realistic model considers the system to consist of a sphere which can turn about its center. At one point on the surface of the sphere, a massless line of length l is fastened. A point mass payload is secured to

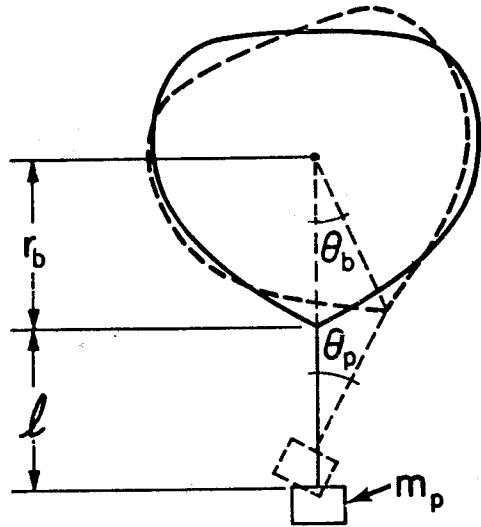


Fig. D-1. A sketch of a balloon system showing the nomenclature used in considering the system as a pendulum.

the other end of the line. The addition of a viscous force to dampen the motion of either the sphere or the payload or both adds still more realism.

A further simplification may be made by substituting a wheel for the balloon and restricting the motion to the plane of the wheel. The system is thus reduced to one having two degrees of freedom. Also, let the wheel's mass be uniformly distributed about its rim, its radius be given by the equation $4\pi r_B^3/3 = V_B$ (where V_B is the volume of gas in the balloon), and its moment of inertia be equal to that of the sphere. Since a fully-inflated balloon is approximately a sphere and since the moment of inertia of a thin shelled hollow sphere about an axis through its center is $2/3 mr^2$, while that of a wheel of the type assumed here is mr^2 , the mass of the wheel is taken as $2/3$ the mass of the balloon.

The equations of motion of the model for small displacements are

$$\left. \begin{aligned} \left(\frac{2}{3} m_B + m_p\right) r_B \ddot{\theta}_B + m_p l \ddot{\theta}_p + m_p g \theta_B &= 0 \\ r_b \ddot{\theta}_b + l \ddot{\theta}_p + g \theta_p &= 0 \end{aligned} \right\} \quad (D-1)$$

or if the motion of both the balloon and payload are viscously damped and

c_B and c_p are their respective damping coefficients

$$\left. \begin{aligned} \left(\frac{2}{3}m_B + m_p\right)r_B \ddot{\theta}_B + m_p l \ddot{\theta}_p + c_B r_B \dot{\theta}_B + m_p g \theta_B &= 0 \\ r_B \ddot{\theta}_B + l \ddot{\theta}_p + c_p l r_B \dot{\theta}_B + c_p l^2 \dot{\theta}_p + g \theta_p &= 0 \end{aligned} \right\} \text{(D-2)}$$

Either set of equations may be solved analytically. Both sets yield oscillatory solutions, and the frequency equation for each set is a quartic equation. The frequency equation for set (D-1) is quadratic in ω^2 where ω is the angular frequency, while the equation for set (D-2) is not. Therefore, the solution equations for set (D-1) are simpler and more amenable to intuitive understanding than those for set (D-2). They do, however, contain the principal features of the motion; consequently, they alone are given as set (D-3):

$$\left. \begin{aligned} \theta_B &= A_1 \sin(\omega_1 t + \psi_1) + A_2 \sin(\omega_2 t + \psi_2) \\ \theta_p &= B_1 \sin(\omega_1 t + \psi_1) + B_2 \sin(\omega_2 t + \psi_2) \end{aligned} \right\} \text{(D-3)}$$

in which

$$\omega^2 = \left(\frac{g}{l}\right) \frac{\left[\frac{2}{3}m_B r_B + m_p (r_B + l)\right] \pm \sqrt{\left[\frac{2}{3}m_B r_B + m_p (r_B + l)\right]^2 - \frac{8}{3}m_B m_p r_B l}}{\frac{4}{3}m_B r_B} \quad \text{(D-4)}$$

The frequency ω_1 is given when the (+) sign is used before the radical;

ω_2 is given when the (-) sign is used. Negative frequencies are not allowed.

If $m_B \gg m_p$ and r_B is not small compared to l , Eq. (D-4) reduces to approximately $\omega_1 = \sqrt{g/l}$ and $\omega_2 = 0$.

It can be shown that

$$\left. \begin{aligned} \frac{A_1}{B_1} &= \frac{-(l\omega_1^2 - g)}{r_B \omega_1^2} \\ \frac{A_2}{B_2} &= \frac{-(l\omega_2^2 - g)}{r_B \omega_2^2} \end{aligned} \right\} \text{(D-5)}$$

Therefore, if $\omega_1^2 = g/l$ and $\omega_2^2 = 0$, B_2 is zero and from set (D-3)

$$\theta_p = B_1 \sin\left(\sqrt{\frac{g}{l}} t + \psi_1\right)$$

which is the solution equation for a simple pendulum of length l . If

$r_B \approx l$, as it usually is in a scientific balloon system, m_B must be at

least two orders of magnitude larger than m_p for this approximation to be

reasonable. Since it rarely is, however, the simple pendulum model is not

a good one.

The values of B_1 and B_2 (or A_1 and A_2) and ψ_1 and ψ_2 must be determined from the initial conditions of the system. In large balloon systems, θ_p

rarely exceeds a few minutes of arc after the system has reached a steady state float condition.

2. Compound Pendulum

The payload may vibrate as a compound pendulum, and this vibration may be nearly independent of the pendulation of the entire balloon system. On the other hand, energy may be exchanged between the two modes of vibration. Figure D-2 illustrates a payload which cannot be suspended from its top. If a substantial portion of the mass is above the suspension point, the distance d from the suspension point to the center of gravity may be small. The equation of motion of such a system, if it is not damped, is

$$J \ddot{\theta} + m_p g d \sin \theta = 0 \quad (D-6)$$

where J is the moment of inertia of the payload about the axis of suspension, m_p is the payload mass, g is the acceleration due to gravity, and θ and d are defined in Fig. D-2. If θ is small so that $\sin \theta \approx \theta$, the solution of Eq. (D-6) is

$$\theta = C \sin (\omega t + \psi) \quad (D-7)$$

and

$$\omega = \sqrt{mgd/J} \quad (D-8)$$

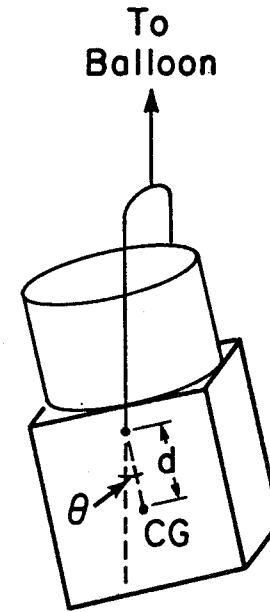


Fig. D-2. A balloon payload acting as a compound pendulum.

Assume that $t = 0$, $\theta = 0$, and $\dot{\theta} = \dot{\theta}_0$. With these initial conditions $\psi = 0$ and $C = \dot{\theta}_0 / \omega = \dot{\theta}_0 \sqrt{J/mgd}$. Since $J = md^2 + J_0$, where J_0 is the moment of inertia of the payload about its center of gravity, the ratio $J/d = md + J_0/d$ becomes very large as d becomes small. Thus, the amplitude C of any oscillation, and consequently the excursions θ , may become large if d is small. On the other hand, the torque required to change (e.g., stop) any motion is $J\ddot{\theta}$ or $(md^2 + J_0)\ddot{\theta}$ which becomes a minimum when the suspension point coincides with the center of gravity.

3. Torsional Pendulum

A balloon system may also act as a torsional pendulum which may be simulated by a horizontal wheel of radius r_B joined co-axially to a second wheel of radius r_p by the suspension system. In this model, r_B is the radius of the balloon from the equation $4\pi r_B^3/3 = V_B$ and r_p is the radius of gyration of the payload. Figure D-3 illustrates the model.

The suspension system usually consists of two or more lines separated by a small distance, and the spring constant K of such a system can be calculated from the relationship between torque and displacement given in Fig. 1 of Section VII. For a suspension system consisting of n identical

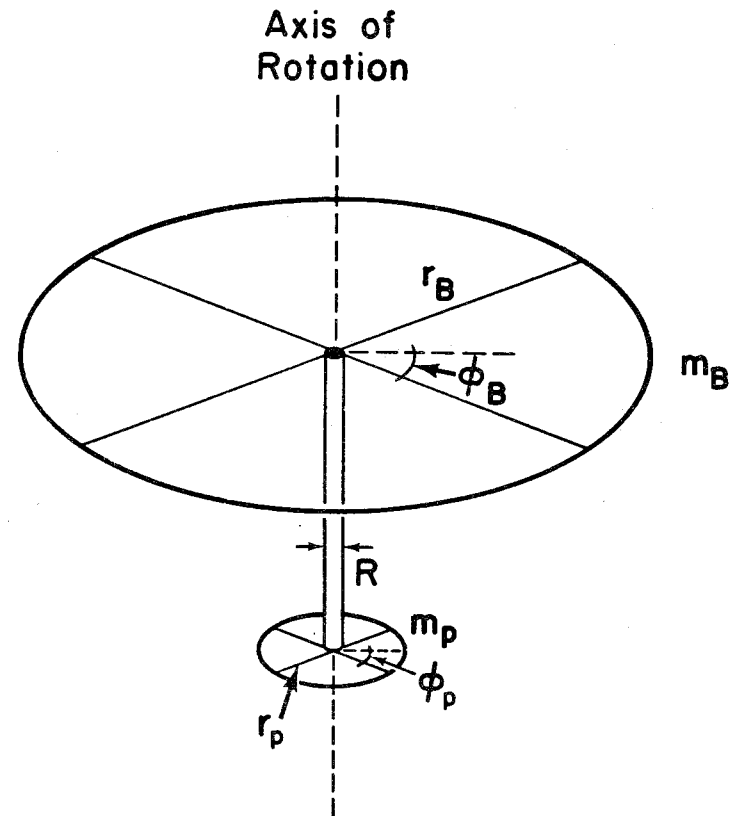


Fig. D-3. Torsional pendulum model of a balloon system.

prismoidal sections of radius R joined end to end,

$$K = \frac{-m_p g R^2}{l} \quad (D-9)$$

where l is the overall length of the suspension and the maximum twisting of any section is so small that $\sin \phi \approx \phi$ and $\cos \phi \approx 1.0$.

The equations of motion of the model are

$$\left. \begin{aligned} J_B \ddot{\phi}_B + \eta_B \dot{\phi}_B + K (\phi_B - \phi_P) &= 0 \\ J_P \ddot{\phi}_P + \eta_P \dot{\phi}_P + K (\phi_P - \phi_B) &= 0 \end{aligned} \right\} \quad (D-10)$$

where η_B and η_P are the torsional damping coefficients of the balloon and payload, respectively. The solution equations are

$$\left. \begin{aligned} \phi_B &= B_1 + f_2 B_2 e^{k_2 t} + C_1 e^{k_3 t} \sin(\omega t + \varphi_1) \\ \phi_P &= B_1 + B_2 e^{k_2 t} + C_2 e^{k_3 t} \sin(\omega t + \varphi_2) \end{aligned} \right\} \quad (D-11)$$

In scientific balloon systems the value of C_1 is normally so small that it may be equated to zero. Also, if the suspension system is not to become twisted, $f_2 \approx 1$. Therefore, the solution equations may be written

$$\left. \begin{aligned} \phi_B &= B_1 + B_2 e^{k_2 t} \\ \phi_P &= B_1 + B_2 e^{k_2 t} + C e^{k_3 t} \sin(\omega t + \varphi) \end{aligned} \right\} \quad (D-12)$$

The sum $(B_1 + B_2)$ is the value of ϕ_B at $t = 0$, and B_1 is the value of ϕ_B when translatory rotation has ceased. The total rotational translation which the balloon will undergo is therefore B_2 . Also the rate of rotation of the balloon at $t = 0$ is $B_2 k_2$.

The amplitude of the undamped oscillation of the payload is given by C .

The frequency of set (D-11) can be determined by solving the characteristic equation of the system. This involves solving a cubic equation and the expression is complicated. Morris and Stefan (1) have shown that the following simple expressions for ω , k_2 , and k_3 are adequate approximations for use in set (D-12):

$$\omega = \frac{R}{r_p} \sqrt{\frac{g}{l}} \quad (D-13)$$

$$k_2 = -\eta_B / J_B \quad (D-14)$$

$$k_3 = -\eta_P / 2J_P \quad (D-15)$$

Values for B_1 , B_2 , C and φ must be determined from initial conditions.

The value of η is a function of air density, air viscosity, and the radius of the balloon. The following equation has been found to give reasonable values of η_B for four flights for which rotation rates were measured:

$$\eta_B = 6 (\mu \rho)^{\frac{1}{2}} r_B^4 \quad (D-16)$$

The form of the equation was suggested by the work of Germeles et al. (2), but as used here, it is strictly an empirical equation. The numerical coefficient, which has the dimensions of $t^{-\frac{1}{2}}$, was determined from about a dozen instances where the rotation decayed monotonically with time. There was no way to assure that the decay rate was not speeded or impeded by relative air motion on the balloon. Therefore, values of η_B computed from the equation should be regarded as crude approximations. The air viscosity μ and the air density ρ may be determined from Tables J-11 and K-1, respectively, or from the U.S. Standard Atmosphere, 1962, (3).

The value of η_p is small for most scientific payloads, and the energy loss in the suspension system may be more effective in damping payload oscillations than energy loss to the atmosphere. Damping is observed, however, and $\eta_p \approx 10^{-3} \eta_B$ appears to give an order-of-magnitude approximation to η_p .

REFERENCES

- (1) Morris, Alvin L. and Karl H. Stefan, 1969: High Altitude Balloons as Scientific Platforms, unpublished NCAR paper presented at The American Society of Photogrammetry Symposium on Earth Observations from Balloons, 6 and 7 Feb. 1969, Washington, D.C.
- (2) Germeles, A. E., R. M. Lucas, E. R. Benton, 1963: Rotation of Balloons at Floating Altitudes. A. D. Little, Inc. Tech Rept. III to Office of Naval Research.
- (3) U.S. Standard Atmosphere, 1962: U.S. Government Printing Office, Washington, D.C., pp 278.

E. GAS FLOW THROUGH AN ORIFICE

Gas will flow through an orifice in a balloon with a speed v_g given by the equation

$$\frac{1}{2} \rho_g v_g^2 = p_g - p_a \quad (E-1)$$

where ρ_g is the density of the gas and p_g and p_a are the pressures of the gas and air, respectively.

Also

$$\frac{dV_g}{dt} = -A_e v_g = -A_e \sqrt{\frac{2(p_g - p_a)}{\rho_g}} \quad (E-2)$$

where dV_g/dt is the volume rate of gas flowing through the orifice and A_e is the effective area of the orifice. Normally, CA is substituted for A_e . In the product CA , A is a nominal area (πr^2 for a circular orifice) while C is an orifice coefficient which accounts for any obstructions that may exist in the orifice as well as for all deviations of the actual flow from the theoretical flow. The value of C must be determined empirically; it is rarely below 0.5 and it cannot exceed 1.0. The negative sign is used to indicate that when $(p_g - p_a) > 0$, the flow is a loss of gas by the balloon. The equations above are not valid if $(p_g - p_a) < 0$.

At an orifice on top of a balloon $(p_g - p_a) = g(\rho_a - \rho_g) D_g$ if D_g is the vertical distance from the zero-pressure level to the orifice.

Assuming the gas bubble to be spherical and the zero-pressure level to be at its bottom makes D_g the diameter of the gas bubble. The mass of gas in such a bubble is $m_g = \pi \rho_g D_g^3/6$ and its volume is $V_g = \pi D_g^3/6$. Therefore, the volume rate of flow through an orifice at the top of a balloon may be written in the following forms:

$$\frac{dV_g}{dt} = -CA \sqrt{\frac{2g(\rho_a - \rho_g) D_g}{\rho_g}} \quad (E-3)$$

$$\frac{dV_g}{dt} = -1.58 CA \sqrt{g \left(\frac{\rho_a - \rho_g}{\rho_g} \right) V_g^{1/3}} \quad (E-4)$$

$$\frac{dV_g}{dt} = -1.58 CA \sqrt{g \left(\frac{\rho_a - \rho_g}{\rho_g} \right) \left(\frac{m_g}{\rho_g} \right)^{1/3}} \quad (E-5)$$

Also, if $p_g = p_a$ and $T_g = T_a$ for the purpose of computing density and $g = 9.8$

$$\frac{dV_g}{dt} = -12.3 CA \left(\frac{m_g}{\rho_g} \right)^{1/6} = -12.3 CA V_g^{1/6} \quad (E-6)$$

for helium, and

$$\frac{dV_g}{dt} = -18.1 CA \left(\frac{m_g}{\rho_g} \right)^{1/6} = -18.1 CA V_g^{1/6} \quad (E-7)$$

for hydrogen.

F. VERTICAL CUTOFF RIGIDITY

The vertical cutoff rigidity of a charged particle is defined as the lowest rigidity that particle can possess and still arrive at a specific point on the earth's surface from the zenith, Shea et al. (1). Only particles having a high rigidity can penetrate the earth's magnetic field near the geomagnetic equator, while particles with very low rigidity can penetrate the field at the geomagnetic poles. Figure F-1 is a world map of vertical cutoff rigidities based on charged particle trajectory calculations by Shea and Smart (2) for particles reaching a point 20 km above sea level from the zenith.

According to Haymes (3) cosmic rays are defined as those charged particles that reach the earth's magnetosphere with velocities greater than the solar wind velocity. Cosmic rays are then affected by the earth's magnetic field, and as shown by various studies, e.g., Kent and Pomerantz (4), cosmic ray intensity is highly correlated with the vertical cutoff rigidity. This effect of the magnetic field makes the earth useful as a charged particle energy analyzer. For some experiments high rigidity is preferred; for others, low rigidity will be necessary.

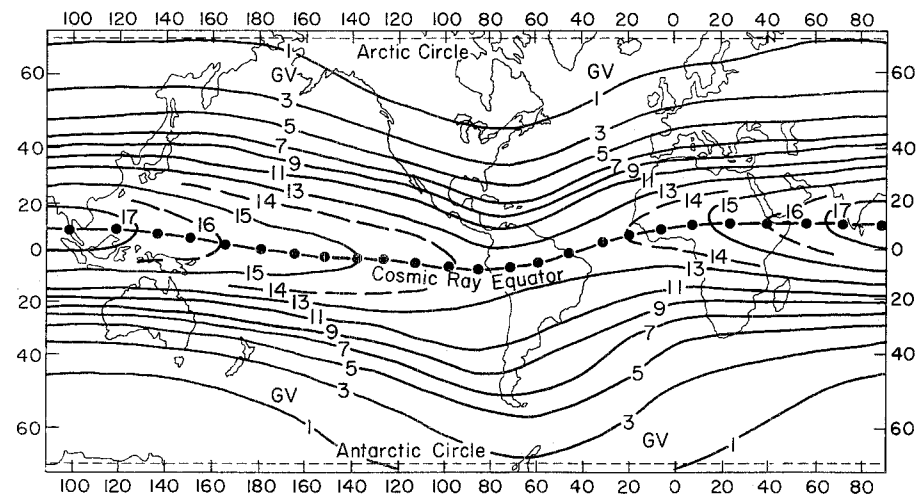


Fig. F-1. Vertical cutoff rigidity. The curves are isolines of vertical cutoff rigidity in gigavolts.

REFERENCES

- (1) Shea, M. A., D. F. Smart, K. G. McCracken, 1965: A Study of Vertical Cutoff Rigidities Using Sixth Degree Simulations of the Geomagnetic Field. Journal of Geophysical Res., Vol. 70, 4117-4130.
- (2) Shea, M. A. and D. F. Smart, 1967: Worldwide Trajectory-Derived Vertical Cutoff Rigidities and Their Application to Experimental Measurements. Journal of Geophysical Res., Vol. 72, 2021-2027.
- (3) Haymes, Robert C., 1971: Introduction to Space Science, John Wiley and Sons, Inc., New York, 369-400.
- (4) Kent, D. W. and M. A. Pomerantz, 1971: Cosmic Ray Intensity Variations in the Lower Atmosphere. Journal of Geophysical Res., Vol. 76, 1652-1661.

G. LANDING ENERGY ABSORBERS1. Landing Energy

If v_i is the vertical velocity of a parachute system at the time the payload touches earth, the energy due to vertical motion which must be dissipated in bringing the payload to a complete stop is $\frac{1}{2}mv_i^2$, where m is the mass of the payload. Likewise, if v_x is the horizontal motion of the payload, it will have a horizontal energy of $\frac{1}{2}mv_x^2$ which must be dissipated. Many types of energy absorbers have been suggested and several have been used in scientific ballooning. None have been entirely satisfactory. Only two will be discussed here, but the problems which are pointed out and much of the discussion will be applicable to others. The one which has been most widely used is a crush pad made from paper honeycomb.

2. Energy and Acceleration

If the acceleration which a payload experiences upon landing were not important, the energy could be absorbed by the gondola and landing surface directly. This would result, in most instances, in destruction or severe damage to the gondola and perhaps to the scientific and control equipment in the gondola. Therefore, it is desirable to limit the acceleration to

some preassigned maximum value while the kinetic energy of the payload is being dissipated.

The relationship $d^2 z/dt^2 = dv/dt = a$ may be integrated between limits as follows:

$$\int_{v_i}^{v_r} dv = \int_{t_i}^{t_r} a dt$$

to yield

$$v_i = - \int_{t_i}^{t_r} a dt = -\bar{a}t_r \quad (G-1)$$

where v_i is the velocity at the time of initial impact t_i , and $v_r = 0$ is the velocity at t_r , the time at which the kinetic energy has been expended. Also, \bar{a} is the average value of acceleration during the period $(t_r - t_i)$. Ideally the acceleration should be constant during that period, because if it is not, then at some time during the period a must be larger than \bar{a} .

Also, $d^2 z/dt^2 = a$ may be integrated twice with limits $z = z_i$, $v = v_i$ at $t = 0$, and $z = z_r$, $v = 0$ at $t = t_r$ to give

$$(z_i - z_r) = \frac{1}{2} \bar{a} t_r^2 \quad (G-2)$$

The height difference $(z_i - z_r)$ is the vertical distance the payload mass

travels from time of first impact with the earth until motion ceases.

If time is eliminated between Eqs. (G-1) and (G-2)

$$(z_i - z_r) = \frac{1}{2} \frac{v_i^2}{\bar{a}} \quad (G-3)$$

This, upon multiplying by m and rearranging, becomes

$$m\bar{a}(z_i - z_r) = \frac{1}{2} m v_i^2 \quad (G-4)$$

Thus, any braking device capable of exerting a force $m\bar{a}$ through a distance $(z_i - z_r)$ can completely dissipate the kinetic energy of mass m moving at a velocity v_i at the instant braking starts.

3. Energy Absorbers

Paper honeycomb is a light, inexpensive material which typically yields to a compressive force acting in a direction parallel to its tubes, as shown by the solid curve in Fig. G-1. The abscissa of Fig. G-1 is the ratio of the relative displacement of the two surfaces to the uncrushed thickness of the material. The ordinate is the ratio of the pressure required to crush the material to the nominal compressive strength. Compressive strength is defined here as the force which must be exerted per unit area to cause the material to yield. More important is the continuing

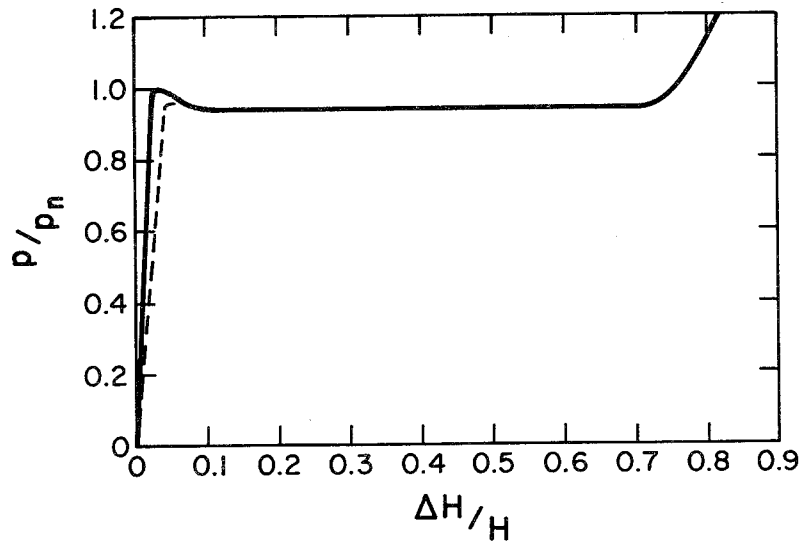


Fig. G-1. Typical stress-strain curve for paper honeycomb.

strength of the material after yield has started and before the cellular structure is so destroyed that the paper itself starts being compressed. If a sheet of paper honeycomb is precrushed, that is, crushed just enough to start the yield, its subsequent yield can be made nearly equal to its continuing strength. It will then have a nearly constant crush strength through about two-thirds of its thickness. The dashed line in Fig. G-1 is a typical stress-strain curve for precrushed paper honeycomb. The constant compressive strength which is a characteristic of good paper honeycomb makes it a good energy absorber.

A rod and die arrangement like that shown in Fig. G-2 may also be used as an energy absorber. The rod is drawn through the die when the drawing force becomes equal to the design actuating force of the rod and die combination. The stress-strain curve is almost identical to that for precrushed honeycomb except that if a uniform rod is used and the die slips off the end, the curve goes down abruptly instead of up when $\Delta H/H$ approaches one. Enlarging the rod near the end, however, will cause the curve to rise as the die approaches the end of the rod.

Consider a load of mass m which is supported on a light, rigid plate.

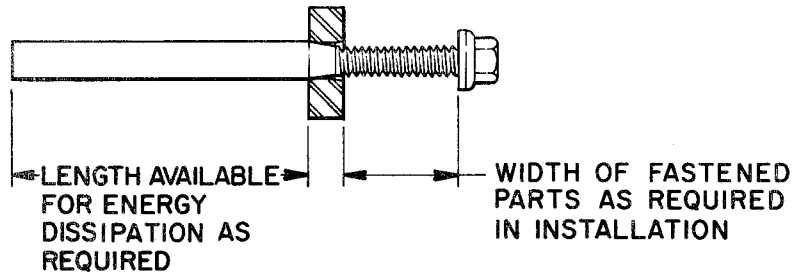


Fig. G-2. Rod and die energy absorber.

Assume that paper honeycomb is available which has a continuing crush pressure (strength) of p_c . Also assume that the maximum acceleration which can be tolerated by the load on landing is ng , where g is the acceleration due to gravity. Then the force required to produce that acceleration of the mass m is mng . That force can be supported by honeycomb having an area A , such that

$$p_c A = mng \quad (G-5)$$

If p_c is constant, then the acceleration ng may be expected to be constant.

From Eq. (G-5) the honeycomb area needed to produce an acceleration ng may be determined.

If the acceleration ng is substituted for \bar{a} in Eq. (G-3), the thickness $(z_i - z_r) = \Delta H$ of honeycomb which must be crushed may also be determined. Because p/p_n starts to grow rapidly for $\Delta H/H > 2/3$, the total thickness H of honeycomb needed is $1.5 \Delta H$. Therefore, Eq. (G-3) written in terms of H is

$$H = 0.75 \frac{v_i^2}{ng} \quad (G-6)$$

Equation (G-5) may be written

$$A = \frac{mg}{P_c} \quad (G-7)$$

Equations (G-6) and (G-7) permit one to calculate the area and thickness of paper honeycomb needed to absorb the energy of a load of mass m moving vertically downward at an initial speed v_i while accelerating the load at the rate ng .

It is interesting that the product AH is the volume of the energy absorber needed and that it is not a function of acceleration. This may be seen by multiplying Eqs. (G-6) and (G-7) together. The resulting equation is

$$Vol = HA = \frac{1.5}{P_c} \left(\frac{1}{2}mv_i^2 \right) \quad (G-8)$$

Equation (G-8) is written in such a way that the kinetic energy is readily identifiable. From Eq. (G-8) it is apparent that one can reduce the area and increase the thickness of a crush pad and not change the quantity of energy which it can absorb. On the other hand, reducing the area will reduce the acceleration during the energy absorption process according to Eq. (G-7). Therefore, subject to the requirement for adequate base area to give the

assemblage stability and the possible requirement to keep it short, a crush pad having a small horizontal area and great vertical depth is preferable to one having a large horizontal area and small vertical depth. An example is useful.

Example: A load of 1000 kg is expected to descend vertically at 7.5 m/sec upon a solid, hard-packed surface. Paper honeycomb which has a compressive strength of 5×10^4 N/m² is available in sheets 10 cm thick. How can a crush pad be designed to absorb the kinetic energy and avoid an acceleration of more than 15 g?

Solution: Using Eq. (G-6) and a slide rule,

$$H = 0.75 \times 7.5 \times 7.5 / (15 \times 9.8) = 0.29 \text{ m}$$

Using Eq. (G-7),

$$A = 10^3 \times 15 \times 9.8 / 5 \times 10^4 = 2.94 \text{ m}^2$$

Three layers of honeycomb formed into a square 1.71 m on a side would meet the requirements if they were mounted in such a way that the compressive forces were uniformly distributed over the surfaces. A larger area would cause an excessive acceleration throughout the energy absorption period. A crush pad having a smaller area and the same thickness would be

crushed completely before all the kinetic energy could be absorbed, and the acceleration would then exceed 15 g.

The volume of crush material required in this example is $2.94 \times 0.29 \text{ m}^3$. If a pad is made four layers or 0.4 m thick, the area can then be reduced to $2.94 \times 0.29/0.40 = 2.13 \text{ m}^2$. Entering this number in Eq. (G-7) yields

$$ng = \frac{2.3 \times 5 \times 10^4}{10^3} \approx 106$$

or $n = 10.8$

This is 28% below the allowable acceleration. Therefore, if an area of 2.13 m^2 provides an adequate base and the added layer of honeycomb does not cause a height problem, the same volume of material provides better protection to the payload in this configuration than in the first configuration. A larger area using four layers could be employed (up to 2.94 m^2) without causing acceleration to exceed 15 g. Doing so would waste material if the energy absorber worked perfectly, but it might provide some assurance of keeping acceleration within 15 g if the energy absorber were to fail to meet expectations.

Paper honeycomb is available in a number of strengths. Select data from one manufacturer are provided in Table 1. The strength of a specific type and sample of honeycomb which is to be used on a gondola should be obtained from the manufacturer or determined by experiment. Occasionally the area of a crush pad may be determined by the restrictions of the experiment on which it is to be used. If so, it will be necessary to select the strength to satisfy Eq. (G-7). For a given area, one may use a lower strength material than that which satisfies Eq. (G-7) if a greater thickness is employed.

If the area of material required according to Eq. (G-7) is smaller than the area desired for a crush pad, a pad may be built up as a multi-layer sandwich. Each layer should consist of two light, rigid plates between which the proper area of honeycomb is placed. The honeycomb should be dispersed symmetrically about the center of gravity of the load and bonded securely to the plates. Figure G-3 illustrates one layer of such a sandwich. Except for the top one, all plates may be made of very strong metal or paper-faced honeycomb or of plywood. The top one will normally be fastened to the gondola and will be made of metal.

Table G-1

Paper Honeycomb Strength Data

Verticel* Designation	Shear Strength**		Compression Strength	
	N/m ² x 10 ⁻⁴	lb/in. ²	N/m ² x 10 ⁻⁴	lb/in. ²
½" 40-50-15%	22.7	33.0	21.6	31.4
½" 60-80-20%	42.5	61.6	42.6	61.8
3/8" 40-50-15%	31.4	45.5	27.1	39.3
3/8" 60-80-20%	69	100	52.1	75.6
¼" 40-50-15%	78	113	71	103
¼" 60-60-20%	102	148	96	140
½" 30-30- 0%	--	--	4.8	7.0
½" 60-80- 0%	--	--	14.8	21.5
¼" 60-60- 0%	--	--	44.5	64.6

*Data courtesy The Verticel Co., Englewood, Colo. The designation numbers indicate the cell size, basis weight, and percent impregnation.

**The shearing forces were contained in parallel planes which cut the honeycomb normal to the axis of the tubes.

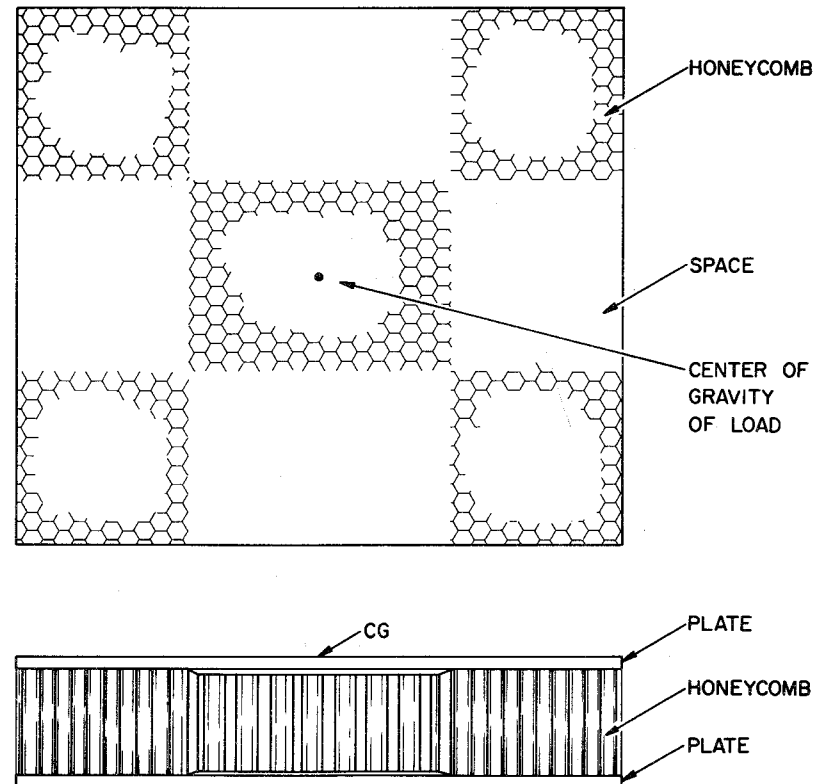


Fig. G-3. Plan view (upper) and side view of a single layer of a crush pad made of sections of honeycomb between light, rigid plates.

4. Horizontal Motion

When a descending system is drifting horizontally at the time of landing, the problem of absorbing the kinetic energy is vastly more complicated than when the motion is vertical. Present landing techniques do not allow the orientation of the impressed force relative to the gondola to be known in advance; therefore, an attempt must be made to make the crush pad absorb energy equally well regardless of the direction of relative horizontal motion. Further, the mechanism for absorbing the energy of horizontal motion must act independently of the mechanism for absorbing the energy of vertical motion, or the two must interact in a known way. Finally, regardless of how well the system is engineered to absorb the energy of a landing on a flat surface, design considerations are not likely to have been adequate if it lands on a steep slope or in a tree top.

The solution most often adopted is to use additional material, such as paper honeycomb, in exactly the same manner as it is used to absorb the energy of vertical motion. This relies on the shearing strength of the honeycomb to reduce the horizontal motion. Unfortunately, the stress-strain curve for the shearing motion involved does not contain a plateau like the

one which characterizes the stress-strain curve for compressive motion. Instead, stress builds nearly linearly until yield starts, and then it rapidly falls to zero as the material tears apart. The solution most often accepted is, therefore, not a good one. If enough area is added to assure that the crush pad has the strength to absorb the energy of horizontal motion without being torn away, resistance to vertical motion will be too large.

A crush pad may be made up as a multi-layered sandwich and made so that both the shear and compressive strengths of the layers increase from layer to layer, with the lowest layer being the weakest. This permits the weaker links in the chain of layers to be used, broken, and lost without losing the benefit of the crush pad. If the top layer were weakest, the entire crush pad might be torn away from the load without having slowed it appreciably. A difference of 3 to 5% in strength between successive layers is adequate.

As an alternative to losing the lower layers of a crush pad progressively, a crush pad may be bound together by bands, or sturdy top and bottom plates may be fastened together by cables as shown in Fig. G-4. Conceptually, this type of construction uses the shearing strength of the honeycomb to

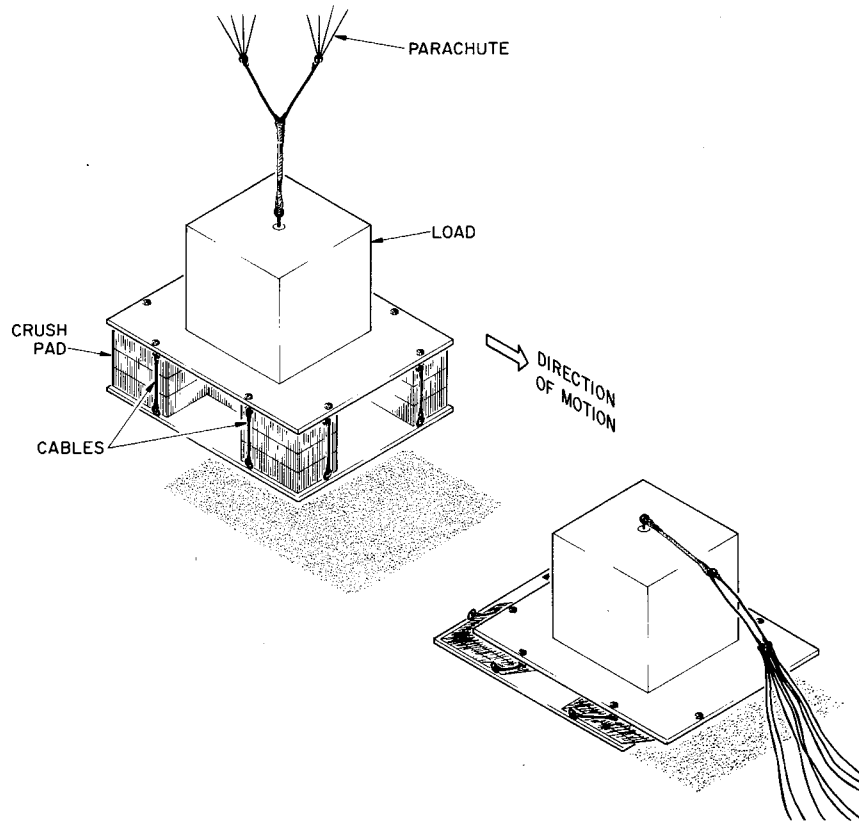


Fig. G-4. A multilayer honeycomb crush pad bound by vertical cables--
before and after landing.

absorb horizontal motion initially, but the cables prevent the paper from tearing apart as the displacement grows and converts horizontal motion into vertical motion. Thus, to a great extent, the horizontal and vertical energy are both absorbed in crushing the honeycomb, and appropriate adjustments to the thickness of the pad must be made. The honeycomb area should not be larger than the maximum allowable for a vertical descent, however, to provide for the contingency of no horizontal motion. The total area of the crush pad should be great enough to prevent the tipping moment caused by horizontal motion from overturning the gondola upon landing. If such a large base is not feasible, protective pads must be used to protect the gondola as it overturns.

Some crush pads were made and tested by Krog (1) in which paper honeycomb was added to the layers with its tubes oriented horizontally. He found that when honeycomb was subjected to shearing forces along its tubes, especially while also being compressed, it absorbed the energy of horizontal motion well and helped prevent the shearing motion from destroying the pad before it had accomplished its purpose. The compressive strength of honeycomb in a direction normal to the tubes is very low through most of its

thickness. Therefore, honeycomb with its tubes oriented parallel to the plates may be added to a sandwich without seriously affecting its reaction to vertical motion.

Practically, the problems of energy absorber design have been solved chiefly through a combination of inspiration (backed by efforts to make engineering approximations) and trial and error. A model energy absorber can readily be fabricated, loaded, and dropped from a truck in motion to simulate a landing. An accelerometer may be used to check the accelerations, and the crush pad may be inspected and its faults corrected. A natural inclination to correct a design by reinforcing the energy absorber to prevent it from being destroyed in such a test must be overcome. It is the load and not the energy absorber which is to be protected.

REFERENCES

- (1) Krog, D. L., 1972: Ball Brothers Research Corp., private communication.

H. PARACHUTE COMPUTATIONAL AIDS

1. Selecting a Parachute

To select a parachute for use with a balloon flight (see Section X for discussion):

- a. Determine m_p , the mass of the payload to be lowered by parachute. The masses of the scientific equipment, flight control equipment, and ballast are usually included.
- b. Multiply m_p by 1.05 to obtain a first approximation of the total parachute system mass m_s .
- c. Decide what vertical landing speed v_T will be acceptable at the altitude where the landing is anticipated. A speed of 7-8 m/sec (~25 ft/sec) is usually acceptable.
- d. From v_T determine $v_{T,o}$ -- the vertical speed the system would have at sea level. It may be approximated satisfactorily by the equation $v_{T,o} = v_T / (1 + 5 \times 10^{-5} H)$, where H is the height of the landing site above sea level in meters or by $v_{T,o} = v_T / (1 + 1.52 \times 10^{-5} H)$, where H is in feet.
- e. Enter Fig. H-1 with the value of m_s from step b and $v_{T,o}$ from step d and determine $C_D A$.

f. Using the value of $C_D A$ obtained in step e and the appropriate pseudo drag coefficient for the parachutes available, enter Fig. H-2 and determine an approximate value of the nominal diameter D' of a parachute. Some typical pseudo drag coefficients are given in the caption to Fig. H-2. Others may be provided by the parachute manufacturer.

g. If a parachute is available which has a nominal diameter near the value of D' determined in step f, use its actual mass, pseudo drag coefficient, and nominal diameter and proceed to step h. If no available parachute is large enough, proceed to step m.

h. Enter Fig. H-2 with the actual nominal diameter and pseudo drag coefficient and determine $C_D A$.

i. Using the $C_D A$ determined in step h and the actual mass of the parachute system (the payload mass including all initial ballast plus the actual mass of the parachute, extension lines, etc.) enter Fig. H-1 and determine $v_{T,o}$.

j. Convert $v_{T,o}$ to v_T using the equations $v_T = v_{T,o}(1 + 5 \times 10^{-5}H)$ for H in meters or $v_T = v_{T,o}(1 + 1.52 \times 10^{-5}H)$ for H in feet.

k. Repeat steps i and j except in step i use the parachute system mass without the ballast.

l. If the range of v_T determined in steps i through k is acceptable, the parachute selected in step g is tentatively acceptable. If v_T from either step j or step k is too large to be acceptable, start over at step g and select a larger parachute. If v_T from step j or k is too small, repeat step g and succeeding steps with a smaller parachute.

If a good selection of sizes is available so that the first parachute selected can have characteristics like those assumed in going through the first six steps, the first selection will probably be suitable. Rarely will it be necessary to go through steps g and h more than twice. If a large part of the initial payload is ballast, the difference in the vertical landing speeds with and without ballast may be so great that the two speeds cannot both be within the range of acceptability. If so, other measures will have to be taken, e.g., measures to assure that the ballast will be dropped in nearly any conceivable circumstance before landing. When a parachute has been tentatively selected on the basis of the steps outlined above, it is necessary to perform a check of the parachute itself to be assured that

it was designed to carry a load as large as the one to be flown and that it is in a good state of repair.

m. If the largest parachute available is not acceptable, consider using a cluster of several parachutes. As a first step in determining the number and size of parachutes, divide D' as determined from step f in turn by $\sqrt{2}$, $\sqrt{3}$, ... \sqrt{N} , where N is the number of identical parachutes which may conceivably be used in a cluster to lower the load. Two identical parachutes having diameter $D'/\sqrt{2}$ or three having diameter $D'/\sqrt{3}$ can be substituted for one having diameter D' if $C'_{D'}$ is the same for each of the parachutes in the cluster as for the entire cluster.

n. Select N identical parachutes, each having a nominal diameter near D'/\sqrt{N} . Multiply the nominal diameter of one of the parachutes by \sqrt{N} to determine the nominal diameter of the cluster. For example, if two 30-meter parachutes are to be used together, the nominal diameter of the cluster is $1.4 \times 30 = 42$ m.

o. If the N parachutes selected have flat, circular canopies, use the equation $C'_{D'} = (0.95 - 0.03N) C'_{D,i}$ to determine the value of $C'_{D'}$ for a cluster where $C'_{D,i}$ is the pseudo drag coefficient of each of the N identical

parachutes of the cluster. This equation is valid for values of N from 2 through 6. For canopies with large geometric porosity such as ribbon, ring slot, or cross-shaped parachutes use $C'_{D,i}$ as the value of $C'_{D'}$ for the cluster.

p. Using the product obtained in step n as a new nominal diameter and the value of $C'_{D'}$ for the cluster obtained in step o, enter step h and proceed through step k. Then proceed to step q.

q. If the range of v_T determined in step p is acceptable for the cluster of N parachutes tested, that cluster may be used; if not, other clusters should be tested via steps n through p until an acceptable cluster is found. Then each of the parachutes to be used in the cluster should be thoroughly checked for strength and state of repair. If a cluster of parachutes is to be used, each parachute should be capable of carrying the entire load at opening because they are not likely all to open simultaneously.

2. Terminal Velocity and Time of Descent

In Fig. H-3 the curve labeled v_T is a plot of $(v_T/v_{T,o})$ vs height in the U.S. Standard Atmosphere, 1962. At any level up to 52 km $(v_T/v_{T,o})$ may

be read from the graph and multiplied by $v_{T,o}$ as determined from either step i or k above to yield v_T at that level. Indeed, $v_{T,2}$ at any level 2 may be determined if $v_{T,1}$ at any other level is known. It is

$$v_{T,2} = \frac{v_{T,1} \left(\frac{v_T}{v_{T,o,2}} \right)}{\left(\frac{v_T}{v_{T,o,1}} \right)} \quad (H-1)$$

where $(v_T/v_{T,o})_2$ and $(v_T/v_{T,o})_1$ are values of $(v_T/v_{T,o})$ read from the graph at levels 2 and 1, respectively. Note the arrow on the v_T curve indicating that it is referred to the abscissa scale along the base of the chart. Height is given in meters on the left ordinate scale and in feet on the right ordinate scale. An equivalent pressure scale parallels the meter height scale.

The curve labeled t is referred to the abscissa scale at the top of the chart as indicated by the arrow. That scale is a plot of $v_{T,o}(t_H - t_o)$ which has the dimensions of length. The quantity $(t_H - t_o)$ is the time required for a parachute system to descend from level H to sea level in the U.S. Standard Atmosphere, 1962. It may be determined for any level by reading the value of $v_{T,o}(t_H - t_o)$ for that level and dividing it by $v_{T,o}$.

Also, the time to descend from any level 1 to any lower level 2 may be determined. It is

$$(t_1 - t_2) = \frac{[v_{T,o}(t_H - t_o)]_1 - [v_{T,o}(t_H - t_o)]_2}{v_{T,o}} \quad (H-2)$$

where $[v_{T,o}(t_H - t_o)]_1$ and $[v_{T,o}(t_H - t_o)]_2$ are read for levels 1 and 2, respectively. Through a thin stratum the two values may be nearly equal, and greater accuracy may be gained by estimating a mean value of v_T within the stratum from the v_T curve and dividing that value into the thickness of the stratum. The value of v_T at the middle of the stratum is a good estimate of the mean for layers up to 1 km thick. The units of time are determined by the units of v_T , and the units of v_T and length must be compatible. For example, if the thickness of a stratum is given in meters and v_T is given in m/sec, the ratio $\Delta H/v_T$ will yield time in seconds. Similarly, if $v_{T,o}(t_H - t_o)$ is read in feet and $v_{T,o}$ is in ft/min, the ratio will yield time in minutes.

Although descent speeds and times calculated with the aid of Fig. H-3 are strictly valid only in the U.S. Standard Atmosphere, 1962, they are good approximations to descent times in the real atmosphere. The following

empirical equations may be used in place of Fig. H-3. They fit the curves of Fig. H-3 better near the surface and in the stratosphere than near the tropopause.

$$\frac{v_T}{v_{T,o}} = e^{0.071 H} \quad \text{for } H \text{ in km} \quad (\text{H-3})$$

$$\frac{v_T}{v_{T,o}} = e^{0.0216 H} \quad \text{for } H \text{ in thousands of feet} \quad (\text{H-4})$$

$$v_{T,o}(t_H - t_o) = 15,450 (e^{-0.071 H} - 1) \quad \text{for } H \text{ in km} \quad (\text{H-5})$$

$$v_{T,o}(t_H - t_o) = 50,690 (e^{-0.0216 H} - 1) \quad \text{for } H \text{ in thousands of feet} \quad (\text{H-6})$$

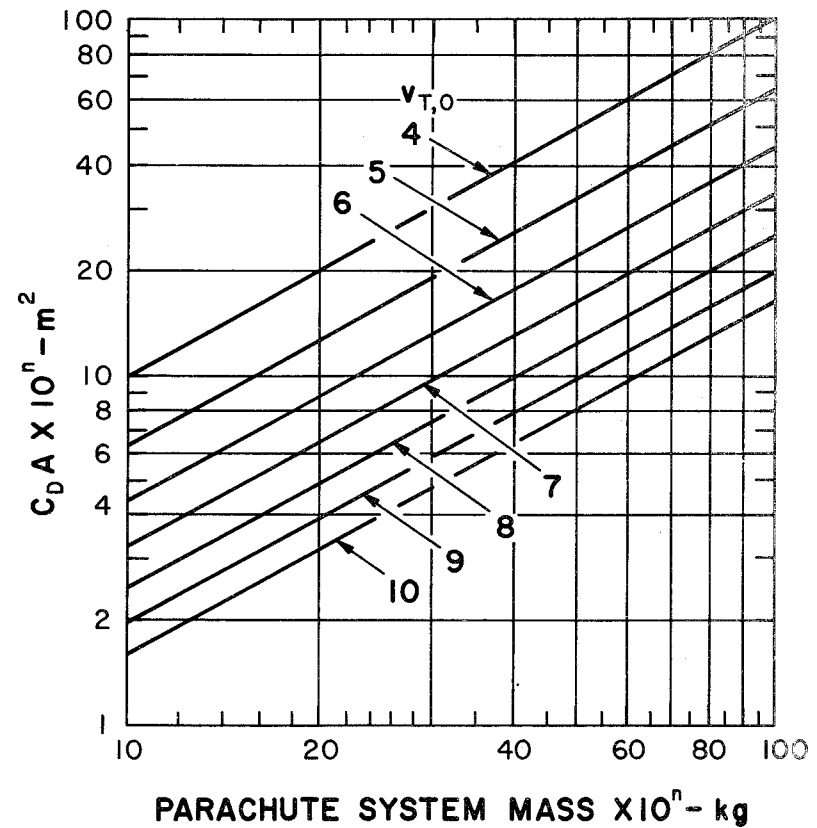


Fig. H-1a. Sea level terminal velocity of a parachute system as a function of system mass and the product of parachute area and drag coefficient.

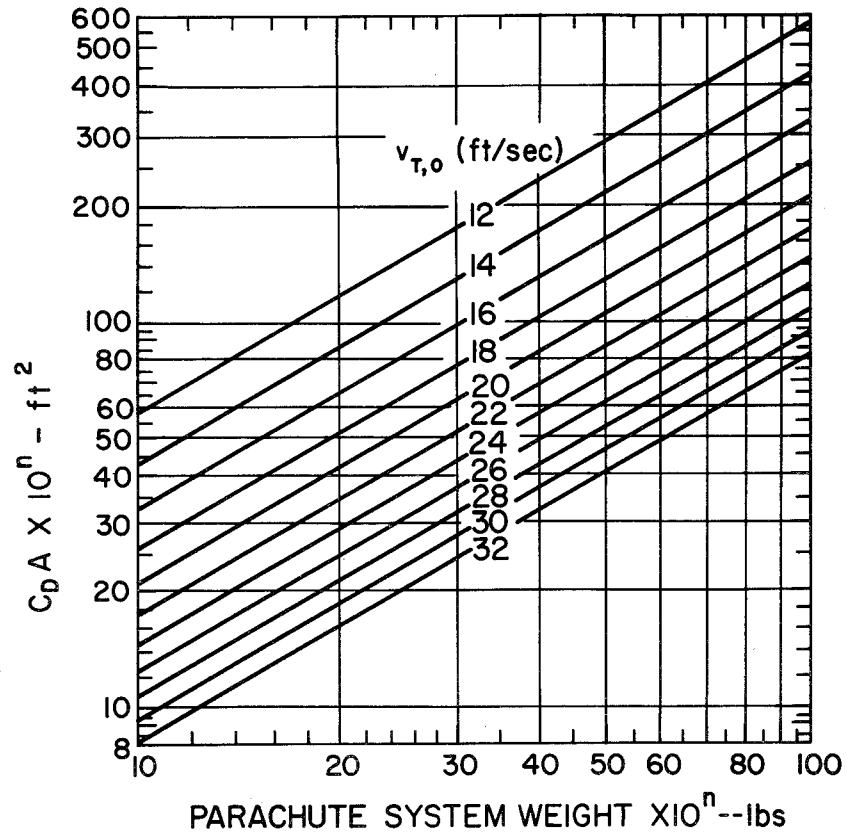


Fig. H-1b. Sea level terminal velocity of a parachute system as a function of system weight and the product of parachute area and drag coefficient.

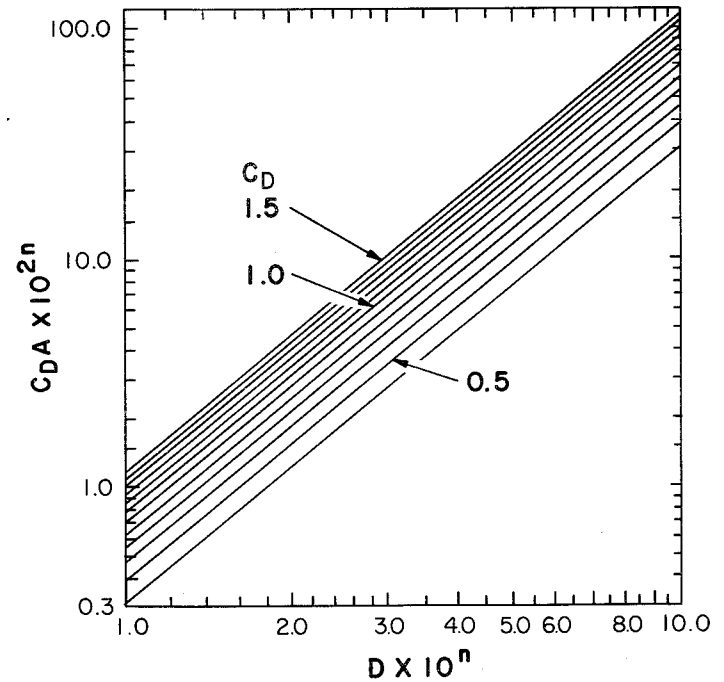


Fig. H-2. Diameter of a parachute as a function of area and drag

coefficient. Diameter is nominal diameter if the pseudo drag coefficient is used. The following are typical pseudo drag coefficients: $C_D' = 0.75$ (design value often quoted for a flat, circular canopy), $C_D' = 0.85$ (empirical value used by NCAR for large flat, circular canopies), and $C_D' = 0.55$ (value quoted by Raven Industries, Inc. for their RAVEN PLUS [®] shape).

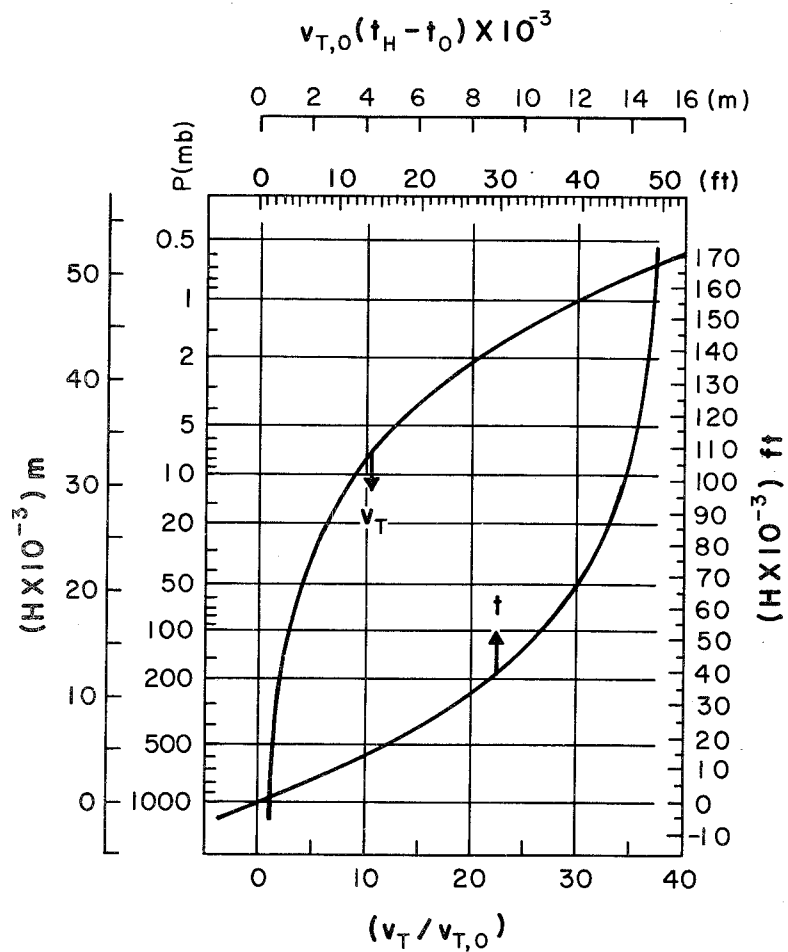


Fig. H-3. Terminal velocity and time of descent as functions of sea level terminal velocity and altitude in the U.S. Standard Atmosphere, 1962.

I. GAS MEASUREMENT AND INFLATION PROCEDURES

Figure I-1 and the tables of this section may be used to compute the lift of the helium or hydrogen contained in an array of cylindrical, steel containers if the total, nominal (water) volume of the array and the pressure and temperature of the gas are known. See Section IV for a discussion of lift gases and gas measurement. A procedure for using the tables and graph to inflate a balloon is given in the following steps:

1. At some time prior to the start of inflation, select enough cylinders of gas to assure that they contain more than the needed lift gas.
2. Arrange them so that the air can circulate freely through them, connect them with a manifold, and place a thermometer in contact with one of them. If a tube trailer like the one shown in Fig. 1 of Section IV is used, the cylinders will already be interconnected by a manifold.
3. At a time when ambient air temperature is not changing significantly with time (a few hours before sunrise is usually satisfactory) read the pressure and temperature. At that time the temperature of the thermometer should be a representative gas temperature. Pressure is always representative if the gas is not flowing and the gage is accurate and is tapped

gently prior to reading. If the temperature is taken during the day, shade the cylinders from the sun and ventilate them long enough prior to the reading to let them and the gas come into thermal equilibrium with the air.

4. Enter the appropriate table (helium or hydrogen in SI or English units) with the temperature and pressure from step 3 to determine the lift per unit of nominal volume of the array of cylinders. Linear interpolation may be used in these tables.

5. Multiply the tabular value obtained in step 4 by the nominal volume of the array to determine the total lift of the gas contained in the array. The nominal volume of each cylinder is usually stamped on it, frequently in cubic inches. To convert in.^3 to ft^3 multiply by 5.787×10^{-4} ; to convert in.^3 to m^3 multiply by 1.6387×10^{-6} . The water volume of the 2260-65# standard bottle is 1.57 ft^3 ($4.45 \times 10^{-2} \text{ m}^3$), on the average.

6. From the total lift contained in the array as determined in step 5 subtract the gross lift of the balloon system to be flown (the free lift plus the gross weight of the system not including the weight of the lift gas). The difference is the lift which should remain in the cylinder ar-

ray after inflation.

7. Divide the difference obtained in step 6 by the nominal volume of the array. This is the lift per unit nominal volume of the gas to be left in the array.

8. Enter the body of the appropriate table with the quotient obtained from step 7 and the temperature obtained in step 3 and obtain a pressure.

9. If the gage pressure obtained from step 8 is not less than $1.5 \times 10^5 \text{ N/m}^2$ (20 psi), the array contains enough gas to provide the required lift without draining the cylinders, and one may proceed to step

10. If the gage pressure obtained in step 8 is less than $1.5 \times 10^5 \text{ N/m}^2$, add additional cylinders and repeat steps 3 through 9 using the new nominal volume, pressure, and temperature of the array. Some prefer to use enough cylinders to leave the post-inflation gage pressure much higher than $1.5 \times 10^5 \text{ N/m}^2$. This assures relatively high flow rates throughout inflation. Others prefer to use just enough cylinders so that all except one must be drained. The latter technique provides greater accuracy of measurement at the expense of longer inflation time. When an array of cylinders has

been finally selected and interconnected by a manifold, all valves should be closed to prevent loss of gas.

10. A short time prior to the start of inflation, open all cylinders of the array selected in step 9 and let the pressure equalize in the array.

Read the initial pressure p_i .

11. Enter the appropriate table with the lift per unit nominal volume determined in step 4 for the final array chosen in step 9 and the pressure determined in step 10, and determine the mean gas temperature. This is a value of temperature taken from the table, not a value measured by thermometer. If post inflation pressure is to be left relatively high in all cylinders, proceed to step 12. If all cylinders except one are to be drained, proceed to step 12a.

12. Using the temperature determined in step 11 and the lift per unit nominal volume which should remain in the array after inflation from step 7, enter the appropriate table and determine the pressure. This is the first estimate of the pressure at which the gas flow should be cut off to end inflation; let it be designated p_f .

13. Divide p_f from step 12 by p_i from step 10; use the quotient and

Fig. I-1 to obtain the ratio p_c/p_f .

14. Multiply p_c/p_f obtained in step 13 by p_f from step 12 to obtain p_c . This is the pressure which the gas in the array should have immediately after the correct amount of lift gas has been removed.

15. When, during inflation, the pressure gage reads the value p_c determined in step 14, cut off the gas flow at the main valve. Let the pressure stabilize and read it. It will be higher than p_c ; call it $p_{c,1}$.

16. Take the difference ($p_{c,1} - p_c$) and subtract it from p_c to obtain $p_{c,2}$.

17. Open the valve again and let the flow continue until the pressure on the gage reads $p_{c,2}$. Close the valve and let the pressure stabilize; it should read very nearly p_c . If it is still slightly higher than p_c , another short burst of flow may be necessary. If it is slightly less than p_c , slightly more gas will have been added to the balloon than was desired. The difference is well within the indeterminacy of the method.

18. Shut off all valves and disconnect all hoses from the balloon.

12a. If all cylinders except one are to be drained during inflation, select the cylinder which is not to be drained. Close its valve and note

its nominal volume.

13a. Subtract the nominal volume of the closed cylinder from the nominal volume of the array as finally determined in step 9. This yields the nominal volume of the cylinders to be drained.

14a. Using the mean temperature of the gas determined in step 11 and a gage pressure of $1.5 \times 10^5 \text{ N/m}^2$, enter the appropriate table and determine the lift per unit nominal volume of the gas to be left in the array.

15a. Subtract the value obtained in step 14a from the value obtained in step 4 and multiply the difference by the nominal volume of the array to be drained from step 13a. This yields the usable lift in the array to be drained.

16a. Subtract the usable lift obtained in step 15a from the gross lift of the balloon system to be flown (used in step 6). The difference is the lift that must be taken from the cylinder which is closed off.

17a. Multiply the lift per unit nominal volume obtained in step 4 by the nominal volume of the cylinder which is closed off. This is the lift contained in that cylinder.

18a. Subtract the lift which must be taken from the cylinder (from step

16a) from the lift contained in the cylinder as determined in step 17a.

This yields the lift to be left in the one cylinder at the end of inflation.

19a. Using the mean temperature of the gas determined in step 11 and the lift to be left in the cylinder from step 18a, enter the appropriate table and determine the final pressure p_f .

20a. Divide p_f from step 19a by p_i from step 10; use the quotient and Fig. I-1 to obtain the ratio p_c/p_f .

21a. Multiply the ratio p_c/p_f obtained in step 20a by p_f from step 19a to obtain p_c . This is the pressure at which gas flow should be cut off in the final cylinder to obtain proper inflation. After the gas in the array (not including the cylinder closed in step 12a) has been allowed to flow into the balloon until the gage pressure has reached $1.5 \times 10^5 \text{ N/m}^2$, all cylinders of the array should be closed off. The one final cylinder is then opened and gas is allowed to flow from it until the pressure reaches the value p_c determined in step 21a above. Then the procedure outlined in steps 15 through 18 should be followed to complete the inflation. Steps 15 through 18 are less critical when only one cylinder is in use at the end than when several are in use. Also it is not necessary to follow that procedure when the final gage pressure is as low as $1.5 \times 10^5 \text{ N/m}^2$.

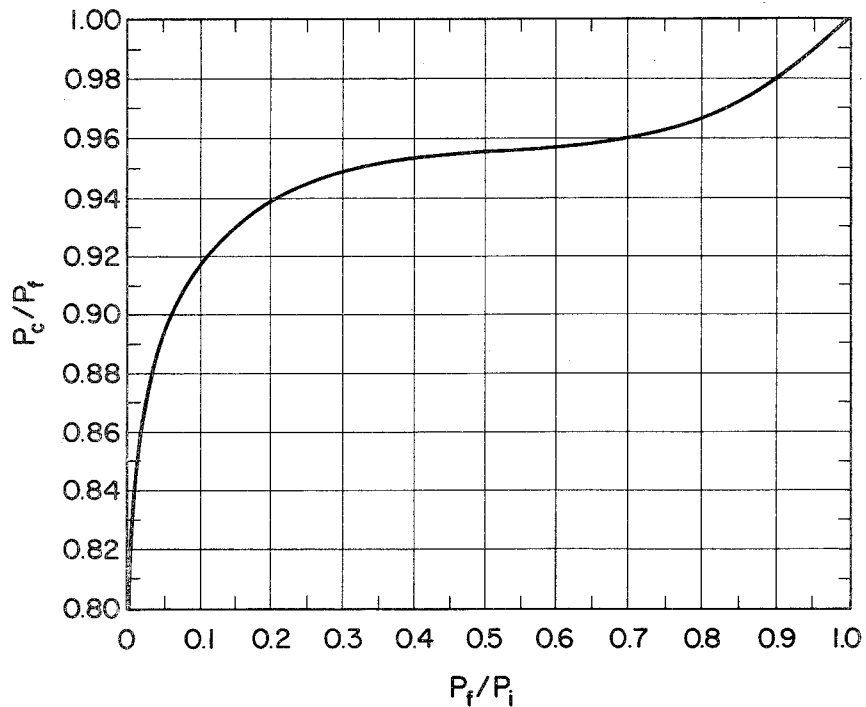


Fig. I-1. Relationship between P_c , P_i , and P_f .

Helium--SI Units

Table I-1

Lift (kg/m^3) of Gas Contained in Steel Cylinders

G.Press. ($\times 10^5$) (N/m^2)	Temperature ($^{\circ}\text{C}$)							
	-25	-20	-15	-10	-5	0	5	10
0.0	1.2235	1.1995	1.1765	1.1544	1.1330	1.1125	1.0927	1.0736
5.0	7.2405	7.0991	6.9633	6.8326	6.7067	6.5855	6.4686	6.3558
10.0	13.224	12.966	12.719	12.481	12.252	12.031	11.818	11.612
15.0	19.174	18.801	18.444	18.099	17.768	17.448	17.140	16.843
20.0	25.090	24.605	24.138	23.688	23.256	22.839	22.437	22.048
25.0	30.974	30.376	29.802	29.248	28.715	28.202	27.707	27.229
30.0	36.826	36.117	35.435	34.779	34.147	33.538	32.951	32.384
35.0	42.645	41.827	41.039	40.282	39.552	38.848	38.170	37.515
40.0	48.433	47.506	46.614	45.756	44.929	44.132	43.363	42.621
45.0	54.189	53.154	52.159	51.202	50.279	49.390	48.531	47.703
50.0	59.914	58.773	57.676	56.620	55.602	54.621	53.675	52.761
55.0	65.608	64.362	63.164	62.010	60.899	59.827	58.793	57.795
60.0	71.271	69.922	68.623	67.373	66.169	65.008	63.888	62.806
65.0	76.904	75.452	74.055	72.710	71.413	70.163	68.957	67.793
70.0	82.507	80.953	79.458	78.019	76.632	75.294	74.003	72.756
75.0	88.080	86.426	84.834	83.302	81.824	80.400	79.025	77.697
80.0	93.624	91.870	90.183	88.558	86.992	85.481	84.023	82.615
85.0	99.138	97.286	95.504	93.788	92.134	90.538	88.998	87.511
90.0	104.62	102.67	100.80	98.992	97.251	95.571	93.950	92.383
95.0	110.08	108.04	106.07	104.17	102.34	100.58	98.878	97.234
100.0	115.51	113.37	111.31	109.32	107.41	105.57	103.78	102.06
105.0	120.91	118.68	116.52	114.45	112.45	110.53	108.67	106.87
110.0	126.28	123.95	121.71	119.56	117.47	115.47	113.53	111.65
115.0	131.63	129.21	126.88	124.63	122.47	120.38	118.37	116.42
120.0	136.94	134.43	132.02	129.69	127.44	125.28	123.18	121.16
125.0	142.23	139.63	137.13	134.72	132.39	130.15	127.98	125.88
130.0	147.50	144.81	142.22	139.72	137.32	134.99	132.75	130.58
135.0	152.74	149.96	147.28	144.70	142.22	139.82	137.50	135.26
140.0	157.95	155.08	152.32	149.66	147.10	144.62	142.23	139.92
145.0	163.13	160.18	157.34	154.60	151.95	149.40	146.96	144.56
150.0	168.29	165.25	162.33	159.51	156.79	154.16	151.63	149.18
155.0	173.42	170.30	167.29	164.40	161.60	158.90	156.29	153.77
160.0	178.53	175.32	172.24	169.26	166.39	163.62	160.94	158.35
165.0	183.61	180.32	177.16	174.10	171.16	168.31	165.57	162.91
170.0	188.67	185.30	182.05	178.92	175.90	172.99	170.17	167.45
175.0	193.70	190.25	186.93	183.72	180.63	177.64	174.76	171.97
180.0	198.71	195.19	191.78	188.50	185.33	182.28	179.32	176.47
185.0	203.69	200.08	196.60	193.25	190.01	186.89	183.87	180.95
190.0	208.65	204.95	201.41	197.98	194.68	191.48	188.39	185.41
195.0	213.59	209.82	206.19	202.69	199.32	196.05	192.90	189.85
200.0	218.50	214.66	210.95	207.38	203.94	200.61	197.39	194.28
205.0	223.39	219.47	215.69	212.05	208.54	205.14	201.86	198.69
210.0	228.25	224.26	220.41	216.70	213.11	209.65	206.31	203.07
215.0	233.10	229.03	225.11	221.32	217.67	214.15	210.74	207.44
220.0	237.92	233.77	229.78	225.93	222.21	218.62	215.15	211.79
225.0	242.71	238.50	234.43	230.51	226.73	223.08	219.54	216.12
230.0	247.49	243.20	239.07	235.08	231.23	227.51	223.92	220.44
235.0	252.24	247.88	243.68	239.62	235.71	231.93	228.27	224.74
240.0	256.97	252.54	248.27	244.15	240.17	236.33	232.61	229.02
245.0	261.68	257.18	252.84	248.65	244.61	240.71	236.93	233.28

Helium--SI Units

Table I-1

Lift (kg/m³) of Gas Contained in Steel Cylinders

G. Press. (x10 ⁵) (N/m ²)	Temperature (°C)							
	15	20	25	30	35	40	45	50
0.0	1.0552	1.0374	1.0201	1.0035	.98739	.97179	.95669	.94206
5.0	6.2469	6.1418	6.0401	5.9418	5.8467	5.7546	5.6653	5.5789
10.0	11.414	11.222	11.037	10.858	10.684	10.516	10.354	10.196
15.0	16.556	16.279	16.011	15.751	15.503	15.257	15.022	14.794
20.0	21.674	21.312	20.962	20.623	20.295	19.978	19.671	19.372
25.0	26.767	26.321	25.890	25.473	25.069	24.678	24.299	23.932
30.0	31.837	31.308	30.796	30.301	29.822	29.358	28.908	28.472
35.0	36.882	36.271	35.680	35.108	34.554	34.018	33.498	32.994
40.0	41.904	41.212	40.542	39.893	39.266	38.658	38.068	37.497
45.0	46.903	46.130	45.382	44.658	43.957	43.278	42.619	41.981
50.0	51.878	51.025	50.200	49.401	48.628	47.878	47.152	46.447
55.0	56.831	55.898	54.997	54.124	53.278	52.459	51.665	50.895
60.0	61.760	60.750	59.772	58.826	57.909	57.021	56.160	55.325
65.0	66.667	65.579	64.527	63.507	62.520	61.564	60.636	59.736
70.0	71.552	70.387	69.260	68.169	67.112	66.088	65.094	64.130
75.0	76.414	75.173	73.973	72.810	71.684	70.593	69.534	68.507
80.0	81.254	79.938	78.665	77.432	76.237	75.079	73.956	72.866
85.0	86.073	84.682	83.336	82.033	80.771	79.547	78.359	77.207
90.0	90.869	89.405	87.988	86.615	85.285	83.996	82.745	81.531
95.0	95.645	94.107	92.619	91.178	89.781	88.427	87.114	85.838
100.0	100.40	98.789	97.231	95.721	94.259	92.840	91.464	90.129
105.0	105.13	103.45	101.82	100.25	98.717	97.236	95.798	94.402
110.0	109.84	108.09	106.39	104.75	103.16	101.61	100.11	98.658
115.0	114.53	112.71	110.95	109.24	107.58	105.97	104.41	102.90
120.0	119.20	117.31	115.48	113.71	111.98	110.32	108.70	107.12
125.0	123.85	121.89	119.99	118.15	116.37	114.64	112.96	111.33
130.0	128.48	126.45	124.49	122.59	120.74	118.95	117.21	115.52
135.0	133.09	131.00	128.97	127.00	125.09	123.24	121.44	119.70
140.0	137.68	135.52	133.42	131.39	129.42	127.51	125.66	123.85
145.0	142.25	140.02	137.86	135.77	133.74	131.77	129.86	128.00
150.0	146.80	144.51	142.28	140.13	138.04	136.01	134.04	132.13
155.0	151.33	148.97	146.69	144.47	142.32	140.23	138.21	136.24
160.0	155.85	153.42	151.07	148.79	146.58	144.44	142.36	140.33
165.0	160.34	157.85	155.44	153.10	150.83	148.63	146.49	144.41
170.0	164.81	162.26	159.79	157.39	155.06	152.81	150.61	148.48
175.0	169.27	166.65	164.12	161.66	159.28	156.96	154.72	152.53
180.0	173.70	171.03	168.43	165.92	163.48	161.11	158.80	156.57
185.0	178.12	175.38	172.73	170.16	167.66	165.23	162.88	160.59
190.0	182.52	179.72	177.11	174.38	171.82	169.34	166.94	164.59
195.0	186.90	184.04	181.27	178.58	175.97	173.44	170.98	168.59
200.0	191.26	188.34	185.51	182.77	180.11	177.52	175.01	172.56
205.0	195.61	192.63	189.74	186.94	184.23	181.59	179.02	176.53
210.0	199.94	196.90	193.96	191.10	188.33	185.64	183.02	180.47
215.0	204.24	201.15	198.15	195.24	192.41	189.67	187.00	184.41
220.0	208.54	205.38	202.33	199.36	196.49	193.69	190.97	188.33
225.0	212.81	209.60	206.49	203.47	200.54	197.69	194.93	192.23
230.0	217.07	213.80	210.64	207.57	204.58	201.68	198.87	196.13
235.0	221.31	217.99	214.77	211.64	208.61	205.66	202.79	200.00
240.0	225.53	222.16	218.88	215.70	212.62	209.62	206.70	203.87
245.0	229.74	226.31	222.98	219.75	216.61	213.57	210.60	207.72

Helium--Eng. Units

Table I-2

Lift (lb/ft³) of Gas Contained in Steel Cylinders

Gage Press. (lb/in. ²)	Temperature (°F)					
	0	10	20	30	40	50
0	.07424	.07268	.07118	.06974	.06836	.06703
50	.32616	.31929	.31271	.30640	.30034	.29451
100	.57712	.56499	.55337	.54222	.53152	.52123
150	.82714	.80980	.79317	.77722	.76190	.74718
200	1.0762	1.0537	1.0321	1.0114	.99150	.97238
250	1.3244	1.2967	1.2702	1.2447	1.2203	1.1968
300	1.5716	1.5388	1.5074	1.4773	1.4483	1.4205
350	1.8179	1.7801	1.7438	1.7090	1.6756	1.6435
400	2.0633	2.0205	1.9794	1.9399	1.9021	1.8657
450	2.3078	2.2600	2.2141	2.1701	2.1278	2.0871
500	2.5514	2.4986	2.4480	2.3994	2.3527	2.3079
550	2.7942	2.7364	2.6811	2.6280	2.5769	2.5279
600	3.0360	2.9734	2.9134	2.8557	2.8004	2.7472
650	3.2769	3.2095	3.1448	3.0827	3.0231	2.9658
700	3.5170	3.4447	3.3755	3.3089	3.2451	3.1836
750	3.7562	3.6792	3.6053	3.5344	3.4663	3.4008
800	3.9945	3.9127	3.8343	3.7591	3.6868	3.6172
850	4.2320	4.1455	4.0626	3.9830	3.9065	3.8330
900	4.4686	4.3775	4.2901	4.2062	4.1255	4.0480
950	4.7043	4.6086	4.5168	4.4286	4.3439	4.2624
1000	4.9393	4.8389	4.7427	4.6503	4.5615	4.4760
1050	5.1733	5.0685	4.9678	4.8712	4.7783	4.6890
1100	5.4066	5.2972	5.1922	5.0914	4.9945	4.9013
1150	5.6390	5.5251	5.4158	5.3109	5.2100	5.1129
1200	5.8706	5.7522	5.6387	5.5296	5.4248	5.3239
1250	6.1014	5.9786	5.8608	5.7476	5.6388	5.5342
1300	6.3314	6.2042	6.0821	5.9649	5.8522	5.7438
1350	6.5605	6.4290	6.3028	6.1815	6.0649	5.9527
1400	6.7889	6.6530	6.5226	6.3974	6.2769	6.1610
1450	7.0165	6.8763	6.7418	6.6125	6.4883	6.3687
1500	7.2433	7.0988	6.9602	6.8270	6.6989	6.5757
1550	7.4693	7.3206	7.1779	7.0408	6.9089	6.7821
1600	7.6945	7.5416	7.3948	7.2538	7.1183	6.9878
1650	7.9189	7.7618	7.6111	7.4662	7.3269	7.1928
1700	8.1426	7.9814	7.8266	7.6779	7.5349	7.3973
1750	8.3655	8.2002	8.0415	7.8890	7.7423	7.6011
1800	8.5876	8.4182	8.2556	8.0993	7.9490	7.8043
1850	8.8090	8.6355	8.4690	8.3090	8.1550	8.0069
1900	9.0296	8.8521	8.6817	8.5180	8.3605	8.2088
1950	9.2495	9.0680	8.8938	8.7263	8.5652	8.4101

Helium--Eng. Units

Table I-2

Lift (lb/ft³) of Gas Contained in Steel Cylinders

Gage Press. (lb/in. ²)	Temperature (°F)					
	60	70	80	90	100	110
0	.06575	.06452	.06334	.06220	.06110	.06004
50	.28891	.28352	.27834	.27333	.26851	.26386
100	.51134	.50182	.49265	.48381	.47529	.46707
150	.73303	.71941	.70629	.69364	.68145	.66968
200	.95399	.93630	.91925	.90282	.88697	.87168
250	1.1742	1.1525	1.1315	1.1114	1.0919	1.0731
300	1.3938	1.3680	1.3432	1.3192	1.2962	1.2739
350	1.6126	1.5828	1.5541	1.5265	1.4998	1.4741
400	1.8306	1.7969	1.7644	1.7331	1.7029	1.6737
450	2.0480	2.0104	1.9741	1.9391	1.9054	1.8728
500	2.2647	2.2231	2.1831	2.1445	2.1072	2.0712
550	2.4807	2.4352	2.3915	2.3492	2.3085	2.2691
600	2.6960	2.6467	2.5992	2.5534	2.5091	2.4664
650	2.9106	2.8575	2.8062	2.7569	2.7092	2.6632
700	3.1245	3.0676	3.0127	2.9598	2.9087	2.8593
750	3.3377	3.2770	3.2185	3.1620	3.1076	3.0549
800	3.5503	3.4858	3.4237	3.3637	3.3059	3.2500
850	3.7622	3.6940	3.6282	3.5648	3.5036	3.4445
900	3.9734	3.9015	3.8322	3.7653	3.7007	3.6384
950	4.1839	4.1083	4.0355	3.9652	3.8973	3.8318
1000	4.3938	4.3146	4.2382	4.1645	4.0933	4.0246
1050	4.6030	4.5202	4.4403	4.3632	4.2888	4.2169
1100	4.8116	4.7251	4.6418	4.5613	4.4836	4.4086
1150	5.0195	4.9295	4.8426	4.7589	4.6780	4.5998
1200	5.2268	5.1332	5.0429	4.9558	4.8717	4.7904
1250	5.4334	5.3363	5.2426	5.1522	5.0649	4.9805
1300	5.6394	5.5387	5.4417	5.3480	5.2576	5.1701
1350	5.8447	5.7406	5.6402	5.5433	5.4497	5.3592
1400	6.0494	5.9419	5.8381	5.7380	5.6412	5.5477
1450	6.2535	6.1425	6.0355	5.9321	5.8322	5.7357
1500	6.4570	6.3426	6.2322	6.1256	6.0227	5.9232
1550	6.6598	6.5420	6.4284	6.3187	6.2126	6.1101
1600	6.8621	6.7409	6.6240	6.5111	6.4020	6.2966
1650	7.0637	6.9392	6.8190	6.7030	6.5909	6.4825
1700	7.2647	7.1368	7.0135	6.8944	6.7793	6.6680
1750	7.4651	7.3339	7.2074	7.0852	6.9671	6.8529
1800	7.6649	7.5305	7.4007	7.2755	7.1544	7.0373
1850	7.8641	7.7264	7.5935	7.4652	7.3412	7.2212
1900	8.0627	7.9218	7.7857	7.6544	7.5274	7.4046
1950	8.2607	8.1165	7.9774	7.8431	7.7132	7.5876

Helium--Eng. Units

Table I-2

Lift (lb/ft³) of Gas Contained in Steel Cylinders

Gage Press. (lb/in. ²)	Temperature (°F)					
	0	10	20	30	40	50
2000	9.4686	9.2832	9.1051	8.9340	8.7694	8.6100
2050	9.6870	9.4976	9.3158	9.1410	8.9729	8.8110
2100	9.9047	9.7114	9.5258	9.3474	9.1757	9.0105
2150	10.122	9.9245	9.7351	9.5531	9.3780	9.2094
2200	10.338	10.137	9.9438	9.7582	9.5796	9.4077
2250	10.553	10.348	10.152	9.9626	9.7806	9.6054
2300	10.768	10.559	10.359	10.166	9.9810	9.8025
2350	10.982	10.770	10.566	10.370	10.181	9.9990
2400	11.195	10.979	10.772	10.572	10.380	10.195
2450	11.408	11.188	10.977	10.774	10.579	10.390
2500	11.620	11.397	11.182	10.975	10.777	10.585
2550	11.831	11.604	11.386	11.176	10.974	10.779
2600	12.042	11.811	11.589	11.376	11.171	10.973
2650	12.252	12.017	11.792	11.575	11.367	11.166
2700	12.461	12.223	11.994	11.774	11.563	11.359
2750	12.669	12.428	12.196	11.972	11.758	11.550
2800	12.877	12.632	12.397	12.170	11.952	11.742
2850	13.084	12.836	12.597	12.367	12.146	11.933
2900	13.291	13.039	12.797	12.564	12.339	12.123
2950	13.497	13.241	12.996	12.759	12.532	12.313
3000	13.702	13.443	13.194	12.955	12.724	12.502
3050	13.907	13.644	13.392	13.149	12.916	12.690
3100	14.110	13.845	13.589	13.343	13.107	12.879
3150	14.314	14.044	13.786	13.537	13.297	13.066
3200	14.516	14.244	13.982	13.730	13.487	13.253
3250	14.718	14.442	14.177	13.922	13.676	13.440
3300	14.919	14.640	14.372	14.114	13.865	13.626
3350	15.120	14.838	14.566	14.305	14.054	13.811
3400	15.320	15.035	14.760	14.496	14.241	13.996
3450	15.520	15.231	14.953	14.686	14.429	14.180

Helium--Eng. Units

Table I-2

Lift (lb/ft³) of Gas Contained in Steel Cylinders

Gage Press. (lb/in. ²)	Temperature (°F)					
	60	70	80	90	100	110
2000	8.4581	8.3108	8.1686	8.0312	7.8984	7.7700
2050	8.6549	8.5044	8.3591	8.2188	8.0832	7.9519
2100	8.8512	8.6975	8.5492	8.4059	8.2674	8.1334
2150	9.0468	8.8900	8.7387	8.5925	8.4511	8.3143
2200	9.2419	9.0820	8.9277	8.7785	8.6343	8.4948
2250	9.4364	9.2735	9.1161	8.9641	8.8171	8.6748
2300	9.6304	9.4643	9.3040	9.1491	8.9993	8.8544
2350	9.8238	9.6547	9.4914	9.3336	9.1810	9.0334
2400	10.017	9.8444	9.6782	9.5176	9.3623	9.2120
2450	10.209	10.034	9.8646	9.7011	9.5431	9.3901
2500	10.401	10.222	10.050	9.8841	9.7234	9.5677
2550	10.592	10.411	10.236	10.067	9.9032	9.7449
2600	10.782	10.598	10.420	10.249	10.082	9.9216
2650	10.972	10.785	10.605	10.430	10.261	10.098
2700	11.162	10.972	10.789	10.611	10.440	10.274
2750	11.351	11.158	10.972	10.792	10.618	10.449
2800	11.539	11.344	11.155	10.972	10.795	10.624
2850	11.727	11.529	11.337	11.151	10.972	10.798
2900	11.914	11.713	11.519	11.331	11.149	10.972
2950	12.101	11.897	11.700	11.509	11.325	11.146
3000	12.288	12.081	11.881	11.687	11.500	11.319
3050	12.473	12.264	12.061	11.865	11.675	11.492
3100	12.659	12.446	12.241	12.042	11.850	11.664
3150	12.843	12.628	12.420	12.219	12.024	11.836
3200	13.027	12.810	12.599	12.395	12.198	12.007
3250	13.211	12.991	12.777	12.571	12.371	12.178
3300	13.394	13.171	12.955	12.746	12.544	12.348
3350	13.577	13.351	13.133	12.921	12.717	12.518
3400	13.759	13.531	13.310	13.096	12.889	12.688
3450	13.941	13.710	13.486	13.270	13.060	12.857

Hydrogen--SI Units

Table I-3

Lift (kg/m³) of Gas Contained in Steel Cylinders

G. Press. (x10 ⁶) (N/m ²)	Temperature (°C)							
	-25	-20	-15	-10	-5	0	5	10
0.	1.3216	1.2957	1.2708	1.2469	1.2238	1.2017	1.1803	1.1596
5.	7.8184	7.6655	7.5185	7.3772	7.2411	7.1100	6.9836	6.8617
10.	14.274	13.996	13.728	13.470	13.222	12.983	12.752	12.530
15.	20.689	20.286	19.898	19.525	19.166	18.820	18.487	18.165
20.	27.064	26.537	26.030	25.543	25.074	24.622	24.187	23.766
25.	33.397	32.747	32.123	31.523	30.945	30.389	29.852	29.335
30.	39.689	38.919	38.178	37.466	36.781	36.120	35.484	34.869
35.	45.941	45.050	44.195	43.372	42.580	41.816	41.081	40.371
40.	52.151	51.142	50.173	49.240	48.343	47.478	46.644	45.843
45.	58.321	57.195	56.113	55.072	54.070	53.104	52.174	51.276
50.	64.450	63.208	62.014	60.866	59.761	58.696	57.669	56.679
55.	70.539	69.182	67.878	66.624	65.416	64.253	63.131	62.049
60.	76.587	75.117	73.704	72.344	71.036	69.775	68.560	67.387
65.	82.595	81.013	79.492	78.029	76.620	75.263	73.955	72.693
70.	88.563	86.869	85.242	83.677	82.169	80.717	79.317	77.966
75.	94.490	92.687	90.955	89.288	87.683	86.137	84.646	83.208
80.	100.376	98.467	96.630	94.863	93.162	91.523	89.943	88.418
85.	106.225	104.208	102.269	100.403	98.606	96.875	95.206	93.596
90.	112.034	109.911	107.870	105.906	104.016	102.194	100.437	98.742
95.	117.802	115.575	113.434	111.374	109.391	107.479	105.636	103.857
100.	123.532	121.202	118.962	116.807	114.732	112.731	110.803	108.941
105.	129.222	126.791	124.454	122.204	120.038	117.951	115.937	113.994
110.	134.874	132.343	129.909	127.567	125.311	123.137	121.040	119.016
115.	140.487	137.857	135.328	132.894	130.550	128.291	126.111	124.008
120.	146.062	143.334	140.711	138.187	135.756	133.412	131.151	128.969
125.	151.598	148.775	146.059	143.445	140.928	138.501	136.160	133.900
130.	157.097	154.178	151.371	148.670	146.067	143.558	141.137	138.800
135.	162.558	159.546	156.649	153.860	151.173	148.583	146.084	143.671
140.	167.981	164.877	161.891	159.016	156.247	153.577	151.000	148.513
145.	173.367	170.172	167.099	164.139	161.288	158.539	155.886	153.324
150.	178.716	175.432	172.272	169.229	166.297	163.470	160.742	158.107
155.	184.029	180.656	177.411	174.286	171.274	168.370	165.567	162.861
160.	189.305	185.845	182.515	179.309	176.220	173.239	170.363	167.585
165.	194.545	190.999	187.587	184.301	181.133	178.078	175.129	172.281
170.	199.749	196.118	192.624	189.259	186.016	182.887	179.866	176.949
175.	204.917	201.203	197.629	194.186	190.867	187.665	184.574	181.588
180.	210.050	206.254	202.600	199.081	195.687	192.414	189.253	186.200
185.	215.148	211.271	207.539	203.944	200.477	197.133	193.903	190.783
190.	220.211	216.254	212.445	208.775	205.237	201.822	198.525	195.339
195.	225.239	221.204	217.319	213.576	209.966	206.482	203.118	199.867
200.	230.234	226.121	222.161	218.345	214.665	211.114	207.684	204.369
205.	235.194	231.005	226.971	223.084	219.335	215.716	212.221	208.843
210.	240.120	235.856	231.750	227.793	223.975	220.290	216.731	213.290
215.	245.013	240.676	236.498	232.471	228.586	224.836	221.213	217.711
220.	249.873	245.463	241.214	237.119	233.168	229.354	225.668	222.106
225.	254.700	250.218	245.900	241.737	237.721	233.843	230.097	226.474
230.	259.495	254.942	250.556	246.327	242.246	238.306	234.498	230.817
235.	264.257	259.634	255.181	250.886	246.742	242.740	238.873	235.133
240.	268.987	264.296	259.776	255.417	251.211	247.148	243.221	239.424
245.	273.685	268.927	264.342	259.919	255.651	251.528	247.544	243.690

Hydrogen--SI Units

Table I-3

Lift (kg/m³) of Gas Contained in Steel Cylinders

G. Press. ($\times 10^6$) (N/m ²)	Temperature (°C)							
	15	20	25	30	35	40	45	50
0.	1.1397	1.1205	1.1019	1.0839	1.0665	1.0496	1.0333	1.0175
5.	6.7440	6.6303	6.5204	6.4142	6.3114	6.2119	6.1155	6.0221
10.	12.316	12.108	11.908	11.714	11.527	11.346	11.170	11.000
15.	17.854	17.555	17.265	16.984	16.713	16.451	16.196	15.950
20.	23.361	22.969	22.591	22.225	21.870	21.527	21.195	20.873
25.	28.835	28.352	27.886	27.435	26.998	26.576	26.167	25.770
30.	34.277	33.704	33.151	32.615	32.098	31.596	31.111	30.640
35.	39.686	39.024	38.385	37.766	37.168	36.588	36.027	35.483
40.	45.064	44.314	43.589	42.888	42.210	41.553	40.917	40.300
45.	50.409	49.572	48.763	47.988	47.223	46.490	45.779	45.091
50.	55.723	54.799	53.906	53.043	52.208	51.399	50.615	49.855
55.	61.005	59.996	59.020	58.077	57.164	56.280	55.424	54.594
60.	66.255	65.162	64.105	63.082	62.093	61.134	60.206	59.306
65.	71.474	70.297	69.159	68.058	66.993	65.962	64.962	63.993
70.	76.662	75.402	74.184	73.006	71.866	70.762	69.692	68.655
75.	81.819	80.477	79.180	77.925	76.711	75.535	74.395	73.290
80.	86.945	85.522	84.147	82.816	81.528	80.281	79.073	77.901
85.	92.040	90.538	89.085	87.679	86.319	85.001	83.724	82.486
90.	97.105	95.523	93.994	92.514	91.082	89.694	88.350	87.047
95.	102.139	100.479	98.874	97.321	95.818	94.362	92.951	91.582
100.	107.143	105.406	103.726	102.100	100.527	99.003	97.525	96.093
105.	112.117	110.303	108.549	106.852	105.209	103.618	102.075	100.579
110.	117.061	115.172	113.345	111.577	109.865	108.207	106.600	105.041
115.	121.976	120.012	118.112	116.274	114.495	112.771	111.100	109.479
120.	126.861	124.823	122.852	120.945	119.098	117.309	115.575	113.893
125.	131.716	129.606	127.564	125.589	123.676	121.822	120.025	118.282
130.	136.543	134.360	132.249	130.206	128.227	126.310	124.451	122.648
135.	141.340	139.087	136.907	134.796	132.753	130.773	128.853	126.991
140.	146.109	143.785	141.537	139.361	137.253	135.211	133.231	131.310
145.	150.849	148.456	146.140	143.899	141.728	139.624	137.584	135.605
150.	155.561	153.099	150.717	148.411	146.178	144.013	141.914	139.878
155.	160.245	157.715	155.268	152.898	150.603	148.378	146.220	144.127
160.	164.900	162.304	159.792	157.359	155.003	152.718	150.503	148.354
165.	169.528	166.866	164.290	161.795	159.378	157.035	154.762	152.558
170.	174.129	171.401	168.761	166.205	163.729	161.328	158.999	156.739
175.	178.702	175.910	173.208	170.591	168.055	165.597	163.212	160.898
180.	183.248	180.392	177.628	174.951	172.357	169.842	167.403	165.035
185.	187.766	184.848	182.023	179.287	176.636	174.065	171.571	169.150
190.	192.259	189.278	186.393	183.598	180.890	178.264	175.716	173.243
195.	196.724	193.683	190.738	187.886	185.121	182.440	179.839	177.314
200.	201.163	198.061	195.058	192.149	189.328	186.593	183.940	181.364
205.	205.576	202.415	199.353	196.388	193.513	190.724	188.019	185.392
210.	209.963	206.743	203.624	200.603	197.674	194.833	192.076	189.399
215.	214.324	211.046	207.871	204.794	201.812	198.919	196.111	193.385
220.	218.660	215.324	212.093	208.963	205.927	202.983	200.125	197.350
225.	222.970	219.578	216.292	213.107	210.020	207.025	204.117	201.294
230.	227.255	223.807	220.467	217.229	214.090	211.045	208.088	205.217
235.	231.515	228.012	224.615	221.328	218.138	215.043	212.038	209.120
240.	235.750	232.192	228.746	225.405	222.164	219.020	215.968	213.003
245.	239.961	236.349	232.850	229.453	226.168	222.976	219.876	216.865

Hydrogen--Eng. Units

Table I-4

Lift (lb/ft³) of Gas Contained in Steel Cylinders

Gage Press. (lb/in. ²)	Temperature (°F)					
	0	10	20	30	40	50
0	.08021	.07851	.07689	.07534	.07384	.07241
50	.35226	.34484	.33772	.33090	.32434	.31805
100	.62316	.61003	.59746	.58539	.57381	.56269
150	.89289	.87410	.85610	.83883	.82226	.80634
200	1.1615	1.1370	1.1136	1.0912	1.0697	1.0490
250	1.4289	1.3989	1.3701	1.3425	1.3161	1.2906
300	1.6951	1.6595	1.6255	1.5928	1.5614	1.5313
350	1.9602	1.9191	1.8798	1.8420	1.8058	1.7710
400	2.2241	2.1775	2.1329	2.0902	2.0491	2.0097
450	2.4868	2.4349	2.3851	2.3373	2.2914	2.2474
500	2.7484	2.6911	2.6361	2.5833	2.5327	2.4841
550	3.0089	2.9461	2.8860	2.8284	2.7730	2.7199
600	3.2681	3.2001	3.1349	3.0723	3.0123	2.9546
650	3.5263	3.4529	3.3827	3.3153	3.2506	3.1884
700	3.7833	3.7047	3.6294	3.5572	3.4878	3.4212
750	4.0391	3.9553	3.8750	3.7980	3.7241	3.6531
800	4.2938	4.2048	4.1196	4.0378	3.9594	3.8840
850	4.5473	4.4532	4.3631	4.2766	4.1936	4.1139
900	4.7997	4.7005	4.6055	4.5144	4.4269	4.3429
950	5.0509	4.9467	4.8469	4.7511	4.6592	4.5709
1000	5.3010	5.1918	5.0872	4.9869	4.8905	4.7979
1050	5.5500	5.4359	5.3265	5.2216	5.1208	5.0240
1100	5.7979	5.6788	5.5647	5.4552	5.3501	5.2492
1150	6.0446	5.9206	5.8019	5.6879	5.5785	5.4734
1200	6.2902	6.1614	6.0380	5.9196	5.8059	5.6966
1250	6.5346	6.4011	6.2731	6.1502	6.0323	5.9190
1300	6.7780	6.6397	6.5071	6.3799	6.2578	6.1404
1350	7.0202	6.8772	6.7401	6.6086	6.4822	6.3608
1400	7.2614	7.1137	6.9721	6.8362	6.7058	6.5804
1450	7.5014	7.3491	7.2030	7.0629	6.9283	6.7990
1500	7.7403	7.5834	7.4329	7.2886	7.1499	7.0167
1550	7.9782	7.8167	7.6619	7.5133	7.3706	7.2335
1600	8.2149	8.0489	7.8897	7.7370	7.5903	7.4493
1650	8.4506	8.2801	8.1166	7.9598	7.8091	7.6643
1700	8.6851	8.5102	8.3425	8.1816	8.0270	7.8783
1750	8.9186	8.7393	8.5674	8.4024	8.2439	8.0915
1800	9.1510	8.9674	8.7913	8.6222	8.4599	8.3038
1850	9.3823	9.1944	9.0141	8.8411	8.6749	8.5151
1900	9.6126	9.4204	9.2360	9.0591	8.8891	8.7256
1950	9.8418	9.6454	9.4569	9.2761	9.1023	8.9352

Hydrogen--Eng. Units

Table I-4

Lift (lb/ft³) of Gas Contained in Steel Cylinders

Gage Press. (lb/in. ²)	Temperature (°F)					
	60	70	80	90	100	110
0	.07103	.06970	.06842	.06719	.06600	.06486
50	.31200	.30617	.30056	.29516	.28995	.28492
100	.55199	.54170	.53179	.52224	.51303	.50415
150	.79103	.77629	.76211	.74844	.73526	.72254
200	1.0291	1.0100	.99152	.97376	.95663	.94010
250	1.2662	1.2427	1.2200	1.1982	1.1771	1.1568
300	1.5023	1.4745	1.4476	1.4218	1.3968	1.3727
350	1.7375	1.7053	1.6743	1.6444	1.6156	1.5878
400	1.9718	1.9353	1.9001	1.8663	1.8336	1.8021
450	2.2050	2.1643	2.1250	2.0872	2.0507	2.0155
500	2.4374	2.3924	2.3493	2.3073	2.2670	2.2282
550	2.6687	2.6195	2.5722	2.5265	2.4825	2.4400
600	2.8992	2.8458	2.7944	2.7449	2.6971	2.6510
650	3.1286	3.0711	3.0157	2.9624	2.9109	2.8612
700	3.3572	3.2956	3.2362	3.1790	3.1238	3.0706
750	3.5848	3.5191	3.4558	3.3948	3.3359	3.2792
800	3.8115	3.7417	3.6745	3.6097	3.5472	3.4870
850	4.0372	3.9634	3.8923	3.8238	3.7577	3.6940
900	4.2620	4.1842	4.1093	4.0371	3.9674	3.9002
950	4.4859	4.4041	4.3254	4.2495	4.1762	4.1056
1000	4.7089	4.6232	4.5406	4.4610	4.3843	4.3102
1050	4.9309	4.8413	4.7550	4.6718	4.5915	4.5140
1100	5.1520	5.0585	4.9685	4.8817	4.7979	4.7171
1150	5.3722	5.2749	5.1811	5.0908	5.0036	4.9194
1200	5.5916	5.4904	5.3930	5.2990	5.2084	5.1209
1250	5.8099	5.7050	5.6039	5.5064	5.4124	5.3216
1300	6.0274	5.9187	5.8140	5.7131	5.6156	5.5216
1350	6.2440	6.1316	6.0233	5.9189	5.8181	5.7208
1400	6.4597	6.3436	6.2317	6.1238	6.0197	5.9193
1450	6.6745	6.5547	6.4393	6.3280	6.2206	6.1169
1500	6.8885	6.7650	6.6461	6.5314	6.4207	6.3139
1550	7.1015	6.9744	6.8520	6.7340	6.6200	6.5100
1600	7.3137	7.1830	7.0571	6.9357	6.8186	6.7055
1650	7.5249	7.3907	7.2614	7.1367	7.0164	6.9001
1700	7.7353	7.5976	7.4649	7.3369	7.2134	7.0941
1750	7.9449	7.8036	7.6676	7.5363	7.4096	7.2873
1800	8.1535	8.0088	7.8694	7.7349	7.6051	7.4798
1850	8.3613	8.2132	8.0704	7.9328	7.7998	7.6715
1900	8.5683	8.4167	8.2707	8.1298	7.9938	7.8625
1950	8.7744	8.6195	8.4701	8.3261	8.1871	8.0528

Hydrogen--Eng. Units

Table I-4

Lift (lb/ft³) of Gas Contained in Steel Cylinders

Gage Press. (lb/in. ²)	Temperature (°F)					
	0	10	20	30	40	50
2000	10.070	9.8693	9.6769	9.4921	9.3146	9.1439
2050	10.297	10.092	9.8958	9.7072	9.5260	9.3517
2100	10.523	10.314	10.114	9.9214	9.7365	9.5587
2150	10.748	10.535	10.331	10.135	9.9461	9.7648
2200	10.972	10.755	10.547	10.347	10.155	9.9700
2250	11.195	10.974	10.762	10.558	10.363	10.174
2300	11.417	11.192	10.976	10.769	10.570	10.378
2350	11.638	11.409	11.189	10.978	10.776	10.581
2400	11.858	11.625	11.402	11.187	10.981	10.782
2450	12.077	11.840	11.613	11.395	11.185	10.983
2500	12.294	12.054	11.823	11.602	11.389	11.184
2550	12.511	12.267	12.033	11.808	11.591	11.383
2600	12.727	12.479	12.241	12.013	11.793	11.581
2650	12.942	12.690	12.449	12.217	11.994	11.779
2700	13.156	12.901	12.656	12.420	12.194	11.976
2750	13.369	13.110	12.861	12.622	12.393	12.172
2800	13.581	13.318	13.066	12.824	12.591	12.367
2850	13.792	13.526	13.270	13.025	12.789	12.561
2900	14.002	13.732	13.473	13.224	12.985	12.755
2950	14.211	13.938	13.675	13.423	13.181	12.948
3000	14.419	14.142	13.877	13.621	13.376	13.140
3050	14.626	14.346	14.077	13.819	13.570	13.331
3100	14.832	14.549	14.277	14.015	13.764	13.521
3150	15.037	14.751	14.475	14.211	13.956	13.711
3200	15.242	14.952	14.673	14.405	14.148	13.900
3250	15.445	15.152	14.870	14.599	14.339	14.088
3300	15.647	15.351	15.066	14.792	14.529	14.275
3350	15.849	15.549	15.261	14.985	14.718	14.462
3400	16.050	15.747	15.456	15.176	14.907	14.647
3450	16.249	15.943	15.649	15.367	15.094	14.832

Hydrogen--Eng. Units

Table I-4

Lift (lb/ft³) of Gas Contained in Steel Cylinders

Gage Press. (lb/in. ²)	Temperature (°F)					
	60	70	80	90	100	110
2000	8.9796	8.8213	8.6688	8.5216	8.3795	8.2423
2050	9.1840	9.0224	8.8666	8.7164	8.5713	8.4311
2100	9.3875	9.2227	9.0637	8.9103	8.7623	8.6193
2150	9.5903	9.4221	9.2600	9.1036	8.9526	8.8067
2200	9.7921	9.6207	9.4555	9.2960	9.1421	8.9934
2250	9.9932	9.8186	9.6502	9.4878	9.3309	9.1794
2300	10.193	10.016	9.8442	9.6787	9.5190	9.3646
2350	10.393	10.212	10.037	9.8689	9.7063	9.5492
2400	10.591	10.407	10.230	10.058	9.8930	9.7331
2450	10.789	10.602	10.421	10.247	10.079	9.9163
2500	10.986	10.796	10.612	10.435	10.264	10.099
2550	11.182	10.989	10.802	10.622	10.449	10.281
2600	11.378	11.181	10.992	10.809	10.632	10.462
2650	11.572	11.373	11.180	10.995	10.816	10.642
2700	11.766	11.564	11.368	11.180	10.998	10.822
2750	11.959	11.754	11.556	11.364	11.180	11.001
2800	12.151	11.943	11.742	11.548	11.361	11.180
2850	12.342	12.131	11.928	11.731	11.541	11.357
2900	12.533	12.319	12.113	11.913	11.721	11.534
2950	12.723	12.506	12.297	12.095	11.900	11.711
3000	12.912	12.692	12.480	12.276	12.078	11.887
3050	13.100	12.878	12.663	12.456	12.256	12.062
3100	13.288	13.063	12.845	12.635	12.433	12.236
3150	13.475	13.247	13.027	12.814	12.609	12.410
3200	13.661	13.430	13.207	12.992	12.784	12.583
3250	13.846	13.612	13.387	13.170	12.959	12.756
3300	14.030	13.794	13.566	13.346	13.134	12.928
3350	14.214	13.975	13.745	13.523	13.307	13.099
3400	14.397	14.156	13.923	13.698	13.480	13.270
3450	14.579	14.336	14.100	13.873	13.653	13.440

J. GAS DATA

Gas data which are of frequent use in scientific ballooning are given here. To keep the tables brief and yet provide the data in several of the more commonly used unit systems, the data are given in dimensionless form in some of the tables. For example, the ratio C_p/R is given in Table J-4, and values of R are given in six systems of units in Table J-3. The two tables contain more information than six tables of C_p values alone would contain, but to determine a value of C_p , it is necessary to select a number from each of the two tables and multiply them together.

Specific heat, thermal conductivity, viscosity, and the Prandtl number of the gases listed here all vary significantly with temperature but not with pressure in the range likely to be encountered in scientific ballooning. This variation is shown by the tables, but in many cases equations are more convenient than tables. Therefore, equations which correlate specific heat, etc., with temperature are given wherever possible. Since the equations are empirical, care should be taken not to use them for calculations outside of the range of validity specified in the description of the tables.

For convenience, references to data sources are given immediately following each table.

1. Miscellaneous Gas Data

Table J-1 lists useful gas data in both SI and English units. Some tabular entries have been shortened through multiplication by a factor 10^n . When this has been done, the multiplying factor is shown in the "Units" column. For example, all values of density given in lbm/ft^3 have been multiplied by 10^2 , and it is necessary to divide by 10^2 to recover the correct value. Thus, the density of dry air is $8.07 \div 10^2 = 0.0807 \text{ lbm/ft}^3$.

REFERENCES

- (1) Kaye, G.W.C. and T. H. Laby, 1966: Tables of Physical and Chemical Constants, John Wiley and Sons, Inc., New York.
- (2) Reid, Robert C. and Thomas K. Sherwood, 1966: The Properties of Gases and Liquids, 2nd ed., McGraw Hill Book Co., New York.
- (3) Weast, Robert C. and Samuel M. Selby, 1967-1968: Handbook of Chemistry and Physics, 48th ed., The Chemical Rubber Co., Cleveland, Ohio.

2. Gas Constant and Specific Heat Data for Selected Gases

The specific heat of all of the gases listed here is nearly independent of pressure under the pressure and temperature conditions they are likely to be subjected to in the atmosphere. Specific heat does vary with temperature in most of the gases, although helium is an exception, and the variation in nitrogen and air is not great. Also, if ammonia should reach the temperature of its normal boiling point (238.9°K) at a pressure near one atmosphere, its specific heat may be expected to be a strong function of both pressure and temperature.

Specific heat can be correlated with temperature for the gases listed over the range given in Table J-4 with deviations of less than 5% by means of an equation of the type

$$\frac{C_p}{R} = a + b \times 10^{-2}T + c \times 10^{-6}T^2 \quad (\text{J-1})$$

where C_p is the specific heat at constant pressure, R is the gas constant, and a , b , and c are arbitrary constants, chosen to give an adequate fit to the data. The fit is precise at $T = 273.15^\circ\text{K}$. The specific heat at constant volume C_v and the ratio C_p/C_v are both of frequent interest. For an

ideal gas $C_p - C_v = R$ or $C_v/R = (C_p/R) - 1$ and $C_p/C_v = (C_p/R)/[(C_p/R) - 1]$.

Table J-2 provides values of the constants a , b , and c , which may be used with the correlating equation to calculate C_p/R . Table J-3 lists values of R in several of the more commonly used systems of units. In Table J-4 are found values of C_p/R for each of the gases for the temperature range over which the correlating equation may be safely used. Finally, Table J-5 gives values of C_p/C_v .

From the entries in Tables J-3 and J-4 it is easy to determine either C_p or C_v in any of the systems of units given in Table J-3. To calculate C_p , multiply together appropriate entries from the two tables; to determine C_v , multiply the entry from Table J-3 by the entry from Table J-4 less one, that is, $C_v = R [(C_p/R) - 1]$.

For many purposes in scientific ballooning, an average value of specific heat may be satisfactory even though changes of temperature occur. The specific heats of air and nitrogen, for example, undergo such slight changes below 300°K that a constant value is often adequate, and the specific heat of helium is essentially constant to 50°K or lower.

The specific heat data for the mixture of hydrogen and nitrogen were

computed from the data for the component gases by the method recommended by Reid and Sherwood (1).

Example: Determine the specific heat at constant volume (C_v) at 250°K of the mixture of gases which results from the decomposition of ammonia and write an equation expressing C_v as a function of absolute temperature. The specific heat is desired in cal/gm°K.

Solution: When ammonia is decomposed into nitrogen and hydrogen, the mixture is essentially 3/4 hydrogen and 1/4 nitrogen by volume. Thus, from the column headed $3H_2 + N_2$ in Table J-3 the desired value of R is 0.23338 cal/gm°K. From Table J-4, C_p/R at $T = 250^\circ\text{K}$ is found to be 3.419. Then, to slide rule accuracy,

$$C_v = 0.23 (3.42 - 1) = 0.56 \text{ cal/gm}^\circ\text{K}$$

Alternatively, from Table J-2, a , b , and c are seen to be 2.72, 0.419, and -5.54, respectively. Substituting these and R into the correlating equation yields

$$\begin{aligned} C_v &= 0.233 (1.72 + 0.419 \times 10^{-2}T - 5.54 \times 10^{-6}T^2) \\ &= 0.56 \text{ cal/gm}^\circ\text{K} \end{aligned}$$

Note that 1.0 was subtracted from the value of a to change the equation

from an equation in C_p to one in C_v .

Table J-1

Miscellaneous Gas Data

	Units	Dry Air	Helium	Hydrogen	Nitrogen	Ammonia	Decomp. Ammonia	Methane	Oxygen
Chemical Formula	--	*	He	H ₂	N ₂	NH ₃	3H ₂ +N ₂	CH ₄	O ₂
Molecular Wt. (M)	kg/kg-Mol lb/lb-Mol	28.964	4.0026	2.0159	28.013	17.031	8.515	16.043	32.000
Gas Constant (R/M)	J/kg-Mol ^o K ft lb/lb-Mol ^o R	287.06 53.36	2077.2 386.1	4124.4 766.6	296.80 55.17	488.19 90.74	976.43 181.5	518.25 96.33	259.82 48.29
Density 273.15 ^o K, 101325 N/m ² 491.67 ^o R, 14.696 lbf/in ²	kg/m ³ lbm/ft ³ (x10 ³)	1.292 8.07	0.1786 1.11	0.0899 0.561	1.250 7.80	0.760 4.74	0.380 2.37	0.716 4.47	1.428 8.91
Density 288.15 ^o K, 101325 N/m ² 518.67 ^o R, 14.696 lbf/in ²	kg/m ³ lbm/ft ³ (x10 ³)	1.225 7.65	0.1693 1.057	0.0853 0.532	1.185 7.40	0.720 4.49	0.360 2.25	0.679 4.24	1.353 8.45
Density of Liquid at Normal Boiling Point	kg/m ³ lbm/ft ³	--	128 7.99	71.5 4.46	811 50.6	682 42.6	--	426 26.6	1090 68.0
Normal Boiling Point at 101325 N/m ² 14.696 lbf/in ²	^o K ^o R	78.8 141.8	4.21 7.58	20.4 36.7	87.4 157.3	239.6 431.3	--	111.6 200.9	90.2 162.4
Latent Heat of Vaporization at B.P.	J/kg (x10 ³) BTU/lbm	--	20.3 8.73	448 193	199 85.6	1370 589	--	510 219	213 91.6
Flammable limits in air	% by volume	--	--	4-75	--	15-28	7-73	5.3-14	--
Critical Temp	^o K ^o R	132.5 238.5	5.25 9.45	33.3 59.9	126.2 227.2	405.4 729.7	--	190.6 343.1	154.8 278.6
Critical Pressure	N/m ² (x10 ⁶) lbf/in ² (x10 ²)	3.77 5.47	0.229 0.332	1.297 1.88	3.39 4.92	11.30 16.4	--	4.62 6.70	5.08 7.37
Critical Density	kg/m ³ lbm/ft ³	312 19.5	69.3 4.33	31.0 1.94	311 19.4	235 14.7	--	162 10.1	410 25.6
Critical Volume	m ³ /kg-Mol ft ³ /lb-Mol	0.090 1.44	0.058 0.93	0.065 1.04	0.090 1.44	0.072 1.15	--	0.099 1.59	0.078 1.25
Critical Compressibility	--	0.318	0.307	0.304	0.291	0.243	--	0.288	0.308

*Dry air is a mixture of nitrogen (78.084% by volume), oxygen (20.950%), argon (0.934%), carbon dioxide (0.031%), and traces of other gases.

Table J-2

Constants for the Specific Heat-Temperature Correlating Equation

	Air	Helium	Hydrogen	Nitrogen	Ammonia	Mixture 3H ₂ +N ₂	Methane
a	3.54	2.50	2.463	3.503	2.93	2.72	2.10
b	-0.0438	0.	0.562	-0.00335	0.45	0.419	0.735
c	1.06	0.	-7.45	+0.112	-0.03	-5.54	-0.039
*Source	(1)(5)	(4)	(2)	(1)(3)	(1)	(1)(2)(3)	(1)(3)

*The numbers refer to the references which follow Table J-5.

Table J-3

Gas Constant R in Various Systems of Units

	Air	Helium	Hydrogen	Nitrogen	Ammonia	Mixture 3H ₂ +N ₂	Methane
J/(kg-Mol) ^o K	8314.3	8314.3	8314.3	8314.3	8314.3	8314.3	8314.3
J/kg ^o K	287.06	2077.2	4124.4	296.80	488.19	976.43	518.25
*Cal/(g-Mol) ^o K	1.9872	1.9872	1.9872	1.9872	1.9872	1.9872	1.9872
Cal/g ^o K	0.06861	0.49648	0.98576	0.07094	0.11668	0.23338	0.12387
BTU/(lb-Mol) ^o R	1.9859	1.9859	1.9859	1.9859	1.9859	1.9859	1.9859
BTU/lb ^o R	0.06856	0.49615	0.98512	0.07089	0.11661	0.23322	0.12379

*The calories used here are gram calories.

Table J-4

Values of C_p/R for Select Gases as a Function of Temperature

Temp °K	Air	Helium	Hydrogen	Nitrogen	Ammonia	Mixture 3H ₂ +N ₂	Methane	Temp °R
150	3.501	2.501	3.138	3.500	--	3.222	3.202	270
160	3.500	2.501	3.171	3.500	--	3.246	3.275	288
170	3.499	2.501	3.203	3.500	--	3.270	3.348	306
180	3.498	2.501	3.233	3.501	--	3.293	3.422	324
190	3.498	2.501	3.261	3.501	--	3.314	3.495	342
200	3.497	2.501	3.289	3.501	--	3.334	3.568	360
210	3.497	2.501	3.314	3.501	--	3.354	3.642	378
220	3.498	2.501	3.338	3.501	--	3.372	3.715	396
230	3.498	2.501	3.361	3.501	--	3.389	3.788	414
240	3.498	2.501	3.382	3.501	--	3.405	3.861	432
250	3.499	2.501	3.402	3.502	4.059	3.419	3.935	450
260	3.500	2.501	3.420	3.502	4.104	3.433	4.008	468
270	3.502	2.501	3.437	3.502	4.149	3.446	4.081	486
280	3.503	2.501	3.452	3.502	4.194	3.457	4.155	504
290	3.505	2.501	3.466	3.503	4.240	3.467	4.228	522
300	3.506	2.501	3.478	3.503	4.285	3.477	4.301	540
310	3.509	2.501	3.488	3.503	4.330	3.485	4.374	558
320	3.511	2.501	3.498	3.504	4.375	3.492	4.447	576
330	3.513	2.501	3.505	3.504	4.420	3.498	4.521	594
340	3.516	2.501	3.512	3.504	4.465	3.503	4.594	612
350	3.519	2.501	3.517	3.505	4.510	3.506	4.667	630

Table J-5

Values of C_p/C_v for Select Gases as a Function of Temperature

Temp °K	Air	Helium	Hydrogen	Nitrogen	Ammonia	Mixture 3H ₂ +N ₂	Methane	Temp °R
150	1.400	1.666	1.468	1.400	--	1.450	1.454	270
160	1.400	1.666	1.461	1.400	--	1.445	1.440	288
170	1.400	1.666	1.454	1.400	--	1.441	1.426	306
180	1.400	1.666	1.448	1.400	--	1.436	1.413	324
190	1.400	1.666	1.442	1.400	--	1.432	1.401	342
200	1.400	1.666	1.437	1.400	--	1.428	1.389	360
210	1.400	1.666	1.432	1.400	--	1.425	1.379	378
220	1.400	1.666	1.428	1.400	--	1.422	1.368	396
230	1.400	1.666	1.424	1.400	--	1.419	1.359	414
240	1.400	1.666	1.420	1.400	--	1.416	1.349	432
250	1.400	1.666	1.416	1.400	1.327	1.413	1.341	450
260	1.400	1.666	1.413	1.400	1.322	1.411	1.332	468
270	1.400	1.666	1.410	1.400	1.318	1.409	1.325	486
280	1.400	1.666	1.408	1.400	1.313	1.407	1.317	504
290	1.399	1.666	1.406	1.400	1.309	1.405	1.310	522
300	1.399	1.666	1.404	1.400	1.304	1.404	1.303	540
310	1.399	1.666	1.402	1.399	1.300	1.402	1.296	558
320	1.398	1.666	1.400	1.399	1.296	1.401	1.290	576
330	1.398	1.666	1.399	1.399	1.292	1.400	1.284	594
340	1.397	1.666	1.398	1.399	1.289	1.400	1.278	612
350	1.397	1.666	1.397	1.399	1.285	1.399	1.273	630

REFERENCES

- (1) Reid, Robert C. and Thomas K. Sherwood, 1966: The Properties of Gases and Liquids, Second Edition, McGraw-Hill, New York, 169-196, 300-370.
- (2) Woolley, Harold W., Russell B. Scott, and F. G. Brickwedde, 1948: Compilation of Thermal Properties of Hydrogen in Its Various Isotopic and Ortho-Para Modifications, NBS Research Paper RP 1932, Vol. 4.
- (3) Rossini, Frederick D., Kenneth S. Pitzer, William J. Taylor, Joan P. Ebert, John E. Kilpatrick, Charles W. Beckett, Mary G. Williams, and Helene G. Werner, 1947: Selected Values of Properties of Hydrocarbons, NBS Circular C461.
- (4) Kropschot, R. H., B. W. Birmingham, and D. B. Mann, 1968: Technology of Liquid Helium, NBS Monograph 111, Supt. of Documents, U.S. Govt. Printing Office, Wash. D.C., 33-53.
- (5) Kreith, Frank, 1967: Principles of Heat Transfer, International Textbook Company, Scranton, Pa., 595.

3. Thermal Conductivity of Selected Gases

The thermal conductivity of most gases at pressures ranging from about 75 N/m² (~ one mm of H_g) to several atmospheres is only very slightly dependent on pressure. It is dependent on temperature, however, and increases with increased temperature. Tsederberg (1) suggests that over a range of temperature from 273°K to 775°K, thermal conductivity and temperature data are correlated well for many uses by means of the following equation:

$$\frac{k}{k_0} = \left(\frac{T}{T_0}\right)^n \quad (J-2)$$

where k_0 is the thermal conductivity at temperature T_0 and n is a constant which must be determined for each gas. Tsederberg (1) also lists a number of gases and gives values of the constants n and k_0 at $T_0 = 273^\circ\text{K}$ for them. Tables J-6 and J-7 provide similar data for a few gases which are most likely to be of concern to scientific ballooning. In Table J-7 values of k_0 are given in several of the more commonly used systems of units.

The constants listed in Tables J-6 and J-7 do not always agree with those given by Tsederberg. In scientific ballooning, interest is more

often focused on temperatures below 300°K than on higher temperatures. Therefore, an effort was made to find experimental data in the range $150^{\circ} - 350^{\circ}\text{K}$ and to fit the correlation equation to those data. Within that range of temperature, except for the mixture of hydrogen and nitrogen, the correlation equation with the constants given in Tables J-6 and J-7 fits the data to within 5%. Extrapolations beyond that temperature range should not be attempted unless comparison can be made between some of the extrapolated values and reliable data to assure that extrapolation is valid. Although Tsederberg listed a value of k_0 for the mixture of hydrogen and nitrogen, it was necessary to calculate values at other temperatures to compute n . These calculations employed the technique of Brokaw described in Reid and Sherwood (2). The accuracy of the data for the mixture is therefore less certain than for the other gases.

Table J-8 was computed from the correlating equation using the constant n given in Table J-6. Tables J-7 and J-8 together provide a means of quickly obtaining thermal conductivity in any of the more commonly used systems of units for the selected gases. Note that each value of k_0 has been multiplied by the factor given in the units column prior to listing it

in Table J-7; therefore, the correct value of k_0 is the tabular entry divided by that factor.

Example: Determine the value of thermal conductivity in $\text{BTU}/\text{ft hr}^{\circ}\text{R}$ for hydrogen at 380°R and write an equation for the thermal conductivity of hydrogen as a function of temperature in degrees Rankine.

Solution: Since 380°R is not given directly in Table J-8, interpolation yields a value of 0.803 for k/k_0 . The accuracy of the table does not warrant retaining the third place number to the right of the decimal. From Table J-7, k_0 is found to be 9.72×10^{-2} , and $9.72 \times 10^{-2} \times 0.80$ yields $7.8 \times 10^{-2} \text{ BTU}/\text{ft hr}^{\circ}\text{R}$.

From Table J-6, n for hydrogen is found to be 0.85. Using that value and k_0 , the desired equation is found to be

$$k = 9.72 \times 10^{-2} \left(\frac{T}{491.67} \right)^{0.85}$$

Table J-6

Values of n for Selected Gases

	Air	Helium	Hydrogen	Nitrogen	Ammonia	Mixture 3H ₂ +N ₂	Methane
n	0.90	0.70	0.85	0.80	1.53	0.84	1.33

Table J-7

Values of k₀ for Selected Gases
 k₀ is the value of k at T = 273.15°K (491.67°R)

	Air	Helium	Hydrogen	Nitrogen	Ammonia	Mixture 3H ₂ +N ₂	Methane
Watts/m ² K (×10 ³)	2.41	14.40	16.82	2.42	2.10	9.8	3.07
Cal/cm sec °K (×10 ⁵)	5.77	34.4	40.18	5.78	5.03	23.4	7.33
k Cal/m hr °K (×10 ²)	2.08	12.38	14.46	2.08	1.81	8.4	2.64
BTU/ft hr °R (×10 ²)	1.40	8.32	9.72	1.40	1.22	5.7	1.77
*Source	(1)(6)	(4)(5)	(1)(6)	(1)(5)	(1)	(1)	(1)(5)

*The numbers refer to the references which follow Table J-8.

Table J-8

Thermal Conductivity Ratios (k/k₀) for Selected Gases as a
 Function of Temperature

Temp °K	Air	Helium	Hydrogen	Nitrogen	Ammonia	Mixture 3H ₂ +N ₂	Methane	Temp °R
150	.612	.657	.601	.619	--	.604	.451	270
160	.645	.688	.635	.652	--	.638	.491	288
170	.678	.718	.668	.684	--	.671	.532	306
180	.710	.747	.702	.716	--	.704	.574	324
190	.743	.776	.735	.748	--	.737	.617	342
200	.774	.804	.767	.779	--	.770	.661	360
210	.806	.832	.800	.810	--	.802	.705	378
220	.837	.859	.832	.841	--	.834	.750	396
230	.868	.887	.864	.871	--	.866	.796	414
240	.899	.913	.896	.902	--	.897	.842	432
250	.930	.940	.927	.932	.873	.928	.889	450
260	.960	.966	.959	.961	.927	.959	.936	468
270	.991	.992	.990	.991	.982	.990	.985	486
280	1.021	1.017	1.021	1.020	1.039	1.021	1.033	504
290	1.050	1.043	1.052	1.049	1.096	1.052	1.083	522
300	1.080	1.068	1.083	1.078	1.154	1.082	1.133	540
310	1.109	1.093	1.114	1.107	1.214	1.112	1.183	558
320	1.139	1.117	1.144	1.135	1.274	1.142	1.234	576
330	1.168	1.142	1.174	1.163	1.335	1.172	1.286	594
340	1.197	1.166	1.205	1.191	1.398	1.202	1.338	612
350	1.225	1.190	1.235	1.219	1.461	1.232	1.391	630

REFERENCES

- (1) Tsederberg, N. V., 1965: The Thermal Conductivity of Gases and Liquids, The MIT Press, Cambridge, Mass., 88-97 and 144-165.
- (2) Reid, Robert C. and Thomas K. Sherwood, 1966: The Properties of Liquids and Gases, 2nd ed., McGraw-Hill, New York, 456-519.
- (3) The U.S. Standard Atmosphere, 1962, U.S. Govt. Printing Office, Washington, D.C., 1 and 91.
- (4) Kropschot, R. H., B. W. Birmingham, D. B. Mann, Editors, 1968: Technology of Liquid Helium, NBS Monograph 111, U.S. Govt. Printing Office, Washington, D.C., 50-51.
- (5) Ho, C. Y. and R. E. Taylor, 1969: Thermal Conductivity, Proceedings of the Eighth Conference, Plenum Press, New York, 76, 119, 125, 229.
- (6) Hilsenrath, Joseph, Charles W. Beckett, William S. Benedict, Lilla Fano, Harold J. Hoge, Joseph F. Masi, Ralph L. Nuttall, Yeram S. Touloukian, Harold W. Woolley, 1955: Tables of Thermal Properties of Gases, NBS Circular 564, U.S. Govt. Printing Office, Washington, D.C., 269 and 285.

4. Viscosity of Selected Gases

The dynamic viscosity of gases at low pressure (two atmospheres or less) is very nearly independent of pressure, but it is a function of temperature, and the viscosity increases with temperature. For most of the gases listed here, the two-constant Sutherland equation has been shown to be a highly reliable equation for correlating viscosity-temperature data.

It is

$$\mu = bT^{1.5} / (S + T) \quad (J-4)$$

where b and S are arbitrary constants which may be determined by any satisfactory curve fitting technique. The equation, in the form

$$\frac{\mu}{\mu_0} = \left(\frac{T}{273.15} \right)^{1.5} \frac{S + 273.15}{S + T} \quad (J-5)$$

in which T must be entered in degrees Kelvin, was used to compute the data of Table J-11 for all gases except hydrogen and helium. The value of S is given in Table J-9.

The hydrogen and helium data were computed using the following equations:

$$\text{Hydrogen} \quad \frac{\mu}{\mu_0} = 460 \left(\frac{T}{273.15} \right)^{1.5} \frac{T + 650.4}{(T + 19.6)(T + 1176)} \quad (J-6)$$

$$\text{Helium} \quad \frac{\mu}{\mu_0} = \left(\frac{T}{273.15} \right)^{0.647} \quad (\text{J-7})$$

Within the temperature range used in Table J-11, the tabulated values and the equations yield viscosity data which rarely differ more than 5% from the data used to determine the constants. Viscosity values for the mixture of hydrogen and nitrogen were computed using the Wilke method for estimating the viscosity of gas mixtures as described in Reid and Sherwood (1), and the Sutherland equation was fitted to the estimated data. Errors may be as large as 10%. The equations for hydrogen and helium may be used for values of T as low as 30°K without excessive error.

Kinematic viscosity η may be determined from μ if the gas density is known since $\eta = \mu/\rho$.

Example: Determine the viscosity of ammonia in lbf sec/ft² at T = 450°R. Also write an equation which may be used in a computer program to compute the viscosity in lbf sec/ft² using T in degrees Rankine.

Solution: The value of μ/μ_0 for ammonia at 450°R is selected directly from Table J-11. It is 0.898. The value of μ_0 for ammonia from Table J-10 is 1.881×10^{-7} lbf sec/ft². Their product is 1.69×10^{-7} lbf sec/ft².

Note that each value of μ_0 given in Table J-10 has been multiplied by the

factor (10^7 in this example) which is shown in the units column. Therefore, the tabular entry must be divided by this factor.

The desired equation is

$$\mu = 1.881 \times 10^{-7} \left(\frac{5/9 T}{273.15} \right)^{1.5} \frac{670 + 273.15}{670 + 5/9 T}$$

where S = 670 is determined from Table J-9 and $5/9 T(^{\circ}\text{R}) = T(^{\circ}\text{K})$.

Table J-9

Values of S for Selected Gases

	Air	Helium	Hydrogen	Nitrogen	Ammonia	Mixture 3H ₂ +N ₂	Methane
S	110.4	--	--	100.1	670	98.9	93.5

Table J-10

Values of μ_0 for Selected Gases
 $\mu_0 = \mu$ when $T = 273.15^\circ\text{K}$

	Mixture						
	Air	Helium	Hydrogen	Nitrogen	Ammonia	$3\text{H}_2 + \text{N}_2$	Methane
kg/m sec ($\times 10^6$)	1.716	1.895	0.841	1.652	0.900	1.43	1.089
*poise ($\times 10^4$)	1.716	1.895	0.841	1.652	0.900	1.43	1.089
lbm/ft sec ($\times 10^5$)	1.153	1.273	0.565	1.110	0.605	0.96	0.732
lbm/ft hr ($\times 10^7$)	4.152	4.586	2.035	3.998	2.178	3.46	2.635
lbf sec/ft ² ($\times 10^7$)	3.586	3.961	1.758	3.453	1.881	2.99	2.276
slug/ft hr ($\times 10^4$)	12.90	14.25	6.324	12.42	6.768	10.75	8.189
**Source	(2)(5)	(3)	(4)(5)	(5)	(1)	(1)	(1)

*1 poise = 1 dyne sec/cm² = 1 gm/cm sec = 0.1 kg/m sec.

**The numbers refer to the reference which follow Table J-11.

Table J-11

Values of μ/μ_0 for Selected Gases as a Function of Temperature

Temp °K	Air	Helium	Hydrogen	Nitrogen	Ammonia	Mixture $3\text{H}_2 + \text{N}_2$	Methane	Temp °R
150	.599	.679	.666	.631	--	.642	.613	270
160	.635	.707	.696	.666	--	.676	.648	288
170	.671	.736	.726	.699	--	.709	.683	306
180	.706	.764	.755	.732	--	.740	.717	324
190	.740	.791	.783	.763	--	.771	.750	342
200	.773	.817	.811	.794	--	.801	.783	360
210	.806	.844	.838	.824	--	.830	.814	378
220	.838	.869	.865	.854	--	.859	.845	396
230	.870	.895	.892	.882	--	.886	.876	414
240	.901	.920	.918	.911	--	.914	.905	432
250	.931	.944	.943	.938	.898	.940	.934	450
260	.961	.969	.969	.965	.942	.966	.963	468
270	.990	.993	.994	.992	.986	.992	.991	486
280	1.019	1.016	1.018	1.018	1.030	1.017	1.019	504
290	1.047	1.039	1.043	1.043	1.075	1.042	1.046	522
300	1.075	1.063	1.067	1.068	1.119	1.066	1.072	540
310	1.102	1.085	1.091	1.093	1.163	1.089	1.098	558
320	1.129	1.108	1.114	1.117	1.208	1.113	1.124	576
330	1.155	1.130	1.137	1.141	1.252	1.136	1.150	594
340	1.181	1.152	1.161	1.164	1.297	1.158	1.174	612
350	1.207	1.174	1.183	1.187	1.341	1.180	1.199	630

REFERENCES

- (1) Reid, Robert C. and Thomas K. Sherwood, 1966: The Properties of Gases and Liquids, 2nd ed., McGraw-Hill, New York, 395-455.
- (2) The U.S. Standard Atmosphere, 1962, U.S. Govt. Printing Office, Washington, D.C., 14.
- (3) Kropschot, R. H., B. W. Birmingham, D. B. Mann, Editors, 1968: Technology of Liquid Helium, NBS Monograph 111, U.S. Govt. Printing Office, Washington, D.C., 50.
- (4) Woolley, Harold W., Russell B. Scott, F. G. Brickwedde, 1948: Compilation of Thermal Properties of Hydrogen in its Various Isotopic and Ortho-Para Modifications, NBS Research Paper, RP 1932, Vol. 41, 446-447.
- (5) Hilsenrath, Joseph, Charles W. Beckett, William S. Benedict, Lilla Fano, Harold J. Hoge, Joseph F. Masi, Ralph L. Nuttall, Yeram S. Touloukian, Harold W. Woolley, 1955: Tables of Thermal Properties of Gases, NBS Circular 564, U.S. Govt. Printing Office, Washington, D.C.

5. Prandtl Number of Selected Gases

The Prandtl number is frequently used in heat transfer correlations.

Because it is a dimensionless number which is determined by the characteristics of the fluid and not by the heat transfer application, it can be tabulated for each fluid. The equations

$$\text{Pr} = \frac{C_p \mu}{k} \quad \text{and} \quad \text{Pr} = \frac{C_p \mu}{kM} \quad (\text{J-8})$$

define the Prandtl number Pr. In the first equation the specific heat C_p must be expressed in terms of energy per unit of mass per degree, while in the second it must be expressed in terms of energy per mol per degree. The variable μ is the dynamic viscosity, k is the thermal conductivity, and M is the molecular weight. Since all of these variables except M are functions of temperature only (or nearly so) at pressures equal to or less than one atmosphere, Pr is also a function of temperature. In fact, Pr can readily be computed from the data in the tables of sub-sections J.2, J.3, and J.4, and a correlating equation for Pr may be derived from the correlating equations given in those sub-sections.

For the gases listed here in the range of temperatures mostlikely to

be encountered in ballooning, Pr is nearly constant, and for many engineering applications an average value is adequate. For those applications which require greater precision, the following equation has been found to correlate Pr well with temperature for the gases listed here.

$$Pr = a + b \times 10^{-4}T \quad (J-9)$$

Table J-12 lists values of a and b for each gas. Temperature must be entered in °K. The equation yields values of Pr which differ from the data used to derive them by not more than 3% over the temperature range shown in Table J-13 for each gas.

Table J-13 gives values of Pr as a function of temperature for several gases. These values were computed by means of the correlating equation given above.

Table J-12

Constants for the Prandtl Number-Temperature Correlating Equation

	Air	Helium	Hydrogen	Nitrogen	Ammonia	Mixture 3H ₂ + N ₂	Methane
a	0.804	0.729	0.744	0.821	0.889	0.501	0.837
b	-3.25	-1.60	-1.25	-3.64	-0.71	-0.53	-2.90
*Source	(1)	(2)	(1)	(1)	**	**	**

*The numbers refer to the references which follow Table J-13.

**These constants are based on values of Pr computed from the data of subsections J.2, J.3, and J.4. The low values of Pr for the mixture of hydrogen and nitrogen have been verified in a study by Colburn and Coghlan (3).

Table J-13

Prandtl Numbers for Selected Gases as a Function of Temperature

Temp °K	Air	Helium	Hydrogen	Nitrogen	Ammonia	Mixture 3H ₂ +N ₂	Methane	Temp °R
150	.755	.705	.725	.766	--	.493	.793	270
160	.752	.703	.724	.763	--	.493	.791	288
170	.749	.702	.723	.759	--	.492	.788	306
180	.745	.700	.721	.755	--	.491	.785	324
190	.742	.699	.720	.752	--	.491	.782	342
200	.739	.697	.719	.748	--	.490	.779	360
210	.736	.695	.718	.745	--	.490	.776	378
220	.732	.694	.716	.741	--	.489	.773	396
230	.729	.692	.715	.737	--	.489	.770	414
240	.726	.691	.714	.734	--	.488	.767	432
250	.723	.689	.713	.730	.871	.488	.764	450
260	.719	.687	.711	.726	.871	.487	.762	468
270	.716	.686	.710	.723	.870	.487	.759	486
280	.713	.684	.709	.719	.869	.486	.756	504
290	.710	.683	.708	.715	.868	.486	.753	522
300	.706	.681	.706	.712	.868	.485	.750	540
310	.703	.679	.705	.708	.867	.485	.747	558
320	.700	.678	.704	.705	.866	.484	.744	576
330	.697	.676	.703	.701	.866	.484	.741	594
340	.693	.675	.701	.697	.865	.483	.738	612
350	.690	.673	.700	.694	.864	.482	.735	630

REFERENCES

- (1) Hilsenrath, Joseph, Charles W. Beckett, William S. Benedict, Lilla Fano, Harold J. Hoge, Joseph F. Masi, Ralph L. Nuttall, Yeram S. Touloukian, Harold W. Woolley, 1955: Tables of Thermal Properties of Gases, NBS Circular 564, U.S. Govt. Printing Office, Washington, D.C., 14-74, 254-368.
- (2) Kropschot, R. H., B. W. Birmingham, D. B. Mann, Editors, 1968: Technology of Liquid Helium, NBS Monograph 111, U.S. Govt. Printing Office, Washington, D.C., 35-53.
- (3) Colburn, A. P. and C. A. Coghlan, 1941: Trans. ASME, 63:561.

K. SPECIFIC LIFT OF HELIUM AND HYDROGEN AND PROPERTIES OF THE U.S. STANDARD

ATMOSPHERE, 1962

Table K-1 is an abridged version of a table contained in an NCAR Technical Note by Warren et al. (1). The basis for calculating the specific lift of a gas in the atmosphere is given in Section IV, and a discussion of the atmosphere, including the U.S. Standard Atmosphere, 1962, may be found in Section XI.

Although the original table has been reduced for inclusion here, linear interpolation is permissible throughout the abridged table. The variables presented in columns 6-10 are valid in any atmosphere in which the mixture of atmospheric gases has the same molecular weight as air, and in which both the pressure-to-temperature ratio in the lift gas and the atmosphere equal the tabulated value. Since gas and air pressure are very nearly equal in zero-pressure balloons during flight, the air and gas temperature must also be nearly equal if the tabulated specific lift values (columns 8-10) are to be valid. An error caused by a difference in temperature between the air and gas is not usually serious from the point of view of the balloon designer or the scientist, but flight operations

personnel must keep such differences in mind. See Sections II and III for a discussion of the consequences of differing gas and air temperatures during flight.

Columns 1 and 3 through 5 are derived directly from the definition of the U.S. Standard Atmosphere, 1962. Column 2 is calculated from an empirical equation derived by Morris (2). The equation is

$$m_n = 10 p_n (1.03751 - 5.27 \times 10^{-3} \log_{10} p_n) \quad (K-1)$$

where p_n is atmospheric pressure in mb at level n in the atmosphere and m_n is the total mass of air in kg in a one m^2 column extending from level n upward through the balance of the atmosphere. A similar equation,

$$p_n = m_n / (1.03757 - 5.27 \times 10^{-3} \log_{10} m_n)$$

in which m_n is given in gm/cm^2 and p_n is in mb, may be used to convert from the usual integrated mass units to pressure.

The following examples illustrate the use of this table:

1. Determine the altitude at which a balloon system having a gross mass m_G of 2721 kg and a volume V of $10^6 m^3$ will float when the balloon is inflated with helium.

Solution: The mass per unit volume (specific lift) which must be supported by the balloon is $m_G/V = m$. Note that m_G is the gross mass of the balloon system excluding the mass of the enclosed lift gas but including the mass of the balloon; m is then $2.721 \times 10^{-3} \text{ kg/m}^3$. Column 9 of the table lists values of $2.8360\text{E-}03$ (2.8360×10^{-3}) and $2.5812\text{E-}03$, corresponding to air densities of $3.2909\text{E-}03$ and $2.9952\text{E-}03$, respectively. Linear interpolation yields a density of 3.1574×10^{-3} corresponding to the specific lift of 2.721×10^{-3} , and the balloon system will float in the atmosphere at the level at which the air density is $3.1574 \times 10^{-3} \text{ kg/m}^3$. If density is known as a function of height, the height at which the balloon will float may be determined. If density is not known as a function of height in the real atmosphere, the height in a model atmosphere can serve as an approximation to the height in the real atmosphere. In this example the height in the U.S. Standard Atmosphere, 1962, is found in column 3 by interpolation to be 41,367 m.

2. Determine the volume of a helium-filled balloon required to support a gross mass of 6000 lb at a height of 135,600 ft in the U.S. Standard Atmosphere, 1962.

Solution: From the definition of specific lift, $V = m_G/m$; from column 10, interpolation yields $m = 1.7057 \times 10^{-4} \text{ lbs/ft}^3$ at 135,600 ft. Then $V = 6000/1.7057 \times 10^{-4}$, or approximately $35.2 \times 10^6 \text{ ft}^3$.

3. Another method of determining volume is to multiply the gas expansion factor for the desired height by the product of the gross mass and the volume of gas required to support a unit mass at sea level.

Solution: From column 7, the gas expansion is found to be 386.8; from Table 2 of Section IV, or by taking the reciprocal of the specific lift at sea level, the volume of helium required to lift a mass of one pound is found to be 15.17. Then $V = 6000 \times 15.17 \times 386.8 = 35.2 \times 10^6 \text{ ft}^3$.

4. A parachute has been selected to lower a payload, and the entire system will have a descent velocity of 22 ft/sec at sea level in the U.S. Standard Atmosphere, 1962. Compute its terminal descent velocity at 2.4 mb in that standard atmosphere.

Solution: Equation (21) of Section X, $v_T = v_{T,0} \sqrt{\rho_0/\rho}$, may be used in this case. The ratio of densities may be determined from the table by division, but the gas expansion factor found in column 7 is that ratio. Thus, $v_T = 22 \sqrt{372.2} = 424 \text{ ft/sec}$.

Table K-1

Specific Lift of Helium and Hydrogen and Properties of the U.S. Standard Atmosphere, 1962									
(1)	(2)	(3)	(4)	(5)	(6)	(7)	(8)	(9)	(10)
p Press. (mb)	Integrated Air Mass (kg/m ²)	H Geopot. Alt. (m)	H Alt. (ft)	T Temp. (°C)	ρ Density (kg/m ³)	Gas Ex- pansion	Lift H ₂ Pure (kg/m ³)	Lift He Grade A (kg/m ³)	Lift He Grade A (lb/ft ³)
1050	1.073E+04	-302	-989	16.96	1.2609E+00	.972	1.1731E+00	1.0866E+00	6.7832E-02
1040	1.062E+04	-220	-723	16.43	1.2511E+00	.979	1.1640E+00	1.0782E+00	6.7308E-02
1030	1.052E+04	-139	-454	15.90	1.2414E+00	.987	1.1550E+00	1.0698E+00	6.6784E-02
1020	1.042E+04	-56	-184	15.36	1.2316E+00	.995	1.1459E+00	1.0614E+00	6.6258E-02
1010	1.032E+04	27	89	14.82	1.2218E+00	1.003	1.1368E+00	1.0529E+00	6.5732E-02
1000	1.022E+04	111	364	14.28	1.2120E+00	1.011	1.1277E+00	1.0445E+00	6.5204E-02
990	1.012E+04	195	641	13.73	1.2022E+00	1.019	1.1185E+00	1.0360E+00	6.4676E-02
980	1.001E+04	281	920	13.18	1.1923E+00	1.027	1.1094E+00	1.0275E+00	6.4146E-02
970	9.911E+03	366	1202	12.62	1.1825E+00	1.036	1.1002E+00	1.0190E+00	6.3616E-02
960	9.809E+03	453	1486	12.06	1.1726E+00	1.045	1.0910E+00	1.0105E+00	6.3084E-02
950	9.707E+03	540	1773	11.49	1.1627E+00	1.054	1.0818E+00	1.0020E+00	6.2551E-02
940	9.605E+03	628	2062	10.92	1.1528E+00	1.063	1.0725E+00	9.9343E-01	6.2018E-02
930	9.503E+03	717	2353	10.34	1.1428E+00	1.072	1.0633E+00	9.8486E-01	6.1483E-02
920	9.401E+03	807	2647	9.76	1.1329E+00	1.081	1.0540E+00	9.7628E-01	6.0947E-02
910	9.299E+03	897	2944	9.17	1.1229E+00	1.091	1.0447E+00	9.6768E-01	6.0420E-02
900	9.197E+03	989	3243	8.57	1.1129E+00	1.101	1.0354E+00	9.5906E-01	5.9872E-02
890	9.096E+03	1081	3545	7.98	1.1029E+00	1.111	1.0261E+00	9.5042E-01	5.9333E-02
880	8.994E+03	1173	3850	7.37	1.0928E+00	1.121	1.0168E+00	9.4176E-01	5.8792E-02
870	8.892E+03	1267	4157	6.76	1.0828E+00	1.131	1.0074E+00	9.3309E-01	5.8251E-02
860	8.790E+03	1362	4468	6.15	1.0727E+00	1.142	9.9802E-01	9.2439E-01	5.7708E-02
850	8.688E+03	1457	4781	5.53	1.0626E+00	1.153	9.8861E-01	9.1568E-01	5.7164E-02
840	8.586E+03	1554	5098	4.90	1.0524E+00	1.164	9.7918E-01	9.0695E-01	5.6619E-02
830	8.484E+03	1651	5417	4.27	1.0423E+00	1.175	9.6973E-01	8.9820E-01	5.6073E-02
820	8.382E+03	1749	5740	3.63	1.0321E+00	1.187	9.6026E-01	8.8942E-01	5.5525E-02
810	8.280E+03	1849	6065	2.98	1.0219E+00	1.199	9.5077E-01	8.8063E-01	5.4976E-02

113

Table K-1

Specific Lift of Helium and Hydrogen and Properties of the U.S. Standard Atmosphere, 1962									
(1)	(2)	(3)	(4)	(5)	(6)	(7)	(8)	(9)	(10)
p Press. (mb)	Integrated Air Mass (kg/m ²)	H Geopot. Alt. (m)	H Alt. (ft)	T Temp. (°C)	ρ Density (kg/m ³)	Gas Ex- pansion	Lift H ₂ Pure (kg/m ³)	Lift He Grade A (kg/m ³)	Lift He Grade A (lb/ft ³)
800	8.178E+03	1949	6394	2.33	1.0117E+00	1.211	9.4125E-01	8.7182E-01	5.4426E-02
790	8.076E+03	2050	6727	1.67	1.0014E+00	1.223	9.3171E-01	8.6298E-01	5.3874E-02
780	7.974E+03	2153	7063	1.01	9.9113E-01	1.236	9.2215E-01	8.5413E-01	5.3321E-02
770	7.872E+03	2256	7402	.34	9.8083E-01	1.249	9.1256E-01	8.4525E-01	5.2767E-02
760	7.770E+03	2361	7745	-.34	9.7050E-01	1.262	9.0296E-01	8.3635E-01	5.2211E-02
750	7.668E+03	2466	8091	-1.03	9.6015E-01	1.276	8.9332E-01	8.2743E-01	5.1654E-02
740	7.566E+03	2573	8442	-1.72	9.4977E-01	1.290	8.8367E-01	8.1848E-01	5.1096E-02
730	7.464E+03	2681	8796	-2.43	9.3936E-01	1.304	8.7398E-01	8.0951E-01	5.0536E-02
720	7.362E+03	2790	9154	-3.14	9.2893E-01	1.319	8.6428E-01	8.0052E-01	4.9975E-02
710	7.260E+03	2901	9516	-3.85	9.1847E-01	1.334	8.5454E-01	7.9151E-01	4.9412E-02
700	7.158E+03	3012	9882	-4.58	9.0798E-01	1.349	8.4479E-01	7.8247E-01	4.8848E-02
690	7.056E+03	3125	10253	-5.31	8.9746E-01	1.365	8.3500E-01	7.7340E-01	4.8282E-02
680	6.954E+03	3239	10628	-6.06	8.8692E-01	1.381	8.2519E-01	7.6432E-01	4.7715E-02
670	6.852E+03	3355	11008	-6.81	8.7634E-01	1.398	8.1535E-01	7.5520E-01	4.7146E-02
660	6.749E+03	3472	11392	-7.57	8.6573E-01	1.415	8.0548E-01	7.4606E-01	4.6575E-02
650	6.647E+03	3591	11780	-8.34	8.5510E-01	1.433	7.9558E-01	7.3689E-01	4.6003E-02
640	6.545E+03	3711	12174	-9.12	8.4443E-01	1.451	7.8566E-01	7.2770E-01	4.5429E-02
630	6.443E+03	3832	12573	-9.91	8.3373E-01	1.469	7.7570E-01	7.1848E-01	4.4853E-02
620	6.341E+03	3955	12977	-10.71	8.2300E-01	1.488	7.6572E-01	7.0923E-01	4.4276E-02
610	6.239E+03	4080	13386	-11.52	8.1223E-01	1.508	7.5570E-01	6.9996E-01	4.3697E-02
600	6.137E+03	4206	13801	-12.34	8.0143E-01	1.529	7.4565E-01	6.9065E-01	4.3116E-02
590	6.035E+03	4335	14221	-13.17	7.9060E-01	1.549	7.3557E-01	6.8131E-01	4.2533E-02
580	5.933E+03	4464	14647	-14.02	7.7973E-01	1.571	7.2546E-01	6.7195E-01	4.1948E-02
570	5.831E+03	4596	15079	-14.87	7.6883E-01	1.593	7.1532E-01	6.6255E-01	4.1362E-02
560	5.729E+03	4730	15517	-15.74	7.5789E-01	1.616	7.0514E-01	6.5312E-01	4.0773E-02

114

Table K-1

Specific Lift of Helium and Hydrogen and Properties of the U.S. Standard Atmosphere, 1962

(1)	(2)	(3)		(4)	(5)	(6)	(7)	(8)	(9)	(10)
p Press. (mb)	Integrated Air Mass (kg/m ²)	H Geopot. Alt. (m) (ft)		T Temp. (°C)	ρ Density (kg/m ³)	Gas Ex- pansion	Lift H ₂ Pure (kg/m ³)	Lift He Grade A (kg/m ³)	Lift He Grade A (lb/ft ³)	
550	5.627E+03	4865	15962	-16.62	7.4691E-01	1.640	6.9493E-01	6.4366E-01	4.0183E-02	
540	5.525E+03	5003	16413	-17.52	7.3590E-01	1.665	6.8468E-01	6.3417E-01	3.9590E-02	
530	5.423E+03	5142	16871	-18.43	7.2484E-01	1.690	6.7439E-01	6.2464E-01	3.8995E-02	
520	5.321E+03	5284	17336	-19.35	7.1375E-01	1.716	6.6407E-01	6.1508E-01	3.8398E-02	
510	5.219E+03	5428	17809	-20.28	7.0261E-01	1.743	6.5371E-01	6.0549E-01	3.7799E-02	
500	5.116E+03	5574	18289	-21.23	6.9144E-01	1.772	6.4331E-01	5.9586E-01	3.7198E-02	
490	5.014E+03	5723	18777	-22.20	6.8022E-01	1.801	6.3287E-01	5.8619E-01	3.6595E-02	
480	4.912E+03	5874	19273	-23.18	6.6895E-01	1.831	6.2239E-01	5.7648E-01	3.5989E-02	
470	4.810E+03	6028	19777	-24.18	6.5765E-01	1.863	6.1187E-01	5.6674E-01	3.5380E-02	
460	4.708E+03	6184	20290	-25.20	6.4629E-01	1.895	6.0131E-01	5.5695E-01	3.4769E-02	
450	4.606E+03	6344	20812	-26.23	6.3489E-01	1.929	5.9070E-01	5.4713E-01	3.4156E-02	
440	4.504E+03	6506	21344	-27.29	6.2344E-01	1.965	5.8005E-01	5.3726E-01	3.3540E-02	
430	4.402E+03	6671	21886	-28.36	6.1195E-01	2.002	5.6935E-01	5.2735E-01	3.2922E-02	
420	4.299E+03	6839	22438	-29.45	6.0040E-01	2.040	5.5861E-01	5.1740E-01	3.2300E-02	
410	4.197E+03	7011	23000	-30.57	5.8879E-01	2.081	5.4781E-01	5.0740E-01	3.1676E-02	
400	4.095E+03	7185	23574	-31.71	5.7714E-01	2.123	5.3697E-01	4.9736E-01	3.1049E-02	
390	3.993E+03	7364	24160	-32.87	5.6543E-01	2.167	5.2607E-01	4.8727E-01	3.0419E-02	
380	3.891E+03	7546	24758	-34.05	5.5366E-01	2.213	5.1512E-01	4.7712E-01	2.9786E-02	
370	3.789E+03	7732	25369	-35.26	5.4183E-01	2.261	5.0412E-01	4.6693E-01	2.9150E-02	
360	3.687E+03	7923	25993	-36.50	5.2994E-01	2.312	4.9306E-01	4.5669E-01	2.8510E-02	
350	3.584E+03	8117	26631	-37.76	5.1799E-01	2.365	4.8194E-01	4.4639E-01	2.7867E-02	
340	3.482E+03	8316	27285	-39.06	5.0597E-01	2.421	4.7076E-01	4.3603E-01	2.7221E-02	
330	3.380E+03	8520	27954	-40.38	4.9389E-01	2.480	4.5951E-01	4.2562E-01	2.6570E-02	
320	3.278E+03	8729	28640	-41.74	4.8174E-01	2.543	4.4821E-01	4.1514E-01	2.5917E-02	
310	3.176E+03	8944	29343	-43.14	4.6951E-01	2.609	4.3683E-01	4.0461E-01	2.5259E-02	

115

Table K-1

Specific Lift of Helium and Hydrogen and Properties of the U.S. Standard Atmosphere, 1962

(1)	(2)	(3)		(4)	(5)	(6)	(7)	(8)	(9)	(10)
p Press. (mb)	Integrated Air Mass (kg/m ²)	H Geopot. Alt. (m) (ft)		T Temp. (°C)	ρ Density (kg/m ³)	Gas Ex- pansion	Lift H ₂ Pure (kg/m ³)	Lift He Grade A (kg/m ³)	Lift He Grade A (lb/ft ³)	
300	3.073E+03	9164	30065	-44.57	4.5721E-01	2.679	4.2538E-01	3.9401E-01	2.4597E-02	
290	2.971E+03	9390	30807	-46.04	4.4483E-01	2.754	4.1387E-01	3.8334E-01	2.3931E-02	
280	2.869E+03	9623	31570	-47.55	4.3236E-01	2.833	4.0227E-01	3.7260E-01	2.3261E-02	
270	2.767E+03	9862	32355	-49.10	4.1982E-01	2.918	3.9060E-01	3.6179E-01	2.2586E-02	
260	2.664E+03	10109	33164	-50.71	4.0718E-01	3.008	3.7884E-01	3.5090E-01	2.1906E-02	
250	2.562E+03	10363	33999	-52.36	3.9445E-01	3.106	3.6700E-01	3.3993E-01	2.1221E-02	
240	2.460E+03	10626	34861	-54.07	3.8163E-01	3.210	3.5507E-01	3.2887E-01	2.0531E-02	
230	2.358E+03	10898	35753	-55.83	3.6870E-01	3.322	3.4304E-01	3.1773E-01	1.9836E-02	
220	2.255E+03	11180	36679	-56.50	3.5575E-01	3.463	3.2913E-01	3.0485E-01	1.9031E-02	
210	2.153E+03	11475	37646	-56.50	3.3767E-01	3.628	3.1417E-01	2.9100E-01	1.8166E-02	
200	2.051E+03	11784	38662	-56.50	3.2159E-01	3.809	2.9921E-01	2.7714E-01	1.7301E-02	
190	1.948E+03	12109	39729	-56.50	3.0552E-01	4.010	2.8425E-01	2.6328E-01	1.6436E-02	
180	1.846E+03	12452	40854	-56.50	2.8944E-01	4.232	2.6929E-01	2.4943E-01	1.5571E-02	
170	1.744E+03	12815	42043	-56.50	2.7336E-01	4.481	2.5433E-01	2.3557E-01	1.4706E-02	
160	1.641E+03	13199	43304	-56.50	2.5728E-01	4.761	2.3937E-01	2.2171E-01	1.3841E-02	
150	1.539E+03	13608	44647	-56.50	2.4120E-01	5.079	2.2441E-01	2.0785E-01	1.2976E-02	
140	1.437E+03	14046	46082	-56.50	2.2512E-01	5.442	2.0945E-01	1.9400E-01	1.2111E-02	
130	1.334E+03	14516	47624	-56.50	2.0904E-01	5.860	1.9449E-01	1.8014E-01	1.1246E-02	
120	1.232E+03	15024	49290	-56.50	1.9296E-01	6.349	1.7953E-01	1.6628E-01	1.0381E-02	
110	1.129E+03	15575	51100	-56.50	1.7688E-01	6.926	1.6457E-01	1.5243E-01	9.5157E-03	
100	1.027E+03	16180	53083	-56.50	1.6080E-01	7.618	1.4961E-01	1.3857E-01	8.6506E-03	
95	9.757E+02	16505	54150	-56.50	1.5276E-01	8.019	1.4213E-01	1.3164E-01	8.2181E-03	
90	9.245E+02	16848	55275	-56.50	1.4472E-01	8.465	1.3465E-01	1.2471E-01	7.7856E-03	
85	8.732E+02	17210	56464	-56.50	1.3668E-01	8.963	1.2716E-01	1.1778E-01	7.3530E-03	
80	8.220E+02	17595	57726	-56.50	1.2864E-01	9.523	1.1968E-01	1.1086E-01	6.9205E-03	

116

Table K-1

Specific Lift of Helium and Hydrogen and Properties of the U.S. Standard Atmosphere, 1962									
(1)	(2)	(3)	(4)	(5)	(6)	(7)	(8)	(9)	(10)
p Press. (mb)	Integrated Air Mass (kg/m ²)	H Geopot. Alt. (m)	H Alt. (ft)	T Temp. (°C)	ρ Density (kg/m ³)	Gas Ex- pansion	Lift H ₂ Pure (kg/m ³)	Lift He Grade A (kg/m ³)	Lift He Grade A (lb/ft ³)
75	7.707E+02	18004	59069	-56.50	1.2060E-01	10.158	1.1220E-01	1.0393E-01	6.4880E-03
70	7.195E+02	18442	60504	-56.50	1.1256E-01	10.883	1.0472E-01	9.6999E-02	6.0554E-03
65	6.682E+02	18912	62046	-56.50	1.0452E-01	11.720	9.7244E-02	9.0070E-02	5.6229E-03
60	6.169E+02	19419	63711	-56.50	9.6478E-02	12.697	8.9763E-02	8.3142E-02	5.1904E-03
55	5.656E+02	19971	65522	-56.50	8.8439E-02	13.851	8.2283E-02	7.6213E-02	4.7578E-03
50	5.143E+02	20576	67507	-55.92	8.0185E-02	15.277	7.4605E-02	6.9101E-02	4.3138E-03
45	4.630E+02	21247	69708	-55.25	7.1945E-02	17.027	6.6937E-02	6.2000E-02	3.8705E-03
40	4.116E+02	22000	72177	-54.50	6.3731E-02	19.221	5.9295E-02	5.4921E-02	3.4286E-03
35	3.603E+02	22856	74987	-53.64	5.5547E-02	22.053	5.1681E-02	4.7868E-02	2.9883E-03
30	3.089E+02	23849	78244	-52.65	4.7397E-02	25.845	4.4098E-02	4.0845E-02	2.5499E-03
29	2.986E+02	24068	78962	-52.43	4.5772E-02	26.763	4.2586E-02	3.9445E-02	2.4625E-03
28	2.884E+02	24294	79706	-52.21	4.4148E-02	27.747	4.1075E-02	3.8045E-02	2.3751E-03
27	2.781E+02	24530	80478	-51.97	4.2526E-02	28.806	3.9566E-02	3.6648E-02	2.2878E-03
26	2.678E+02	24774	81280	-51.73	4.0906E-02	29.947	3.8059E-02	3.5251E-02	2.2007E-03
25	2.575E+02	25029	82115	-51.47	3.9287E-02	31.180	3.6553E-02	3.3857E-02	2.1136E-03
24	2.473E+02	25294	82984	-51.21	3.7671E-02	32.518	3.5049E-02	3.2464E-02	2.0266E-03
23	2.370E+02	25570	83892	-50.93	3.6056E-02	33.975	3.3547E-02	3.1072E-02	1.9398E-03
22	2.267E+02	25860	84841	-50.64	3.4444E-02	35.565	3.2047E-02	2.9683E-02	1.8530E-03
21	2.164E+02	26163	85836	-50.34	3.2833E-02	37.309	3.0548E-02	2.8295E-02	1.7664E-03
20	2.061E+02	26481	86881	-50.02	3.1225E-02	39.231	2.9052E-02	2.6909E-02	1.6799E-03
19	1.958E+02	26816	87981	-49.68	2.9620E-02	41.358	2.7558E-02	2.5525E-02	1.5935E-03
18	1.856E+02	27170	89142	-49.33	2.8016E-02	43.725	2.6066E-02	2.4144E-02	1.5072E-03
17	1.753E+02	27545	90371	-48.95	2.6416E-02	46.374	2.4577E-02	2.2764E-02	1.4211E-03
16	1.650E+02	27943	91678	-48.56	2.4818E-02	49.360	2.3090E-02	2.1387E-02	1.3351E-03

117

Table K-1

Specific Lift of Helium and Hydrogen and Properties of the U.S. Standard Atmosphere, 1962									
(1)	(2)	(3)	(4)	(5)	(6)	(7)	(8)	(9)	(10)
p Press. (mb)	Integrated Air Mass (kg/m ²)	H Geopot. Alt. (m)	H Alt. (ft)	T Temp. (°C)	ρ Density (kg/m ³)	Gas Ex- pansion	Lift H ₂ Pure (kg/m ³)	Lift He Grade A (kg/m ³)	Lift He Grade A (lb/ft ³)
15	1.547E+02	28368	93071	-48.13	2.3223E-02	52.750	2.1606E-02	2.0012E-02	1.2493E-03
14	1.444E+02	28823	94564	-47.68	2.1631E-02	56.632	2.0125E-02	1.8641E-02	1.1637E-03
13	1.341E+02	29313	96170	-47.19	2.0042E-02	61.121	1.8647E-02	1.7272E-02	1.0782E-03
12	1.238E+02	29843	97909	-46.66	1.8457E-02	66.370	1.7173E-02	1.5906E-02	9.9296E-04
11	1.135E+02	30420	99804	-46.08	1.6876E-02	72.588	1.5701E-02	1.4543E-02	9.0790E-04
10.0	1.032E+02	31055	101885	-45.45	1.5299E-02	80.07	1.4234E-02	1.3184E-02	8.2307E-04
9.5	9.807E+01	31397	103008	-45.10	1.4512E-02	84.41	1.3502E-02	1.2506E-02	7.8074E-04
9.0	9.292E+01	31758	104193	-44.74	1.3727E-02	89.24	1.2771E-02	1.1829E-02	7.3848E-04
8.5	8.777E+01	32141	105448	-44.11	1.2928E-02	94.75	1.2028E-02	1.1141E-02	6.9552E-04
8.0	8.262E+01	32548	106785	-42.97	1.2107E-02	101.18	1.1265E-02	1.0434E-02	6.5136E-04
7.5	7.747E+01	32984	108215	-41.74	1.1291E-02	108.50	1.0505E-02	9.7301E-03	6.0743E-04
7.0	7.231E+01	33453	109753	-40.43	1.0479E-02	116.90	9.7494E-03	9.0302E-03	5.6374E-04
6.5	6.716E+01	33959	111414	-39.01	9.6713E-03	126.66	8.9982E-03	8.3344E-03	5.2030E-04
6.0	6.200E+01	34509	113220	-37.47	8.8690E-03	138.12	8.2517E-03	7.6430E-03	4.7714E-04
5.5	5.685E+01	35112	115196	-35.79	8.0721E-03	151.76	7.5103E-03	6.9563E-03	4.3427E-04
5.00	5.169E+01	35777	117377	-33.93	7.2812E-03	168.2	6.7744E-03	6.2747E-03	3.9172E-04
4.80	4.963E+01	36063	118317	-33.12	6.9666E-03	175.8	6.4817E-03	6.0036E-03	3.7479E-04
4.60	4.756E+01	36362	119299	-32.29	6.6531E-03	184.1	6.1900E-03	5.7334E-03	3.5792E-04
4.40	4.550E+01	36676	120329	-31.41	6.3407E-03	193.2	5.8994E-03	5.4642E-03	3.4112E-04
4.20	4.344E+01	37006	121411	-30.48	6.0294E-03	203.2	5.6098E-03	5.1960E-03	3.2437E-04
4.00	4.137E+01	37353	122551	-29.51	5.7194E-03	214.2	5.3213E-03	4.9288E-03	3.0769E-04
3.80	3.931E+01	37720	123753	-28.48	5.4106E-03	226.4	5.0340E-03	4.6627E-03	2.9108E-04
3.60	3.724E+01	38108	125027	-27.40	5.1032E-03	240.0	4.7480E-03	4.3978E-03	2.7454E-04
3.40	3.518E+01	38520	126379	-26.24	4.7972E-03	255.4	4.4633E-03	4.1340E-03	2.5808E-04
3.20	3.312E+01	38959	127820	-25.01	4.4926E-03	272.7	4.1799E-03	3.8716E-03	2.4169E-04

118a

Table K-1

Specific Lift of Helium and Hydrogen and Properties of the U.S. Standard Atmosphere, 1962										
(1)	(2)	(3)		(4)	(5)	(6)	(7)	(8)	(9)	(10)
p Press. (mb)	Integrated Air Mass (kg/m ²)	H Geopot. Alt. (m) (ft)		T Temp. (°C)	ρ Density (kg/m ³)	Gas Ex- pansion	Lift H ₂ Pure (kg/m ³)	Lift He Grade A (kg/m ³)	Lift He Grade A (lb/ft ³)	
3.00	3.105E+01	39429	129362	-23.70	4.1896E-03	292.4	3.8980E-03	3.6104E-03	2.2539E-04	
2.80	2.898E+01	39935	131019	-22.28	3.8882E-03	315.1	3.6176E-03	3.3507E-03	2.0918E-04	
2.60	2.692E+01	40481	132810	-20.75	3.5886E-03	341.4	3.3389E-03	3.0926E-03	1.9306E-04	
2.40	2.485E+01	41074	134757	-19.09	3.2909E-03	372.2	3.0619E-03	2.8360E-03	1.7705E-04	
2.20	2.279E+01	41723	136887	-17.28	2.9952E-03	409.0	2.7868E-03	2.5812E-03	1.6114E-04	
2.00	2.072E+01	42440	139238	-15.27	2.7018E-03	453.4	2.5137E-03	2.3283E-03	1.4535E-04	
1.80	1.865E+01	43239	141859	-13.03	2.4107E-03	508.2	2.2429E-03	2.0774E-03	1.2969E-04	
1.60	1.658E+01	44140	144815	-10.51	2.1222E-03	577.2	1.9745E-03	1.8289E-03	1.1417E-04	
1.40	1.451E+01	45172	148202	-7.62	1.8367E-03	666.9	1.7089E-03	1.5828E-03	9.8814E-05	
1.20	1.245E+01	46378	152158	-4.24	1.5546E-03	788.0	1.4464E-03	1.3397E-03	8.3634E-05	
1.00	1.038E+01	47820	156890	-2.50	1.2872E-03	951.7	1.1976E-03	1.1092E-03	6.9247E-05	
.90	9.340E+00	48655	159629	-2.50	1.1584E-03	1057.5	1.0778E-03	9.9830E-04	6.2322E-05	
.80	8.304E+00	49588	162690	-2.50	1.0297E-03	1189.6	9.5805E-04	8.8738E-04	5.5397E-05	
.70	7.268E+00	50646	166161	-2.50	9.0101E-04	1359.6	8.3830E-04	7.7646E-04	4.8473E-05	
.60	6.232E+00	51867	170167	-2.50	7.7229E-04	1586.2	7.1854E-04	6.6553E-04	4.1548E-05	
.50	5.195E+00	53305	174885	-5.11	6.4984E-04	1885.1	6.0461E-04	5.6001E-04	3.4960E-05	
.40	4.158E+00	55044	180592	-8.59	5.2671E-04	2325.8	4.9005E-04	4.5390E-04	2.8336E-05	
.30	3.121E+00	57254	187840	-13.01	4.0174E-04	3049.2	3.7378E-04	3.4621E-04	2.1613E-05	
.20	2.082E+00	60305	197850	-19.11	2.7426E-04	4466.5	2.5517E-04	2.3635E-04	1.4755E-05	
.10	1.043E+00	65281	214176	-37.62	1.4791E-04	8282.1	1.3762E-04	1.2746E-04	7.9573E-06	

REFERENCES

- (1) Warren, J.C., J. H. Smalley, A. L. Morris, 1971: Aerostatic Lift of Helium and Hydrogen in the Atmosphere. NCAR-TN/TA-69, National Center for Atmospheric Research, Boulder, Colo., 79 pp.
- (2) Morris, Alvin L., 1970: Atmospheric Mass above Balloon Payloads, Facilities for Atmospheric Research. 14, Sept. 1970. National Center for Atmospheric Research, Boulder, Colo., 21-24.

L. BASIC NATURAL-SHAPE BALLOON PARAMETERS

The principles of balloon design are discussed in detail in Section V, and the history of the development of the natural-shape balloon is reviewed in Section I. For nearly two decades a set of "Sigma Tables" was an indispensable tool of the balloon designer, and, although digital computers now enable a design engineer to by-pass the tables, many uses are still found for them. Table L-1, which was computed by Smalley (the author of Section V) is valid for zero-pressure, fully tailored balloons carrying the full payload at the nadir. All parameters are non-dimensional except the angle, which is in degrees. Lengths have been non-dimensionalized by dividing by λ , forces by dividing by P. Examples of the use of the table are given in Section V.

Terms used in the table are defined as follows:

$$\text{SIGMA} = (2 \pi)^{1/3} (w/b \lambda)$$

where w is film weight per unit area, b is specific buoyancy of lifting gas, λ is $(P/b)^{1/3}$, and P is total payload (located at nadir).

GORE STA.--curvilinear coordinate measured from nadir.

RADIUS--Radial coordinate measured horizontally from axis of rotation.

HEIGHT--Height coordinate measured vertically from nadir.

ANGLE--angle of tangent to curve measured with respect to the axis of rotation.

FILM LOAD--totalized meridional film stress.

PARTIAL AREA--area of balloon below the gore station.

PARTIAL VOLUME--volume of balloon below the gore station.

$$A/S^{*2} = A/S^2 = (\text{total area})/(\text{total gore length})^2$$

$$V/S^{*3} = V/S^3 = (\text{total volume})/(\text{total gore length})^3$$

Note: A constant gore station increment has been used for each SIGMA value. The RADIUS and HEIGHT are given, however, at the level where RADIUS is maximum, i.e., where ANGLE is zero.

TABLE 1
 (continued)

BASE ANGLE = 54.39144 SIGMA = 0.10						
GOPE STA.	RADIUS	HEIGHT	ANGLE	FILM LOAD	---PARTIAL---	---
					AREA	VOLUME
0.00000	0.00000	0.00000	50.149	1.56056	0.00000	0.00000
.03999	.03062	.02556	50.146	1.56056	.00384	.00003
.07978	.06124	.05110	50.130	1.56056	.01535	.00020
.11960	.09185	.07671	50.034	1.56056	.03453	.00068
.15955	.12242	.10232	49.995	1.56056	.06139	.00161
.19944	.15295	.12800	49.849	1.56056	.09589	.00314
.23933	.18339	.15374	49.630	1.56056	.13804	.00544
.27922	.21371	.17964	49.325	1.56056	.18781	.00866
.31911	.24388	.20579	48.918	1.56056	.24515	.01296
.35899	.27383	.23212	48.396	1.56056	.31003	.01851
.39888	.30351	.25878	47.744	1.56056	.38239	.02550
.43877	.33285	.28580	46.946	1.56056	.46214	.03410
.47866	.36177	.31327	45.988	1.56056	.54919	.04452
.51855	.39019	.34126	44.855	1.56056	.64343	.05696
.55843	.41801	.36985	43.533	1.56056	.74472	.07164
.59832	.44510	.39912	42.005	1.56056	.86290	.08878
.63821	.47135	.42915	40.258	1.56056	.99776	.10861
.67810	.49660	.46002	38.278	1.56056	1.08908	.13135
.71799	.52071	.49180	36.050	1.56056	1.21659	.15720
.75788	.54349	.52454	33.561	1.56056	1.34997	.18634
.79776	.56474	.55825	30.800	1.56056	1.48888	.21892
.83765	.58426	.59307	27.755	1.56056	1.63291	.25502
.87754	.60182	.62888	24.420	1.56056	1.78158	.29462
.91743	.61716	.66569	20.789	1.56056	1.93438	.33761
.95732	.63005	.70344	16.859	1.56056	2.09073	.38376
.99721	.64021	.74203	12.634	1.56056	2.24997	.43267
1.03769	.64741	.78122	8.121	1.56056	2.41139	.48378
1.07698	.65141	.82090	3.332	1.56056	2.57422	.53640
1.11687	.65218	.84743	0.000	1.56056	2.73762	.59164
1.15676	.65199	.86077	-1.713	1.56056	2.73762	.59164
1.19665	.64897	.90053	-5.986	1.56056	2.90073	.64255
1.23654	.64225	.93983	-12.456	1.56056	3.06261	.69406
1.27642	.63176	.97830	-18.080	1.56056	3.22234	.74315
1.31631	.61751	1.01553	-23.313	1.56056	3.37897	.78885
1.35620	.59959	1.05115	-29.003	1.56056	3.53156	.83035
1.39609	.57817	1.08478	-35.393	1.56056	3.67922	.86703
1.43598	.55348	1.11603	-41.126	1.56056	3.82104	.89957
1.47586	.52580	1.14476	-46.742	1.56056	3.95640	.92489
1.51575	.49549	1.17070	-52.185	1.56056	4.08443	.94616
1.55564	.46231	1.19368	-57.400	1.56056	4.20454	.96277
1.59553	.42841	1.21368	-62.338	1.56056	4.31630	.97529
1.63542	.39236	1.23074	-66.955	1.56056	4.41919	.98435
1.67530	.35511	1.24495	-71.213	1.56056	4.51288	.99026
1.71519	.31693	1.25649	-75.081	1.56056	4.59711	.99473
1.75508	.27810	1.26557	-78.534	1.56056	4.67168	.99728
1.79497	.23881	1.27244	-81.553	1.56056	4.73646	.99873
1.83486	.19923	1.27739	-84.123	1.56056	4.79136	.99949
1.87475	.15948	1.28071	-86.234	1.56056	4.83631	.99983
1.91463	.11965	1.28273	-87.880	1.56056	4.87123	.99999
1.95452	.07977	1.28377	-89.057	1.56056	4.89623	.99999
1.99441	.03989	1.28415	-89.764	1.56056	4.91128	1.00000
1.99441	-.00000	1.28421	-93.000	1.56056	4.91628	1.00000

A/S**2 = 1.23597 V/S**3 = .12605 HEIGHT = 0.00000

TABLE 1

BASE ANGLE = 54.39144 SIGMA = 0.10						
GOPE STA.	RADIUS	HEIGHT	ANGLE	FILM LOAD	---PARTIAL---	---
					AREA	VOLUME
0.00000	0.00000	0.00000	54.391	1.71749	0.00000	0.00000
.04309	.03363	.02909	54.382	1.71764	.06974	.00603
.08618	.06705	.05820	54.342	1.71809	.01837	.00226
.12927	.10505	.09534	54.257	1.71834	.04267	.00887
.17236	.13999	.13055	54.111	1.71983	.07585	.00207
.21545	.17486	.16588	53.867	1.72125	.11847	.00405
.25855	.20960	.19130	53.571	1.72292	.17052	.00762
.30164	.24418	.17708	53.140	1.72491	.23196	.01119
.34473	.27854	.20308	52.938	1.72722	.30273	.01678
.38782	.31262	.22945	51.910	1.72987	.38276	.02403
.43091	.34635	.25627	51.067	1.73288	.47198	.03319
.47400	.37963	.28364	50.054	1.73627	.57027	.04453
.51709	.41238	.31164	49.856	1.74034	.67750	.05834
.56018	.44449	.34037	47.457	1.74424	.79352	.07493
.60327	.47584	.36994	45.844	1.74837	.91813	.09462
.64636	.50628	.40044	44.002	1.75288	1.05110	.11775
.68946	.53565	.43197	41.917	1.75957	1.19218	.14465
.73255	.56379	.46460	39.576	1.76568	1.34104	.17568
.77564	.59049	.49842	36.968	1.77233	1.49734	.21105
.81873	.61554	.53347	34.304	1.77953	1.66064	.25116
.86182	.63870	.56980	30.915	1.78729	1.83043	.29608
.90491	.65973	.60740	27.457	1.79560	2.00630	.34592
.94800	.67835	.64626	23.706	1.80446	2.18750	.40660
.99109	.69429	.68628	19.666	1.81382	2.37339	.45988
1.03418	.70726	.72736	15.342	1.82362	2.56319	.52331
1.07727	.71700	.76933	10.746	1.83380	2.75607	.59203
1.12036	.72325	.81195	5.894	1.84420	2.95113	.66572
1.16346	.72578	.85495	.868	1.85487	3.14737	.73070
1.20655	.72583	.86163	0.000			
1.24964	.72441	.89801	-4.484	1.86550	3.34378	.80188
1.29273	.71951	.94074	-9.948	1.87601	3.53928	.87188
1.33582	.70351	.98275	-15.545	1.88623	3.73275	.93928
1.37891	.68593	1.02363	-21.232	1.89602	3.92311	1.00276
1.42200	.66783	1.06295	-26.963	1.90523	4.10924	1.06116
1.46509	.64929	1.10030	-32.686	1.91373	4.29080	1.11355
1.50818	.63189	1.13537	-38.352	1.92142	4.46463	1.15935
1.55127	.60355	1.16781	-43.911	1.92825	4.63195	1.19830
1.59437	.57224	1.19739	-49.312	1.93418	4.79118	1.23043
1.63746	.53833	1.22395	-54.505	1.93920	4.94158	1.25627
1.68055	.50220	1.24741	-59.460	1.94336	5.08249	1.27627
1.72364	.46423	1.26776	-64.124	1.94672	5.21335	1.29124
1.76673	.42477	1.28506	-68.468	1.94934	5.33373	1.30202
1.80982	.38416	1.29944	-72.462	1.95132	5.44326	1.30944
1.85291	.34268	1.31110	-76.082	1.95277	5.54167	1.31431
1.89600	.30058	1.32025	-79.308	1.95377	5.62827	1.31731
1.93909	.25806	1.32718	-82.125	1.95444	5.70440	1.31902
1.98218	.21526	1.33218	-84.522	1.95484	5.76848	1.31991
2.02528	.17230	1.33551	-86.490	1.95506	5.82095	1.32031
2.06837	.12926	1.33755	-88.024	1.95517	5.86177	1.32046
2.11146	.08618	1.33859	-89.122	1.95521	5.89093	1.32050
2.15455	.04309	1.33895	-89.780	1.95522	5.90843	1.32051
2.15455	-.00000	1.33903	-90.000	1.95522	5.91427	1.32051

A/S**2 = 1.27406 V/S**3 = .13203 HEIGHT = .32051

Table L-1

BASE ANGLE = 58.88617 SIGMA = .20						
GORE STA.	RADIUS	HEIGHT	ANGLE	FILM LOAD	-----PARTIAL----- AREA	-----VOLUME
0.00000	0.00000	0.00000	58.886	1.93521	0.00000	0.00000
.04701	.04024	.02430	58.867	1.93554	.00594	.00004
.09402	.08047	.04862	58.798	1.93654	.02377	.00033
.14103	.12065	.07302	58.663	1.93821	.05347	.00112
.18803	.16076	.09754	58.444	1.94056	.09504	.00265
.23504	.20075	.12224	58.125	1.94361	.14843	.00520
.28205	.24058	.14721	57.689	1.94736	.21361	.00903
.32906	.28019	.17253	57.121	1.95185	.29052	.01444
.37607	.31951	.19828	56.403	1.95711	.37910	.02173
.42308	.35847	.22459	55.521	1.96318	.47923	.03124
.47009	.39698	.25155	54.458	1.97012	.59081	.04334
.51709	.43494	.27928	53.199	1.97798	.71369	.05844
.56410	.47222	.30791	51.728	1.98683	.84768	.07697
.61111	.50870	.33755	50.033	1.99673	.99256	.09940
.65812	.54422	.36834	48.097	2.00777	1.14809	.12623
.70513	.57862	.40038	45.909	2.02003	1.31394	.15800
.75214	.61168	.43379	43.457	2.03357	1.48976	.19521
.79915	.64321	.46866	40.731	2.04848	1.67513	.23838
.84616	.67295	.50505	37.723	2.06480	1.86955	.28795
.89316	.70064	.54303	34.427	2.08257	2.07245	.34428
.94017	.72600	.58260	30.841	2.10180	2.28320	.40759
.98718	.74874	.62374	26.967	2.12246	2.50106	.47792
1.03419	.76893	.66636	22.809	2.14449	2.72521	.55506
1.08120	.78508	.71035	18.379	2.16777	2.95474	.63892
1.12821	.79808	.75551	13.699	2.19213	3.18863	.72750
1.17521	.80724	.80161	8.760	2.21733	3.42580	.82087
1.22222	.81232	.84832	3.617	2.24311	3.66509	.91719
1.26923	.81334	.88837	0.000	2.26912	3.90524	1.01478
1.31624	.81311	.89531	-1.711	2.29502	4.14498	1.11174
1.36325	.80948	.94216	-7.190	2.32042	4.38298	1.20614
1.41026	.80133	.98844	-12.783	2.34493	4.61790	1.29610
1.45727	.78869	1.03369	-18.449	2.36820	4.84844	1.37990
1.50428	.77162	1.07747	-24.145	2.38991	5.07330	1.45617
1.55128	.75030	1.11935	-29.828	2.40980	5.29126	1.52389
1.59829	.72495	1.15891	-35.452	2.42767	5.50118	1.58251
1.64530	.69587	1.19583	-40.973	2.44341	5.70200	1.63191
1.69231	.66342	1.22981	-46.350	2.45699	5.89279	1.67240
1.73932	.62798	1.26067	-51.541	2.46845	6.07271	1.70462
1.78633	.58994	1.28826	-56.509	2.47788	6.24106	1.72945
1.83334	.54973	1.31254	-61.224	2.48545	6.39725	1.74795
1.88034	.50766	1.33355	-65.642	2.49136	6.54081	1.76121
1.92735	.46417	1.35136	-69.748	2.49581	6.67134	1.77033
1.97436	.41955	1.36615	-73.515	2.49906	6.78857	1.77628
2.02137	.37410	1.37812	-76.923	2.50131	6.89227	1.77994
2.06838	.32805	1.38751	-79.958	2.50279	6.98241	1.78204
2.11539	.28158	1.39461	-82.605	2.50369	7.05859	1.78312
2.16240	.23485	1.40315	-84.856	2.50419	7.12103	1.78361
2.20941	.18797	1.40315	-86.704	2.50442	7.16962	1.78380
2.25642	.14101	1.40523	-88.145	2.50451	7.20433	1.78384
2.30342	.09402	1.40630	-89.175	2.50453	7.22515	1.78385
2.35043	.04701	1.40670	-89.794	2.50453	7.23210	1.78385
A/S**2 = 1.30909	V/S**3 = .13738	WEIGHT = .78385				

Table L-1

BASE ANGLE = 63.46893 SIGMA = .30						
GORE STA.	RADIUS	HEIGHT	ANGLE	FILM LOAD	-----PARTIAL----- AREA	-----VOLUME
0.00000	0.00000	0.00000	63.469	2.23872	0.00000	0.00000
.05176	.04630	.02313	63.438	2.23927	.00753	.00005
.10351	.09258	.04631	63.333	2.24092	.03011	.00042
.15527	.13879	.06961	63.137	2.24367	.06774	.00141
.20703	.18491	.09311	62.833	2.24756	.12037	.00336
.25879	.23107	.11691	62.403	2.25261	.18798	.00660
.31054	.27662	.14110	61.830	2.25889	.27051	.01152
.36230	.32210	.16582	61.099	2.26645	.36787	.01849
.41406	.36722	.19117	60.193	2.27538	.47997	.02798
.46582	.41189	.21732	59.096	2.28579	.60666	.04046
.51757	.45600	.24439	57.792	2.29779	.74780	.05651
.56933	.49943	.27254	56.266	2.31153	.90317	.07672
.62109	.54203	.30193	54.564	2.32717	1.07254	.10179
.67285	.58365	.33270	52.492	2.34487	1.25960	.13246
.72460	.62408	.36500	50.218	2.36481	1.45201	.16951
.77636	.66312	.39898	47.671	2.38715	1.66135	.21378
.82812	.70052	.43474	44.841	2.42108	1.88313	.26607
.87987	.73602	.47240	41.723	2.43972	2.11677	.32718
.93163	.76931	.51202	38.313	2.47019	2.36160	.39776
.98339	.80008	.55363	34.612	2.50356	2.61686	.47833
1.03515	.82799	.59720	30.622	2.53981	2.88166	.56913
1.08690	.85269	.64267	26.354	2.57886	3.15504	.67010
1.13866	.87383	.68990	21.820	2.62053	3.43587	.78078
1.19042	.89106	.73869	17.037	2.66452	3.72295	.90124
1.24218	.90406	.78877	12.029	2.71146	4.01496	1.02710
1.29393	.91254	.83981	6.821	2.75784	4.31046	1.15950
1.34569	.91628	.89141	1.446	2.80606	4.60796	1.29518
1.39745	.91646	.90510	0.000	2.85447	4.90588	1.43155
1.44920	.91511	.94314	-4.064	2.90234	5.20261	1.56591
1.50096	.90893	.99450	-9.671	2.94897	5.49651	1.69552
1.55272	.89773	1.04901	-15.338	2.99366	5.78596	1.81786
1.60448	.88159	1.09917	-21.025	3.03579	6.06937	1.93079
1.65623	.86366	1.14148	-26.692	3.07481	6.34524	2.03262
1.70799	.83518	1.18651	-32.300	3.11032	6.61211	2.12226
1.75975	.80546	1.22886	-37.810	3.14203	6.86868	2.19924
1.81151	.77185	1.26819	-43.185	3.16981	7.11375	2.26365
1.86326	.73475	1.30426	-48.390	3.19365	7.34624	2.31610
1.91502	.69459	1.33689	-53.391	3.21367	7.55223	2.35761
1.96678	.65180	1.36597	-58.158	3.23010	7.73939	2.38945
2.01854	.60680	1.39151	-62.662	3.24325	7.90969	2.41309
2.07029	.55998	1.41354	-66.880	3.25348	8.13398	2.42998
2.12205	.51171	1.43224	-70.788	3.26119	8.29239	2.44156
2.17381	.46233	1.44767	-74.369	3.26679	8.43659	2.44912
2.22556	.41211	1.46018	-77.604	3.27067	8.56036	2.45376
2.27732	.36130	1.46999	-80.483	3.27322	8.66954	2.45641
2.32908	.31008	1.47740	-82.993	3.27478	8.76201	2.45778
2.38084	.25860	1.48273	-85.126	3.27564	8.83771	2.45840
2.43259	.20697	1.48631	-86.877	3.27604	8.89661	2.45863
2.48435	.15526	1.48848	-88.242	3.27620	8.93869	2.45870
2.53611	.10351	1.48960	-89.219	3.27623	8.96394	2.45871
2.58787	.05176	1.49001	-89.805	3.27623	8.97235	2.45871
A/S**2 = 1.33975	V/S**3 = .14187	WEIGHT = 1.45871				

Table L-1

BASE ANGLE = 67.91954 SIGMA = .40						
GORE STA.	RADIUS	HEIGHT	ANGLE	FILM LOAD	---PARTIAL--- AREA	---PARTIAL--- VOLUME
0.00000	0.00000	0.00000	67.920	2.66022	0.00000	0.00000
.05741	.05319	.02159	67.875	2.66101	.00999	.00066
.11482	.10635	.04328	67.730	2.66336	.03837	.00051
.17223	.15943	.06514	67.467	2.66732	.08631	.00174
.22964	.21239	.08732	67.069	2.67294	.15338	.00417
.28705	.26516	.10995	66.519	2.68030	.23951	.00824
.34446	.31767	.13312	65.861	2.68951	.34464	.01445
.40187	.36986	.15705	64.898	2.70072	.46865	.02336
.45928	.42161	.18188	63.795	2.71411	.61141	.03561
.51669	.47284	.20781	62.476	2.72991	.77275	.05194
.57409	.52339	.23501	60.926	2.74837	.95245	.07318
.63150	.57313	.26367	59.130	2.76979	1.15024	.10029
.68891	.62188	.29398	57.075	2.79447	1.36580	.13435
.74632	.66944	.32614	54.749	2.82276	1.59874	.17692
.80373	.71556	.36031	52.146	2.85501	1.84858	.22808
.86114	.75999	.39666	49.240	2.89155	2.11477	.29032
.91855	.80243	.43531	46.045	2.93270	2.39663	.36453
.97596	.84253	.47638	42.552	2.97873	2.69380	.45191
1.03337	.87995	.51940	38.763	3.02981	3.00443	.55345
1.09078	.91429	.56590	34.684	3.08603	3.32783	.66986
1.14819	.94515	.61429	30.327	3.14734	3.66331	.80140
1.20560	.97213	.66495	25.717	3.21351	4.00923	.94780
1.26301	.99483	.71766	20.844	3.28416	4.36812	1.10813
1.32042	1.01287	.77214	15.764	3.35868	4.72637	1.28076
1.37783	1.02592	.82803	10.495	3.43631	5.09423	1.46338
1.43524	1.03370	.88488	5.069	3.51609	5.46586	1.65298
1.49265	1.03601	.94223	-.479	3.59695	5.83931	1.84607
1.55006	1.03603	.93730	0.000	3.67770	6.21259	2.03881
1.60747	1.02378	1.05620	-11.800	3.75712	6.58366	2.22728
1.66488	1.00927	1.11172	-17.499	3.83403	6.95050	2.40769
1.72228	.98932	1.16553	-23.176	3.90730	7.31112	2.57667
1.77969	.96417	1.21711	-28.793	3.97596	7.66360	2.73144
1.83710	.93413	1.26601	-34.318	4.03921	8.00612	2.87003
1.89451	.89957	1.31183	-39.716	4.09645	8.33697	2.99115
1.95192	.86091	1.35424	-44.958	4.14734	8.65460	3.09455
2.00933	.81860	1.39301	-50.012	4.19171	8.95762	3.18059
2.06674	.77309	1.42799	-54.853	4.22966	9.24478	3.25032
2.12415	.72486	1.45910	-59.454	4.26143	9.51502	3.30528
2.18156	.67435	1.48636	-63.792	4.28743	9.76744	3.34730
2.23897	.62198	1.50985	-67.846	4.30819	10.00129	3.37840
2.29638	.56813	1.52971	-71.598	4.32432	10.21598	3.40058
2.35379	.51314	1.54617	-75.031	4.33646	10.41102	3.41576
2.41120	.45730	1.55946	-78.132	4.34526	10.58607	3.42565
2.46861	.40085	1.56988	-80.889	4.35137	10.74086	3.43172
2.52602	.34398	1.57775	-83.292	4.35538	10.87520	3.43518
2.58343	.28686	1.58341	-85.335	4.35782	10.98898	3.43698
2.64084	.22958	1.58721	-87.011	4.35917	11.08213	3.43779
2.69825	.17221	1.58952	-88.318	4.35981	11.15460	3.43809
2.75566	.11482	1.59071	-89.252	4.36005	11.20637	3.43819
2.81306	.05741	1.59114	-89.813	4.36010	11.23743	3.43819
2.87047	-.00000	1.59121	-90.000	4.36011	11.24778	3.43819

A/S**2 = 1.36508 V/S**3 = .14537 WEIGHT = 2.42819

Table L-1

BASE ANGLE = 72.01204 SIGMA = .50						
GORE STA.	RADIUS	HEIGHT	ANGLE	FILM LOAD	---PARTIAL--- AREA	---PARTIAL--- VOLUME
0.00000	0.00000	0.00000	72.012	3.23816	0.00000	0.00000
.06396	.06083	.01977	71.953	3.23919	.01222	.00008
.12792	.12162	.03968	71.767	3.24228	.04889	.00062
.19188	.18232	.05985	71.435	3.24750	.10997	.00210
.25584	.24287	.08046	70.942	3.25497	.19542	.00505
.31980	.30321	.10168	70.273	3.26484	.30516	.01005
.38376	.36326	.12371	69.411	3.27734	.43910	.01777
.44772	.42294	.14674	68.342	3.29277	.59710	.02898
.51168	.48212	.17100	67.048	3.31147	.77899	.04463
.57564	.54069	.19670	65.517	3.33387	.98455	.06581
.63960	.59849	.22409	63.733	3.36045	1.21350	.09378
.70356	.65535	.25340	61.682	3.39175	1.46549	.13004
.76752	.71104	.28486	59.351	3.42826	1.74011	.17625
.83148	.76531	.31869	56.731	3.47090	2.03684	.23427
.89544	.81789	.35510	53.812	3.52001	2.35544	.30666
.95940	.86845	.39428	50.590	3.57628	2.69399	.39369
1.02336	.91660	.43636	47.062	3.64026	3.05278	.49915
1.08732	.96196	.48144	43.231	3.71240	3.43038	.62427
1.15128	1.00408	.52957	39.105	3.79238	3.82557	.77054
1.21524	1.04249	.58069	34.696	3.88209	4.23696	.93890
1.27920	1.07674	.63469	30.022	3.97956	4.66297	1.12959
1.34316	1.10635	.69127	25.106	4.08493	5.10182	1.34195
1.40712	1.13088	.75042	19.974	4.19744	5.55157	1.57431
1.47108	1.14992	.81146	14.657	4.31601	6.01009	1.82393
1.53504	1.16314	.87402	9.187	4.43924	6.47510	2.08705
1.59900	1.17027	.93756	3.600	4.56551	6.94421	2.35911
1.66296	1.17155	.97823	0.000	4.69299	7.41492	2.63453
1.72692	1.17113	1.00149	-2.070	4.82279	7.88471	2.90798
1.79088	1.16564	1.016519	-7.746	4.95977	8.35102	3.17374
1.85484	1.15383	1.02803	-13.513	5.09389	8.81133	3.42658
1.91880	1.13581	1.03938	-19.219	5.22352	9.26113	3.66196
2.00000	1.11181	1.04864	-24.868	5.34816	9.69128	3.87629
2.08112	1.08213	1.05527	-30.431	5.46279	10.10228	4.06712
2.16224	1.04710	1.05886	-35.877	5.56737	10.49328	4.23313
2.24336	1.00731	1.05881	-41.179	5.66195	10.86428	4.37417
2.32448	.96338	1.05499	-46.319	5.74653	11.21528	4.49106
2.40560	.91497	1.04712	-51.242	5.82111	11.54628	4.58547
2.48672	.86349	1.03505	-55.956	5.88569	11.85728	4.65965
2.56784	.80914	1.01873	-60.427	5.94027	12.14828	4.71625
2.64896	.75238	1.00821	-64.637	5.98485	12.41928	4.75804
2.73008	.69368	1.00358	-68.567	6.01943	12.67028	4.78782
2.81120	.63343	1.00452	-72.201	6.04401	12.90128	4.80816
2.89232	.57198	1.01027	-75.524	6.05859	13.11228	4.81910
2.97344	.50965	1.02102	-78.524	6.06317	13.30328	4.82144
3.05456	.44669	1.03677	-81.190	6.05775	13.47428	4.82553
3.13568	.38329	1.05661	-83.514	6.04233	13.72528	4.83147
3.21680	.31962	1.07921	-85.489	6.01691	13.95628	4.83657
3.29792	.25579	1.10401	-87.110	6.00149	14.16728	4.83765
3.37904	.19188	1.12981	-88.373	6.00607	14.35828	4.83806
3.46016	.12792	1.15077	-89.277	6.02065	14.51928	4.83817
3.54128	.06396	1.17114	-89.819	6.03523	14.65028	4.83818
3.62240	-.00000	1.17113	-90.000	6.04981	14.76128	4.83818

A/S**2 = 1.38484 V/S**3 = .14790 WEIGHT = 3.85818

M. BUOYANT EQUILIBRIUM DIAGRAMS

A floating balloon is in a precarious state of equilibrium, and a slight decrease in the ratio of gas to air temperature or a slight loss of gas will cause it to accelerate downward unless corrective measures are taken. Figures M-1 and M-2 provide graphical solutions to the equation of buoyant equilibrium for balloons inflated with helium and hydrogen, respectively. The theory upon which these diagrams are based and some examples of their use are given in Section II.I.4.a.

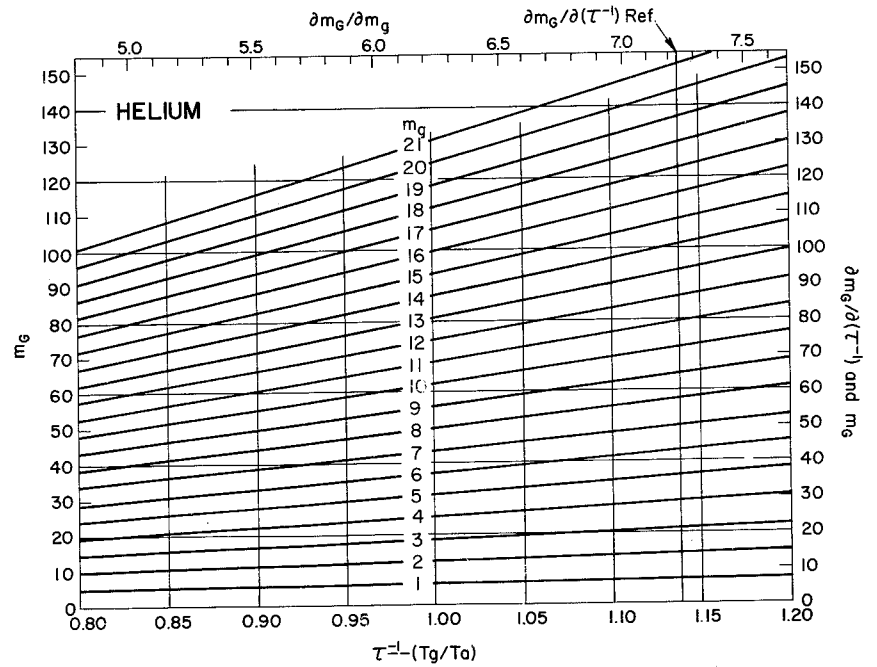


Fig. M-1. Buoyant equilibrium diagram for helium.

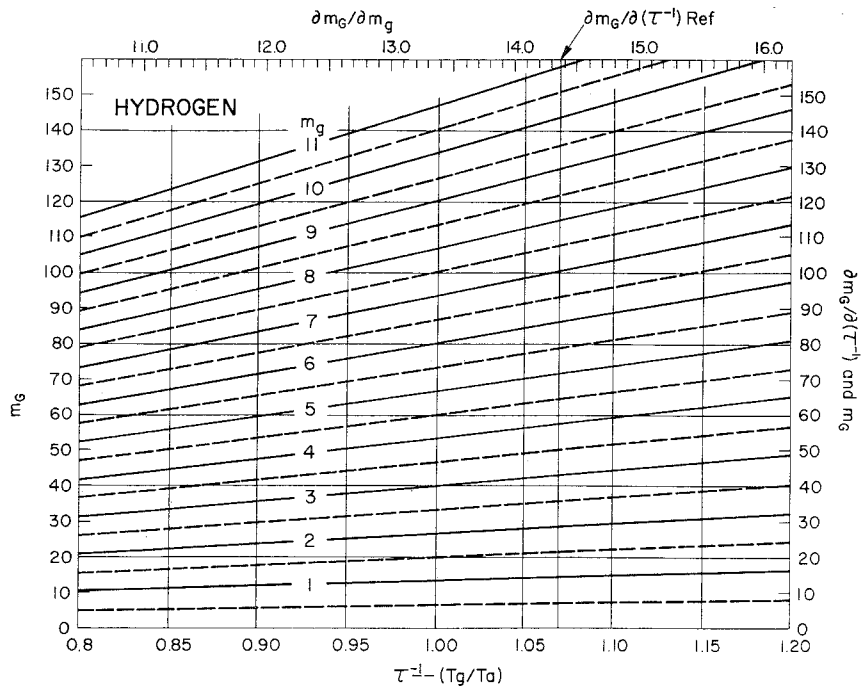


Fig. M-2. Buoyant equilibrium diagram for hydrogen.

N. SUNRISE AND SUNSET

The times of sunrise and sunset, both at the ground and on a floating balloon, are often important. If a nautical almanac is available, it is a relatively simple matter to determine sunrise and sunset at the surface. If it is more convenient, however, the local hour angle of sunrise and sunset at the surface may be approximated by the formula

$$(\text{LHA})_S = \cos^{-1} \left[\frac{-0.01 - \sin \lambda_1 \sin \delta_s}{\cos \lambda_1 \cos \delta_s} \right] \quad (\text{N-1})$$

in which λ_1 is the latitude of the observer and δ_s is the solar declination. Both λ_1 and δ_s are positive north of the equator and negative south of the equator. The formula includes a coarse correction for the apparent diameter of the sun and atmospheric refraction. The $(\text{LHA})_S$ in degrees divided by 15 is the time in hours by which the sunrise precedes true solar noon or the sunset follows true solar noon.

Similarly, the formula

$$(\text{LHA})_B = \cos^{-1} \left[\frac{-\sqrt{\frac{2H}{r}} - 0.016 - \sin \lambda_1 \sin \delta_s}{\cos \lambda_1 \cos \delta_s} \right] \quad (\text{N-2})$$

gives approximately the local hour angle of sunrise or sunset on a balloon

floating at height H where r is the radius of the earth; H and r must be expressed in the same length units.

The time difference in minutes between sunrise (or sunset) at the surface and sunrise (or sunset) at a floating balloon is

$$\Delta t = 4 [(LHA)_B - (LHA)_S] \quad (N-3)$$

if the LHA values are determined in degrees.

The value of δ_s is a function of time; it is given approximately by the formula

$$\delta_s = -23.45 \cos \frac{360}{365} (n + 10) \quad (N-4)$$

in which n is the number of the day in the year counting 1 January as n = 1, 2 January as n = 2, etc. to 31 December = 365.

0. STAR CHARTS

The appearance of the brighter stars in the sky at any hour of the night and any time of the year may be visualized by referring to Figs. 0-1 and 0-2. These star charts may also be used to determine the approximate positions (declination and local hour angle) of any of the charted stars, day or night.

A star chart provides the most direct visual simulation of the star pattern when it is "set" against the sky. To set a chart for midnight, hold it directly overhead facing downward so that it can be read and turn it until an imaginary line drawn from the time of year on the outer ring through the pole on the chart points toward the earth's pole. The star pattern on the chart will then correspond to the midnight star pattern in the heavens at the observer's location at the time of year for which the chart was set.

An observer at a Northern Hemisphere site where there are no obstructions on the horizon should be able to see stars on the northern horizon which are below Polaris at a co-latitude equal numerically to his latitude. He should see stars on the southern horizon which are at a southern latitude

equal to his co-latitude. The stars on his eastern and western horizon will be directly over the equator, and their local hour angle will be 90° , i.e., they will pass over his meridian in six hours. By using these four points, the horizon can be visualized on the charts. Note that latitude is used when discussing the angular displacement of a star from the equator although declination is the proper term. A northern latitude corresponds to a positive declination, and a southern latitude to a negative declination.

There are 24 alternately shaded and unshaded hour segments in the ring just inside the month ring. The arrows indicate the direction of apparent turning of the celestial sphere. A chart may be set for n hours before midnight by first setting it to simulate the midnight sky and then turning it back n hours, i.e., n segments in the direction opposed to the arrows. Likewise, turning a chart set for midnight n hour segments in the direction of the arrows sets it for n hours after midnight.

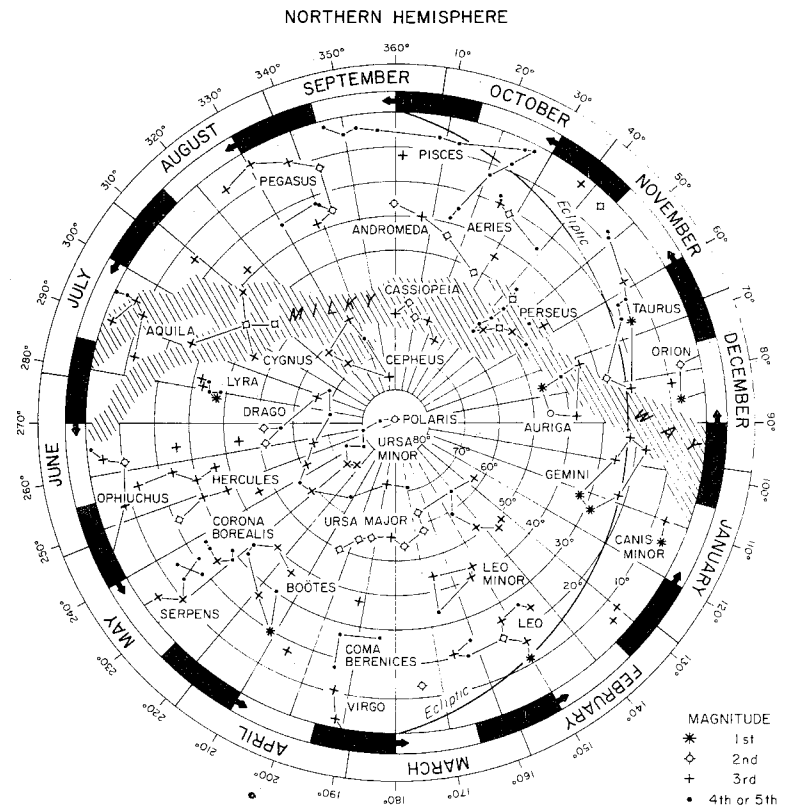


Fig. 0-1. Northern Hemisphere star chart.

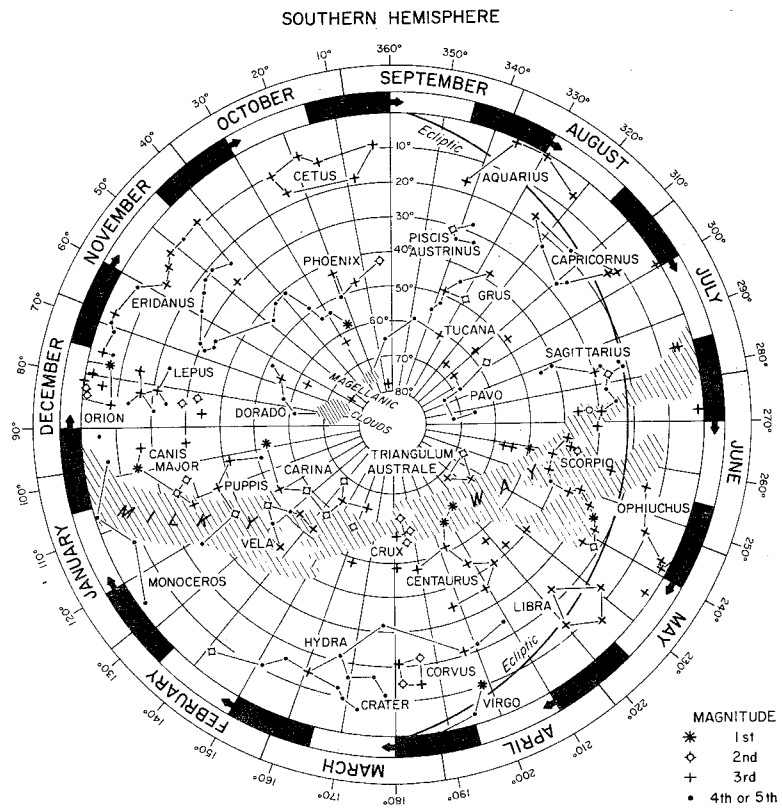


Fig. 0-2. Southern Hemisphere star chart.